MARTIN MARIETTA ENERGY SYSTEMS LIBRARIES
3 4456 0059678 1

ORNL-3189
UC-41 – Health and Safety
TID-4500 (16th ed., Rev.)

HEALTH PHYSICS DIVISION
ANNUAL PROGRESS REPORT
FOR PERIOD ENDING JULY 31, 1961

OAK RIDGE NATIONAL LABORATORY
operated by
UNION CARBIDE CORPORATION
for the
U.S. ATOMIC ENERGY COMMISSION

CENTRAL RESEARCH LIBRARY
DOCUMENT COLLECTION
LIBRARY LOAN COPY
DO NOT TRANSFER TO ANOTHER PERSON
If you wish someone else to see this document, send in name with document and the library will arrange a loan.

Printed in USA. Price $3.50. Available from the

Office of Technical Services
Department of Commerce
Washington 25, D.C.

LEGAL NOTICE

This report was prepared as an account of Government sponsored work. Neither the United States, nor the Commission, nor any person acting on behalf of the Commission:

A. Makes any warranty or representation, expressed or implied, with respect to the accuracy, completeness, or usefulness of the information contained in this report, or that the use of any information, apparatus, method, or process disclosed in this report may not infringe privately owned rights; or

B. Assumes any liabilities with respect to the use of, or for damages resulting from the use of any information, apparatus, method, or process disclosed in this report.

As used in the above, "person acting on behalf of the Commission" includes any employee or contractor of the Commission, or employee of such contractor, to the extent that such employee or contractor of the Commission, or employee of such contractor prepares, disseminates, or provides access to, any information pursuant to his employment or contract with the Commission, or his employment with such contractor.

ORNL-3189
UC-41 – Health and Safety
TID-4500 (16th ed., Rev.)

Contract No. W-7405-eng-26

HEALTH PHYSICS DIVISION ANNUAL PROGRESS REPORT

For Period Ending July 31, 1961

K. Z. Morgan, Director

DATE ISSUED

OCT 24 1961

MARTIN MARIETTA ENERGY SYSTEMS LIBRARIES

3 4456 0059678 1

OAK RIDGE NATIONAL LABORATORY
Oak Ridge, Tennessee
operated by
UNION CARBIDE CORPORATION
for the
U. S. ATOMIC ENERGY COMMISSION

HEALTH PHYSICS DIVISION ANNUAL PROGRESS REPORT

SUMMARY

1. RADIOACTIVE WASTE DISPOSAL

Low-Level Waste Water Treatment

The process waste treatment plant at ORNL employs $CaCO_3$ precipitation for removal of Sr^{90} and addition of clay for removal of Cs^{137}. Laboratory studies and plant tests include classification of solids in the plant effluent, use of phosphates as a supplement to normal lime-soda softening, and use of natural minerals for second-stage treatment. Their purpose is to investigate methods of increasing fission-product removals by use of the plant facilities that are available.

Study of White Oak Creek Drainage Basin

A number of monitoring stations have been installed to describe the release of radionuclides to the White Oak Creek drainage basin, and to delineate their accumulation and transport in the physical and chemical environment. The quantity of radionuclides contributed from the laundry and burial ground 4 is small, even though some leaching of buried solid waste by recharging rainfall is evident. Approximately 150,000 ft^3 of contaminated silt has been washed from the bed of White Oak Lake since 1953, due primarily to channel erosion. Preliminary analyses of sediment cores from the lake bed show that most of the gross gamma activity is contained in the upper 12 in. of soil.

Clinch River Study

Water sampling and stream gaging stations and analytical procedures have been established to provide information about flow, discharge, stable and radioactive ion concentrations, and sediment load in the Clinch River. A preliminary estimate has been made of the radionuclide distribution and accumulation in bottom sediments of the Clinch River from Clinch River Mile (CRM) 21.6 to CRM 4.7. This estimate, based on the results of core samples, collected from 19 cross sections, shows that Cs^{137}, Ru^{106}, Co^{60}, and total rare earths exhibit concentration maxima at CRM 20.8 and CRM 11.0. A comparison of the calculated total activity in the Clinch River with the core-sample estimate shows that approximately 14% (184 curies) of the total activity (1300 curies) is associated with bottom sediments. The estimated amounts of radioactivity in bottom sediments as determined by analysis of the core samples are: Cs^{137} = 99.48 curies; TRE = 37.64 curies; Ru^{106} = 33.20 curies; Co^{60} = 11.64 curies; and Sr^{90} = 1.86 curies.

Fundamental Studies of Sorption by Minerals

Removal of fixed cesium was significant only when cations capable of expanding the collapsed lattice were used. Intensive cropping by oats grown on vermiculite with fixed cesium released only about 1% of the sorbed cesium.

In reactions involving strontium removal, the ion-exchange capacity, saturating cation, and surface characteristics of sorbent influenced the degree of sorption. Precipitation reactions involving calcium and phosphate ions were also important in removing strontium.

Ruthenium removals were increased when reducing conditions were imposed on the system; chalcopyrite ($CuFeS_2$) was found to be one of the more effective minerals for sorbing ruthenium.

Soil Column Studies

Particle diffusion coefficients have been estimated for the migration of cesium to the interior of vermiculite platelets, and the effects of particle diffusion on column operation have been discussed. Improvement of vermiculite column operation, based on an understanding of the reaction mechanism, has been demonstrated.

Disposal in Salt Formations

The field experiments in the Carey Salt Mine have been completed and the results analyzed. The

thermal data from the experiments agree quite well with the theoretical calculations, and the plastic flow around the heated cavities gave no indication that the stability of the room had been disturbed.

Primary program emphasis has been changed from studies of direct-liquid disposal in salt to solids disposal.

Laboratory studies on the control and elimination of radiolytic off-gases have been continued. A study has been initiated on the mechanisms responsible for the changes observed in the shape and size of liquid-waste-filled salt cavities.

Disposal in Deep Wells

In a full-scale experiment, two separate batches of grout, totaling over 200,000 gal, were injected into the local shale formation at depths of roughly 700 and 1000 ft. Test drilling, not yet completed, has shown that the grout formed generally horizontal fractures extending out 400 to 500 ft from the injection well. Work has been started on a test well, 3000 ft deep, to explore potential disposal formations not exposed at the surface; and a preliminary design and cost estimate of a disposal plant and well system to dispose of the Laboratory's medium-level waste stream has been prepared.

Evaluation of Engineering, Economics, and Hazards

A more thorough examination has been made of tank storage hazards. The consequences of tank-cooling system failure were studied in detail.

A study has been undertaken, in cooperation with the ORNL Chemical Technology Division, to evaluate, first from economics and later from hazards standpoints, the various methods of high-activity liquid and solid waste disposal being investigated by the Laboratory. As a necessary part of this study, the various operations leading to these ultimate disposal methods will also be evaluated. The economics studies of interim liquid storage and conversion to solids by pot calcination have been completed.

Related Cooperative Projects

A number of investigations have been made by and in cooperation with other groups, both governmental and private. Five engineers and scientists from other countries have worked for varying lengths of time as members of the Radioactive Waste Disposal Section.

2. ECOLOGICAL RESEARCH

White Oak Lake Bed Studies

Research in White Oak Lake bed and the surrounding contaminated environs takes advantage of the presence of mixed radioisotopes, both as a source of radiation and as a tool for studying the behavior of these radioelements in the environment. During the past two years there has been virtually no change in the over-all distribution of plant communities on the ecology study area in the lower section of White Oak Lake bed. The major changes that are developing represent invasion by low-land moist-soil and upland woody vegetation. The former are becoming dominant along the creek shore and the latter in the higher areas adjacent to the original lake shore. Soil-to-plant studies of uptake of radionuclides included an experiment on rate of uptake by *Lespedeza* during the growing season. There was a fivefold increase in Sr^{90} accumulation during the 1960 growing season which resulted in a total of $(157.0 \pm 9.7) \times 10^3$ (s.e.) $\mu\mu c$ of Sr^{90} per m^2 of vegetation. Based on the total number of days in the growing season this accumulation represented an uptake rate of 1300 ± 81 $\mu\mu c$ of Sr^{90} per m^2 per day. *Lespedeza* was compared with *Polygonum* (smartweed) harvested the previous year by using a coefficient of transfer, which is the ratio of the uptake rate to the soil burden per unit area. On this basis *Polygonum* as a vegetation unit seems to be approximately 4.5 times more effective than *Lespedeza* in accumulating Sr^{90}. Use of massive doses of phosphate fertilizer showed encouraging results in decreasing the total uptake of Sr^{90} in proportion to increase in total yield. Increases in total radiostrontium were 136, 237, and 266% (in terms of controls) compared to yield increases of 223, 453, and 568%.

The rates of elimination of radioisotopes by insects can be used to estimate the rates of feeding. Better estimates of an average λ (the elimination constant) for cesium were the result of analyses of the relationship between weight of insect and rate of elimination. The elimination

rate for cesium decreased as size of insect increased, when different insect species were compared. Immature stages had lower rates of elimination than their smaller size would suggest. Estimates of the annual consumption of vegetation by insects were increased from 3 to 5% of annual plant production, by refined estimates of λ.

Few cotton rats out of 180 on the lake bed were trapped for periods of over 6 months, and only 1 was present for over a year. The sex ratio of males (178) to females (137) differed significantly from 1:1 for the lake bed, but not for an uncontaminated old field. The average number of young per litter was smaller at the lake bed (5.4) than at the old field (7.7). Weighted incidences of injuries and abnormalities for both areas were about the same.

Whole-body dose rates calculated for muskrats from the radioactive settling basin ranged from 15.1 rems/week (contents of GI tract not included) to 112 rems/week (contents of GI tract included). Calculations show that a person eating 1 lb of muskrat meat would have received a whole-body dose rate of 0.023 rem/week at $t = 0$, and 0.034 rem/week shortly after ingestion of the second pound of meat one week after the first ingestion. For cotton rats living in an area with an average external radiation field of 15 mr/hr, the integrated whole-body dose rate from internal and external sources was estimated to be 2.6 rems/week; 86% of this dose rate was due to the radiation field above the lake bed, 10% was due to radionuclides in the tissues, and the remaining 4% was due to radioisotopes in the contents of the GI tract. Body burdens of Sr^{90}, Cs^{137}, Ru^{106}, and Co^{60} determined by radioassay of known-age cotton rats were lower than predicted for each isotope.

Few gross pathologies have been observed so far in mammals from radioactive and nonradioactive areas, but examination of tissues revealed an unexpected number of generalized pathologies, none of which could be positively related to radiation exposure.

Forest Ecology

Complex ecological systems like forests are maintained by a natural flux of energy and a circulation of chemical elements. Botanical, forestry, soils, zoological, microbiological, geochemical, and mathematical studies contribute to an understanding of these systems and the implications of their processes for the dispersal of environmental radioactivity.

In addition to small acreages already contaminated by waste disposal, the Oak Ridge Reservation includes over 25,000 acres of land, in many stages of forest development, which is suitable for research. Residual, colluvial, and alluvial soils are derived from Paleozoic sandstones, shales, dolomites, and limestones. Permanent forest plots, sampling of forest biomass and productivity, and chemical analysis of plant and soil materials aid in planning for use of this Reservation and also provide information and samples that are needed for interpretation of tracer experiments. Biogeochemical studies include activation analyses showing environmental levels of stable cesium (2 to 9 μg per gram of soil), cobalt (6 to 50 μg per gram of soil and 0.02 to 0.12 μg/g in pine needles and boles), and cerium (40 to 400 μg per gram of soil and usually <0.25 μg/g in pine boles).

Tracer experiments continue to follow the rapid ecological cycle of Cs^{134} in and near 12 white oak trees. Sampling indicates more rapid movement of cesium into and out of natural soils than might be expected from the high capacity of their illite or vermiculite clays to fix cesium. Other experiments with tagged leaves indicate leaching rates for Cs^{134} several times as rapid as decay rates of organic litter. Releases of Ru^{106}, Co^{60}, and Sr^{85} or Sr^{90} occurred at rates comparable with rates of litter breakdown for various leaf species.

Arthropods and microorganisms hasten the breakdown of litter and the important natural cycle of nutrients and of isotopes. Changes in populations, respiratory activity, and litter weight loss are partly accounted for by the annual cycle of temperature, week-to-week or day-to-day fluctuations in moisture, and diurnal cycles of temperature. Mite and insect species also show striking differences related to stage in litter breakdown and to forest association (white oak vs pine). Fungi and bacterial counts varied over several orders of magnitude between leaf species (mulberry, redbud, oak, pine). Various microorganisms showed concentration factors of 2 to 48 for Co^{60} and smaller values for Cs^{134} in aqueous shaking cultures; in soil, however, concentration factors were higher for Cs^{134} than for Co^{60}. High uptake, rapid turnover, and frequent prompt release by microbial death from dessication

or freezing suggest a greater role of microorganisms in isotope cycling than is indicated by their small biomass.

Formulation of theoretical models for ecosystems has been aided by simulating such a system on a large analog computer. One console was devised to simulate the transfer of biomass, while a second console was connected to record changes in radioactivity of plants, animals, and litter and soil materials. Selection of positive and negative feedback parameters offers possibilities for simulating diverse ecosystems when enough data on the pool sizes and turnover rates of their compartments can be synthesized.

Clinch River Studies

Bottom organisms are being used to determine both the fate and radiation effects of radionuclides released to the Clinch River. A model using parameters obtained from laboratory experimentation and field observation showed that the feeding activities of tubificid worms did not contribute significantly to the downstream movement of radioactive river bottom sediments. The bottom-dwelling organisms in the Clinch River received an average dose which is 20 times that from naturally occurring radiation and in White Oak Creek the dose is about 1000 times background. *Chironomus tentans* Fabr. (midge) is a dipteran species with larval stages living in bottom muds. The use of sensitive cytogenetic techniques and analysis of the salivary gland chromosomes of this species has shown a high frequency of chromosomal aberrations, including a number of individuals with three chromosomes instead of the usual four.

About 40% of the Co^{60} taken up by crayfish was by adsorption on the exoskeleton and the uptake was directly proportional to the concentration in the environment. The rate of Co^{60} uptake was more rapid for hard-shelled individuals and large individuals. The excretion of Co^{60} was more rapid for small specimens and for those which had been tagged by injection rather than in a radioactive solution. In the latter instance there was little or no Co^{60} associated with the exoskeleton from which loss of Co^{60} was slow. Radioassay of crayfish showed that the highest concentration of Co^{60} g^{-1} was in the exoskeleton. The hepatopancreas contained 86%, gut 49%, muscle, gonad, and blood each 0.14% as much Co^{60} as did the exoskeleton.

A study of the strontium and calcium in the shells of Tennessee River clams showed that the calcium content was constant and constituted 40% of the shell. The strontium content was proportional to the growth rate of the clam's shell and varied from 150 to 500 ppm. The laboratory releases of Sr^{90} were considered as a tracer and the Sr^{90}–stable strontium atom ratios in clam shells downstream from White Oak Creek could be explained solely on the basis of the dilution of Sr^{90}-contaminated Clinch River water by non-contaminated Tennessee River water. This shows that Sr^{90} released to a surface water stream moves downstream in solution and there is little or no ionic exchange between the strontium in solution and that in the bottom sediments.

Tagging fish with numbered tags has shown that the white crappie tends to remain in the vicinity of initial capture. This species has been selected for a study of fission-product element metabolism. During five months of tagging in 1960 and 1961, 5245 fish have been tagged, and there have been 150 returns by fishermen and our own netting operations. The fishermen returns show a movement by white bass from the Clinch River downstream into the Tennessee River portion of Watts Bar Reservoir.

3. RADIATION PHYSICS AND DOSIMETRY

Theoretical Physics of Dosimetry

Fundamental investigation of the properties of classical plasmas has been continued. A new instability in the interaction of a beam and a stationary plasma has been discovered. A phenomenological description of the space dispersive properties of plasma, based on the existence of the Doppler effect, has been given. The emission of optical photons from solids irradiated by charged particles has been analyzed theoretically, and a code for detailed computation has been written. Interest in the analysis of swarm experiment data on the transport of electrons in gases had led to the computation of equilibrium distribution functions in diatomic gases employing theoretical predictions of relevant cross sections available in the literature. A new method of analyzing swarm data in polyatomic gases is proposed and is being tested numerically. Monte Carlo results

or the computation of neutron penetration in an air-over-ground geometry is given. A generalized principle of radiation dosimetry is formulated and examined in a number of special cases.

Experimental Physics of Dosimetry

The spectral distribution of the light emitted from foils irradiated by electron beams has been measured. It was found that the "color" of the light depends strongly on the metal being studied, the thickness of the foil, the beam energy, and the angle of observation. Experimental results are in approximate agreement with a theory based on the exchange of energy between the beam electrons and the conduction electrons of the foil acting collectively. Such collective interactions are thought to occur in irradiated biological systems as well.

Dosimetry Methods

A fast neutron dosimeter has been developed using a silicon-gold surface barrier to detect fission recoils from a foil containing U^{235}, Np^{237}, and U^{238}. Proper choice of the mass ratios and shielding with B^{10} produced a response which gives a direct indication of fast neutron tissue dose.

Extensive airborne measurements of plane and point ground sources of gamma radiation have been carried out at the Nevada Test Site. The dependence of spectral distributions and gamma ray intensity with altitude has been developed, and is useful in connection with airborne surveys of radioactivity.

Dosimetry Applications

The primary objective of the Dosimetry Applications Group is the accumulation of radiation exposure data for humans as a part of the Nuclear Energy Civil Effects Program. Specific projects include the "Ichiban" project to determine the radiation exposure of the survivors of the nuclear bombings of Hiroshima and Nagasaki, Japan, and the nuclear accident studies. Related work includes the development of special radiation measurement instruments and techniques, special shielding studies, and the research at the Fast Burst Reactor at ORNL.

Progress this year includes the development of neutron and gamma ray spectrometers, better gamma ray dosimeters for mixed radiation dosimetry, and preparation for extensive experiments at the Nevada Test Site in late 1961.

Physics of Tissue Damage

Spectral studies were undertaken of the light emitted in fluorescence and thermoluminescence from trypsin, spores of bacillus megaterium, and the amino acids L-tyrosine, L-phenylalanine, and L-tryptophan. In all cases spectral bands were found which were characteristic of the material irradiated and its temperature. The data revealed the existence and depth of metastable energy levels into which charge carriers are excited by the passage of x and gamma rays through these biochemicals.

In particular:

1. Those electronic rearrangements which are initiated in the interaction of ionizing radiation with trypsin become preferentially localized in a very restricted number of metastable configurations.
2. The thermoluminescence from the molecular crystals of aromatic amino acids is not attributable to those electronic transitions which account for fluorescence and phosphorescence due to ultraviolet excitation.
3. The energy resulting from the decay of the metastable configuration in trypsin may very well appear as tryptophan phosphorescence. Thus the recombination might involve either tyrosine or phenyalanine, and energy transfer to tryptophan would then account for the predominant emission at 4600 A.
4. With increasing temperature, the spectral distribution shifts toward longer wavelengths. The fact that these bands are shifted by as much as 0.6 ev makes it seem somewhat unlikely that this would represent an increasing partition of recombination energy into nonradiative modes.
5. There has been considerable controversy as to whether conduction bands exist in proteins. The present studies do not resolve this question. If such do exist, however, these results indicate that the conduction and filled bands must be separated by at least 2.7 ev in trypsin.

4. INTERNAL DOSIMETRY

Estimation of Internal Dose

A formula for estimating body burdens of Pu from urinary excretion data has been derived and

programmed on the IBM 7090 computer. The formula demands data for urinary excretion as a continuous function of time. Although the values of the urinary excretion are known only at discrete times, these are regarded as sample values, and the continuous case is obtained by a linear interpolation. Several methods of interpolating have been explored, and thus far no substantial difference in the estimates of retention has resulted.

An MPC_w for Rn^{222} has been estimated from the data available in the literature and compared with naturally occurring levels. It is indicated that a level of 5×10^{-6} $\mu c/cc$ delivers 3 millirems per week to yellow marrow, which, if considered in the same category as the bloodforming organs, is the critical organ.

An MPC_a for insoluble Ra^{226} compounds was calculated. An experimental measurement of the retention of Ra^{226} daughter products in lung tissue was required, and even though no adequate experimental data could be found, some estimates of the greatest and least retention, which bracketed the most reasonable retention, were made. The values corresponding to these two estimates were 1×10^{-10} $\mu c/cc$ and 5×10^{-11} $\mu c/cc$ (40-hr occupational exposure), different from each other by a factor of only 2. The lower value was recommended for application pending more experimental data.

Stable Element Metabolism by Man

The techniques in the spectrographic determination of trace elements in human tissue performed by the ORNL Analytical Chemistry Division including the methods of sample preparation, the problem of cross-contamination of samples, instrumentation involved, standards preparation, exposure conditions, precision and sensitivity of the method, and the photographic exposure work are discussed. The trace element concentrations of ~ 17 elements in brain, diaphragm, and heart of 28 cadavers from San Francisco are presented.

The median, 10th, and 90th percentiles for the trace metal concentrations in organs and tissues of U.S. adults (>20 years of age) have been determined. Studies of the age trend of trace metal concentrations in liver, lung, and kidney were carried out. Also, a nonparametric statistical method has been applied to the measurements of Cu, Al, and Zn concentrations in human kidneys to estimate the maximum per cent of the population which exceeds the mean sample concentration by a factor of three. At the 95% confidence level, this study indicates that not more than 9% of the adult urban population exceeds three times the sample mean. The effect of the size of sample on this estimate is discussed.

Microscopic and Autoradiographic Studies of Uranium Distribution in Rat Kidney

Studies of the distribution of uranium in rat kidney at the microscopic level were carried out to obtain more information relating to the phenomenon of prolonged retention of uranium by kidneys of animals given an intraveneous administration of a large mass of uranium. The distribution of uranium in the cortex of rat kidney has been determined at different times after injection and for different injected amounts of uranium. Log-normal distribution curves could not always be fitted to the data. Data obtained in studies of leaching of uranium from kidney tissue into the formalin fixative and the dehydrating solutions indicated that very little uranium was leached. Distribution curves determined from measurements made on autoradiographs of kidney tissues prepared with the freeze-dry method were similar to the curves determined from data derived from formalin-fixed and dehydrated tissue. The diameters of tubules from kidneys of uranium-injected rats did not differ significantly from those of the controls or correlate with the amount of uranium injected. The diameters of the glomeruli, however, decreased with increasing levels of uranium injection. More data on the nonuniform distribution factor are presented. These data indicate that the cortex contains ~ 1.4 times the average amount in the kidneys.

5. HEALTH PHYSICS TECHNOLOGY

The ORNL whole-body counter, in operation with a 4×4-in. NaI(Tl) crystal since June 1960, is now shut down during the changeover to an 8×4-in. NaI(Tl) crystal system. An auxiliary scintillation counter, having the same shielding as the big room, is used to monitor for transient changes in the general background. Air from the room is treated and recirculated, with makeup air being provided from cylinders of aged breathing-air. Of the 208 persons checked in the routine program, 7.2% showed gamma-ray

spectra different from those of unexposed individuals; furthermore, the most significant internal deposit was less than 20% of the maximum permissible body burden (Hg^{203}).

Urinary and fecal excretion rates of Sr^{90} and Ca^{45} were determined for an employee who sustained a percutaneous exposure. The rate function of Sr^{90} excretion in the urine was seen to be very similar to that of two experimental subjects receiving single intravenous injections of Sr^{85}. On the third day after exposure, the employee increased his calcium intake to above 4 g/day (via milk), and this action resulted in doubling the stable calcium and also the Ca^{45} urinary excretion rates. There was no significant change observed in the Sr^{90} excretion rate. For the first 22 days, 61% of the total Ca^{45} excreted was in the urine, while at 60 days about 90% of the total excreted Sr^{90} had been eliminated via the urine.

An exploding-wire aerosol generator, consisting of a 4000-joule capacitor bank and a triggered sphere gap, has been applied to the production of aerosols of 14 different metals by exploding them in air or argon gas. Particles are spherical and are predominantly in the range of 0.01 to 0.10 μ. An aerosol of isolated U_3O_8 particles was produced as the result of stirred settling to remove chains and agglomerates.

Attempts to compare radioactive contamination control criteria for different installations have led to a study of the methods available for measuring "removable" surface contamination. Thorium dioxide dust, 3 μ in diameter, was allowed to settle onto representative test surfaces and the degree of removability was determined by each of three methods – smears (abrasion), adhesive papers, and a new method employing air impingement to redisperse particles from the surface (the "smair" sample). In general, no one mechanism for particle removal was equivalent to the other methods. Factors variously affecting the fraction removed per sample included size of the area sampled, dustiness, aging the deposit, composition of the surface, and surface roughness. Adhesive paper samples consistently removed the largest fraction of the total contamination. Smear samples were the most variable, while smair sample yield was practically unaffected by any of these factors except the surface composition.

Beef-cattle thyroid samples and samples of pasture grasses have been collected from areas within a 100-mile radius of ORNL and analyzed for I^{131}. Although the grass samples generally did not contain detectable amounts of I^{131}, 85% of the thyroid samples did show measurable amounts. A general ambient level of 2 $\mu\mu$c per gram of thyroid was observed at large distances from ORNL, and this level remained essentially unchanged from July 1960 through October 1960. The amounts of I^{131} expected to be deposited on the ground were calculated using stack release data and a modified form of Sutton's equation. For sampling stations in the prevailing wind directions, the ratio of the total amount of I^{131} found in the thyroid to the predicted deposition per square meter averaged 550. There was a general decrease in the amounts of I^{131} in cattle thyroids after November, possibly a result of increased supplementary feeding during the winter months.

A method is being evaluated for estimating fast-neutron dose (>2.5 Mev) by the analysis of hair samples for P^{32}. The analysis of body hair can provide valuable supplementary information with regard to the dose from fast neutrons, and, also, it can give an indication of the orientation of the person during exposure. Samples of hair were attached in the appropriate locations on four man-simulating phantoms, and these assemblies were exposed to a field of mixed neutron and gamma radiation at the Tower Shielding Reactor. There is excellent agreement, down to about 5 rads, between the fast-neutron dose estimated from a 1-g sample of hair compared with the analysis of large sulfur pellets located near the packets of hair during exposure. For phantoms facing the reactor, the average front-to-back ratio is about 10. Studies now under way are aimed at improving the discrimination against possible fission product contamination on the hair.

6. EDUCATION, TRAINING, AND CONSULTATION

The need for trained health physicists, both in this country and abroad, continues. Again this year, several foreign students completed the AEC

Fellowship Program at Vanderbilt University and Oak Ridge. A combined lecture and laboratory course covering the principal aspects of health physics has become an integral part of the ORSORT program. To provide training in health physics for AEC personnel and personnel from state departments of health, a ten-week course in health physics has been established.

It is anticipated that in the future more training in health physics will be provided for ORNL personnel and for foreign students on an individual basis.

CONTENTS

SUMMARY iii

1. RADIOACTIVE WASTE DISPOSAL 1

Low-Level Waste Water Treatment 1
- Classification of Effluent Solids 1
- Phosphate Coagulation 1
- Natural Minerals for Second-Stage Treatment 4

Study of White Oak Creek Drainage Basin 6
- Sources of Contamination 6
- Solid Waste Burial 9
- White Oak Lake Bed 11

Clinch River Studies 13
- Hydrology 13
- Water Sampling and Analysis 15
- Estimate of Radioactivity in Bottom Sediments 19

Fundamental Studies of Sorption by Minerals 27
- Structural Relationships in Cesium Sorption 27
- Strontium Reactions with Minerals 32
- Removal of Ruthenium 37
- Removal of Nuclides Using Organic Minerals 38
- Biological Recovery of Cesium Sorbed on Vermiculite 40

Soil Column Studies 42
- Particle Diffusion Processes 43
- Potassium Treatment for Optimizing Cesium Removal 46
- Large-Scale Testing of Vermiculite Columns 47
- Summary 48

Disposal in Salt Formations 49
- Large-Scale Field Experiments 49
- Plastic Flow Studies 52
- Thermal Studies 56
- Cavity Alteration Studies 62
- Off-Gas Studies 67
- Test of New Concepts 68

Disposal in Deep Wells 69
- Disposal of Radioactive Waste by Hydraulic Fracturing 69
- Injection of Radioactive Waste into Deep Permeable Formations 71

Evaluation of Engineering, Economics, and Hazards 72
- Hazards of Tank Storage 72
- Economics of High-Level Waste Treatment and Disposal 76

Related Cooperative Projects 77
- Geologic and Hydrologic Studies by U.S. Geological Survey 77
- Cooperation of Other Agencies in ORNL Studies 78
- Visiting Investigators from Abroad 79
- Nuclear Safety Review 79
- Committee Work 79
- Participation in Educational Programs 79

2. ECOLOGICAL RESEARCH 81
White Oak Lake Bed Studies 81
Changes in Vegetation 81
Uptake of Radionuclides by *Lespedeza* 87
Fertilizer Studies 90
Insect Studies 91
Mammalogy 95
Forest Ecology 105
Studies of the Oak Ridge Reservation 105
Tracer Experiments and Ecological Cycles 113
Biological Populations and Processes Affecting the Movement of Elements and Isotopes 120
Compartment Models and Analog Computer Simulation 124
Clinch River Studies 129
Bottom Organism Studies 129
Fish Studies 137
Related Activities 138
Committee Work 138
Participation in Educational Programs 139
3. RADIATION PHYSICS AND DOSIMETRY 140
Theoretical Physics of Dosimetry 140
Electromagnetic Interaction of a Beam of Charged Particles of Plasma 140
Space Dispersive Properties of Plasma 140
Optical Emission from Irradiated Solids 141
Analysis of Swarm Experiment Data on the Transport of Electrons in Gases 142
The Energy Distribution of Slow Electrons in Gases 143
Neutron Penetration in an Air-over-Ground Geometry 145
Pulse Height from an Ionization Chamber Containing an Attaching Gas 149
Some General Remarks on Radiation Dosimetry 149
Experimental Physics of Dosimetry 155
The Spherical Electrostatic Analyzer 155
Ionization of Gas Mixtures 156
Dissociative Electron Capture in Water Vapor 157
Low Energy Electron Attachment and Drift Velocity in Gas Mixtures Containing Water Vapor 158
The Interference Filter Spectrograph 160
Measurement of Light Emission from Irradiated Metal Foils 162
Dosimetry Methods 166
Silicon-Gold Surface Barrier Fission Dosimeter 166
Radiation Measurements over Simulated Plane Sources 166
Dosimetry Applications 172
Ichiban Program – the Atomic Bomb Hypocenter at Nagasaki 172
Evaluation of the Residual Radiation in Hiroshima and Nagasaki 173
Fast Burst Reactor (Fast Critical Assembly) 173
Metaphosphate Glass Microdosimeters (Fluorods) 175
Compton Gamma-Ray Spectrometer 176
Neutron Spectrometer 177
Physics of Tissue Damage 179
Emission Spectra of the Low Temperature Thermoluminescence from Gamma-Irradiated Biochemicals 179

4. INTERNAL DOSIMETRY 191
Estimation of Internal Dose 191
Estimation of Pu Body Burdens on the Basis of Urinalysis Data 191
On the $(MPC)_w$ for Rn^{222} and Its Comparison with Naturally Occurring Levels 192
$(MPC)_a$ for Insoluble Ra^{226} Compounds 196
Stable Element Metabolism by Man 197
The Spectrographic Determination of Trace Elements in Human Tissue 197
Statistical Interpretation of Trace Element Concentrations in Human Tissue 203
Variability of Relative Organ Concentration of Trace Elements in Human Tissue 206
Microscopic and Autoradiographic Studies of Uranium Distribution in Rat Kidney 210
Introduction 210
Distribution of Uranium in Rat Kidneys 211
Studies to Determine Leaching of Uranium from Quartered Rat Kidney 217
Distribution of Uranium in Rat Kidney Tissues Prepared by the Freeze-Dry Method Compared with Formalin-Fixed Tissues 217
Histological Changes in Proximal Tubules and Glomeruli of Uranium-Injected Rats 218
Nonuniform Distribution Factor 219

5. HEALTH PHYSICS TECHNOLOGY 222
The ORNL *In Vivo* Gamma-Ray Spectrometer Facility 222
Introduction 222
The IVGS Facility 222
Routine Program 222
Status 223
The Excretion Pattern of Sr^{90} and Ca^{45} in Man 224
Ca^{45} Excretion 226
Discussion 226
Exploding Wire Aerosol Generator 227
Studies of Surface Contamination 230
Introduction 230
Intercomparison of Methods for Measuring "Removable" Contamination 230
Effect of Surface Roughness on the Fraction Removable 230
A Study of Methods for Monitoring the I^{131} Contamination in the Environment 232
Estimation of Fast Neutron Dose to Man by the Analysis of Hair for P^{32} 234
Introduction 234
Analytical Procedure 234
Exposure Studies 235
Results 235

6. EDUCATION, TRAINING, AND CONSULTATION 236
AEC Fellowship Program 236
Other Activities 236

PUBLICATIONS 237

PAPERS 240

LECTURES 243

1. RADIOACTIVE WASTE DISPOSAL

E. G. Struxness R. J. Morton

LOW-LEVEL WASTE WATER TREATMENT

K. E. Cowser

T. Tamura D. A. Gardiner[1]
O. H. Myers H. J. Wyrick

The process waste treatment plant at ORNL employs $CaCO_3$ precipitation for removal of Sr^{90} and addition of clay for removal of Cs^{137} (refs 2, 3). Laboratory studies and plant tests include classification of solids in the plant effluent, use of phosphates as a supplement to normal lime-soda softening, and use of natural minerals for second-stage treatment. Their purpose is to investigate methods of increasing fission-product removals by use of the plant facilities that are available.

Classification of Effluent Solids

Preliminary investigation of the distribution of radionuclides in the plant effluent showed that 40 to 50% of the Sr^{90}, Cs^{137}, and gross beta activity is associated with the suspended solids in the effluent. During normal operation the effluent contains an average of 35 ppm of suspended material.

Dorr-Oliver, Inc., under a contract with the AEC, developed a sampling train to classify the solids in ORNL's low-level liquid waste stream. The unit included a Merco Bantam Strainer and four separate Dorr Clone systems (identified as P-100, P-50, P-25, and TM-1) with an over-all capacity of 24 gpm. A Merco Centrifuge (C-9), having a capacity of 8 gpm, was used to classify the solids passing through the sampling train.

Representatives of Dorr-Oliver, Inc., completed a series of five operating runs on the treatment plant effluent to classify the suspended solids and their associated activity.[4] A total of 64,000 gal of waste, containing 30 ppm of suspended solids, was passed through the hydroclones; a smaller volume of hydroclone effluent was treated with the centrifuge.

The median diameters of the solids removed were as follows: 25 microns by the P-100, 15 microns by the P-50, 11 microns by the P-25, 7.9 microns by the TM-1, and 6.5 microns by the centrifuge. These suspended solids contained 48% of the gross gamma activity, 59% of the Cs^{137}, and 34% of the Sr^{90}. Thus, by reducing the amount of suspended solids in the effluent, it would be possible to increase the efficiency of the treatment plant. The use of coagulant aids, another approach to increased removals of suspended solids, had been investigated previously.[5]

Phosphate Coagulation

The successful experience in other countries with phosphate coagulation for the removal of strontium from low-level liquid wastes and the possibility of increasing strontium removal from ORNL process waste by the formation of apatite in the existing $CaCO_3$ treatment system prompted an investigation of the use of phosphates. Previous studies of phosphate coagulation had demonstrated the need for close control of pH and of the PO_4^{3-}/Ca^{2+} ratio in the waste.[6-10] Nesbitt[7]

[1] Mathematics Panel, ORNL.

[2] K. E. Cowser and R. J. Morton, *Proc. Am. Soc. Civil Engrs.* 85 (SA 3), 55–76 (1959).

[3] M. C. Culbreath, *Proc. Am. Soc. Civil Engrs.* 85 (SA 3), 41–53 (1959).

[4] Dorr-Oliver, Inc., Stamford, Conn., *Informational Report*, Atomic Energy Commission, Research and Development Contract No. AT-(40-1)-2746 (Jan. 5, 1961).

[5] T. Subbaratnam, K. E. Cowser, and E. G. Struxness, *Studies on the Use of Coagulant Aids in the Lime-Soda Treatment of Large-Volume, Low-Level Radioactive Liquid Waste*, ORNL CF-60-7-17 (August 1960).

[6] R. A. Lauderdale, *Studies on the Removal of Radioisotopes from Liquid Wastes by Coagulation*, ORNL-932 (January 1951).

[7] J. B. Nesbitt *et al.*, *The Removal of Radioactive Strontium from Water by Phosphate Coagulation*, NYO-4435 (February 1952).

[8] R. H. Burns, *Radioactive Waste Control at the United Kingdom Atomic Energy Research Establishment Harwell*, AERE-M649 (March 1960).

[9] R. H. Burns and E. Glueckauf, *Proc. UN Intern. Conf. Peaceful Uses Atomic Energy, 2nd, Geneva, 1958*, 18, 161 (1958).

[10] K. G. Seedhouse, J. Monhahan, and G. Wallie, *The Removal of Fission Products from Solution with a Precipitator — Column Treatment*, AERE-2220 (1958).

found that strontium removal decreased as the pH increased from 10.4 to 11.4, presumably due to the presence of small quantities of a stable calcium phosphate sol in the supernatant liquid. Centrifugation of the settled supernatant removed most of the stabilized material.

The variable chemical quality of ORNL process waste, the lack of a recording pH meter at the plant, and the single-stage treatment facility suggested the use of phosphates as a supplement to normal lime-soda softening rather than as a replacement of it. Tap water spiked with Sr^{85} was treated with various amounts of phosphate, by a jar-test procedure, to duplicate the contact time and agitation sequence of the treatment plant. The maximum removal of strontium occurred at about 125 ppm of PO_4^{3-} (Fig. 1.1) with little difference noted whether the phosphates were added during flash mixing or after 11 min of flocculation. A phosphate concentration above 200 ppm hindered settling of the flocculent material. In all cases the floc formed was easier to resuspend by slight agitation than in the control jars containing only $CaCO_3$.

The removal of strontium by primary phosphate coagulation with various PO_4^{3-}/Ca^{2+} ratios was compared to that of lime-soda softening with 95 ppm and 125 ppm of phosphate added (Table 1.1). For effective removal of strontium by phosphate coagulation, it was necessary to adjust the pH of the system. At pH 10.2, the removal of strontium was generally increased by filtering the supernatant. The comparison showed that lime-soda softening with added phosphate did not require adjustment of pH, produced a floc of better settling character, and removed as much strontium as the most efficient straight phosphate treatment.

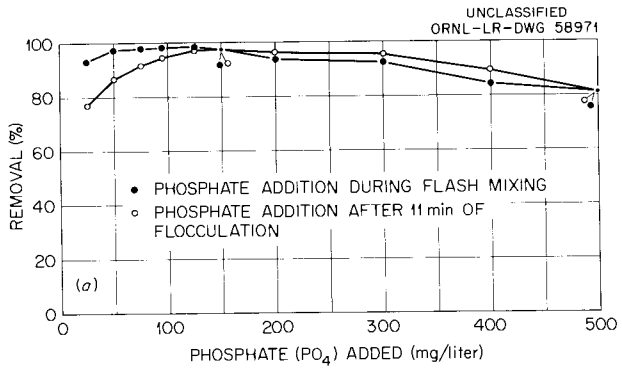

Fig. 1.1. Effect of Phosphates on Strontium Removal.

Table 1.1. Comparison of Phosphate Coagulation with Lime-Soda Softening and Supplemental Phosphate in Strontium Removal

Phosphate (ppm)	PO_4^{3-}/Ca^{2+}	pH	Strontium Removal (%)			
			No pH Adjustment		pH Adjustment (10.2)	
			Settling	Settling and Filtration	Settling	Settling and Filtration
47.4	1.6[a]	8.8	51.0	53.8	72.6	66.5
63.4	2.1	9.0	58.7	61.5	85.3	78.0
69.5	2.3[b]	9.1	71.1	74.4	80.0	94.1
85.9	2.9[c]	9.3	81.1	83.0	82.6	97.2
147.4	5.0[d]	9.8	95.4	96.0	83.1	99.0
95[e]		10.4	96.3	97.7		
125[e]		10.4	96.4	97.5		

[a] Stoichiometric omount of phosphate and calcium.
[b] Optimum PO_4^{3-}/Ca^{2+} ratio according to Lauderdale.[6]
[c] Optimum PO_4^{3-}/Ca^{2+} ratio according to Nesbitt.[7]
[d] 100 ppm excess PO_4^{3-}.
[e] Stoichiometric lime, 200 ppm excess soda ash, and 200 ppm clay.

In anticipation of difficulty in obtaining a settleable floc during test operations in the treatment plant, a number of coagulant aids were investigated. These included $FeCl_3$, $Fe_2(SO_4)_3$, $Th(NO_3)_4$, additional clay, and Hagan aids 2, 18, 50, and 323 (ref 11). A combination of 0.5 to 1.0 ppm Hagan 323 and 1.0 to 2.0 ppm Hagan 2 gave the best results.

To determine the optimum combination of lime, soda ash, clay, and phosphate for the most effective removal of strontium and cesium, a series of laboratory tests with actual process waste was started. The same experimental procedure was employed as that previously applied to lime-soda softening.[12] Although the laboratory experiments have not been completed, the most effective combination of treatment variables used thus far (lime, 0.83 times stoichiometric; soda ash, 200 ppm excess; phosphate, 250 ppm; and clay, 117 ppm) removed 99.0% of the strontium and 87.7% of the cesium.

The results of plant tests to date are summarized in Table 1.2. Average removals of gross beta activity, Sr^{89+90}, and Cs^{137} are listed for periods immediately preceding each of the two test periods (August 22 to October 9, 1960, and March 20 to April 30, 1961) and during the time of the tests (October 10–16, 1960, and May 2–7, 1961). The efficiency of plant operation was lower during the October test because of a slowly settling floc with substantial quantities of solids remaining in the plant effluent. Two tests were then run with coagulant aids to determine the proper concentration and point of addition of these materials and to evaluate their performance. By introducing 1.0 ppm of Hagan 323 before the flash mixer and 2.0 ppm of Hagan 2 to the flash mixer, removal of solids was improved considerably. The average concentration of suspended solids in the effluent during the May test was 15 ppm (as compared with 35 ppm during normal operation), and the analyses of filtered and unfiltered samples showed that the radionuclides were associated principally with the liquid phase. Strontium and Cs^{137} removals were 87 and 97% respectively.

Earlier plant tests showed that removals of strontium and cesium can be increased for short periods of time, when needed, by optimizing the amounts of lime, soda ash, and clay. However, as a routine practice, it is not desirable to optimize the chemical dosages because this increases the volume of sludge. Coogulant aids, adding only 1-to-2¢/1000 gal to the cost of treatment, will improve the clarity of the plant effluent and increase plant efficiency. The addition of phosphates will also improve plant efficiency, but adds to the cost of treatment by about 16¢/1000 gal. To obtain over-all removals greater than 95% routinely, second-stage treatment is necessary.

[11] Hagan Chemicals and Controls, Inc., Pittsburgh, Pa.

[12] D. A. Gardiner and K. E. Cowser, *Health Phys.* 5, 70–78 (1961).

Table 1.2. Process Waste Water Treatment Plant Tests; Removals (%) of Gross Beta Activity, Sr^{89+90}, and Cs^{137}

Period	Gallons Treated	Gross Beta	Sr^{89+90}	Cs^{137}
	$\times 10^6$			
Aug. 22, 1960–Oct. 9, 1960[a]	23.1	77	77	79
Oct. 10, 1960–Oct. 16, 1960[b]	3.3	78	67	78
Mar. 20, 1961–Apr. 30, 1961[a]	12.3	77	79	85
May 2, 1961–May 7, 1961[c]	1.7	96	87	97
		97[d]	89[d]	98[d]

[a] Lime, stoichiometric; soda ash, 200 ppm excess; clay, 200 ppm; effluent sample not filtered.

[b] Same as (*a*) with addition of 130 ppm PO_4; operating rate 330 gpm; effluent sample not filtered.

[c] Same as (*a*) with addition of 125 ppm PO_4, 1.0 ppm Hagan 323, and 2.0 ppm Hagan 2; operating rate 200 gpm.

[d] Same as (*c*) except effluent sample filtered.

Natural Minerals for Second-Stage Treatment

The use of natural minerals as sorptive material for second-stage treatment of ORNL process waste is predicated on their ability to sorb and retain radionuclides and on the safety and economy of ultimate disposal of the contaminated solid without additional treatment. Regeneration and re-use of such mineral columns would not be necessary because of their low cost.

To assess the suitability of various natural minerals for second-stage column operation, the quantity of strontium and cesium removed and the rates of removal were evaluated by slurry tests. Small quantities of these minerals were contacted for various periods of time with 30 ml of a synthetic waste typical of the effluent from the ORNL treatment plant. A phosphate-treated waste was simulated by addition of 100 ppm of phosphate. Results of the slurry tests are summarized in Table 1.3. Of the minerals tested, vermiculite ore is one of the most promising with respect to efficiency, availability, and cost.

It is necessary to pretreat raw vermiculite and remove the readily replaceable calcium and magnesium, thus preventing their later interference with column operation. Sodium chloride is effective for this pretreatment, and distribution coefficients of 5000 and greater were attained with BO-4, sodium-treated vermiculite.[13] The presence of 100 ppm of phosphate interfered with strontium removal by all minerals tested, but had a negligible effect on cesium removal. From control systems

[13] Zonolite Company, Travelers Rest, S. C.

Table 1.3. Cesium and Strontium Distribution Coefficients[a] (Effluent of Process Waste Treatment Plant)[b]

Material	Cesium				Strontium			
	Sodium Treated		Natural		Sodium Treated		Natural	
	PO_4[c]	No PO_4	PO_4[c]	No PO_4	PO_4[c]	No PO_4	PO_4[c]	No PO_4
Vermiculite BO-1		180		300				
Vermiculite BO-2	170	180		340	110	60	40	
Vermiculite BO-3	1100	1200			430	2,700		
Vermiculite BO-4								
1 *M* NaCl	3200	5000			4700	13,000		
0.9 *M* NaCl, 0.1 *M* NaOH					3400	22,000		
5 *M* NaCl					6100	14,000		
Vermiculite BE-3	3700	3200	2900	2700	280	6,000		
Clinoptilolite			2900	2900			1700	3900
Rock Phosphate								
Fine							300	400
Coarse							130	
Al_2O_3							300	700
Bauxite							490	1600

[a] Distribution coefficient (2-hr contact time) = $\frac{\text{radionuclide sorbed per gram of material}}{\text{radionuclide unsorbed per milliliter of solution}}$.

[b] Waste composition: 8.0 ppm Ca^{2+}; 2.9 ppm Mg^{2+}; 235 ppm Na_2CO_3; and 100 ppm PO_4^{3-} where indicated.

[c] 100 ppm PO_4.

where no phosphate was added, removal by vermiculite and clinoptilolite of about 95% of the strontium was rapid (Fig. 1.2), an important factor in effective column operation; after 30 min of contact time, there was little additional removal of strontium.

As shown in Fig. 1.3, phosphates inhibited the rate of strontium removol by both vermiculite and clinoptilolite, but not as severely in the case of clinoptilolite. The rate of cesium removal by vermiculite and clinoptilolite was not affected when phosphates were present (Fig. 1.4).

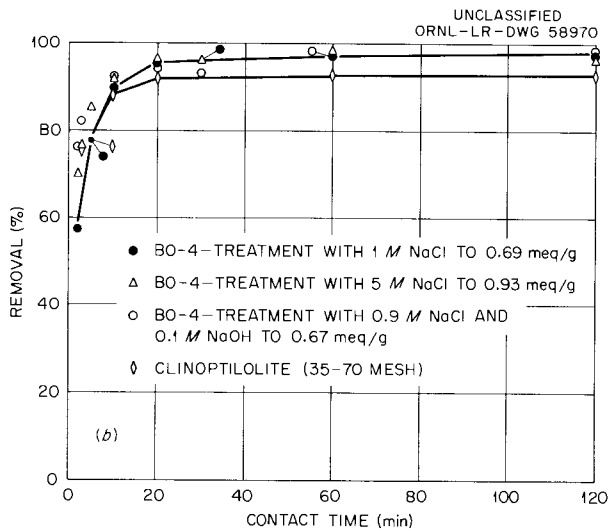

Fig. 1.2. Strontium Removal by Vermiculite (BO-4) and Clinoptilolite (Nonphosphated System).

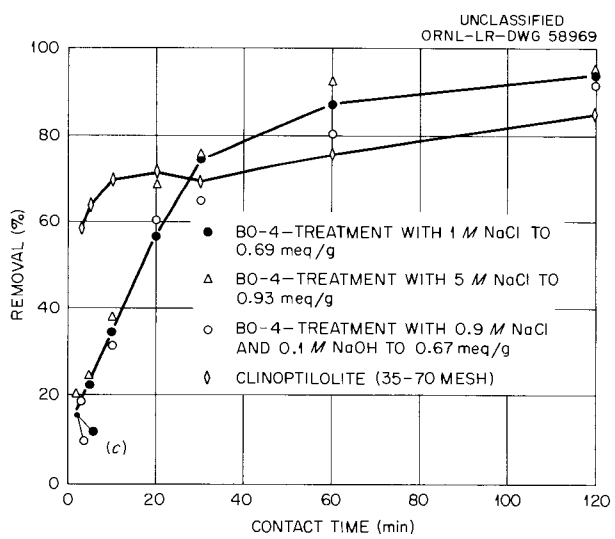

Fig. 1.3. Strontium Removal by Vermiculite (BO-4) and Clinoptilolite (Phosphated System).

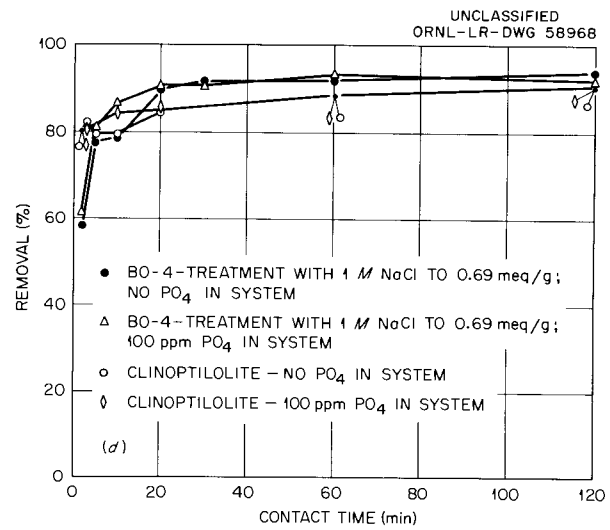

Fig. 1.4. Cesium Removal by Vermiculite and Clinoptilolite.

From slurry tests it was observed that particle size is an important parameter in the use of natural minerals, the smaller particles being the most efficient. The range in size of the vermiculites, rock phosphates, and clinoptilolite that were tested is shown in Table 1.4. In the design of a column to contain one or more natural minerals, the head-loss characteristics of the materials must be known. Also physical breakdown of the mineral materials on contact with water, as experienced with Conasauga shale, would make its texture unsuitable for use in columns. Resistance to the flow of water was assessed by small columns, either 1 or 2 in. in diameter, containing 18 in. of the material. The loss-of-head data in Table 1.4 are in centimeters of water per foot of bed depth for two different rates of flow. In all cases, the head loss through the column was linear with flow rate. Under the conditions of the loss-of-head test, none of the materials tested were unacceptable.

The physical characteristics of vermiculite are likely to change as a result of bed compaction or chemical treatment. A 2-in.-diam × 12-ft-long glass column was charged with 9 ft of vermiculite (BO-4 grade), and the loss of head determined

Table 1.4. Physical Characteristics of Natural Minerals

	Particle Size			Loss of Head (cm/ft)	
	Effective Size (mm)	Uniformity Coefficient	10% and 90% Passing Size (mm)	Flow Rate (0.5 gal min^{-1} ft^{-2})	Flow Rate (1.0 gal min^{-1} ft^{-2})
Vermiculite BO-1	2.1	1.3	2.1–3.8	0.75	1.5
Vermiculite BO-2	2.0	1.1	2.0–2.6	1.1	2.2
Vermiculite BO-3	0.41	2.4	0.41–1.6	5.0	11.0
Vermiculite BO-4	0.17	2.3	0.17–0.49	10	20
Rock Phosphate					
Fine	0.25	1.9	0.25–0.80	16	32
Coarse	1.1	2.8	1.1–4.0	1.5	3.0
Clinoptilolite			0.21–0.50*		

*Size range represents lower and upper limit of the clinoptilolite studied.

with a fluid typical of process waste. The resistance to flow during upflow operation agreed with results obtained with a 1½-ft column of vermiculite; channeling began at a flow rate of 2.5 ml min^{-1} cm^{-2}. However, during downflow operation, the loss of head (37.5 cm of water per ft of vermiculite at 4 ml min^{-1} cm^{-2}) was twice that observed in the shorter columns. After the vermiculite was treated with NaCl (80 liters of 12% solution) and NaOH (35 liters of 0.2 *M* solution), the loss of head increased to 120 cm of water per ft of vermiculite at 2 ml min^{-1} cm^{-2}, primarily because of breakdown of the particles by the caustic treatment. Although the head loss was reduced by backwashing to remove the excess fine material, full recovery did not occur; the head loss remained 1.6 times the head loss before treatment. Since mechanically cleaned vermiculite does not require a caustic treatment, its use should obviate this difficulty.

These natural minerals appear to have application in waste treatment. To demonstrate the extent and limitation of their use in second-stage treatment of ORNL process waste, laboratory scale columns are being evaluated, and a pilot plant, capable of treating up to 3 gal per min of treatment plant effluent, is now under construction.

STUDY OF WHITE OAK CREEK DRAINAGE BASIN

T. F. Lomenick K. E. Cowser
H. J. Wyrick

Sources of Contamination

A study of the nature and extent of fission-product accumulation and transport in the White Oak Creek drainage system resulting from general fallout, Laboratory fallout, and waste disposal operations at ORNL, is in progress. The drainage basin encompasses an area of about 6 square miles. Other than general fallout, the principal contamination sources include those of the central off-gas facility, the process waste system, the solid waste burial grounds (Nos. 2, 3, 4, and 5), the liquid waste seepage pits (Nos. 2, 3, 4, and 5), and the contaminated sediments of White Oak Lake and the Intermediate Pond; smaller contributors are the laundry, sewage treatment plant, and cooling water from reactors.

Techniques and Equipment Employed in Assessing Sources. – Temporary water sampling stations have been installed at White Oak Creek Mile (WOCM) 2.6 and 3.9 and the tributary stream draining the northwest portion of the area to determine the amount and type of activity contributed

to the system from fallout and other sources that cannot be monitored directly. In addition, these stations provide information as to the chemical composition of creek water, transport of sediments, and flow in the creek. Representative samples of the effluent from the laundry and the sewage treatment plant are also taken.

The sampling devices at the creek stations and sewage treatment plant consist of battery-operated scoop-type devices that take samples continually and in proportion to the head behind weirs or Parshall flumes (see Fig. 1.5). By use of water-level recorders, a continuous record of the discharge at each station is obtained.

Findings at Monitoring Stations. – A summary of findings at the creek sampling stations is shown in Table 1.5. Although a limited amount of information is available at this time, it is seen that Sr^{89+90} and Cs^{137} are the principal radionuclides detected; other radionuclides included are: Ru^{106}, $Zr\text{-}Nb^{95}$, Co^{60}, Zn^{65}, and the rare earths. Included in the drainage area of the northwest tributary stream, which comprises approximately 15% of the total area of the drainage basin, are solid waste burial ground No. 3 and the extreme northwest portion of the ORNL plant site. Approximately 40% of the watershed is located above the sampling station at WOCM 2.6. Burial ground No. 2 and the cooling water ponds of the LITR and ORR are

Fig. 1.5. Temporary Stream Sampling Station.

Table 1.5. Radioactivity Measured at Stream Sampling Stations

Sample Date	Volume Discharge (gal)	Activity (μc)						
		Sr^{89-90}	TRE*	Ru^{106}	Cs^{137}	$ZrNb^{95}$	Co^{60}	Zn^{65}
	$\times 10^3$							
				Northwest Tributary				
Apr. 20–27, 1961	5,429	2,219	659	796	2,648	463	241	
Apr. 27–May 4, 1961	4,713	1,695	482	1,004	1,061		24	
May 4–11, 1961	8,912	2,294	5,162	1,337	4,377			
Totals	19,054	6,208	6,303	3,137	8,086	463	265	
				White Oak Creek Mile 2.6				
Apr. 28–May 5, 1961	19,836	34,841	24,329	10,283	21,040	4803	4939	5649
May 5–12, 1961	23,398	8,414	5,935	5,985	25,816	3591	3791	
May 12–19, 1961	26,150	1,782	2,277		5,530			
Totals	69,384	45,037	32,541	16,268	52,386	8394	8730	5649
				White Oak Creek Mile 3.9				
May 31–June 9, 1961	2,805	48			277			

*Exclusive of Y^{90}.

located within this area. The drainage area of the sampling station at WOCM 3.9, which comprises about 10% of the White Oak Creek watershed, does not contain any Laboratory facilities or waste disposal areas. Thus, the activity at this station is the result of rainfall and surface runoff leaching and transporting soils contaminated by Laboratory fallout and general fallout (approximately 3 curies $year^{-1}$ $mile^{-2}$). The contamination detected at other stream sampling points includes that associated with fallout, with discharges or seepage from known sources located within the drainage areas, and as yet unknown or undefined sources.

About 3000 lb of contaminated clothing is washed each week at the laundry. All wash water from the laundry drains into a storm sewer which in turn empties into White Oak Creek. A 100-ml sample of the effluent is taken from each contaminated wash, composited, and then analyzed. A summary of the activity released to White Oak Creek from the laundry for the period November 1, 1960, to April 30, 1961, is shown in Table 1.6. Approximately 50 millicuries of gross activity was detected for the six-month period.

Water entering the sewage treatment plant is normally uncontaminated. However, radionuclides have inadvertently entered the sewer system in the past. Approximately 100,000 gal of waste water is discharged from the plant to White Oak Creek each day. A portable weir box and a scoop-type sampler were installed on the effluent from this facility.

It is too early to draw any firm conclusions from the limited amount of data gathered and analyzed for the temporary stream monitoring stations. Eventually, information from the temporary monitoring stations will be integrated with that from other monitoring stations and other related studies

Table 1.6. Total Activity Released to White Oak Creek from ORNL Laundry
(Microcuries)

Date	Gallons	TRE*	Sr^{89}-Sr^{90}	Ce^{144}	Ru^{106}	Cs^{137}	Zr^{95}-Nb^{95}
Nov.–Dec. 1960	40,800	4,737	2567	3253	3411	4047	824
Jan.–Feb. 1961	42,500	2,839	2670		3840	1661	
Mar.–Apr. 1961	44,500	5,291	2514		2095	3143	1105
Totals	127,800	12,867	7751	3253	9346	8851	1929

Date	Gallons	Co^{60}	Zn^{65}	U^{233}	Pu^{239-40}	Pu^{238}	Unidentified Alpha
Nov.–Dec. 1960	40,800	1,885		101	259	28	19
Jan.–Feb. 1961	42,500	1,371		69	50		17
Mar.–Apr. 1961	44,500	1,780	1481				111
Totals	127,800	5,036	1481	170	309	28	147

*Exclusive of Y^{90}.

to establish a budget of activity in the creek and to define the mechanisms of movement and rates of movement of the radioactive materials discharged to White Oak Creek.

Solid Waste Burial

Radionuclides have been detected in seeps, in streams, and in 8 of the 16 wells located within the recently abandoned burial ground No. 4 (see Fig. 1.6).[14,15] The concentration of activity observed in the wells varies with the sampling date. By comparing gross beta counts with ground-water elevations in the wells at the time the samples were taken, some correlation is noted. In wells 194 and 185, the rise in water level during the wet season is accompanied by an increase in gross counts (see Figs. 1.7 and 1.8). In wells 182, 191, 196, and 197, the trend is toward lower concentrations of activity as the water level rises. The concentrations of activity in wells 186 and 195 are so low and erratic that no relation with ground-water elevation is apparent.

Although there seems to be a direct relationship between the concentration of activity in some of the contaminated wells and ground-water elevation, the reasons for this are not clear. Perhaps the additional amount of water accompanying a rise in water level is simply diluting the waste solution, or the rise in water level may cause additional leaching of the waste, resulting in greater concentrations of radionuclides. Other conditions further complicate the interpretation of these data. The heterogeneous nature of the waste, the lack of detailed information of burial operations, and the lack of specific information concerning the waste, such as the type, concentration, chemical state, and amount of activity, prevent a more complete understanding of these relations.

In Table 1.7 the chemical analyses of composite well samples, as well as seep and stream samples, are compared to the analyses of uncontaminated well samples taken at burial ground No. 5 prior to its use. The relatively high concentration of Na^+, Cl^-, NO_3^-, and SO_4^{2-} ions found in the contaminated water samples show that chemical ions are also being leached from the buried material.

[14] E. G. Struxness *et al.*, *Health Phys. Div. Ann. Progr. Rept. July 31, 1960*, ORNL-2994, p 20–32.

[15] T. F. Lomenick and K. E. Cowser, *Status Report on Evaluation of Solid Waste Disposal at ORNL: II* (in review).

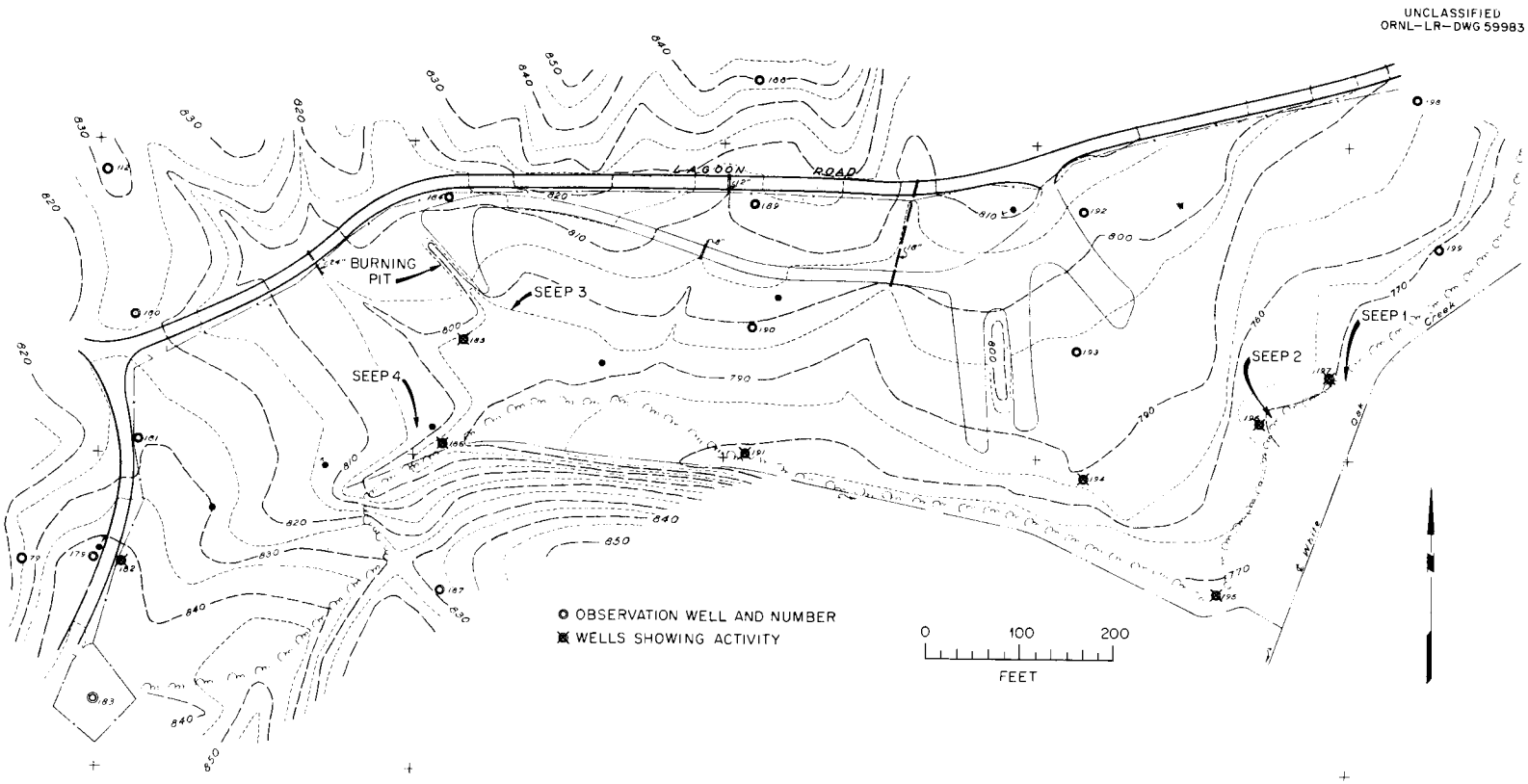

Fig. 1.6. Burial Ground No. 4.

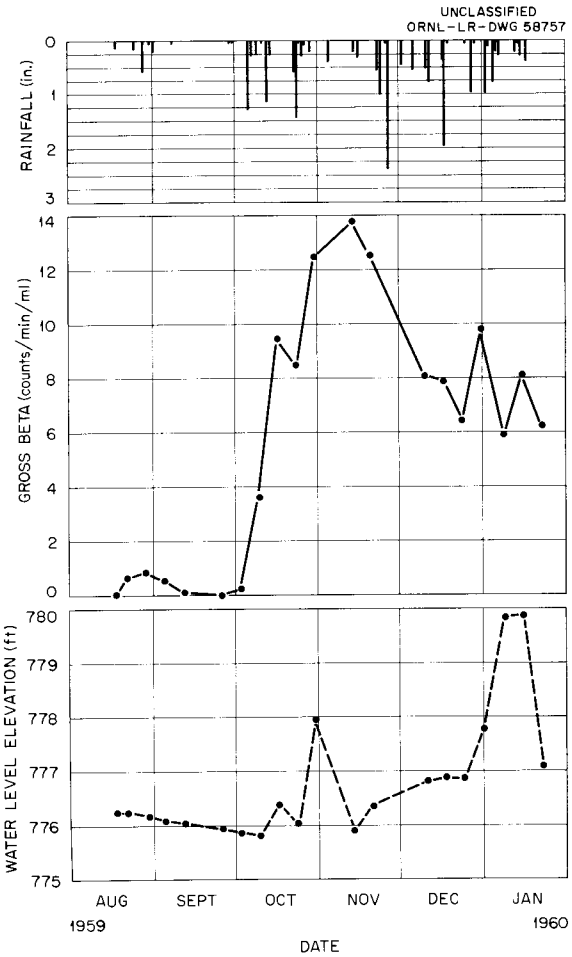

Fig. 1.7. Comparison of Gross Beta Activity and Water Level Elevations in Well 194.

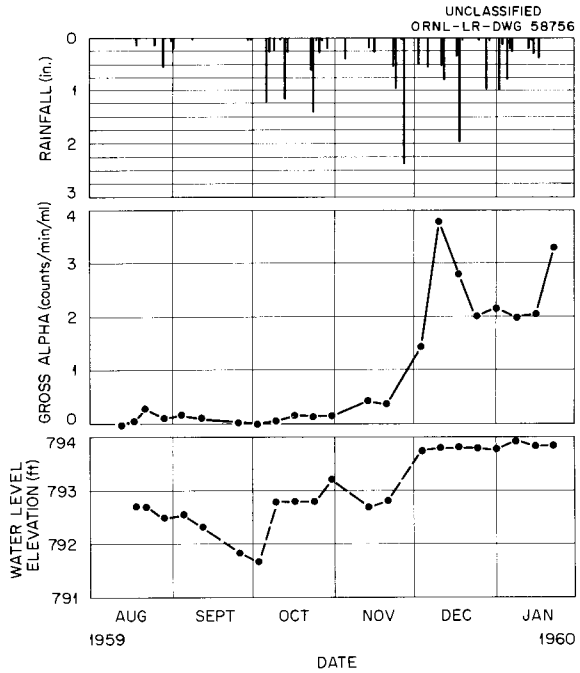

Fig. 1.8. Comparison of Gross Alpha Activity and Water Level Elevations in Well 185.

Table 1.7. Chemical Analyses of Water from Auger Wells, Seep, and Stream in Burial Ground No. 4 and Noncontaminated Auger Wells in Burial Ground No. 5

	Analyses (ppm)					
	Ca^{2+}	Na^{+}	NO_3^-	Cl^-	SO_4^{2-}	Total Hardness as $CaCO_3$
Contaminated Wells in Burial Ground No. 4						
Wells						
182	50	92	24	74	800	749
191	30	34	20	32	71	211
194	394	58	88	674	780	1420
196	40	56	19	59	143	295
197	67	56	29	87	163	270
Seep 2	26	72	32	78	78	194
Stream	25	41	35	39	51	147
Noncontaminated Wells in Burial Ground No. 5*						
Composite Sample of 4 wells	68	2.1	1.2	1.3	8.7	193

*Samples at burial ground No. 5 taken prior to burial

White Oak Lake Bed

White Oak Lake formerly served as a final settling basin for low-level radioactive wastes discharged from ORNL. White Oak Dam, a highway fill located 0.6 mile upstream from the confluence of White Oak Creek and the Clinch River, was closed in October 1943. The lake extended about 1 mile upstream and covered an area of about 44 acres. The temporary holdup afforded some dilution and a period for the decay of short-lived radionuclides before release to the Clinch River; it also allowed the deposition and accumulation of contaminated sediments. Draining the lake in 1955 and allowing the gate at the dam to remain open permitted the creek to flow unimpeded into the river. At present there is a 100,000-cu-ft impoundment behind the dam. Seepage from the waste pits flow onto the

lake bed and radionuclides from the lake bed enter the creek.

To determine the nature and extent of fission-product accumulation and transport in the lake bed, geologic and hydrologic investigations are needed, as is information on the quantity and distribution of radionuclides already in the bed.

Geology and Hydrology. – The lake bed is underlain by 6 to 12 ft of alluvial material and the Conasauga shale formation of Cambrian age. The alluvial material consists mostly of silts and clays; however, some sands and gravels are present. Core samples, taken to a depth of 6 ft along transects at the upper, middle, and lower parts of the bed, and auger samples, taken at depths below 6 ft, are being mechanically analyzed to determine the distribution of the various sizes of individual particles within the alluvial material.

To define the configuration of the water table, 31 shallow observation wells have been completed in the lake bed. These wells, which vary from 5 to 6 ft in depth, consist of a perforated casing surrounded by gravel. The direction and rate of ground-water movement within the area will be assessed by mapping the water table and by laboratory and field tests of soil permeability.

Silt Range Investigation. – An investigation is being made to determine the extent of sediment deposition and/or losses in the lake bed since it was drained in 1955. A previous investigation by the Tennessee Valley Authority showed that as of June 1953 the lake bed contained 1,030,000 ft^3 of sediment with an average annual buildup of 100,000 ft^3 per year. By comparing recent measurements of the depth of sediment with measurements made in 1953 at seven of the monumented ranges established by TVA, it was found that (1) the channel of White Oak Creek, which was filled with sediments before the lake was drained, has for the most part eroded to its preimpoundment

Table 1.8. Distribution of Gross Gamma Activity in the Bed of White Oak Lake

Depth (in.)	Gross Gamma Activity (counts min^{-1} g^{-1} wet weight)									
	Upper Transect (White Oak Creek Mile 1.3)					Lower Transect (White Oak Creek Mile 0.9)				
	Distance from Left Bank (ft)									
	50	80	140	190	240	90	190	250	340	410
0–1	21,300	36,500	16,700	32,500	18,500	3000	14,000[a]	15,700	8,000	8,700
1–2	19,800	30,600	29,400	28,000	13,700	6000		14,400	9,600	13,400
2–3	19,600	20,500	29,200	27,000	21,400	2100	13,800[b]	13,400	18,100	13,700
3–4	190	18,400	31,700	28,000	21,000	450		18,700	24,500	14,400
4–5	110	23,800	27,800	25,000	20,500	15	17,300[c]	1,300[c]	26,100	16,500
5–6	10	63,000	21,400	43,100	11,000	15			24,400	13,000
6–9	10	57,900	23,500	21,000	4,900	230	2,100	65	3,300	2,900
9–12	6	8,700	28,600	5,500	3,200	5	450	10	100	700
12–18	35	1,400	6,800	2,000	1,500	15	300		80	95
18–24	30	800	1,800	500	1,400	5	7	450	7	30
24–36	2	600	300	400	1,400	5	100	6	10	5
36–48	2	180	100	270	750	5	3	10	7	5
48–60	750	50	75	170	630	2	3	2	8	6
60–72	90	25	85	200	700	3	5	3	3	15

[a] Total for depth of 0 in. to 2 in.
[b] Total for depth of 2 in. to 4 in.
[c] Total for depth of 4 in. to 6 in.

depth; (2) the depth of sediments over the lower one-third of the bed, with the exception of the stream channel, is approximately the same as that reported in 1953; and (3) the middle and upper two-thirds of the lake has slightly less sediment than that reported in 1953. Approximately 150,000 ft^3 of silt has left the lake bed due to channel erosion. Distances along the silt ranges were obtained by tag line, and soundings were made with a rod every 10 ft. Ranges not located in the normal impoundment area were surveyed during times of unusually high water.

Distribution of Radionuclides. – An area sampling program has been initiated to determine the vertical and lateral distribution of radionuclides in the lake bed. For the first phase of this program, 15 six-ft-deep core samples were taken along three monumented silt ranges: one at the upper end, one in the middle, and one at the lower end of the lake. These samples were recovered with a 2-in.-diam thin wall tube that was manually pressed into the soil. The cores were sliced and segmented into various increments for radionuclide analyses. In general, for the first 6 in. of soil, each inch was analyzed separately. At greater depths larger increments were used. A summary of the gross gamma activity found in the cores, taken along the upper and lower ranges, is shown in Table 1.8. From these data it is noted that, in general, (1) more gamma activity per gram of soil was detected at the upper transect than at the lower one; (2) most of the gamma activity is contained in the first 12 in. of soil; and (3) activity in the upper few inches of each core is rather uniformly distributed. A more complete understanding of the distribution of radionuclides will be obtained by analyzing these cores for specific radionuclides.

CLINCH RIVER STUDIES

P. H. Carrigan[16]	E. E. Eastwood
E. G. Struxness	J. A. Payne[18]
F. L. Parker[17]	W. E. Parker[19]
R. J. Morton	T. Tamura
W. B. Nix	L. Hemphill

Comprehensive studies of the physico-chemical environment of Clinch River downstream from ORNL have been continued in cooperation with the following state and federal agencies: U.S. Atomic Energy Commission, U.S. Public Health Service, U.S. Geological Survey, Tennessee Valley Authority, Tennessee Game and Fish Commission, and Tennessee Stream Pollution Control Board. The purpose of these studies is to determine the capacity of the river for continuous release of low-level radioactive wastes and to assess the long-term effects of radioactive contamination on this environment.

The Clinch River Study Steering Committee, which is comprised of a representative from each cooperating agency, directs, coordinates, and advises the various investigators in their conduct of the Study. Meetings of the Steering Committee have been held on September 22, 1960, and May 4, 1961. During these meetings progress on the Studies has been reported, future plans discussed and implemented, and objectives defined. An immediate objective in the investigation has been to determine the fate of radioactive materials currently released to the river from White Oak Creek. To meet this objective a program of measuring flow, stable and radioactive chemical load, and suspended-sediment load has been intensively prosecuted.

Work done on sorption capacity of river-borne sediments and on distribution of radioactivity in bottom sediments has been directed toward evaluating the usefulness of Clinch River for radioactive-waste disposal.

Hydrology

Flow Measurements. – Records of flow in Clinch River were obtained at the gaging station near Scarboro, Tennessee. Those for White Oak Creek were obtained at the station at White Oak Dam. Locations of these stations are shown in Fig. 1.9. In Table 1.9 mean monthly flows for these two stations during the fiscal year are listed. The station on White Oak Creek was re-established at the beginning of the present fiscal year.

Comparison of mean monthly discharges for the two streams shows that the monthly dilution factor varies from 93 to 1010. The maximum daily discharges observed during the period of concurrent

[16] U.S. Geological Survey.

[17] Presently on leave of absence with the International Atomic Energy Agency, Vienna, Austria.

[18] Temporary summer employee, University of Tennessee, Knoxville.

[19] Temporary summer employee, Haverford College, Haverford, Pa.

operation were 21,900 cfs for Clinch River and 217 cfs for White Oak Creek. The minimum daily discharge for Clinch River occurred during a three-week period in which no releases were made from Norris Reservoir. Although these maximum and minimum daily discharges did not occur concurrently, the variation in magnitude of flows does illustrate the range in dilution factor which might occur.

Measurements of velocity and temperature distribution at many sections in the Study Reach of Clinch River were made by the U.S. Geological Survey. Results of these measurements are being used to establish flow characteristics of the river

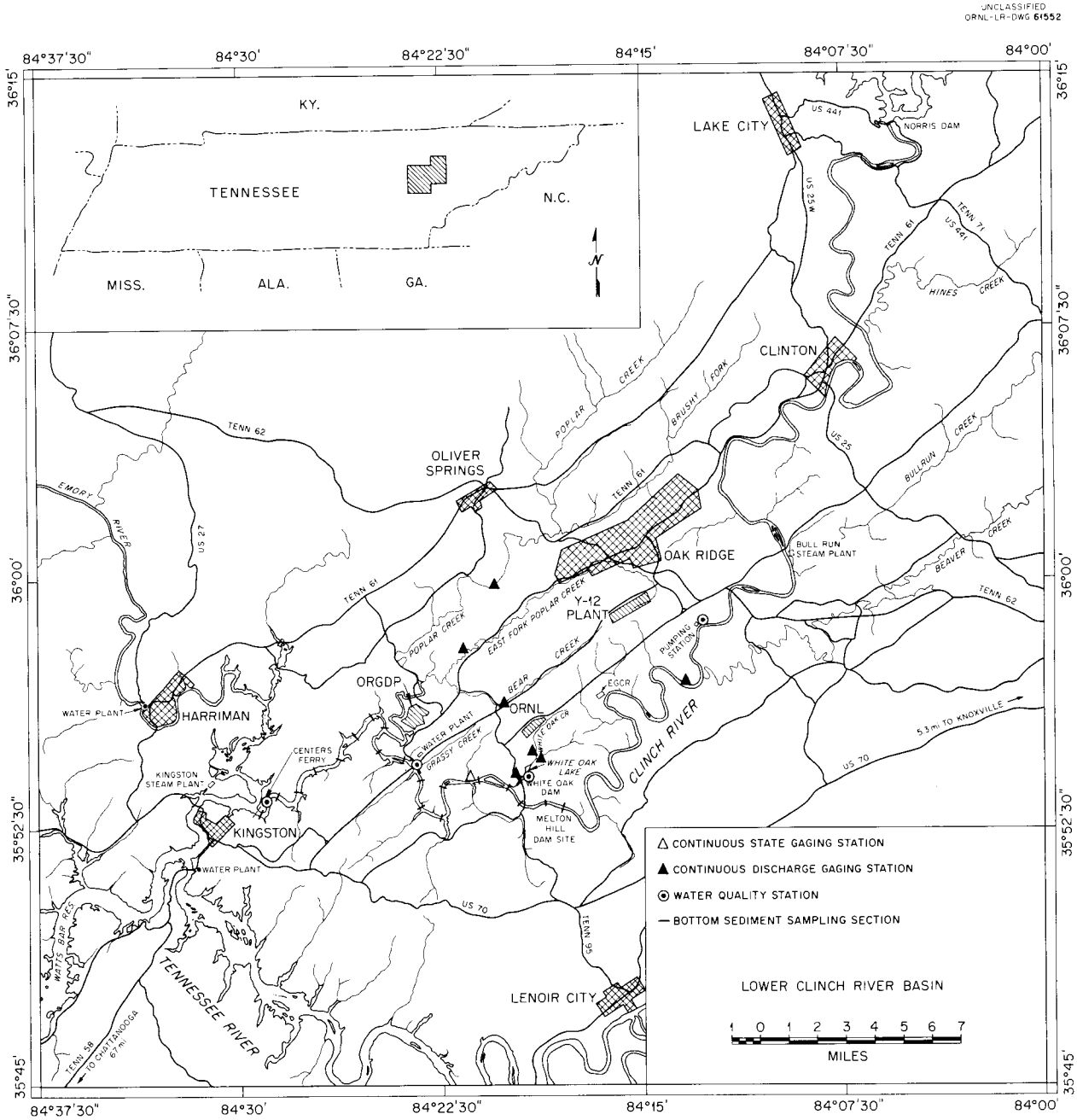

Fig. 1.9. Map of Clinch River Basin Showing Locations of Sampling Stations.

and to assist the planning of the water quality sampling program. Later, results of these measurements will be used in a study of dispersion.

Table 1.9. Mean Monthly Flow for Clinch River near Scarboro, Tennessee, and for White Oak Creek at White Oak Dam*

Month	Mean Monthly Discharge (cfs)	
	Clinch River Near Scorboro	White Oak Creek At White Oak Dam
1960		
July	4491	
August	5839	5.8
September	4764	6.0
October	3537	8.4
November	2711	6.6
December	4823	11.9
1961		
January	4027	13.4
February	3346	36.0
March	9507	28.7
April	2803	20.3
May	3617	12.9
June	2880	9.9

*Tentative records of discharge furnished by U.S. Geological Survey.

Melton Hill Dam Construction. – Construction operations at the Melton Hill Dam site (see Fig. 1.9) began in the spring of 1961. At that time excavation of a diversion canal around the construction site was started. The canal has been completed and water diverted from the river channel in the vicinity of the site. Construction activities during this early period and during the next fiscal year are not expected to affect the flow in the Study Reach. In August 1962 the diversion canal will be filled in, and water will flow through the navigation lock and over the spillway. Some minor changes in flow characteristics in the Study Reach may be expected when the flow is returned to the channel.

Establishment of Gaging Stations. – Gaging stations were established on Poplar Creek, East Fork Poplar Creek, and Bear Creek during the summer of 1960 by the U.S. Geological Survey (see Fig. 1.9). Records of flow for these streams will be used to determine tributary inflow to Clinch River in the Study Reach. Continuous records of stage are being collected at these stations. Measurements of flow are being made to establish the stage-discharge relations. Once the relations are defined, continuous records of discharge will be computed.

A continuous stage-gaging station was constructed by ORNL on the Clinch River, 1.7 miles downstream from the mouth of White Oak Creek (see Fig. 1.10). Stage records at this site will have many uses. The records will be useful, especially in "time of travel" studies. Instruments for installation at this station have been designed to permit the determination of discharge.

Water Sampling and Analysis

Sampling Stations. – In the spring of 1960, water-quality sampling stations were established at three sections on the Clinch River. Samples from the stations are analyzed for concentrations of suspended sediments, stable chemical constituents, and long-lived, radioactive constituents. One station was relocated at a more favorable section in November 1960. At the same time a station on White Oak Creek at White Oak Dam and three stations on the Tennessee River were established. The stations in the Clinch River basin are shown in Fig. 1.9. Those in the Tennessee River basin are shown in Fig. 1.11. Improved sample collection equipment was installed at some stations in November 1960.

Samples of White Oak Creek are collected continuously in proportion to the flow. Weekly composites of these samples are submitted to U.S. Public Health Service for radioactive chemical analyses. Daily samples are collected at the other stations, and weekly composites are prepared so that the daily samples are in proportion to the daily flow except for the station on the Clinch River at the Gaseous Diffusion Plant. The daily samples are collected automatically from the discharge line of a continuously operated pump by the time-sequence operated solenoid valves shown in Fig. 1.12. Samples are submitted to the Tennessee Stream Pollution Control Board Laboratory, Nashville, Tennessee, for stable chemical analyses and the U.S. Public Health Service, Robert A. Taft Sanitary Engineering Center Laboratory, Cincinnati, Ohio, for radiochemical

Fig. 1.10. Continuous Stage Gaging Station on Clinch River.

analyses. Samples from the station on Clinch River near ORGDP are reserved for analysis by ORNL. Samples at stations on the Tennessee River are collected by Visking Corporation and TVA.

Scope of Analyses. – The analyses[20] of water samples collected in previous years by the Applied Health Physics Section have indicated that the major long-lived radionuclides released to the Clinch River are: Sr^{90}-Y^{90}, Cs^{137}-Ba^{137}, Co^{60}, Zr^{95}-Nb^{95}, Ce^{144}-Pr^{144}, and Ru^{106}-Rh^{106}. Thus, the analyses for these radionuclides may be accomplished by gamma spectroscopy except for Sr^{90}-Y^{90}. Concentration of Sr^{90}-Y^{90} is determined by radiochemical separation and beta counting. Before submission for radiochemical analysis the samples are filtered; the filtrate and filter residue are analyzed separately.

Suspended sediment concentrations are determined routinely as a part of the stable chemical analyses. Particle-size distribution of the suspended sediment will be determined only four or five times a year.

Various investigators associated with the Clinch River Studies met in conference to discuss the scope of stable chemical analyses. The analyses presently undertaken are those selected by this group.[21]

Results of Analyses. – *Stable Chemical Analyses.* – A summary of the results of stable chemical analyses are summarized in Table 1.10. At the

[20] W. D. Cottrell, *Radioactivity in Silt of the Clinch and Tennessee Rivers,* ORNL-2847 (Nov. 18, 1959).

[21] Minutes of Clinch River Meeting, Sept. 22, 1960.

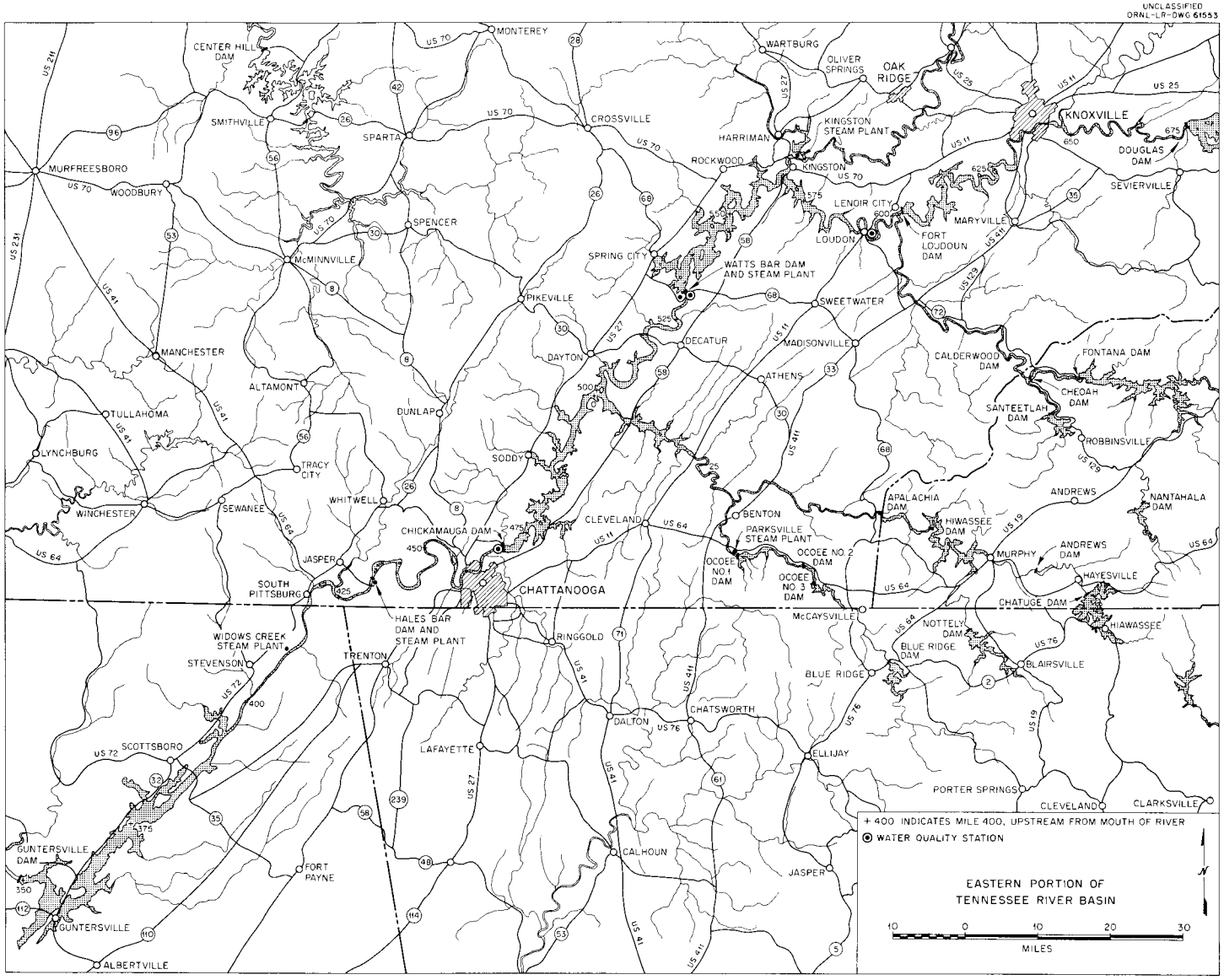

Fig. 1.11. Map of Tennessee River Basin Showing Water Quality Stations.

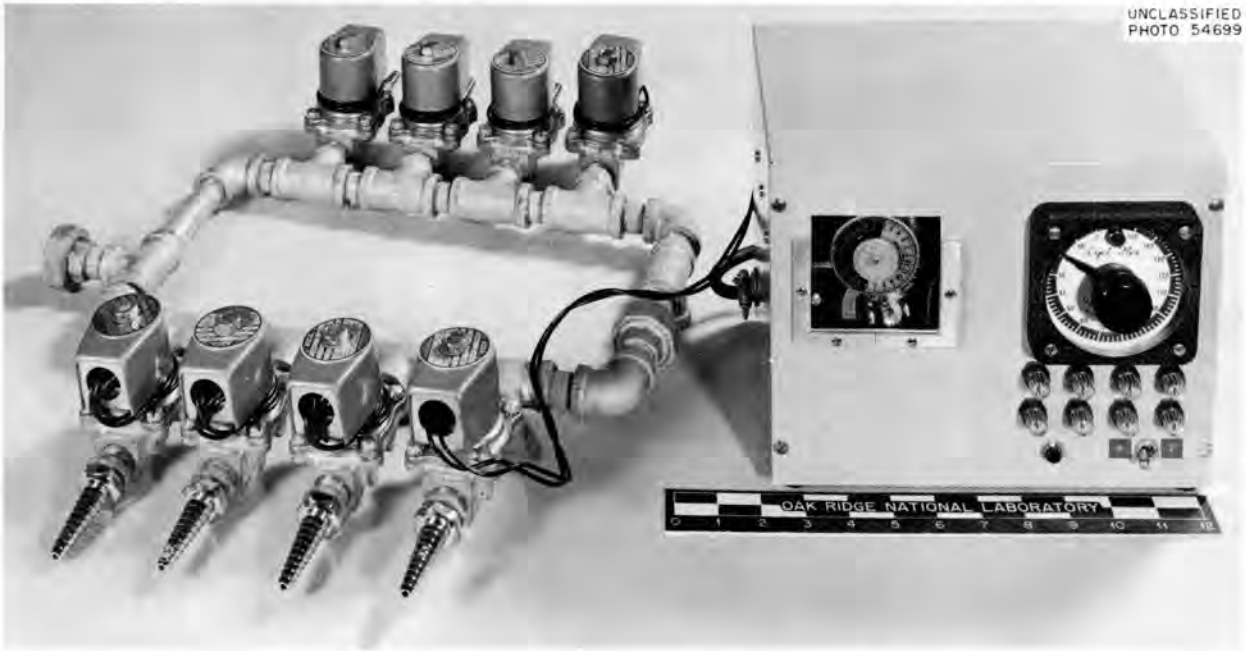

Fig. 1.12. Sequency-Timer-Operated Automatic Water Sampler.

bottom of Table 1.10 several constituents are listed for which the concentrations in the samples were below detectable limits. The limits of detection are shown in the column titled: "Average Concentration."

The stable chemical analytical program will be continued until a full year of collection has been completed at all stations. At the end of this year the number of stations will be reduced to one or two "control" stations. Interpretative studies of the data will then be undertaken.

Radioactive Chemical Analyses. – The results of radiochemical analyses of weekly composite samples from all stations on White Oak Creek, Clinch River, and Tennessee River are available for the period November 1, 1960, to February 18, 1961. Radionuclides found in the samples of water are Ru^{106}, Co^{60}, Cs^{137}, Sr^{89}, and Sr^{90}. The analytical data are summarized in Table 1.11. The results from February 18, 1961, to June 30, 1961, have not been reported by the cooperating laboratories.

Trace concentrations of cesium were detected in three weekly composite samples of water – two from Clinch River at Oak Ridge Water Plant and one from Tennessee River at Loudon, Tennessee. Results of five analyses for radiostrontium are available from four of the stations listed in Table 1.11.

Sufficient data are available to compute the radioactive chemical load at several sampling stations. Load is the total curies transported in the water past the station in a period of time and is equal to the product of radionuclide concentration, discharge, and time. These computations are shown in Table 1.12. The distance between stations is large enough so that time-of-flow must must be considered. Therefore, the periods for which load is computed at the various stations are not absolutely concurrent. The load of Co^{60} was not computed for the Tennessee River, because it was not detected (see Table 1.11).

Results of filtrate and filter residue analyses are available only for samples collected at the Gaseous Diffusion Plant. All the Cs^{137} detected was in the filter residue. Ruthenium-106 was detected in all filtrate samples and in about 25% of the filter residue samples. The maximum activity found in the filter residue was about 40% of the activity in the total sample. Strontium-90 was detected in about 50% of the filter residue samples and in all of the filtrate samples; the maximum activity found in the filter residue was about 25% of the activity in the total sample.

Table 1.10. Summary of Stable Chemical Analyses for Clinch River at Oak Ridge Gaseous Diffusion Plant

Constituent	Average Concentration (ppm)	Range in Concentration (ppm)
Sodium	2.6	1.8–4.7
Potassium	1.4	1.1–2.3
Calcium	22.4	17–48
Magnesium	6.8	<2–9.8
Strontium	0.063	0.04–0.08
Chloride	1.7	1.2–4.5
Nitrate	2.8	1.1–14.0
Sulfate	11.1	0.8–27.0
Phosphate	0.24	<0.003–0.75
Bicarbonate	110	87–134
Zirconium	0.04	
Copper	0.06	<0.01–0.10
Zinc	0.15	0.06–0.32
Iron	0.12	0.01–0.37
Aluminum	0.16	<0.01–0.34
Silicon	1.8	1.7–2.0
Titanium	0.03	0.01–0.08
Fluoride	0.24	0.22–0.26
Constituents Not Detected		
Rubidium	<0.005	
Cesium	<0.01	
Ammonium	<0.2	
Barium	<0.3	
Manganese	<0.01	
Cobalt	<0.02	
Nickel	<0.01	
Bromide	<1.0	
Iodide	<2.0	
Ruthenium	<0.1	
Suspended Sediment	24	1–104

Table 1.11. Summary of Radiochemical Analyses[a]

Radionuclide	Average Concentration ($\mu\mu$c/liter)	Range in Concentration ($\mu\mu$c/liter)
Clinch River at Oak Ridge Water Plant		
Ruthenium 106	48	*b*–210
Cobalt 60	*b*	
White Oak Creek at White Oak Dam		
Ruthenium 106	177,000	116,000–274,000
Cobalt 60	4,240	2,500–7,700
Clinch River at Oak Ridge Gaseous Diffusion Plant Water Plant		
Ruthenium 106	246	76–383
Cobalt 60	*b*	Tr[c]
Strontium 90	23.3	4.5–70
Cesium 137	11.9	*b*–32
Clinch River at Centers Ferry		
Ruthenium 106	381	*b*–1,500
Cobalt 60	9.9	*b*–33
Tennessee River at Watts Bar Dam		
Ruthenium 106	78	8–139
Cobalt 60	*b*	
Tennessee River at Chickamauga Dam		
Ruthenium 106	95	*b*–290
Cobalt 60	*b*	

[a]Results of radioactive chemical analyses furnished by U.S. Public Health Service for all stations except Clinch River at Oak Ridge Gaseous Diffusion Plant Water Plant.

[b]Concentration is too low for detection.

[c]Cobalt 60 detected in suspended sediment of one sample.

Estimate of Radioactivity in Bottom Sediments

During July and August of 1960, concurrent with the Applied Health Physics Survey, samples were taken of the Clinch River bottom sediments from CRM 21.6 to CRM 4.7. Both survey groups sampled the same sections; however, additional intermediate sections were sampled by the Radioactive Waste Disposal Section. The additional sections were included in order to provide better development of the longitudinal distribution of radioactivity; also, core samples of the bottom sediment, rather than Eckman dredge samples, were obtained in order to provide better development of the vertical distribution of radioactivity.

Core sampling was attempted at approximately eight to ten equally spaced intervals within each cross section. This operation consisted of plunging a $\frac{3}{4}$-in.-ID × 14-in.-long plastic tube, contained in a weighted stainless steel tube, into the sediment. The sampling apparatus is shown in Fig. 1.13.

Table 1.12. Total Radiochemical Load in a Period of Eleven Weeks

Station	Period Included	Total Curies
	Ruthenium-106	
White Oak Creek at White Oak Dam	Nov. 13, 1960–Jan. 28, 1961	381
Clinch River at Centers Ferry	Nov. 13, 1960–Jan. 28, 1961	377
Tennessee River at Watts Bar Dam	Nov. 20, 1960–Feb. 4, 1961	341
Tennessee River at Chicamauga Dam	Nov. 27, 1960–Feb. 11, 1961	425
	Cobalt-60	
White Oak Creek at White Oak Dam	Nov. 13, 1960–Jan. 28, 1961	8.7
Clinch River at Centers Ferry	Nov. 13, 1960–Jan. 28, 1961	9.8

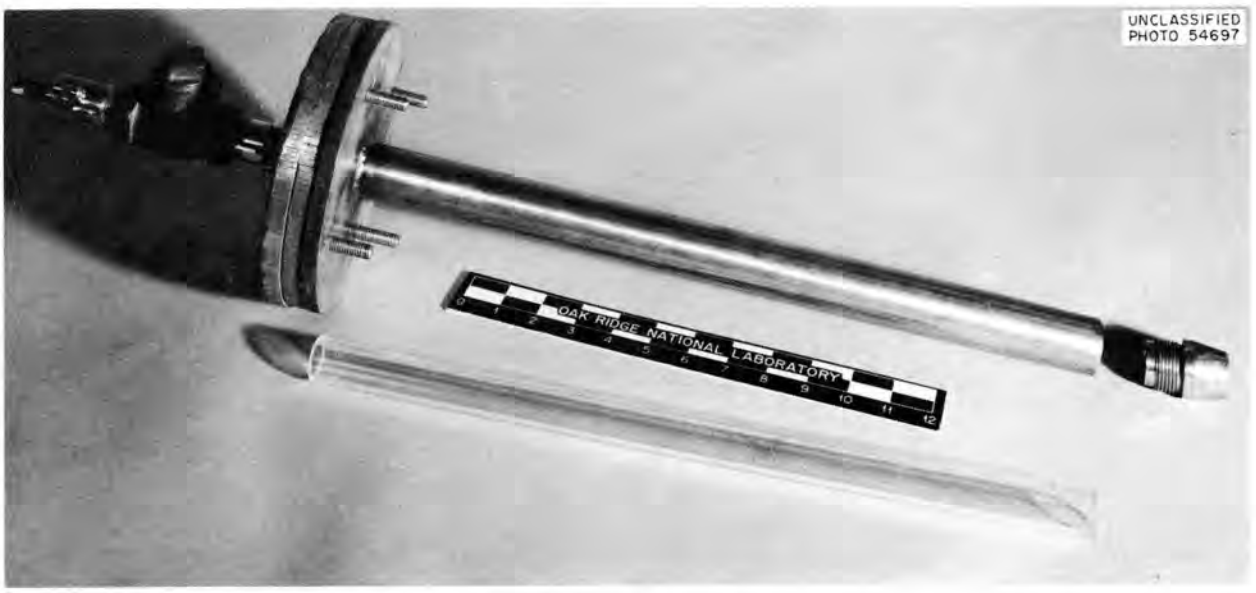

Fig. 1.13. Core Sampling Apparatus.

Following completion of sampling, the samples were prepared for radiochemical analyses according to the following procedure:

(1) Each core was frozen in its plastic tube, (2) extruded from the tube, (3) sliced into 1-in.-long × $^4/_5$-in.-diam cylindrical segments on a cutting block, (4) transferred to a labeled test tube, and (5) weighed and stoppered.

Cores were cut into segments for use in studies of depth and distribution of activity in the cross section. The relative gross gamma activity of each 1-in. sample was measured with a gamma scintillation detector and scaler. Each sample and control (background sample) was counted for a 10-min interval in order to provide reasonable counting statistics.

A preliminary examination of the gross gamma results indicated that many of the 1-in. segments were too low in activity for individual radiochemical or gamma spectrometric analysis. Because of these low activities and the expense of analyzing 870 separate 1-in. segments, all of the

segments from a cross section were mixed to form a homogeneous composite sample. The composited samples were dried at 100°C, sealed in 3-in.-diam × 1.5-in.-high plastic containers, and counted in a 256-channel gamma spectrometer. Strontium-90 and TRE (total rare earths) of each composite were determined by radiochemical separation and beta counting.

Data collected during core-sampling operations – section width, water depth, and sediment depth – were incorporated into scale drawings of each section. Calculation of section area and sediment volume for the sampled stations in the 17.8-mile reach of the river was accomplished by point-to-point numerical integration. The results of these calculations, along with the average sediment density of each section, are listed in Table 1.13.

The scaled sections and the calculated areas in Table 1.13 show that the river channel changes in shape and width around CRM 16.9. Upstream from this section the channel is relatively narrow and deep with nearly vertical sides. The shallow sediment deposits in this area are located very close to the sides. By comparison, the sections downstream from CRM 16.9 are wide and shallow. The sediment deposits in this region are thick and continuous across the entire channel width. This situation suggests that the calculated sediment volume for the sediment deposits was realistic. The sediment volume calculated for the region downstream from CRM 16.9 may be low, because the depth of the sediment deposits in this region exceeded the core sampler length.

The relative gross gamma activity of each core was calculated on a gram basis by correcting for background activity and sample weight. A value of the relative gross gamma activity per section was calculated by substituting the corrected

Table 1.13. Clinch River Cross Sections

Total silt volume: 491 acre-ft

Location (CRM)	Width[a] (ft)	Cross Sectional Silt Area[b] (ft^2)	Cross Sectional Water Area[b] (ft^2)	Average Silt Density[c] (g/cm^3)
4.7	600	325	16,350	1.4339
5.8	670	375	13,525	1.3210
6.9	800	473	15,025	1.4813
8.0	705	419	14,225	1.3596
9.0	525	318	14,975	1.3139
10.0	1050	581	13,650	1.4450
11.0	630	375	10,795	1.1731
12.0	480	143	11,655	1.3079
13.0	430	267	8,644	1.2430
14.0	500	192	8,725	1.2913
14.6	400	114	7,275	1.3448
15.3	420	113	7,797	1.3650
16.0	660	307	8,310	1.5161
16.9	350	58.7	6,115	1.2210
18.1	365	73.3	6,090	1.4887
19.5	350	50.0	5,730	1.2361
20.8	400	49.6	4,773	1.4024
21.6	370	113	3,630	1.3833
22.5	400		4,490	1.1660

[a]Measured at surface of water.

[b]Calculated from field measurements collected during core sampling.

[c]Wet weight sample.

counting data in a point-by-point area and mass integration calculation. An explanation of the calculation, including units, approximations, and procedure, is shown in the sample calculation (Table 1.14). The tabulated results of the gross gamma analyses are shown in Table 1.15, along with the results of the 1960 Applied Health Physics "Flounder" instrument survey.

A qualitative comparison of the "Flounder" and core gross gamma data is shown in Fig. 1.14. Both sets of data were plotted with reference to maximum "Flounder" readings at CRM 11.0. This point occurred as a low order maximum in the core analysis data, exceeded by CRM 20.8 and 14.0. The shapes of the two curves are similar; however, there are obvious areas of disagreement about

Table 1.14. Sample Calculation of Gross Gamma Activity in CRM 11.0 Section

Distance from Initial Point (ft)	Width (ft)	Depth (ft)	Mean Core Depth (ft)	Sediment Area (ft^2)	Gross Gamma Count per Total Core Depth (counts min^{-1} ft^{-1})	Mean Gross Gamma Count (counts min^{-1} ft^{-1})	Total Gamma Count (counts/min)
					$\times 10^3$	$\times 10^3$	$\times 10^6$
0 LB	0	0	0	0	0	0	0
50	50	0.750	0.375	10.4	87.4	43.7	2.18
150	100	0.417	0.583	58.3	73.4	80.4	8.04
250	100	0.667	0.542	54.1	153	113	11.30
350	100	0.917	0.792	79.2	135	144	14.39
450	100	0.667	0.792	79.2	160	148	14.77
550	100	0.667	0.667	66.7	145	153	15.26
630 RB	80	0	0.333	26.7	0	72.5	5.80
				374.6			71.74

Specific Activities:

Area:

$$K_A = \frac{71.7 \times 10^6 \text{ counts/min}}{375 \text{ ft}^2} = 191 \times 10^3 \ \frac{\text{counts/min}}{\text{ft}^2} .$$

Gravimetric:

$$K_g = \frac{71.7 \times 10^6 \text{ counts/min}}{4.7 \times 10^5 \text{ g}} = 152 \text{ counts min}^{-1} \text{ g}^{-1} .$$

Equation:

$$K_A = \int C \left(\frac{\text{counts/min}}{\text{ft}^2} \right) dA \, (\text{ft}^2) \approx \sum C \left(\frac{\text{counts/min}}{\text{ft}^2} \right) \Delta W \, (\text{ft}) \, \Sigma \, y \, (\text{ft})$$

$$= \sum \left[C \, \Delta y \left(\frac{\text{counts/min}}{\text{ft}} \right) \right] \Delta W \, (\text{ft}), \ \Delta y = \text{constant.}$$

CRM's 20.8, 16.9, 14.0, 10.0, 9.0, and 8.0. To a large extent, this disagreement is most pronounced in areas where sampling cross sections in the two surveys do not coincide. There is also some disagreement at coincident sampling sections, probably arising from the difference in measurement techniques. The "Flounder," constructed with 12 GM tubes, detects the activity within a relatively large volume near the surface of the silt. In contrast, the core data are essentially a number of measurements of weighted point sources averaged over the whole cross section.

Gross gamma measurements of the 1-in. core samples showed no uniform or continuous vertical distribution pattern. In general, there was a decrease in activity with depth; however, the rate of decrease was too irregular to define the lowest horizon of activity in the sediment.

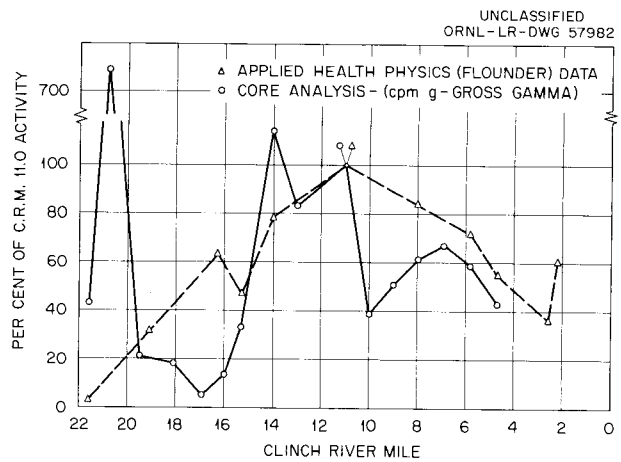

Fig. 1.14. Comparison of Core Data (Gross Gamma) and "Flounder" Data.

Table 1.15. Distribution of Gross Gamma Activity in Clinch River Bottom Sediment from Mile 21.6 to 4.7

Cross Section Location (CRM)	1960 Applied Health Physics "Flounder" Data (counts/min)	1960 Clinch River Study Core Analysis Data (activity, counts min^{-1} g^{-1})
2.1	9,120	
2.6	5,460	
4.7	8,280	66.1
5.8	10,860	89.2
6.9		102
8.0	12,780	92.5
9.0		78.0
10.0		59.7
11.0	15,180	152
12.0		103
13.0		127
14.0	11,800	173
14.6		4.1
15.2	7,080	
15.3		50.6
16.0		20.9
16.3	9,540	
16.9		7.2
18.1		27.9
19.1	4,860	
19.5		32.0
20.8		1,080.
21.5	360	
21.6		66.3
27.5	240	

Gamma spectrometric analysis showed that Cs^{137}, Ru^{106}, and Co^{60} were present in all composited samples. Spectrometric data were compared with standard soil samples containing known amounts of the nuclides to determine absolute activities of each sample. Results of these analyses, expressed in microcuries per kilogram, are given in Table 1.16. Each datum was transformed to activity per mile by the following calculation:

Let $N(X)$ = average specific activity ($\mu c/kg$) of the silt at CRM X;

$\rho(X)$ = average silt density (g/cm^3); and

$A_s(X)$ = silt cross section (ft^2) at the same point.

Thus

$$\frac{dc}{dX}(X) = \text{number of curies per mile of river}$$

$$= N(X)\ (\mu c/kg) \times 10^{-6}\ \text{curies}/\mu c \times 10^{-3}\ kg/g \times \rho(X)\ (g/cm^3) \times (30.5\ cm/ft)^3 \times A_s(X)\ (ft^2) \times 5280\ ft/mile$$

$$= 0.1489\ N(X)\ \rho(X)\ A_s(X).$$

Results of this calculation for each nuclide and for each sample section are listed in Table 1.16 and shown in Figs. 1.15–1.19.

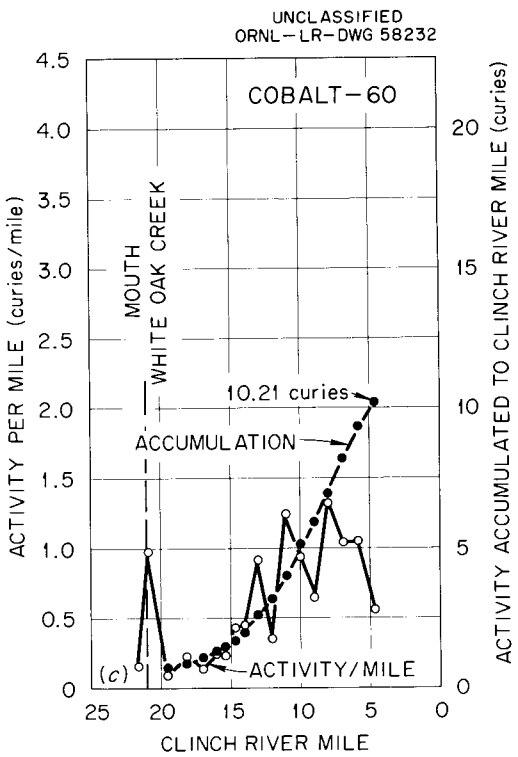

Fig. 1.16. Co^{60} Activity per Mile.

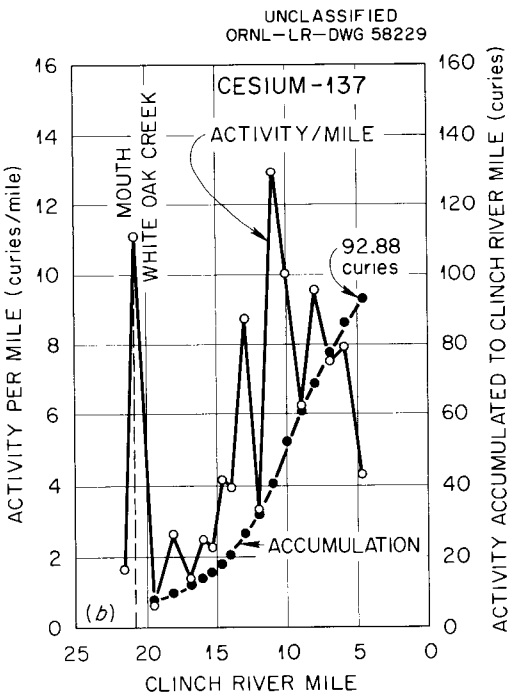

Fig. 1.15. Cs^{137} Activity per Mile.

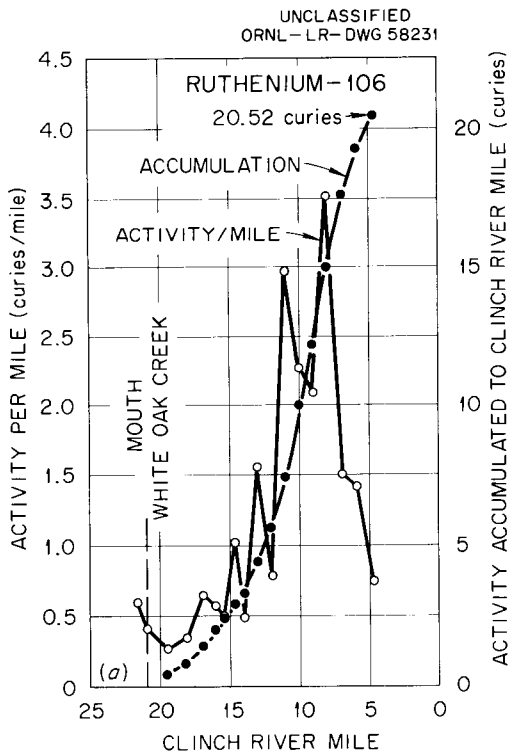

Fig. 1.17. Ru^{106} Activity per Mile.

Table 1.16. Analysis of Clinch River Silt for Specific Radionuclides

Clinch River Mile	Ru^{106} [a]		Cs^{137} [a]		Co^{60} [a]		Sr^{90} [b]		Total Rare Earths	
	Specific Activity (μc/kg)	Activity per Mile (curies/mile)	Specific Activity (μc/kg)	Activity per Mile (curies/mile)	Specific Activity (μc/kg)	Activity per Mile (curies/mile)	Specific Activity (μc/kg)	Activity per Mile (curies/mile)	Specific Activity (μc/kg)	Activity per Mile (curies/mile)
	$\times 10^{-2}$		$\times 10^{-1}$		$\times 10^{-2}$		$\times 10^{-3}$		$\times 10^{-2}$	
4.7	1.05	0.734	0.622	4.33	0.788	0.549	0.856	0.060	0.99	0.69
5.8	1.91	1.41	1.06	7.87	1.42	1.05	1.94	0.144	2.28	1.69
6.9	1.43	1.50	0.721	7.55	0.995	1.04	1.58	0.165	1.3	1.4
8.0	4.13	3.52	1.12	9.51	1.55	1.32	1.89	0.161	4.86	4.15
9.0	3.34	2.09	0.995	6.22	1.03	0.644	1.71	0.107	4.42	2.77
10.0	1.81	2.27	0.797	10.02	0.752	0.944	1.13	0.141	2.14	2.70
11.0	4.50	2.96	1.97	12.96	1.89	1.24	4.23	0.278	7.03	4.63
12.0	2.81	0.783	1.19	3.33	1.24	0.345	2.12	0.059	5.40	1.51
13.0	3.12	1.55	1.76	8.71	1.84	0.912	2.52	0.125	7.66	3.81
14.0	1.33	0.492	1.06	3.94	1.19	0.442	1.94	0.072	2.9	1.1
14.6	4.41	1.01	1.81	4.14	1.85	0.423	3.47	0.080	5.63	1.29
15.3	2.16	0.497	0.977	2.25	0.977	0.225	1.49	0.034	3.11	0.718
16.0	0.815	0.568	0.354	2.46	0.347	0.241	0.766	0.053	1.5	1.0
16.9	5.99	0.642	1.32	1.41	1.22	0.131	1.40	0.015	5.86	0.627
18.1	2.12	0.346	1.61	2.63	1.29	0.211	2.30	0.037	3.59	0.585
19.5	2.79	0.258	0.712	0.658	0.923	0.0857	1.08	0.010	2.28	0.211
20.8	3.90	0.405	10.6	11.05	8.32	0.970	16.8	0.175	20.4	2.12
21.6	2.54	0.594	0.703	1.64	0.653	0.153	1.44	0.034	3.07	0.718
22.5	1.36		0.248		0.334		0.090		1.4	
Total [c]	20.52		92.88		10.21		1.75		29.66	
Total [d]	20.92		97.96		10.66		1.83		30.79	
Total [e]	33.20		99.48		11.64		1.86		37.64	

[a] Gamma spectrometer analysis.
[b] Chemically separated before counting.
[c] Total activity (curies) between CRM 20.8 and 4.7.
[d] Total activity (curies) between CRM 21.6 and 4.7.
[e] Total (*d*) adjusted for decay.

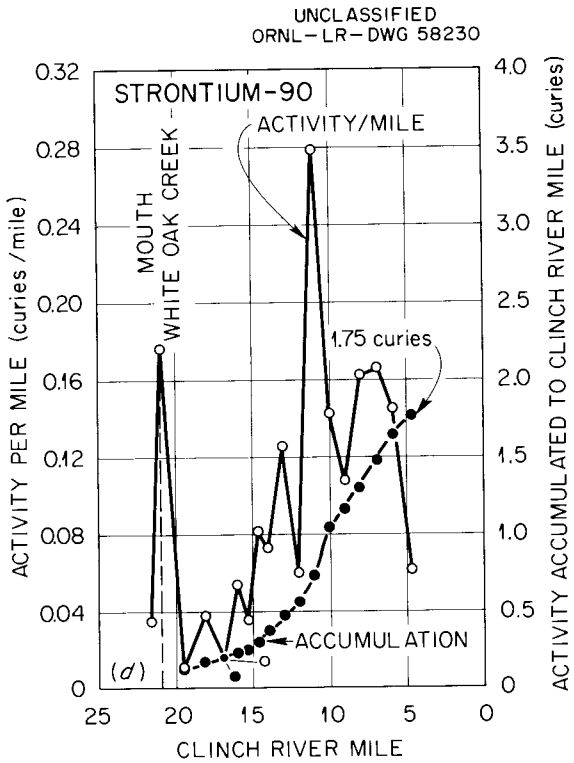

Fig. 1.18. Sr^{90} Activity per Mile.

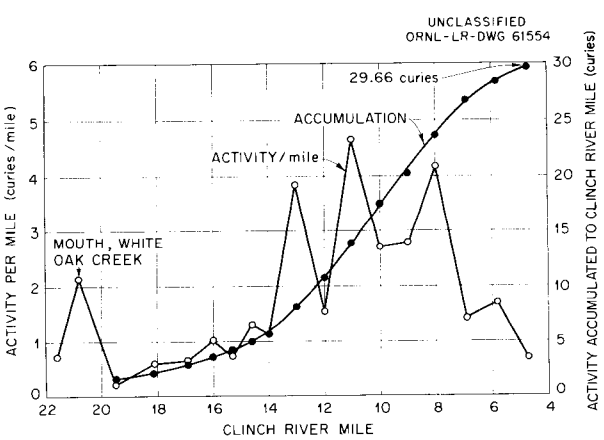

Fig. 1.19. TRE Activity per Mile.

Cesium-137 is shown to be the predominant nuclide at all sections downstream from CRM 21.6. The linear distribution (curies/mile) patterns of Cs^{137}, Ru^{106}, and Co^{60} are similar to each other from CRM 16.0 to 4.7. Both Cs^{137} and Co^{60} show a sharp maximum at CRM 11.0, greater than the 20.8 maximum. Ruthenium-106 also shows a maximum at CRM 11.0. Secondary maxima for Cs^{137} activity at CRM 8.0 and 13.0 are greater than the corresponding secondary maxima for Co^{60}. Generally, Ru^{106} exhibits a regular increase in concentration from CRM 19.6 to 8.0 and a sharp decrease from CRM 8.0 to 4.7. The Cs^{137} and Co^{60} distribution curves also show a general decrease in activity past CRM 8.0, but not as drastic as that shown by the Ru^{106} curve. Unlike the distribution pattern of the other two nuclides, the Ru^{106} linear activity curve shows a symmetrical increase above and below CRM 19.6; thus, the linear activities at CRM 21.6 and 16.9 are approximately equal.

Results of Sr^{90} and TRE radiochemical analyses are seen in Table 1.16 in the same form as the gamma spectrometric analysis. The downstream linear distribution of Sr^{90} (Fig. 1.18) and TRE (Fig. 1.19) shows a similarity to the Cs^{137} (Fig. 1.15) and Co^{60} (Fig. 1.16) curves. Points of maximum activity for the five radionuclides coincide. For Sr^{90} and TRE, the maxima, in order of decreasing magnitude, fall at CRM 11.0, 8.0, and 13.0.

To obtain the number of curies of any nuclide in a given reach of river, the above expressions were integrated over the area of interest.

$$C(\text{curies}) = 0.1498 \int N(X)\, \rho(X)\, A_s(X)\, dX.$$

This calculation was performed numerically, point-by-point, for all four nuclides identified. The integration was carried out from CRM 20.8 to each sampling section. These integrations, and the activity accumulated to each section, are plotted in Figs. 1.15–1.19. Implicit in these calculations is the assumption that $(N\rho A_s)$ for a river bend lies on a straight line between the values in the neighboring straight reaches.

Total activity calculated for each of the radionuclides is given at the bottom of Table 1.16. Between CRM 21.6 and 4.7, the amounts are 20.92, 97.96, 30.79, 10.66, and 1.83 curies for ruthenium, cesium, TRE, cobalt, and strontium, respectively, for a total of 162.16 curies. Correcting these data for decay since sampling brings the total to 184 curies.

For comparison with activity found in river sediment, a sophisticated guess was made of the total amount of each nuclide which has gone over White Oak Dam, corrected for decay. For the calculation, two assumptions were made:

1. For a period of five years, a total of five curies per day was released to Clinch River. For the following ten years, up to the date of sediment sampling, one curie per day was released.

2. The proportion of this activity due to each isotope was uniform over the whole 15-year period. These proportions were assumed to be the average of the analyses made by Applied Health Physics on White Oak Creek water in 1960.[22]

For calculation of the amount of TRE (excluding Ce^{144}), additional assumptions were made:

1. The activity of each rare earth was initially proportional to its fission yield.

2. The rare earths released from White Oak Creek were one year old.

3. By the time of sediment sampling, the activities of all rare earths, except Pm^{147}, Sm^{151}, and Eu^{155}, are negligible.

These assumptions, although questionable, lead to a rough "frame of reference" for the core-analysis estimate. Table 1.17 lists the two sets of values. It is indicated that approximately 14% (184 curies) of the total activity (1300 curies) is associated with the bottom sediment. A comparison of the relative amounts of each nuclide in the two estimates shows that Cs^{137}, Ru^{106}, and TRE's make up 92% of the sediment activity; whereas, they contribute only 75% of the total activity. The most prevalent nuclide in the calculated estimate, Sr^{90} (27%), constitutes only 1% of the activity in the bottom sediments. In addition, these values show that approximately 20% of the Cs^{137}, 5% of the Ru^{106}, 48% of the TRE's, and 6% of the Co^{60} released to the river are associated with the bottom sediments.

[22] W. D. Cottrell, "Area Monitoring Data" (unpublished data), 1960.

Table 1.17. Comparison of Calculated Total Released Activity and Bottom Sediment Activity in the Clinch River

Nuclide	Calculated Total Activity		Bottom Sediment Activity	
	Curies	Per Cent	Curies	Per Cent
Cs^{137}	285	21.9	99.5	54.1
Sr^{90}	346	26.6	1.86	1.0
Co^{60}	199	15.3	11.6	6.3
Ru^{106}	381	29.2	33.20	18.1
TRE	77.6	6.0	37.64	20.5
Ce^{144}	6.6	0.5		
Zr^{95}	3.7	0.3		
Nb^{95}	2.7	0.2		
Total	1301.6		183.8	

FUNDAMENTAL STUDIES OF SORPTION BY MINERALS

T. Tamura
F. S. Brinkley
D. Catron
O. M. Sealand
D. G. Jacobs
S. Amarantos[23]
A. L. Mohan[24]
J. Murdock[25]
Y. Nakayama[26]

Structural Relationships in Cesium Sorption

Earlier studies showed that lattice closure improved the ability of minerals to selectively sorb cesium from simulated waste solutions.[27,28] In this section the effect of expanding the *c*-axis spacing on cesium sorption is reported; in addition, the leachability of sorbed cesium by different cations is discussed.

Lattice Expansion by Removal of Structural Potassium. – Biotite is a mineral whose formula may be written as $KAlSi_3(Fe,Mg)_3O_{10}(OH)_2$. On weathering, the potassium is leached from the structure, and the more highly hydrated magnesium, calcium, or sodium ions satisfy the negative charge requirement. When the more highly hydrated ions substitute for potassium, the volume required to accommodate the hydrated ions is greater; this requirement is satisfied by an increase in the distance separating the unit

[23] Alien guest from Democritus Nuclear Center, Greek Atomic Energy Committee, Athens, Greece.

[24] Alien guest from Atomic Energy Establishment, Trombay, Bombay, India.

[25] ORINS research participant, University of Wisconsin.

[26] Alien guest from Nippon Atomic Industry Group Company, Ltd., Tokoyo, Japan.

[27] T. Tamura and D. G. Jacobs, *Health Phys.* 2, 391 (1960).

[28] T. Tamura and D. G. Jacobs, *Health Phys.* 5, 149 (1961).

sheets. By x-ray diffraction tests one can determine the distance separating the sheets and thus confirm that substitution has been accomplished.

Normally, weathering is a slow process. In the laboratory the process can be accelerated by leaching with concentrated solutions of salts. In these tests, 50 g of natural vermiculite containing approximately 40% biotite was leached with 9 liters of 5 *N* NaCl solution.[29] After passage of the solution, which required 9 days, the vermiculite was pushed out of the column and the material separated into four approximately equal segments. The portions were washed free of excess NaCl and air-dried.

Another method for accelerating the removal of potassium is to treat with sodium tetraphenylboron. Since potassium tetraphenylboron is relatively insoluble, lattice potassium is removed. The treatment consisted in mixing an equal weight of vermiculite or pure biotite with sodium tetraphenylboron. The mixture was wetted to give a pasty consistency and then dried in the oven at 100°C. When cool, acetone (approximately five times the volume of solid) was added, the suspension was mixed, and the supernatant decanted. This washing procedure was repeated three or four times.

In Table 1.18 the potassium concentrations and the ion exchange capacities of the materials leached with sodium tetraphenylboron are listed. The potassium concentrations show that tetraphenylboron treatment did remove potassium; noteworthy was the low removal from muscovite. The ion exchange capacity of each material was increased by the treatment. On the basis of the amount of potassium leached from the material, the exchange capacity was calculated. The vermiculite sample should have gained 64 meq/100 g, the biotite sample 94 meq/100 g, and the muscovite sample 20 meq/100 g. The observed differences were 71, 92, and 13 meq/100 g respectively. Although no potassium measurements were made for the NaCl-leached vermiculite, the exchange capacity measurements suggest that removal of the lattice potassium was accomplished by leaching.

Substitution of hydrated sodium for potassium should increase the *c*-axis spacing; x-ray diffraction patterns were made and confirmed the increased spacing. The type of response noted is illustrated by biotite, whose pattern is given in Fig. 1.20. Note that the increase is approximately 2 A (12 A − 10 A) even with the addition

[29] This material, commonly referred to as vermiculite, is a hydrobiotite and contains approximately 40% biotite.

Table 1.18. The Potassium Content and Cation-Exchange Capacity of Several Minerals

Material*	Treatment	K (ppm)	Cation Exchange Capacity (meq/100 g)
Vermiculite	None	36	69
Vermiculite	2 × Na-tetraphenylboron	11	140
Biotite	None	70	4.5
Biotite	2 × Na-tetraphenylboron	34	97
Muscovite	None	75	3.3
Muscovite	2 × Na-tetraphenylboron	67	16
Vermiculite	Leaching		
	Influent end		95
	Second quarter		90
	Third quarter		83
	Effluent end		84

*The vermiculite sample is a hydrobiotite and contains approximately 40% biotite.

of glycerol. This suggests that the expanded material (14 A) occurs interstratified with unexpanded biotite (10 A) and not as discrete units of expanded material. The ineffectiveness of the tetraphenylboron treatment to remove potassium from muscovite was verified by x-ray diffraction tests. The 10-A spacing remained unaltered after the treatment. Studies are in progress to determine the cause of the difference between biotite and muscovite.

Cesium Sorption by Expanded Materials. – To determine the effectiveness of the expanded biotite and vermiculite to sorb cesium from simulated waste solutions, the materials were tested in 0.1 *M* NaCl solutions. The solutions were first spiked with a very low concentration of cesium (Cs^{137} was used as tracer). The amount of cesium sorbed by 1 meq of the material after 24 hr of contact was determined; then the cesium concentration was increased and the amount sorbed redetermined. Since natural biotite possesses only 4.5 meq per 100 g of cation exchange capacity, the amount of material used was kept at the same level as the expanded biotite (1.4 g based on 72 meq per 100 g) instead of using 20–25 g per 50 ml of solution.

The data obtained for four materials are shown in Fig. 1.21. Several interesting relationships are noted from the figure. With an increase in ion exchange capacity, the amount of cesium sorbed

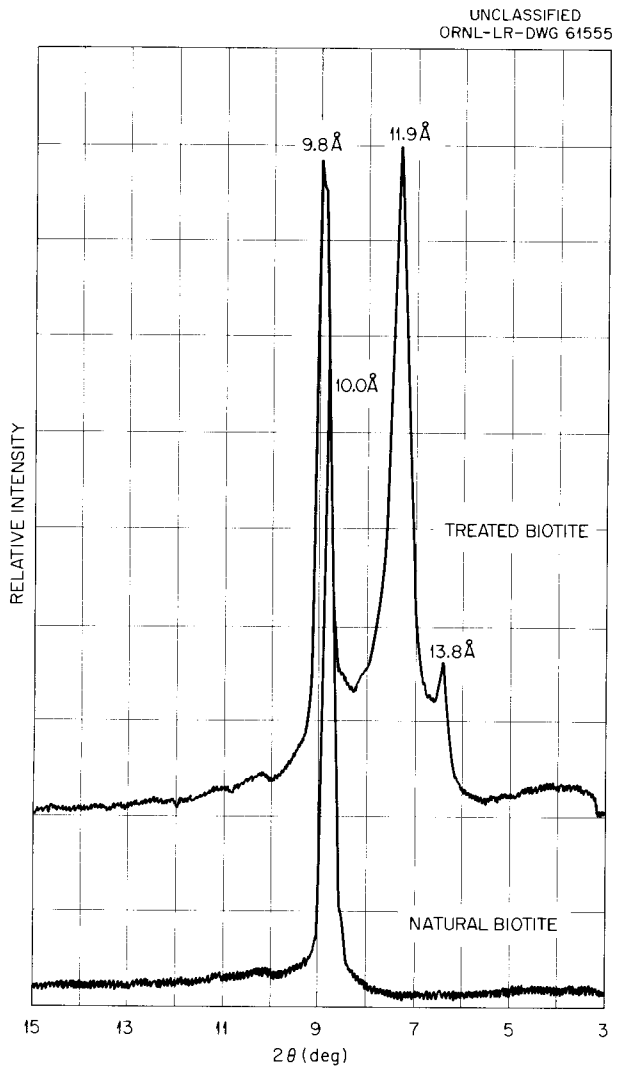

Fig. 1.20. The X-Ray Diffraction Tracings of Natural Biotite and Biotite Treated with Sodium Tetraphenylboron.

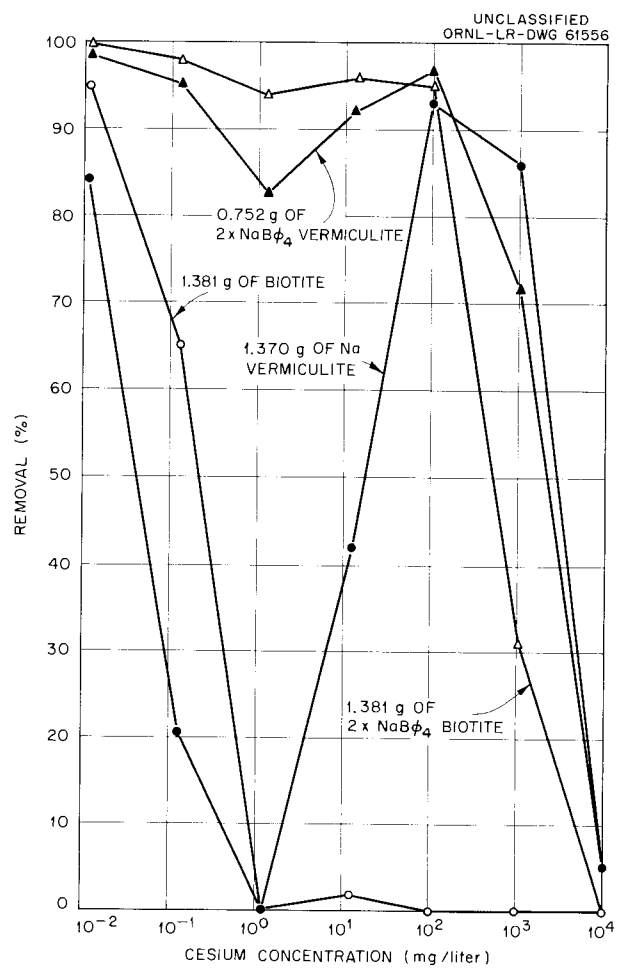

Fig. 1.21. Removal of Cesium by Biotite and Vermiculite Before and After Treatment with Sodium Tetraphenylboron. 50 ml of 0.1 *M* $NaNO_3$ solution per meq of material.

is also increased. However, the superior performance of natural biotite compared with Na-vermiculite in the low cesium concentration ranges (1.4 mg cesium per liter = 5×10^{-4} meq per meq of material) emphasizes the importance of the closed sheets of layer-lattice silicates for selective removal of cesium from waste solutions having high salt concentrations.

The exchange sites produced by the treatment appear to be more selective for cesium than the original exchange sites. This is particularly evident in the vermiculite curves. Both curves represent 1 meq of exchange material; the Na-vermiculite sorbed very little cesium at a 1.4-mg level whereas the treated material sorbed most of the cesium. Even greater concentrations of cesium (> 1.4 mg) induced collapse of the lattice, and the structure reverted to the closed-lattice biotite type except that cesium is in the interlayer position instead of potassium.[30]

Another particularly interesting response was the increase for natural biotite at a cesium concentration of 13 mg per liter. Several tests were made in addition to that reported in Fig. 1.21; in each case the sorption at a cesium concentration of 13 mg was higher than that at larger or smaller concentrations. This strongly suggests that the observed response is real and not due to error in the experiment. If the response is real, then this procedure may serve as a tool to establish collapsible layers in biotites which more conventional identification techniques would classify as completely closed-lattice minerals.

Desorption Studies. – Sorption of cesium by layer-lattice clay minerals is effected by three ion exchange mechanisms: (1) reversible ion exchange at freely accessible charged surfaces, (2) sorption at sterically favorable exchange sites at the edges of collapsed lattices (edge fixation), and (3) interlayer entrapment caused by collapsing of the layer lattice during the exchange process (interlayer fixation). The mechanism of the exchange reaction should be influential in determining the effectiveness of various cations for replacement of the sorbed cesium. Desorption data obtained using a number of leaching solutions show this to be true.

Illite and vermiculite were treated with $CsNO_3$, tagged with Cs^{137}, to obtain different levels of cesium saturation. Edge fixation was responsible for a high percentage of sorption at low concentrations of cesium in both cases. Sorption by illite at the low concentration of cesium is higher than by vermiculite because of the greater number of collapsed lattices affording sites for edge fixation; approximately 40% of the material in the vermiculite sample are collapsed biotite lattices. Because almost all the illite lattices are in the collapsed state, no interlayer fixation by illite is observed; the cesium beyond the amount necessary to satisfy edge fixation sites is reversibly sorbed at the freely accessible exchange sites. The cesium sorbed by vermiculite at the higher concentration does not exceed the interlayer fixation capacity of approximately 45 meq/100 g so that no easily exchangeable cesium is present on the vermiculite.

Portions of the illite (4 g) and vermiculite (2 g) representing approximately 1 meq exchange capacity were thoroughly mixed for 1 hr in a centrifuge tube containing 40 ml of various leaching solutions specified in the discussion below. The suspension was centrifuged, two aliquots of the supernatant were removed for counting, and the supernatant liquid decanted. Ten successive leaches were made using 0.025 *M* solution (1 meq), followed by nine leaches with 0.25 *M* solution and ten leaches with 1.0 *M* solution. Leaches with these higher concentrations were not made using $CsNO_3$ or RbCl. After a desorption series, portions of the leached clay were counted and the count rate compared with that of the unleached clay.

Desorption of Cesium from Edge Fixation Sites of Illite. – Cesium sorbed at edge fixation sites of illite is most effectively desorbed by cations having steric favorableness for the fixation sites (Table 1.19). Rubidium chloride and potassium nitrate were about 92% as effective as cesium nitrate for removal of the cesium from these exchange sites while hydrochloric acid was only about 7.4% as effective. Desorption studies using NaCl as a leaching solution resulted in dispersal of the fine particles of illite. Therefore, samples free from suspended solids could not be obtained for assay, though it was estimated that NaCl was approximately 10% as effective as $CsNO_3$ for removal of cesium. Only about 20% of the

[30] D. G. Jacobs and T. Tamura, "The Mechanism of Ion Fixation Using Radioisotope Technique," presented at the 7th International Congress of Soil Science, Aug. 14–24, 1960, Madison, Wis.

total cesium held at edge fixation sites by illite could be removed by leaching with 500 meq of various solutions.

Desorption of Easily Exchangeable Cesium from Illite. – All the leaching solutions employed were effective in removing easily exchangeable cesium from illite, though approximately 3–3.5% of the cesium had not been removed after leaching with 500 meq of leaching solution (Table 1.19). It can be postulated that this portion of the cesium was retained at edge fixation sites. Combining this data with that obtained from the leaching of cesium sorbed at edge fixation sites of the illite, one can estimate that the edge fixation capacity of the illite is about 0.0026 meq/g, corresponding to about 1% of the total number of exchange sites. This is consistent with the number of fixation sites that must be assumed in order to reconstruct cesium sorption curves previously obtained for illite.

Table 1.19. Desorption of Cesium from Vermiculite and Illite

Leaching Agent (meq)	Cesium Leached (%)			
	Illite		Vermiculite	
	a	*b*	*c*	*d*
$CsNO_3$				
1	55.2	3.6	0.14	3.07
10	92.5	13.7	0.51	4.21
RbCl				
1	41.0	3.1	0.08	0.62
7	87.2	9.4	0.19	1.14
KNO_3				
1	1.8	6.7	0.19	0.26
10	74.6	11.3	2.03	0.54
100	96.2	18.8	11.3	1.04
500	96.9	20.8	31.3	1.99
HCl				
1	27.8	0.15	0.10	1.04
10	82.2	1.05	0.86	6.82
100	94.0	4.1	3.41	39.7
500	96.6	16.7	11.2	70.8
NaCl				
1	10.5		0.20	1.59
10	61.1		1.17	8.92
100	87.8		4.05	32.5
500	96.5		9.05	58.4

[a]Four-gram sample containing 0.272 meq cesium.

[b]Four-gram sample containing 0.990×10^{-5} meq cesium.

[c]Two-gram containing 0.518 meq cesium.

[d]Two-gram sample containing 0.619×10^{-5} meq cesium.

Desorption of Cesium from Edge Fixation Sites of Vermiculite. – The data from this series of desorption studies show that two mechanisms are operating in the system (Table 1.19). The leaching ability of the cations having steric favorability for the edge fixation sites (Cs^+, Rb^+, and K^+) is offset, especially after the initial leach, by the ability of these same ions to cause collapse of the vermiculite lattice with the resultant entrapment of the remaining cesium by interlayer fixation. On the other hand, HCl and NaCl do not cause lattice collapse and they continue to remove cesium from the vermiculite.

Assuming that the edge fixation sites available in the vermiculite sample have the same affinity for cesium as those in the illite sample, it can be estimated from the sorption of cesium from the dilute cesium solution that 20 g of vermiculite has 16.5% as many edge fixation sites as does 40 g of illite. The greater removal of cesium from edge fixation sites of vermiculite compared with that from illite by HCl seems to bear this out; that is, the leaching of the vermiculite is greater because of the presence of a smaller number of fixation sites.

Desorption of Cesium from Interlayer Fixation Sites of Vermiculite. – Cesium held at interlayer fixation sites is much less subject to leaching than that held at other exchange positions (Table 1.19). Rubidium chloride was less effective than $CsNO_3$ for the removal of this cesium, but HCl and NaCl, which will allow lattice expansion, were more effective. However, the interlayer cesium is so tenaciously held that it would require prolonged or drastic leaching to effect complete lattice expansion.

Leaching with 500 meq KNO_3 removed over 30% of the cesium, even though potassium would be expected to maintain a collapsed lattice system. The reason for this behavior is not quite clear, unless it can be assumed that the potassium combines a steric favorability for the interlayer fixation sites with the ability to diffuse into the basal spacings and displace the cesium. It is

also possible that at least a portion of the collapsed lattices have a distinct preference for potassium over cesium and that a more stable state is attained by the replacement of cesium by potassium within these basal spacings.

Strontium Reactions with Minerals

In characterizing the reactions of strontium with sorbent materials, four possible mechanisms were suggested: (1) ion exchange as an absorption process exemplified by the resins, clinoptilolite, and the clay minerals; (2) ion exchange as an adsorption process characterized by the reaction of alumina; (3) metasomatic replacement as characterized by the $CaCO_3$-phosphate reactions; and (4) precipitation reactions as evidenced by natural vermiculites and clinoptilolite in contact with phosphated waste.

The slurry tests consisted in adding a known weight of material to a beaker containing a measured volume of simulated waste solution. For most tests this was 0.5 g in 50 ml of 0.1 *M* $NaNO_3$ solution containing 0.05 mg of strontium. The pH of the suspension was adjusted with NaOH or HNO_3 as desired; after 1 hr of contact the pH was redetermined and adjusted if necessary. Depending on the sampling schedule, periodic pH checks and adjustments were made. Strontium removals were based on Sr^{85}-tagged solutions. All samples were counted in a well-type gamma scintillation counter equipped with an NaI crystal.

Ion Exchange by Absorption. – Selected materials which were tested are shown in Table 1.20. These include the low ion exchange kaolinite, which shows a relatively low removal of strontium, and the high ion exchange Dowex 50W, which removes a higher percentage of the strontium. In general the higher the exchange capacity the higher the removal of strontium; the highest K_d (distribution coefficient) is 9800 ml/g for Dowex 50W based on the oven-dried weight, and the lowest is about 15 ml/g for kaolinite.

Included in the table are data for natural materials which have been treated to increase the exchange capacity. Note the increase for both biotite and vermiculite which (by removal of lattice potassium by the sodium tetraphenylboron

Table 1.20. Per Cent Removal of Strontium from Simulated Waste by Selected Materials

Material	Size (mesh)	Ion Exchange Capacity (meq/100 g)	pH*	Strontium Removed (%)			
				1-hr Contact	4-hr Contact	24-hr Contact	72-hr Contact
Dowex 50W-X12	50–100	500	5.2 ± 0.2	50.4	74.0	93.4	98.2
Duolite C-3	35–70	250	3.0 ± 0.3	29.1	52.1	84.9	90.5
Kaolinite	170–200	13	7.5 ± 0.5	11.7	10.7	12.1	13.8
Nontronite	60–170	98	7.0 ± 0.3		19.2	48.4	53.4
Vermiculite	35–70	67	7.5 ± 0.5	10.5	16.1	30.8	36.3
Montmorillonite	200–270	91	8.4 ± 0.3	35.0	44.0	44.3	43.6
Clinoptilolite	35–70	200	7.0 ± 0.5		34.7	74.5	89.6
			8.5 ± 0.5		43.9	77.5	90.8
2 × Na-tetraphenylboron vermiculite	35–70	140	8.5 ± 0.5	37.5	51.0	74.9	79.9
2 × Na-tetraphenbyboron biotite	35–70	97	8.5 ± 0.5	38.1	52.7	68.5	66.9
Biotite	35–70	4	8.5 ± 0.5	2.20	2.30	3.37	2.31

*Deviations refer to maximum change noted during the experiment after pH adjustment.

treatment) had been increased in exchange capacity. The results with the treated biotite and vermiculite emphasize the importance of the cation exchange capacity for strontium sorption.

Ion Exchange by Adsorption. – In a previous report[31] promising results were reported for alumina in the removal of strontium from simulated waste solutions. Several other oxides were tested, and cerium dioxide showed similar behavior (Fig. 1.22). These materials were found to have very low ion exchange capacities; alumina, for example, showed less than 1 meq/100 g. Although the cause of the selectivity for strontium is not known, it is thought that the amphoteric qualities of alumina and cerium dioxide are responsible.

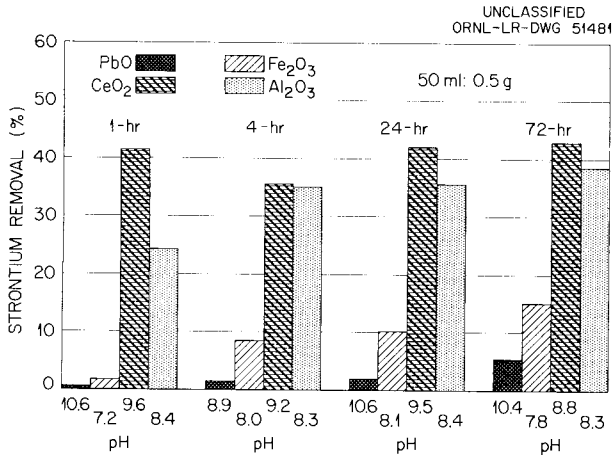

Fig. 1.22. Removal of Strontium from Simulated Waste by Several Oxides.

To establish the influence of pH on the performance of alumina and cerium dioxide, tests were run at several pH levels. The results are shown in Fig. 1.23. It is obvious that the alumina response is greatly influenced by pH. The number associated with each experimentally determined point refers to the pH at that contact time.

A significant difference between alumina and vermiculite in removing strontium is shown in Fig. 1.24. Evidence accumulated thus far suggests that alumina removes by a surface reaction and that vermiculite removes by absorption. It is premature to offer a more detailed explanation

[31] E. G. Struxness *et al.*, *Health Phys. Div. Ann. Progr. Rept. July 31, 1960*, ORNL-2994, p 70–78.

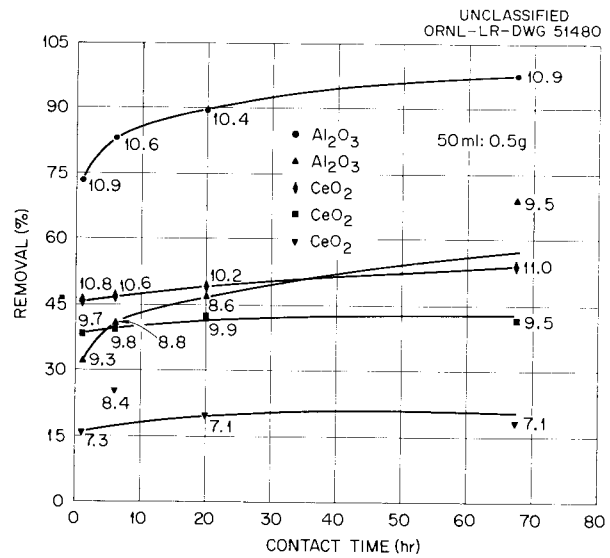

Fig. 1.23. Comparison of Strontium Removals by Al_2O_3 and CeO_2.

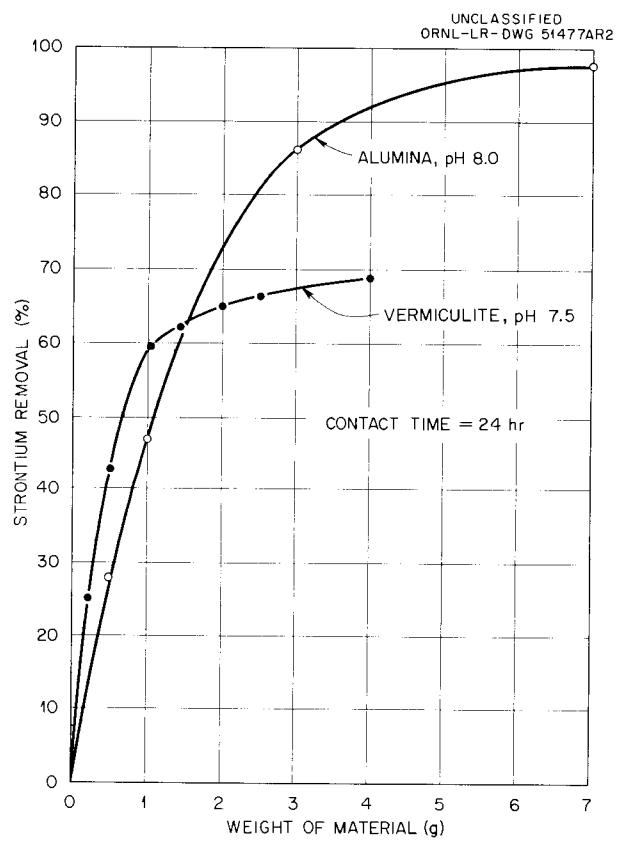

Fig. 1.24. Removal of Strontium by Al_2O_3 and Na-Vermiculite in 50 ml of 0.1 *N* $NaNO_3$ Containing 1 mg Sr^{2+} per Liter.

for the difference; however, the curves suggest that surface reactive materials such as alumina may be useful in removing traces of strontium from wastes. Further tests are now being conducted in order to explain the difference in response.

Metasomatic Replacement and Precipitation Reactions with Phosphate Ions. – In Table 1.21 results are shown for several materials tested when phosphate was added to the waste. The influence of phosphate on $CaCO_3$ has been studied intensively; the reaction which removes strontium was reported to be a metasomatic replacement reaction.[32]

The beneficial influence of phosphate on strontium removal by natural vermiculite is caused by the formation of magnesium phosphate precipitate; the magnesium is present as an exchangeable ion on the natural material. After substitution of sodium ions for magnesium on the exchange site, vermiculite no longer shows any benefit from the addition of phosphate. With 5000 ppm of phosphate a detrimental effect is observed; this is likely due to formation of collodial strontium phosphate which prevents the strontium from entering into the ion exchange reaction. By saturating the exchange site with calcium, the removal of strontium was reduced to 27.1% after 24 hr; by adding 100 ppm the removal was increased to 37.4% after 24 hr. These tests not only demonstrate the influence of insoluble phosphate precipitation but also show the superiority of calcium phosphates for removing strontium. In soils where most of the saturating cations are calcium, the influence of phosphate will be an important consideration.

The influence of phosphate on strontium removal by clinoptilolite was investigated. Since the material contains calcite impurities, it was suggested that the metasomatic replacement reaction was responsible for the removal.[33] That the addition of phosphate ions is beneficial to the natural clinoptilolite system is apparent from the data in Table 1.22. With as low as 100 ppm of phosphate at pH 10.5, removal was improved. Calcium vermiculite also showed improvement when 100 ppm phosphate was added at pH 9.0.

Since sodium saturation of vermiculite eliminated the benefit of phosphate, the clinoptilolite

[32] L. L. Ames, *Econ. Geol.* 55, 354 (1960).

[33] J. F. Honstead *et al.*, "Fixation on Minerals," p 263 in *Report of Second Working Meeting on Radioactivity in Stable Solid Media*, TID-7613 (1961).

Table 1.21. The Effect of Adding Sodium Phosphate on the Per Cent Removal of Strontium (pH = 9.0)

Material	Contact Time (hr)	Strontium Removed (%) at a Phosphate Concentration (ppm) of:				
		0	100	500	1000	5000
$CaCO_3$	1	1.31	0.31	1.18	3.22	5.24
	4	0.62	0.32	10.3	21.5	42.7
	24	0.00	1.57	75.6	91.3	98.7
	72	0.00	29.2	95.9	99.1	99.8
Natural vermiculite	1	9.62	6.80	7.44	12.5	12.8
	4	17.2	14.4	15.5	23.9	24.6
	24	30.8	32.0	28.8	34.5	54.9
	72	36.3	38.4	41.7	44.0	68.4
Sodium vermiculite	1	14.6	14.9	12.4	10.8	7.37
	4	19.5	22.4	20.6	12.0	8.35
	24	40.0	40.5	38.2	41.5	22.4
	72	49.7	51.0	49.9	47.2	29.4
Alumina	1	25.8	29.9	26,2	35.4	33.7
	4	31.8	44.2	44.4	54.9	46.7
	24	40.1	60.1	66.9	71.2	62.3

Table 1.22. The Per Cent Removal of Strontium by Natural and Na-Clinoptilolite as a Function of Phosphate (Na_2HPO_4) Concentration*

Contact Time (hr)	Strontium Removal (%) at a Phosphate Concentration (ppm) of: 0	100	500	1000
	Natural Clinoptilolite			
1	33.7	55.5	71.2	65.5
4	61.2	76.1	90.9	89.7
46	91.8	93.9	96.3	96.0
95	94.2	95.0	97.4	97.2
	Na-Clinoptilolite			
1	39.3	28.8	31.9	26.9
4	59.6	55.0	56.4	57.6
24	86.1	85.3	86.8	87.0
72	92.5	93.1	93.7	93.9
96	92.6	93.4	94.0	94.0

*Fifty milliliters of 0.1 *M* $NaNO_3$ containing 1 mg Sr per liter contacted with 0.5 g of natural clinoptilolite and 0.25 g of Na-clinoptilolite at pH 10.5.

was treated with sodium chloride solutions to form the sodium clinoptilolite. The results (Table 1.22) show that there was no improvement from the addition of phosphate. The amount of material used in the test was reduced because sodium ions on exchange sites offer less competition than calcium ions; a sorption test with twice this amount had shown over 90% removal.

If the sodium chloride during saturation had dissolved the calcite impurity and eliminated the metasomatic replacement reaction, the addition of calcite to sodium clinoptilolite should have restored the strontium removal capacity to its original level. In Table 1.23 several combinations of calcite addition to sodium and natural clinoptilolite are shown. The addition of 500 ppm of phosphate to natural clinoptilolite containing 10% limestone showed the same removal as the natural clinoptilolite without added limestone. When the limestone was added to sodium clinoptilolite, removal was less than that for natural clinoptilolite.

From these tests one might deduce that the exchangeable calcium on the ion exchange material, under some conditions, may be more influential than the calcite crystals in removing strontium by the phosphate reaction. Determination of the calcium concentration of the clinoptilolite showed approximately 20 meq of calcium per 100 g of material.

Table 1.23. The Influence of Limestone and Sodium Acetate Washings on the Per Cent Removal of Strontium by Clinoptilolite

Fifty milliliters of 0.1 *M* $NaNO_3$ solution containing 1 mg Sr per liter and 500 ppm phosphate ions. pH adjusted to 10.5.

Contact Time (hr)	Strontium Removal (%) Na-Clinoptilolite A		B		Natural Clinoptilolite B	
1	58.6	61.4*	51.3	59.5*	82.0	58.6*
4	82.2	80.1*	76.4	78.8*	91.0	80.6*
24	94.6	93.0*	93.4	93.4*	95.7	92.9*
72	97.2	96.8*	96.7	96.6*	97.8	97.0*
96	97.6	97.0*	97.0	97.0*	98.1	97.2*

A = 0.450 g clinoptilolite, 0.050 g limestone.

B = 0.495 g clinoptilolite, 0.050 g limestone.

*Washed with NaOAc.

Influence of pH on Strontium Sorption by Vermiculite. – There are several reasons to suspect that pH plays an important role in strontium sorption by vermiculite and other clay minerals. With acid pH, clay will release aluminum ions from its lattice and become hydrogen-aluminum-saturated. Clays not only contain hydroxyl ions in their crystal makeup but are hydroxylated at the edges of the crystals due to unsatisfied charges of the terminal oxygen ions. The hydrogen ions of the hydroxyls, especially those at the edges of the crystals, are capable of ionization and can contribute to the ion exchange capacity of the mineral.

The influence of pH is illustrated in Fig. 1.25. Note that the material is sodium vermiculite; for natural vermiculite containing magnesium ions, reactions at high pH are complicated by the precipitation of $Mg(OH)_2$. The data show that pH 9 is superior to pH 4 in removal of strontium. After 72 hr contact the suspension pH was reversed from pH 9 to pH 4 and from pH 4 to pH 9. Whereas the adjustment to an acid pH reduced the sorption to the same value as for the originally acid sample, the sample adjusted to pH 9 did not reach the same value as that obtained for the sample originally at pH 9. The reason for this behavior is thought to be alumination of the vermiculite in acids.

The known characteristics of clay suggest two possible reasons for improved removal at high pH. One may be that at high pH the hydrogen ions of hydroxyls are ionized, leaving the surface free for strontium. The other reason may be the alumination of the clay in acids.

Other tests have shown that there is a gradual increase in strontium removal between pH 4 through 11. To investigate the effect on strontium sorption of substituting the ionizable hydrogen ions with sodium, sodium vermiculite was treated with a solution containing 0.9 *M* NaCl and 0.1 *M* NaOH. Part of the sample was then treated with 1 *M* NaCl and washed. These samples were tested for strontium removal over a wide range of pH. In Fig. 1.26 data are given for the material treated with NaCl-NaOH but not with the additional NaCl. The additional NaCl treatment reduced the sorption by about 3–5% as compared to the sample without the added treatment.

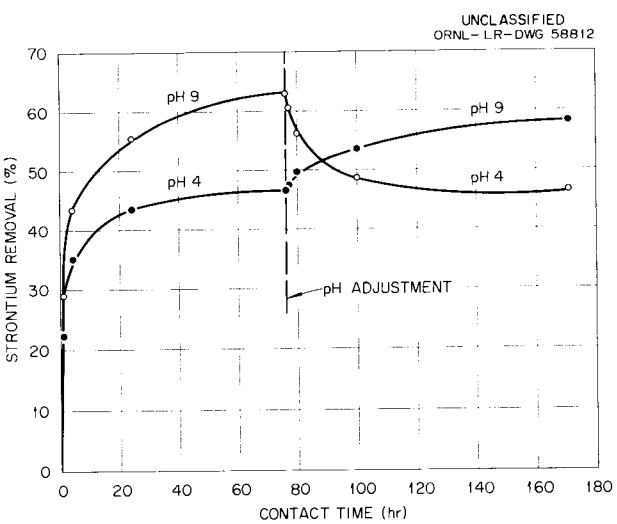

Fig. 1.25. Removal of Strontium by Na-Vermiculite as Related to pH.

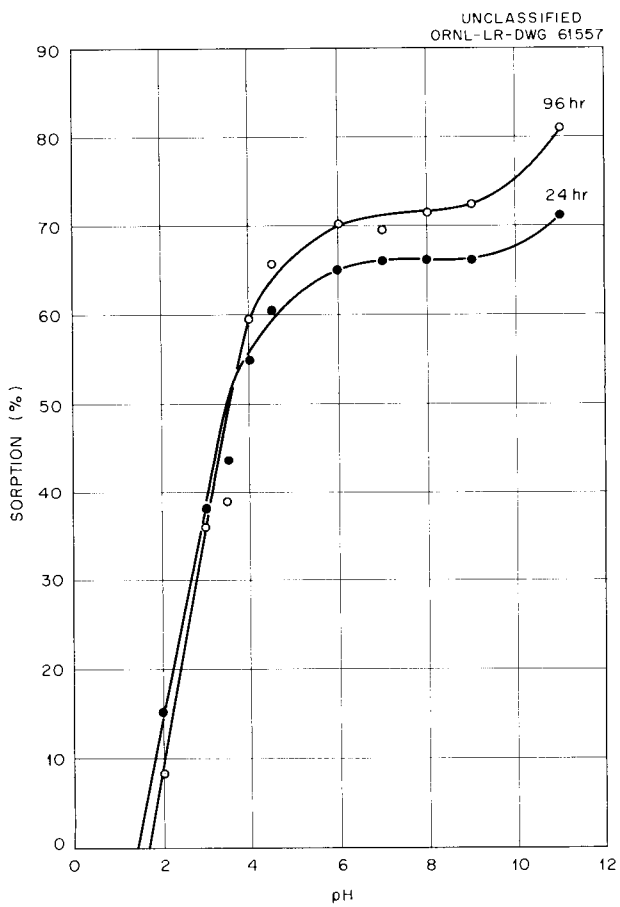

Fig. 1.26. Removal of Strontium by NaCl:NaOH-Treated Vermiculite as a Function of pH. 0.1 *N* $NaNO_3$ containing 1 mg Sr^{2+}/liter. 50 ml solution to 0.5 g vermiculite.

This suggests that the NaOH did have a direct influence on the clay. Comparing the data in Figs. 1.25 and 1.26, one can see that the NaCl-NaOH treatment did improve strontium removal. Furthermore, the data in Fig. 1.26 show that between pH 6 and 9 there was very little difference in sorption. The rise noted at pH 11 is not yet explained.

Below pH 4, strontium sorption is reduced with longer contact time. At pH 4, the highest sorption (61.1%) was observed after 48 hr; thus, the value at 96 hr, though greater than that observed after 24 hr, indicates that a slow decomposition of the clay was occurring. The extreme reduction in strontium sorption at pH 2 noted for vermiculite is not shown by the resins (Dowex 50W and Duolite C-3) nor by clinoptilolite.

Removal of Ruthenium

Ruthenium is not strongly sorbed from the intermediate-level waste stream as it seeps through the Conasauga shale at ORNL. Therefore it moves some distance from the waste seepage pits and is readily detected in the monitoring wells. Fortunately it is not an especially hazardous radionuclide, but if it moves freely in the ground water, increased releases of this nuclide could pose a problem.

Because it is a transition element, ruthenium exists in numerous oxidation states, and anionic species probably predominate in the intermediate-level waste stream. Its ability to be reduced suggested that ruthenium might be removed from the waste stream by reduction followed by a sorption process.

Solution was collected from a seep near pit No. 4. A scan of the gamma spectrum indicated that Ru^{106} was the only radionuclide of consequence in the solution.

Manganese Precipitation. – Fifty milliliters of solution was brought to pH 1.5 using concentrated HCl. One ml 50% $Mn(NO_3)_2$ was added and was precipitated as MnO_2 by raising the pH to 11.5. The suspension was centrifuged after 1 hr and the supernatant was decanted and counted for Ru^{106}. This was followed by successive treatments of the solution phase. About 17% of the ruthenium in solution was brought down with each MnO_2 precipitation.

Sorption on Metal. – Increments of the untreated waste solution were passed through a column composed of 20 g Ottawa sand, 8 g iron powder (40 mesh), and 2 g aluminum (40 mesh). Based on the 50% breakthrough volume, a K_d of 20 ml/g was obtained. The Ottawa sand does not sorb Ru^{106} and was added only to permit flow of solution through the column. The leakage of Ru^{106} through the column before the breakthrough wave was quite high.

Dithionite Reduction. – Dithionite ($Na_2S_2O_4$), a strong reducing reagent in alkaline media, was used to reduce Ru^{106} for subsequent sorption on vermiculite and on metal powders. The results of these studies, using 100 ml solution and 10 g sorbent, are shown in Table 1.24. The dithionite causes reduction of the ruthenium if sufficiently high concentrations are employed, but the amount necessary seems excessive for routine use. Removal by the metal powder was considerably higher than removal by vermiculite, and both sorbent media showed strong time dependence.

Sorption by Minerals. – Increased removal of ruthenium as the pH is lowered and as conditions are made favorable for reduction suggested that a satisfactory method for decontamination of intermediate-level wastes might be to pass the basic waste stream through mineral-filled columns for removal of cesium and strontium. At this point the pH could be lowered and the effluent pumped into a seepage pit filled with reducing minerals, such as chalcocite (CuS), chalcopyrite ($CuFeS_2$), or pyrite (FeS). The ruthenium not removed from solution in the seepage pit might be in a form that could be removed as the solution percolates through the formation to surface waterways.

Several sulfide minerals were checked for their abilities to remove ruthenium from the seep solution. Highest removals were obtained using chalcopyrite ($CuFeS_2$), so this mineral was selected for more intensive investigation.

Removal of ruthenium from 100 ml solution by 0.1 g chalcopyrite continued beyond 96 hr contact time, pointing out the necessity for long residence times for ruthenium decontamination. Increasing the amount of chalcopyrite gave the surprising result of depressing ruthenium sorption when more than 1 g of sorbent was added to 100 ml of solution. This condition persisted with increased contact time, indicating a probable change in solution conditions. Measurement of Cu^{2+}, Fe^{3+}, and S^{2-} showed no discontinuity in the concentration of these ions at this point. As a check,

Table 1.24. Removal of Ru^{106} from Solution by Reduction and Sorption

Contact Time (hr)	pH	Ruthenium Removed from Solution (%)			
		Untreated Waste	0.001 *M* $Na_2S_2O_4$	0.01 *M* $Na_2S_2O_4$	0.1 *M* $Na_2S_2O_4$
			10 g Vermiculite		
1	10.5	2.8	4.3	34.5	43.8
70	10.5	4.0	5.8	44.5	63.5
130	10.5	0.0	1.5	43.5	69.2
264	10.5	0.0	0.0	43.0	69.2
288	9.0	0.0	0.4	40.2	76.2
312	6.0	0.7	0.4	34.9	76.6
336	3.0	0.0	0.1	20.0	63.2
			5 g Iron plus 5 g Copper		
1	10.5	3.4	5.3	43.2	41.6
70	10.5	12.0	16.2	55.8	81.4
130	10.5	19.0	27.0	60.6	88.2
264	10.5	16.4	33.8	60.8	88.8
288	9.0	28.4	44.5	72.4	90.7
312	6.0	40.7	58.4	77.4	93.6
336	3.0	61.8	72.3	91.2	93.0

systems were investigated to which 100 ppm Cu^{2+}, Fe^{3+}, and S^{2-} were added. The break in the sorption curve persisted when copper or iron salts were added, though both these ions had a moderate depressing effect on ruthenium removal. In the system where 100 ppm S^{2-} was added, a severe depressing effect was noted and the sorption curve was smoothed out at a lower level of ruthenium sorption. Additions of dithionite, to maintain strong reducing conditions, also smoothed out the response curve with no inhibition of ruthenium removal. This suggested that there had been sufficient change in the oxidation-reduction potential to cause a break in the sorption curve. This seems more likely than inhibition by increased concentration of S^{2-}, as no increase in the sulfide-ion concentration was found in the supernatant at the break in the sorption curve.

Studies of pH effects under various conditions showed that optimum removal is attained at near-neutral conditions with the addition of 0.01 *M* $Na_2S_2O_4$. The use of other strong reducing reagents which are more effective in acidic solutions would probably change the optimum pH range.

Removal of Nuclides Using Organic Minerals

Slurry and column techniques were used to study the sorption of radionuclides by natural organic materials. Preliminary slurry tests showed that the removal from aqueous solutions of Ru^{106}, Cs^{137}, Sr^{85}, and Co^{60} by bituminous and anthracite coals was very poor. Peat and lignite effectively sorbed strontium and cobalt from demineralized water, the sorption reaction reaching equilibrium after 3 to 4 hr. Ion impurities of Na^+ and Ca^{2+} interferred with the sorption of all elements except ruthenium.

For column experiments, lignite, peat, and vermiculite were used. Mixed-bed columns of peat and vermiculite, peat and lignite, and lignite and vermiculite were tested. The lignite-vermiculite columns performed most effectively.

The radioactive solutions used in these tests were prepared with trace amounts of the four radionuclides. The radioactivity of the spiked, master solution varied from 1×10^4 to 4×10^4 counts min^{-1} ml^{-1}. Unless otherwise specified, the suspension of sorbent was stirred with a stirring device during the slurry tests. Acidity was controlled using either HNO_3 or NaOH for pH adjustments.

Slurry Studies. – The results from slurry studies show that peat and lignite sorb strontium and cobalt much more effectively than they sorb cesium. With inorganic minerals, cesium was sorbed most effectively, and strontium and cobalt were sorbed less efficiently. Ruthenium removals were lower than those for strontium and cobalt; however, its removal was influenced least by stable ion impurities.

Although cobalt has been reported to be subject to hydrolysis under certain conditions, results showed that ion exchange materials of organic origin are more effective in removal of cobalt than the poor ion exchange bituminous and anthracite coals. Both peat and lignite are effective removal agents over a wide pH range; bituminous and anthracite coals are not effective.

Column Studies. – Slurry tests gave fairly promising results for the sorption of strontium and cobalt from demineralized water by peat and lignite. However, stable ion impurities had a substantial effect on their sorptive capacities, particularly in the case of peat. To test the performance of the organic material in columns, combinations of peat, lignite, and vermiculite (grade BO-3) were used.

Three columns, operated simultaneously, contained the following: column 1, ~20 g peat (10–30 mesh) and ~30 g vermiculite; column 2, ~20 g peat (10–30 mesh) and ~30 g lignite (28–48 mesh); and column 3, ~40 g lignite (28–48 mesh) and ~10 g vermiculite. The columns were 185, 196, and 86 cm^3 in volume respectively. The low-density peat occupied a much larger volume than lignite or vermiculite. The influent solution was demineralized water containing 1000 ppm $NaNO_3$ and 100 ppm $CaCl_2$, spiked with Cs^{137} (~36%), Sr^{85} (~42%), and Co^{60} (~22%). Initially the pH was 2.5, but because activity started passing through the columns almost immediately, the pH was readjusted to pH 10. The gamma activity in the influent varied from 5×10^4 to 7×10^4 counts min^{-1} ml^{-1}, measured in a well-type gamma scintillation counter. The operation of the columns was not continuous, and the flow rates ranged from 4 to 11 ml cm^{-2} min^{-1}.

The effluent was collected continuously during operation and composited in 1-hr batches, from which two 1-ml samples were pipetted and counted. The per cent removal was estimated by comparing the activity in the effluent with that in the influent solution. In addition, each sample was scanned for gamma emissions, using a single-channel analyzer to identify the radionuclides in the effluent.

Table 1.25 shows column removals after passage of a certain number of bed volumes. As was mentioned, the columns were operated discontinuously; on one occasion it was necessary to stop for 96 hr. After that interruption, the columns showed better performance, especially the columns

Table 1.25. Removal of Gross Gamma Activity by Ion Exchange Columns After Passage of Various Amounts of Solution

Column 1 (peat-vermiculite)		Column 2 (peat-lignite)		Column 3 (lignite-vermiculite)	
Bed Volumes	Removal (%)	Bed Volumes	Removal (%)	Bed Volumes	Removal (%)
8	92.2	6	94.4	18	98.8
17	90.1	13	87.0	41	98.6
30	88	22	81.5	66	97.1
53	85.9	38	64.5	110	90.1
75	82.2	54	61.5	150	80
		After Rest for 96 hr			
92	88.5	66	56.6	175	84.1
110	88.1	79	54.6	208	75.3

containing vermiculite (columns 1 and 3). Probably the activity had time to diffuse farther into the material during the interruption, as was shown by the cesium-vermiculite reaction.[34]

Column 3 showed a sharp breakthrough. However, column 1 was better with respect to the total percolated volume. Column 2 gave fairly poor results. Observations made during the operation of the columns may be summarized as follows:

1. In column 1 (peat-vermiculite), while the pH was low, all three radionuclides passed through the column. Later, when the pH was readjusted to 10 and until the end of the experiment, strontium and cesium passed through (mostly strontium).
2. In column 2, at the acid pH, both strontium and cesium passed through. Later, at alkaline pH only cesium passed through. Strontium was identified only in the last two samples.
3. In the effluent of column 3, when the pH was low, strontium (predominantly) and cesium were identified. Later at pH 10 cesium (predominantly) and cobalt passed through. After that only cesium was identified, and in the end cesium (predominantly) and a little strontium passed through.

Some K_d values were calculated using the activity in the upper increment of each column expressed as counts min^{-1} g^{-1} (assumed to be saturated) and the activity in the influent as counts min^{-1} ml^{-1}. These K_d's were as follows: column 1, ~2000 ml/g; column 2, ~1000 ml/g; and column 3, ~1800 ml/g.

Biological Recovery of Cesium Sorbed on Vermiculite

Vermiculite, containing 40% biotite impurity, was collapsed with either potassium or cesium ions; the material was then treated with either cesium, potassium, or ammonium ions to saturate the easily exchangeable ion exchange sites. These materials were used to determine the rate and total amount of cesium or potassium recovered by vegetation from the treated vermiculite. Autoradiographic technique was used to examine the Cs^{137}-treated vermiculite in an attempt to "locate" the ions under various conditions.

[34] T. Tamura and D. G. Jacobs, *Health Phys.* 2, 391 (1960).

Saturation Studies. – To compare the reactions of Cs and K with vermiculite and subsequently to recover the Cs and K by intensive cropping, several types of vermiculite samples were prepared. In general all experimental work was done with two types of samples: those which were saturated with either Cs or K and those in which the saturating cation was removed from the exchange material.

The vermiculite was treated by refluxing with 1 *M* NaCl for 32 hr, with periodic changes of the refluxing solution. The sample was washed with 95% ethanol until free of chlorides. Two 80-g samples of the Na-vermiculite were treated with 200 ml of 0.3 *M* $CsNO_3$ and 200 ml of 0.3 *M* KCl respectively. The mixture was stirred magnetically for 4 hr, the supernatant removed, and the sample washed with ethanol and dried. The saturating solutions were made radioactive so that the specific activities of the solutions were 1.43 mc/g of Cs and 9.76 mc/g of K; the total cation added was approximately 1.25 times that required for complete saturation. Subsamples of 25 g each were then taken for exchange reactions with 50 ml of 1 *M* NH_4Ac, 50 ml of 1 *M* Cs^{137}-labeled $CsNO_3$, or 50 ml of 1 *M* K^{42}-labeled KCl, depending on the previous treatment. The exchange reaction was carried out in a manner similar to that of the saturating procedure but was allowed to react for only 5 min. The resulting treatments were as follows:

1. K-saturated vermiculite with K on the exchange position,
2. Cs-saturated vermiculite with Cs on the exchange position,
3. K-saturated vermiculite with NH_4 on the exchange position,
4. Cs-saturated vermiculite with NH_4 on the exchange position,
5. K-saturated vermiculite with Cs on the exchange position,
6. Cs-saturated vermiculite with K on the exchange position.

These samples were used in all subsequent experiments. The data in Table 1.26 show that the K saturating solution was much more effective in saturating the Na-vermiculite than was the Cs solution. Vermiculite sorbed 63.4 meq of K during the 4-hr reaction period while it sorbed

Table 1.26. Sorption of Cesium and Potassium from 0.3 *M* Saturating Solutions and 1 *M* Exchange Solutions by Sodium-Treated Vermiculite

Sample Number	Treatment: Saturating Cation	Treatment: Exchange Cation	mg of Cation Sorbed per g of Vermiculite: K	mg of Cation Sorbed per g of Vermiculite: Cs	meq of Cation Sorbed per 100 g of Vermiculite: K	meq of Cation Sorbed per 100 g of Vermiculite: Cs
1	K	K	24.2		63.5	
2	Cs	Cs		43.4		32.6
3	K	NH_4	20.0		52.8	
4	Cs	NH_4		41.4		31.1
5	K	Cs	20.4	8.0	52.6	6.0
6	Cs	K	7.6	41.2	19.5	30.9

only 32.6 meq of Cs. Jacobs and Tamura[35] report a total sorption of 60.2 meq of Cs with similar treatment using a 24-hr reaction time. Thus, the differences in total amount of Cs and K sorbed apparently represent a rate function. Given adequate time either cation will completely saturate the vermiculite. X-ray diffraction patterns showed that upon K treatment the *c*-spacing of the vermiculite was closed to 10.0-A spacing. These results indicate that a longer period of time was needed in order to completely saturate the vermiculite with Cs.

The exchange reactions removed only small amounts of Cs from the Cs-vermiculite while they replaced a larger quantity of K from the K-vermiculite. Conversely, the Cs-vermiculite removed approximately 3 times as much of the cation from the exchange solution as did the K-vermiculite. The *c*-spacings of the K-vermiculite were not changed by the exchange treatments; however, the spacings of the Cs-vermiculite show some collapse with either the NH_4 or K treatments.

Short-Term Uptake by Oats. – Short-term uptake methods of Stanford and DeMent were used.[36] Thirty oat seeds (*Avena sativa*) were planted in 12-oz cottage cheese cartons containing 500 g of sand and 75 ml of minus-K nutrient solution. The plants were grown in the sand culture for two weeks to produce potassium-deficient plants with a good mat of roots. The bottoms were then removed from the cartons containing the plants and were nested in a second carton containing the mixture of sand and treated vermiculite. The mixture in the second carton was prepared in two layers, each containing 1 g of vermiculite and 50 g of coarse sand. The two layers were separated by a cheesecloth disk. The lower layer contained the labeled vermiculite, and the upper layer contained stable K or Cs vermiculite, depending on the cation in the lower layer. This was done in order to equate the total quantity of K or Cs added to each carton. The vermiculite in the upper layer also acted as a buffer to prevent cations in the solution above from moving into the layer containing the labeled vermiculite.

Inspection of the recovery data showed that only minute quantities of Cs were taken up by the crop during the first week. This corresponds with the time required for the plant roots to penetrate the sand layer containing the Cs-labeled vermiculite. Starting on the sixth day the uptake of Cs from sample 5 (K-vermiculite, Cs exchange) rose sharply. This rapid increase continued for 1 week at which time the recovery rate decreased substantially. A similar uptake pattern was obtained with sample 4 (Cs-vermiculite, NH_4 exchange) except that uptake lagged as compared with that of sample 5 by 3 to 4 days. The uptake

[35] D. G. Jacobs and T. Tamura, "The Mechanism of Ion Fixation Using Radioisotope Technique," presented at the 7th International Congress of Soil Science, Aug. 14–24, 1960, Madison, Wis.

[36] G. Stanford and J. D. DeMent, *Soil Sci. Soc. Am. Proc.* 21, 612 (1957).

curve for sample 2 (Cs-vermiculite, Cs exchange) also lagged as compared with sample 5; however, the rapid rate of recovery from this sample continued for a longer period of time. Consequently the total uptake was greater for sample 2. A longer period of time was required for the crop to remove measurable quantities of Cs from sample 6 (Cs-vermiculite, K exchange); this sample also gave the lowest total uptake of Cs.

The percentage of the total Cs removed by the crop was 9.4, 2.5, 1.8, and 1.1% for samples 5, 2, 4, and 6 respectively. The fact that so little cesium was removed by this intensive cropping procedure indicates that Cs, especially that in the interlayer spaces, is "fixed" very tightly. The only sample which released a substantial amount of Cs to the crop was sample 5 in which the Cs was on the "exchange" site of a K-saturated vermiculite.

It should be pointed out that if the applied Cs had been readily available to the crop, almost all of it would have been removed. The Cs levels in crop plants may run 20% or higher. Thus, these samples, some of which weighed as much as 2.0 g, could have easily taken up to 40 mg of Cs, and the highest rate of cesium application was 43.4 mg per carton.

Autoradiographic Studies. – Cesium^{137}-labeled vermiculite was placed on a microscope slide in a layer thin enough that individual particles were easily distinguishable. The vermiculite was then fixed to the slide with a fine spray of clear plastic. The remainder of the slide was also coated with the plastic in order to prevent the separation of the plastic film during development.

Nuclear track emulsion NTB-3 obtained from the Eastman Kodak Co. was used. The emulsion was heated to 46°C to liquefy the gel; the slide was then dipped into the emulsion, removed, and held in an upright position for 5 sec to allow excess emulsion to drain. The slide was then placed in a light-tight box and refrigerated in order to slow down the decomposition of the emulsion.

Samples that had an activity of approximately 0.1 mc/g of vermiculite were exposed for one day, and the sample having a specific activity of approximately 0.01 mc/g of vermiculite was exposed for 6 days. The latter exposure time was too short for the low concentration. After exposure the samples were developed for 10 min in D-19 developer, fixed in Kodak acid fixer for 5–10 min, and dipped in a pan of water to wash. A Wratten series 6B safe-light was used when needed, although a Wratten series 2 was recommended.

Although this experiment was conducted primarily to work out the technique, several interesting changes were observed. Autoradiographs developed from sample 2 (Cs-vermiculite, Cs exchange) showed that most of the particles were completely covered with Cs. A few of the larger particles appeared to have a higher concentration of Cs on the outer edges of the platelet; these particles may be those which were not completely collapsed when examined by x-ray diffraction.

Autoradiographs of particles from samples 4 and 6 showed a ring of Cs around the edges and center but an area near the edge free of cesium. Apparently the NH_4 and K had removed the cesium from the outer region but some of the cesium had remained tightly bound to the extreme edge of the plate.

SOIL COLUMN STUDIES

D. G. Jacobs O. M. Sealand

In the operation of an ion exchange column, when the solute obeys a linear or near-linear adsorption isotherm, the concentration history of the effluent can be typified by an error function,[37]

$$c/c^0 = q/q^0 = 1/2 + \mathcal{A}\{(N/V\bar{V})^{1/2}(V - \bar{V})\}\,, \quad (1)$$

where

c = concentration of the exchanging species in the effluent,

c^0 = concentration of the exchanging species in the influent,

q = concentration of the exchanging species in the sorbent phase,

q^0 = concentration of the exchanging species in the sorbent phase at the equilibrium with c^0,

$$\mathcal{A}\{y\} = \frac{1}{\sqrt{2\pi}} \int_0^y \exp\left(\frac{-y^2}{2}\right) dy\,,$$

[37] E. Glueckauf, *Trans. Faraday Soc.* 51, 1540 (1955).

N = number of theoretical plates in the column,

V = throughput volume,

$\bar{V}$ = throughput volume at the inflection point of the curve, where $c/c^0 = 1/2$.

$$\bar{q}_t = q_t - \frac{6}{\pi^2} \int_{\tau=0}^{\tau=t} \left(\frac{dq}{dt}\right)_\tau \sum_{n=1}^{\infty} \frac{1}{n^2} \left\{\exp[-n^2 \pi^2 \epsilon (t - \tau)]\right\} d\tau . \qquad (4)$$

When the column is operated at a constant flow rate, F, $V = tF$, and $\bar{V} = \theta F$, where θ is the time at the point of inflection. Near the point of inflection $(\bar{V} V)^{1/2} \cong \bar{V} = K_d X$, where X is the weight of the column bed, so that Eq. (1) can be written:

$$c/c^0 = q/q^0 = 1/2 + \mathcal{A}\{\beta(t - \theta)\} , \qquad (2)$$

where $\beta = \sqrt{NF}/K_d X$.

Particle Diffusion Processes

Cesium breakthrough curves obtained from vermiculite-filled[38] columns are complicated by a particle diffusion rate-controlling process. This is manifested by the prolonged time required for the concentration of the effluent to reach zero gradient after the inflection of the curve and results in increased loading of cesium on the column with increased time of operation.

Particle Diffusion into a Sphere. – Glueckauf[37] has given a mathematical treatment for the effect of spherical particle diffusion on column operation. When steady external conditions are maintained, there is, at time $t = 0$, a surface concentration jump from $q_s = q_0$ to $q_s = q_1$, after which the surface concentration remains at q_1. In this case the mean internal concentration of the particle, $\bar{q}$, is given by:

$$\bar{q}_t = q_0 + (q_1 - q_0) \left[1 - \frac{6}{\pi^2} \sum_{n=1}^{\infty} \frac{1}{n^2} \exp(-n^2 \pi^2 \epsilon t) \right] , \qquad (3)$$

where

$\epsilon = D/r^2$,

D = diffusion coefficient for the ion in the particle (assumed constant),

r = particle radius.

If the surface concentration is not constant but varies in a continuous manner, the expression of the mean internal concentration of the particle takes the form:

When the transient surface concentration can be expressed by Eq. (2), Glueckauf[37] gives the solution of this integral as

$$q - \bar{q} = \frac{6q^0}{\pi^2} \sum_{n=1}^{\infty} \frac{1}{n^2} \left[\frac{1}{2} + \mathcal{A}\left\{\beta(t - \theta) - \frac{n^2 \pi^2 \epsilon}{\beta}\right\} \right] \times \exp\left[\frac{n^4 \pi^4 \epsilon^2}{2\beta^2} - n^2 \pi^2 \epsilon (t - \theta) \right] . \qquad (5)$$

Figure 1.27 shows the effect of particle diffusion into a sphere on the concentration history of effluent from an exchange column. An increase of β/ϵ is equivalent to assuming a smaller particle diffusion coefficient and requires a longer period of time for attainment of equilibrium between the surface and the interior of the particle.

Particle Diffusion into a Platelet. – The vermiculite particles are not spherical in shape but are flaky like mica (isinglass). The exchanging cesium must find its way to basal exchange sites by migrating from the edges of the vermiculite flakes; migration through the faces of the sheets is prevented (or at least is held to a much lower order of magnitude) by the crystal structure of the vermiculite. When steady external conditions are maintained, the mean internal concentration of the particle, $\bar{q}$, is given by:[39]

$$\bar{q}_t = q_0 + (q_1 - q_0) \left[1 - \sum_{n=1}^{\infty} \frac{4}{\xi_n^2} \exp(-\xi_n^2 \epsilon t) \right] , \qquad (6)$$

where ξ_n are the roots of the equation $J_0(X) = 0$, where $J_0(X)$ is the Bessel function of zero order. For continuously variable surface conditions, the

[38] Hydrobiotite obtained from the Zonolite Co., Traveler's Rest, S.C.

[39] W. Jost, *Diffusion in Solids, Liquids, Gases*, Academic Press, New York, 1952.

equation takes the form:

$$\bar{q}_t = q_t - 4 \int_{\tau=0}^{\tau=t} \left(\frac{dq}{dt}\right)_\tau \sum_{n=1}^{\infty} \frac{1}{\xi_n^2} \times \exp[-\xi_n^2 \epsilon (t - \tau)]\, d\tau . \quad (7)$$

When the variation of the surface concentration is given by Eq. (2), integration yields an equation analogous to (5):

$$q_t - \bar{q}_t = 4q^0 \sum_{n=1}^{\infty} \frac{1}{\xi_n^2} \left[\frac{1}{2} + \mathcal{A}\left\{\beta(t - \theta) - \frac{\xi_n^2 \epsilon}{\beta}\right\}\right] \times \exp\left[\frac{\xi_n^4 \epsilon^2}{2\beta^2} - \xi_n^2 \epsilon (t - \theta)\right] . \quad (8)$$

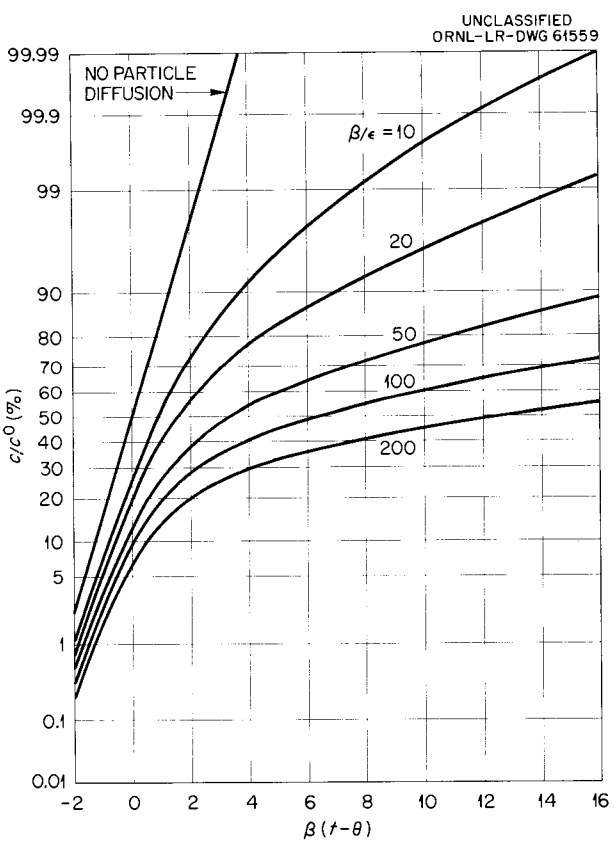

Fig. 1.27. The Effect of Particle Diffusion into a Sphere on the Concentration History of the Effluent from an Ion Exchange Column.

The interior of a platelike particle reaches equilibrium more slowly than does the interior of a spherical particle of the same radius and having the same particle diffusion coefficient (compare Fig. 1.28 to Fig. 1.27 for similar values of β/ϵ).

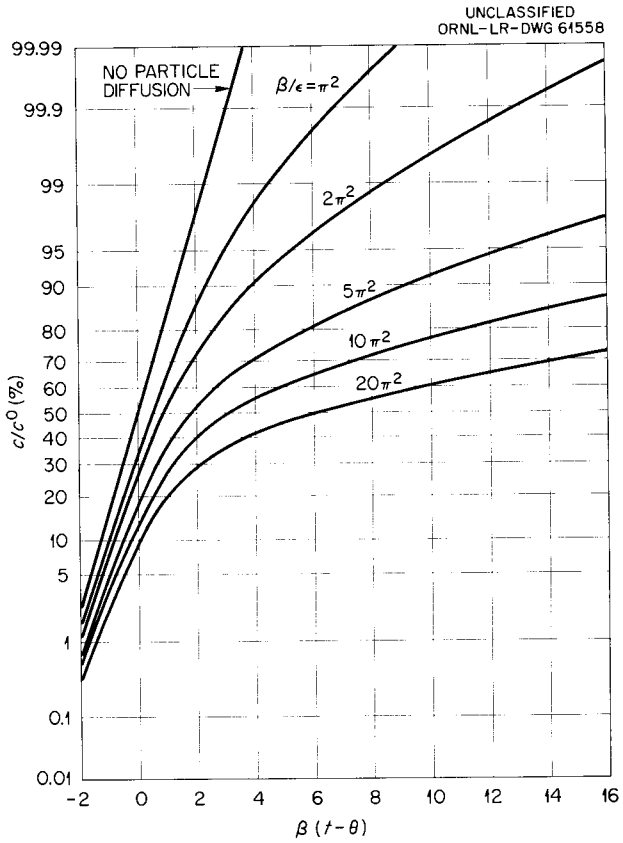

Fig. 1.28. The Effect of Particle Diffusion into a Platelet on the Concentration History of the Effluent from an Ion Exchange Column.

Estimation of Particle Diffusion Coefficients. – Estimates of particle diffusion coefficients were made by comparing the concentration histories of experimental columns with the theoretical curves. This was done by a comparison of slopes at various points along the breakthrough curve and allowed estimation of β/ϵ, θ, and β from the effluent data. From these estimations one can further estimate ϵ, N, and the surface K_d. These estimates are tabulated in Table 1.27. An estimate was made for the particle diffusion coefficient, D, using the radius of particle at the 50% passing point in the size analysis of BO-4 vermiculite, 0.02 cm.

Table 1.27. Estimation of Particle Diffusion Coefficients, D, from Experimental Concentration Histories

	Column Number*							
	2	3	4	5	6	7	8	9
Weight, g	94.7	99.0	98.4	97.6	48.1	54.2	190.5	291.6
Height, cm	18.9	19.3	21.7	~20	11.8	11.5	45.8	70.9
Flow rate, ml/min	3.8	7.6	16.7	57.7	5.2	4.8	5.1	5.2
	Estimated Values							
β/ϵ	50	50	73	32	33	38	51	53
θ, hr	63	25	8.6	1.96	20	24	98	230
β, hr^{-1}	0.085	0.234	0.520	1.92	0.276	0.212	0.087	0.085
ϵ, $sec^{-1} \times 10^{-6}$	0.47	1.3	2.0	16	2.3	1.6	0.47	0.45
N	30	35	32	14	30	28	118	295
HETP, cm	0.63	0.55	0.69	1.40	0.39	0.42	0.39	0.24
Surface K_d, ml/g	162	119	100	77	137	134	202	226
$\epsilon\,\theta$	0.106	0.118	0.062	0.112	0.163	0.134	0.166	0.374
D**, $cm^2/sec \times 10^{-10}$	1.9	5.2	7.9	65	9.3	6.2	1.9	1.8

*Data from column 1 was not included because operation of this column was suspended at ~30% breakthrough.
**The particle radius was assumed to be 0.02 cm.

A constant value for ϵ is not obtained from the experimental data, but rather ϵ decreases with time. Some factors possibly accounting for this may be: (1) The vermiculite is a natural exchanger material having more than one type of exchange site; thus the kinetics observed for the system are the net result of those of several separate processes. (2) The exchanger particles are not of a uniform particle size but differ in size over a considerable range (0.0147 to 0.083 cm diam); thus, for a constant D, the value of β/ϵ would increase with an increase in particle size. After the smaller particles had attained equilibrium with the surface concentration, nonequilibrium would persist at the interior of the larger particles. Thus, for increased time of column operation, ϵ would seem to decrease, while the apparent surface K_d would appear to increase, as noted in Table 1.27. (3) In the collapsed layer lattice minerals, it is not uncommon for the periphery of the particle to have a somewhat greater basal spacing than the core of the particle, due to a gradually increasing degree of hydration toward the outside of the particle.[40] This would mean less steric impedance to the diffusing ion near the periphery of the particle; thus D would apparently decrease as the diffusing species moved toward the interior of the particle with time. (4) Initially, the major saturating cations of the vermiculite are magnesium and potassium. As column operation proceeds, these cations are gradually replaced by sodium, the major cationic constituent of the influent solution. Thus the ion population in the zone of restricted cesium movement is being continuously altered and would undoubtedly affect the diffusion of the cesium, because the ion population of the exchange sites measurably affects the interlayer spacing.

All these factors could be operative, and the net effect would be an increase in the apparent surface K_d and a decrease in ϵ with increased times of column operation.

Effects of Particle Diffusion on Column Operation. – One of the effects of particle diffusion on the concentration history of the effluent from

[40] D. M. C. MacEwan, *J. Soil Sci.* 1, 90 (1950).

an ion exchange column has already been seen; that is, at high per cent breakthrough the concentration gradient diminishes but approaches zero gradient rather slowly. This is of little concern in the loading operation of an ion exchange column, where the concern is only with very low breakthrough per cents. A second effect, increased loading of the column with increased operating time, would be of concern, however. Table 1.28 shows the time required to attain a given per cent of equilibrium between the mean particle concentration and the surface concentration for various grades of commercially available Zonolite.

Table 1.28. The Effect of Particle Size on the Time Required to Attain Equilibrium Between the Surface and the Interior of Vermiculite Particles (the particle diffusion coefficient is assumed to be 1.8×10^{-10} cm^2/sec)

Vermiculite Grade	Median Particle Radius (cm)	Time Required to Attain Various % Equilibrium (days)		
		50%	90%	95%
BO-1	0.134	72	388	521
BO-2	0.128	65	352	473
BO-3	0.050	10	54	72
BO-4	0.020	1.6	8.6	11.6
BO-5	0.018	1.3	6.9	9.3

Another interesting point is that particle diffusion will result in "recovery" of a column. When the loading operation is temporarily halted a portion of the surface cesium migrates to the interior exchange sites, resulting in cesium deficiency at the particle surface. Replenishment of the surface cesium, when operations are resumed, results in a decrease in the effluent activity from what it had been immediately before operations had been stopped. This behavior will continue until the total operating time equals approximately r^2/D. Flow rate also has a pronounced effect on the effluent quality, because it affects the time allowed for diffusion of the cesium to the interior exchange sites of the vermiculite.

Potassium Treatment for Optimizing Cesium Removal

Early studies of sorption by Conasauga shale showed that sorption of cesium by illitic-type clay minerals (i.e., those 2:1 layer lattice minerals having a nonexpanding crystal lattice) was seriously inhibited by cations having steric favorableness for "edge fixation" sites. Further studies with reference-clay minerals showed that potassium, rubidium, and ammonium ions normally inhibit the sorption of cesium to a marked degree, as cesium is generally removed from solution by "edge fixation" by the illitic-type clay minerals or by simple ion exchange in the freely expanding clay minerals.

The Mechanism of Cesium Removal by Vermiculite. – Extension of cesium sorption studies to vermiculite systems revealed that a third sorption mechanism was operative. In this case, high concentrations of cesium or potassium result in a reduction of the lattice c-spacing from $\sim$ 14.2 A to $\sim$ 10 A, causing a physical entrapment of interlayer exchangeable cations. This entrapment process may be called "interlayer fixation" to differentiate it from the "edge fixation" mechanism. Analysis of the data obtained in studies of the mechanism of "interlayer fixation" indicated that below critical concentrations of ions which induce lattice collapse, no lattice collapse occurs. Inspection of the data suggests that it is first necessary to satisfy "edge fixation" sites before any appreciable quantities of the collapse-inducing ions are available for interlayer exchange. Thus the number and the selectivity of "edge fixation" sites for various collapse-inducing cations would control the minimum concentration of the cation necessary to initiate lattice collapse and interlayer fixation. Also the concentration of cations necessary to initiate collapse is not sufficient to effect collapse of all lattices, even when the solution is continually replenished by column operation. It is speculated that all interlayer spacings are not equivalent in this system, and it is suspected that interlayer charge density plays an important role in determining which interlayer spacings will be most easily collapsed.

The Effect of Potassium Treatment of Vermiculite on Cesium Sorption. – Natural Zonolite is an interlayering of biotite and vermiculite. The biotite, with potassium occupying the interlayer

exchange positions, has a collapsed lattice of ~ 10-A c-spacing, while the vermiculite lattice with magnesium, and some calcium, occupying these basal exchange sites has a c-spacing of ~ 14.2 A. The biotite impurity, which amounts to about 40% of the material, is responsible for the edge fixation of cesium. Replacing the magnesium and calcium of the vermiculite lattices with potassium results in a collapse of the vermiculite lattices and the formation of new edge-fixation sites. After potassium saturation, one would expect the cesium K_d to be approximately 2.5 times that of the natural vermiculite, provided the selectivity of the newly formed edge-fixation sites is the same as those previously existent. Previous column testing of BO-4 vermiculite and potassium-treated BO-4 vermiculite showed an increase from 29.6 ml/g to 77.6 ml/g upon potassium treatment, or an increase of 2.6 times.

The Effect of Potassium Additions to the Waste Stream on Cesium Sorption by Vermiculite. – For reasons of safety, it would be an advantage to seal cesium in the "interlayer fixation" sites where the possibility of its desorption is markedly decreased. Also, from the point of view of a waste-disposal operation, it would be desirable to lengthen the life of a cesium-sorbing exchange column. Both objectives can be attained by adjusting ion concentrations to induce interlayer fixation rather than edge fixation. It is not practical to consider increasing cesium concentrations in waste streams, due to the prohibitive costs of cesium salts. However, the same ends can be realized by using increased concentrations of potassium. Potassium would serve to collapse the vermiculite lattice, and interlayer cesium would be entrapped along with it. Although the potassium would compete with cesium for interlayer exchange sites subjected to interlayer fixation, there are approximately 45 meq per 100 g of these sites compared with approximately 0.015 meq per 100 g of the edge-fixation sites. The net effect is greatly increased capacity of a column for fixation of cesium (Table 1.29).

Because collapse of all interlayer spacings does not occur at the minimum concentration for initiating lattice collapse and because increases in potassium concentration increase competition with cesium for exchange sites, it would be necessary to optimize the potassium to sodium ratio for best cesium removal. It appears that optimum conditions would be to operate at the minimum $(K^+)/(Na^+)$ until the easily collapsed lattices are all in the collapsed state. This would be evident from an increase in the cesium activity of the effluent. Gradual increases of the $(K^+)/(Na^+)$ would result in more and more lattice collapse and increased cesium sorption, until finally a state would be reached where all possible collapse had been accomplished. Beyond this point, increases in potassium concentration would merely interfere with cesium sorption, though desorption studies have shown that little of the fixed cesium would be desorbed by the increased amounts of potassium.

Table 1.29. The Effect of Potassium Ion Concentration on the Sorption of Cesium by Zonolite* (BO-3) from 0.5 M $NaNO_3$ Containing the Mass Equivalent of 2 μc Cs^{137} per ml

Potassium Concentration (M)	Cesium K_d (ml/g)	Observation
10^{-4}	15	Apparently no collapse
10^{-3}	9.5	Apparently no collapse
10^{-2}	925	Some indication of interstratification with a small amount of 10-A spacing
10^{-1}	44	Nearly perfect 10-A spacing

*Hydrobiotite obtained commercially from the Zonolite Company, Traveler's Rest, South Carolina.

Large-Scale Testing of Vermiculite Columns

Four test columns (2 in. ID and 10 ft in length) filled with vermiculite were tested for removal of cesium and strontium from simulated ORNL intermediate-level waste. The solution used was essentially 0.32 M $NaNO_3$, 0.22 M NaOH, and contained the mass equivalent of 2 μc Cs^{137} per ml and 0.1 μc Sr^{90} per ml.

The vermiculite for the first column was treated with NaOH-NaCl solution to remove the easily exchangeable magnesium. Enough potassium was added to the suspension to result in approximately 10% potassium saturation. The column was charged with 4167 g of this vermiculite and was filled

to a depth of 8.5 ft. Six hundred liters of simulated waste, to which was added 3×10^{-3} *M* KH_2PO_4, was passed through the column intermittently over a three-week period. No strontium was detected in the effluent, but cesium commenced breakthrough after the passage of 350 liters. The pressure drop across the column was 1 ± 0.2 psi.

After completion of the run, the column was sampled at various points to obtain the cesium and strontium distribution along the column. Cesium loading was rather uniform over the first 80% of the column bed with an average loading of 306 μc/g, corresponding to a K_d of 153 ml/g, in this range. The strontium loading diminishes rapidly and cannot be detected at all in the last quarter of the column. A maximum loading of 57 μc Sr^{90} per g, equivalent to a K_d of 570 ml/g, was observed for the initial increment of vermiculite. The passage of more solution through the column might have resulted in a higher loading for strontium.

The second column was charged with 6878 g of NaOH-NaCl treated vermiculite which filled the column to its full 10-ft depth. Two hundred liters of simulated waste, to which was added 3×10^{-3} *M* KH_2PO_4, was passed through the column continuously at a flow rate of 40.0 ± 2.0 ml/min. The head loss across the column, which was quite densely packed, was about 50 psi. Neither cesium nor strontium appeared in the effluent. Based on the loading of the initial increment of vermiculite in the column, the column was only about 30% saturated with respect to cesium and 20% with respect to strontium; thus the estimates for K_d, 83 ml/g for cesium and 151 ml/g for strontium based on the maximum loading, may be conservative.

The third column was also charged with sodium-vermiculite (6092 g), but no KH_2PO_4 was added to the influent. Two hundred liters of solution passed through the column at a steady flow rate of 38.0 ± 1.5 ml/min. The observed pressure drop across the column was 5 psi. Strontium breakthrough began immediately, and cesium appeared in the effluent after the passage of 120 liters of solution. Both the cesium and the strontium K_d's were quite low, 15.4 ml/g and 13.4 ml/g respectively. Referring to Table 1.29, we note that the cesium K_d is nearly the same as that obtained for a 10-g BO-3 vermiculite column where 10^{-4} *M* potassium had been added to the influent. It appears that the addition of 3×10^{-3} *M* potassium is beneficial for cesium removal, but is less than the optimum concentration. Addition of phosphate to this system appears to be necessary for adequate removal of strontium.

The fourth column was charged with 975 g sodium-treated, exfoliated vermiculite (BE-3). Two hundred liters of solution, to which was added 10^{-2} *M* Na_3PO_4, was passed through the column at a flow rate of 38.1 ± 3.3 ml/min. The pressure drop across the column was too small to be measured. Most of the cesium and strontium was found near the influent end of the column. From the loading of the initial increment, K_d's were estimated to be 772 ml/g for cesium and 1160 ml/g for strontium.

Summary

Particle diffusion processes have a pronounced influence on cesium breakthrough curves obtained from small columns operated for rather short periods of time. Extrapolation from bench-scale experiments to field scale may require correction for this phenomenon, as the cesium loading increases with increased time of column operation. For prolonged times of column operation, the effects of particle diffusion are not so pronounced. The choice of particle size for an operating column may be determined, in part at least, by the kinetics of the exchange reaction.

An understanding of the reaction mechanisms involved in the sorption of cesium by vermiculite permits a good evaluation of column behavior. Improvement in operation can be predicted from theoretical considerations, then checked empirically. For example, it was possible to predict that additions of potassium salts to the influent waste solution would improve cesium sorption by changing the reaction mechanism from edge fixation to interlayer fixation. Experimental data was necessary to establish the minimum and optimum concentration of potassium necessary to effect this change and to optimize cesium removals, as well as to determine the degree of benefit derived.

Further work is contemplated for optimizing cesium removal through additions of potassium salts to the influent solutions in column studies.

For a full explanation, the potassium behavior in the system will be explored and related to the cesium behavior.

DISPOSAL IN SALT FORMATIONS

W. J. Boegly, Jr. F. M. Empson
R. L. Bradshaw B. L. Houser
D. G. Catron H. Kubota[41]
E. G. Struxness

Laboratory and field studies conducted to date have placed prime importance on the problems related to the direct disposal of high-level radioactive liquids in natural salt formations. It is now apparent that high-level wastes will be converted to solids by the various calcination schemes in the next few years, and, further, that some safe ultimate disposal site for these solids must be developed. Because of its many advantages,[42] salt is felt to be one of the most promising media for this disposal. As a result, primary emphasis has now been changed to studies relating directly to solids disposal or to studies that are applicable to disposal of both solids and liquids. The laboratory studies on the interaction between salt and liquid wastes are being continued, but field testing of liquid disposal schemes has been temporarily discontinued.

Use of the two large-scale test cavities described in previous reports[43,44] has been terminated, and the wastes removed from the cavities. Detailed measurements and photographs have been made of the walls of both cavities for comparison with similar data taken prior to adding the wastes. Analysis of the thermal and plastic flow data from the tests is almost complete.

If a large number of waste containers are placed in the floor of a salt mine, the heat sources can be considered as a flat slab of finite thickness generating heat homogeneously throughout the slab. Calculations and field studies of heat transfer around single cylinders of various diameters and lengths have also been performed. More accurate calculations on the waste and salt temperatures can be obtained by deriving an equation for a number of cylindrical heat sources spaced or arrayed at various intervals. This is now in progress and field experiments to verify the calculations are being planned.

The plastic flow studies are being expanded to include all the variables known to affect the rate of flow. Previous studies have been concerned only with the flow of salt in the vicinity of the test cavities and do not encompass any variable other than temperature. More detailed studies on the effect of temperature on plastic flow will be conducted in the field. Since the concentration of radioactivity which can be stored is higher for solid wastes than for liquids, studies on the effect of gamma radiation on the structural properties of rock salt will be expanded to higher doses than previously studied.[45]

Laboratory studies on interaction of liquid wastes and salt have been continued. No work has been performed on chemically produced off-gases since the previous report;[46] however, further work has been under way on the radiolytic off-gases. Small cavities have been excavated and operated to study the mechanisms of cavity alteration, and laboratory tests have been initiated in an attempt to control or eliminate these phenomena.

Large-Scale Field Experiments

Completion of Experiments. – Heating of the acid waste cavity was terminated on August 2, 1960, after 197 days of operation, and of the neutralized cavity on February 1, 1961, after 392 days of operation. Temperatures in the two systems were allowed to fall naturally until both the waste solutions and the surrounding salt returned to ambient. This required approximately 100 days. After the solutions reached ambient temperature, the acid waste was pumped into polyethylene carboys and the neutralized waste into steel drums for removal from the mine. The waste solutions were disposed of in the industrial waste treatment facilities designed to handle plating wastes and

[41] Member of Analytical Chemistry Division.

[42] F. L. Parker, L. Hemphill, and J. Crowell, *Status Report on Waste Disposal in Salt Formations*, ORNL-2560, pp 11-21 (Aug. 14, 1958).

[43] E. G. Struxness *et al.*, *Health Phys. Ann. Progr. Rept. July 31, 1959*, ORNL-2806, p 85.

[44] F. M. Empson (ed.), *Status Report on Waste Disposal in Natural Salt Formations: III*, ORNL-3053, pp 22–56 (July 11, 1961).

[45] B. D. Gunter and F. L. Parker, *The Physical Properties of Rock Salt as Influenced by Gamma Rays*, ORNL-3027 (Mar. 6, 1961).

[46] E. G. Struxness *et al.*, *Health Phys. Div. Ann. Progr. Rept. July 31, 1960*, ORNL-2994, p 96.

similar industrial wastes at the Boeing Airplane Company, Wichita, Kansas.

Following removal of both pit covers and associated equipment, photographs and measurements were made of the cavity walls. Recrystallized salt and other loose materials were removed from the walls and floor of the cavities and weighed. After the cleaned cavities were rephotographed, they were filled and covered with fine salt to return the mine floor to its original condition.

Observation of Cavity Changes. – Changes in the cavities were documented in three ways: (1) by photographs, (2) by direct measurements, and (3) by weighing the salt redeposited during the experiment. Changes in the cavity walls can be seen most graphically in the photographs. Determination of the weight of material dissolved and redeposited gives an average value for the enlargement of the cavity, but does not give any indication of variations in dissolution from one area to another.

Acid-Waste Cavity. – Figure 1.29 is a photograph of the top of the acid-waste cavity after removal by hand chipping of the recrystallized salt, loose shale, and salt deposited on the floor. Very little shale seems to be missing from the wall, but chemical action with the acid Purex waste has made it weak and spongy. There is practically no change from the original dimensions in the salt and anhydrite in the upper 12 in. The pure salt, 12 to 18 in. down from the floor, is undercut 1 to 2 in., due to vapor condensing on the wall. Beginning at 18 to about 24 in., there is closely bedded shale and salt from which the salt has been partially dissolved; below this and continuing to the liquid level, there is a lacy area of anhydrite and/or shale from which the salt has been dissolved.

Fig. 1.29. View of the Acid Waste Cavity After Removal of Recrystallized Salt.

From the liquid level at $2\frac{1}{2}$ to about 9 ft below the mine floor, the wall was partially covered with large crystals deposited from the waste solution. Localized attack has resulted in pitting to as much as 8 to 9 in. There is no apparent system to these points of deep attack.

The bottom of the cavity was covered by a thick layer of dense recrystallized salt. The material reached a depth of 16 in. near the wall, and was about 4 in. thick near the center.

It is of interest to note in Figure 1.29 that no change occurred in the dimensions of the cavity rim or in the seal trench. The cavity wall was most affected in the area in direct contact with the acid waste. Above the liquid level, there were only superficial changes. Marked pitting and formation of recrystallized salt occurred over the remainder of the wall, except the area near the floor where the original wall surface was present when the bottom layer was chipped away.

Approximately 7400 lb of material (recrystallized salt and some shale) was chipped from the walls and floor of the acid pit. If this amount of material is considered to have dissolved from the walls, it represents an average penetration of 1.9 in. If the unattacked area at the bottom of the cavity is eliminated from the computation, the average penetration is 2.5 in.

Neutralized-Waste Cavity. – Figure 1.30 is a view of the neutralized-waste cavity before removal of the cover and electrodes. The large amount of recrystallized salt bridging out from the wall to the electrodes is shown, as well as deposits on the walls below the bridge and over the sludge layer in the bottom of the cavity. Figure 1.31 is a top view of the cavity after removal of the cover and recrystallized salt from the side-walls. This view

Fig. 1.30. Interior of the Neutralized-Waste Cavity Before Cover Removal.

Fig. 1.31. View of the Neutralized-Waste Cavity After Removal of Recrystallized Salt.

shows the deep erosion of the wall just below the rim of the cavity. The anhydrite band, beginning about 10 in. below the floor, is undisturbed. Below the anhydrite band (15 to 21 in. down) salt mixed with shale is eroded to maximum depths of 15 to 18 in. Bridging out recrystallized salt occurred from 21 in. down to the liquid level (30 in. down). Below this the wall was covered by 1 to 2 in. of crystalline salt down to the precipitate occupying 24 to 30 in. at the bottom. It is obvious that the condensate collection system was not as effective in preventing erosion of the upper part of the cavity as was the system on the acid cavity. Possibly differences in the cover and off-gas system may be responsible for this, although the installations were supposed to have been identical. Support is lent to this hypothesis by the fact that condensate collection, at peak waste temperature, from the neutralized cavity averaged about 0.5 gal per day, while condensate collection from the acid cavity was 1.5 gal per day.

It was not possible to secure an accurate figure for the amount of recrystallized salt deposited in the neutral cavity, as there was a considerable amount of salt in the sludge which could not be separated. After removal of the waste, approximately 5600 lb of salt were chipped from the walls. If this were removed evenly from the upper two feet of the walls, the depth of erosion would be about 8 in.

Plastic Flow Studies

Analysis of Field Data. – Dial-gage extensometers were installed in the vicinity of the waste cavities to measure the plastic flow occurring during the field experiments. The gages around the neutralized-waste cavity were installed for ORNL by the Geotechnical Corporation, and those around

the acid-waste cavity were installed by the University of Texas.[47] Figure 1.32 shows the relative positions of the gages. Installation of the gages was completed after the cavities were excavated, and data was collected on the rate of movement of the salt prior to heating the cavities.

The rate of movement (in. in.$^{-1}$ yr^{-1}) obtained from the ORNL gages during this initial period was almost constant for each gage, and the results are summarized in Table 1.30. Gages 9105 – Nos. 2 and 3, which were located near the columns, showed a rate of movement which was about 50% of the movement in the center of the room (9100 – No. 3). As expected, the rate of vertical movement observed at each gage location is a function of the distance from the center line of the room (see Fig. 1.33); that is, the movement is greatest in the center of the room and least at the columns. Although the total column-to-column movement (Table 1.30) was approximately equal to one-half the floor-to-ceiling movement in the center of the room, the change in length per unit length (unit deformation) was much less, only about 13% of the unit deformation in the center of the room.

When heat was applied to the cavity at start-up, the rate of movement increased rapidly due to increased creep and thermal expansion of salt (see Fig. 1.34). This apparent increased rate of movement slowly decreased until, at constant temperature, the rate was approximately equal to that observed prior to heating. After the heaters were turned off, the salt contracted, causing an increase in room dimensions. This effect is now disappearing. The latest gage readings indicate that, although the total movement was greater than normal, the heated cavities did not significantly upset the rate of movement or the stability of the experimental room. As an example, the total observed movement during the heating cycle for the

[47] T. D. Reynolds and E. F. Gloyna, *Reactor Fuel Waste Disposal Project, Permeability of Rock Salt and Creep of Underground Salt Cavities – Final Report*, University of Texas, AEC Contract AT-(11-1)-490, p 86 (Dec. 30, 1960).

UNCLASSIFIED
ORNL-LR-DWG 61560

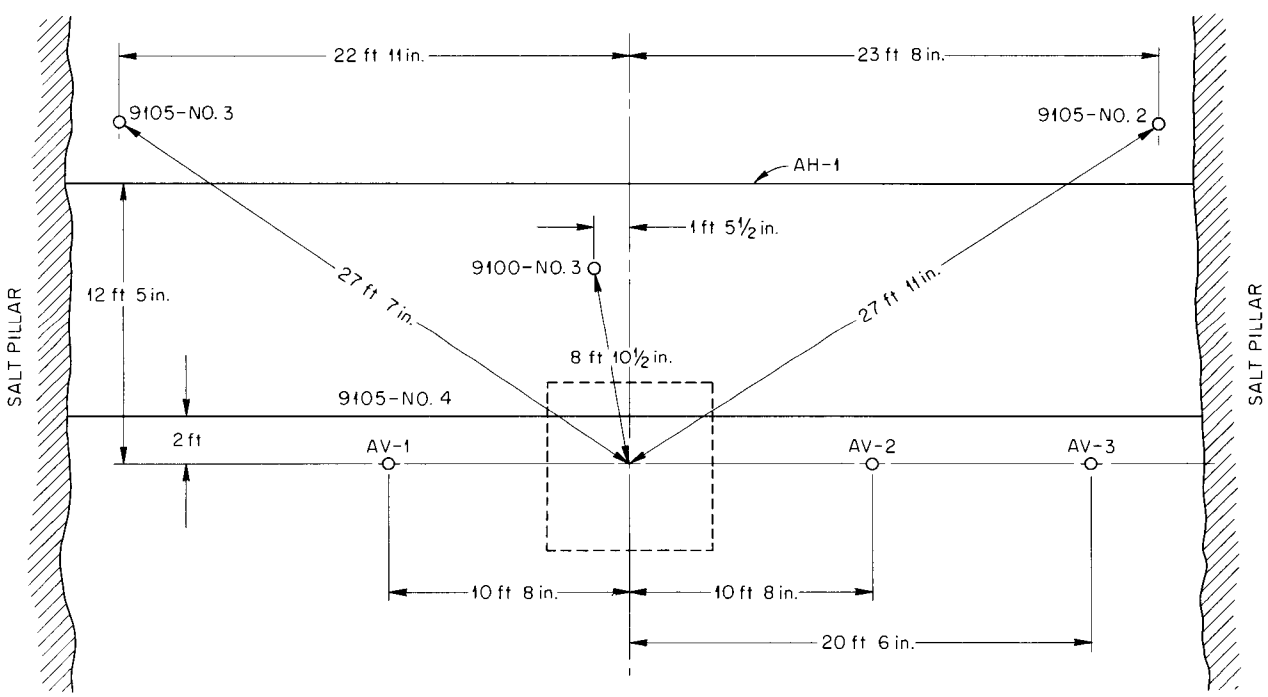

AV-1, AV-2, AV-3, AND AH-1, ARE UNIVERSITY OF TEXAS GAGES LOCATED AROUND ACID WASTE CAVITY.
9100-NO. 3, 9105-NO. 2, 9105-NO. 3, AND 9105-NO. 4 ARE ORNL GAGES LOCATED AROUND NEUTRALIZED WASTE CAVITY.

Fig. 1.32. Plan View Showing Relative Locations of ORNL and University of Texas Gages.

Table 1.30. Extensometer Results for Period Prior To Heating of Waste Cavities

Gage	Distance from Center of Room	Rate of Movement* (in. in.$^{-1}$ yr^{-1})
		($\times 10^{-4}$)
	ORNL Extensometers	
9105–No. 2	27 ft 11 in.	5.0
9105–No. 3	27 ft 7 in.	5.4
9105–No. 4	Horizontal gage	1.4
9100–No. 3	8 ft 10½ in.	11.1
	University of Texas Extensometers	
AV–1	10 ft 8 in.	9.9
AV–2	10 ft 8 in.	9.5
AV–3	20 ft 6 in.	6.1
AH–1	Horizontal gage	1.0

*Average rate for measuring period.

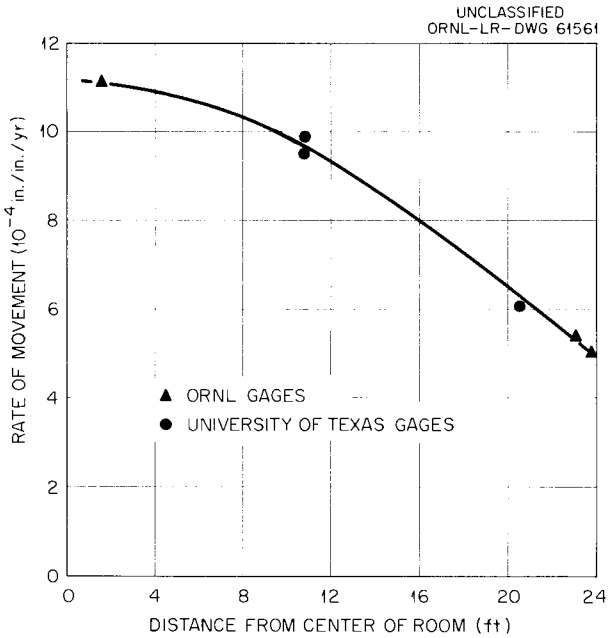

Fig. 1.33. Relationship Between Distance from Center of Experimental Room and the Rate of Plastic Flow for Time Prior to Startup.

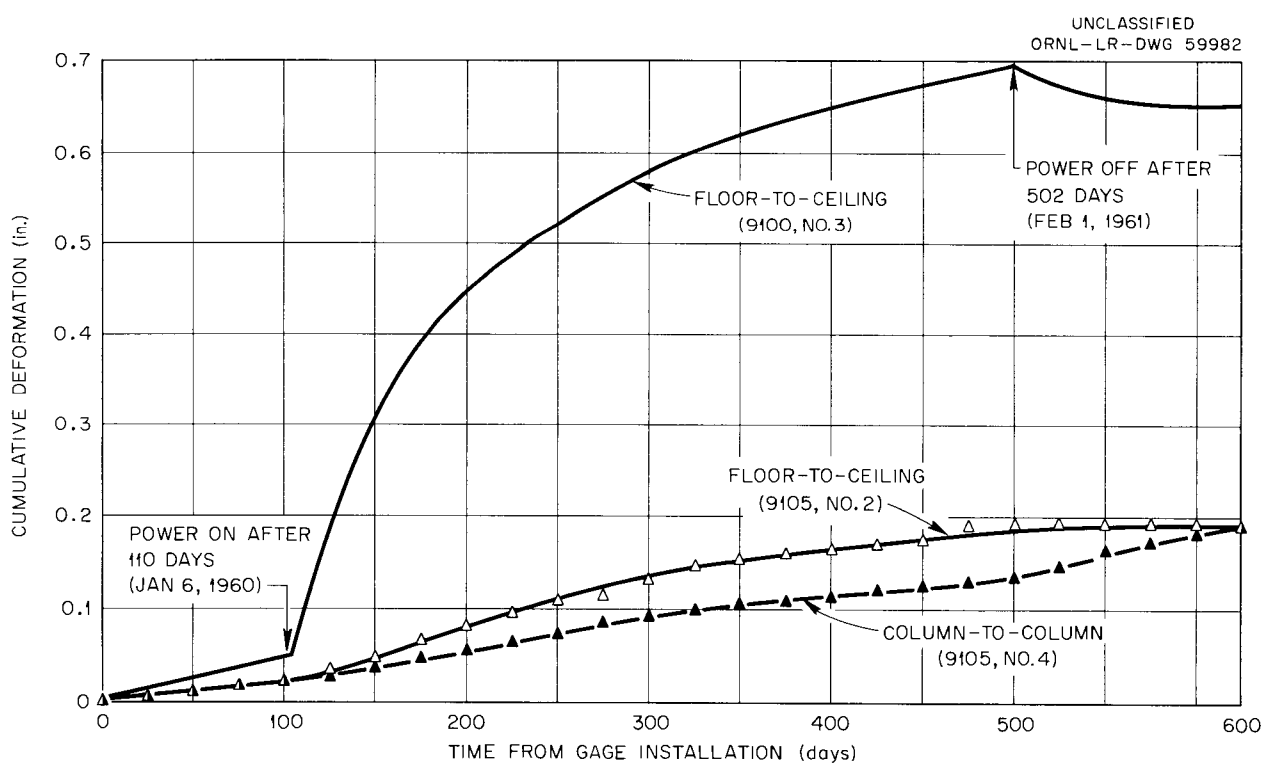

Fig. 1.34. Extensometer Results for ORNL Gages Surrounding Neutralized-Waste Cavity.

vertical gage in the center of the room (9100 – No. 3) was 0.65 in., whereas, if heating had not taken place, the expected movement would have been 0.15 in. Thus 0.5 in. of total movement above normal movement was produced by the thermal expansion of salt and increased creep of salt with temperature. However, the rate of movement prior to the tests was 0.0005 in. per day, and at the time the heaters were turned off was 0.0004 in. per day, meaning that the long-term rate of movement was not significantly upset by the heating of the cavities.

At approximately 500 days after installation, the gage measuring column-to-column movement started to show an unexpected increase in rate of movement (from 0.0003 in. per day to about 0.0005 in. per day). Later, during the disassembly of test equipment, it was discovered that two of the wires which supported the gage from the ceiling were broken. This may account for the apparent increase in movement of about 0.03 in. in the last 125 days as shown in Fig. 1.34. The column-to-column curve will be analyzed further to verify this.

The strain seismographs installed to determine if the salt moves with constant or variable velocity for short time increments have been disassembled and the recording charts analyzed. The previously reported indication[48] that the salt was not moving with a constant velocity has been found to be incorrect and was caused by an extraneous signal from the power controllers being picked up by the velocity transducer. It is now apparent after reviewing all charts that there was no rapid acceleration occurring, meaning that there was no fracturing or cracking of the salt.

Future Program. – At the present time, sufficient information is not available to adequately predict the rate and total amount of plastic flow which will occur in a mined opening in rock salt. The time required for a mined opening to close is dependent on the mine depth, size and shape of the opening, nature of the overlying rock, age of the opening, temperature, and structural properties of the salt. The field studies conducted to date have been concerned with flow around the large cavities and, thus, provide data for only one set of mine variables.

An expanded study is being initiated which will consist of making field measurements of flow in various mines, using rooms of different size, shape, and age. By using a number of mines, the effects of mine depth, overburden pressure, and structural properties can be evaluated. Gages of the "Reidometer" type which are capable of measuring movement in the floor and/or the ceiling will be used in this study. Whenever possible, the stresses in the pillars and in the salt surrounding the room will be measured at the gage stations, and the structural properties of the salt will be determined with the salt in place or on samples removed from near the stations. The data from this study will be analyzed to determine the effect of each of the variables on the rate of flow and the time required to close the mined opening. All measurements will be made at ambient mine temperature.

In order to determine more accurately the effect of temperature on the rate of plastic flow, a series of small experiments called "heated rooms" will be performed. These rooms, approximately 2 ft high by 6 ft wide by 8 ft deep will be excavated in the pillars of the Carey Mine. Immediately upon excavating the rooms, the overburden pressure will be measured and gages installed to measure the flow at ambient temperature. The rooms will then be heated to various predetermined temperatures and the increase in flow measured. Careful selection of the pillars used for the rooms will permit different stress conditions to be obtained and thus measurement of flow at various combinations of temperature and stress. It is anticipated that this information can then be included in the studies made at ambient temperature to define the thermal effect on plastic flow.

Concurrently with the field work, theoretical calculations will be made in an attempt to mathematically relate the factors affecting flow and the observed flow rate. At the present time, it is not apparent whether these calculations can be carried to the degree of accuracy obtained in the field measurements, but it is anticipated that they can be used as a check on, or in conjunction with, the field data.

Laboratory studies on the effect of gamma radiation on the structural properties of rock salt will be expanded to cover doses greater than 5×10^8 r. Some indication that a decrease in structural strength occurs at Co^{60} gamma dosages of 5×10^8 r and greater can be detected, and further study in the laboratory will be required to adequately define

[48] E. G. Struxness *et al.*, *Health Phys. Div. Ann. Progr. Rept. July 31, 1959*, ORNL-2806, p 123.

this decrease. If there is a significant decrease, this effect must also be combined into the data from the other studies.

The over-all objective of this phase of the program is to derive equations for predicting the rate and total movement in rock salt openings which will take into account the properties of the salt, the characteristics of the mine, and the effects of temperature and radiation. These equations can than be used to design openings suitable for radioactive waste-disposal operations, or to check existing mine openings for possible usefulness.

Thermal Studies

Analysis of Large-Scale Field Data. – A comparison of the time-space-temperature rises obtained in the 7½-ft-cube waste cavities and the surrounding salt with theoretical rises calculated for a 5-ft-radius sphere (same surface area as the cube) has been made previously.[49] The agreement was quite good, considering the fact that the sphere only roughly approximates the cube and the presence of the mine floor invalidates the infinite-medium assumption for all but short periods of time.

[49] E. G. Struxness *et al.*, *Health Phys. Div. Ann. Progr. Rept. July 31, 1960*, ORNL-2994, pp 119–20.

The theoretical time-space-temperature rise about a sphere with constant heat generation can be normalized in a manner such that the temperature rise as a function of heat generation rate, sphere radius, and thermal conductivity of the infinite medium can be plotted against time as a function of the sphere radius and the thermal diffusivity of the medium (Fig. 1.35). A family of temperature-rise-vs-time curves is thus obtained which apply for distances from the sphere in terms of sphere radii. When plotted on log graph paper, the thermal conductivity and diffusivity of the infinite medium can be determined by superimposing experimental time-space-temperature rises obtained about spheres. In the case of the 7½-ft cube of neutralized waste, the localized heating in the precipitate phase makes such a comparison invalid, but the acid-waste cavity data (Fig. 1.36) gives a reasonably good check if the comparison is confined to those portions of the curves which represent a temperature rise greater than 1°C and time less than 20 days after startup (the accuracy of the temperature recordings is approximately ± ½°C; and after about 20 days, the floor influence is felt, in addition to the fact that the power input is reduced). When the acid-waste cavity wall temperature is matched with the theoretical curve for $r = a$ (Fig. 1.35), then the 2.5-ft-,

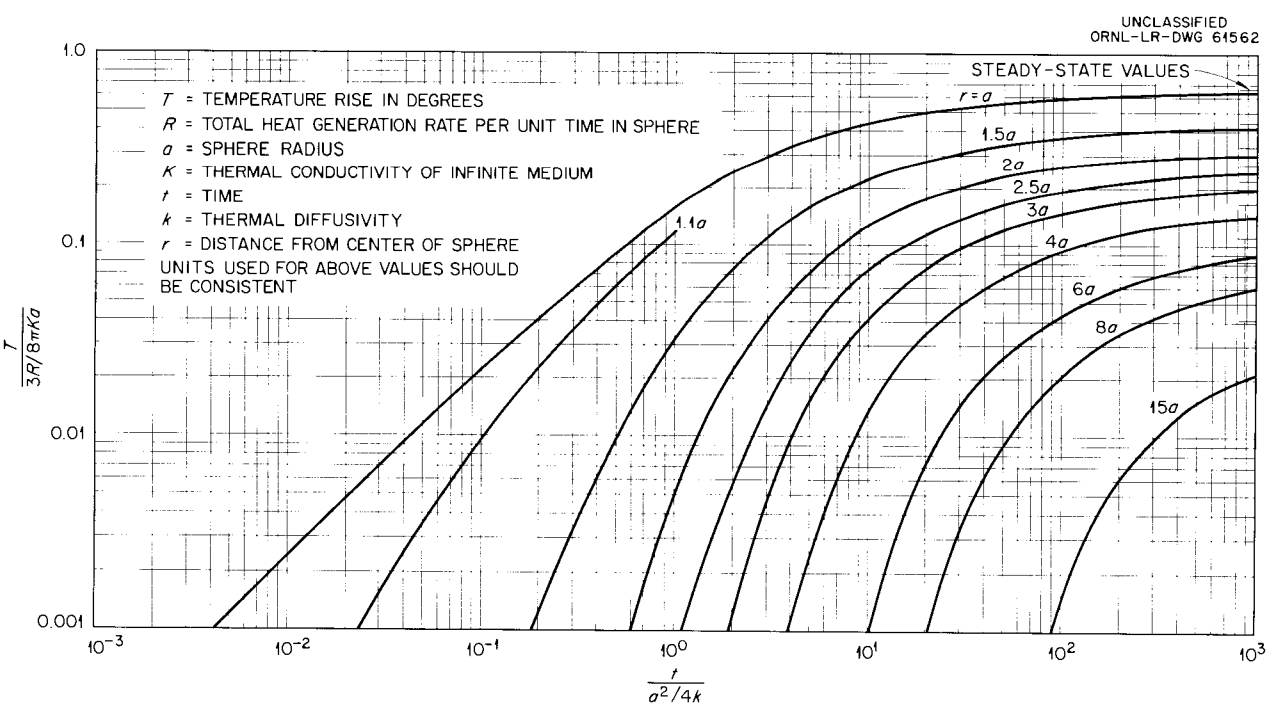

Fig. 1.35. Temperature Rise Around a Sphere with a Constant Heat Generation Rate.

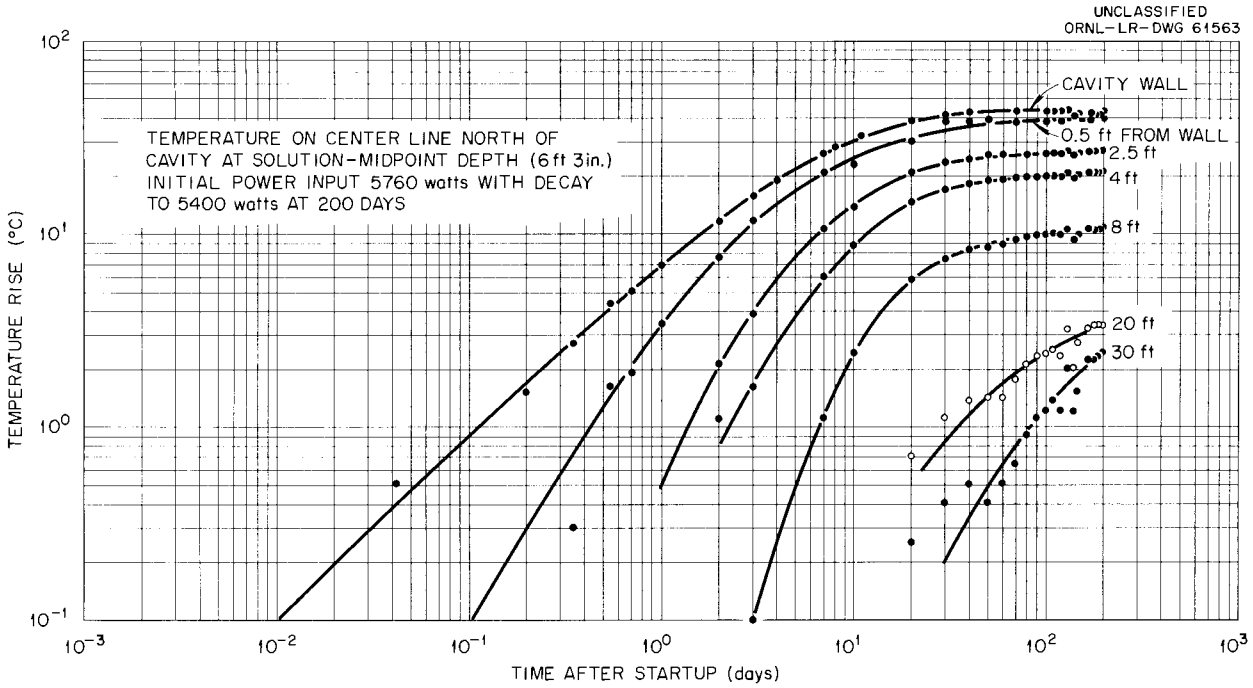

Fig. 1.36. Temperature Rise – 7½-ft Cube Acid Waste Experiment.

4-ft-, and 8-ft-out curves (Fig. 1.36) agree closely with the $r = 1.5a$, $1.8a$, and $2.6a$ curves respectively; that is, with the theoretical curves for a 5-ft-radius sphere. The 0.5-ft-out curve does not agree as well, perhaps due to a nonvertical thermocouple hole. From this comparison, the calculated thermal conductivity is 2.6 Btu hr^{-1} ft^{-1} $(°F)^{-1}$, and the diffusivity 0.099 ft^2/hr which corresponds to the Birch values[50] for single pure-salt crystals, at 80°C and 65°C respectively. The peak salt temperature over the portions of the curves compared was about 60°C and the minimum 22°C, perhaps indicating that the bedded Kansas salt is a somewhat poorer heat conductor than pure salt crystals.

In the 1959 Annual Report,[51] an equation was given for determining the power input as a function of depth, with the electrode configuration used in the 7½-ft-cube tests, and a calculation was presented which assumed that the power input would be 15 kw. The actual power input was 5.8 kw, and the calculated power variation with solution depth for this input is shown in Fig. 1.37. For comparison, data on a 10-in. laboratory block experiment are also shown. The vertical temperature-rise profile actually obtained in the 7½-ft cube acid-waste cavity is also shown in Fig. 1.37 and indicates that convection currents set up by the localized heating

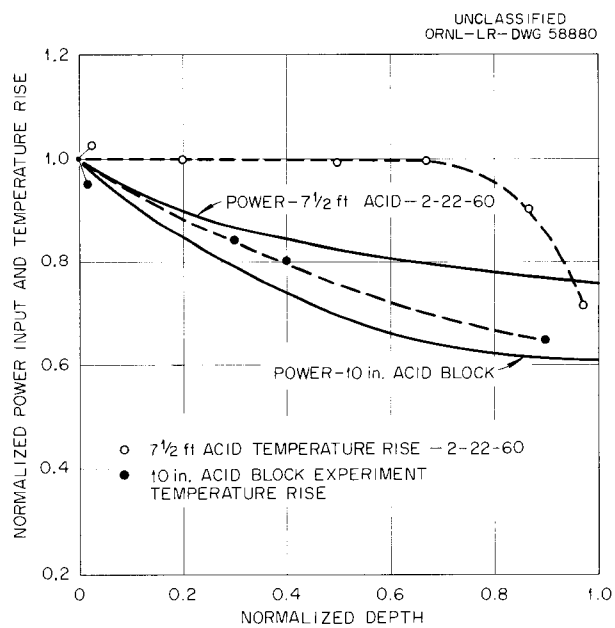

Fig. 1.37. Power Input and Temperature Rise vs Depth.

[50] F. Birch and H. Clark, *Am. J. Sci.* **238**, 529–58, 613–35 (1940).

[51] E. G. Struxness *et al.*, *Health Phys. Div. Ann. Progr. Rept. July 31, 1959*, ORNL-2806, pp 81–83.

immediately around the electrodes tended to equalize the temperature throughout the cavity. The bottom foot or so seems to be much cooler than the rest, and is apparently explained by the fact that the thermocouples located at points 3 in. and 1 ft off the bottom of the cavity were actually in redeposited salt. In the top 6 ft of solution, there was only a degree or so variation in either the horizontal or vertical directions.

In the neutralized waste there was a viscous precipitate which settled to occupy approximately 30% of the solution volume. Heating was nearly all confined to this region, since most of the fission products would be scavenged by the precipitate. There was little or no convection in the precipitate, and, consequently, temperatures as high as 120°C were recorded near the center; however, a steep gradient existed, and temperatures at the cavity wall were approximately the same as in the supernatant region. There was free convection in the supernatant, and, thereby, a uniform temperature distribution.

In September of 1960 (approximately 8 months after the start of the test) five additional thermocouple holes were drilled to a depth of 30 ft on the north side of the neutralized-waste cavity. Thermocouples in these holes made possible the construction of a vertical temperature profile around the cavity. Figure 1.38 shows the vertical temperature distribution obtained within the cavity and out into the salt at the center of the north wall of the neutralized cavity. Temperature contours in the precipitate are based on data from five fixed-position thermocouples and vertical traverses made with two thermocouples and, thus, are not as accurate as the salt temperature contours. The contours in the salt were constructed from data obtained from 44 thermocouples. An insufficient number of thermocouples was installed to construct salt temperature contours around the acid cavity, but a comparison of existing thermocouples indicated that the salt temperature profile was approximately the same as for the neutralized cavity.

Slab Heat Sources. – An actual disposal operation will consist of a number of waste cavities spaced as closely as possible without exceeding the allowable temperature rise. If it is assumed that the disposal operation is handling the output from a fuel reprocessing plant serving the entire United States power reactor economy circa 1970, wastes will be produced at a rate such that the number of heat sources can be represented by a slab of infinite horizontal dimensions. The infinite slab calculation will be conservative in that wastes will be produced at a finite rate, and, thus, the actual slab will contain wastes whose average heat generation rate may be considerably lower than that which is currently being added. Additionally, probably not more than 60% of the gross mine area will actually contain wastes, the remainder being taken up by passageways and roof supports. On the other hand, the infinite slab calculation assumes that the waste is uniformly distributed in the slab so that if the waste is contained in discrete containers, say vertical cylinders, a correction should be made for the temperature perturbations produced. In any event, the solution to the slab problem is relatively easy, allowing an estimate to be made of the amount of mine space which is required. This information is needed for the economic study of waste-disposal methods currently in progress (see section on Evaluation of Engineering, Economics, and Hazards) and may be adequate for studies on the disposal of liquids in thin layers recessed in the mine floor.

A code designed for monitor runs on the IBM 7090 computer has been written by W. D. Powers (formerly of the Reactor Experimental Engineering Division) to evaluate the temperatures in an infinite slab with a variable heat source. The code is formulated so that the temperature rise is evaluated as a function of time for waste whose age at the time of burial varies. The temperature at any number of points in the heat-generating layer (waste mixed with salt) and in the infinite medium (salt) may be calculated. The vertical thickness of the heat-generating layer may also be varied. An assumption is made that equal amounts of heat flow upward and downward, so that the problem resolves itself to the semi-infinite region bounded by the plane $x = 0$, where x is depth below the center of the waste layer. The general heat-conduction equations were thus set up with the following boundary conditions: (1) for $t \leq 0$, the temperature is zero throughout the region $0 \leq x < \infty$, (2) for $t > 0$, there is no flow of heat across the boundary at $x = 0$, (3) for $t > 0$ in the region $0 < x < a$ (where $2a$ = thickness of waste layer), heat is generated which is independent of position but dependent upon time. The method used to solve these equations is as follows. The total

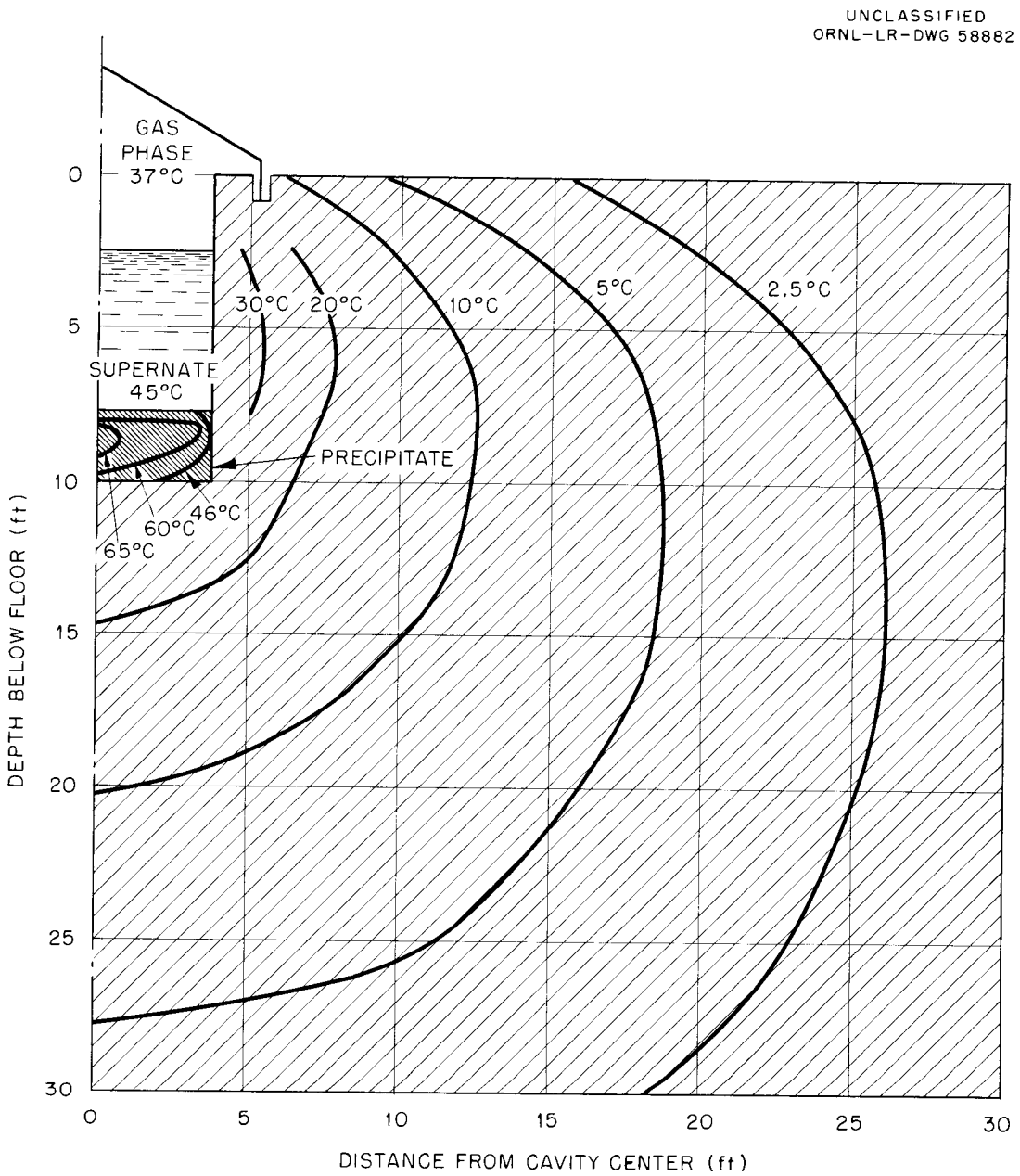

Fig. 1.38. Vertical Temperature Rise Contours – 7½-ft Neutralized-Waste Experiment – October 1960.

time in which the temperature structure is desired is divided into finite intervals of length Δt. The rate of heat generation is first assumed to be constant, and the differential equations are solved and the temperatures calculated at the end of each of these time intervals. The temperatures due to impulses of heat, starting at $t = n\Delta t$ and ending at $t = (n + 1)\Delta t$, are then derived from the first result. The mean value of the heat input in each of the time intervals, Δt, is calculated. By means of a finite approximation to a convolution integral, the last two results are combined to yield the temperature rise due to the variable heat source.

In Fig. 1.39 are shown peak temperature rises at the center of the heat-generating layer ($x = 0$), as a function of cooling time before storage, obtained with the slab code. The rate of heat generation decay used was that produced by natural or slightly

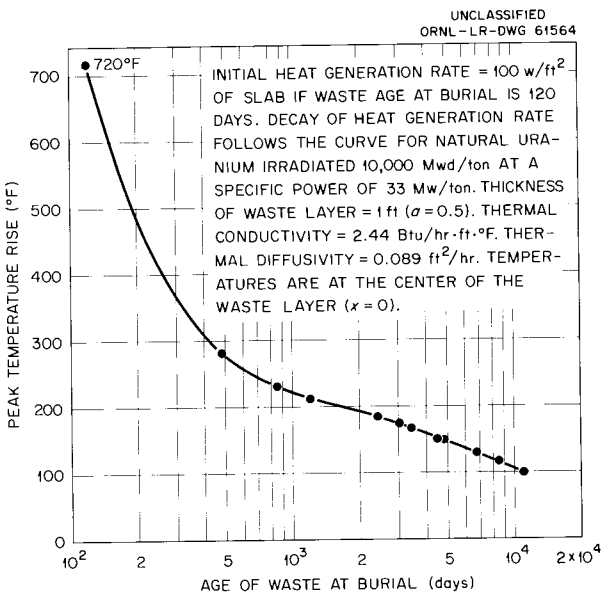

Fig. 1.39. Peak Slab Temperature Rise as a Function of Age of Waste at Burial.

enriched uranium fuel irradiated to 10,000 Mwd/ton at a specific power of 33 Mw/ton. The heat-generation rate in the slab was arbitrarily assumed to be 100 w/ft^2 for wastes of 120 days age at the time of burial, and the 100 w/ft^2 was assumed to be contained in a slab 1 ft thick (a = 0.5 ft). Thermal constants used were those for salt at a temperature of 100°C.[52] The temperature rise is a linear function of the heat-generation rate per unit of slab area; therefore, rises for wastes of different heat-generation rates per unit area may be obtained by multiplying by the appropriate factor. It is apparent from Fig. 1.39 that it would be wasteful of mine space to store wastes which have been cooled for less than 1 yr.

Cylindrical Heat Sources. – The slab calculation gives a conservative estimate of space requirements for an evenly distributed heat source; but if discrete sources are used, it is necessary to correct for the temperature perturbations around the sources. It would appear that the most likely storage-container shape for solid wastes is the cylinder. R. E. Glover of Denver, Colorado, a consultant, has developed an equation for a line source of constant heat-generation rate. If the cylindrical source is long compared with its diameter, this gives a good approximation of the temperature rises in the medium surrounding the cylinder (other equations are available for obtaining the temperature profile within the cylinder itself). This equation requires a numerical integration and produces only the results for a steady heat-generation rate; however, it should be relatively easy to apply the superposition principle and program the varying-heat-source solution in a manner similar to that which was done for the infinite slab.

Glover has calculated the time-temperature profile on a line perpendicular to the center of the constant heat source at distances from the center of $1/24$, 0.5, 1.0, 1.5, 2.0, and 3.0 times the length of the source. These are shown in Fig. 1.40 along with curves for additional values of x/L which were obtained from a cross-plot.

Two tests were made in the Carey Mine using Calrod-type heating units to obtain data on the time-space-temperature profiles near an isolated cylindrical heat source. One heater was located in the center in the floor of the corridor leading to the ORNL room, and the other was located halfway up the wall of a pillar. Each heater was placed in a sand-filled iron pipe, and this assembly was located in a $1\frac{3}{4}$-in.-diam hole and the hole backfilled with sand.

The heaters had an active heating length of 6 ft and were located with their centers 10 ft below the salt surface. Thermocouples were inserted in polyethylene tubing and backfilled with sand in $1\frac{3}{4}$ in. holes. Figures 1.41 and 1.42 show the temperature rises obtained at distances of 2, 4, 8, and 16 ft on a line perpendicular to the centers of the heaters at a constant power input of 2000 w. The points shown were obtained in three different runs, with the salt being allowed to return to ambient temperature between runs. Although the wall and floor test results do not agree exactly, it appears that there is no great difference in the heat-transfer capabilities of the two locations, even though there is considerable shale and anhydrite in the floor and the wall is nearly pure salt. A comparison of the measured temperature rises with the theoretical curves of Fig. 1.40 shows reasonable agreement. The scatter in the experimental data (and perhaps the accuracy of the calculations and the cross-plots used to obtain the theoretical curves) does not permit an accurate determination of the thermal properties of the salt, but the conductivity appears to be approximately

[52] Birch and Clark, *loc. cit.*

3.5 Btu hr^{-1} ft^{-1} $(°F)^{-1}$ and the diffusivity 0.10 ft^2/hr.

Future Program. – Future theoretical studies will be concerned with modifying the infinite slab calculations to take into account the finite dimensions of an actual disposal operation and the development of a solution for arrays of cylindrical heat sources.

Laboratory measurements of the thermal properties of single pure-salt crystals indicate that the conductivity and diffusivity decrease rapidly with increasing temperature (a factor of 2 between 0 and 200°C). The previous experiments have indicated that the thermal properties of natural salt in place, even with as much as 25% impurities, at temperatures slightly above ambient are not very different from the pure crystal values; however, with solid wastes in discrete packages, temperatures in the salt may be allowed to rise to as much as 200°C,

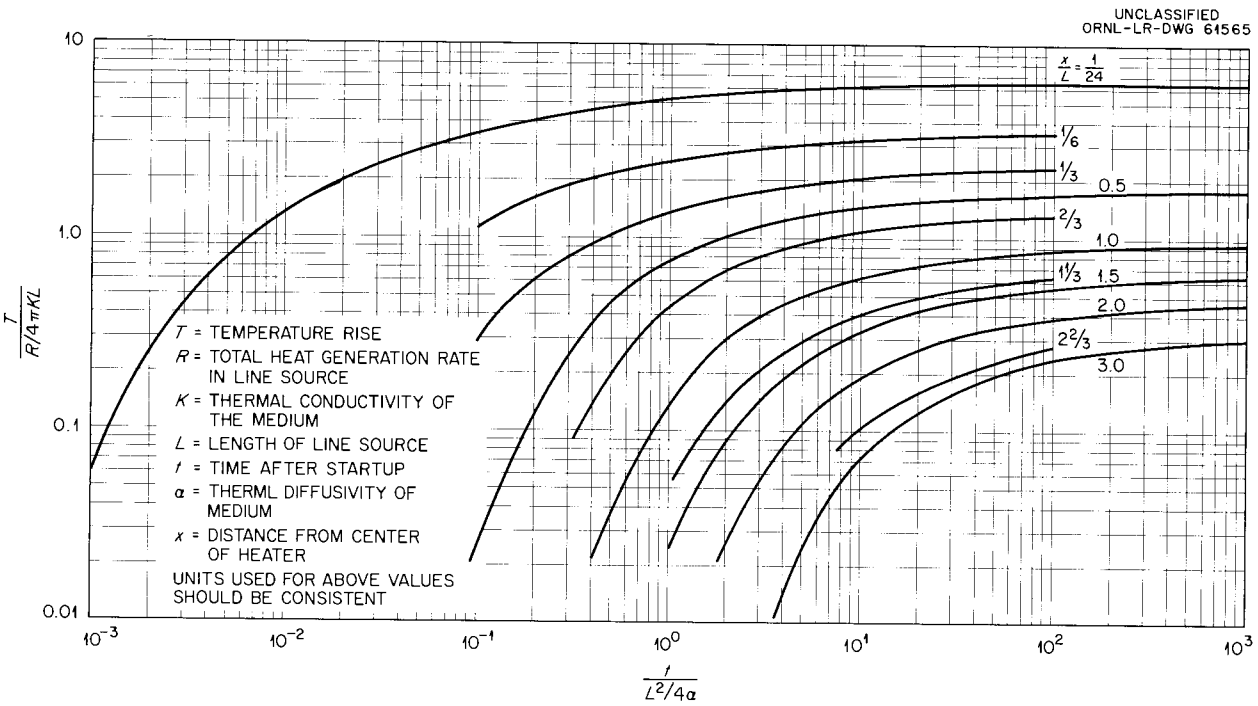

Fig. 1.40. Temperature Rise Around a Line Source with a Constant Heat Generation Rate in an Infinite Medium.

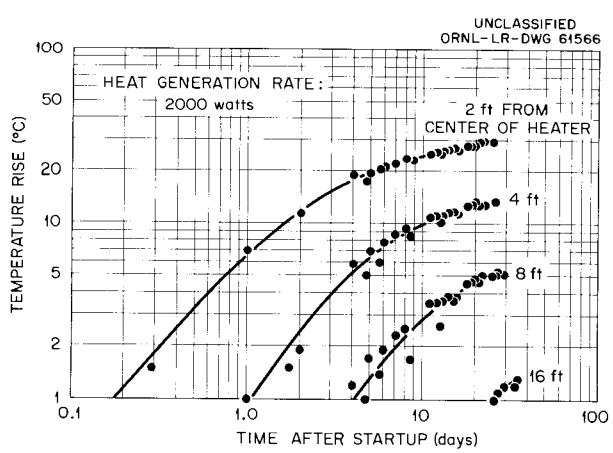

Fig. 1.41. Temperature Rise Around a 6-ft Rod Heater in Floor of Salt Mine.

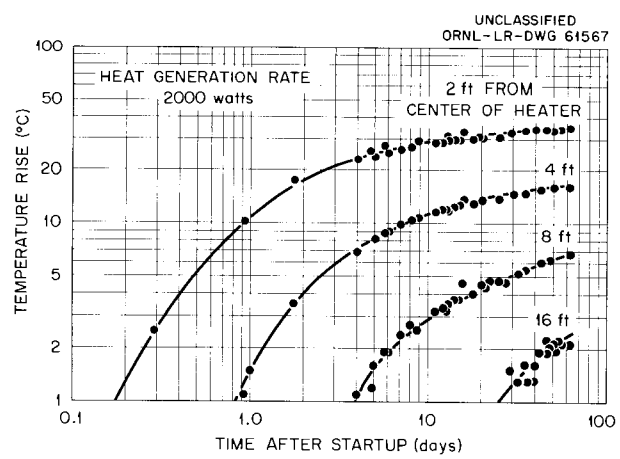

Fig. 1.42. Temperature Rise Around a 6-ft Rod Heater in Wall of Salt Mine.

and it is desirable to ascertain the relationship between temperature and thermal properties for salt *in situ*. An experiment is planned to obtain this information during the coming year.

Also planned for the coming year is a test of simulated cylindrical sources in an array perhaps 20 ft square. In addition to allowing a check of theoretical calculations, this will also permit an observation of the effect of elevating the temperature of a large section of salt floor. Core samples heated in a muffle furnace have been found to shatter violently when the temperature is raised above 200°C. This is believed to be a thermal stress relief phenomenon which will not occur when the salt is restrained *in situ*; however, a field demonstration is desirable.

Further in the future will be a confirmatory and demonstration test utilizing containers of actual solid radioactive waste.

Cavity Alteration Studies

Field Experiments. – One of the major problems in the disposal of liquid waste into salt is the effect of the heated waste on the integrity of the cavity. In order to study this problem a series of experiments was performed. Each experiment consisted of a cylindrical hole, 3 in. in diameter by 36 in. deep, sealed at the top by a 12-in. square plug of rock salt cemented in place by tamped fine salt. One cylinder was completely filled with salt-saturated acid Purex waste and one to a depth 6 in. below the plug. The liquid temperature was held at approximately 85°C for 4 months, using a tantalum-sheathed resistance heater. The heater, a vent tube, and thermocouples were inserted in the cavities through holes sealed with tamped salt. A small amount of vapor leakage occurred around the vent line and stains appeared around the plug near the end of the experiments, indicating that the seals leaked slightly. A combination off-gas-vent system was provided to scrub any off-gas with NaOH solution and to allow air to be drawn in through a water bubbler if negative pressures developed. No indication of pressures significantly different from atmospheric was observed during the experiment.

The experiments were terminated by allowing them to cool, drawing out as much of the solution as possible, and splitting away the front of the stage in which the holes were excavated. In general, the difference in liquid level seemed to have no significant effect. The increase in cavity diameter above the heaters (approx $2\frac{1}{2}$ in. maximum) was the same in each experiment.

Both cavities had several inches of salt recrystallized at the bottom. A bridge of recrystallized salt closing the cavity about 4 in. below the plug was observed in each case at the same elevation. This occurred at approximately the liquid level in the partially full experiment, but apparently does not indicate a marked difference in behavior since it happened in both cases. A third test of this type, with approximately 7 in. of freeboard, is continuing. This test was initiated at a location remote from those reported here when it became apparent that thermal or blasting cracks existed between the two plugs.

It may be concluded from these qualitative tests that a slender cylinder is probably not a good shape in which to study cavity migration if the results are to be extrapolated to larger cavities, since the cavity changes noted in the large acid experiment were not of a similar nature. The experiments have shown, however, that in a slender cylinder the fullness of the cavity does not have a significant effect on the final cavity shape.

Laboratory Studies. – A laboratory study was initiated in an effort to resolve the factors that are responsible for cavity alteration, particularly the mechanism by which the cavity walls were eroded in the presence of a saturated salt solution. Since the alteration was believed to be a temperature effect (the result of vaporization and condensation) tests were run at 25 and 75°C. The first, at 25°C, was intended simply to establish a reference point, to verify the assumption that the solubility of the mine-salt samples was not significantly affected by impurities in the salt or the presence of other ions in the solutions.

Since radioactive material has not been used in this work, the results do not indicate the possible effect of radiation. It is thought, however, that radiation effects upon cavity alteration are of little consequence.

A system consisting of a cylindrical block of salt partially immersed in liquid and contained in a closed glass vessel was utilized in this study. Salt cylinders $2\frac{1}{2}$ in. in diameter from cores taken

at the Carey Mine were cut into sections about 6 in. long for this purpose.

Measurements at 25°C. – Initial studies were made at 25°C, a temperature at which it is relatively easy to maintain isothermal equilibrium between solid, liquid, and vapor phases. This condition is desirable in order to approach ideal equilibrium exchange of water between the liquid and vapor phases. The salt block was weighed and placed upright in the glass container. Where solutions were salt-saturated, 10 g of sodium chloride (analytical-grade fine crystals) was placed in the bottom of the bottle. In each test 100 ml of the test solution was carefully poured into the bottle so that the salt block was not wet at any point above the final liquid level. The bottle was sealed and immersed in a water bath kept at 25°C.

Four test solutions were used: (1) water, (2) saturated sodium chloride, (3) saturated sodium chloride and sodium nitrate, and (4) saturated sodium chloride–5 *N* hydrochloric acid. Solution 3 contained an anion whose sodium salt is more soluble than sodium chloride, while solution 4 contained the hydronium cation whose compound with chloride is more soluble than sodium chloride.

The period of immersion was 27 days. No special significance is attached to this time period; however, all subsequent tests were continued over the same time span. At the end of the period the blocks were removed, wiped free of adhering liquid, air-dried for 24 hr, and weighed. Density measurements were made of each solution before and after the runs. The experimental data are tabulated in Table 1.31. The photographs of the dried blocks after the experiment are shown in Fig. 1.43.

Water (solution 1) was the only medium in which any noticeable change had taken place. The diameter of the immersed portion was reduced uniformly to $2\frac{3}{16}$ in., except at the water line where it was 2 in. The excessive erosion at the water line is due to surface motion of the liquid imparted by the water-bath stirrer. The 35-g weight loss approximates the solubility of sodium chloride in water at 25°C (35.9 g/100 ml). Visual inspection, followed by a check with a pair of calipers, corroborated the weight figures.

It was concluded that, in an isothermal system at 25°C, a salt cavity can be expected to resist any attack by an aqueous solution as long as the solution is saturated with respect to salt and regardless of the presence of other ions.

Measurements at 75°C. – A salt block was partially immersed in a saturated salt solution which was maintained at 75°C. Since only the solution portion was heated, the vapor phase was cooler than the liquid phase. As a result, considerable condensation of vapor took place, and moisture dropped back or flowed down the sides of the bottle into the liquid.

A photograph of the block at the end of the run is shown in Fig. 1.44. The salt block has been eroded just at the water line. Recrystallized salt is deposited upon the block below the liquid level. Salt is also recrystallized and laid down on the block in the vapor area.

It was assumed that the loss of water vapor caused an oversaturation within the liquid. Salt, therefore, selectively crystallized out on the salt wall. When condensate which contained very little solute returned to the surface of the liquid, there

Table 1.31. Erosion of Salt Blocks at 25°C

Salt cylinders $2\frac{1}{2}$ in. in diameter by 6 in. long partially immersed 27 days

Medium	Weight of Block (g)		Weight Loss (g)	Density of Medium (g/cm^3)	
	Before	After		Before	After
1. H_2O	665	630	35	0.998	1.194
2. Sat. NaCl	762	762	0	1.193	1.194
3. Sat. NaCl–$NaNO_3$	703	704	– 1	1.333	1.333
4. Sat. NaCl–5 *N* HCl	735	735	0	1.116	1.116

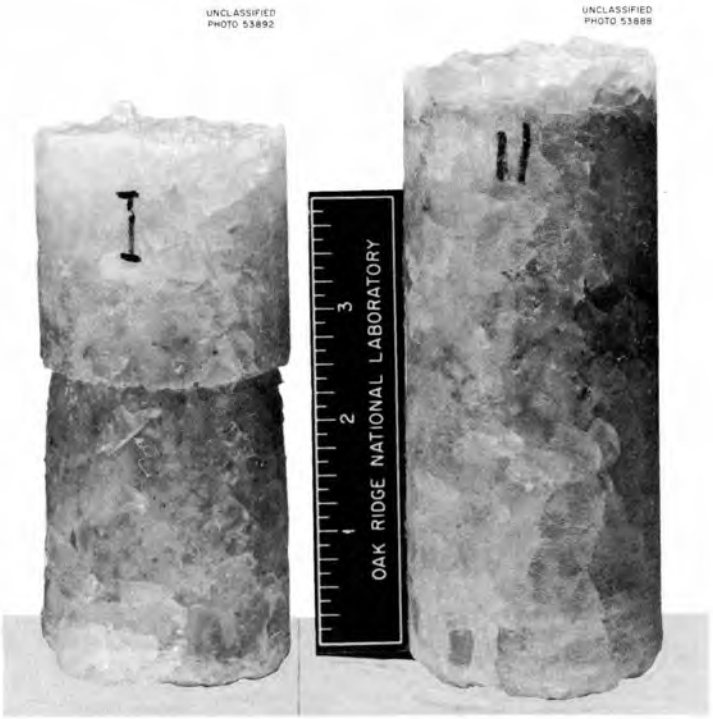

DISTILLED WATER SATURATED NaCl SOLUTION

SATURATED $NaCl-NaNO_3$ SOLUTION SATURATED NaCl - 5*N* HCl SOLUTION

Fig. 1.43. Erosion of Salt Blocks at 25°C.

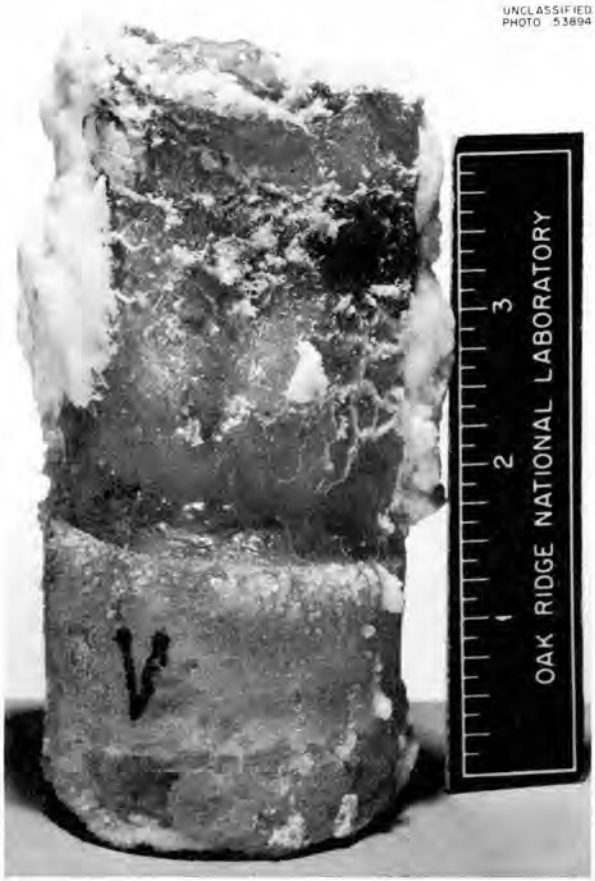

Fig. 1.44. Erosion of Salt Block in Saturated NaCl Solution at 75°C.

Fig. 1.45. Erosion of Salt Block at 75°C with Protective Collar Around Block.

was an unsaturation just at the surface. This results in an erosion at the water line.

In order to test this hypothesis, another test was run in which the salt block was encased in a glass collar, $2\frac{1}{2}$ in. in diameter, which extended $\frac{1}{2}$ in. above the liquid surface. A funnel was inverted over the block in the vapor area so that any vapor condensing in the gas phase would drop back into the solution outside the collar. This prevented any contact between unsaturated solution and the salt block. The solution outside the collar can dissolve some of the salt placed at the bottom to return to a saturated state.

The result of this test is shown in Fig. 1.45. The erosion at the water line is not seen in this case. There is a more pronounced deposit of salt below the liquid level. Some solution of the salt block in the gas phase is also seen. This is attributed to the dissolution of salt by water vapor. This phenomenon is not observed at 25°C, because the vapor pressure of water is too low to cause visible evidence of dissolution.

The behavior of a salt block kept in a system where all three phases are in thermal equilibrium at 75°C is shown in Fig. 1.46. There is no erosion at the water line. There is evidence of an exchange of salt between the solid and liquid phases, since the solid in the portion below the water line has become more white and appears to be more uniformly crystalline than that in the vapor area. The salt in contact with the vapor phase shows signs of partial dissolution, but the degree of dissolution is much less than when the solution alone was heated.

When the liquid phase alone is heated, as is the case with a high-level waste solution, changes in salt concentration at the liquid-vapor interphase cause salt deposition when the solution is temporarily oversaturated and dissolution of salt from

Fig. 1.46. Isothermal Erosion at 75°C.

the solid phase at the junction of the solid-liquid-vapor phases when unsaturated condensate returns to the liquid surface. Water vapor dissolves salt that is in contact with the vapor at a rate that is accelerated by temperature, but this rate is less rapid when all three phases are in thermal equilibrium. When the solution is maintained at a temperature greater than that of the environment, condensation of vapor results which is followed by cavity deformation in the areas in contact with both the vapor and liquid phases.

Storage in Crushed Salt. – Radiolytic studies now under way indicate that radiolysis may be minimized by storing the waste solutions in the interstices of crushed salt. The results of a cavity stability study of this type of disposal are shown in Fig. 1.47. No changes in the wall of the block either

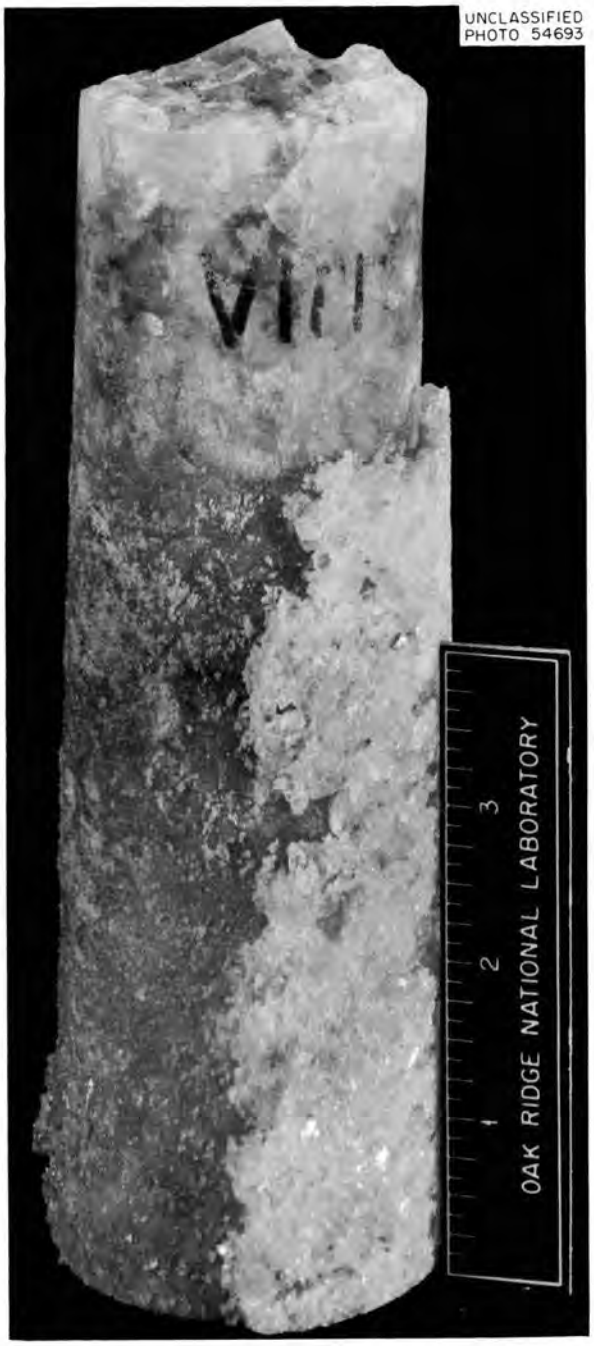

Fig. 1.47. Erosion in Crushed-Salt Solution Storage.

in the liquid or vapor area are apparent. The liquid level at the termination of the test had dropped to about 80% of the original level. The lost liquid was distributed throughout the salt layer over the liquid. One of the mechanisms of water movement evidently was vaporization followed by condensation

on the cooler salt. There was considerable cohesion of the original loosely packed particles which could have resulted from a partial solution of salt followed by drying, so that neighboring particles were fused together. Capillary forces must also come into play, because the face of the block, as well as areas of the crushed salt, are mottled by the color of the synthetic waste solution up to the upper level of the crushed salt. To date this study indicates that very little cavity alteration can be expected in this type of disposal.

Off-Gas Studies

Studies on the radiolytic decomposition of synthetic waste solutions have been continued using a Co^{60} source. Synthetic Purex waste partially neutralized to 1.2 *M* acid and formaldehyde-denitrated Purex (0.5 *M* acid) were used in order to avoid the possibility of chemical gas production.

A waste solution kept in a confined system will approach a steady-state condition where the recombination of product gases balances the radiolytic dissociation and maintains this condition over wide dose range. This steady state is attained at a pressure which varies with the composition of the solution and is of the order of 3–10 atmospheres. It is not feasible to maintain a pressure head of a few atmospheres in salt structures over long periods of time; therefore, containment in closed systems with the expected pressure buildup has to be ruled out. It has been found that a hydrogen atmosphere over the solution will reduce the steady-state pressure to the atmospheric level, but this too is impractical. The presently known recombination catalysts increase their efficiency with increasing pressure, and the minimum pressure at which favorable rates of recombination are promoted are again too high for use in salt structures. At the present time, therefore, the containment of liquid wastes in salt cavities can be expected to result in the production of a steady stream of radiolytic gases, principally hydrogen and oxygen.

In a different approach to minimizing radiolysis, the effect of suspending the waste solution as a surface film on crushed salt was studied. Waste solution was poured over crushed salt in the ratio of one milliliter of waste to 5 g of salt. The salt and solution were contained in an irradiation tube of the type shown in Fig. 1.48. Upon exposure to Co^{60} radiation, no pressure buildup was seen as

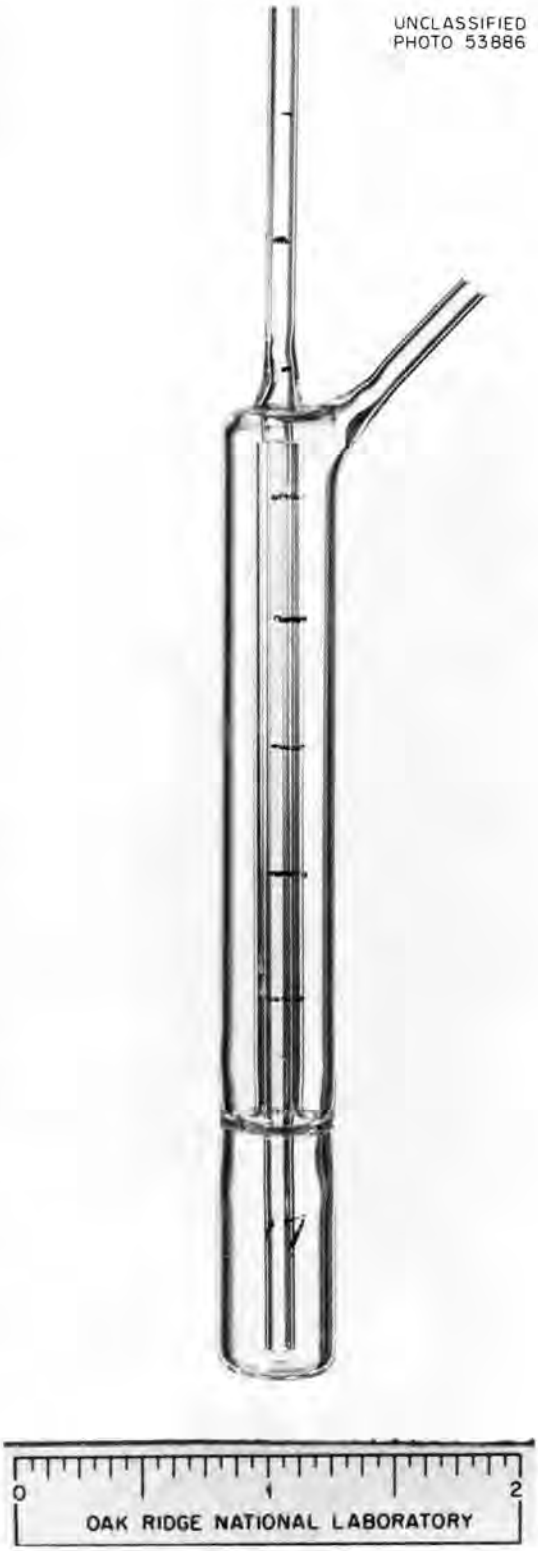

Fig. 1.48. Radiation Cell, 5-ml Capacity.

long as the liquid remained suspended on the solid phase. As the dose approached 10^9 rads, a liquid phase was found to form over the solid salt layer in most of the tubes. This phase separation was accompanied by a buildup in pressure. In order to minimize possible wall effects, the same irradiation was repeated using larger tubes containing five times more material. The same behavior was observed, which strengthens the thought that phase separation is more closely tied in with radiation effects than container wall effects. Varying the particle size caused no change in the radiolytic process. When coarse salt particles ($\frac{1}{4}$-in. mesh) were used, there were relatively large volumes of free solution in the voids between the particles. Despite the existence of such locales of free solution, no radiolytic pressure buildup was observed as long as the free liquid was overlain by a layer of salt.

When waste solution was sorbed in the lattices of vermiculite and attapulgite, a similar radiolytic behavior was observed. The maximum pressure buildup was 20 mm Hg at 10^9 rads.

The work thus far has been limited to the effects of gamma radiation from an external Co^{60} source. Studies are now under way using Pu^{235} as an internal alpha source. Hot-cell experiments using radioactive cesium and strontium are also planned.

Test of New Concepts

This test ("Room and Puddle") was designed to provide information which will assist in evaluating the feasibility of storing liquid radioactive waste in mine rooms with recessed floors. It is envisioned that in such an operation a thin layer (perhaps a foot thick) of crushed salt would be placed in the floor recess and waste piped in to fill the voids in the crushed salt. The entryway would be sealed before introduction of the waste, and the only penetration would be lines for waste injection and off-gas removal. Two possible modes of operation are: (1) no off-gas flow other than that caused by pressure buildup in the room and (2) off-gas flow augmented by external means. In the first case, there may be alteration of the cavity due to the evaporation-condensation-dissolution-recrystallization process. In the second case, the off-gas system will continuously remove the vapor, thus preventing cavity alteration and resulting in a solid waste. The condensate from the off-gas would be expected to be orders of magnitude less active than the original waste and might be disposed of in various ways. A third, and perhaps more promising, mode of operation would be to place a layer of water-absorbing material on top of the crushed salt. Assuming no chemical or radiolytic gases, the off-gas system would thus have to handle only thermal expansion gases, and cavity alteration would be prevented.

For the test an 18-in.-square horizontal cavity was cut into the face of a pillar to a depth of 24 in. Then, starting 6 in. in from the face, the floor of the cavity was recessed to a depth of 5 in., producing a recess with dimensions 18 × 18 × 5 in. The cavity recess was filled with crushed salt ($\frac{1}{8}$- to $\frac{1}{4}$-in. size), having a void volume of approximately 40%, and 2 gal of salt-saturated 3.5 *M* acid Purex waste added, bringing the liquid level up to approximately $1\frac{1}{2}$ in. below the top of the recess. A salt block was then sealed into the entry hole with a fine salt mortar. The only opening was provided by a $\frac{1}{2}$-in. polyethylene tube which vented the off-gas into a soda-lime trap. The solution was heated electrolytically by means of two comb-type graphite electrodes, with six teeth each, located on opposite sides of the cavity.

The test was operated for $4\frac{1}{2}$ months, with the waste temperature in the center of the recess maintained between 80 and 90°C; however, on the third night of operation, an increased supply voltage allowed the waste to boil (107°C was recorded). A small amount of solution leaked out of the wall below the cavity, presumably due to the presence of blast cracks, and a smaller amount came out around the bottom of the block, probably due to the boiling. An examination of the soda-lime from the off-gas trap, after termination of the test, showed no indication of color and that only a very small amount of water had escaped the cavity via the off-gas line. The only change in cavity appearance was the presence of small stalactites and stalagmites. There appeared to be only a very slight general surface erosion with no pitting effects. Thus, the storage of liquid waste in granular-salt-filled floor recesses appears to be feasible.

DISPOSAL IN DEEP WELLS

W. de Laguna D. G. Jacobs

Disposal of Radioactive Waste by Hydraulic Fracturing

The purpose of this investigation is to determine the feasibility of disposing of liquid radioactive waste by mixing it with cement or some other hardening agent and then injecting it, while still fluid, deep into a bedded rock by pumping it down a specially constructed well. The pressure developed at the bottom of the well forces the rock to fracture and separate, after which the waste-cement mixture flows out into the rock in a thin sheet where it hardens. Two years ago a preliminary field experiment was conducted by pumping some 27,000 gal of cement grout into a local shale formation at a depth of 300 ft.

The second experiment in hydraulic fracturing was carried out early in September of 1960 very much as planned.[53] A total volume of 91,567 gal of grout containing 222 tons of cement, 12,500 lb of bentonite and 25 curies of Cs^{137} was injected into the shale at a depth of 934 ft on September 3d, and a second batch of 132,770 gal containing 416 tons of cement, 17,000 lb of bentonite, 25 curies of Cs^{137} and about one curie of Co^{60} was injected into the same well at a depth of 694 ft on September 10th. This work was performed under an ORNL subcontract by the Halliburton Company of Duncan, Oklahoma. The pressures required were somewhat higher than anticipated; 1700 to 2000 psig (surface) for a pumping rate of up to 150 gpm for the first injection, and 2000 to 2300 psig for a pumping rate of up to 300 gpm for the second injection. These pressures are more than the static weight of the overburden and, even allowing for friction losses, it is probable that some force was required to bend or compress the overlying rock as well as to lift it. Each injection required 11 hr of pumping although they could have been made more rapidly.

Precise measurements of the elevations of a net of bench marks before and after each injection showed a clear pattern of uplift on each occasion of up to about $\frac{1}{8}$ in. and extending out after the first injection to distances of from 350 to 750 ft and after the second injection to distances of from about 700 to 1000 ft. Precise measurements were also made of the very slight tilting of the land during each of the injections. These surface measurements were made by the U.S. Geological Survey.

Provision had been made to measure separately the fluid pressure in each of the two grout sheets following the injections. The pressure in the lower sheet fell from 575 psig (surface) on September 10th, to 380 psig on October 12th, due presumably to a very slow loss of water to the shale formation immediately adjacent to the grout sheet. The pressure in the upper sheet, which was 580 psig 12 hr after the injection had ended, fell to 225 psig by October 5th, also presumably as the result of a slow loss of water to the shale. Direct communication between either of the grout sheets and the surface would, of course, have produced a much more rapid drop in pressure, and, as the grout had hardened a few hours after the injection had stopped, the observed drops in pressure represent a relatively small fluid loss.

By the end of June 1961, a total of 18 test wells, varying in depth from 714 to 1035 ft, had been drilled in an effort to determine the extent, depth, and thickness of the two grout sheets. These wells were located from 100 to 600 ft from the injection well. The rocks present in the area consist, from the surface down, of about 300 ft of thin-bedded and somewhat shaly limestone, which grades down into interbedded limestone and shale about 350 ft thick, this underlain by very thin-bedded red shale 300 ft thick, and at the bottom, at a depth of about 950 ft, at least 40 ft of dense, hard, light-gray quartzite. The two grout sheets were both injected into the thin-bedded red shale, the upper one at 694 ft, about 58 ft below the lowest bed of limestone which forms a recognizable horizon marker, and the lower sheet, at 934 ft, about 20 ft above the quartzite which is also easily recognized. Two types of drill bit were used, a tri-cone bit which cuts 10 to 20 ft an hour in shale or limestone, but which does not give a rock core, and a diamond coring bit, which will cut 2 to 4 ft an hour. Because of the difference in cutting rates an attempt was made in each hole to drill down with the tri-cone bit to a point just above the upper grout sheet, then core through the grout sheet in order to determine its thickness, then again drill with the tri-cone bit to a point just above the lower grout sheet which was cored in its turn. The holes were completed by

[53] E. G. Struxness *et al.*, *Health Phys. Div. Ann. Progr. Rept. July 31, 1960*, ORNL-2994, p 134.

extending them down a few feet into the quartzite largely for purposes of stratigraphic correlation on which an analysis of the structure depends.

In a disappointingly large proportion of the early holes the drilling was carried down through one or even both of the grout sheets with the tri-cone bit before the coring bit was put on. Although the stratigraphic correlations and analysis of the structure have not yet been completed it is apparent that the injection well, quite by chance, was located in a narrow down-folded or down-faulted block, at least as represented by the position of the surface of the quartzite. This structure extends up through but largely dies out in the 300 ft of overlying red shale, and appears to be represented by rather minor variations in the position of the lowest limestone bed. However, this structure, which in the upper part of the red shale is probably a fold, served to deflect the upper grout sheet upward about 35 to 40 ft. Because the structure, whether fold or fault, is more pronounced in depth, the lower grout sheet was deflected upward about 80 ft. In each case this was enough to upset calculations as to the expected depths of the sheets, and drilling in some of the first holes was carried below the sheet with the tri-cone bit. The only loss, however, was an inability to determine the detailed structure of the sheet and its thickness. The position of the sheet, and the possible presence of multiple sheets if they are not too close together, can be determined by a gamma-ray log of the hole whether a core is recovered or not. The gamma-ray log also distinguishes between shale and limestone or quartzite on the basis of their natural radioactivity which depends largely on their potassium content. It is possible to trace some individual beds with the gamma-ray logs and so map the underground structure, although not always in as much detail as could be desired.

The down-folded or down-faulted block in which the injection well was by chance located was only some 200 ft wide, and the upward deflections referred to above took place within 100 ft or less of the point of injection. Out beyond this, to a distance of between 500 and 600 ft, the upper grout sheet followed very much the same stratigraphic horizon and was found at approximately the depths anticipated. This was true also of the lower sheet which has been found out to a distance of 400 ft from the injection well.

The structures within the shale not only deflected the grout sheets upward a short distance but also appear to have determined the general direction of easiest relief and therefore the general direction in which each sheet extended outward. For the upper sheet this was to the east and northeast, and for the lower sheet to the north and possibly the northwest, although the drilling has not yet been completed and the full extent of the sheets remains to be defined.

One point, however, has already been clearly established and that is the poor correlation between the amount and extent of the observed vertical uplift of the land surface and the thickness and extent of the grout sheets. In several places cores of the upper grout sheet show that it consists at these points of four sheets with a total thickness of $\frac{1}{2}$ in., while the surface uplift at these points measured only 0.1 in. or less. On the other hand, the surface uplift extended in all directions out beyond the limits of the grout sheets and is much more regularly and symetrically arranged around the injection well than are the grout sheets. It is clear from this data and also from the magnitude of the injection pressures required, that the deformation on the rock is, in part at least, the elastic response of a body which has some shearing strength. Under these circumstances the surface uplift is a poor guide to the location and extent of the grout sheet, and it is not possible to map the position and area underlain by a grout sheet from surface measurements.

With this possible exception the second fracturing experiment appears at this stage to have given results favorable to the possibility of actually disposing of radioactive waste at Oak Ridge by hydraulic fracturing. We now know that it is possible to inject into the shale, at depths up to at least 1000 ft, individual batches of liquid-cement mixtures of over 100,000 gal, and that the fractures formed by the injection, even when located in relatively unfavorable local structures, extend outward laterally and show no inclination to break up toward the surface even when forced upward for short distances by sharp folds or faults. This is what was hoped might be the case, and there is no serious doubt that completion of the drilling now in progress will confirm this opinion.

Because the method shows such practical promise three further lines of investigation have been

initiated. At the request of the Atomic Energy Commission the American Petroleum Institute arranged a meeting between representatives of the petroleum industry and of the Oak Ridge National Laboratory to discuss possible programs for research and development work by certain oil-company laboratories to find mixes of waste, clay, and cement which would be suitable for use in waste disposal by hydraulic fracturing. It is expected that suitable arrangements for this work can be made shortly. Second, a deep test well has been started at ORNL to core the rocks below the quartzite to a total depth of about 3000 ft to see if any of these deeper formations, which are not exposed at the surface, would be suitable for this method of waste disposal. Third, the Laboratory's Engineering and Mechanical Division has prepared a conceptual design of a possible waste disposal plant to handle the current medium-level waste stream by hydraulic fracturing, largely for purposes of a budget estimate. The cost of the complete plant was estimated at $860,000.

The Laboratory is at present producing an average of 7,000 gal a day of medium-level waste, which is to be reduced in volume by a factor of 10 by evaporation. In two months this would result in some 42,000 gal of waste concentrate containing about 1800 to 2000 curies of activity. This, mixed with clay, cement, and possibly other additives, would make up a total volume of some 60,000 gal. This would be injected as a single sheet at the bottom of the disposal well, which would then be plugged back upward a distance of about 10 ft with neat cement. Two months later the next batch would be injected 10 ft above the first, and so on, until five years later, 30 individual batches would have been injected at 10-ft intervals into the 300 ft of suitable shale.

If the deep test hole shows additional suitable rock in depth, the life of the original disposal well can be correspondingly increased if this should appear desirable. In any case when the first well must be abandoned several more, drilled some 600 or 700 ft from the first, can be each used in turn, and eventually the injection plant itself can be moved to a new location. Initially the disposal cost will probably fall between fifty cents and a dollar a gallon of waste concentrate although this will depend very largely on operating, maintenance, and amortization costs which have not yet been determined. This is, however, the total and final cost for permanent disposal. It should not be compared directly with such alternatives as tank storage or even conversion to a solid, unless the cost of storing and monitoring the solid is also included.

Injection of Radioactive Waste into Deep Permeable Formations

A number of problems likely to be encountered in the discharge of radioactive waste solution to deep permeable formations have been noted by the American Petroleum Institute's Subcommittee on Disposal of Radioactive Waste.[54] In order to avoid unnecessary duplication in the solution of these problems, preliminary discussions have been held with representatives of the University of California and the U.S. Bureau of Mines regarding establishment of cooperative programs with consistent objectives and comprehensive consideration of the problems involved.

The University of California group, under the direction of W. J. Kaufman, has made substantial progress in studies of the theoretical and practical aspects of radionuclide dispersion in porous media under various operating conditions. The U.S. Bureau of Mines' program, directed by J. W. Watkins and J. B. F. Champlin, has been primarily concerned with the physical aspects of injection, as limited by the presence of suspended solids and flocs in the discharge solution or by chemical reactions in the receiving formation.

The laboratory and field measurements necessary for successful planning, operation, and evaluation of a field test are being outlined by representatives of these agencies.

Comparison of Ion Exchange Chromatography in Linear and Radial Flow Systems. – A mathematical treatment of the concentration history of the effluent from an ion-exchange column operated under conditions of linear flow has been given by Glueckauf.[55] In the discharge of radioactive waste solutions to deep permeable formations, however, the outward flow from an injection well is more closely described by radial flow than by linear flow. We are

[54] T. V. Moore (Chairman) *et al.*, *Problems in the Disposal of Radioactive Waste in Deep Wells*, Division of Production, American Petroleum Institute, Dallas, Texas (October 1958).

[55] E. Glueckauf, *Trans. Faraday Soc.* 51, 34 (1955).

further concerned with the buildup of activity on the sorbent phase at various distances from the injection well.

Glueckauf's solution of the mass balance equation for the continuous flow of solution with concentration c^0 through a previously empty column is:

$$c/c^0 = q/q^0 = \frac{1}{2} - \mathcal{A}\left\{\frac{N-M}{\sqrt{M}}\right\} + \left[\exp(2N)\right]\left[\frac{1}{2} - \mathcal{A}\left\{\frac{N+M}{\sqrt{M}}\right\}\right], \quad (1)$$

where

$$\mathcal{A}\left\{y\right\} = 1/\sqrt{2\pi}\int_0^y \exp(-y^2/2)\,dy,$$

c' = concentration of solute in solution at point x,

q = amount of solute per unit volume of sorbent at point x,

q^0 = amount of solute per unit volume of sorbent at equilibrium with solution of concentration c^0,

$N = x/\Delta x$, the number of theoretical sorbent volumes up to point x,

$M = v/a\Delta x$, number of theoretical plate elution volumes contained in the volume of solution injected,

$\bar{x}$ = point at which $q = q^0/2$,

v = volume of solution injected into the column.

For $N > 3$, the second term of Eq. (1) is negligible, and in a linear flow system $N = b/\Delta b$ and $M = \bar{b}/\Delta b$, so we can write

$$q/q^0 = \frac{1}{2} - \mathcal{A}\left\{\sqrt{M}\left(\frac{b-\bar{b}}{\bar{b}}\right)\right\}, \quad (2)$$

to describe the concentration of activity along a linear column. $\sqrt{M}$ is directly proportional to $\sqrt{v}$, and $\bar{b}$ is directly proportional to v; so Eq. (2) can be expressed:

$$q/q^0 = \frac{1}{2} - \mathcal{A}\left\{\frac{k_b}{\sqrt{v}}(b-\bar{b})\right\}. \quad (3)$$

From this equation we see that the general concentration gradient along the sorption column diminishes with increased injection of solution.

In the case of radial flow, $N = r/2\Delta r$ and $M = \bar{r}/2\Delta r$. M and $\bar{r}$ are both directly proportional to the volume of injected solution. Thus, we can write, for radial flow:

$$q/q^0 = \frac{1}{2} - \mathcal{A}\left\{k_r(r-\bar{r})\right\}. \quad (4)$$

Once the concentration gradient is established in a radial flow system [that is, when the exponential term of Eq. (1) becomes negligible], it is maintained with continued injection of solution.

If the movement of liquid in a deep-well disposal operation can be described by a radial flow system, a monitoring well in line with a pressure relief well, but near the injection well, could be used to observe the buildup of activity in the formation. Activity buildup at greater distances from the point of injection could be estimated from simple extrapolations, provided the formation characteristics remain the same at increased distances from the injection well. In the case of a nonhomogeneous formation, deviation from the ideal behavior must be accounted for in terms of solution travel-time distribution; the solution travel-time distribution to a given point can be estimated by observing the arrival of tritiated water at that point.[56] The arrival of various radionuclides can then be estimated after taking into account their retention by ion-exchange processes in the formation.

EVALUATION OF ENGINEERING, ECONOMICS, AND HAZARDS

R. L. Bradshaw W. B. Nix

Hazards of Tank Storage

A previous study[57] of the hazards of storing high-activity wastes in steel-lined concrete tanks showed that the apparent safety could be misleading. The limited lifetime of the tanks, plus the large volume of highly concentrated radionuclides could lead to a serious contamination hazard.

[56] W. J. Kaufman *et al.*, *J. Water Pollution Control Fed.* 33(1), 73 (1961).

[57] E. G. Struxness *et al.*, *Health Phys. Div. Ann. Progr. Rept. July 31, 1959*, ORNL-2806, pp 106–17.

Since the previous report, a more thorough examination has been made of tank hazards, especially with respect to the manner and probability of tank failure. Also examined was the possibility of predicting the manner in which released wastes would be dispersed throughout the environment; on the surface, in the atmosphere, and in ground and surface waters. The emphasis of this report is on methods of analysis applicable to any site. The various factors affecting tank hazards are discussed, and, where possible, typical calculations are given.

Inherent Hazards. – The first phase of a tank hazards evaluation concerns the waste itself and the probability of tank rupture. Obviously, if the tank and cooling system maintains its integrity there is no hazard. However, it is not expected that any tank will have a lifetime as long as the wastes contained in it. For instance, according to the previous study[57] a 4.5×10^4-gal tank would still contain a total of 10^3 curies of activity after more than 10^6 yr. In contrast, tank lifetime is assumed, in most studies, to be about 50 yr.

Characteristics of the waste tending to increase the probability of tank rupture are its corrosiveness, radiation field, and self-heating. The age of the nuclear industry has not been sufficient for development of accurate information on tank mortality. Data from the oil industry are inapplicable due to the differences in tank construction and contents; however, experience with fuel reprocessing plants indicates that acid Purex wastes will corrode stainless-steel-lined tanks only about one mil per year.[58] Corrosion by neutralized wastes would be expected to be much less. Structural weakening by the radiation field, at this time, eludes prediction. Only self-heating is immediately amenable to analysis.

To illustrate the calculation of temperature rise due to self-heating, assume a 45,000-gal tank receiving the high-activity wastes from the nuclear industry predicted for 1970. Results of the calculation of radionuclide content and power generation rate were reported by Emerson[57] and are repeated here as Figs. 1.49 and 1.50. Using this power generation rate as a function of time, Birch's equation for a sphere,[59] and several simplifying assumptions, the temperature rise in a tank was calculated.

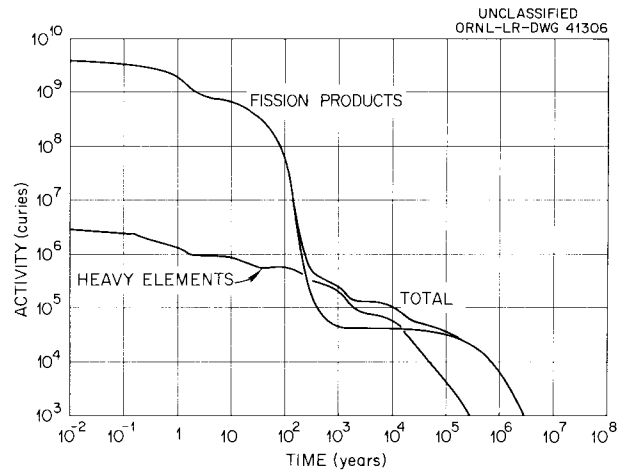

Fig. 1.49. Fission Product and Transuranic Activity.

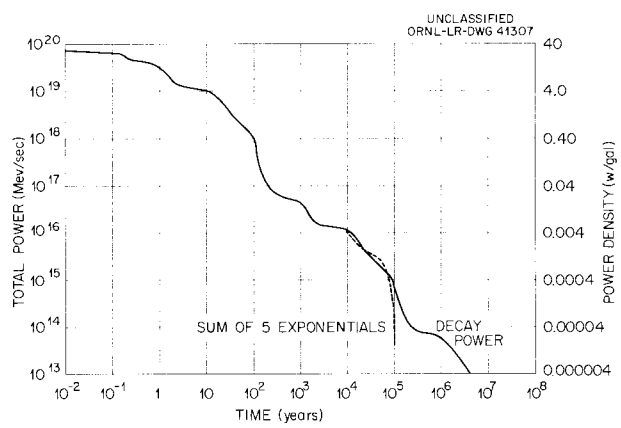

Fig. 1.50. Heat Source from Radioactive Decay.

The tank is assumed to be spherical with uniform temperature inside, and embedded in an infinite conducting medium with thermal properties those of the average of the earth's crust (conductivity = 0.004 cal $(°C)^{-1}$ cm^{-1} sec^{-1}, diffusivity = 0.012 cm^2/sec).[60] The waste is presumed to be cooled until, at some time after filling, the cooling system breaks down or is deliberately shut down. The temperature will then rise. Figure 1.51 shows the length of time required for the waste to boil as a function of the age of the waste and the difference between cooling temperature and boiling point (100 – 114°C).

[58] F. M. Empson, personal communication, 1961.

[59] F. Birch, *Thermal Considerations in Deep Disposal of Radioactive Wastes*, NAS-NRC 588, p 18 (1958).

[60] C. D. Hodgman (ed.), *Handbook of Chemistry and Physics*, 39th ed., p 2255, 2104, Chemical Rubber Publishing Co., Cleveland, 1957.

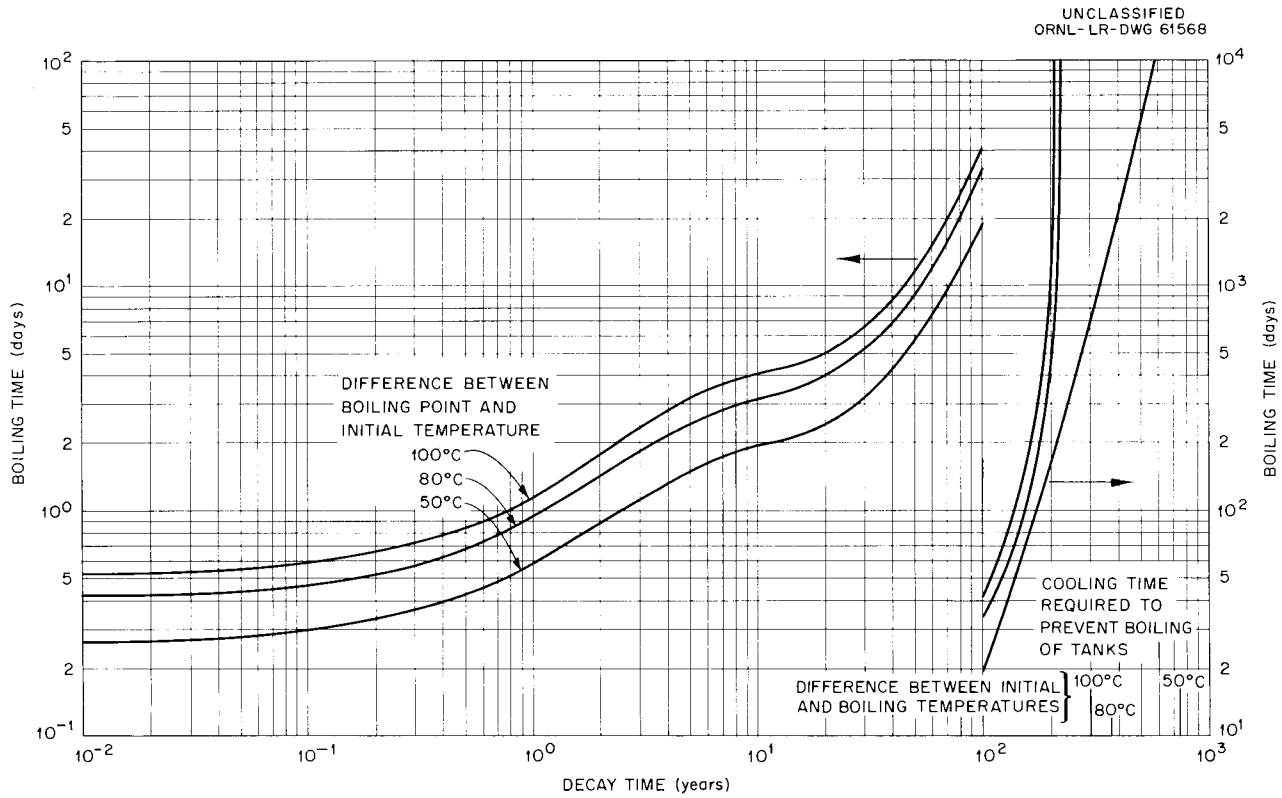

Fig. 1.51. Time Required for Waste to Boil After Cooling System Failure.

It is apparent that the most danger of boiling occurs in the first several hundred years of storage. For instance, if wastes are cooled to 80°C below boiling (approximately 20°C, probably the average ambient temperature) and the cooling system breaks down at age 50 yr, the contents will boil in 2.4 days, a relatively short time in which to correct the situation. Also shown by Fig. 1.51 is the length of time the wastes must be cooled to prevent boiling. This was calculated, again with Birch's equation. This cooling time is such that, if the cooling system is turned off permanently, the steady-state temperature rise will just barely reach the boiling point.

It has been implicitly assumed throughout this discussion that, in the event of boiling, the tank will be forced to rupture. The probability of tank rupture due to boiling decreases with increasing age of the waste. Counteracting this trend is the increasing decrepitude of the tanks with age. In addition to the weakening due to corrosion and radiation field, the tank will become weakened by settling, cracking, and weathering normal to concrete structures. It seems reasonable, therefore, to expect the maximum probability of waste escape at some time toward the end of a tank lifetime and early in the life of the wastes.

Provision for off-gas and pressure-relief mechanisms will alleviate the danger of pressure rupturing the tank. Still, if boiling occurs in the first hundred years, boiling of a full tank should be violent enough to force some of the liquid out of the tank.

There are other possibilities for release of tank contents, most of them rather catastrophic. Coming to mind are seismic disturbances, sabotage, physical shock due to explosions other than at the tank, tidal waves near oceans, etc. The probability of seismic rupture can be estimated from seismic tables for the given tank site. The others present more difficulty. Probably, there would be no small leaks due to this last group of causes; disturbances large enough to break the tank walls would release a large fraction of the contents.

Environmental Contamination. – Upon rupture of the storage tank, the released waste can be distributed in three general media. The waste may be dispersed into the atmosphere; into the ground, thence into ground and surface waters; or, by a

relatively direct route, into surface water. Atmospheric contamination represents the case of most rapid contact with the population, but also, due to dilution and precipitation, the most rapid dimunition of hazard. Spillage into the ground can form an external hazard if, by capillary action or other mechanism, the wastes reach the surface of the soil. Such wastes will be sorbed to some extent by soils and will be diluted by ground waters. Surface-water contamination is a direct hazard via drinking water. It is also an indirect hazard due to inclusion of the radionuclides in aquatic food chains.

The problem of atmospheric dispersion has received detailed consideration from groups concerned with release of stack gases and with reactor hazards. The equations used are either those of Sutton's model[61] or the interpolation formula used in Cramer's work.[62] The latter is derived solely from the requirement of mass continuity and a Gaussian distribution function for the concentration. The equation is (including a factor of 2 for reflection in the ground plane):

$$X(x)/Q = (\pi\sigma_y\sigma_z u)^{-1} \exp -\frac{1}{2}(y^2/\sigma_y^2 + z^2/\sigma_z^2) ,$$

where

$X(x)$ = concentration at a distance $x(m)$ downwind from the contamination source, curies/m^3,

Q = rate of contaminant release, curies/sec,

u = wind velocity, m/sec.

The dispersion coefficients, σ_y and σ_z, are both functions of x and of atmospheric conditions. These coefficients have been determined empirically and are summarized by Gifford.[63,64]

Because of the availability of meteorological data for ORNL, this site was chosen to illustrate an atmospheric dispersion calculation. Wind velocity is chosen to be 5 miles/hr, approximately the median annual velocity for ORNL.[65] The most probable wind direction is along the axis of Bethel Valley.[66] The vertical distance, z, was chosen to be 66 in. (1.68 m) to give the concentration at the height of an average man's head. Figure 1.52 shows a plot of $X(x)/Q$ calculated with these assumptions. In this form, the plot is independent of the rate of contaminant release and is expressive of the amount of atmospheric dilution.

The quantity Q may be estimated for the case where the waste is being vaporized by its own heat. It will be assumed for calculation purposes that the vapor is not recondensed by the tank soil-cover. Assume again the 4.5×10^4-gal tank with its radionuclides and heat load calculated by Emerson.[57] Suppose the tank contents are allowed to boil 40 yr after filling. At this time, the total heat power is 1.83×10^5 cal/sec. It is calculated that approximately 60% of the power goes into heating the waste.

[66] *Ibid.*, p 565.

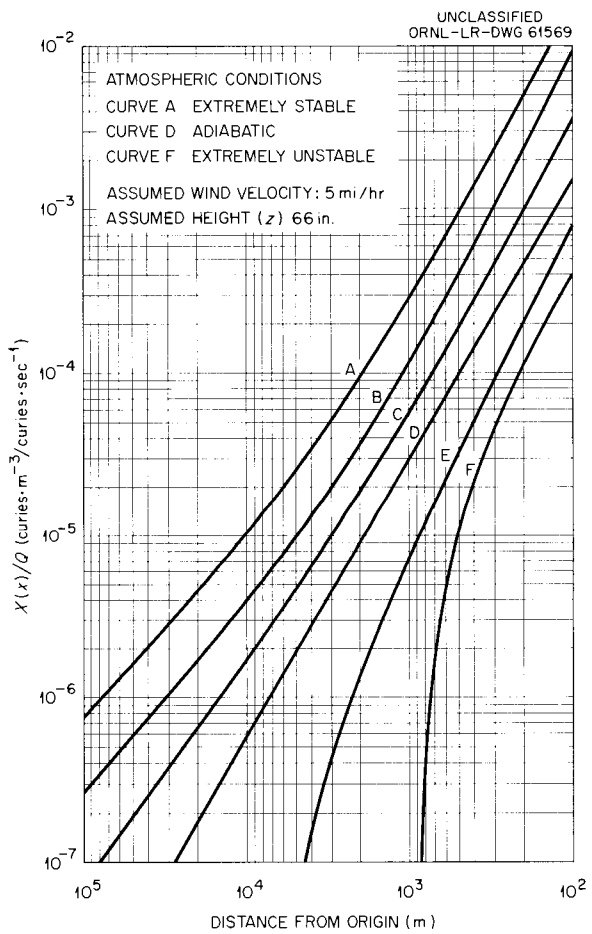

Fig. 1.52. Atmospheric Dispersion of Contamination.

[61] O. G. Sutton, *Proc. Roy. Soc. (London)*, **135A**, 143 (1932).

[62] H. E. Cramer, *Bull. Am. Meteoral. Soc.* 40(4), 165–71 (1959).

[63] F. A. Gifford, *Nuclear Safety* 1(3), 56–62 (1960).

[64] F. A. Gifford, personal communication, 1961.

[65] J. Z. Holland *et al.*, *A Meteorological Survey of the Oak Ridge Area*, ORO-99, p 577 (1953).

Let

D = power density going into heating the waste
$= 6.7 \times 10^{-4}$ cal cm^{-3} sec^{-1},

H = heat of vaporization
$= 6.5 \times 10^{2}$ cal/cm^{3} (estimated).

The fraction of the volume, V, of waste evaporating per unit time will be

$$f_v = D/H$$
$$= 3.7 \times 10^{-3}\ \mathrm{hr}^{-1}.$$

Then

$$Q = -\alpha\ dV/dt$$
$$= \alpha f_v V \quad ,$$

where α = specific activity, curies/cm^3. Therefore

$$Q = \alpha f_v V_0 \exp(-f_v t) \equiv Q_0 \exp(-f_v t)\ ,$$

where V_0 = original total volume of waste. From Emerson's data

$$\alpha V_0 = 6.4 \times 10^{5} \text{ curies (transuranics)}$$
$$= 2.9 \times 10^{8} \text{ curies (fission products).}$$

Therefore

$$Q_0 = 6.6 \times 10^{-1} \text{ curie/sec (transuranics)}$$
$$= 3.0 \times 10^{2} \text{ curies/sec (fission products).}$$

Using the MPC$_a$'s for a 168-hr/week exposure, it is found that

$$\Sigma_i\ Q_{0i}\,(\mathrm{MPC}_a)_i^{-1} = 1.1 \times 10^{12}\ \mathrm{m}^3/\mathrm{sec}\ ,$$

approximately 72% of this value being from Sr^{90}. Looking again at Fig. 1.52, one sees that under adiabatic conditions (curve D), air contamination 28 km downwind will be, at its maximum, about 1.1×10^{5} MPC. This number is expected to be an overestimate. The assumption of no condensation on the way to the surface is improbable. Also expected is a large, rapid fallout of the activity onto the surface. Prediction of the magnitude of these two events has not been attempted because of their lack of definition.

The previous tank hazards report discussed the consequences of spillage into the ground with contamination of ground waters. This problem was discussed in general terms with hydrological systems of assumed simple geometry. Since that time no known methods have been developed to analyze dilution and soil sorption processes for arbitrary conditions. Analysis of this portion of the hazard has, thus, been frustrated. So, also, has the problem of surface water contamination. Since the likelihood of a direct channel to surface waters is highly unlikely, prediction of surface water contamination is dependent on the ground-water movement. Much further study is needed on these two problems.

Economics of High-Level Waste Treatment and Disposal

A study has been undertaken in cooperation with the ORNL Chemical Technology Division to evaluate, first from economics and later from hazards standpoints, the various methods of high-activity liquid and solid waste disposal being investigated by the Laboratory. As a necessary part of this study, the various operations leading to those ultimate disposal methods will also be evaluated.

In the study, the disposal operation is assumed to be handling the high-activity waste output from a 6-ton/day fuel reprocessing plant which processes 1500 metric tons per yr of uranium converter fuel with a burnup of 10,000 Mwd/ton and 270 tons per yr of thorium converter fuel with a burnup of 20,000 Mwd/ton. This hypothetical plant would be processing all the fuel from a 15,000 Mw$_e$ nuclear economy which may be in existence in the 1970's.

Handling the wastes in either the acidic or neutralized state will be considered. Purex waste is assumed to be 50 gal/ton acidic or 60 gal/ton neutralized. Thorex is 400 gal/ton acidic and 642 gal/ton neutralized. Decladding and other low-activity wastes are assumed to be treated separately and will not be included in this study.

The preliminary operations to be evaluated are (1) interim liquid storage, (2) conversion to solids by pot calcination, (3) interim storage of solids in pots, and (4) shipment as either liquids or calcined solids.

The ultimate disposal methods to be evaluated are (1) liquids in salt formations, (2) liquids in deep porous formations, (3) liquids in hydrofractures, (4) liquids in tanks, (5) calcined solids in salt formations, (6) calcined solids in vaults, and (7) calcined solids in vertical shafts.

The cost study of interim liquid storage has been completed. Costs for storage of acidic and alkaline Purex and Thorex wastes were estimated for storage

times from 0.5 to 30 yr. Tanks of Savannah River design were assumed, with stainless steel construction for acid wastes and mild steel for alkaline wastes. Tanks and buildings were amortized over a period of 60 yr at 4% interest. Tank farm equipment, such as heat exchangers and cooling towers, was amortized over 20 yr. Total yearly costs, including capital and operating expenses, ranged from $263,000 to $1,214,000 for acidic wastes stored 0.5 to 30 yr and from $199,000 to $619,000 for alkaline wastes stored for the same periods. In terms of cost per unit of electric power, for storage times of 0.5 to 30 yr, costs ranged from 2.0×10^{-3} to 9.3×10^{-3} mills per kwh_e for storage of acidic wastes and from 1.5×10^{-3} to 4.7×10^{-3} mills per kwh_e for alkaline wastes. Details of this study are published in ORNL-3128, "Evaluation of Ultimate Disposal Methods for Liquid and Solid Radioactive Wastes – Part I, Interim Liquid Storage," by R. L. Bradshaw, J. J. Perona, J. T. Roberts, and J. O. Blomeke.

The economic study of the second preliminary step, conversion to solids by pot calcination, has also been completed, and a report is in preparation. Costs of the calcination plant building as a function of cell block size (which varies with different combinations of acid and alkaline wastes and with different calcination vessel sizes) and as a function of shielding wall thickness (which varies according to the length of interim liquid storage) were estimated. Building costs were amortized over 50 yr at 4% interest. Process equipment costs were broken down into two categories and amortized over periods of 20 and 10 yr. Building costs ranged from about $\$1.5 \times 10^6$ to $\$4 \times 10^6$, resulting in annual costs ranging from $70,000 to $185,000. Total capital costs per year, including process equipment, ranged from about $150,000 to $375,000 per year.

Yearly operating costs ranged from about $600,000 to $1,400,000 (40 to 90 man-years/year plus maintenance and overhead).

Calcination pots were assumed to be 10 ft in length and 6 in., 12 in., or 24 in. in diameter. The number of pots required per year ranged from a minimum of 145 if 24-in. pots were used to a maximum of 9660 if 6-in. pots were used, depending on the waste combinations and cooling times chosen.

Total yearly cost (capital, operating, and pots) of operation of the calcination plant was evaluated for each of 12 waste combinations with up to 9 combinations of pot diameter (a total of 90 combinations) for interim liquid storage periods of 0 to 30 yr. These costs ranged from $\$3.1 \times 10^6$ per year using 24 in.-pots to $\$6.6 \times 10^6$ per year using 6-in. pots, depending on waste and pot size combinations chosen, for 120-day cooled wastes (no interim liquid storage), and from $\$1.1 \times 10^6$ to $\$6.6 \times 10^6$ per year for 30-yr cooled wastes. The corresponding ranges per unit of electric power are 2.4×10^{-2} to 5.0×10^{-2} mills/kwh_e for 120-day cooled wastes and 0.87×10^{-2} to 5.0×10^{-2} mills/kwh_e for 30-yr cooled wastes.

RELATED COOPERATIVE PROJECTS

Geologic and Hydrologic Studies by U.S. Geological Survey

In order to understand the movement of radioactive materials through the environment, it is necessary to know how water, the principal natural vehicle transporting the materials, moves through the environment. Information on the magnitude and variability of stream flow is obtained through operation of gaging stations, where a continuous record of discharge is obtained, and from partial-record, low-flow, and crest stage stations, which supplement the regular gaging station network.

During the past year, the Survey has continued operation of stream gaging stations on the Clinch River near Scarboro, White Oak Creek below ORNL, Melton Branch near White Oak Lake, and the Settling Basin effluent into White Oak Creek, and has reactivated the station on White Oak Creek at White Oak Dam. Operation of these stations provides flow information necessary for the Clinch River Study and waste disposal operation at ORNL.

To obtain a more complete picture of the characteristics of stream flow in the Oak Ridge Reservation, gaging stations were constructed and put into operation on Bear Creek, East Fork Poplar Creek, and Poplar Creek near Oak Ridge during July and August 1960. In addition, 25 sites were selected for a network of partial-record, low-flow, and crest stage stations on principal and selected streams within and adjacent to the ORNL area. These stations will be activated in Fiscal Year 1962.

As part of the fracturing experiment described earlier, under "Disposal in Deep Wells," the Geological Survey determined precisely the elevations of bench marks in the vicinity of the injection well before and after grout injection. The Survey

also provided tiltmeters to measure relative movement of the land surface in the vicinity of the well during the period of injection.

Cooperation of Other Agencies in ORNL Studies

The research and development program of the Radioactive Waste Disposal Section of this Division is of special interest to various public and private agencies. Several study projects provide an opportunity for others to participate both to supplement the Laboratory's research effort and to gain information and experience of value to the other agency. The ways in which another agency may cooperate include assignment of on-loan personnel as temporary additions to the ORNL Staff, performance of specific work under cooperative agreements to augment ORNL programs, work authorized under ORNL subcontracts and performed by the contracting agency, or coordination of related work projects with ORNL projects for the mutual benefit of both.

Clinch River Study. – This is a cooperative study under the guidance of the Clinch River Study Steering Committee which coordinates arrangements for participation of the agencies represented by membership on the Committee. These include, in addition to ORNL, the U.S. Geological Survey, the U.S. Public Health Service, the Tennessee Valley Authority, the Tennessee State Department of Public Health and Stream Pollution Control Board, the Tennessee State Fish and Game Commission, the Divisions of Reactor Development and Biology and Medicine of the U.S. Atomic Energy Commission, Washington, D.C., and the Biology Division of the U.S. Atomic Energy Commission, Oak Ridge Operations. The activities of the Steering Committee, participation by the several agencies, and the results during the past year are presented in a following section of this report ("Clinch River Studies").

Disposal in Salt Formations. – Agencies participating in this program during the past year have included the Geotechnical Corporation of Dallas, Texas, under an ORNL subcontract; the Department of Sanitary Engineering of the University of Texas by cooperative agreement; the Bartlesville Petroleum Research Center of the U.S. Bureau of Mines, Bartlesville, Oklahoma, by cooperative agreement; and the Carey Salt Company of Hutchinson, Kansas, ORNL subcontractor. The results of this cooperative program are given in a preceding section of this report ("Disposal in Salt Formations").

Disposal in Deep Wells. – The *ad hoc* committee of the American Petroleum Institute, formed at the request of the U.S. Atomic Energy Commission to advise on the apparent feasibility of disposing of fluid radioactive waste into deep permeable formations, having submitted its report, is no longer active. However, as the direct result of recommendations contained in the report, several organizations are cooperatively investigating certain aspects of the general problem. At the request of the AEC, the Oak Ridge National Laboratory is informally serving as a coordinator of these efforts.

A subcommittee of the Committee on Research of the American Association of Petroleum Geologists is studying the fifty-odd deep sedimentary basins in the United States to determine those best suited for waste disposal. The U.S. Geological Survey is actively participating in this study. Certain aspects of the problem of basin evaluation, in particular those related to abnormally high or low fluid pressures in the deep formations; have been discussed and studied for several of the deep basins by the Petroleum Research Corporation of Denver, Colorado. The theoretical aspects of fluid dispersion due to flow and ion exchange in permeable media are presently under study at the University of California. Problems of injectivity have been under investigation by the U.S. Bureau of Mines Petroleum Experiment Station at Bartlesville, Oklahoma. Through the combined efforts of these groups, the general program of study recommended by the API committee has been initiated.

Low-Level Waste Water Treatment. – As reported a year ago in the Annual Progress Report of the Division,[67] Dorr-Oliver, Inc., has conducted studies under sponsorship of the AEC and with assistance from the staff of the Radioactive Waste Disposal Section. The proposed studies described in the report last year have been completed, including the quantity and particle-size distribution of suspended solids in low-level wastes at ORNL, the relationship of particle size to activity level, and an evaluation of certain special equipment for improving clarification of the effluent and increasing the the efficiency of plant operation. Results of these studies are to be reported to the AEC, but the types

[67] E. G. Struxness *et al.*, *Health Phys. Div. Ann. Progr. Rept. July 31, 1960*, ORNL-2994, pp 137–46.

of equipment and the preliminary results are summarized briefly in this report under the section on Low-Level Waste Water Treatment.

Visiting Investigators from Abroad

During the year, five "noncitizen guests," doing investigative work at ORNL, were on assignment as temporary members of the research staff of the Section. Three of these, namely, K. T. Thomas of India, S. Amarantos of Greece, and Y. Nakayama of Japan, reported last year, and have completed their assignment.[68] Two other investigators were assigned to the section during the year; namely, Shinji Okuyama of Japan and A. L. Mohan of India. Mr. Okuyama was assigned for approximately four months and worked principally in assembling information regarding regulatory problems related to nuclear energy programs in Japan. Mr. Mohan, assigned to ORNL for approximately six months and still in this Section, is conducting laboratory studies on the removal of ruthenium from solutions by mineral sorption.

Nuclear Safety Review

Two members of the Section served on the staff of *Nuclear Safety* as assistant editor, each for a part of the year. During the year, several individuals in the Section contributed review articles which were published under the category, "Consequences of Activity Release."

Committee Work

American Standards Association. – Two of the staff have served on ASA Sectional Committee N5, "Nuclear Fuel Cycle Engineering," as representatives of professional organizations and of the Laboratory. These and two others of the staff, a total of four, have served as members of ASA Subcommittee N5.2, "Radioactive Waste Disposal," one continuing to serve as secretary of the Subcommittee. One of the four has served as leader and two others as members of Working Group N5.2.2, "Site Selection Criteria." This group is developing information and a descriptive outline or check list of features of nuclear energy sites related to radioactive wastes which should be considered prior to final selection of the site. A statement will be submitted later for consideration and approval by the American Standards Association.

[68] *Ibid.*, pp 141–42.

American Public Health Association Committee on Radiological Health. – As described in the report a year ago,[67] one member of the Section has continued to serve on the APHA Program Area Committee on Radiological Health and has attended two meetings of this Committee. The Committee has: (1) assembled information and is preparing program guides to aid public health departments in dealing with health problems of nuclear energy; (2) reviewed drafts of regulations proposed for adoption by state and local health departments; and (3) held one of its meetings at the University of Chicago to confer on a proposed training program in radiological health for personnel of public health agencies.

ORNL Committees and Special Working Groups. – One member of the Section is serving on the "Laboratory Director's *Ad Hoc* Water Committee." This committee was organized to consider expansion of work at ORNL to cover saline water conversion and to recommend regarding the feasibility of setting up a National Water Laboratory at ORNL. A report on this assignment has been prepared and proposed work programs are being formulated.

Two sanitary engineers of the staff have been designated to provide advisory service to engineering design groups regarding protection of the potable water supply of the Laboratory against "crossover" contamination where it is necessary to lay water mains and waste pipes across one another or in close proximity. Upon request of the design engineers during the year, a number of designs have been reviewed and discussed in the preliminary stages and final plans checked for approval of the methods of protection provided.

Participation in Educational Programs

The Section leader gave two 2-hr lectures in the AEC Fellowship Course in Radiological Physics, conducted by the Education and Training Section of the Division at Vanderbilt University in Nashville, Tennessee. Also during the ten weeks of field training in this course given at ORNL, two students per week were assigned to work one week in the waste disposal section under the supervision of three staff members.

The Section leader participated in the Second Colloquim on Public Health and the Problems of Radioactive Waste Disposal, conducted by the Section of Nuclear Medicine, University of Chicago, November 30 to December 2, 1960. He presented a

lecture and led a detailed discussion on the subject, "Subterranean Disposal of Radioactive Wastes." The announced purpose of these colloquia is to acquaint science writers representing publicity media with the principles of nuclear energy and of public protection against radiation exposure.

In the Health Physics Course primarily for foreign students conducted by the Health Physics Division in the Oak Ridge School of Reactor Technology, five members of the Section gave five lectures and a field tour on radioactive waste problems and waste disposal studies at ORNL. Also the course in physical geology conducted by the Oak Ridge School of Reactor Technology, given again by one member of the waste disposal staff, comprised approximately 30 lectures to the class of about 60 students, some American and some from other countries.

In the short course in health physics for public health personnel, conducted for AEC by ORINS and the Education and Training Section of this Division at ORNL during April and May 1961, seven members of the waste disposal section staff presented lectures dealing with the major aspects of waste handling, treatment, and disposal, dispersion of waste in surface waters, and evaluation of radioactive-waste engineering problems and disposal hazards.

Four lectures and a field tour of the Laboratory's waste disposal facilities and ecological research activities were provided at ORNL by the staff of the Section as part of the course conducted by the U.S. Public Health Service on "Reactor Safety and Environmental Health Problems," in May 1961.

Two staff members gave two lectures on "Radiation Problems Related to Public Health" for the College of Education, University of Tennessee, as part of the program in public health education for teachers.

2. ECOLOGICAL RESEARCH

WHITE OAK LAKE BED STUDIES

S. I. Auerbach

D. A. Crossley, Jr.
H. E. Childs, Jr.[1]
P. B. Dunaway
S. V. Kaye
G. L. Plummer[2]
J. A. Sealander[1]
R. M. Anderson
U. S. Davis, Jr.[3]
V. I. Dodson
L. L. Smith
W. L. Tietjen[2]
D. C. Walton[2]

Research in White Oak Lake bed and the surrounding environs takes advantage of the presence of mixed radioisotopes, both as a source of radiation and as a tool for studying the behavior of these radioelements in the environment. This research encompasses the following phases: (1) movement of mixed radionuclides from soil to vegetation and related applications, (2) the ecological relationships between insects and plants utilizing the contaminants as tracers, (3) equilibrium relationships between radioisotopes in herbivorous mammals and their food, and (4) effects of chronic radiation upon native mammals.

Changes in Vegetation

Knowledge of changes in the plant and animal communities comprising a part of the landscape is prerequisite to continuing studies of the plant and animal populations contained therein. After the draining of White Oak Lake in October 1955, plant succession and concomitant animal succession was rapid for approximately three years. The major features of these successions during the years 1956–58 have been reported previously.[4–7] During 1956–58 detailed studies on changes in plant ecology of the lake bed have been conducted by the Botany Department, University of Tennessee, under contract with the AEC. The purpose of the present report is to summarize the vegetational analyses conducted by ORNL personnel for the years 1959–60.

During the past two years there has been virtually no change in the over-all distribution of plant communities on the lower lake bed. Evidence for this conclusion is illustrated in Figs. 2.1 and 2.2, which are vegetation maps of the ecology grid area on the lower lake bed. These maps are for the years 1959 and 1960, respectively, and show the patterns of distribution for the major plant populations. The mapping was done in late summer, at the end of the growing season, so that dominant and subdominant species are included. However, a large number of species which may or may not be present as discrete associations are not included, since they were small and evidently had small coverage. Consequently, many plants, such as mosses, small herbs, etc., which may form an important constituent below the larger herbaceous vegetation, are not shown.

The subdominants primarily are the large and relatively abundant forbs (*Solidago* spp., *Oenothera* spp., and *Aster* spp.), which tend to be scattered throughout the bed and do not become prominent until they flower, usually in August. The dominant herbaceous vegetation consists of sedges (*Carex* spp. and *Cyperus* spp.), and rushes (*Juncus* spp.), which have maintained their relative positions and approximately the same amount of areal coverage during the past two years. The dominant woody vegetation is the black willow (*Salix nigra* Marsh.), which is occupying more and more of the grid area. This increase in population density can be seen by comparing the willow distribution around the photo reference pole for the two years. Up to this time the increase in willow density has been at the expense of plant associations such as smartweed (*Polygonum* spp.), *Bidens* spp., and *Eupatorium* spp., which were dominant associations in parts of the bed during 1957 and 1958.

---

[1] Research participant.

[2] Summer employee.

[3] Temporary employee.

[4] S. I. Auerbach *et al.*, *Health Phys. Div. Ann. Progr. Rept. July 31, 1957*, ORNL-2384, pp 10–11.

[5] S. I. Auerbach *et al.*, *Health Phys. Div. Ann. Progr. Rept. July 31, 1958*, ORNL-2590, p 30.

[6] S. I. Auerbach *et al.*, *Health Phys. Div. Ann. Progr. Rept. July 31, 1959*, ORNL-2806, pp 20–24.

[7] D. A. Crossley, Jr., and H. F. Howden, *Ecology* 42, 302 (1961).

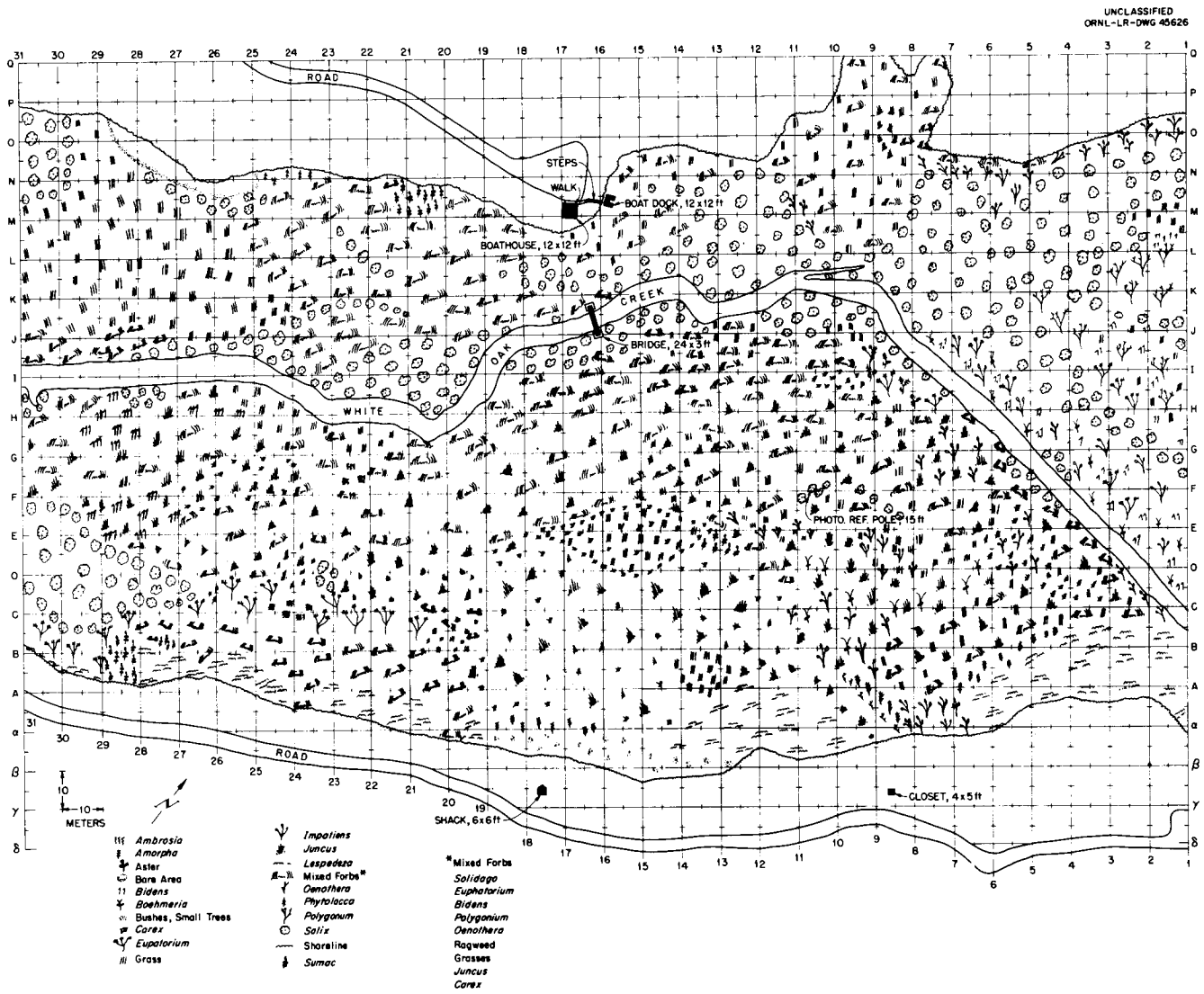

Fig. 2.1. Distribution of Vegetation, August–September 1959, Ecology Study Area. (Ten-meter grid of lower White Oak Lake bed.)

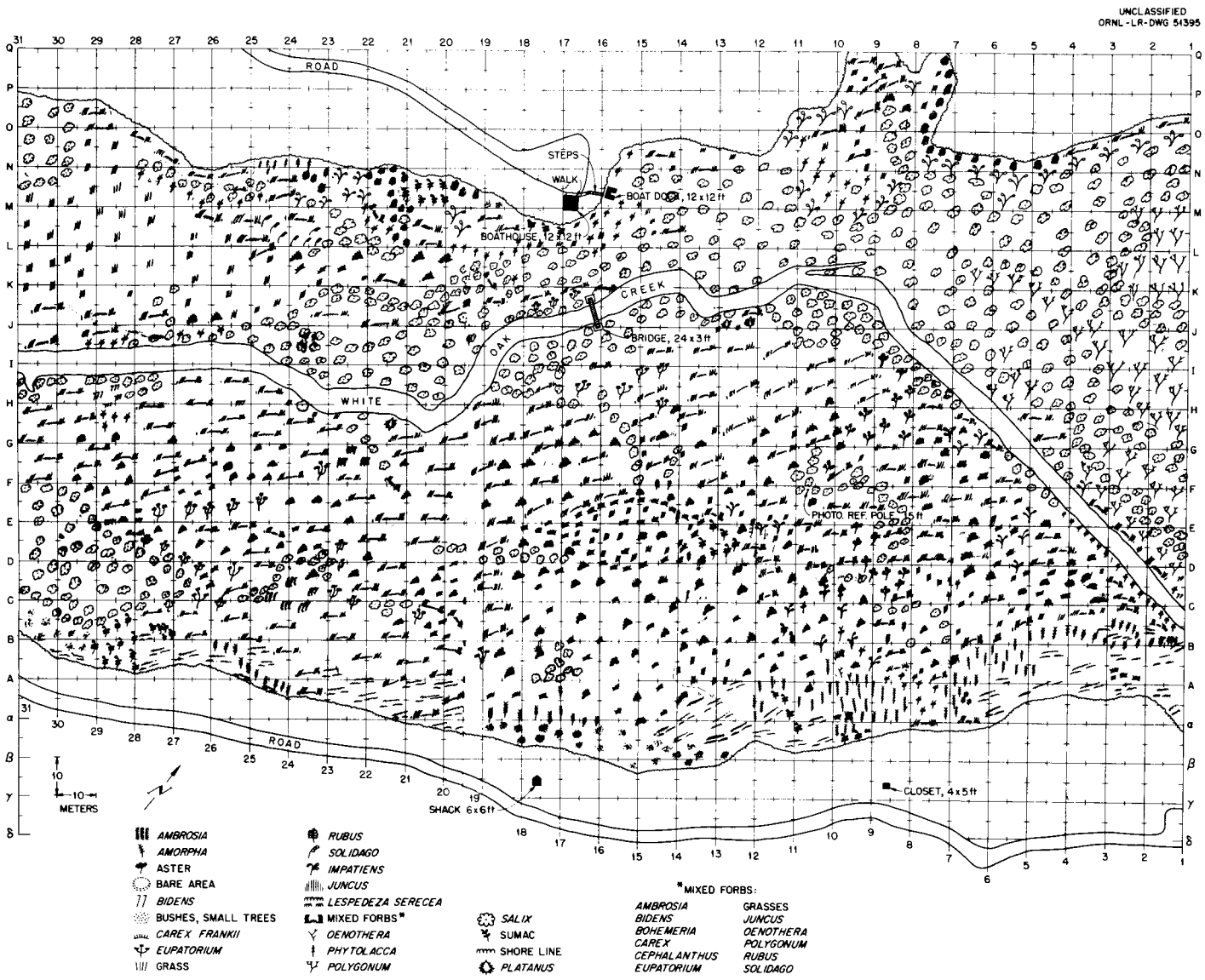

Fig. 2.2. Distribution of Vegetation in the Ecology Study Area of Lower White Oak Lake Bed, August 1960.

The rapid growth of the willows has contributed to the striking change in the aspect of the lower lake bed. Figure 2.3 is a view of this area taken in June 1961. The margins of the area along both banks of White Oak Creek are almost completely occupied by willow, many of which are now over 12 ft in height. Essentially the lower bed has become a swamp meadow characterized by the combination of lowland wet soil vegetation and the large variety of flowering forbs. The swamp character of the vegetation can be expected to be enhanced during the next several years as a result of the modification of the gates of White Oak Dam.[8] The purpose of the modification was to maintain a constant head of water behind the dam so that there would always be flow over the dam regardless of changes in water level below the dam resulting from the operation of the TVA Watts Bar Dam. The standing pool thus created will tend to back up water into the lower lake bed and will thus serve to maintain a more constant and higher water table throughout the growing season than has been the case during the past five years.

While the herbaceous vegetation has undergone little change during the past two years, invasion of the bed by woody vegetation has been continuing. The succession and increasing complexity of woody vegetation is illustrated in Figs. 2.4 and 2.5. These maps show only the patterns on the area south of the creek. The area on the north bank has been occupied mainly by willow during this time. Two patterns of invasion are evident. Lowland moist-soil species are predominant in the areas adjacent to the creek where the water table tends to remain high throughout the growing season. Upland species have invaded along the original lake shore and moved into the areas where the water table tends to drop below the 2-ft layer during the summer months.

Table 2.1 lists the species of woody plants on this area as of autumn 1960. Of the 17 species listed, about half are lowland species and the remainder upland. The characteristic lowland species besides willow are the sycamore (*P. occidentalis* L.) and box elder (*A. negundo* L.).

[8] K. Z. Morgan *et al.*, *Applied Health Phys. Ann. Progr. Rept. for 1960*, ORNL-3159, p 4.

Fig. 2.3. Panoramic View of the Ecology Grid Area of Lower White Oak Lake Bed, June 1961. View is toward the northeast. Black and white photo reference pole may be seen in center of photograph. Pole is 15-ft tall and marked in alternate 1-ft black and white bands.

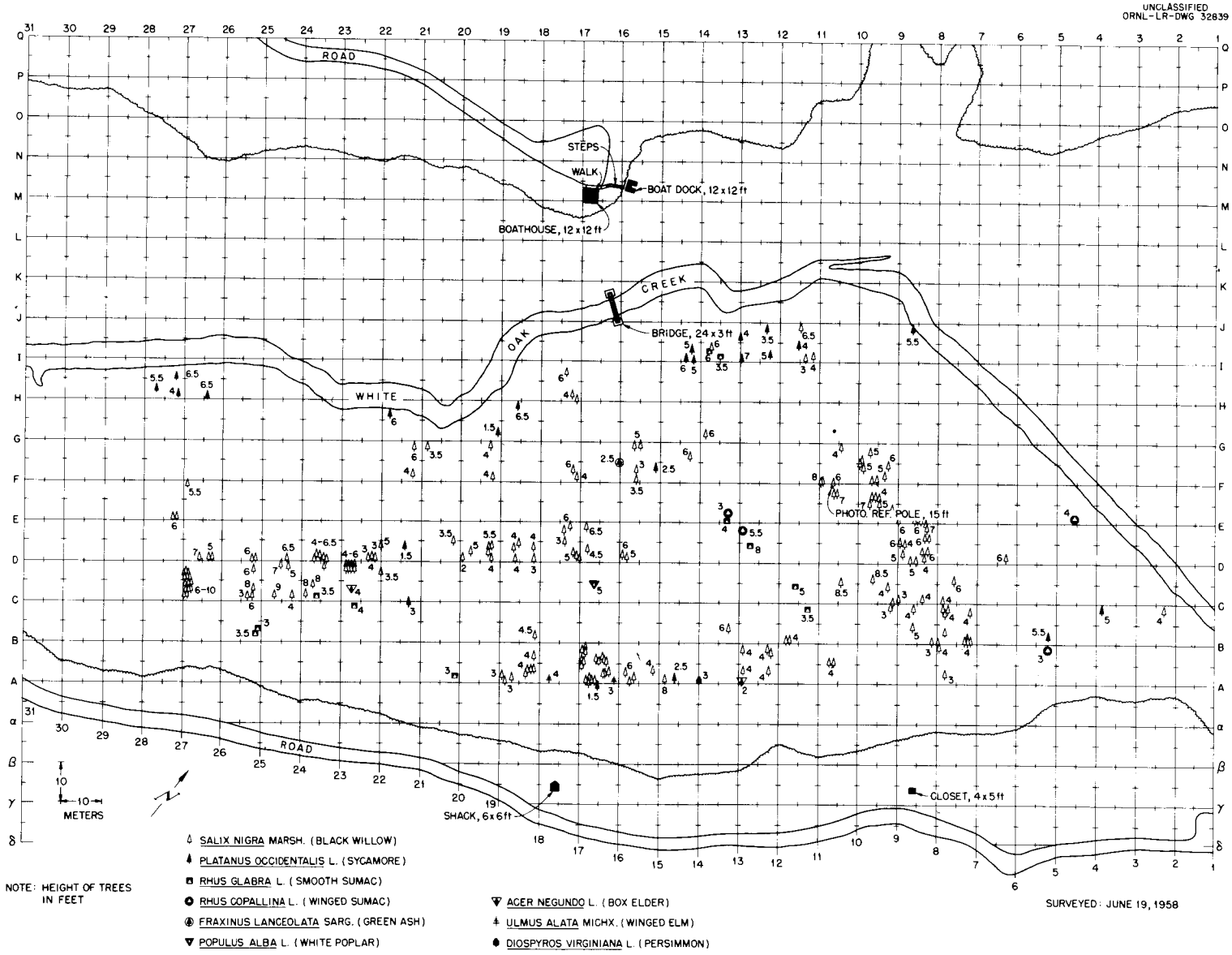

Fig. 2.4. Distribution of Trees, September 1958, Ecology Study Area. (Ten-meter grid of lower White Oak Lake bed.)

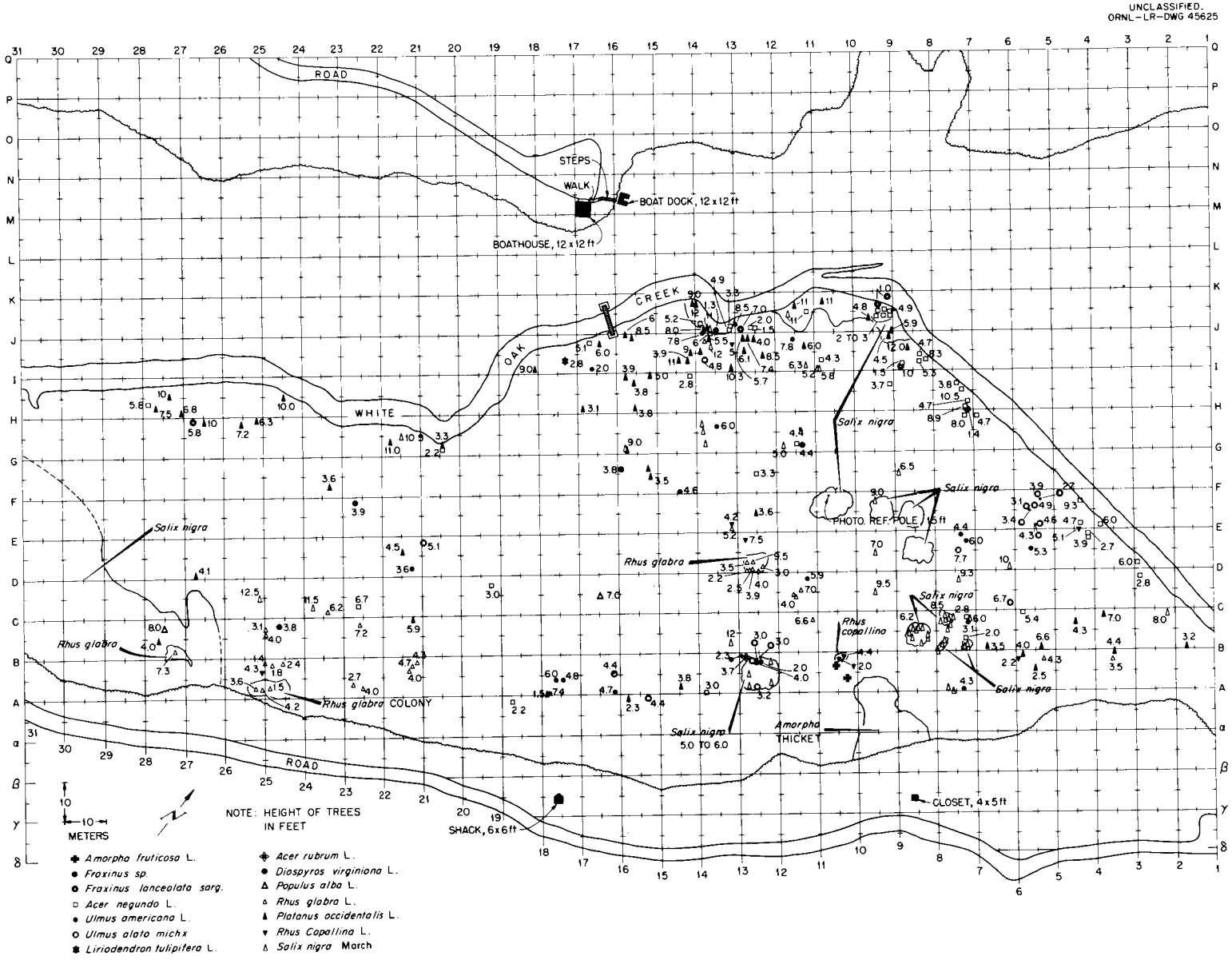

Fig. 2.5. Distribution of Trees, August–September 1959, Ecology Study Area. (Ten-meter grid of lower White Oak Lake bed.)

Table 2.1. Species of Trees and Shrubs Growing in the Lower Bed of Former White Oak Lake as of August–September 1960

Scientific Name	Common Name
Acer negundo L.	Box Elder
Acer rubrum L.	Red Maple
Amorpha fruticosa L.	Dull-leaf Indigobush
Cephalanthus occidentalis L.	Buttonbush
Cercis canadensis L.	Redbud
Cornus ammomum Mill.	Silky Dogwood
Diospyros virginiana L.	Persimmon
Fraxinus pennsylvanica var. *subintegerrima* fern.	Green Ash
Hypericum densiflorum Pursh.	Dense St. Johnswort
Platanus occidentalis L.	Sycamore
Populus alba L.	White Poplar
Rhus copallina L.	Winged Sumac
Rhus glabra L.	Smooth Sumac
Salix nigra Marsh.	Black Willow
Ulmus alata Michx.	Winged Elm
Ulmus americana L.	American Elm
Ulmus rubra Muhl.	Slippery Elm

In future years the presence of a relatively high and stable water table will probably result in the elimination of many of the upland species now on the bed with subsequent replacement by lowland types.

Uptake of Radionuclides by *Lespedeza*

Knowledge of the uptake of mixtures of radionuclides by vegetation throughout the growing season has two important implications. First, it may provide further insight into the contamination of man's food. It is not enough to have data merely on the behavior of a single isotope applied by sprays or even by plowing into the soil. If there will be contamination of man's food, most likely it will consist of mixtures of radioisotopes. Second, transfer of different radioelements from one ecological level to another in different ecological situations is applicable to further understanding of the basic functioning of complex ecosystems.

Previous studies[9] on one of the native plants of the lake bed (smartweed) showed that uptake of radiostrontium and radiocesium decreased relative to rate of plant growth through the growing season. These results were based on random harvesting of such smartweed stands that were growing in the vicinity of the lake bed agricultural plot. The availability of the agricultural plot made it opportune to test these results under more controlled conditions.

In the summer of 1959, the agricultural area was laid out in a row and column design consisting of four rows, each containing four plots 10 × 50 ft. Eight of the plots were used for this experiment. Two varieties (Korean and Kobe) of the common forage legume *Lespedeza* were planted in alternate plots in each column. In this way no plot was adjacent to another either in the column or in the row. The crop was allowed to grow the rest of the summer and autumn. By the following spring the crop was sufficiently established to start harvesting.

The first harvest was taken on May 20, 1960, about thirty days after the start of the growing season. A total of four harvests were taken, each on the 20th of the month.

Harvesting was accomplished by staking out two quadrats, each $\frac{1}{2}$ m^2, at opposite ends of the plot. Subsequent harvests were taken by staking similar quadrats adjacent to those harvested previously. In this way replicate harvests representing two ends of the plot could be obtained with allowance for disturbance due to harvesting operations, servicing, etc. Plants were clipped about 1 in. above ground surface. The plant material (leaves and stems) was washed to remove surface contamination, dried at 110°C by standard methods, ground in a Wiley mill, and aliquots were taken for radioanalysis.[10] After harvesting, ten 6-in. soil cores were taken from each quadrat and composited for radio- and stable-chemical analysis. Because of the large number of samples only the first and third soil samples have been analyzed to date, and only for Sr^{90}.

Differences between the mean radionuclide contents and between the mean yields of the two

[9] S. I. Auerbach *et al.*, *Health Phys. Div. Ann. Progr. Rept. July 31, 1960*, ORNL-2994, p 149.

[10] Radioanalyses were made by the Low Level Radioanalytical Laboratory of the Analytical Chemistry Division.

varieties were not found to be significant. Consequently, the sixteen samples per harvest were treated as replicates. The changes in radionuclide concentration as a function of time are plotted in Fig. 2.6. Yield (g/m^2) is also plotted on the same graphs as a function of time. Yields for the four harvests were (mean ± s.e.) 38 ± 4.3, 201 ± 22.5, 151 ± 12.9, and 334 ± 20.7 g/m^2. The anomalous lower yield for the third harvest probably resulted from a combination of circumstances derived from a flooding of the lake bed which occurred less than two weeks before the third harvest. On July 10 and 11, 1960, 3.74 in. of precipitation occurred in the ORNL area. This downpour completely flooded the lake for two days. In addition to coating the plants with silt the flood may have redistributed quantities of the radionuclides which had entered the upper lake bed from the liquid waste pits. Because of this possibility the third harvest was processed differently. Instead of treating the stems and leaves as a unit, we attempted to separate the two parts. The purpose of this change in procedure was to see if there was differential contamination between the stems and leaves, since part of the latter contained new growth which took place after the flooding. The small size of the leaves made separation difficult, and under the duress of processing, a large amount of sample material was lost.

That the flooding effected a redistribution of the radionuclides is most strikingly evident in the case of Ru^{106} (Fig. 2.6*c*). During the previous two years there was a considerable increase in the quantity of Ru^{106} released to the liquid waste pits and subsequently to the upper lake bed via the east and west seeps. In 1959 the quantity moved to the lake bed was estimated to be 1300 curies.[11] All the other radioisotopes showed a similar increase with the third harvest. The quantity of Sr^{90} moved was relatively small, reflecting the smaller quantities present in the bed. Radiocesium shift is probably exaggerated because spectrometric analysis for Cs^{137} was complicated by the presence of the large quantities of Ru^{106}.

The pattern of uptake for the first two harvests is essentially the same for all four radionuclides. Strontium-90, which can be expected to be metabolized by this calcium-utilizing plant, has the highest initial concentration of the four isotopes. Subsequent production of new cellulose does not seem to be accompanied by further uptake of radiostrontium. As a result there appears to be an inverse relationship between uptake and rate of growth. Ruthenium-106 and cobalt-60 also show evidence of this inverse relationship for harvests 1 and 2. Radiocesium, on the other hand, does not show a decrease with yield for the same two harvests, which corresponds with the results obtained with smartweed last year.

The concentrations of radionuclides in the vegetation after the flooding would include foliar absorption, and therefore reduction in concentration in the 4th harvest does not necessarily reflect a change in uptake in relation to growth. If the decrease in uptake of Sr^{90} is not related to a lack of available Sr^{90}, then the results suggest that it would be advantageous to utilize crops with long growth periods and large yields in those soils which may be subjected to contamination by Sr^{90}.

The accumulation of radionuclides by the vegetation biomass is more directly related to problems of ecological transfer and to cycling of radionuclides in differing ecosystems. Quantities of radionuclides per square meter of vegetation were computed using the data on yield and the concentrations per unit weight of plant material. The total accumulations are summarized in Table 2.2. The data for Sr^{90} are least dependent on the effects of flooding and therefore are most illustrative. With these data and the soil burden two kinds of uptake rates can be determined: (1) the activity uptake rate which measures the increase of activity per unit of biomass per unit time and (2) a coefficient of transfer rate, which is the ratio of the activity uptake rate to the soil burden per unit area, and which may be used to compare different vegetation units.

There was a fivefold increase in Sr^{90} accumulation during the 1960 growing season (Table 2.2) which resulted in a total of $(157.0 \pm 9.7) \times 10^3$ $\mu\mu c$ of Sr^{90} per m^2 of vegetation. If a growth period of 120 days (April 20–August 20) is assumed prior to the 4th harvest, an activity uptake rate of 1300 ± 81 $\mu\mu c$ of Sr^{90} per m^2 per day is obtained. This rate is considerably less than that obtained for smartweed the previous year, which was approximately 4430 $\mu\mu c$ of Sr^{90} per m^2 per day. The difference between the two reflects the greater production of smartweed per

[11] K. E. Cowser, *Potential Hazard of Ruthenium in the ORNL Waste Pit System*, ORNL CF-60-3-93 (Mar. 11, 1960).

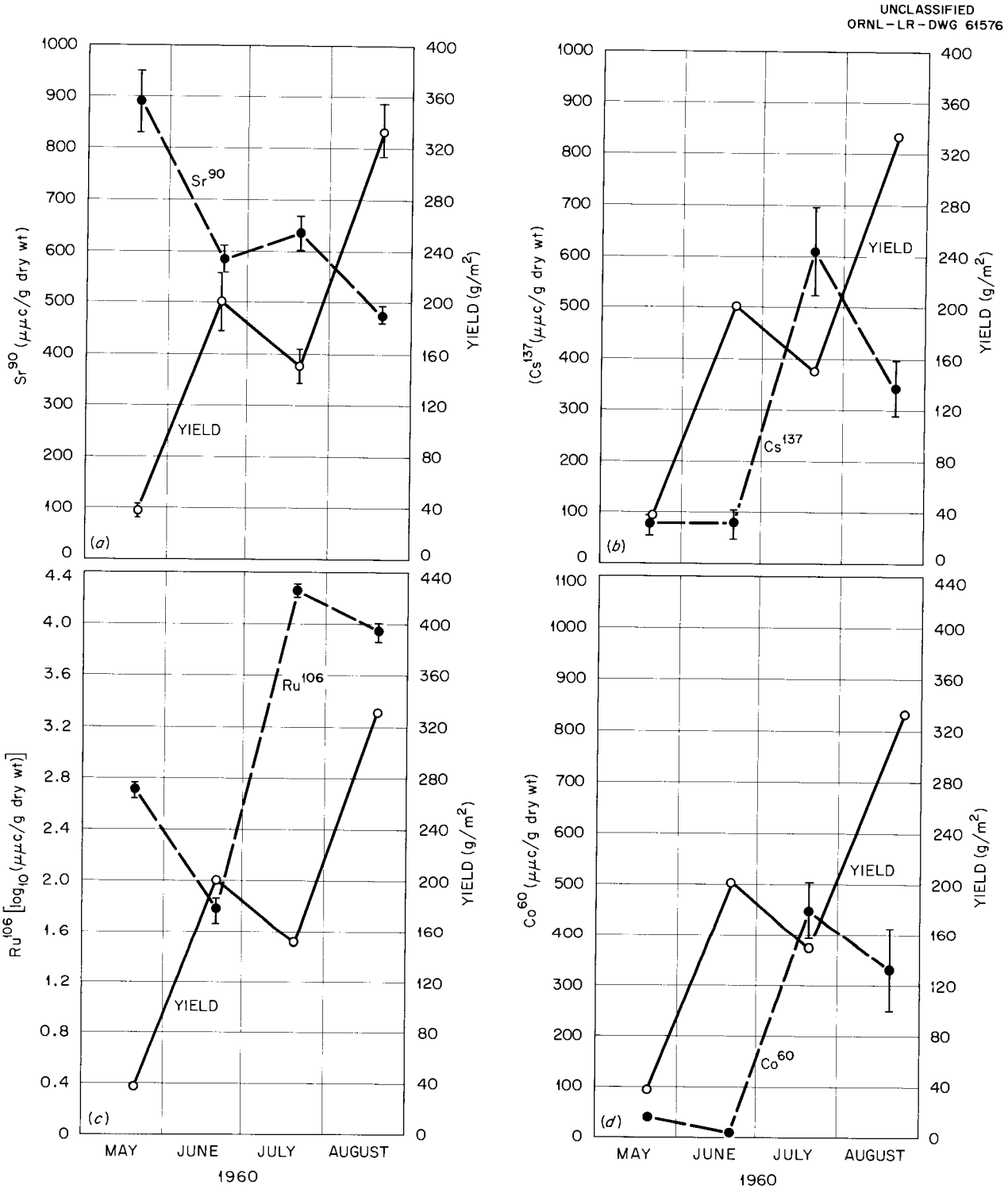

Fig. 2.6. Changes in Concentration of Four Radionuclides and Increase in Yield of *Lespedeza* Grown on the White Oak Lake Bed Agricultural Plot, Summer 1960. Points represent the mean (n = 16) ± one s.e.

Table 2.2. Accumulation of Radionuclides in *Lespedeza*

Mean ± s.e. (n = 16)

	$\mu\mu$c per m^2 of Vegetation			
	Sr^{90}	Cs^{137}	Co^{60}	Ru^{106}
	$\times 10^4$	$\times 10^4$	$\times 10^3$	$\times 10^4$
1st harvest May 20, 1960	3.30 ±0.40	0.29 ±0.10	1.50 ±0.20	1.40 ±0.35
2d harvest June 20, 1960	11.3 ±1.3	1.40 ±0.51	2.00 ±0.22	0.75 ±0.17
3d harvest July 30, 1960	10.6 ±1.3	10.3 ±2.5	75.1 ±15.2	211 ±46.1
4th harvest Aug. 19, 1960	15.7 ±0.97	11.0 ±1.80	105 ±24.0	201 ±36.8

unit area. Activity uptake rates for the two vegetation types may be compared more validly by computing the rates of uptake for the growing period prior to each harvest. These are shown below (units are $\mu\mu$c of Sr^{90} per m^2 per day):

	May	June	July	August
Lespedeza (1960)	1100	2670		720*
Smartweed (1959)		3620*	1670	5230

The rates marked with (*) were computed on a 60-day basis. Omission of the June 20–July 20 period for *Lespedeza* was necessary because of the faulty data on yield of the third harvest. No harvest of smartweed was taken in May.

The two vegetation types may also be compared by means of the coefficient of transfer rate which is expressed by the following equation:

$$\text{Coefficient of } Sr^{90} \text{ transfer} = \frac{\mu c \text{ of } Sr^{90} \text{ (m}^2 \text{ plant)}^{-1} \text{ days}^{-1}}{\mu c \text{ of } Sr^{90} \text{ (m}^2 \text{ soil)}^{-1}} . \quad (1)$$

The ratio provides a means for comparing efficiencies of transfer for different vegetation units. Coefficients were calculated for *Lespedeza* and smartweed for the two harvest periods which were comparable in time. These are as follows:

	June	August
Lespedeza	2.0×10^{-5}	1.4×10^{-5}
Smartweed	5.1×10^{-5}	6.3×10^{-5}

The June harvest represented the first 60 days of growth. Smartweed appears to be about 2.5 times more effective in accumulating Sr^{90} during this part of the growing season. The August harvest would include most of the growing season and here represents 120 days of growth. On this basis smartweed as a vegetation unit seems to be approximately 4.5 times more effective than *Lespedeza* in accumulating Sr^{90}.

Fertilizer Studies

Most of the investigations on uptake of Sr^{90} and other potentially hazardous radionuclides by plants have treated these elements independently, even though they frequently occur together, as in fallout. The presence of at least four such isotopes (Sr^{90}, Cs^{137}, Ru^{106}, and Co^{60}) in the calcareous soils of White Oak Lake bed affords an opportunity to obtain information on total radionuclide uptake by plants of several species of radioelements. Likewise the bed may be useful for testing various methods of reducing uptake from contaminated soils.

Use of phosphates to form insoluble strontium compounds has been suggested as a possible

method of treating calcareous soils[12] in order to reduce uptake of Sr^{90}. Another related aspect, based on harvest studies,[13] is the development of soil treatments which would also increase crop yield without resulting in a proportionate increase of hazardous isotopes.

Two plots in the White Oak Lake bed agricultural area were subdivided into 24 subplots, each 16 in. by 6 ft 5 in. Eighteen of the plots, selected at random, were treated with a commercial fertilizer (Armour Big Crop 20% superphosphate). Six subplots were used as controls. Treatments were applied at a rate of 1000, 2000, and 3000 lb of phosphorus per acre. After application the fertilizer was mixed in the top 3 in. of soil. At the same time top soil was removed from an adjacent plot, homogenized, air dried, and potted. Pots were given the same fertilizer doses as the field plots. Two series, each consisting of 12 pots with three replications per treatment, were prepared for seeding. Both pots and field plots were seeded with Sudan grass (*Sorghum sudanense* × *saccaratum*) and *Lespedeza*. Sudan grass grew successfully and was harvested in the greenhouse after 36 days. The field plots were harvested 47 days after seeding.

The effect of the fertilizer treatment was pronounced both in the field and the greenhouse (Table 2.3). Significant reductions in Sr^{90} and Cs^{137} were obtained under greenhouse conditions by treatment I (1000 lb of P per acre). Radiostrontium in fact appears to have been appreciably reduced by all treatments. In this respect it is unique among the four radioisotopes. The reduction in radiocesium by treatment I was greatest in the greenhouse series; the heavier treatments had little further effect on radiocesium uptake, whereas there appears to be continuing reduction with increased dose in the field tests. The effects on cesium may be related to the potassium content of the fertilizer. Aliquots of the latter are being analyzed currently for this and other macronutrients. Quite unexpected is the almost geometrical increase of Co^{60} with increased dose. The explanation for this phenomenon may be related to the fact that the ash contents of the greenhouse plants also increased linearly with fertilizer dose. Soil deficiency in cobalt and a metabolic requirement for this element in a rapidly growing plant may be the cause.

Agreement between field and laboratory results was unusually good. The only exception was the uptake of radiocobalt which under field conditions was neither enhanced nor diminished.

These reductions in uptake were accompanied by significant increases in yield (Table 2.4). Under field conditions yield was doubled for fertilizer treatments I and II. Previous analyses[14] had indicated that phosphorus content of the lake bed soils was somewhat low by agricultural standards. Consequently, the control yield (*ca.* 1600 lb/acre) was rather poor. The three fertilizer amendments resulted in increases to 3600, 7300, and 9100 lb/acre, respectively. Most encouraging is the fact that the increase in yield is not accompanied by a proportionate increase in total uptake of Sr^{90} and Cs^{137}. For example, the increases in total radiostrontium (using values of Table 2.3 and the yields cited above) were 136, 237, and 266% respectively compared to yield increases (Table 2.4) of 223, 453, and 568%. If greenhouse data are used the results are even more striking. Contrary to work reported elsewhere[15,16] these results indicate that phosphate fertilizers may be useful in treating contaminated soil and massive treatments may be justifiable economically in situations where the land is valuable, the increased crop production is needed, and where fission products in the crop may be expected to undergo further reduction due to the various discrimination mechanisms present in the several links of the food chain leading to man.

Insect Studies

Ecological research on insects is developing data pertaining to basic aspects of insect ecology, as well as information on the role of insects in the redistribution and spread of radioactive contamination. White Oak Lake bed is being used as a large-scale tracer experiment to resolve questions concerning the amount of plant

[12] R. L. Uhler and F. P. Hungate, *Nature* **187**, 252 (1960).

[13] S. I. Auerbach *et al.*, *Health Phys. Div. Ann. Progr. Rept. July 31, 1960*, ORNL-2994, p 150.

[14] S. I. Auerbach *et al.*, *Health Phys. Div. Ann. Progr. Rept. July 31, 1958*, ORNL-2590, p 33.

[15] R. G. Menzel, pp 37–46 in *Radioisotopes in the Biosphere*, University of Minnesota, Minneapolis, 1960.

[16] R. L. Uhler and F. P. Hungate, *op. cit.*

Table 2.3. Effect of Fertilizer (20% Superphosphate) upon Uptake of Radionuclides by Sudan Grass (*Sorghum sudanense* × *saccaratum*)

Radionuclide	Radionuclide Content ($\mu\mu$c/g dry wt)			
	Control	Treatment I 1000 lb P per Acre	Treatment II 2000 lb P per Acre	Treatment III 3000 lb P per Acre
		Greenhouse, mean ± s.e., $n = 3$		
Sr^{90}	645.3 ± 58.3	153.4 ± 10.1	84.4 ± 8.6	44 ± 4.6
Cs^{137}	380.7 ± 37.2	19.6 ± 8.4	12.3 ± 0.84	18.6 ± 1.9
Ru^{106}	35.9 ± 18.4	10.2 ± 2.3	10.7 ± 2.0	13.7 ± 2.3
Co^{60}	7.8 ± 7.8*	10.5 ± 0.67	23.7 ± 1.9	52.7 ± 3.5
		Lake Bed Plot, mean ± s.e., $n = 6$		
Sr^{90}	338.5 ± 14.1	206.8 ± 9.8	177.0 ± 9.5	158.6 ± 11.9
Cs^{137}	121.3 ± 10.1	77.0 ± 15.1	38.5 ± 4.7	40.5 ± 8.9
Ru^{106}	62.0 ± 11.2	60.0 ± 11.8	38.5 ± 3.0	33.2 ± 2.7
Co^{60}	22.4 ± 2.5	25.0 ± 4.4	21.2 ± 1.5	20.2 ± 1.8

*Co^{60} not detected in two replicates.

Table 2.4. Change in Concentration of Radionuclides and in Yield of Standing Crop of Sudan Grass as a Function of Fertilizer Treatments

	Per Cent of Control		
	Treatment I 1000 lb P per Acre	Treatment II 2000 lb P per Acre	Treatment III 3000 lb P per Acre
	Greenhouse		
Yield (standing crop)	+479	+483	+462
Sr^{90}	−76	−87	−93
Cs^{137}	−95	−97	−95
Ru^{106}	−72	−70	−62
Co^{60}	+135	+304	+676
	Field Plot		
Yield (standing crop)	+223	+453	+568
Sr^{90}	−39	−48	−53
Cs^{137}	−37	−68	−67
Ru^{106}	−3	−38	−46.5
Co^{60}	+112	−5	−11

material eaten by insects during a growing season.[17] Measurements of such quantities provide information essential to an understanding of the interrelationships between components of an ecosystem. These measurements estimate the flow of materials and energy from one ecological level to another. Consumption of plants by insects is difficult to measure with any known technique, but it can be approximated from the relationship

$$ra = \lambda Q_e , \qquad (2)$$

where r is the rate of ingestion of a given radionuclide, a is the proportion absorbed from the intestines, λ is the ratio of ln 0.5 to the biological half-life T_b (or the effective half-life if the physical half-life is short) for the given radionuclide, and Q_e is the body concentration at equilibrium of that nuclide in the insects. Estimates of r can be obtained, based on samples of insects from White Oak Lake bed, and λ and a estimated in the laboratory. With this information, together with data on the concentrations of radionuclides in the plant food and biomasses of plants and insects, the consumption of plants by insects can be approximated.

Current work on insects is proceeding along two lines: (1) comparison of the rate of feeding, r, as estimated from Eq. (2) and as measured in laboratory experiments for a single insect species (*Chrysomela knabi*) and (2) investigation of rate of elimination of radioisotopes as a function of size of insect.

Studies on *Chrysomela knabi*. – The purpose of these investigations is to test the precision of Eq. (2) for estimating food consumption by insects. Measurements of the feeding rate made under laboratory conditions will be compared with estimates of r from Eq. (2), based upon field measurements of the equilibrium concentration of Cs^{137} in White Oak Lake bed specimens and laboratory estimates of the elimination rate for Cs^{134}. *Chrysomela knabi*, the beetle chosen for these experiments, feeds upon willow leaves. All stages in the life history can be collected and the insect is easily reared and handled. The period of activity is short, however (4 to 6 weeks).

This year, laboratory measurements of feeding rates and elimination rates were made for both larvae and adults. Field collections were not completed; beetle populations were small due to cool weather in the spring and heavy rains in the summer.

Feeding rates were established for third-instar larvae and adults. There are 3 larval instars of 1, 1–2, and 4–6 days duration. First- and second-instar larvae were small (1–3 mg, wet wt) and ate less than 10 mg (fresh wt) per day of willow leaves, or less than 30 mg total for this period. Data on feeding rates of third-instar larvae are summarized in Table 2.5. The amount consumed increased with increasing size of insect until the day before pupation, when consumption dropped. Food consumption averaged about 20 mg per day for these third-instar larvae and about 45 mg per day for adults. Feeding activities of the adults did not necessarily result in weight gains.

Table 2.5. Average Weights of Food Consumed by Third-Instar Larvae of *Chrysomela knabi*

Averages of 12 individuals

Days Before Pupation	Mean Fresh Weight of Food Eaten (mg)	Meon Weight of Beetles (mg)
5	11.6	5.0
4	19.8	6.5
3	27.8	12.4
2	28.6	19.9
1	9.9	24.2

Elimination of Cs^{134} occurred at rates corresponding to a 7-hr biological half-life for first-instar larvae (mean of 4 individuals), an 8-hr T_b for third-instar larvae (14 individuals), and a 10-hr T_b for newly-emerged adults (8 individuals). Within each stage the data were well fit by a straight line function (Fig. 2.7); there was no indication of additional components of elimination as in studies on *Romalea*[18] or *Melanoplus*.[19] Figure 2.7 illustrates elimination by one individual; loss during the third instar, retention during pupation, and further loss during the adult stage are shown.

[17] D. A. Crossley, Jr., and H. F. Howden, *Ecology* 42, 302 (1961).

[18] D. A. Crossley, Jr., and M. E. Pryor, *Health Phys.* 4, 16–20 (1960).

[19] D. A. Crossley, Jr., and J. H. Schnell, *Ann. Entomol. Soc. Am.* 54, 459–61 (1961).

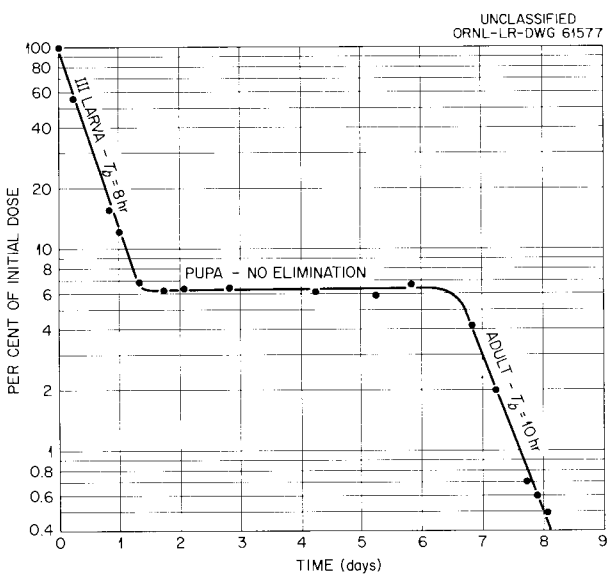

Fig. 2.7. Elimination of Cs^{134} by a Specimen of *Chrysomela knabi*. Third-instar larva, pupa, and adult stages are shown.

These short biological half-lives suggest that, under conditions of a constant rate of feeding, equilibration with isotope concentrations in food would occur in less than 2 days. As shown above, however, feeding rates increase as the insect grows. First-instar larvae ate less than 10 mg per day, whereas third-instar larvae ate about 20 mg per day. Equilibration could occur in the third instar (except for the last day of that instar), since it lasts for an average of 5 days. And adults several days old should equilibrate with their rates of feeding. Rates for adults, as measured in the laboratory, were more variable than those for larvae, and larger field collections would be required.

The feeding rate was reduced on the day preceding pupation, but no such decrease in the rate of elimination of cesium was found. Presumably, therefore, field populations of these insects would have a reduction in body concentration of cesium in the day preceding pupation, and pupae would have lower body concentrations than would be expected from the average feeding rates of the third-instar larvae.

The insects overwinter as adults, and year-old individuals were available for comparison with newly-emerged individuals. No comparable estimates of food consumption were obtained, but elimination rates were different: the average T_b was 10 hr for new adults but only 7–8 hr for year-old ones. This difference is probably a reflection of the metabolic status of the individuals. New adults are accumulating materials to prepare for hibernation, whereas year-old ones are mating, seeking oviposition sites, and laying eggs.

Relation of Size to Elimination Rate. – A more important case for application of the isotope-equilibrium method of measuring plant consumption is one where many different insect species are involved. With a single species such as *Chrysomela knabi* the consumption of food can be measured directly in the laboratory, but this is impossible in natural systems such as White Oak Lake bed which contains several hundred species.[20] Preliminary estimates of consumption of plants by this insect community have been reported[21] using different assumptions of λ and a.

The selection of an average λ, the elimination constant, for the insect species resident on White Oak Lake bed is necessary for estimates of feeding rates. This year's work has been directed toward quantifying the relationship between size of insect and rate of elimination so that insect weights may be utilized as a basis for choosing an average λ.

Figure 2.8 shows the relation of T_b to body weight for four species of insects studied previously. Values used are average T_b's and average body weights for adults. Although only four points are involved, the linear regression of elimination rate on body weight is highly significant statistically ($P = 0.01$), whether arithmetic or logarithmic values are used.

Table 2.6 shows the weight composition of insect samples taken in September 1960. The size classes used were those most convenient for grouping the insects. In terms of numbers of individuals, the smallest were the most numerous; more than 60% weighed less than 1 mg. However, these minute insects contributed only 4% to the weight of the sample. The modal class for insect weights was in the 20–50 mg size; that is, these

[20] H. F. Howden and D. A. Crossley, Jr., *Insect Species on Vegetation of the White Oak Lade Bed, Oak Ridge, Tennessee*, ORNL-3094 (Apr. 6, 1961).

[21] S. I. Auerbach *et al.*, *Health Phys. Div. Ann. Progr. Rept. July 31, 1960*, ORNL-2994, p 156.

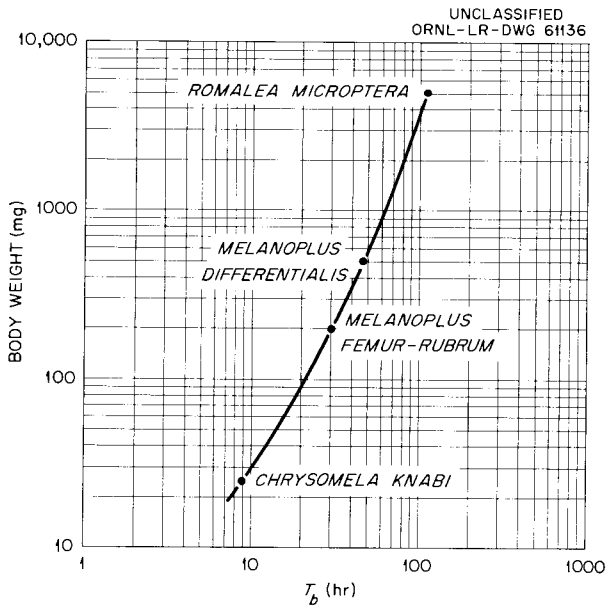

Fig. 2.8. Relation of Biological Half-Life (T_b) of Cesium to Body Weight of Insects.

Table 2.6. Weight Composition of Insect Samples from White Oak Lake Bed

Weight Class (mg)	Per Cent of Total Number	Per Cent of Total Weight
Below 1	63.1	4.3
1–10	22.5	13.5
10–20	8.5	22.6
20–50	4.4	29.3
50–100	1.1	15.7
Above 100	0.4	14.6
	100.0	100.0

insects made the greatest contribution to the weight of the sample.

On the assumption that the 20–50 mg size class represents the average for the community, the average λ would then be based on a T_b of about 9–15 hr (Fig. 2.8). This is lower than the average T_b of about 1 day used in a previous report,[21] and suggests that insect consumption of the plant crop during a growing season amounts to about 5%, rather than the 3% estimate based on a 1-day T_b.

The relationship of size to biological half-life was also investigated for within-species correlations. Biological half-lives of Cs^{134} were found for a series of grasshoppers (*Melanoplus* spp.) of different ages. The range of sizes extended from about 30 mg to 1 g, and 26 individual curves were obtained. Two-component curves were necessary for these data; a shorter component (T_1) averaging about 8 hr and a longer component (T_2) averaging about 47 hr were found. T_1 was correlated significantly with log body weight ($P = 0.05$) but the scatter of values was large. No correlation between body weight and T_2 was found. Since errors in estimates of one component were reflected in estimates of the other, a harmonic sum of the two components was calculated:

$$T_s = \frac{T_1 T_2}{T_1 + T_2} . \qquad (3)$$

Correlation of this harmonic sum with log body weights was highly significant ($P = 0.01$). Thus the relationship of T_b to body weight within the species is not the simple linear one obtained between different species.

Elimination curves for *Chrysomela knabi* consisted of but one component and the relationship between individual T_b's and weights could be examined more readily. However, the smaller size categories were inadequately represented in the data, so that the range of values was smaller than that available for *Melanoplus* spp. For the data at hand, mostly based on third-instar larvae and adults, no correlation between weight and elimination rate was found for *Chrysomela*.

Variation in the rate of elimination between members of the same insect species seems to be influenced more by other factors than by body weight. Such factors as stage of life history, age of individual, metabolic state, and fecundity all induce variations in the T_b which seem to conceal variations due to differences in body weight. In general, the immatures, though smaller, seem to have elimination rates lower than would be expected from the weight-T_b curve in Fig. 2.8.

Mammalogy

Studies of wild-mammal populations in contaminated habitats have progressed according to planned steps prerequisite for design of a program to investigate the somatic effects of environmental

radiation correlated with dose rates and the isotopic equilibrium relationships related to the biogeochemical cycling of radionuclides. The prerequisite steps have been completed and are (1) a description of population dynamics on the contaminated White Oak Lake bed and an uncontaminated old field to obtain necessary basic information over a period of several years on population parameters[22,23] and (2) a pilot-scale study of bioaccumulation of radioelements by mammals in radioactive habitats to determine the spectrum of radionuclides in tissues and to make preliminary estimates of dose rates and radioisotope equilibrium relationships between the animals and their food. The completion of the preliminary studies has resulted in the design of the third planned step, which will be a hematological study of White Oak Lake bed mammals supported by studies of internal and external dose rates. Much of this hematological work will be accomplished with the use of a Coulter electronic blood cell counter to analyze the blood-cell response of animals from uncontaminated areas introduced into pens on the White Oak Lake bed. The use of pens will result in accurate estimates of external radiation doses as well as exposure times. Internal doses will be calculated after radioassay of the animals.

Further processing of data collected during the population dynamics study and stored on IBM cards has revealed some interesting population phenomena.[22,23] Some of these findings, as well as the principal results of the bioaccumulation study and the design for future studies, are discussed in the following sections.

Dynamics of Cotton Rat Populations. – *Trap-Revealed Longevity.* – Survival of cotton rats, *Sigmodon hispidus komareki* Gardner, on the two areas can be inferred from trapping results. Figure 2.9 shows that few individuals were trapped on the lake bed for periods of over six months between first and last captures. Five females and two males were present for over 10 months, and only one of these, a female, was present for over a year (403 days). Of course, most of the animals

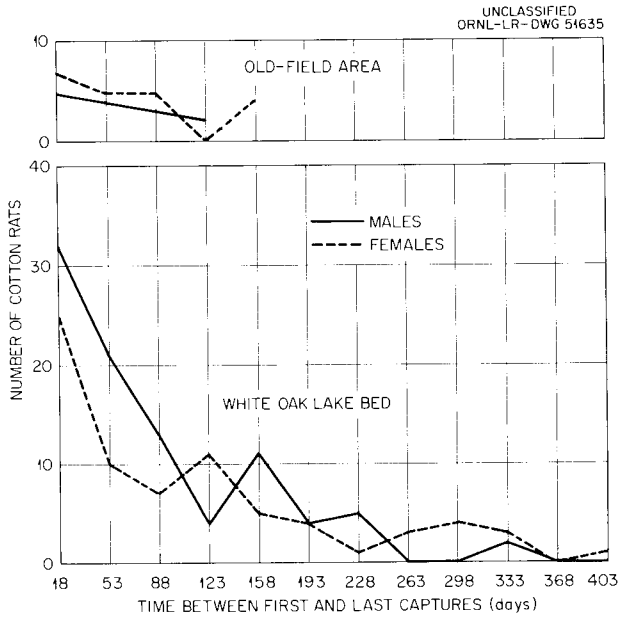

Fig. 2.9. Times Between First and Last Captures for Cotton Rats. Only those individuals with more than seven days between captures are included. Number of individuals: White Oak Lake bed, 180; old-field area, 36.

trapped for the first time were at least a month old and many were probably several months old so that perhaps several of the 180 individuals were actually over a year old. The population at the old field was not present long enough for comparisons of trap-revealed longevity to be made with the lake bed population. Many of the animals trapped in the areas were probably transients. Of the total 248 rats trapped on the lake bed, 35% were caught only once. On the old-field area, 27% of 48 rats were trapped only once.

Sex Ratios. – The sex ratios of the old-field *Sigmodon* were equal when the total number for both sexes were considered (41 males, 39 females); however, the total number of cotton rats on the lake bed from 1957 to 1960 was 178 males and 137 females. A chi square test showed these differences to be significant ($\chi^2 = 5.336$, $P = 0.025$). On the lake bed, more females than males were caught from July to December in 1958 and from May to November (except July) in 1959 (Fig. 2.10). Although these monthly differences were not statistically significant when tested by the nonparametrical runs method, there seems to be a tendency for females to be more numerous from late spring or summer to late fall or early winter.

[22] P. B. Dunaway and S. V. Kaye, *J. Mammalogy* **42**, 265–68 (1961).

[23] P. B. Dunaway and S. V. Kaye, *Transactions Twenty-Sixth North American Wildlife and Resources Conference*, in press.

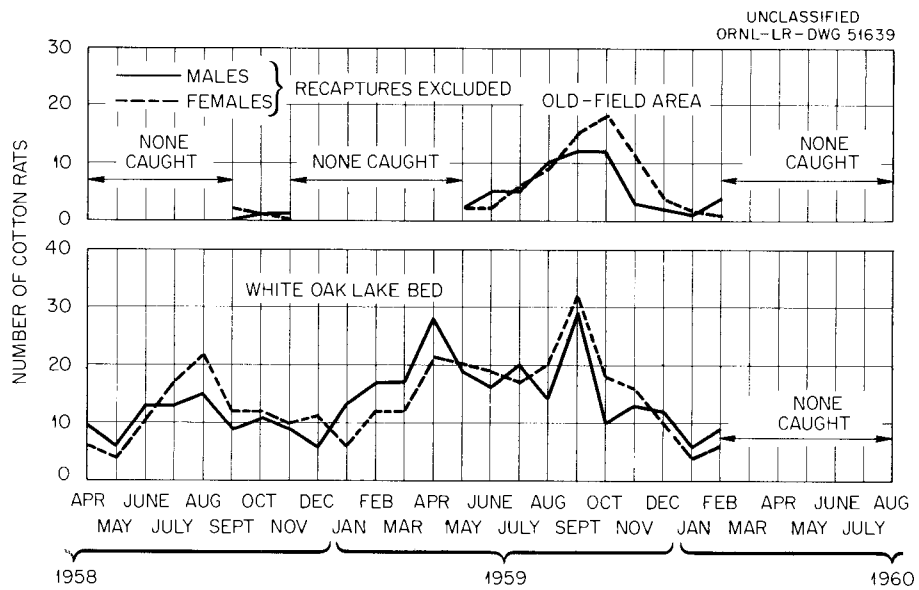

Fig. 2.10. Cotton Rat Males and Females Caught Per Month on the White Oak Lake Bed and Old-Field Areas.

Determining the relative abundances of the sexes in an area is apparently a difficult process, considering that we found that adult males range for distances covering hundreds of feet during the warm months of the year and that adult females are relatively sedentary.[23] More males than females were trapped only once at each area (lake bed, 55 males vs 32 females; old field, 9 males vs 4 females). On the other hand, more females were trapped a greater number of times. In general, the reason for the greater number of captures for females is that more females lived longer on the areas (Fig. 2.9). It seems somewhat paradoxical that more females than males were caught during most of the breeding season in view of the greater mobility of the males during this time. However, males were more numerous during the first part of the breeding season, and it may be that they are exposed to more predation, because of their travels, and eventually become less numerous than the females.

Reproduction. – Reproduction occurred chiefly from about April to October (Fig. 2.11). Pregnancies were determined by consideration of weights before and after a suspected pregnancy, palpation, and condition of mammae. Testes were noted as "descended" or "undescended." Percentages of males with descended testes are usually much higher than the corresponding percentages for pregnant females because of the difficulties of detecting early stages of pregnancy (Fig. 2.11). In general, there is a correspondence between pregnancies and descended testes. Sporadic breeding occurred on the lake bed area during the winter of 1958–59. No pregnant females were noted in June 1959 at the old field; the reason for this lack of detectable pregnancies may have been that the small females (all were less than 101 g) that appeared on the area in June had not bred in time for the pregnancies to be apparent. A pregnant female was present at the old field in November 1959, one month after pregnant females ceased to be detected at the lake bed. Males with scrotal testes were recorded at the old field also in November, *two* months later than at the lake bed.

Litters were born in traps, born in cages to pregnant females removed for a few days from the areas, and some were born in the field and found in nests. These litters are listed in Table 2.7. The average number of young per litter was smaller at the lake bed (5.4) than at the old field (7.7). More males than females were born at the lake bed (42 males, 32 females), while at the old field the division was more nearly equal (22 males, 24 females).

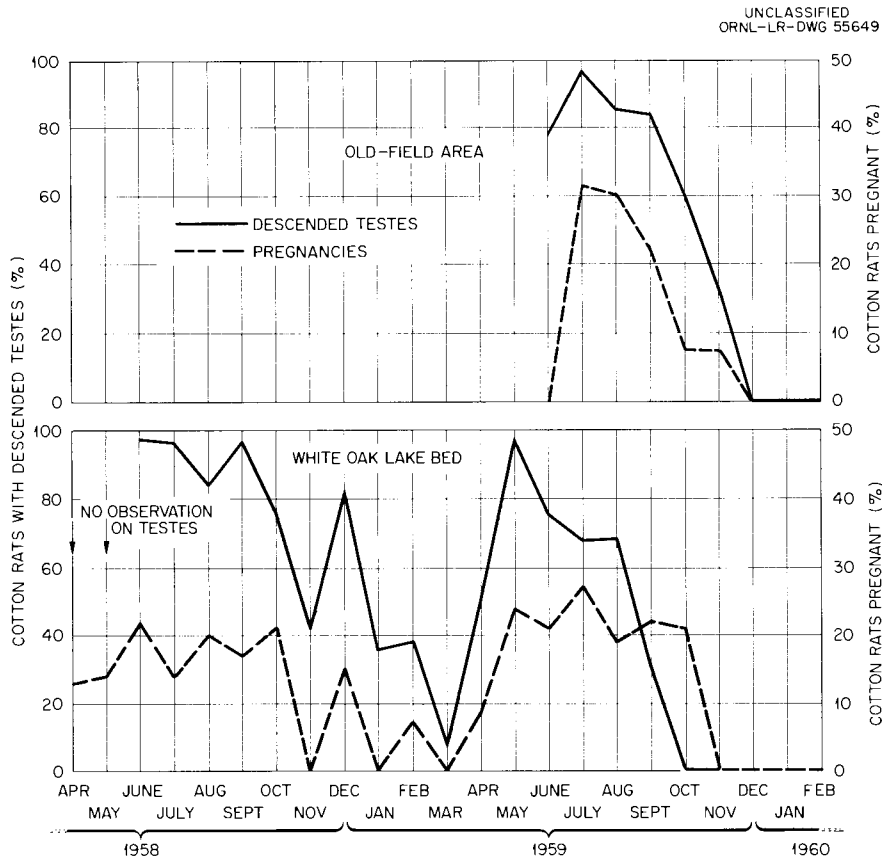

Fig. 2.11. Cotton Rats Pregnant and Cotton Rats with Descended Testes.

Injuries and Abnormalities. – Notes on external injuries and abnormalities were recorded as mammals were examined. The ears of most of the adult and many of the younger cotton rats were the sites of most injuries. Damage ranged from small notches in the margins of the pinnae to one case where practically all of a pinna was missing. Other injuries are listed in Table 2.8. The weighted incidence of injuries and abnormalities for the two areas is about the same. It might be argued that some of the items cited are not abnormalities. For instance, in view of the well-known propensity of the tail skin of *Sigmodon* to slip off when the tail is seized, perhaps it is not an abnormal situation for many individuals of a wild population to have parts of their tails missing. The part of the tail exposed when the skin slips off disappears, usually within a few days, and healing may be complete within a month. Predation, fighting, and accidents may result in tail injuries. It is not very likely that any of the injuries were caused by trapping. No "freaks" were noticed among the cotton rats examined, although an individual from the lake bed did have an area of white hairs around its nose.

Interpretation of Population Data for Radiation Effects. – Although the study was designed to investigate population dynamics, external examinations were made to determine if radiation effects possibly were manifested. Analyses of population data for cotton rats show that some differences did exist between the populations of White Oak Lake bed and the old field. It is well known that reproduction is a process which seems to be relatively sensitive to radiation. No males with descended testes were recorded at the White Oak Lake bed during October and November 1959, but males with scrotal testes were present during these months at the old field. No pregnant females were noted during November 1959, at the lake bed, but a gravid female was present during this month at the old field. The average litter size in the lake bed was 5.4 as compared with 7.7 in the old field. More males than females (42 males, 32 females)

Table 2.7. Cotton Rat Litters Born in Traps, Cages, and on the Study Areas

White Oak Lake Bed				Old Field			
Date	No. in Litter	♂♂	♀♀	Date	No. in Litter	♂♂	♀♀
			Born in Traps				
9-2-57	7			8-13-59	12	7	5
6-18-58	5	3	2	10-9-59	4	3	1
6-30-58	5	3	2				
8-13-58	6	4	2				
4-1-59	3	1	2				
5-12-59	6	3	3				
9-25-59	5	2	3				
9-25-59	5	5	0				
	42	21	14		16	10	6
			Born in Cages				
9-14-59	4	3	1	10-12-59	6	4	2
10-5-59	5	4	1				
10-16-59	6	3	3				
11-4-59	7	1	6				
	22	11	11		6	4	2
			Born on Area				
6-3-59	7	5	2	8-13-59	9	3	6
7-1-59	5	4	1	9-29-59	7	3	4
9-16-59	5	1	4	10-9-59	8	2	6
	17	10	7		24	8	16
Grand totals	81	42	32		46	22	24
Av No. in litter	5.4	3.1	2.3		7.7	3.7	4.0

were found in the litters at the lake bed, while at the old field the division was more nearly equal (22 males, 24 females). More males than females were trapped at the lake bed. Most of the differences noted were not statistically significant. In addition, the effects produced by the differences in habitat, location, and population densities and structures would be difficult to separate from the effects of radiation.

Bioaccumulation. – Part of the data on bioaccumulation of radioisotopes has been reported previously.[24] These data and subsequent radioassays have been used to calculate whole-body dose rates to some of the animals from the settling basin and lower lake bed.

Settling Basin. – The ORNL settling basin for liquid wastes has a capacity of about one million gallons, and its primary purposes are (1) to allow

[24] S. I. Auerbach *et al.*, *Health Phys. Div. Ann. Progr. Rept. July 31, 1960*, ORNL-2994, p 162.

the settling out of particulates to which radionuclides are sorbed and (2) to provide a hold-up time for radioactive decay of short-lived isotopes. The liquid wastes which drain from the settling basin are a principal source of radioactive contamination in White Oak Creek and the Clinch River.[25] In 1954 a muskrat from the vicinity of the settling basin was found to have a high body burden of Sr^{90} and an osteogenic sarcoma of the right tibiofibula.[26] Body burdens for four muskrats trapped from the settling basin for the pilot study are shown in Table 2.9. Variations of radionuclide burdens are small within each of the two fractions except for specimen 204SVK which has a high quantity of Co^{60} and Sr^{90} in the GI tract.

Table 2.8. Injuries or Abnormalities of Cotton Rats

Condition	Number of Cases	
	Lake Bed*	Old Field**
Missing, swollen, or twisted toes	19	3
Part of tail missing	12	8
Large cuts or scars	11	2
Broken or badly swollen leg or foot	3	0
Swollen area around pectoral mammae	2	0
Subcutaneous lump anterior to vagina	2	0
Miscellaneous	10	1

*Total number of examinations, 1153.
**Total number of examinations, 199.

The whole-body dose rate to each muskrat was calculated for radionuclides deposited in the tissues only, and for radionuclides in tissues and GI tract with contents. The dose rate, R rems/week, to an organ of m g having a burden of qf_2 μc of a radioisotope may be expressed by

$$R = qf_2 \xi / mK \quad , \tag{4}$$

where $\xi = \Sigma EF(\text{RBE})n$ as defined by the ICRP.[27] K is a constant equal to 2.8×10^{-3}. The fraction of the whole-body burden in the organ of reference is f_2 and therefore is equal to 1 if the dose rate is calculated for the whole body. For determining the dose to the whole body when several isotopes

[25] E. G. Struxness, *Detailed Assessment of Solid and Liquid Waste Systems — Hazards Evaluation, vol 4*, ORNL CF-60-5-29 (May 31, 1960).

[26] L. A. Krumholz and J. H. Rust, *A.M.A. Arch. Pathol.* 57, 270–78 (1954).

[27] "Report of Committee II on Permissible Dose for Internal Radiation (1959)," *Health Phys.* 3, 1–233 (1960).

Table 2.9. Body Burdens of Radionuclides for Muskrats from ORNL Settling Basin

Identification Number	Burden of Radionuclides (μc)					
	Cs^{137}	Co^{60}	Ru^{106}	Zn^{65}	Ce^{144}	Sr^{90}
GI tract with contents						
202SVK	0.639	0.859	0.394			1.370
204SVK	0.976	67.600				12.400
279SVK	0.122	0.089	0.014	0.560	0.077	0.214
280SVK	0.478	0.207	0.045	Trace	0.285	0.174
Residual carcass						
202SVK	3.710	0.098		0.053		13.800
204SVK	1.140	0.122		0.193		8.370
279SVK	0.312	0.071	0.152	0.274	0.116	8.790
280SVK	2.040	0.094	0.450	0.029	0.054	6.540

are present, Eq. (4) may be rewritten

$$R = \sum_{i=1}^{k} \frac{q_i \xi_i}{mK} , \qquad (5)$$

where $i = 1, 2, \ldots k$ radioisotopes. In applying this equation to muskrats from the settling basin we have assumed that the animal may be represented by a 10-cm-diam cylinder for the purpose of determining the effective absorbed energies. Values for ξ_i used in the calculations are Sr^{90}-Y^{90}, 1.1; Cs^{137}, 0.41; Co^{60}, 0.72; Ru^{106}-Rh^{106}, 1.4; Zn^{65}, 0.15; and Ce^{144}-Pr^{144}, 1.3.

When the radionuclides in the contents of the GI tract are excluded from the calculations, the resulting estimates are probably minimum values. Equation (5) also may be used to calculate the whole-body dose rate resulting when the contents of the GI tract are considered as part of the body burden. This calculation assumes that these nuclides are uniformly distributed throughout the body and that self absorption is negligible. Since in actuality this is not the case, such estimates must be regarded as maximum values. The results of both types of calculations are summarized in Table 2.10. For one animal (202SVK) the relative increase in dose rate is slight when the GI tract is included, but for the other three the increase is larger, especially for 204SVK which is increased 7-fold from 15.1 to 112 rems/week. The true dose-rates probably lie between the two values calculated for each muskrat and would be high enough to suggest that radiation-induced pathologies or premature aging might result from such dose rates. Gross pathological examinations of all four animals and diagnostic x rays of 279SVK and 280SVK did not reveal any lesions. The exposure time is not known for these animals and it may have been short enough that effects did not have sufficient time to be manifested.

When muskrats leave the settling basin they use White Oak Creek as an avenue of dispersal. Since muskrats are an important fur resource and also are utilized as food, more information is needed on muskrat life histories to determine the extent of movements of radioactive animals from controlled areas to uncontrolled areas such as the Clinch River. Table 2.11 lists the concentrations of radioisotopes found in various organs and tissues of a fifth muskrat from the settling basin.

Table 2.10. Whole-Body Dose Rates from Internal Sources for Muskrats from ORNL Settling Basin

Identification No.	Dose Rate to Whole Body from Radionuclides in Residual Carcass (rem/week)	Dose Rate to Whole Body from Radionuclides in Residual Carcass and GI Tract with Contents (rem/week)
202SVK	23.7	27.8
204SVK	15.1	112
279SVK	13.2	21.2
280SVK	8.3	17.8

It is interesting to note that the highest concentration of Cs^{137} is in the muscle, which would be the tissue most certainly utilized for food. In addition to the muscle, it is probable that the liver would also be eaten. By a modification of Eq. (5) it is possible to calculate the dose to a person eating muskrat muscle and liver having the concentrations of radionuclides shown in Table 2.11. The body burden, q_i, of a person ingesting Q_{0i} μc in a given mass of contaminated meat may be estimated from the equation

$$q_i = Q_{0i} f_{1i} (e^{-\lambda_i t}) , \qquad (6)$$

where f_{1i} is the fraction of the ingested isotope reaching the blood from the GI tract and $e^{-\lambda_i t}$ is the expression for elimination (λ = 0.693 per effective half-life and t = days postingestion). Substitution into Eq. (5) for q_i gives

$$R = \sum_{i=1}^{k} \frac{Q_{0i} f_{1i} (e^{-\lambda_i t}) \xi_i}{mK} . \qquad (7)$$

If it is assumed that a person ingests at one meal, 1 lb (454 g) of muscle and the entire liver (22.3 g in the case of 201SVK), his dose rate for t = 0 is 0.023 rem/week, and for t = 7 days his dose rate is 0.019 rem/week. If a second muskrat is eaten (assume the same q_i as for the first ingestion) one week after the first muskrat was eaten, then the dose rate immediately after the second ingestion is 0.023 rem/week plus 0.019 rem/week which equals 0.042 rem/week. The maximum

Table 2.11. Concentrations of Radionuclides in Tissues and Organs of Muskrat ♂ 201SVK from Settling Basin

Sample	Concentration of Radionuclide ($\mu\mu c/g$, dry wt)						
	Cs^{137}	Cs^{134}	Co^{60}	Ce^{144}	Ru^{106}	Zn^{65}	Sr^{90}
Stomach contents	10,700	*	3,620	*	5,480	*	27,300
Small intestine contents	37,600	*	10,500	8,010	11,000	*	44,800
Caecum and large intestine contents	33,000	*	63,800	33,900	37,700	*	70,800
Stomach (washed)	5,250	*	1,160	*	*	1,170	1,290
Small intestine (washed)	6,190	*	2,090	*	786	2,130	3,590
Caecum and large intestine (washed)	3,990	*	8,620	*	3,970	*	3,820
Liver	17,100	*	4,240	*	*	2,120	**
Kidneys	25,800	*	7,560	*	*	*	**
Brain	10,600	*	285	*	*	568	**
Spleen	21,600	*	1,290	*	*	*	**
Muscle	34,200	377	219	*	*	530	**
Eyes	17,300	*	*	*	*	Troce	**
Lungs	21,000	*	1,080	*	*	989	**
Femurs	3,280	*	160	*	*	773	190,000
Lower incisor teeth	1,730	*	*	*	*	697	268,000
Pelt (washed)	5,840	*	494	*	*	*	1,240
Pelt (unwashed)	5,540	*	406	*	*	708	1,000

*None detected.
**Sample not radioanalyzed for this nuclide.

permissible dose rate based upon a 50-yr exposure for persons living in the vicinity of an atomic energy installation is 0.03 rem/week. The estimated dose rates from the hypothetical case do not take into consideration the Sr^{90} and alpha emitters which might have been in the muscle and liver (no analyses were made for them); therefore, the dose rates for the conditions set forth may not be maximum estimates, but relatively conservative estimates. The calculations presented here are based upon a small amount of data, but emphasize the importance of determining whether radioactive muskrats are a part of man's food.

Lower White Oak Lake Bed. – In contrast to the muskrats from the settling basin, the cotton rats from the lower lake bed are exposed to a much lower radiation dose. Dose rates from internal sources were calculated from the body burdens listed in Table 2.12. These body burdens have a small enough variation to permit calculation of an average dose rate. Equation (5) was used by substituting the proper values for ξ_i (based upon a 5-cm-diam organism), q (Table 2.6), and m. The estimated average whole-body dose rate is 0.3 rem/week when only radionuclides in the tissues are considered, but is increased to 2.9 rems/week when the radioactivity in the GI tract and external radiation field is taken into consideration. Total absorption was assumed from a 15 mr/hr average external radiation field. Eighty-six per cent of the 2.9 rems/week dose rate is due to the radiation field above the lake bed, 10% is due to

Table 2.12. Body Burdens of Radionuclides for Cotton Rats from Lower White Oak Lake Bed

Identification Number	Body Burden (exclusive of GI tract contents) ($\mu\mu c$)			
	Sr^{90}	Ru^{106}	Cs^{137}	Co^{60}
155SVK	9,440	1,080	989	451
156SVK	12,800	1,300	1,090	616
157SVK	16,200	932	1,200	460
158SVK	9,420	1,210	998	598

radioisotopes deposited in the tissues, and the remaining 4% is due to radioisotopes in the contents of the GI tract. The Cs^{137}, Ru^{106}, and Co^{60} deposited in the lake bed soil accounts for almost all of the external radiation dose, whereas Sr^{90} accounts for 84% of the dose from radionuclides in the tissues.

Rats 156SVK and 158SVK were known to be 170 days old when collected for radioassay because they were first captured, marked, and released when one day old. Assuming that these animals lived this entire period on the lake bed, it is possible to calculate the theoretical body burden at the time of capture and the theoretical body burden at equilibrium. These estimates may be evaluated by comparing them to the observed values from radioassay. In order to have an equilibrium condition, intake must equal elimination and can be represented by

$$ra = \lambda Q_e \,, \tag{8}$$

where

r = rate of feeding (μc/day),

a = fraction of ingested isotope assimilated by organs,

$\lambda = 0.693/T = 0.693/T_r + 0.693/T_b$,

T = effective half-life (days),

T_r = radiological half-life (days),

T_b = biological half-life (days),

Q_e = body burden at equilibrium (μc).

For the radioisotopes under consideration, $T \cong T_b$ because $T_r \gg T_b$. The body burden at 170 days may be represented by

$$Q_{170} = Q_e(1 - e^{-\lambda t}) \,, \tag{9}$$

where Q_{170} is the theoretical body burden at 170 days (μc), and t is the age of the animal (days). The rationale for use of Eqs. (8) and (9) is that there must be a constant rate of intake of radioactivity. For the animals under discussion, this is assumed. The estimated average daily rate of food intake from 0 to 170 days (6.5 g, dry wt per day) was multiplied by the average radioisotope concentration per gram of stomach contents to obtain r of Eq. (8). Assimilation factors and biological half-lives from the literature are:

Isotope	Assimilation Factor	Biological Half-Life (days)
Sr^{90}	0.15 (ref 28)	350 (ref 28)
Cs^{137}	0.80 (ref 29)	6.5 (ref 29)
Ru^{106}	0.03 (ref 30)	85 (ref 30)
Co^{60}	0.30 (ref 27)	9.5 (ref 31)

The laboratory rat was used as the experimental animal for Sr^{90}, Cs^{137}, and Ru^{106}, whereas the laboratory mouse was used for Co^{60}.

The Q_e and Q_{170} values are equal for both rats in terms of Cs^{137} and Co^{60}, indicating that the radioisotope concentrations in the animals theoretically were at equilibrium with the radioisotope concentrations in the food at the time of capture (Table 2.13). For practical purposes, equilibrium may be assumed to be reached after five biological half-lives ($^{31}/_{32}$ of the final value), which would be a minimum of 33 days and a maximum of 48 days for these two radioisotopes. On the other hand, Table 2.13 shows that the Q_{170} values are slightly more than $^1/_4$ of the Q_e value for Sr^{90} and $^3/_4$ of the Q_e value for Ru^{106}. These differences between estimates of Q_e and Q_{170} are obviously influenced a great deal by the longer biological half-lives. Because of these long biological half-

[28] K. Williams, *Strontium Studies*, AERE-R 3423 (1960).

[29] C. R. Richmond, *Retention and Excretion of Radionuclides of the Alkali Metals by Five Mammalian Species*, LA-2207 (1958).

[30] R. C. Thompson *et. al.*, *Am. J. Roentgenol., Radium Therapy Nuclear Med.* **79**, 1026–44 (1958).

[31] M. J. Cook, K. Z. Morgan, and A. G. Barkow, *Am. J. Roentgenol., Radium Therapy Nuclear Med.* **75**, 1177–87 (1956).

Table 2.13. Calculated and Radioassay Body Burdens of Radionuclides for Two Cotton Rats from Lower White Oak Lake Bed

Isotope	Body Burdens ($\mu\mu c$)			
	Calculated		Radioassay	
	Q_e	Q_{170}	♂ 156SVK	♀ 158SVK
Sr^{90}	57,400	16,400	12,800	9,420
Ru^{106}	11,400	8,520	1,300	1,210
Co^{60}	9,530	~9,530	616	598
Cs^{137}	28,600	~28,600	1,090	998

lives, and the fact that cotton rats on the lake bed rarely live more than one year,[32] Sr^{90} concentrations in cotton rats could not come into equilibrium with concentrations in food; however, Ru^{106} equilibrium would occasionally be possible.

The body burden of each radioisotope determined by radioassay was in all cases lower than the calculated value Q_{170} (Table 2.13). The closest agreement was for Sr^{90} where the radioassay body burdens were about $\frac{3}{4}$ and $\frac{1}{2}$ of the Q_{170} body burden. The much larger differences for the other radionuclides indicate that either the experimental data from the literature do not apply or that the feeding rate and exposure time estimates have significant errors. It seems likely that the most significant error might be in the time of exposure, t. There is an increasing divergence between the radioassay values and Q_{170} values as biological half-life decreases. This condition would be expected if the animals had fed for a period of time on noncontaminated food before they were captured. If $t < 170$ days, then there has not been a constant rate of intake and use of Eqs. (8) and (9) is not valid. Certainly it is possible that these cotton rats could have lived part of the time off the contaminated lake bed.

New Studies of Pathologies and Bioaccumulation. – A two-year investigation initiated last summer on pathologies of mammals from radioactive and nonradioactive areas will be completed in September 1961. Few gross pathological conditions have been observed so far in these mammals, but examination of tissues taken from the major organs revealed an unexpected number of generalized pathologies, none of which could be positively related to radiation exposure. None of the lesions suspected of being tumors upon gross examination were neoplastic.[33] Thirty-four white-footed mice from radioactive areas were examined; 18 (53%) displayed pathologic conditions. Of 52 individuals from nonradioactive areas, 34 (66%) were positive. Table 2.14 is a summary of the lesions observed in the white-footed mice. X rays of 81 mammals revealed no unusual skeletal abnormalities.[34] Final evaluation of the incidence of pathological conditions in the mammals in radioactive and nonradioactive areas must wait until this project has been completed. Data on packed-cell volumes of blood are also being taken this year before animals are autopsied. The Coulter electronic particle counter and cell-size analyzer is being tested and calibrated for studying numbers and size distribution of blood cells. Trial runs on human and rodent blood have given encouraging results on accuracy and reproducibility for determining cell numbers. Studies of size distribution have not progressed far enough for evaluation.

A block of four pens, each 10 × 10 m, has been constructed on both the lower lake bed and on an uncontaminated old field, and similar pens are being built on the upper lake bed and on another uncontaminated area. Adult cotton rats have been introduced into the pens to test for survival and optimum density. Animals of known histories will be placed in the pens and sampled at selected times for blood and radioanalyses of tissues. Bioaccumulation of radionuclides can be ascertained, and effects of radiation on the circulating cells of the blood can be related to radiation dose.

[32] P. B. Dunaway and S. V. Kaye, *Transactions Twenty-Sixth North American Wildlife and Resources Conference*, in press.

[33] W. D. Gude and his associates of the Biology Division prepared the slides. G. E. Cosgrove, Biology Division, examined the slides.

[34] Diagnostic x rays taken and analyzed by M. E. Finkel, Argonne National Laboratory.

Table 2.14. Incidence of Lesions Observed in *Peromyscus leucopus* from Radioactive and Nonradioactive Areas

	Animals with Pathologies			
	Number		Per Cent	
	Contaminated Areas	Noncontaminated Areas	Contaminated Areas	Noncontaminated Areas
Sporozoan cysts	6	15	17.7	28.8
Cuterebra larvae	11	14	32.4	26.9
Liver infiltration	3	11	8.8	21.2
Liver necrosis	1	6	2.9	11.5
Liver nodules	0	3	0	5.8
Spleen, abnormal	2	7	5.9	13.5
Lymph node, hyperplastic	0	2	0	3.8
Glomerulosclerosis	0	1	0	1.9
Bladder, ulcer	1	1	2.9	1.9
Lung, abnormal	2	0	5.9	0
Gastric mucosa, nodule	1	0	2.9	0
Heart, thrombus	1	0	2.9	0
Tail, cutaneous abscess	4	0	11.8	0
Miscellaneous lesions	0	3	0	5.8

FOREST ECOLOGY

J. S. Olson

D. A. Crossley, Jr.
R. L. Doub[35]
M. P. Hoglund
H. D. Waller
M. Witkamp
W. C. Cate
G. Dodson
R. J. Hutnik[36]
R. O. Petty[37]
J. P. Witherspoon[38]

Experimental and field research reported in this section includes (1) characterization of the habitats, biomass, productivity, and chemical turnover of terrestrial ecological systems of Oak Ridge, which are mostly forests; (2) tracer experiments on the ecological or biogeochemical cycles of radioactive isotopes and chemical elements; and (3) biological studies of the soil fauna and microorganisms which participate in the natural circulation of nutrients and radioisotopes. The development of ecological models, with the aid of analog computer simulation of ecological systems, is aimed at synthesis of quantitative information from all parts of the ecology program. These studies of the environmental movements of radioactive isotopes not only provide information needed for health physics predictions of the consequences of release of radioactive materials into the environment but should enhance our understanding of the natural operation and organization of ecological systems (ecosystems).

Studies of the Oak Ridge Reservation

The Oak Ridge Reservation constitutes a large-scale field research facility, analogous to the

[35] Cooperator, Division of Forestry Relations, Tennessee Valley Authority.
[36] Summer employee, 1960.
[37] Visiting investigator, October 1960, Wabash College, Crawfordsville, Indiana.
[38] ORINS Fellow, University of Tennessee.

reactors, cyclotrons, and chemical and biological laboratories of other groups. Studies of the diverse ecosystems represented on or near this area of the southern Appalachian Mountains serve the double purpose of helping to plan the optimal use of this facility and of providing information and materials needed for analysis in the experimental program.

The map of Fig. 2.12 shows the location of several features affecting the research program. Sites influenced by waste disposal are chiefly located in the White Oak Creek Drainage basin. Soils which have developed along the linear outcrop belts of several contrasting geologic formations are extensively represented here and in other parts of the Reservation. These several types of substrate vary in the development of different forest types and conditions, which have been mapped and sampled by the TVA Division of Forest Relations. Several studies of tree biomass and productivity are providing the basis for using stand information for interpreting the rate of movement of materials in the forests. Chemical analyses of the collected samples help to show differences in the rates of cycling of different elements, which are being investigated further by tracer techniques.

Sources of Isotope Contamination at Oak Ridge. – The early phase of orienting the basic research program on isotope movement in forests included a survey of the several pathways by which radioactive contamination was reaching areas outside the White Oak Lake bed and Clinch River; this phase was summarized last year.[39] A report[40] now completed discusses aerial contamination, which involves wider distribution but lower levels of activity than other waste disposal practices. Less survey work was done this year than previously, but the increase in potential sources of radioactivity on the Reservation suggests that ecological monitoring will need to be increased again in the future.

Preliminary sampling of tree foliage near one of the earliest pits in solid-waste burial ground No. 5 (SWB5 on Fig. 2.12) did not reveal conspicuous gamma activity by the autumn of 1960, but increased use of this burial ground for solid wastes from all over the eastern United States will require systematic attention in the future.

The main source of environmental radioactivity around ORNL continues to be low-level and intermediate-level wastes diluted in large volumes of water from the settling basin (SB on Fig. 2.12), the old liquid-waste pits (LWP), the new liquid-waste column (LWC), the Intermediate Pond flood plain (IPF), and the upper and lower sections of the White Oak Lake bed (UWOLB, LWOLB). Effects on these areas and places of several accidental releases of radioactive material are indicated in last year's report and in other sections of the present report.

Soils and Geology. – Conasauga and Rome shales (belts 2 and 6 on Fig. 2.12) underlie several valleys, including many of the older ecology study sites in Melton Valley. Chickamauga limestone and shales (belts 1 and 5) underlie Bethel Valley and East Fork Valley. Separating such valleys are ridges which have resisted erosion, because of either resistant sandstones and siltstones of the Rome formation (as on Haw Ridge and Pine Ridge, belts 3) or deeply weathered cherty soils of the Knox dolomite (as on Melton Hill, Chestnut Ridge, and Black Oak Ridge, belts 1). The sequence of these lower Paleozoic formations is repeated several times because of typical southern Appalachian thrust-fault structure.[41] Limited areas of younger formations are preserved in a synclinal structure, which outcrops mostly outside the Controlled Area portion of the Oak Ridge Reservation (belt 8).

The selection and interpretation of experimental sites for either similarity or contrast of soils developed from these formations have required careful profile study, collection, and mapping of soil types. Soil-profile-horizon samples collected in 1960 have been processed and analyzed in varying degrees of detail (see the subsection, "Biogeochemical Analyses of Plants and Soils"). Field mapping has been restricted to small study areas and belts of special contrast (e.g., the very calcareous Bland and Upshur types in belt 5 on Fig. 2.12). Soil and litter characteristics pertinent to TVA foresters' interests in hydrology and ORNL's interest in forest chemistry have been studied in connection with the selected TVA forest survey plots mentioned below.

Whereas the ridges and certain higher areas within the valley belts of the Reservation are underlain by residual soil profiles, extensive

[39] J. S. Olson *et al.*, *Health Phys. Div. Ann. Progr. Rept. July 31, 1960*, ORNL-2994, pp 179–84.

[40] J. S. Olson, *Ecological Sampling and Meteorological Interpretation of Fallout on Forests Near Oak Ridge*, ORNL-3181 (1961).

[41] W. M. McMaster, *Geologic Map of the Oak Ridge Reservation* (to be published).

UNCLASSIFIED
ORNL-LR-DWG 61579

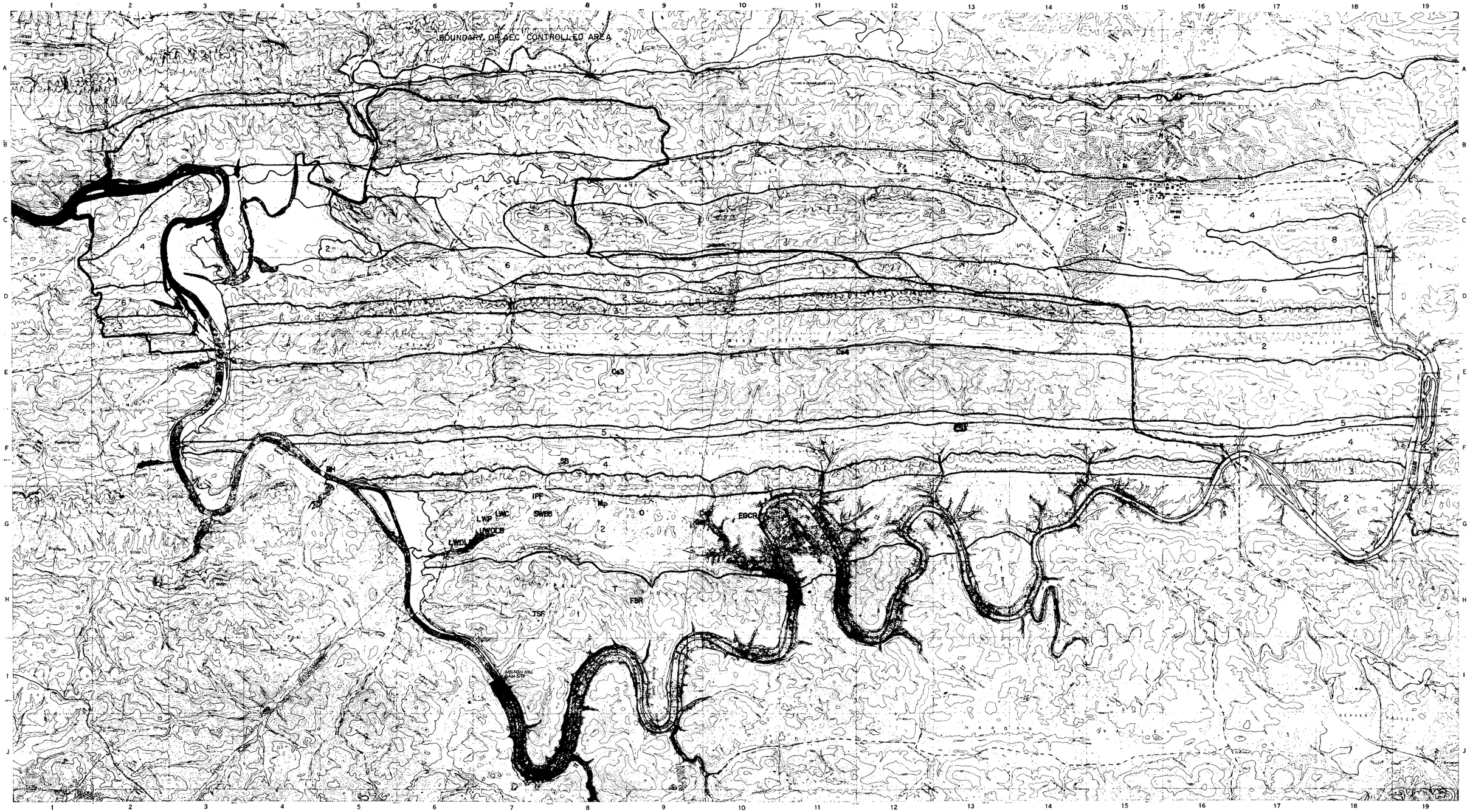

Fig. 2.12. Map of the Oak Ridge Reservation, Showing Features Influencing the Ecological Research Program. (See Table 2.15 for numbered geologic belts.)

gentle valley slopes and benches are underlain by colluvial soils whose upper horizons are influenced by soil creep and wash from nearby higher land. Local alluvial soils are limited to narrow bottom lands of small streams and to sinkholes, while broader terrace and bottom-land soils occur mainly along the Clinch River, chiefly along the southwest border of the Reservation (area 7 on Fig. 2.12). Table 2.15 relates the commoner soils to substrate and topography.

Distribution and Characteristics of Oak Ridge Forests. – Differences in biological composition and characteristics of growth of diverse forest types affect the rate and character of the movement of radioactive materials and must be taken into account systematically in the selection of research areas.

Between November 1960 and April 1, 1961, the TVA Division of Forest Relations extended its survey to the establishment of 226 permanent plots. Diameters, heights, and other data on trees in nested circular plots were recorded and later processed on IBM cards for use in forest management planning and ecological research.

Most of the tree biomass in the Reservation is in "small sawtimber" stands, with tree diameters,

Table 2.15. Relation of Soil Types of the Oak Ridge Area to Parent Material and Normal Topographic Position

Geologic Belt and Typical Lithology	Type of Material and Topographic Position		
	Upland Residual Soil	Bench or Terrace	Bottom-Land Alluvial Soil
		Colluvium	Local Alluvium
1. Knox dolomite	Clarksville		
	Fullerton	Landisburg	Greendale
		Minvale	
	Bolton	Hermitage	Emory
2. Conassauga shale	Montevallo		
	Litz		
	Sequoia	Leadvale	Prader
Limy shale	Armuchee	Muse	
3. Rome sandstone	Muskingum	Jefferson	
	Hartsells	Allen	
Red siltstone	Lehew		
4. Chickamauga limestone	Colbert		
	Talbot	Minvale	Linside
Shale	Sequoia	Leadvale	
5. Red limestone	Bland		
	Upshur		
6. Rome shale	Teas		Camp
		Terrace Deposits	River Bottom*
7. River deposits		Nolichucky	Linside
		Cumberland	Melvin
		Waynesboro	Huntington

*Noncalcareous river deposits of sandstone and shale are sometimes distinguished as Stasser, Hamblen, and Prader.

at 4.5 ft above ground, of 9 to 15 in. for pine and 11 to 15 in. for hardwoods (Table 2.16). "Large sawtimber" stands are mostly limited to a few ridge slopes. It is important for research purposes that examples of such old and relatively undisturbed forests are available on appropriate soil and topographic situations. "Poletimber" and younger stands, mostly on old fields, occupy extensive areas, including gentler slopes and valley bottoms, and are mostly changing rapidly. Aerial photographs taken at various times since 1925, and present data and future remeasurements of the permanent plots document the rate of forest development and succession.

Tree Biomass and Productivity. – In order to translate data on living stands of trees into estimates of the organic material (and chemical or isotopic composition) on a unit area of ground, statistical regressions can be used to relate these characteristics to readily measurable variables such as tree diameter and height. These methods are also being extended for measurements of *increment* of biomass, or growth. Production of

Table 2.16. Approximate Distribution of Cubic Foot Volume of Acreage of Forests by Geologic Belt in the Oak Ridge AEC Controlled Area

For each set of values, the first number is the thousands of cubic feet (gross) for each forest stand size, the second value is the number of acres,[a] and the third value is the number of gross cubic feet per acre[a]

Geologic Belt	Forest Stand Size				Total, All Stand Sizes
	Large Sawtimber	Small Sawtimber	Pole Timber	Young Growth[b]	
1. Knox dolomite	1153	5,463	1921	325	8,862
	582	5,044	2910	3492	12,028
	1981	1,083	660	93	737
2 and 6. Conasauga and Rome shales	286	3,659	481	775	5,201
	194	3,686	1164	2522	7,566
	1474	992	413	307	687
3 and 8. Rome and post-Chickamauga (mostly Rockwood) formations	624	2,410	119	19	3,172
	485	2,619	194	291	3,589
	1287	920	613	65	883
4 and 5. Chickamauga limestone and shale	708	1,832	329	95	2,964
	485	1,348	873	1649	4,355
	1459	1,248	377	57	680
All geologic belts[c]	2771	13,364	2850	1214	20,199
	1746	12,697	5141	7954	27,538
	1585	1,052	553	145	733

[a]Acreage proportions based on grid, points: one plot per 194 acres in belt 1 (Knox dolomite), one plot per 97 acres elsewhere. Areas and total volumes subject to revision based on mapping.

[b]Young growth includes open and closed natural stands or plantations having less than 1500 net board feet or 30 trees >5 in. in diameter at 4.5 ft per acre.

[c]River-bottom alluvium not represented by forested plots.

foliage is also being estimated by collections of recently fallen liter.

Initial sampling of shortleaf pine by methods described earlier[42] was extended in 1960 to the site being cleared at the High-Flux Isotope Reactor site. Preliminary statistical analysis confirmed the linear regression relating logarithm of branch mass to logarithm of branch diameter (Fig. 2.13), except for a few readily recognizable broken branches. This and other results encouraged progress in two directions. More rapid progress on the analysis of a number of deciduous species was possible in 1961, with the cooperation of R. E. Shanks of the University of Tennessee Botany Department, by combining a simplified tree-measurement procedure for most trees with a complete weighing for some. These rapid methods and a slower, intensive analysis of trunk and branch growth in cooperation with R. H. Whittaker of Brooklyn College are being used in the summer of 1961 on Chestnut Ridge. Samples of trunk and branch and foliage materials are selected for subsequent chemical analysis. The more intensive growth analyses are being made on *Pinus echinata*, *Quercus alba*, and *Liriodendron tulipifera*, the species which dominate the forests where major tracer experiments are in progress (see below).

Litter production in several study areas of the Reservation was measured by monthly or more frequent collections from bushel baskets, staked a few inches above ground level. Results in Table 2.17 cover 1 yr for most stands. The six stands included in a study of litter decay rates all had production rates from about 400 to about 600 g m^{-2} yr^{-1}. This variability was not related consistently to forest cover (pine vs deciduous) or slope (north, south, level). These results are consistent with other data indicating production of approximately 500 g m^{-2} yr^{-1}.

Biogeochemical Analyses of Plants and Soils. – All the preceding studies provide steps toward determining inventories of materials stored in ecological systems, particularly in forests where long-term storage is prominent, and estimates of the rates at which these materials move. Chemical analyses of the samples from the collections make possible an evaluation of the processes of movement for many elements. Elements which have hazardous long-lived radioactive isotopes (cesium, cobalt, cerium, strontium) have been singled out for special attention, but information on many additional elements has been made available to aid the basic research program and to help interpret the movement of elements and isotopes in ecosystems.

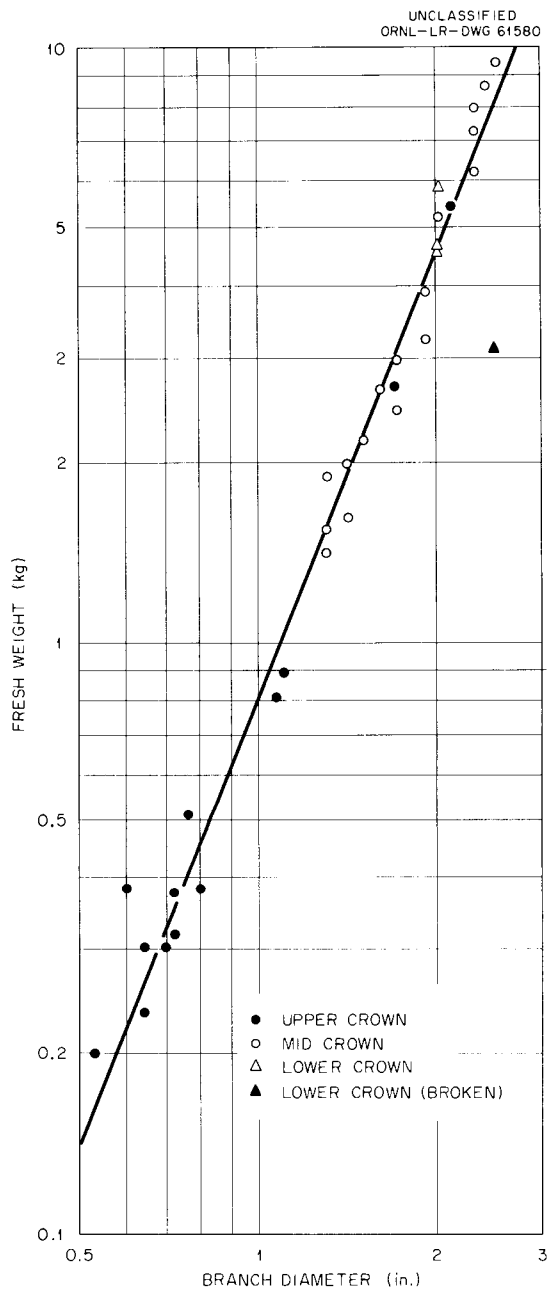

Fig. 2.13. Regression of Branch Mass on Basal Diameter for One Short-Leaf Pine Tree, Shown Separately for Lower, Middle, and Upper Crown Levels.

[42] S. I. Auerbach *et al.*, *Health Phys. Div. Ann. Progr. Rept. July 31, 1959*, ORNL-2806, pp 45–47.

Table 2.17. Litter Fall (g/m^2) in Nine Forests of the Oak Ridge Reservation

Forest Habitat	1960 May–June	1960 July–August	1960 September–October	1960 November–December	1961 January–February	1961 March–April	Total
Conifer							
Pine							
Dry upland-level	34	40	72	73	91	70	380
Upper north slope	165	88	188	100	48	74	663
Upper south slope	64	77	167	97	107	107	618
Mean	87	68	142	90	96	84	554
Lower south slope			121	56	57	88	
Deciduous							
Oak, hickory, tulip							
Dry upland-level	30	66	324	55	29	34	538
Upper north slope	71	84	143	40	24	59	421
Upper south slope	10	96	339	6	24	24	499
Mean	37	82	268	34	26	39	486
Valley	107	50	394	2	25	31	627
Tulip poplar ash							
Sinkhole	25	49	320	41	18	20	472
Red maple, gum							
Valley			312	17	42	35	

Flame-photometric analyses of potassium, sodium, calcium, magnesium, and strontium have been continued in connection with studies of litter breakdown (discussed below) and for ammonium acetate and acetic acid extracts or complete digestates of soil profile horizons. Exploratory activation analyses have been successful in detecting cesium, cobalt, cerium, and many additional elements in soils and plant materials. A few representative analyses are included in Tables 2.18 and 2.19 to indicate some of the elements covered and their approximate levels in local materials. Since these methods are still being tested and developed, the results are subject to revision prior to further publication.[43]

Relatively few studies report the naturally occurring levels of cesium in plants and soils.[44,45] Both nondestructive and radiochemical separation methods confirm that cesium is commonly present in Oak Ridge soils at uniform levels of a few micrograms per gram. Studies of cesium in biological samples are still in progress.

Cobalt concentrations are higher but more variable (6 to 50 or more $\mu g/g$) in soils, with sufficient variability among some duplicate or triplicate samples to suggest the possibility that inclusions of individual grains of material with high or low cobalt content are substantially

[43] Parts of the activation analyses have been supported by Isotopes Development funds, with the cordial cooperation of G. W. Leddicotte and L. C. Bate. We are also indebted to T. C. Raines for flame-photometric studies and to many other members of the Analytical Chemistry Division for other help.

[44] N. Yamagata *et al.*, *Bull. Chem. Soc. Japan* 32, 407–14 (1959).

[45] A. P. Vinogradov, *The Geochemistry of Rare and Dispersed Chemical Elements in Soils*, 2d ed., translated by Consultants Bureau, Inc., New York, 1959.

Table 2.18. Activation Analyses[a] of Cesium, Cobalt, and Cerium in Soil Profile Horizons from the Oak Ridge Reservation (Values in $\mu g/g$)

Geologic Belt and Soil Series	Soil Profile Horizon[b]						
	A_1	A_2	A_3	B_1	B_2	B_3	C_1
A. Cesium							
1. Knox dolomite							
Fullerton[c]	2.9	3.6	5.1	6.4	8.5	8.4	7.9
Landisburg[c]	2.4	2.9	3.6	3.9	3.9	3.7B3M1	3.6B3M2
Emory	3.4	9.2		9.3B		7.0	8.0
2. Conasauga shale							
Sequoia 1[c]	1.8	2.4		4.6	5.4		5.7
Sequoia 2	2.6	1.7	3.9	3.6	3.5	4.4	
Monongahela[c]		3.3AP		4.1	4.9	5.4	7.4
Prader		3–5A				3.3C11	3.3C12
3. Rome formation							
Muskingum		5–7				2–6BC	3.9
Lehew	3.5	4–6				4–2 BC	4–6
4. Chickamauga							
Leadvale		3.2AP		3.9		3.7B3M1	5.6
B. Cobalt							
1. Fullerton	26	16	13	9.5	16		15
Emory	38	37		44B		36	51
2. Sequoia 1	6.9	8–13		17	21		17
Sequoia 2	33	35	48	35		18	
Prader		7.9A				11C11	7.1C12
3. Muskingum		6.5				9.1BC	17
Lehew	6.1	6.2				5.9BC	9.3
4. Leadvale		7.6AP		6.0	16		31–83
C. Cerium							
1. Fullerton	185	42	99–124	68	314		314–419
Emory	83	113		153B		165	170
2. Sequoia 1	334	316–397		291	251		162–227
Sequaia 2	33	57	54	63	86	54	
Prader		83				50C11	64C12
3. Muskingum		96				93BC	75–110
Lehew	63	53				16BC	44
4. Leadvale		97AP		60		55B3M	68

[a]These values are subject to change prior to further publication.

[b]Except for profile horizons otherwise designated.

[c]Four profiles were analyzed for cesium by radiochemical separation of scandium and iron. All others were analyzed by nondestructive gamma spectrometry with complement subtraction, following one week of irradiation and several weeks of decay of shorter lived nuclides.

Table 2.19. Some Trace Elements in Pine Trees, Tentatively Estimated[a] by Activation Analysis (Values in μg/g)

Element	Material and Crown Position[b]										
	New Needles			Old Needles			Old Twigs[c]			Boles[d]	
	Lower	Middle	Upper	Lower	Middle	Upper	Lower	Middle	Upper	Lower	Upper
Co	0.024	0.022	0.029	0.039	0.023	0.039	0.017	0.024	0.022	0.117	0.125
Ce										0.25?	0.11
Sc	0.15	0.20	0.15	0.25	0.25	0.25	0.18	0.27	0.23		
Zn	42	34	36	47	36	48	18	39	75	14	19
Cu	2.85	3.17	3.23	2.52	3.68	2.79	4.13	5.25	5.25	0.40	0.51
Cr	2.36	5.21	2.69	4.15	3.58	4.16	2.73	3.37	4.09	0.42	0.77
Br	19.4	19.5	15.9	21.6	18.8	22.3	2.93	3.73	4.85	0.97	0.87

[a]These values are subject to change prior to further publication.
[b]Lower, middle, and upper thirds of crown.
[c]Material less thon 0.5 in. in diameter, excluding first-year shoots.
[d]Averages for six trees – three lower bole and three upper bole slabs of each.

modifying the results. Table 2.19 shows consistently lower cobalt contents of pine tree materials (tenths of a microgram per gram for boles, a few hundredths of a microgram per gram for foliage and branches), spanning the range of values which Beeson, Lazar, and Boyce[46] found for coastal-plain vegetation other than for species showing a specific capacity for concentrating cobalt.

Cerium showed still higher values in soils (50 to 350 μg/g in most cases). Lanthanum, another rare earth, varied from 25 to 90 μg/g in these samples, while the chemically similar scandium was consistently lower. Values of a fraction of a microgram per gram for both cerium and scandium in pine samples (Table 2.19) are consistent with the concept of low biological availability of rare earths and similar elements for most plant species, and possibly low biological hazard of radioisotopes of these elements after their incorporation into the soil.

While early analyses of zinc vary from 1 to 20 μg/g in soils, the plant analyses are in the range of 10 to 40 or more μg/g (Table 2.19), consistent with Beeson's values for all species except the zinc accumulator *Clethra alnifolia*. Another essential micronutrient, copper, showed plant values of 2 to 5 μg/g, slightly lower than Beeson's values for needle and branch samples, and considerably lower for bole samples. Chromium similarly showed a difference of several micrograms per gram for needle and branch samples, and tenths of a microgram per gram for branches. One of the surprising results was for bromine, which was slightly above or below 1 μg/g in 12 bole samples, but which showed foliage values of 15 to 22 μg/g.

Tracer Experiments and Ecological Cycles

The prediction of movement of radioactive isotopes of an element and an understanding of the ecology and biogeochemistry of the element are closely related problems. More extensive chemical analyses like those given above, supported by field data on the amounts of materials and rates of movements involved, are prerequisites for measuring the specific activity of hazardous isotopes in different parts of an ecosystem and for interpreting the reasons for their environmental movements. Conversely, the use of radionuclides as tracers provides a tool for basic research on the natural circulation of the elements they represent. They not only indicate the dominant pathways of movement but allow measurement of rates of transfer through the several stages of a complete cycle.

Cesium-134 Cycle Involving White Oak Trees. – The study of natural cycling of Cs^{134} continues around three inoculated white oak trees growing on

[46]K. C. Beeson, V. A. Lazar, and S. G. Boyce, *Ecology* 36, 155–56 (1955).

each of four contrasting soils (Monongahela and Sequoia on Conasauga shale and Landisburg and Fullerton on Knox dolomite soils, in wet and dry sites, respectively). These sites are labeled Cs 1, Cs 2, Cs 3, and Cs 4 on Fig. 2.12.

Rapid initial movement of this radioisotope into the leaves and prompt removal of portions by rain leaching were reported last year.[47] Total leaf uptake was greater in trees on the dolomitic sites, but it is not yet known whether this was due to some site characteristic or to the fact that trees on the shale sites happened to be inoculated before or after the time in the growing season most favorable for uptake. Subsequent work has shown that leaf radioactivity increased up to about 30 days after inoculation, but then decreased until the end of the growing season, when a reduction of 39 to 72% [mean (62.6 ± 3.2%)] was observed (Fig. 2.14). While 9 to 18% of the reduction in leaf contents of Cs^{134} was estimated to be due to rain leaching, the remainder was presumably translocated back into the woody tissue (Table 2.20).

[47] J. S. Olson *et al.*, *Health Phys. Div. Ann. Progr. Rept. July 31, 1960*, ORNL-2994, pp 172–74.

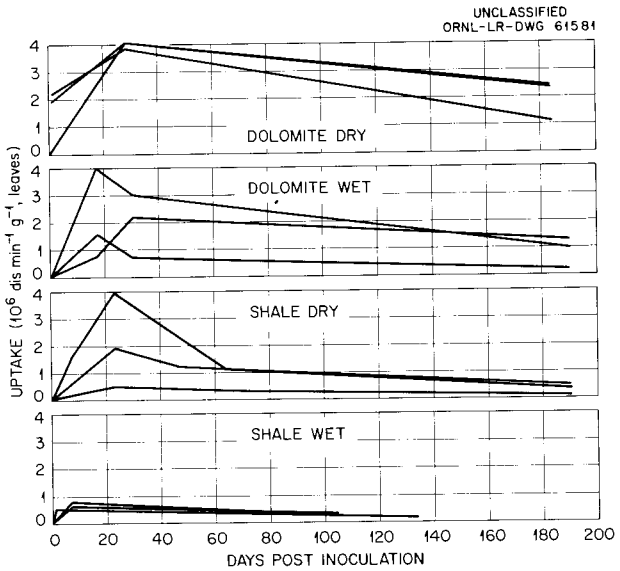

Fig. 2.14. Uptake and Depletion of Cesium-134 in White Oak Foliage – 1960 Growing Season.

This reduction of cesium in the leaves is similar to that reported for potassium (72.5%) by other workers.[48]

[48] H. J. Lutz and R. F. Chandler, *Forest Soils*, Wiley, New York, 1946.

Table 2.20. Stages in Transfer of Cs^{134} In and Around White Oak Trees During 1960 Growing Season

Cesium Distribution	Parent Material, Topography, Soil				Mean Values, All Sites
	Dolomite		Shale		
	Dry	Wet	Dry	Wet	
	1. Fullerton	2. Landisburg	3. Sequoia	4. Monongahela	
Maximum leaf uptake, % of input	45.7	49.3	28.8	6.9	32.7
Per cent of leaf uptake					
In leaves at end of season	42.3	39.8	35.1	32.4	37.4
Returned to tree wood	45.9	49.4	55.5	48.7	49.9
Rained out	11.8	10.8	9.4	18.9	12.7
Per cent of activity rained out					
In understory	2.9	9.2	7.6	5.6	6.3
In litter	27.4	9.4	18.4	10.8	16.5
In soil (0 to 4 in.)	69.7	81.4	74.0	83.6	77.2
Per cent of activity in top 4 in. of soil					
0–1 in.	72.4	65.3	68.7	28.5	58.7
1–2 in.	20.6	12.8	26.1	37.7	24.3
2–4 in.	7.0	21.9	5.2	33.8	17.0

Most of the radiocesium rained out was held only a short time in the litter layer under inoculated trees. By the end of the growing season a large percentage had moved into the mineral soil (Table 2.20). Mobility in the soil profile was significantly greater in the wet soils. The greatest mobility was observed in the wettest soil – the shale wet. With the exception of this wettest situation, over 60% of the total amount of soil radiocesium was still found in the 0 to 1 in. depth.

More recent studies in the summer of 1961 have shown that, after addition of more radiocesium via leaf fall and after overwintering, this element has penetrated to a depth of over 10 in. in wet illitic soil. However, the largest portion of soil Cs^{134} (70%) is still in the 0 to 1 in. layer, because of the addition of a fresh surface supply from the leaching of fallen leaves. X-ray diffraction analyses of clay minerals showed large differences between dominantly illitic clays of the Conasauga soils vs kaolinitic and vermiculite clays of the Knox soils. However, mobility in the soil is influenced not only by clay mineralogy (abundance of cesium-fixing minerals such as illite and vermiculite) but by moisture, presence of open channels, and other physical and biological features of the intact soil profile.

Data on leaf uptake for the 1961 growing season indicate that radiocesium which overwintered in the woody tissue of white oaks is moving into leaves in quantities as great as from the initial inoculations. Thus, trees seem not to offer any great ability to retard the movement of this element in a forest ecosystem for a long period of time.

Last year rapid movement of Cs^{134} from litter into white oak saplings was reported.[49] The total uptake by saplings during the 1960 growing season was small – less than 1% of the amount applied. Total sapling harvests showed that the roots contained most of the activity. Roots less than 0.5 mm in diameter contained 12 times more Cs^{134} on a weight basis than larger roots up to 50 mm. Eleven per cent of the radiocesium which had moved from litter into the top 2 in. of soil was found to be "available" in 1 *N* ammonium acetate (pH 7.0) extraction.

Levels of naturally occurring stable cesium involved in some of the cyclic processes are being investigated. Quantitative determinations have been made by activation analysis for the soil profiles represented on experimental sites (Table 2.18). While stable-cesium values in soil are low (1.8 to 8.5 $\mu g/g$) compared with macronutritional elements such as potassium, they are several orders of magnitude higher than the quantities of radiocesium (1.7 μg of Cs^{134}) inoculated into each tree and subsequently greatly diluted through a large mass of vegetation and soil. Studies are now in progress on the availability of soil stable cesium and levels contained in vegetation.

Weekly Estimates of Leaf Litter Breakdown and Release of Sr^{85}, Co^{60}, and Ru^{106}. – The previously reported experiments[50] involving weekly measurements of weight loss and release of radioisotopes by bagged leaf litter have been continued for more than a year. Although these data were developed primarily to support studies on litter-inhabiting arthropods (see below), the data form an unusually detailed description of weight loss by decomposing leaf litter and approximate the loss of incorporated radioisotopes from litter.

In November 1959, four combinations of leaf and radioisotope (Ru^{106} in pine, Ru^{106} in oak, Co^{60} in oak, and Sr^{85} in dogwood) in 1-dm^2 litter bags were placed in pine and oak stands. Every week a set containing three bags (one each of the leaf species) was collected from each stand, arthropods were extracted, and the bags were weighed, counted for radioactivity, and returned to the field. Eight such sets of bags were placed in the forests, so that each set was brought into the laboratory every eighth week. Thus repeated measurements at eight-week intervals were available for each bag. Bags returned to the field were placed in the identical sites from which they had been collected.

Loss of weight by litter followed a similar pattern in each of the six leaf-species stand combinations (Fig. 2.15). Initially, weight loss was rapid, evidently due to the loss of readily soluble compounds from the leaves. During the winter months the rate of weight loss was slow, since the activity of microbial and faunal elements was inhibited by cold weather (Fig. 2.15). During the spring and summer the rate of decomposition and weight loss again accelerated. Similar curves for loss of weight by ash and oak leaves on a *moder* soil formation were obtained by Bocock

[49] J. S. Olson *et al.*, *Health Phys. Div. Ann. Progr. Rept. July 31, 1960*, ORNL-2994, p 174.

[50] *Ibid.*, pp 177–79.

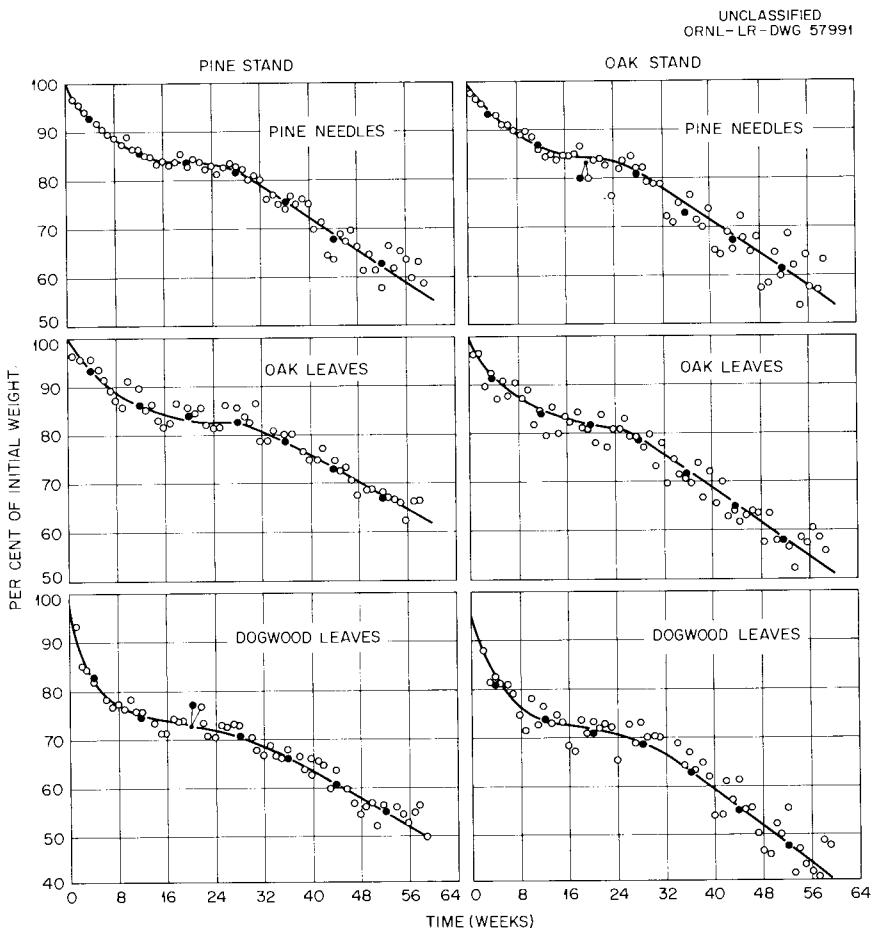

Fig. 2.15. Loss of Weight by Decaying Leaves in Litter Bags as a Function of Time. Three leaf species in two stands. Hollow circles are individual measurements; solid circles are averages for eight-week cycles. Line fitted by eye.

et al.[51] At the end of the year, fractions remaining were: pine, 61–63% of original weight; oak, 58–68%; and dogwood, 48–56%. In each case the litter bags in the oak stand lost more weight than did those in the pine stand. The difference between the species seems to lie in the initial period of weight loss in early winter, rather than in the rates of loss in the summer.

Regression coefficients were calculated for weight loss from each of the 48 bags. A logarithmic transformation that was used should give a linear regression under the ideal assumption that loss of weight is a negative exponential function; the regression approximates the annual trend but does not adequately describe the details of variation within a single year for the species under study (see solid lines in Fig. 2.16). Table 2.21 presents the means of the regression coefficients for weight loss by litter in the two stands. An analysis of variance detected differences between the stands but not between species of leaf. Real differences between rates of breakdown for the leaf species are certainly present, but for adequate treatment they require different analyses that respond to the rapid initial weight loss.

Figure 2.16 shows the count rates, expressed as a ratio of count rate of sample to count rate of standard and normalized to percentages of the initial count, for each of the three radioisotopes in pine and oak stands. Because litter in the bags settled under field conditions, many count rates exceeded 100% of the initial count. More variation exists in estimates of radioactivity than in estimates of weight (compare Figs. 2.15 and 2.16)

[51] K. L. Bocock *et al.*, *J. Soil Sci.* **11**, 1–19 (1960).

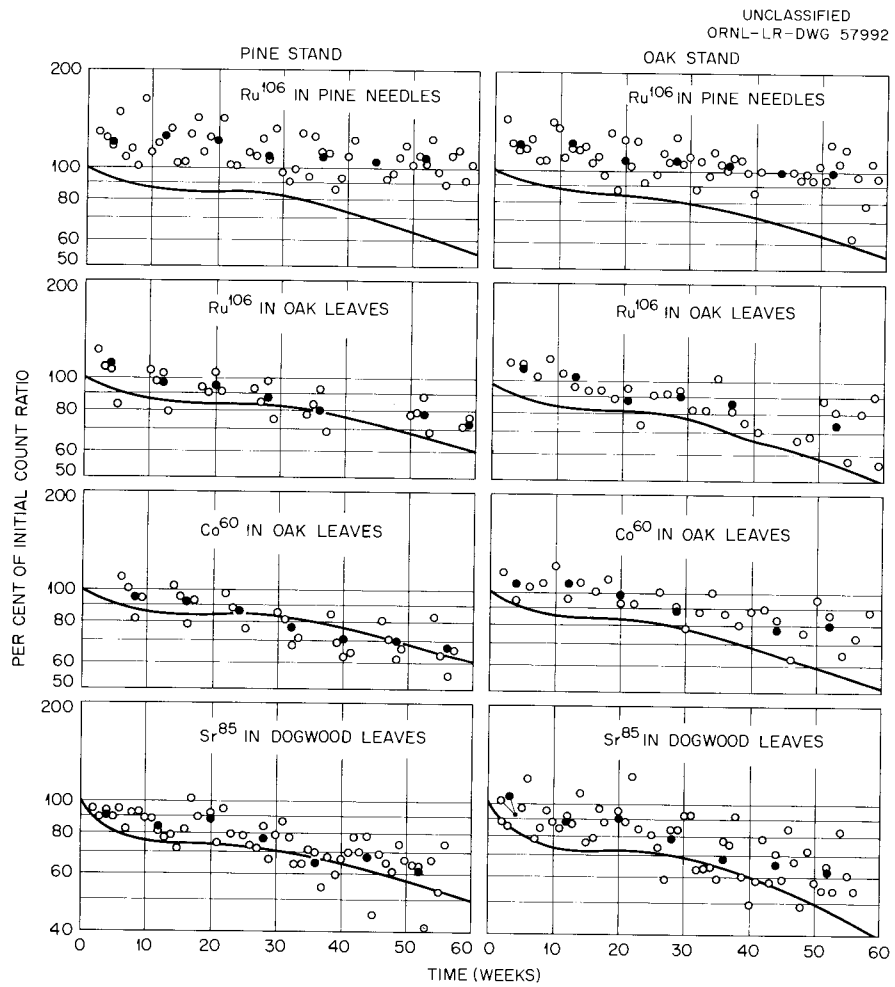

Fig. 2.16. Loss of Radioisotopes from Decaying Leaves in Litter Bags as a Function of Time. Hollow circles are individual measurements; solid circles are averages for eight-week cycles. Solid line represents loss of weight.

Table 2.21. Mean Regression Coefficients for Logarithms of Weights of Litter Contained in Litter Bags as a Function of Time (Weeks); Litter of Three Leaf Species in Two Stands; Values are in Log Grams per Week

	Pine Stand			Oak Stand		
	$\bar{X}$ [a]	S.E.[b]	n [c]	$\bar{X}$	S.E.	n
Pine needles	−0.00376	0.000281	8	−0.00385	0.000686	8
Oak leaves	−0.00276	0.000051	8	−0.00404	0.000141	8
Dogwood leaves	−0.00352	0.000209	8	−0.00468	0.000253	8

[a] Mean.
[b] Standard error.
[c] Number of regression coefficients.

because of the difficulties with repeated counting over many weeks at similar geometries. The solid line in Fig. 2.16 illustrates the loss of weight, to facilitate comparison of losses of radioisotopes and weight by litter. The three phases of weight loss – initially rapid, slower in winter, again more rapid in summer – are not evident in the data from estimates of radioactivity. Generally it appears that the three isotopes are lost at about the same rates at which weight is lost by the leaf litter. Regression coefficients were calculated for the log ratio: (bag count rate)/(standard count rate), and the mean regression coefficients for each isotope–leaf-type–stand combination are shown in Table 2.22. An analysis of variance detected no significant difference between these mean regression coefficients. For isotope loss, coefficients are slightly higher than for weight loss, but other techniques of assaying radioactivity of the bags must be used to measure more precisely the relationship between loss of weight and loss of radioisotopes.

Influence of Climate, Forest Stand, and Leaf Species on Rates of Litter Breakdown. – Before results on the turnover of organic matter, nutrients, and isotopes can be generalized or qualified for application to a wide variety of vegetational and habitat conditions, it is essential to begin establishing the sensitivity of rate parameters to various environmental factors. Results on a cooperative study of first-year litter breakdown of untagged leaves in the contrasting forests of the Great Smoky Mountains and Oak Ridge have been published.[52] A linear regression of per cent breakdown on altitude was equivalent to 1% difference in rate of breakdown per 1°F for the average of five deciduous leaf species. This compares closely with Mikola's difference of 1.75% per 1°C for breakdown of pine needles in Finland, but is slightly lower than his difference of 2.4% per 1°C for birch leaves.[53] These differences in response of breakdown rate to temperature are close enough to be encouraging about the eventual possibility of generalized comparisons of ecological rate parameters over many parts of the world, even though detailed accounting for results of individual areas would obviously involve many local factors.

Among these local factors are the gross vegetational contrasts, such as those between evergreen and deciduous forests, with all the differences in organic activity (see below) and microclimate which such cover differences imply. For the average of five species, there was a difference of 6% in weight loss between spruce and beech forests in the high Smokies (1600 m above sea level), hemlock and cove hardwood forest at midelevations (1040 m), and pine and oak forest at Oak Ridge (260 m). The data of Fig. 2.15 similarly show an average of slightly over 6%

[52] R. E. Shanks and J. S. Olson, *Science* 134, 194–95 (1961).

[53] P. Mikola, *Oikos* 11, 161 (1960).

Table 2.22. Mean Regression Coefficients for Log Count Ratios (Bag Count)/(Standard Count) Against Time (Weeks); Four Isotope-Litter Combinations in Two Stands; Values Are Log Ratio: (Count Rate Bag)/(Count Rate Standard) per Week

	Pine Stand			Oak Stand		
	$\bar{X}$ [a]	S.E.[b]	n[c]	$\bar{X}$	S.E.	n
Ru^{106} in pine needles	−0.00672	0.001532	8	−0.00592	0.001601	8
Ru^{106} in oak leaves	−0.00965	0.004439	4	−0.00665	0.003676	4
Co^{60} in oak leaves	−0.00468	0.002079	4	−0.00689	0.002726	4
Sr^{85} in dogwood leaves	−0.00418	0.000977	8	−0.00534	0.000884	8

[a] Mean.
[b] Standard error.
[c] Number of regression coefficients.

difference between the pine and oak stands, but this average actually represented differences of 2, 10, and 7% for pine, oak, and dogwood.

The great differences between individual species in their rates of breakdown have been recalculated (see Table 2.23) from the data of Shanks and Olson into a form which accounts, in part, for the obvious tendency of detailed data like those of Fig. 2.15 to show more rapid decay in the early phase of breakdown than during the later stages when less material remains to be broken down. Under the exponential model assuming constant fractional breakdown per unit time, the fraction at the end of each year, k', is e^{-kt} for $t = 1$; so $k = -\ln(1 - k')$. Such estimates of k are included in Table 2.23 for comparison between 1959 breakdown in the Smokies and Oak Ridge, with the 1960 values for three additional species in Oak Ridge based on year-end data from Fig. 2.15. The parameter based on year-end breakdown does not differ greatly from that of Table 2.21, but tends to show the difference between species somewhat better because the rapid early weight loss has a strong influence on k' and hence k. The further need to account for seasonal effects is discussed later under the subsection "Compartment Models and Analog Computer Simulation."

Movement of Cs^{134}, Co^{60}, and Sr^{90} from Litter into Soil. – New experiments still in progress are comparing weight losses and isotope release of cesium, cobalt, and strontium from leaves of mulberry, redbud, white oak, and loblolly pine which were tagged in the summer of 1960. The decimeter-bag method of counting was improved by two methods, either allowing for the variation in counting efficiency by measuring the thickness of the bag, or minimizing variations due to this source by gently pressing the leaves to a standardized position in the plastic counting vessel (sandwich box) by insertion of a cellulose sponge. Another addition to the technique in some cases was the inclusion of a layer of natural forest floor material in a plastic box whose bottom was mostly open except for supports and a layer of Fiberglas screen.

Table 2.23. Estimates of Exponential Rate of Litter Breakdown (k) by the Method Based on Year-End Fraction of Litter Remaining ($1 - k'$); $k = -\ln(1 - k')$

Year and Leaf Species	Location and Forest Stand					
	Oak Ridge, 260-m Elevation		Great Smoky Mountains			
			1040-m Elevation		1600-m Elevation	
	Pine	Oak	Hemlock	Cove Hardwood	Spruce	Beech
1959						
Mulberry	1.14	1.11	0.87	1.27	0.87	0.89
White oak	0.48	0.63	0.40	0.44	0.25	0.45
Shumard oak	0.43	0.62	0.40	0.43	0.37	0.49
Sugar maple	0.37	0.51	0.38	0.45	0.24	0.37
Beech	0.30	0.34	0.21	0.25	0.12	0.25
1960						
Dogwood[a]	0.58	0.73				
Southern red oak[b]	0.38	0.54				
Virginia pine[b]	0.46	0.49				

[a]Estimates by this method for dogwood are substantially greater than those obtained by statistical regression (0.45 and 0.46 for pine and oak forest) because of the high initial loss of soluble material in dogwood litter breakdown.

[b]Estimates based on year-end values only slightly greater than those based on statistical regression (0.33 and 0.48 for oak and 0.48 and 0.46 for pine) because of their low initial loss of soluble material.

Early results by these methods with redbud leaves confirmed the rapid leaching of Cs^{134} from litter, at a rate at least twice as great as that for Co^{60} or Sr^{90}. More than half the leached cesium remained in the slabs for four humus types that contained mineral soil horizons, but a pine humus type consisting of only organic L, F, and H layers retained less than half. A much smaller percentage of the Co^{60} was retained. Retention of Sr^{90} appears high, but cannot be estimated well without destructive assay of the materials.

Biological Populations and Processes Affecting the Movement of Elements and Isotopes

While preceding studies measure the rates of movement of tracers and nutrient elements, repeated collections and observations from the same study areas are following the rapidly changing populations of soil animals and of microorganisms which utilize these materials and which hasten their movement during the breakdown of organic litter.

Arthropods Associated with Litter Breakdown and Release of Radioactive Isotopes. – The soil fauna contains many species of animals instrumental in the breakdown of fallen leaf litter, with consequent release of incorporated radioisotopes and other materials to the soil. Soil animals may affect the breakdown of leaf litter in several ways: their feeding processes cause a physical breakdown of the leaves; the material passed through their intestines may be more susceptible to decay by microorganisms; and leaf fragments may become intimately mixed with mineral soil as a result of feeding activities and vertical migration by the animals.

Current studies are attempting to relate the community structure of soil microarthropods to the rates of breakdown of leaf litter and to rates of radioisotope cycling. Present work includes the estimation of populations associated with leaf litter in various stages and with different rates of decay. The more influential species are being discovered, so that their rates of feeding in litter can be investigated. The true role of the microarthropods is one of interaction with the microbial flora in the degradation of leaf litter, and the population studies currently in progress are needed to prepare for further experiments on microarthropod-microbial interactions.

Preliminary results of field experiments on the numbers of arthropods associated with decaying leaf litter and the influence of environmental factors on these numbers were reported previously.[54] Weekly measurements of arthropods numbers (extracted on Tullgren funnels) were taken in connection with the measurements of weight loss and loss of radioisotopes from the litter bags discussed above. Analyses of the arthropod populations are complete for the first eight months of the experiment started in November 1959. Not all the soil arthropod species are active in reduction of fresh leaf litter. In December, collembola and about 25 species of mites invaded the bags of fresh leaves. Many of them were typical soil and litter forms (*Tectocepheus velatus*, *Ceratoppia bipilis*), but others which normally occur in soil and humus rather than fresh litter (such as *Rhodacarus*) did not enter the bags. During the winter months the arthropod community contained few species, some represented by many individuals, and was thus analogous to early successional stages of animal communities. In the oak stand a single species of mite, *Tydeus* sp., completely dominated the winter arthropod populations. Numbers of this mite reached several hundred per litter bag by late December and remained high throughout the winter, but declined in late spring (Fig. 2.17). The species was replaced by *Asca* spp. during the summer, and was absent from the pine stand. During the late spring the arthropods, although represented by small numbers due to low humidities, increased in variety of species. When moisture conditions became favorable, a complex arthropod community entered the litter bags.

Arthropod numbers vary directly with moisture content of the litter bags during the summer months when temperature is not a critical factor. Figure 2.18 shows the highly significant ($P = 0.01$) relationship between moisture and arthropod numbers for samples taken from June 21 through October. If the winter months were included in the calculations, a significant regression would still be present, but there would be considerably more variation, due to measurements during periods such as March 1960 when ice in the litter bags raised the moisture contents but low temperatures resulted in small populations of arthropods.

[54] J. S. Olson *et al.*, *Health Phys. Div. Ann. Progr. Rept. July 31, 1960*, ORNL-2994, pp 177–79.

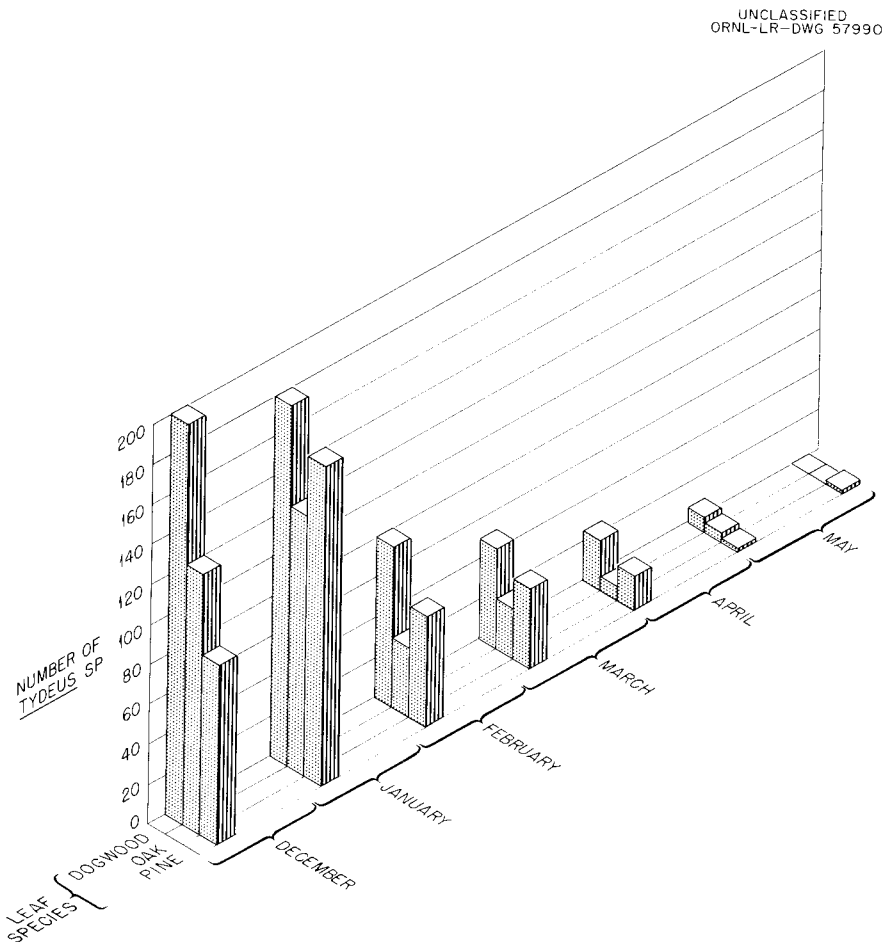

Fig. 2.17. Numbers of *Tydeus* sp. in Pine, Oak, and Dogwood Litter Bags. Values are averages for four-week periods.

The large numbers of *Tydeus* in the oak stand made it possible to examine the efficiency of the litter-bag method for estimating arthropod populations. Bags of two sizes and of three meshes, containing mulberry leaves, were placed in the oak stand for four weeks and then were collected. The results are shown in Table 2.24. Decreasing the mesh size from coarse openings to 1-mm openings produced no increase in numbers of *Tydeus*; evidently *Tydeus* enters and leaves the bags freely, and the populations are not the offspring of a few individuals who happen to gain entrance into the bags. However, the *Tydeus* may tend to retreat into the centers of the samples rather than desert them on the Tullgren funnels: The numbers of *Tydeus* from the larger bags were only twice those from the smaller bags, although the volume of material was four times greater than in the smaller bags. The smaller bags provide little protection from desiccation, but the larger ones may have contained enough material to provide a hiding place.

Litter bags of 1 dm^2 appear to be a better means of sampling for these mites than are collections of loose leaves or core samples. Confinement in litter bags may produce significant effects on populations of this or other mite species, but such effects are minor compared with those produced by environmental and successional phenomena.

A summary of the yearly cycle of microarthropod populations in litter bags is shown in Fig. 2.19, which includes monthly averages of the numbers of arthropods per litter bag; the average moisture content, expressed as per cent of dry weight of the litter; and the average median air temperature 6 in. above the litter, expressed as a monthly

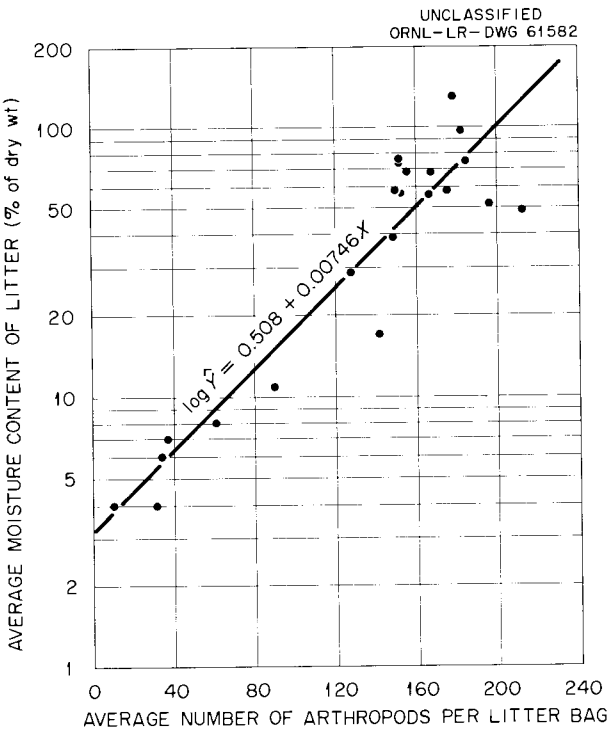

Fig. 2.18. Relation of Number of Arthropods in Litter Bags to Moisture Content of Litter Bags. Data for summer-fall 1960 only.

average of weekly maximum and minimum temperatures. The bags were placed in the field in November and were rapidly invaded by microarthropods. An average of more than 100 arthropods per bag was found in January and February. Numbers of arthropods declined in March due to low temperatures, although moisture contents of the litter bags were high. In April, May, and June, temperatures were favorable, but low-moisture conditions reduced the microarthropod populations. From July through November, both temperature and moisture conditions were favorable and consequently there were high populations of arthropods. These periods of abundance in late fall and early winter, and again in summer and fall, coincide with periods of rapid leaf-litter breakdown, rapid release of nutrients, and high populations and activities of microorganisms discussed below.

Microbial Ecology. – Two kinds of procedures are used to investigate the relationships between microorganisms and the movement of radioisotopes: (1) Field measurements of microbial populations and their respiration in natural environments contribute information about their important role in the breakdown of organic litter and the release of nutrients and isotopes. (2) Laboratory experiments are evaluating the uptake and turnover of tracers by the microorganisms themselves, under varied culture conditions.

Table 2.24. Numbers of *Tydeus* sp. Occurring in Litter Bags of Different Size and Construction; Values Are Included for Duplicate Bags of Each Size and Type

Mesh Description	Bag Size	
	1 dm^2	$(2\ dm)^2$
Fine Fiberglas	194	*a*
(1-mm mesh)	74	*a*
Nylon	78	258
(2.3-mm mesh)	178	238
Coarse Fiberglas[b]	204	327
(2-mm mesh)	152	199

[a]No samples.
[b]Coarse Fiberglas material was loosely woven; many openings exceeded 2 mm.

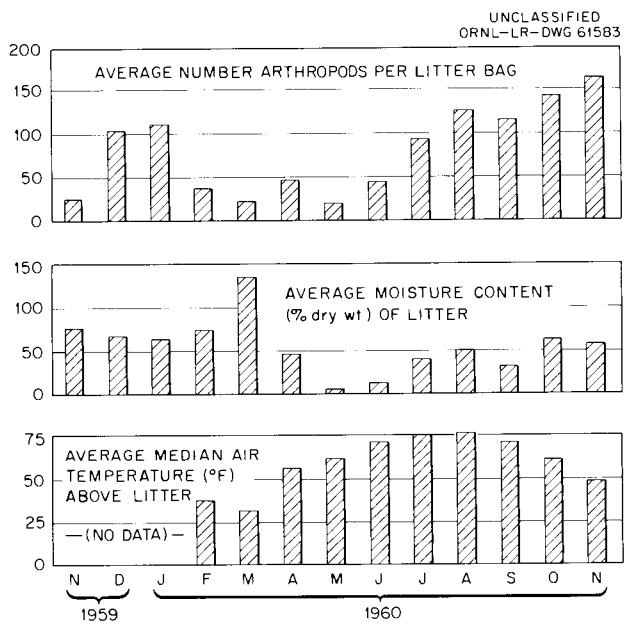

Fig. 2.19. Comparison of Arthropod Numbers, Moisture Content of Litter, and Median Air Temperature Above Litter.

Serial dilution counts of fungal and bacterial populations, increments of growth of fungal hyphae, and CO_2 production have been related to the breakdown of litter. The influences of temperature, moisture, and condition of substrate have been compared during biweekly measurements carried on since November 1960 in red maple, white oak, and pine stands (M, O, and P on Fig. 2.12). Microbial populations promptly rose to high levels on fresh litter in late autumn and fluctuated with temperature and moisture throughout the winter.

The example in Fig. 2.20 for January 26, 1961, illustrates the large population differences typically found between mulberry, redbud, white oak, and pine litter. Average respiration rates for 2 hr, every two weeks, during the whole period of November to July, and the total weight loss during this period decrease in the same order as the numbers of fungi and bacteria in this example:

	Leaf Species			
	Mulberry	Redbud	Oak	Pine
Fungal colonies, $\times 10^6$ per gram of dry weight	38	4.8	3.8	0.24
Bacteria, $\times 10^6$ per gram of dry weight	10,068	1215	29	9.3
Mean respiration (Nov.–July), μl/hr	166	50	40	30
Per cent weight loss (Nov.–July)	72	35	36	26

These and many similar examples emphasize the contrast between rapid breakdown of mulberry leaves, which presumably is hastened by specific chemical factors favoring prompt bacterial decay into black amorphous humus, and the slower decay of oak and pine litter. The latter support a relatively greater participation by fungi, whose hyphae gradually weaken and mat the more or less intact leaves or needles.

As expected, temperature regulates the general annual cycle of potentially rapid decay in summer and slow (but never zero) decay through the winter. During the warm season when temperature is not a limiting factor, desiccation intermittently reduces litter decay rates to levels almost as low as those during the winter. Average litter respiration fell from 250 μl/hr per gram of original dry weight on November 28 to near 15 μl/hr through most of January and February, varied between 140 and 25 in March and April and between 190 and 75 in May, and rose from 130 to 270 in June.

Biweekly measurements of respiration for litter plus soil were consistently higher and less variable than for litter alone, which responds more promptly to desiccation. The prompt response to rain falling after a dry spell is shown by a 15-fold increase in litter respiration within 24 hr, as compared with an increase in soil respiration of only 28% by the mineral soil.

Within a given diurnal cycle when there is little change in moisture conditions of the litter, there are smaller-order fluctuations which again are controlled by temperature. For example, on September 21, 1960, respiration varied gradually between 22 μl hr^{-1} g^{-1} during the night (16.5°C) and 61 μl hr^{-1} g^{-1} during the day (27.5°C).

Concentration factors and release coefficients of Co^{60} and Cs^{134} were determined for several microorganisms. Cobalt-60 concentration factors relative to the nutrient medium were as follows (after growing for six days in shaking cultures): Streptomycete, 32; fungi, 9–22; bacteria, 4–34.

A common fungus, *Trichoderma viride*, had Co^{60} concentration factors which ranged from 12, near neutral pH, to 48 at pH 4 and 22 at pH 8. Concentration factors of Cs^{134} ranged from 3.3 at pH 4 to 4.3 at pH 8. For both nuclides the greatest concentration factor was obtained after 7 to 16 days and decreased after prolonged growth. Concentration factors were not affected by a wide range of initial levels of activity (600 to 80,000 $\mu\mu$c/ml).

Release of Co^{60} and Cs^{134} from intact *Trichoderma* fungus mycelium was only 8–14% and 11–23%, respectively, after shaking with various aqueous leachants at 20°C for 24 hr. However, drying or freezing of mycelium before leaching increased the release to 85–88% for Co^{60} and 91–96% for Cs^{134}. This difference suggests that previous uptake had been more physiological than physical.

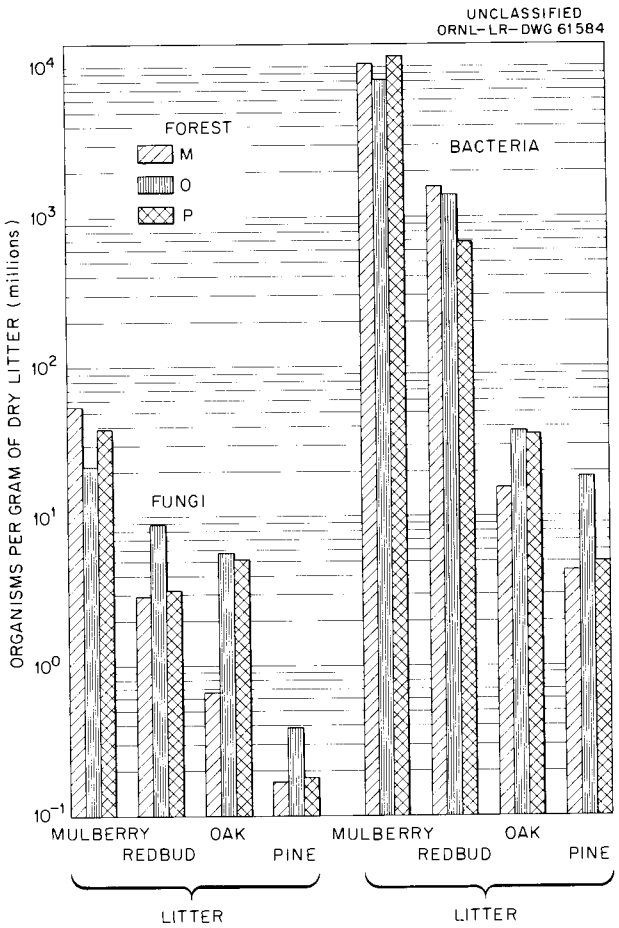

Fig. 2.20. Large Differences in Fungal and Bacterial Populations on Mulberry, Redbud, Oak, and Pine Litter [January 26, 1961, in Red Maple (M), White Oak (O), and Pine (P) Forests].

The maximum uptake rate of Co^{60} by *T. viride* on leaves or leaves plus soil occurred after seven days. A constant level was reached after 17 days of growth at room temperature. At this time the mycelium retained 31% of the activity that could be leached from control leaves without fungus or 12% of the original activity in the substrate. Concentration factors of Co^{60} in sporulating mycelium on soil and leaves, respectively, were 23 and 21. For uptake of Cs^{134} from soil the concentration factor was 158.

These results indicate the extent to which microbial tissue can accumulate and retain environmental radioactivity. Accumulation of radioisotopes was greatest during the period of maximum growth and respiration of the organism. Release by leaching in microbe-containing systems after freezing or drying was moderated by the presence of organic matter or soil. Freezing or drying at the soil surface where most fungi are active will promptly release absorbed isotopes for subsequent movement in the environment.

Compartment Models and Analog Computer Simulation

Many parts of the preceding program directly or indirectly provide information on rates of transfer of chemical elements or their isotopes from one part of an ecosystem to another. Mathematical treatment of compartment models is used increasingly for the physiological or biophysical analysis of movement of materials between cells or between organs of a single individual. The logical extension of this methodology to ecosystems has been explored in anticipation of using analog computer facilities at ORNL for the interpretation of ecological data. Analog simulation of ecosystems should aid the prediction of long-range consequences following from actual or hypothetical conditions of environmental contamination. As computer time permitted in 1961, efforts were made to elaborate the very simple but admittedly unrealistic assumptions that were made in a previous study[55] and to investigate systematically the influence of parameters which affect gross behavior of the model.[56]

Differential Equations for Transfer of Materials. – It is important to consider the changes in total material or mass M of each compartment of an ecosystem (usually expressed in g/m^2 of surface area of the earth), in addition to the changes in some other material – element or isotope – expressed either as concentration U (per gram of material) or as total amount X (per m^2 of surface area) $= MU$. It is also convenient to allow any compartment to be indexed by either the subscript J if the balance of material in this compartment is currently under consideration or by the subscript I for all compartments which are merely being considered as sources or destinations for movement

[55] R. B. Neel and J. S. Olson, *Use of Analog Computers for Simulating the Movement of Isotopes in Ecological Systems*, ORNL-3172 (in press).

[56] The encouragement by E. R. Mann of the Instrumentation and Controls Division of our new application of the Reactor Controls Analog Computer Facility (RCAF-X10) is gratefully acknowledged. O. W. Burke of the Engineering and Mechanical Division provided indispensable aid in the wiring and operation of the computer.

to or from compartment J. Then the rate of change of mass in compartment J is simply the sum of gains minus losses:

$$\frac{dM_J}{dt} = \sum_{I=0}^{i} k_{mIJ}M_I - \sum_{I=0}^{i} k_{mJI}M_J \qquad (J = 1, \ldots, j), \qquad (10)$$

where k_{mIJ} is the fraction of mass in compartment I transferred to compartment J per unit time (instantaneous rate).

Similarly, the rate of change of the material X is:

$$\frac{dX_J}{dt} = \sum_{I=0}^{i} k_{xiJ}X_I - \sum_{I=0}^{i} k_{xJI}X_J \qquad (J = 1, \ldots, j), \qquad (11)$$

where k_{xIJ} is the fraction of material x in compartment I transferred to compartment J per unit time (instantaneous rate).

Special treatment of the case for index $I = 0$ is used to allow for the fact that ecosystems are generally not closed systems. They exchange materials as well as energy with the larger surrounding ecosystem – the environment of the local system – which will be denoted by $I = 0$. Intake of organic matter from the atmosphere in self-supporting systems is mainly by photosynthesis, whose rate is described by the function

$$P = k_{m01}M_0 , \qquad (12)$$

where, in this special case:

k_{m01} = a parameter expressing the level of input to compartment 1 (photosynthetic vegetation),

M_0 = a multiplying factor, commonly a periodic function of time.

Losses of mass of organic matter from individual compartments and from the system as a whole (except for limited recycling of locally respired CO_2) result from respiration.

The ecosystem may or may not be approximately closed with respect to the gains or losses of inorganic elements. Input may be expressed as a fraction k of some large outside reservoir X_o of the element or isotope, or $k_{x0J}X_0$. Losses from the system, $k_{xJ0}X_J$, may include actual exports and additional losses due to radioactive decay in the case of radioisotopes. Many health physics problems of environmental contamination depend on whether the export from some local "regulated" ecosystem is sufficiently great to result in significant contamination of "unregulated ecosystems" in view of the radioactive decay of the isotope in question. Measurement of the movement of radioisotopes (or of the elements they represent) between compartments *within* the local ecosystem is usually necessary for evaluating this kind of problem and may also be required for understanding what is happening to this local system as a result of exposure to contamination.

Analog Computer Simulation of Ecosystems. – Analog computer methods not only help to solve equations such as (10) or (11) above, after they have been formulated mathematically, but have been even more constructive during the present exploratory stage of model building as a means of seeing promptly the total effect of changing the structure or parameters of a model by direct electronic simulation of the model itself. Integrators in the circuit provide a continuous cumulative record of the net balance of gains and losses of Eq. (10) for each compartment of the system. Certain potentiometers control the negative feedback of a certain fraction of the voltage stored on each integrator, which simulates the losses from the compartment, the second term on the right of Eq. (10) or (11). The inputs to each compartment are controlled by additional potentiometers which draw a certain fraction of the voltage from the integrators which simulate the appropriate ecological source compartments.

A report[57] illustrating the methodology and simple applications of analog computer methods for ecosystem models used the example of the element carbon and the redistribution of changes in C^{14} through plants, organic litter, and soil. Simple linear equations with constant coefficients were used previously, but even these became unwieldy when solved analytically for cases of periodic and exponentially varying inputs.

The analog computer offers technical advantages of convenience and speed in exploring the influence of various parameters, even in a fairly small system governed by linear equations with constant coefficients. The advantages have become much greater in dealing with larger numbers

[57] R. B. Neel and J. S. Olson, *op cit.*

of compartments, as in the example outlined below, or more complex ecological problems which can readily be called to mind. The greatest power of the method comes when the restriction of constant coefficients is replaced by allowing for differential equations with variable coefficients, or nonlinear systems of equations. Servomultipliers are especially useful in providing coefficients which vary as a function of time or of the variables for which a solution is sought. Diode limiters have proved valuable in imposing fairly abrupt upper or lower limits on the variables in the problem.

Operationally, the general model outlined below uses two control panels of the Reactor Controls Analog Computer Facility, one to control the changes in biomass represented by Eq. (10) and the other to control changes in isotope distribution represented by Eq. (11). In addition, special sine-generating circuits, servomultipliers, and limiters are used to provide the periodic inputs represented by Eq. (12).

Periodic Input Functions. – An auxiliary circuit which generates sine and cosine functions was utilized to simulate a fluctuating rate of assimilation of organic matter into the circuit which recorded the biomass of the compartments of the system. The function $A \cos \omega t$ and a constant voltage, $-A$, were summed in a summing amplifier and inverted to give one of several functions actually utilized to simulate "gross photosynthesis":

$$P = A(1 - \cos \omega t) \ . \qquad (13)$$

Commonly this was modified in at least two ways. First a positive feedback was provided so that a larger biomass of producing vegetation would lead to a higher rate of photosynthesis. Then an upper limit on the gross photosynthesis function was superimposed to simulate the competition that eventually limits production when vegetation occupies the surface so fully that little remaining solar light is dissipated at the ground surface. The ecosystem is assumed to saturate the level of activity permitted by the incoming energy.

The gross photosynthesis was then fed into a second summing operational amplifier, along with respiration of the producing vegetation (which represents a negative feedback, having opposite sign). The output of this amplifier is then gross photosynthesis minus respiration ($P - R$). Depending on the actual values of positive and negative feedback, and on various elaborations in photosynthesis functions like Eq. (13), many input conditions can be simulated.

Biomass Circuit. – For many exploratory purposes it was sufficient to deal with a "skeleton" model which might approximate a herbaceous ecosystem having only a few compartments:

1 = "herbage," all above-ground vegetation,
2 = roots,
3 = herbivores,
4 = predators feeding on herbivores,
5 = predators feeding on predators,
6 = organic litter lying above mineral soil,
7 = decomposers of litter,
8 = soil organic matter having rapid turnover,
9 = soil organic matter having slow turnover.

The pathways connecting these compartments are shown on Fig. 2.21. Transfers which simply represent a constant fraction of the source compartment are indicated by $k_{mIJ}M_I$. A few transfers which involve periodic functions are written out, with an equation typical of some of these being included. In computer practice, these variable coefficients are obtained by using such a function to drive a servomultiplier, by introducing the other factor on one of the multiplier arms, and by taking off the product at the output corresponding to that arm.

Net photosynthesis served as input to an integrator for the herbage (1). A fraction of the output from herbage served as input to roots (2), to the herbivore compartment (3), and to the organic "litter" compartment (6). The transfer from herbage to litter did not have k_{m16} = constant, but was regulated by a servomultiplier driven by a function such as $A(1 + \cos \omega t)$. This resulted in timing of the death of herbage (and hence fall of litter) occurring in autumn or winter, simulating the seasonal phenomenon actually occurring in nature.

Only three compartments were included initially for the animal trophic levels (3, 4, 5), but it is possible to have additional compartments for dealing separately with individual important species and to combine the possible pathways of food so that omnivores, scavengers, and other special nutritional cases can be simulated as closely as needed.

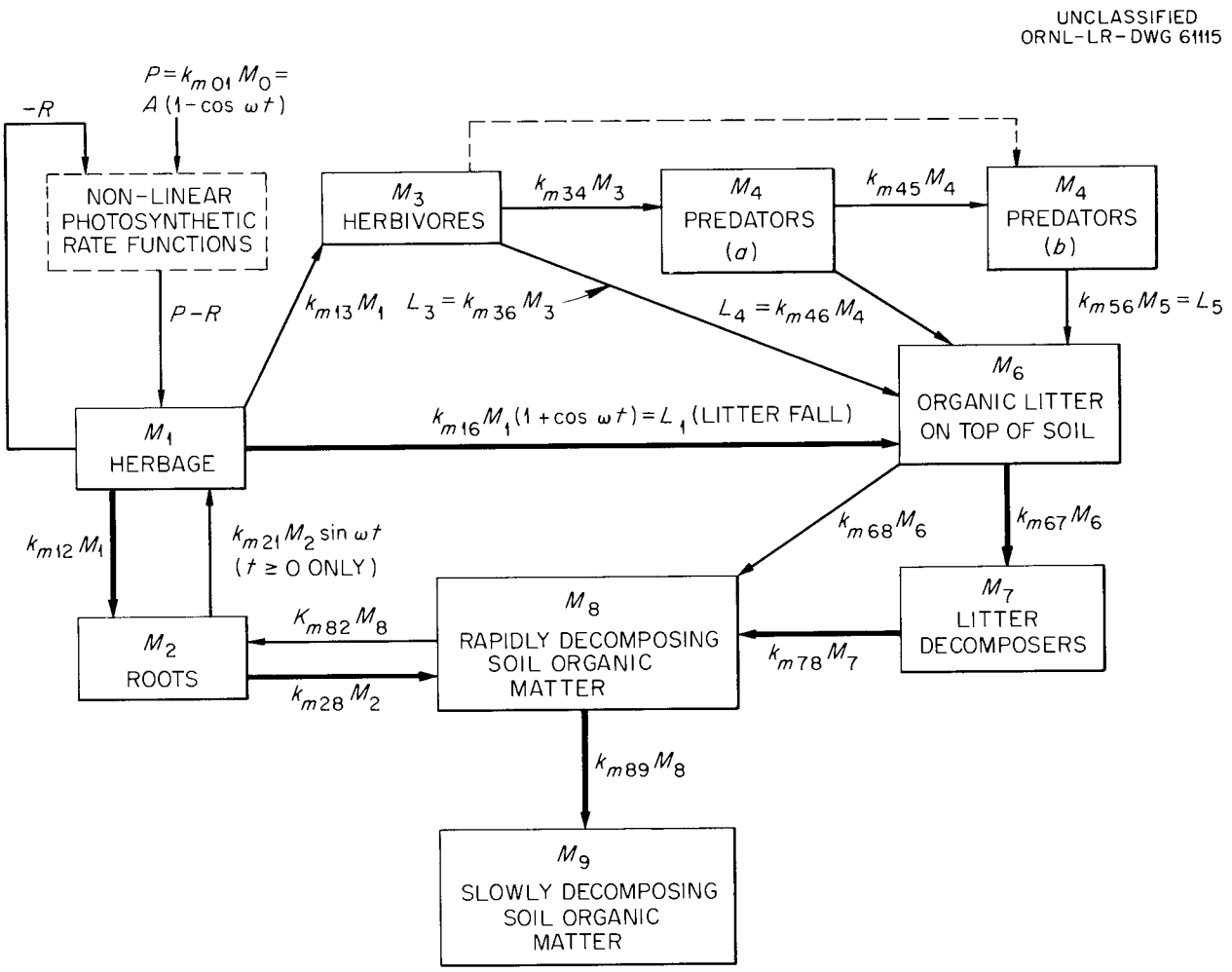

Fig. 2.21. Flow of Biomass in a Simple Model for an Herbaceous Ecosystem.

The rates of production of dead organic matter from plant litter and lesser amounts of animal debris are combined in a summing amplifier representing "litter fall." The integral of this litter fall summarizes the total amount of organic matter which has ever reached the forest floor. The integrator representing organic matter lying unincorporated on top of mineral soil represents what remains of this input as losses from microbial decay and migration into mineral soil are continually subtracted. A separate compartment represents microbial biomass, which is characterized by a very high turnover rate.

Outputs from microbes and from the death of roots are the inputs to the first of two fractions of soil organic matter. This first fraction is assumed to have a relatively rapid turnover rate. A second fraction of soil organic matter is assumed to represent a relatively stable fraction of humus having turnover rate of a century or more.

Circuit for Inorganic Elements and Radioisotopes. – A separate control panel for another part of the computer can be used for simulating the flow of nutrient elements or radioisotopes through the ecosystem. Radioactive decay is allowed for simply by increasing the negative feedback for individual integrators by an amount corresponding to their radioactive decay constant. Except for this loss, or possible losses due to export of the isotopes from the local ecosystem, the export from one compartment of the system must be equal to the gains to other parts of the system. Compartments are labeled as for the biomass circuit, except that the rapid and slow soil compartments are interpreted as exchangeable and relatively

unexchangeable fractions, respectively, of the inorganic element.

One important way in which this circuit differs from that for biomass (see Fig. 2.22) is in the presence of a major pathway of uptake of isotope from a relatively exchangeable fraction in the soil to the plant roots. The major movement then proceeds from plant roots to tops, through the several trophic levels of animals, and to organic litter. For convenience in biological comparisons, radioisotopes in living organisms are expressed in units per gram of organic matter (U). A servo-multiplier is used to multiply activity per gram (U) times the amount of litter fall (L), to express litter activity in dimensions of units per square meter of ground surface (X). Isotopes in microorganisms and in the rapid and slow compartments of soil are also expressed in these units. Hence plant uptake is determined by a parameter k_{xu12} relating uptake (units per gram of root) to (units per square meter of soil).

Most effort to date has been consumed in evaluating the response of the biomass circuit to several positive and negative feedback parameters, in order to select certain combinations which simulate "reasonable" behavior of the system. While further exploration is needed for the behavior of contrasting classes of ecosystems, the techniques developed and tested already should facilitate the simulation of some aspects of realistic field situations, when sufficient empirical data can be organized to suggest the pertinent parameters and boundary conditions.

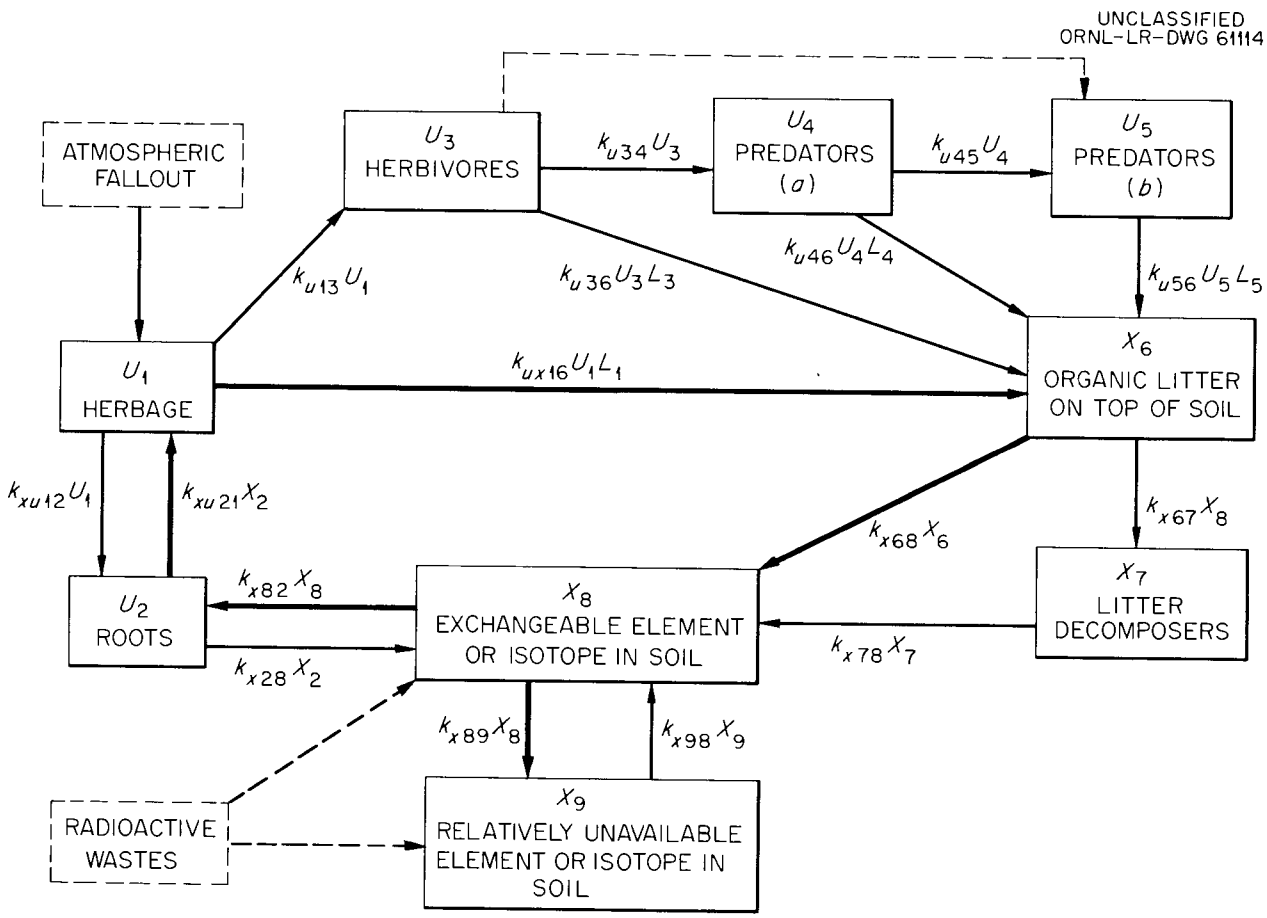

Fig. 2.22. Flow of Inorganic Nutrient and Isotope in a Simple Herbaceous Ecosystem.

CLINCH RIVER STUDIES

D. J. Nelson

R. L. Herman[58] R. C. Early
C. W. Wiser[59] N. A. Griffith

The biological phases of the Clinch River studies are proceeding with a balanced program concerning both the fate of released radioactive isotopes in the river environment and the effects of ionizing radiation from released radioactive wastes on a selected aquatic species. The preliminary characterization of the Clinch River biota was completed last year. The initial work has made it possible to select experimental organisms or groups of organisms suitable for specific studies. These studies will enable us to evaluate the hazard and effects of continuous releases of low-level radioactive wastes to the river system.

Bottom Organism Studies

Worm Studies. – Tubificid worms are the most abundant bottom organism in the Clinch River, and in feeding they bring radioactive bottom sediments into the overlying water. The effect of the worms in the downstream distribution of bottom sediments was evaluated through a mathematical model[60] using these parameters: rate of feeding, rate of fecal pellet fall, height of worm tail above the bottom, depth of burrowing, diameter of feeding worms, mud density, and current velocity. Worm populations in the Clinch River average one worm per 10 cm^2, and on the basis of the observations made for the model, would require 3.33 yr to move the sediment from a cm^2 downstream 9.18 cm. Tubificid populations may be as high as 100 individuals/cm^2 in areas with much organic pollution. With the latter population Cs^{137} adsorbed on mud would be moved downstream about 800 meters during one radioactive half-life. This movement is insignificant when compared with the transport of suspended sediments by water currents.

Diptera Studies. – In a preliminary examination of the salivary-gland chromosomes of *Chironomus tentans* Fabr. larvae from White Oak Creek and the Clinch River, a high frequency of chromosomal aberrations was observed.[60,61] For example, *C. tentans* normally has four chromosomes, but five individuals were found with three chromosomes each. These preliminary results indicated the need for calculations of the radiation dose in the environment which Diptera with bottom-dwelling life stages may be receiving. Organisms living in their natural environments are subject to radiation from three sources: (1) External emitters – there are a large number of naturally occurring radioisotopes which contribute to background radiation.[62] Of these, only the radiation contributed by K^{40} and Rb^{87} has been evaluated because these radioisotopes are the most abundant in the earth's crust[63] and both have high specific activities. (2) Internal emitters – the previously mentioned naturally occurring radioisotopes, when contained in the tissues of organisms, irradiate the animals when these isotopes disintegrate. (3) Cosmic radiation – these sources of radiation have been considered with respect to doses which each may contribute to bottom organisms living in the Clinch River.

Dose Calculations. – Absorbed dose to the bottom organisms was calculated on the assumption that the organisms received a submersion dose for the beta disintegrations and one-half submersion dose for the gamma emissions. The standard dose rate equations were used for these calculations.[64]

$$\text{Dose (rad/week)} = \mu c \times 3.70 \times 10^4 \times 6.05 \times 10^5 \times 1.6 \times 10^{-8} \times Ei \,, \quad (14)$$

[58] Summer employee.

[59] Research participant.

[60] Clinch River Study Steering Committee, *Status Report No. 1 on Clinch River Study*, ORNL-3119 (in press).

[61] S. I. Auerbach *et al.*, *Health Phys. Div. Ann. Progr. Rept. July 31, 1960*, ORNL-2994, p 188.

[62] M. W. Lowder and L. R. Solon, *Background Radiation – A Literature Search*, NYO-4712 (July 1956).

[63] L. T. Alexander, E. P. Hardy, Jr., and H. L. Hollister, "Radioisotopes in Soils: Particularly with Reference to Strontium-90," p 3 in *Radioisotopes in the Biosphere* (ed. by R. S. Caldecott and L. A. Snyder), University of Minnesota, Minneapolis, 1960.

[64] The calculations were done on the basis of advice from W. S. Snyder and the Internal Dose Group of the Health Physics Division.

where

μc = μc/g of mud,

3.70×10^4 = disintegrations sec^{-1} μc^{-1},

6.05×10^5 = sec/week,

1.6×10^{-8} = rad × g/Mev,

Ei = effective absorbed energy per disintegration for a radionuclide.

An empirical formula was used to estimate the average effective absorbed energy of a beta disintegration (p 28, *Report of Committee II on Permissible Dose for Internal Radiation*, ICRP):

$$E_i = 0.33E_m f \left(1 - \frac{\sqrt{Z}}{50}\right)\left(1 + \frac{\sqrt{E_m}}{4}\right), \quad (15)$$

where

E_m = maximum energy of beta disintegration,

f = fraction of disintegrations at a particular energy,

Z = atomic number.

The effective energies of gamma disintegrations were calculated as follows:

$$\text{gamma energy} = 0.5Ef,$$

where

0.5 = for one-half submersion,

E = gamma energy peak,

f = fraction of disintegrations at the energy.

The calculated background radiation to which bottom organisms are exposed was derived as follows: (1) External emitters – the external emitters occur in both the water and mud. An average potassium content of 2.6% for the river sediments has been assumed in lieu of specific analyses. The estimate for potassium content is based on the abundance of elements in various rocks of the earth's crust:[63] igneous 2.6%, sandstone 1.1% shale 2.7%, limestone 2.7%. The sediments in the river bottom are derived primarily from local shale and limestone with an admixture of sand. Potassium with a specific activity of 8.4×10^{-4} μc per g of K gives a dose of 3.6 mrad/week. The average potassium content of the river water is 0.00014% (based on three analyses from the Waste Disposal Section) which would not result in a significant dose. The average rubidium content of river sediments estimated on the same basis as potassium was 0.03%. The specific activity of naturally occurring Rb^{87} is 1.9×10^{-2} μc per g of Rb, which results in a dose of 9.5×10^{-3} mrad/week. The calculated doses are summarized in Table 2.25. (2) Internal emitters – the potassium content of a composited sample of *Chironomus* larvae, whose gastrointestinal tracts were devoid of sediment, was 0.2%. The specific activity of potassium and this potassium content gives a K^{40} activity of 1.74×10^{-6} μc per g of dry weight. The dose from this source is 2.89×10^{-4} mrad/week. (3) Cosmic radiation – the intensity of cosmic radiation decreases rapidly below the surface of water. The following data[65] indicate the extent of this decrease:

Table 2.25. Summary of Natural Background Radiation to Bottom Organisms in the Clinch River

Source	Dose (mrad/week)	Dose (mrad/yr)	Per Cent of Dose
External emitters			
Mud K^{40}	3.6	187.2	88
Rb^{87}	9.5×10^{-3}	0.5	0.2
Water	Insignificant		
Internal emitters			
K^{40}	2.89×10^{-4}	1.5×10^{-2}	
Cosmic radiation	4.8×10^{-1}	25	11.8
Total		212.7	100

Depth in Meters	mrad/year
0	35
10	10.1
20	4.86
50	1.40

Chironomus larvae have been found to depths of about 12 meters in the Clinch River. An estimate of 25 mrad/year of cosmic radiation has been used as this portion of the total background radiation.

[65] T. R. Folsom and J. H. Harley, "Comparison of Some Natural Radiations Received by Selected Organisms," p 28 in *The Effects of Atomic Radiation on Oceanography and Fisheries*, NAS-NRC Pub. 551, Washington, D.C., 1957.

Radioanalyses of bottom sediments by the Applied Health Physics Group[66] have been used in calculating the doses. The samples were collected at eleven transects from Clinch River Mile 21.5 to 1.1, and the average radionuclide content for these transects was used to calculate doses (Table 2.26). The concentration of radioisotopes

Table 2.26. Doses Calculated on the Basis of Radionuclide Content of the Clinch River Bottom Sediments

Isotope	Dose (mrad/week)	Dose (rad/yr)	Per Cent of Dose
$Cs\text{-}Ba^{137}$	50.258	2.613	59.7
Sr^{90}	0.350	0.018	0.4
Y^{90}	1.736	0.090	2.1
$Ce\text{-}Pr^{144}$	1.379	0.072	1.6
TRE	7.852	0.408	9.3
$Ru\text{-}Rh^{106}$	5.965	0.310	7.1
Co^{60}	16.129	0.839	19.2
Zr^{95}	0.371	0.019	0.4
Nb^{95}	0.092	0.005	0.1
Total	84.132	4.374	99.9

from river mile 16.3 to 19.1 is approximately twice the average value for the entire river. Thus, over several miles of river there are areas where doses are about twice as high as the average in the river from mile 21.5 to mile 1.1. Data from the White Oak Creek drainage[67] indicate that the concentration of radioisotopes is approximately 50 times that of the river. The Diptera populations are subject to the following doses of radiation:

	rad/yr	Times Background
Background	0.213	
Average for the river	4.37	20.5
Hottest areas of river	8.52	40
White Oak Creek	213.0	1000

[66] J. C. Hart, *Applied Health Phys. Ann. Rept. for 1959*, ORNL-3073 (Mar. 20, 1961).

[67] E. G. Struxness, *Detailed Assessment of Solid and Liquid Waste Systems — Hazards Evaluation*, vol 4, ORNL CF-60-5-29 (May 31, 1960).

The life cycle of *Chironomus tentans* Fabr. from egg to death of the adult requires from 26 to 61 days.[68] This wide range in time to complete the life cycle is not unusual among insects with aquatic life stages. Most individuals of *C. tentans* Fabr. complete their life cycles in about 30 days, of which 3 days are spent as an adult. Thus, the dose to the population may be reduced by about 10% during the spring, summer, and fall months when there are flying adults. The larvae are found in the bottom sediments throughout the winter.

Indicator Organisms for Radiation Effects. — In looking for an organism which is suitable as an indicator species for radiation effects in aquatic environments one should consider several factors: (1) The species should spend all or most of its life in the aquatic environment. (2) The species should have some characteristics which may be adapted to quantitative measurement. (3) Is one concerned with levels of radiation which will produce somatic effects or genetic effects?

A large number of invertebrate and vertebrate organisms is found in aquatic environments; consequently, there is little restriction from the standpoint of taxonomic representation. Somatic effects have been studied in the laboratory in a number of instances. Bonham and Palumbo[69] reported that doses of 500–100,000 r were necessary to produce 50% mortality in mollusks, crustacea, and algae. These lower forms of life are generally less sensitive to acute doses of radiation than are vertebrates. The LD_{50} dose for fish varies from slightly less than 1000 r to several thousand r. The LD_{50} doses reported are for acute doses of radiation. These acute doses produced gross damage such as hemorrhage in adult rainbow trout. Gonadal hemorrhage was observed in fish exposed to 500 r.[70] The growth rate of fish[71] and the intrinsic rate of natural increase of *Daphnia pulex*[72] have been

[68] W. O. Sadler, *Biology of the Midge* Chironomus tentans *Fabr. and Methods for its Propagation*, Cornell University Agricultural Experimental Station Memorandum 173 (1935).

[69] K. Bonham and R. F. Palumbo, *Growth* 15, 155 (1951).

[70] A. D. Welander *et al.*, *The Effects of Roentgen Rays on Adult Rainbow Trout*, UWFL-17 (1949).

[71] L. A. Krumholz, *Bull. Am. Museum Nat. Hist.* 110, 277 (1956).

[72] J. S. Marshall, *The Effects of Continuous Gamma Radiation on the Intrinsic Rate of Natural Increase of* Daphnia pulex, Thesis, University of Michigan (1960).

used as indices of radiation effects. Growth rate is affected by many environmental factors other than radiation, such as the availability of food and temperature; therefore, it is difficult to make positive statements about the results. The intrinsic rate of natural increase is an ideal tool for laboratory populations, but collecting the precise population data required from field populations is difficult. Relatively high dose rates of 20 r/hr were required to produce detectable effects on *Daphnia pulex*. It appears that the methods used for detecting these radiation effects are relatively insensitive and require doses several orders of magnitude greater than any ever expected in natural environments.

The genetic effect of radiation, according to present evidence, appears to be a linear function of dose. Therefore, under the conditions of the environment in White Oak Creek and the Clinch River, a study of effects which could be related to genetic changes would be a reasonable approach for exploratory studies on radiation effects under field conditions. Geneticists have used *Drosophila* to study heredity because it is possible to examine the giant chromosomes (polytene) in the salivary gland microscopically and relate certain morphological characteristics of the individual to the pattern of banding on the giant chromosomes. The giant chromosomes are characteristic of Diptera and each species has its own typical pattern of banding. Thus, it is logical to use a dipteral species for the study of the genetic effects of radiation in an aquatic environment. Many aquatic Diptera spend most of their life-cycle in bottom sediments where much of the released radioactivity is contained. Since the developmental stages of organisms are more subject to the effects of ionizing radiation than are mature individuals[73,74] and because sensitive cytogenetic techniques can be used to describe the populations, Diptera appear to offer possibilities as indicators of the genetic effects of chronic low-level radiation arising from the release of radioactive wastes to aquatic environments.

Chironomus tentans Fabr. is widely distributed over North America and Europe, a circumstance which offers the potential advantage of having one species which can be used for the study of the genetic effects of radiation in the environments of large, continental areas. Further interesting possibilities for the study of chronic effects arises from the release of mutagenic chemicals in industrial waste effluents to surface water supplies. The concentrations of the chemicals are low, so acute effects are not readily manifested in aquatic organisms. *Chironomus tentans* Fabr. or the more pollution-tolerant species *C. riparius* Meigen may be used as species for studies of this type.

Crayfish Studies. – The uptake of Co^{60} from solution by crayfish (*Cambarus longulus longerostris*) was studied by placing crayfish in 50- or 500-ml volumes of liquid containing from 10 to 10^5 dis min^{-1} ml^{-1} and in a flowing system in which a solution containing 2.52×10^3 dis min^{-1} ml^{-1} was pumped through the containers holding the crayfish.[60] The uptake of Co^{60} was also studied as a function of size of the individuals, and the uptake by living animals was compared with that of animals killed and preserved in a 5% formaldehyde solution. The excretion of Co^{60} was determined by placing the tagged crayfish in one liter of nonradioactive spring water which was changed daily.

The uptake of Co^{60} by crayfish weighing about 0.5 g each was directly proportional to the concentration of Co^{60} in the solution in which the crayfish were maintained. The sample regression equations for the 50- and 500-ml volumes were $y = 61x$ and $y = 201x$ respectively, where y is the uptake per g and x is the initial concentration per ml of solution (Fig. 2.23). The depletion of available cobalt in the 50-ml volume accounts for the lower uptake by a factor of 3.3 from this volume than from the 500-ml volume. The uptake of cobalt from the continuously flowing solution was slightly greater than that obtained with the 500-ml volume for the same size individuals. In uptake studies such as this it is apparent that one should use either large volumes of liquid under static conditions or a continuously flowing system.

The equilibrium level of Co^{60} increased with the increasing size of the individual crayfish, but the uptake per g decreased with increasing size (Fig. 2.24). Crayfish killed and preserved in 5% formaldehyde solution took up about 40% as much Co^{60} as did living crayfish, and this uptake may be attributed to adsorption on the exoskeleton. The

[73] A. D. Welander, *Growth* **18**, 227 (1954).

[74] L. B. Russell and W. L. Russell, *J. Cell. Comp. Physiol.* **43** (Suppl. 1), 103 (1954).

rate of accumulation of Co^{60}, described by a first-order rate equation, varied with several factors. Hard- and soft-shelled animals had half-times for accumulation of 62 and 75 hr respectively. The half-times for accumulation in the flowing system were 70 hr for small animals (0.9 g, av wt) and 66 hr for large ones (6.4 g, av wt); in the static system (500 ml) the half-times were 24 and 16.6 hr respectively. The larger animals accumulated Co^{60} more quickly because the physical adsorption on their exoskeletons was a faster process than metabolic uptake. The shorter half-times for uptake from the static system are due to the limitations imposed by the availability of Co^{60} in the initial supply of solution in the container. The half-time for accumulation of Co^{60} by dead crayfish is about three times that for living ones under similar experimental conditions.

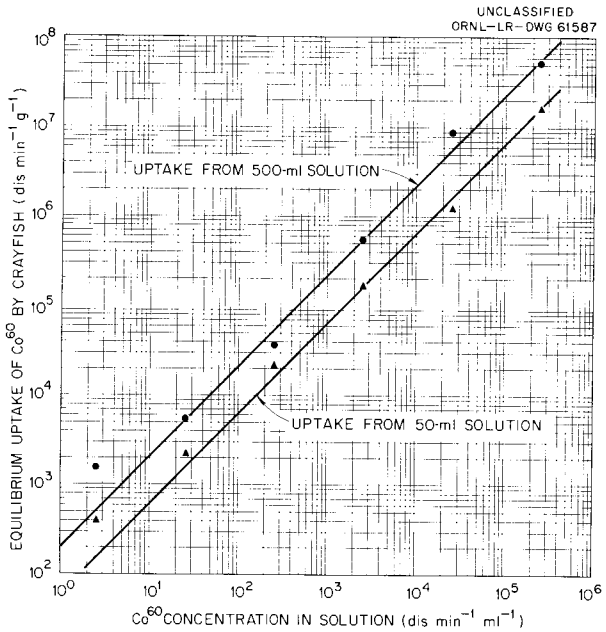

Fig. 2.23. The Uptake of Co^{60} by Similar-Size Crayfish as a Function of Co^{60} Concentration in the Medium.

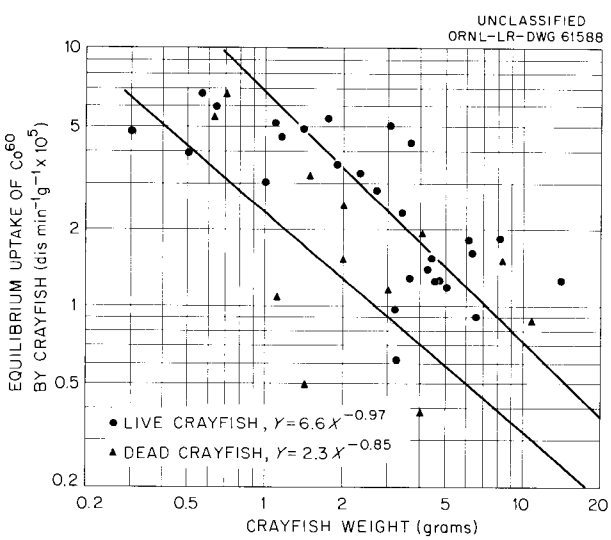

Fig. 2.24. Equilibrium Levels of Ca^{60} Uptake per Gram of Living and Dead Crayfish. The Co^{60} Concentration was 2.54×10^3 dis min^{-1} ml^{-1} and each crayfish was in a 500-ml volume of solution.

Excretion rates, also described by a first-order rate equation were much less than rates of uptake. The biological half-life of Co^{60} ranged from 14 to 70 days and varied with method of dosing and size of the individuals. Cobalt-60 in crayfish (0.87 g, av wt) tagged by placing them in the radioactive solutions had a biological half-life of 37 days, while Co^{60} in crayfish with an average weight of 5.02 g had a biological half-life of 70 days. Small crayfish, having a higher metabolic rate, would excrete mobile Co^{60} more rapidly than the absorbed Co^{60}. Cobalt-60 injected into crayfish had a biological half-life of 14 to 19 days. In this instance little adsorption would occur on the exoskeleton, and virtually all the Co^{60} would be available for excretion; consequently, the shorter biological half-life.

Dissection and radioassay of crayfish tagged with radioactive solutions showed the exoskeleton had the highest concentration per g. Other tissues analyzed and their respective activities as per cent of activity of the exoskeleton were: hepatopancreas 86%; gut 49%; muscle, gonad, and blood (each) 0.14%. The hepatopancreas is a large internal organ, important in mineral metabolism, and probably accounts for most of the Co^{60} which is available for excretion. The gut is lined with a material similar to the exoskeleton, which explains the relatively high concentration of Co^{60} in that tissue.

Strontium and Calcium in Tennessee River Clams. – Fresh-water clams have a shell consisting primarily of $CaCO_3$ and including some strontium. The shell after deposition is unlike bone of vertebrates in that it is not subject to the subsequent metabolism of the clam. New layers of the $CaCO_3$ shell are laid down as the clam grows, and a section through a clam shell contains a history of the mineral deposition of the animal in

successive annual layers. Clams are relatively immobile on the river bottom, and they pump water through their siphons through much of the year although most growth occurs from March through October. The clams are considered as integrating biological samplers of the Sr^{90} content in river waters.

The objectives of the clam study are: (1) to determine the content of stable strontium and calcium and Sr^{90} as a function of species and location in the Clinch and Tennessee Rivers; (2) by considering the Sr^{90} releases from the laboratory as a tracer, to test whether clams may be used as biological samplers of Sr^{90}; (3) to obtain information on long-term changes in stable strontium and calcium in clams by analysis of prehistoric Indian-midden, pre-TVA, and present-day clam shells.

Clams were collected from seven different sites on the Clinch and Tennessee Rivers. Shells of some of the same species of clams were obtained from prehistoric Indian kitchen middens at locations where present-day collections were made. A series of shells representing two species which were collected prior to the construction of TVA dams was obtained from the University of Michigan Museum of Zoology. Clams were identified by comparison with a reference collection from this area.

Chemical analyses for strontium and calcium were made by flame photometry. The strontium determinations were further checked by spectrophotometric methods, and the results from the two methods agreed within 5%. An important point regarding the determination of strontium was the use of calutron-produced Ca^{40} of very high purity in the preparation of standards. A number of common, reagent-grade calcium compounds were analyzed for strontium contamination (Table 2.27); the strontium contamination was of the same order of magnitude as the strontium content of clam shells.[75]

Calcium in Clam Shells. – The aragonite shell of clams is reasonably pure $CaCO_3$ which should yield 400 mg of Ca per g of shell. The initial analyses of the ashed shells showed the calcium content to be as expected; consequently, in subsequent analyses only one in ten shells was analyzed for calcium. A total of 25 shells were analyzed for calcium and the mean content was 401 ±6.51 mg g^{-1} (±s.e.). These deviations from the expected value are within the limits of variability of the analytical techniques.

Table 2.27. Strontium Contamination of Reagent Grade Calcium Compounds

Compound	Sr per g of Ca (μg)	Manufacturer and Lot No.	
Calcium citrate	285	Baker	81844
$CaHPO_4$	500	B&A	N 220
$CaCl_2$	1615	B&A	L 098
$Ca(NO_3)_2 \cdot 4H_2O$	139.5	Mallinckrodt	EXP
CaO	345	Baker	27427
$CaSO_4$	877	Baker	91405
$CaCO_3$	174	Baker	7069
$Ca(OH)_2$	346	Mallinckrodt	GKH

Strontium in Clam Shells. – The clams analyzed in this study were of different ages, although efforts were made to avoid extreme ranges in age. In the collection of *Elliptio crassidens* from TRM 521, the strontium content of 5 clams 4–6 yr old was compared with that of 10 clams 10–15 yr old. The younger clams had a mean strontium content of 204.6 ± 4.87 ppm (±s.e.), and the older clams had a mean content of 214.8 ± 16.2 ppm. These differences are not significant. However, three 2- and 3-yr-old *Anodonta corpulenta* had a strontium content ranging from 232–294 ppm (mean 263 ± 31 ppm), and four 4-yr-old clams of the same species had a strontium content ranging from 353–426 ppm (mean 382 ± 77.6). Since it was not possible to obtain a complete age series of any one species, several *E. crassidens* were sectioned and the annual increment of growth separated in each case. Preliminary data show that the strontium content of the shell deposited when the clam is one and two years old is about one-half as much as the shell deposited in years 5–8. It would not be possible to detect these differences unless clams were analyzed which represented different year classes or the shells were sectioned. The shell

[75] The cooperation of a number of individuals has contributed to the success of this study. Clams were collected by: Paul Bryan, TVA; John Conder, Tennessee Game and Fish Commission; H. E. Voress and E. Kiser, AEC-ORO; H. W. Van der Schalie and J. Burch, University of Michigan; W. D. Cottrell, ORNL. Chemical analyses were done by T. C. Rains, J. A. Norris, and C. L. Burros, Analytical Chemistry Division, ORNL.

growth in the first 2–3 yr, which contains a lesser proportion of strontium, is quantitatively a small part of the shell of a clam 6 or more years old. In the comparison of analyses of clams the age of the clam must be considered in interpreting differences in the stable strontium content.

Table 2.28 summarizes the strontium content of present-day clams collected from six locations on the Clinch and Tennessee Rivers. The strontium content of *E. crassidens* appears to be significantly greater for the specimens collected at CRM 47. However, those clams from the CRM 47 site had a mean age of 23.6 yr, those from TRM 521, 7.5 yr, and those from TRM 425, 14 yr. These differences in strontium content are due to the age difference. In addition, the clams from CRM 47 had a great deal of erosion at the umbo where the early growth was deposited. The difference in strontium content for specimens of *Pleurobema cordatum* from CRM 47 and TRM 425 is significant. The respective ages of these groups are 16.6 and 20.5 yr. The mean growth rate for *P. cordatum* from TRM 425 was 4.9 g/yr and for the CRM 47 collection it was 2.5 g/yr. Approximately same-age (17 and 18.7 yr) *Cyclonaias tuberculata* from TRM 521 with an average growth rate of 2.6 g yr^{-1} have a significantly higher strontium content than do those from TRM 100 which have an average growth rate of 2.4 g/yr. In these species the individual with the fastest growth rate had the highest strontium content. Shell growth rate is the obvious factor controlling strontium deposition in clams. The changes which occur in strontium content of a clam shell with age of the clam can be explained in either of two ways: (1) The clam shell is deposited by the mantle. If there is more mantle per unit of shell to be deposited in a young clam, the rate at which shell-secreting cells would have to lay down shell would be less. (2) The young clams have to compete for food and space in their environment. These clams may have a difficult time surviving the first few years of their life with a resulting slower growth rate.

Strontium-90—Stable Strontium Atom Ratios and the Fate of Sr^{90} in the River System. – The releases of Sr^{90} from the Laboratory have not been constant, nor is it possible to derive adequate quantitative data on Sr^{90} from the early information on monitoring; consequently it is not an ideal tracer experiment. One can assume that Sr^{90} and stable strontium have been taken up by the organisms in proportion to the ratio of these elements in the water. The age of the clams analyzed did not antedate 1943, the time of the first releases. Because of the 28-yr radioactive half-life of Sr^{90}, slight differences in ages of the clams analyzed should not have an appreciable effect on Sr^{90}–stable strontium atom ratios. The average age of the clams analyzed for Sr^{90} was about 15 years. Therefore, the variation in Sr^{90} discharges from the laboratory is of no consequence.

Table 2.28. Mean Strontium Content (ppm) of Present-Day Clams in the Tennessee River System Collected at Different Locations

Species	D* Value	CRM 66	CRM 47	CRM 17	TRM 521	TRM 425	TRM 100
Quadrula pustulosa	49.2			115.9		202.7	119.5
Elliptio dilatatus	27.1	222.0	206.2				
E. crassidens	26.8		260.9		211.4	211.7	228.2
Pleurobema cordatum	18.1		198.5			237.3	
Cyclonaias tuberculata	29.8		213.5		242.6	213.3	208.8
Actinonaias carinata gibba	16.2	198.4	187.5				
Lampsilis ovata	28.6	231.1	224.0				

*The Tukey Test was used to compare means of species from different locations. The difference between means must be greater than this value for significance at the 5% level.

The Sr^{90}–stable strontium atom ratios observed and expected on the basis of dilution of Clinch River water by Tennessee River water are shown in Table 2.29. The Sr^{90}–stable strontium atom ratio upstream from White Oak Creek is due to fallout and may be assumed to be constant for the entire river system. Estimates of the average annual volume of river flow at the various stations were obtained from U.S. Geological Survey stream gaging station data and corrected to the specific collecting locality when necessary. The Sr^{90}–stable strontium atom ratio from clams collected in the Clinch River downstream from White Oak Creek was divided by the dilution factor to obtain the atom ratio expected on the basis of dilution. The agreement between expected and observed atom ratios is excellent considering that we have a tracer experiment over almost 500 river miles. The observed Sr^{90}–stable strontium atom ratio at TRM 521 is about 80% of the expected value. The low value may be explained by a greater than predicted dilution of Tennessee River water in the area of the clam bed. The bed from which the clams were taken at TRM 521 is on a shoal area on the left side of the river, the channel being located on the right. Sewee Creek with an average annual discharge of 190 cfs enters the Tennessee River at TRM 524.5, on the left bank. There are two possible reasons which explain why Sewee Creek water does not disperse completely in the Tennessee River by the time it flows over the bed: (1) the distance between the confluence of Sewee Creek and the Tennessee River and the clam bed is short, and the waters do not have time to mix completely. (2) The flow of water in this reach of the Tennessee River is highly regulated by the discharge from Watts Bar Dam (TRM 530). Therefore, during periods of low flow on the Tennessee River, the Sewee Creek water would dilute the Tennessee River water in the area of the clam bed. In this instance strictly local conditions account for difference in Sr^{90} uptake by a relatively immobile organism as a clam.

Strontium-90 released to surface water streams remains in solution, and concentrations downstream from a release point may be predicted solely on the basis of dilution of the contaminated water by noncontaminated water. These data also indicate that there is very little ion exchange between strontium in the water and the bottom sediments. This conclusion could be anticipated on the basis of radiochemical analyses of the Clinch River bottom sediments.[66] In this respect the behavior of Sr^{90} is much different from that of Cs^{137} which is adsorbed strongly to soil and bottom sediments. The implications for the disposal of atomic wastes are important in the event of multiple atomic energy installations on one river drainage system. The release of low-level wastes by each installation will have to be coordinated

Table 2.29. Observed and Expected Sr^{90}–Stable Strontium Atom Ratios in Clams as a Function of the Dilution of Clinch River Water

Collection Site	Dilution Factor for Clinch River Water	Sr^{90}–Stable Sr Atom Ratio $\times 10^{11}$		Number Analyzed	Fallout Sr^{90}–Laboratory-Released Sr^{90} Atom Ratio
		Expected on the Basis of Dilution	Observed by Stable Chemistry and Radiochemistry		
CRM 47* (Upstream from White Oak Creek)			1.67 ± 0.50	12	
CRM 17–4.7 (Downstream from White Oak Creek)	1	130.8	130.8 ± 22.7	12	1:78
TRM 521	4.2	31.1	25.24 ± 3.36	19	1:15
TRM 425	7.05	18.6	19.78 ± 1.71	19	1:12
TRM 100	12.3	10.6	10.14 ± 1.81	14	1:6

*CRM, Clinch River Mile; TRM, Tennessee River Mile; the Clinch River joins the Tennessee River at TRM 586 (River Miles measured from mouth of the river); ± one standard error of the mean.

in order to avoid exceeding permissible concentrations of Sr^{90}.

The contribution of Laboratory releases of Sr^{90} to the Clinch and Tennessee Rivers may be compared with that from fallout through use of the Sr^{90}–stable strontium atom ratios in clams collected at CRM 47 (upstream from White Oak Creek) and the atom ratio in clams collected downstream from White Oak Creek. The Laboratory contributed 78 atoms of Sr^{90} for each atom of fallout Sr^{90} in the Clinch River. This ratio decreases in proportion to dilution of the Clinch River water.

Strontium Contamination of Reagent Calcium Compounds. – The relatively large amounts of strontium in reagent calcium compounds (Table 2.27) may be of considerable significance in metabolic studies of calcium and strontium. The metabolism of strontium by organisms has been of major concern in connection with fallout and other environmental releases of fission products. Strontium is usually associated with the metabolism of calcium because of its chemical similarity. One of the important factors studied has been the effect of different calcium content in diets on the uptake of strontium. There have been a number of papers on this subject, and one[76] has been selected as an example to compare the quantities of Sr^{90} and contamination strontium present in the diets of rats containing different levels of calcium.

The rats consumed 9.5 g of food per day from diets which contained 0.03, 0.1, 0.5, and 2.0% calcium. There was a daily ingestion of 0.95 μc Sr^{90}. The calcium compound used to adjust the dietary level of calcium in the above experiment was not analyzed (Table 2.27). Since this is a generalization, the average strontium content (535 μg per g of calcium) for all calcium compounds analyzed was used to calculate the atom relationships of contamination stable strontium and Sr^{90} (Table 2.30).

There are present in this instance from 200 to 15,000 times as many stable strontium atoms as there are Sr^{90} atoms. The stable strontium contamination atoms increase in proportion with the calcium content of the diet. Therefore, it would be difficult to differentiate between the effects of calcium and strontium in the uptake of Sr^{90}

[76] R. C. Thompson and R. F. Palmer, *Am. J. Physiol.* 199, 94 (1960).

Fish Studies

Fish-tagging studies were initiated on the Clinch River in the vicinity of White Oak Creek to determine the movement of fish in this portion of the Clinch-Tennessee River system. Fish were caught in hoop nets, marked with number tags, and released at the capture site. Except for gizzard shad, all fish captured were tagged routinely. There have been 150 (2.8%) tag recoveries of 5245 fish tagged (Table 2.31). About two-thirds of the tag recoveries represented white bass and white crappies. Fishermen have recovered twice as many tagged white bass as have been recovered in netting. Over two-thirds of the white bass returns by fishermen have come from the Tennessee River portion of Watts Bar Reservoir. These fish moved an average distance of 28 miles downstream. Fishermen also have accounted for 40% of all white crappies recovered, and all but three of these have been from the Clinch River. The average distance moved by white crappie was 11.8 miles.

Table 2.30. Atoms of Stable Strontium Present as Contamination of Calcium Compounds in Relation to Sr^{90} Added in a Tracer Experiment

Calcium in Diet (%)	Stable Strontium Atoms from Contamination (atoms/day)	Sr^{90} Atoms Added as a Tracer (atoms/day)	$\frac{\text{Stable Sr}}{Sr^{90}}$
0.03	1.05×10^{16}	4.62×10^{13}	2.27×10^{2}
0.1	3.49×10^{16}	4.62×10^{13}	7.55×10^{2}
0.5	1.75×10^{17}	4.62×10^{13}	3.79×10^{3}
2.0	7.01×10^{17}	4.62×10^{13}	1.52×10^{4}

Table 2.31. Kinds and Numbers of Fish Tagged and Numbers of Fish-Tag Recoveries by Fishermen and Netting

Species	Number Tagged	Tag Recoveries	
		Fishermen	Netting
Longnose Gar, *Lepisosteus osseus*	3		
Skipjack Herring, *Alosa chrysochloris*	30	1	
Gizzard Shad, *Dorosoma cepedianum*	577	1	1
Mooneye, *Hiodon tergisus*	12		
Carp, *Cyprinus carpio*	978	3	2
River Carpsucker, *Carpiodes carpio*	183	3	7
Quillback, *Carpiodes cyprinus*	11		
Smallmouth Buffalo, *Ictiobus bubalus*	639	5	7
Bigmouth Buffalo, *Ictiobus cyprinellus*	1		
Black Buffalo, *Ictiobus niger*	6		
River Redhorse, *Moxostoma carinatum*	2		
Black Redhorse, *Moxostoma duquesnei*	1		
Golden Redhorse, *Moxostoma erythrurum*	94		2
Blue Catfish, *Ictalurus furcatus*	24	1	1
Yellow Bullhead, *Ictalurus natalis*	2		
Channel Catfish, *Ictalurus punctatus*	151	9	3
Flathead Catfish, *Pylidictis olivaris*	10		
White Bass, *Roccus chrysops*	812	34	18
Rock Bass, *Ambloplites rupestris*	6		
Bluegill, *Lepomis macrochirus*	149		
Longear Sunfish, *Lepomis megalotis*	2		
Smallmouth Bass, *Micropterus dolomieui*	2		
Spotted Bass, *Micropterus punctulatus*	2	1	
Largemouth Bass, *Micropterus salmoides*	5		
White Crappie, *Pomoxis annularis*	1027	18	27
Black Crappie, *Pomoxis nigromaculatus*	9		
Walleye, *Stizostedion v. vitreum*	1	1	
Sauger, *Stizostedion canadense*	42	1	
Freshwater Drum, *Aplodinotus grunniens*	463	1	3
	5245	79	71

The value of the fish tagging studies will increase as more tags are recovered. It is already evident that fish which have been in the Clinch River in the vicinity of White Oak Creek will move considerable distances in the Tennessee River system. One sauger and a skipjack herring have been recovered almost 100 and 50 miles, respectively, from the location of tagging.

The white crappie is being used as an experimental fish to study fission product element metabolism because, of all the 29 species of fish caught from the Clinch River, it is caught in largest numbers, appears to have a relatively small home range, and is also an important game species.

RELATED ACTIVITIES

Committee Work

American Standards Association. – One member of the staff was appointed to and participated in the activities of the American Standards Association Subcommittee N-5.2 on "Radioactive Waste Disposal – Site Selection Criteria."

Ecological Society of America. – The section leader recently was appointed chairman of the Ecological Society's Committee on Radioecology. A proposal for a summer institute in radioecology was prepared under committee auspices and submitted to the Atomic Energy Commission and the

National Science Foundation. If approved, this institute would be held in Oak Ridge during June–August, 1962, and would be conducted by staff members of the section and staff of the Oak Ridge Institute of Nuclear Studies.

One member of the staff is chairman of a subcommittee on Chemical Cycles in Ecological Systems, sponsored by the Ecology Study Committee of the National Science Foundation and the Ecological Society of America. The organization meeting of this subcommittee was held at ORNL on May 14–16, 1961. Activities include sponsorship of a national symposium in August, 1961, exchange of information, and recommendations on activities in this field.

Civil Defense. – A staff member served on a working group on ecological problems involved in civil defense and nuclear warfare, for the Advisory Committee on Civil Defense of the National Academy of Sciences–National Research Council. A report on research policy relative to damage to and recovery of the environment from blast, fire, and radiation has been submitted.

Participation in Educational Programs

Two members of the section gave lectures and guided field tours to a group of district leaders of the Soil Conservation Service, USDA, who were in Oak Ridge for briefing on studies related to nuclear fallout and agriculture.

Members of the section gave a guided tour of some of the ecology study sites to a group of editors of the national agriculture newspaper, "Prairie Farmer."

Two student groups, representing Emory University, Atlanta, Georgia, and Tennessee Wesleyan College, Athens, Tennessee, visited the ecology laboratories. Members of the staff lectured on various aspects of research under way and the groups were given tours of the field study sites.

Instruction and practice for analyzing radioactivity in vegetation samples, and use of radioisotopes in ecological research, was given to personnel representing three schools which have AEC-supported radioecology programs (Duke University, University of Tennessee, Wabash College).

Two staff members lectured and gave guided field tours to a class of radiological health trainees from the R. A. Taft Sanitary Engineering Center, Cincinnati, Ohio.

3. RADIATION PHYSICS AND DOSIMETRY

THEORETICAL PHYSICS OF DOSIMETRY

J. Neufeld

P. H. Doyle[1] G. S. Hurst
W. D. Moon[1,2] H. B. Eldridge
H. Wright[1,2] R. H. Ritchie
D. W. Forester[1]

Electromagnetic Interaction of a Beam of Charged Particles of Plasma

This investigation deals with the passage of an electron beam through plasma and points out the existence of a new instability caused by electromagnetic interaction between the beam and the stationary plasma.

The plasma-beam instability has been studied by Akhiezer and Fainberg[3] under the assumption that $\theta = 0$, where θ is the angle formed by the direction of the beam and the direction of the growing wave resulting from the instability. Under these conditions the interaction is electrostatic; that is, the wave is longitudinal. In this investigation the above assumption is generalized so as to include the case of $\theta \neq 0$ and the effect of electromagnetic interaction. For $\omega \sim \omega_1$, where ω_1 is the Langmuir frequency of the plasma, the interaction is electrostatic for all values of θ, and the resulting instability which produces a longitudinal wave increases exponentially in accordance with the term $\exp\,(3\sqrt{3}\,\omega_0^2 k v_0 \cos\theta/8)^{1/3}$ (where ω_0 is the Langmuir frequency of the beam). For a frequency range below ω_1 the instability is less pronounced. However, this instability is significant, since the interaction is electromagnetic, and the "growing wave" resulting from this interaction is characterized by an electric vector having both transverse and longitudinal components. In investigating the above instabilities, an assumption was made that the density of the incident beam is small and the results cover all values of θ except those in the immediate neighborhood of $\pi/2$. For θ in the neighborhood of $\pi/2$ the assumption is more general and the results apply to any density of the beam.

Space Dispersive Properties of Plasma

Phenomenological electrodynamics of material media as formulated by Maxwell was based on an assumption that the dielectric and magnetic permeability of matter may be represented by means of suitable constants. An important modification of the macroscopic theory has been introduced by Lorentz who formulated the concept of frequency dispersion. More recently, various types of material media have been described phenomenologically in terms of "space dispersion." Space dispersion – that is, the occurrence of the term k in the dielectric constant $\epsilon(\omega,k)$ – can be attributed either to the Doppler effect or to the magnitude of a term ak that may appear in the formulation of the problem (a is a characteristic distance such as the Debye length). By use of an approach based on the Doppler effect, the macroscopic parameters of a plasma have been represented in the form of four-dimensional tensors of the fourth order (similar to those introduced by Mandelstam and Tamm.)[4]

The phenomenological description of plasma has also been formulated in a three-dimensional space by means of two macroscopic parameters, the electric susceptibility χ_e and the "proper magnetic susceptibility" χ_μ/μ. Expressions for these parameters have been given for the general case of a plasma having an electron velocity distribution $f(v)\,dv$ and for a few typical specific cases. Both parameters are functions of the frequency and of the wave vector. This formulation shows that a plasma is a magnetically polarizable medium and that the term χ_μ/μ vanishes only if the electron velocity distribution is isotropic. In the current literature the existence of the term χ_μ/μ has not been taken into account, since in the use of a

[1] Consultant.

[2] Summer employee.

[3] A. I. Akhiezer and Ia. B. Fainberg, *Zhur. Eksptl. i. Teoret. Fiz.* 21, 1262 (1951).

[4] L. E. Mandelstam and I. E. Tamm, *Math. Ann.* 95, 154 (1925).

"modified representation" of the dielectric constant, the magnetic properties of plasma have not been considered. In the modified representation the dielectric constant ϵ_M is defined by the relationship $k \times B = -(\omega/c)\epsilon_M E$, whereas in the conventional representation the same relationship has the form $k \times B = -(\omega/c)\epsilon E + 4\pi(\chi_\mu/\mu)k \times B$, where $\epsilon = 1 + 4\pi\chi_e$. A general formalism has been developed for deriving the electric and magnetic plasma parameters directly from the Boltzman-Vlasov equations.

Optical Emission from Irradiated Solids

A dielectric theory of coulomb-stimulated photon emission from solids, based on the approach of Frank and Ginsberg,[5] has been described elsewhere.[6] This theory has been generalized to include the wave properties of the incident charged particle. A digital computer code has been written to evaluate the expression for the photon distribution function derived by means of this approach.

Ferrell[7] has considered the specific case of light emission from a thin slab of plasma irradiated by normally incident electrons. He presents a very ingenious nonrelativistic treatment in which the act of energy deposition in the slab is considered separately from the coupling of polarization currents with the transverse electromagnetic field. His approach yields a series of equations which may be combined to give the distribution function

$$n_{\text{Ferrell}}(\theta, \omega; a, \beta) = \frac{\alpha\beta^2}{4\pi^2} \frac{\theta^2\omega_p \sin^2(t/2\beta)}{[(\omega - \omega_p)^2 + \omega_p^2(\epsilon_2 + \theta^2 t/2)^2/4]}, \quad (1)$$

where $n(\theta, \omega; a, \beta)$ is the number of photons emitted per unit solid angle in the direction making the angle θ with the velocity vector of the incident electron, per unit frequency interval at the frequency ω. Also, ω_p is the plasma resonance frequency; β is the velocity of the incident electron divided by c, the velocity of light; a is the foil thickness; ϵ^2 is the imaginary part of the dielectric constant of the plasma at the frequency ω_p, α is the fine structure constant, and $t = a\omega/c$.

The present approach yields a more complicated formula, but one which is applicable to a foil having a general dielectric variation with frequency; that is, $\epsilon(\omega) = \epsilon_1(\omega) + \epsilon_2(\omega)$, and bounded on both sides by vacuum:

$$n(\theta, \omega; a, \beta) = \frac{\alpha\beta^2}{\pi^2\omega} \mu^2(1 - \mu^2) \left|\frac{D}{\Delta}\right|^2, \quad (2)$$

where

$$D = \left(\frac{\beta\sigma - \epsilon}{1 - \mu^2\beta^2} - \frac{1}{1 - \beta\sigma}\right)(\mu\epsilon + \sigma)\, e^{-it\sigma} + \left(\frac{\beta\sigma - \epsilon}{1 - \mu^2\beta^2} + \frac{1}{1 + \beta\sigma}\right)(\mu\epsilon - \sigma)\, e^{it\sigma} - 2\sigma\left(\frac{\epsilon}{1 - \beta\mu} - \frac{1 + \beta\mu\epsilon}{1 - \beta^2\sigma^2}\right) e^{-it/\beta},$$

$$\Delta = (\mu\epsilon - \sigma)^2 e^{it\sigma} - (\mu\epsilon + \sigma)\, e^{-it\sigma},$$

$$\mu = \cos\theta,$$

$$\sigma = [(\epsilon_1 - 1 + \mu^2)^2 + \epsilon_2^2]^{1/4} \exp\left(\frac{i}{2}\tan^{-1}\frac{\epsilon_2}{\epsilon_1 - 1 + \mu^2}\right).$$

Equation (2) is applicable, as it stands, to emission angles $0 \leqq \theta \leqq \pi/2$. If one sets $\mu = |\cos\theta|$, $\beta \to -\beta$, it is valid in the range $\pi/2 \leqq \theta \leqq \pi$. The polarization of these photons is predicted to be entirely in the plane containing the foil normal and the propagation vector of the photon.

Equation (2) includes Ferrell's result as a special case. If one puts $\beta = 0$ in both the D and Δ expressions of Eq. (2), and sets $\epsilon_1 = 1 - (\omega_p/\omega)^2$, and $\omega \sim \omega_p$, corresponding to the case of a classical free-electron plasma close to resonance, assumes ϵ_2, t, and θ are $\ll 1$, but allows t/β to be unrestricted, one finds an expression which differs from Eq. (1) only in terms containing the small quantity ϵ_2.

The present treatment predicts that photon emission occurs at any frequency for which $\epsilon(\omega) \neq 1$ and that a peaking in the emission spectrum should occur wherever $Re[\epsilon(\omega)] \cong 0$, regardless of whether

[5] I. M. Frank and V. I. Ginsberg, *J. Phys. (U.S.S.R.)* 9, 353 (1945).

[6] R. H. Ritchie and H. B. Eldridge, *Bull. Am. Phys. Soc.* 11, 386 (1959); ORNL-2806, p 136.

[7] R. A. Ferrell, *Phys. Rev.* 111, 1214 (1958).

this behavior is due to the excitation of collective oscillations in the solid or whether it is due to a single electron interband (or intraband) transition.

A code to evaluate Eq. (2) for arbitrary values of its argument has been written for the IBM 7090. The optical data of Taft and Phillips[8] on $\epsilon(\omega)$ for Ag have been employed to predict the photon distribution from this metal when irradiated by electrons. Agreement with the experimental data of Arakawa, Birkhoff, and Frank is good as may be seen by referring to Fig. 3.28 of the Experimental Physics of Dosimetry section and the descriptive material accompanying this figure.

Equation (2) is valid in the relativistic range as long as the photon energy, $\hbar\omega$, is much less than the energy of the incident particle. When the bombarding electron energy is in the relativistic range, emission of Cerenkov photons from the foil is possible. Equation (2) also describes the distribution of these photons in energy and angle. Because the foil surfaces are present, these photons are refracted and may be internally reflected many times before emerging. The distinction between Cerenkov photons and "transition" photons is not a clear-cut one at relativistic energies. For example, there may be a relativistic enhancement of emission at angles $\theta < \pi/4$ and at frequencies where the velocity of light in the foil is not greater than c.

A competing process, which may result in the generation of optical photons when charged particles irradiate a solid, is the well-known bremsstrahlung phenomenon. In this case, an incident electron may suffer a deflection in the nuclear field of an atom in the solid and thereby couple with the transverse electromagnetic field. The polarization and particle energy dependence of the light from the bremsstrahlung process are both expected to be different than they would be if the light were generated in the transition radiation process.

Bremsstrahlung in a nuclear encounter with an isolated atom has been investigated extensively. Recent results[9,10] give the distribution of photons averaged over all possible deflections of the incident electron. In the case of optical photons, these authors give for the cross section per atom for finding a photon of frequency ω per unit frequency interval per unit solid angle in the direction θ with respect to the velocity of the incident electron

$$\sigma_{\parallel} = \frac{Z^2\alpha}{2\pi}\left(\frac{e^2}{mc^2}\right)^2 \frac{1-\beta^2}{\beta^2}\,\frac{(\cos\theta-\beta)^2}{(1-\beta\cos\theta)^4}\,\frac{1}{\omega}\,[L + 0_{\parallel}(1)]\,, \quad (3)$$

for photons polarized in the plane containing the initial electron direction and the photon propagation vector and

$$\sigma_{\perp} = \frac{Z^2\alpha}{2\pi}\left(\frac{e^2}{mc^2}\right)^2 \frac{1-\beta^2}{\beta^2}\,\frac{1}{(1-\beta\cos\theta)^2}\,\frac{1}{\omega}\,[L + 0_{\perp}(1)]\,, \quad (4)$$

for photons polarized perpendicular to this plane. The quantity

$$L \equiv \ln\left\{(mc^2)^2\,\frac{\beta^2}{1-\beta^2}\left[(\hbar\omega)^2\left(\frac{1-\beta\cos\theta}{\beta}\right)^2 + \left(\frac{Z\,1/3\,mc^2}{108}\right)^2\right]\right\}, \quad (5)$$

and $0_{\parallel}(1)$ and $0_{\perp}(1)$ are quantities of the order of unity. Z is the atomic number of the nucleus.

A complete theory of optical bremsstrahlung in a finite foil of given optical characteristics does not seem to have been carried out. Work along this line is now being done in our theoretical group.

Analysis of Swarm Experiment Data on the Transport of Electrons in Gases

A new method of analyzing electron swarm data has been formulated, and numerical work is in progress to test its accuracy in cases involving electron transport in molecular gases. Analysis of such experiments in the past has been done by making rather crude assumptions regarding the equilibrium distribution of electron energies. The present method involves a solution of the integral equation which results when one assumes that the swarm electrons are in energetic equilibrium with the field and that the distribution of their velocities is nearly isotropic. Basic electron-molecule cross sections are obtainable directly from the

[8] E. A. Taft and H. R. Phillip, *Phys. Rev.* 121, 1100 (1961).

[9] R. L. Gluckstern, M. H. Hull, Jr., and G. Briit, *Phys. Rev.* 90, 1020 (1953).

[10] R. L. Gluckstern and J. H. Hull, Jr., *Phys. Rev.* 90, 1030 (1953).

field dependence of drift velocity and diffusion coefficient.

Taking such an approach, one finds that the unnormalized equilibrium distribution of electrons in a molecular gas may be written

$$f(y,\epsilon) = \exp(-yx) , \tag{6}$$

where

$$x(\epsilon) = \int_0^{\epsilon} \gamma(\epsilon')\sigma_t^2(\epsilon')\,d\epsilon' ,$$

$\gamma(\epsilon)$ = average energy loss per collision for an energy ϵ,

$\sigma_t(\epsilon)$ = inverse transport mean free path at unit pressure,

$y = (eE/p)$,

E = electric field strength,

e = electronic charge,

p = gas pressure.

This expression is derived assuming that the average fractional energy loss per collision is small and that the average swarm energy is much greater than the thermal energy of the gas.

If $W(y)$ is the drift velocity of a swarm of electrons in a molecular gas and $K(y)$ is its diffusion coefficient, both determined for a particular value of y, then the following nonlinear integral equation for $d\epsilon/dx$ may be proved:

$$\frac{d\epsilon}{dx} = \frac{\int_0^x K(x-x')\,\epsilon^{1/2}(x')\,\frac{d\epsilon}{dx}(x')\,dx'}{\int_0^x W(x-x')\,\epsilon^{1/2}(x')\,\frac{d\epsilon}{dx}(x')\,dx'} , \tag{7}$$

where

$$K(x) = \frac{(9m/2)^{1/2}}{2\pi 6} \int_{C-i\infty}^{C+i\infty} e^{xy}\, pK(y)\,dy , \tag{8}$$

$$W(x) = \frac{(9m/2)^{1/2}}{2\pi i} \int_{C-i\infty}^{C+i\infty} e^{xy}\, y^{-1/2}\, W(y)\,dy , \tag{9}$$

and m is the electron mass. The contours in the complex integration of Eqs. (8) and (9) are to be taken to the right of all singularities in the complex y plane. The evaluation of the complex integrals may be done best by fitting experimental data on $W(y)$ and $K(y)$ with analytical expressions which have easily obtainable Laplace inverses. The integral equation may be then solved by an iterative procedure. Preliminary considerations of cases in which $f(y,\epsilon)$ is known indicate that such a scheme may give rapid convergence.

Once $\epsilon(x)$ is found by numerical means, $\sigma_t(\epsilon)$ and $\gamma(\epsilon)$ are easily obtained. A digital computer code is being written to solve Eq. (7) and will be tested on cases for which the $\epsilon(x)$ relation is known.

The Energy Distribution of Slow Electrons in Gases

In order to infer the energy dependence of experimental parameters characterizing electron transport through a gas, it is necessary to know the form of the energy distribution function of the electrons. Distribution functions for two diatomic gases have been calculated using molecular cross sections for elastic and inelastic collisions from the theories of Fisk[11] and Gerjuoy and Stein,[12,13] respectively.

One may solve the Boltzman transport equation by expanding the unknown electron distribution function $f(v,\theta,\phi)$ into a Taylor's series in v', the speed of the electron before collision with the gas molecule, about the speed v of the electron after collision with the gas molecule. If one retains only the first two terms in the expansion, assumes f is independent of ϕ, and then expands f in a Legendre series in the angle θ, the angle between $\bar{v}$ and the electric field, one obtains the following solution for f_0, the first-order harmonic in the Legendre series,

$$f_0 = C \exp -6 \int_0^{\epsilon} \frac{Q\left(\sigma_1 \gamma x + \frac{1}{2}\sum_i \alpha_i\right) dx}{\xi^2 + 6Q\left(\sigma_1 \gamma x + \frac{1}{2}\sum_i \alpha_i\right) kT} \tag{10}$$

where

$Q(\epsilon)$ = sum of all cross sections for the energy loss processes being considered,

γ = mass of electron divided by mass of molecules,

$\sigma_1(\epsilon)$ = elastic momentum transfer cross section, cm^{-1} at unit pressure,

[11] J. B. Fisk, *Phys. Rev.* **49**, 167 (1936).

[12] E. Gerjuoy and S. Stein, *Phys. Rev.* **98**, 1848 (1955).

[13] E. Gerjuoy and S. Stein, *Phys. Rev.* **97**, 1671 (1955).

ξ = electric field per unit pressure of gas, reduced by pressure

$\alpha_i(\epsilon)$ = energy loss per cm of travel by electron due to the ith inelastic process,

C = normalization constant,

k = Boltzmann constant,

T = absolute temperature.

In order to compare the above distribution with experimental work, $\bar{\epsilon}$, the average swarm energy, W, the drift velocity, and W/pK, the ratio of drift velocity to diffusion coefficient per unit pressure of gas were calculated for nitrogen and hydrogen. The only inelastic process considered is the excitation of rotational levels in the gas since these are the only losses for which cross sections are available. The total elastic cross sections evaluated theoretically by Fisk[11] were used for $\sigma_1(\epsilon)$, and the inelastic cross sections and energy loss functions were evaluated from the work of Gerjuoy and Stein.[12,13] Subject to the above restrictions, the averages are defined by the following integrals:

$$\bar{\epsilon} = \int_0^\infty \epsilon n(\epsilon)\, d\epsilon ,$$

$$W = -\frac{2ma}{3} \int_0^\infty \frac{\epsilon}{Q} \frac{\partial}{\partial \epsilon} \frac{1}{\sqrt{\epsilon}} n_0(\epsilon) ,$$

$$\frac{W}{pK} = -\xi \frac{\displaystyle\int_0^\infty \frac{\epsilon}{Q} \frac{\partial}{\partial \epsilon} \frac{1}{\sqrt{\epsilon}} n(\epsilon)\, d\epsilon}{\displaystyle\int_0^\infty \frac{\epsilon^{1/2}}{Q} n(\epsilon)\, d\epsilon} ,$$

where

$$n(\epsilon)\, d\epsilon = \frac{f_0 \sqrt{\epsilon}\, d\epsilon}{\displaystyle\int_0^\infty f_0 \sqrt{\epsilon}\, d\epsilon} .$$

A program has been developed to evaluate the above averages numerically. All cross sections and energy-loss functions are put into the program as tabulated functions of energy. A plot of the average energy for both nitrogen and hydrogen calculated numerically is shown in Fig. 3.1 as a function of ξ, taking kT = 0.025 ev. Since the first vibrational levels occur at 0.29 and 0.54 ev in nitrogen and hydrogen respectively, one may determine approximately the range of ξ over which the distribution is valid for the two gases by determining the values of ξ at which the average energy becomes equal to the first vibrational level. From Fig. 3.1 the maximum value of ξ for which the distribution is valid is about 0.15 ev cm^{-1} (mm Hg)$^{-1}$ for nitrogen; it is valid for hydrogen up to and beyond 0.5 ev cm^{-1} (mm Hg)$^{-1}$. In Figs. 3.2 and 3.3 the drift velocity is compared with the experimental work of Errett[14] and Bowe.[15] The agreement is fair but the theoretical values are too low for the higher values of ξ. This behavior is expected and may be explained by a simple physical argument. Since inelastic processes other than rotational excitation were neglected in the derived distribution function, it would predict more electrons in the higher energies than is actually the case in the real physical situation. This is to say the derived distribution would have a smaller slope on the high-energy side of the maximum, and since the drift velocity is proportional to the slope of the distribution function, W would be expected to be lower if the derived distribution is used in its evaluation. Figures 3.4 and 3.5 show a comparison between W/pK as evaluated in the above manner and the recent experimental work of Forester, Cochran,[16] and Crompton.[17] The agreement here

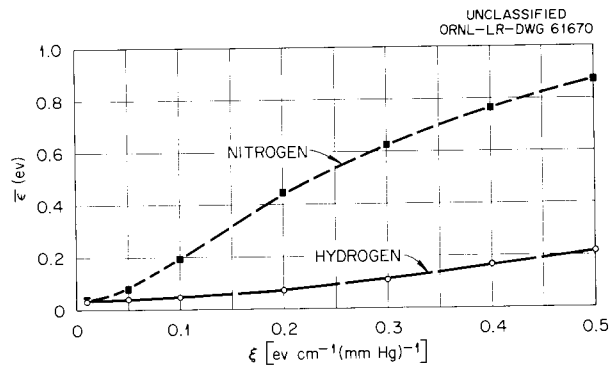

Fig. 3.1. Average Energy of Electrons in Nitrogen.

[14] D. D. Errett, *The Drift Velocity of Electrons in Gases*, Thesis, Purdue University, 1951 (unpublished).

[15] J. C. Bowe, *Phys. Rev.* 117, 1411 (1960).

[16] D. W. Forester and L. W. Cochran, Private Communication.

[17] R. W. Crompton and D. J. Sutton, *Proc. Roy. Soc. (London)* A215, 467 (1952).

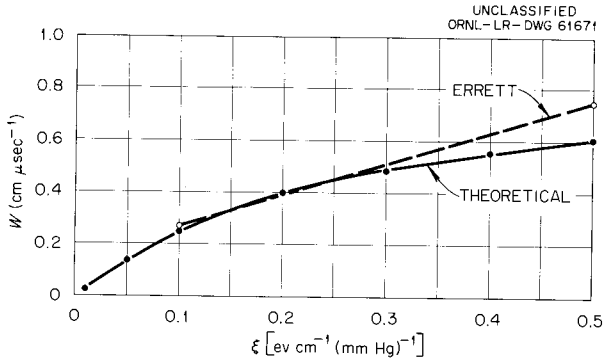

Fig. 3.2. Drift Velocity of Electrons in Hydrogen.

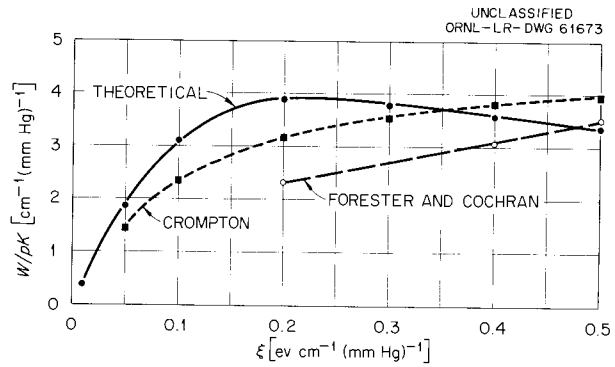

Fig. 3.4. Ratio of Drift Velocity to Diffusion Coefficient of Electrons in Hydrogen at Unit Pressure.

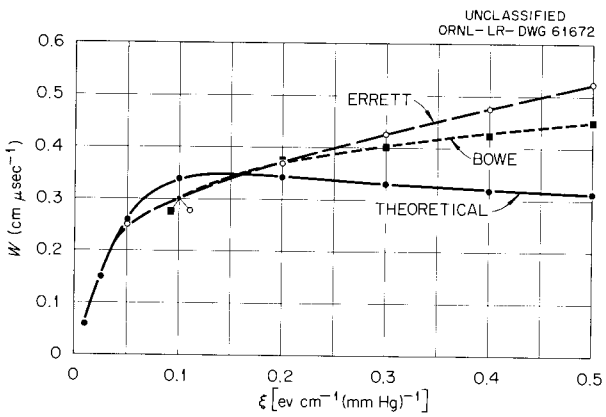

Fig. 3.3. Drift Velocity of Electrons in Nitrogen.

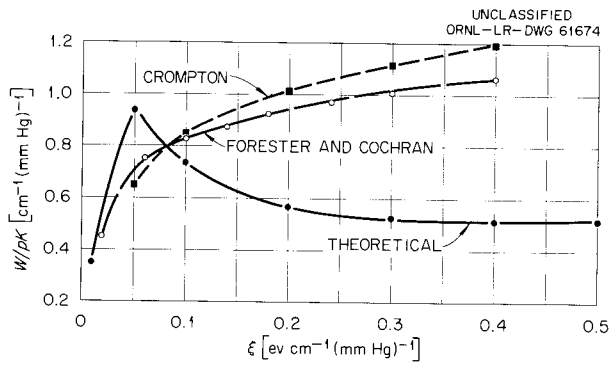

Fig. 3.5. Ratio of Drift Velocity to Diffusion Coefficient of Electrons in Nitrogen at Unit Pressure.

also seems to be reasonable, since at high values of ξ one would expect the numerically evaluated pK to be too large since it varies as $(\epsilon)^{1/2}$, and the derived distribution would predict too large an $\bar{\epsilon}$. Therefore, at high values of ξ, since W is too small and pK is too large, the numerical evaluation of the ratio W/pK should be less than the experimentally measured values.

Neither the Fisk and the Gerjuoy-Stein cross sections are exact. The Gerjuoy-Stein values are based upon the use of the Born approximation, while Fisk's results assume a schematic model of the N molecular potential. In view of this, the agreement between theory and experiment is felt to be satisfactory. Further work is planned to evaluate the pertinent cross sections more accurately.

Neutron Penetration in an Air-over-Ground Geometry

The problem of the penetration of neutrons from a point source in air in an air-over-ground geometry is amenable to a Monte Carlo approach but seems to be very difficult by analytic or numerical means such as the moments method. In view of the importance of this problem in connection with weapons-effect studies being carried out in the Ichiban program, a Monte Carlo study of this problem has been made. A code written at Los Alamos[18] has been adapted and improved for this purpose, and a revision of cross-section input has been effected.

[18] W. A. Biggers *et al.*, *Space Energy and Time Distribution of Neutrons at the Ground-Air Interface*, LA-2390 (1960).

The code, as used in this connection, assumes a point monoenergetic source of neutrons situated in air at a given height above a plane interface separating air and ground. The energy-angle distribution of flux at the interface is computed by the code. In addition, the angle distribution of dose and the energy distribution of flux integrated over all angles is printed out.

Cross sections for air and ground have been taken from the latest compilations.[19,20] Differential elastic scattering has been handled by means of tables of integral scattering probability vs scattering angle, and interpolation between tabulated values is carried out by the program. A total of 32 tables are provided, each appropriate to a different energy interval.

In order to make the results more meaningful, computations of neutron transport have been made both for the air-over-ground geometry and for an infinite air medium using correlated histories. One expects the ratio of these results to be more accurate than either separately.[21]

A comparison of the differential flux spectrum calculated by the Monte Carlo code for source neutrons having the prompt-fission-neutron distribution with a moment-method calculation of the same quantity[22] is shown in Fig. 3.6. The shapes of the energy-dependence curves of the two spectra are seen to agree well. Figure 3.7 shows a comparison of the flux distribution due to a 3-Mev point source in an infinite air medium given in by an independent computation[23] with unsmoothed results given by the present code. Again the agreement is seen to be good, considering the fact that the cross sections used in the two computations differed somewhat.

Figure 3.8 shows the variation of r^2 times the first collision dose with source energy E_0 at

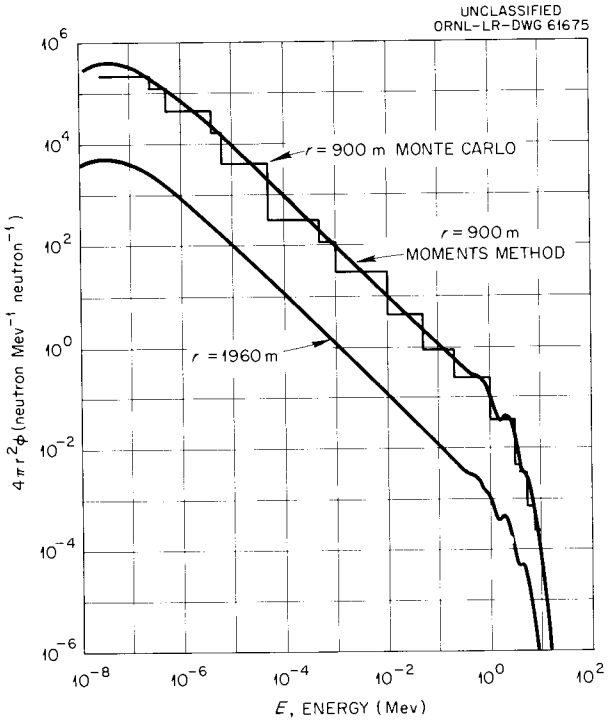

Fig. 3.6. Comparison of Neutron Flux Spectra in an Infinite Air Medium (Density 1.07 g/liter) Due to a Prompt Fission Neutron Source.

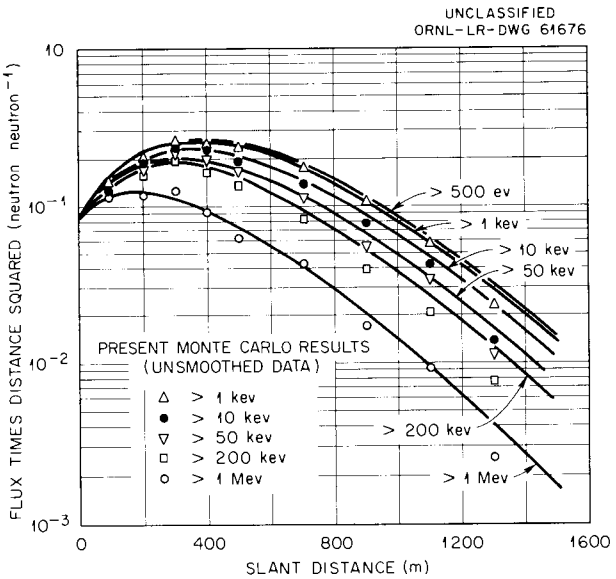

Fig. 3.7. Comparison of Flux Distribution in Infinite Air Medium Computed by Present Method and by Sandia Code. Source energy = 3.0 Mev.

[19] H. Lustig *et al.*, *The Neutron Cross Sections of Nitrogen*, NDA-86-1 (1959).

[20] E. S. Troubetzkoy, *Fast Neutron Cross Sections of Iron, Silicon, Aluminum, and Oxygen*, NDA-2111-3 (1959).

[21] A computation of the air-ground problem for gamma rays has been made by this method by Berger [M. Berger, *J. Appl. Phys.* 28, 1502 (1957)].

[22] D. Spielberg, NROL-OCDM Shielding Symposium, Oct. 31–Nov. 1, 1960.

[23] C. R. Mehl, *A Monte Carlo Calculation of the Neutron Flux from a Monoenergetic Point Source in Air*, SC-4174 (TR) (1958).

fixed values of the slant range r for point isotropic sources at a height of 91.44 m above the air-ground interface. Figure 3.9 shows the same quantity for the infinite air medium. The air density was taken to be 1.075 g/cm^3 in all the computations carried out here. One sees that the effective relaxation length for neutrons having energies above ~3 Mev is approximately constant.

Figure 3.10 shows the result of a series of calculations of the ratio of first collision dose in the finite medium to the dose in the infinite medium as a function of slant range for various source heights. The source energy was 3 Mev in all cases. One sees that the effect of the ground is to raise the dose at points close to the source and to lower it at distant points.

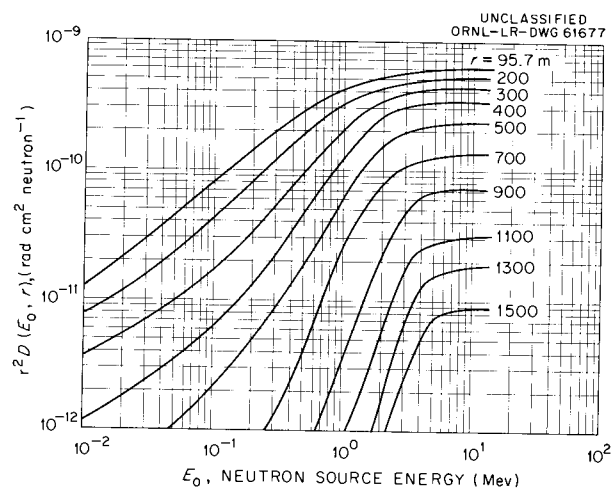

Fig. 3.8. Fast Neutron First Collision Dose as a Function of Source Energy at Various Slant Ranges r. Air density = 1.07 g/liter, height = 91.44 m air-over-ground geometry.

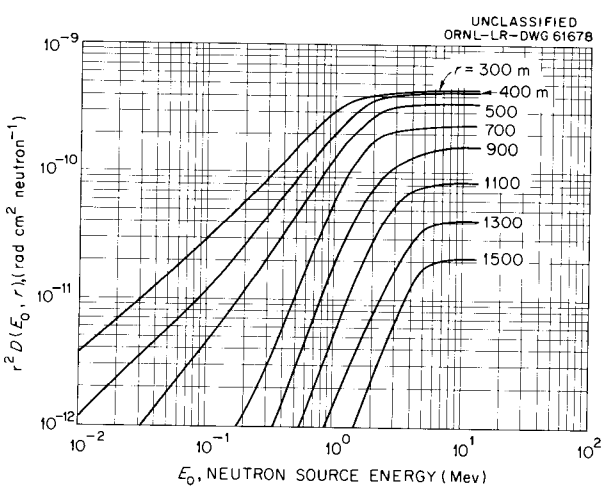

Fig. 3.9. First Collision Dose vs Source Energy at Various Slant Ranges r. Infinite air medium; air density = 1.07 g/liter.

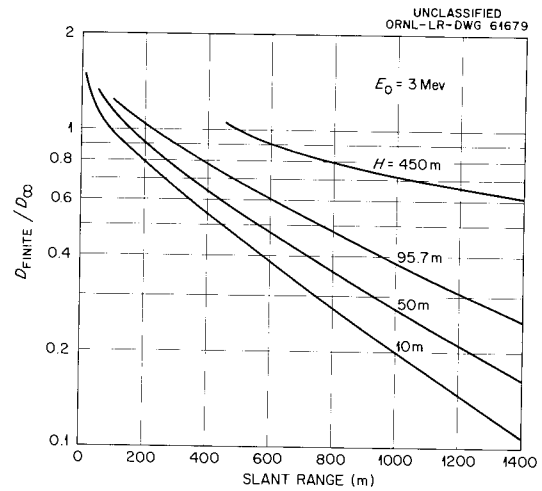

Fig. 3.10. Ratio of First Collision Dose at the Interface in the Finite Medium to That at the Same Slant Range in an Infinite Medium of Air.

The output from various runs made with monoenergetic sources has been stored on tape, and a summary code has been written to combine these cases with various weighting factors in order to allow one to build up arbitrary source distributions as needed. Figure 3.11 shows a plot of dose vs slant range from a prompt fission source distribution for both the air-over-ground geometry at a height of 91.44 m and for an infinite air medium. Figure 3.12 gives a plot of the flux above various energies as a function of slant range for the air-over-ground geometry and the same source while Fig. 3.13 shows similar data for the infinite medium.

Figure 3.14 gives data on the dependence of first-collision dose upon the angle θ between the neutron velocity vector and the source-to-detector line. These data represent a sum over the azimuthal angle. The dependence of dose upon azimuth is obtainable from this code.

The data generated by this code are being compared with field data on weapons tests. The code is being modified to compute the gamma dose due to neutron captures and inelastic scatters in air or ground.

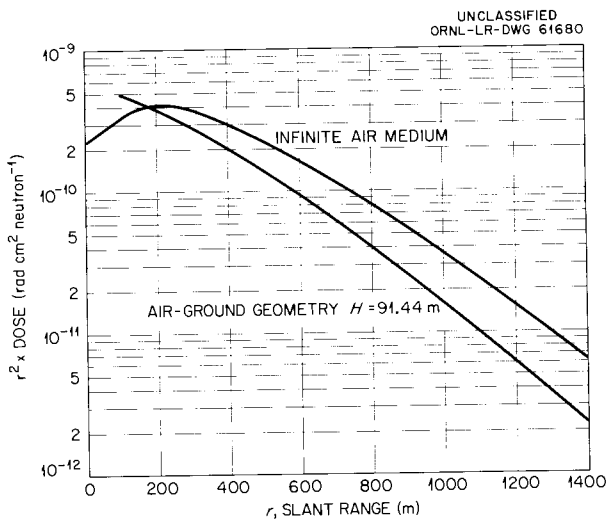

Fig. 3.11. First Collision Dose vs Slant Range for Prompt Fission Source.

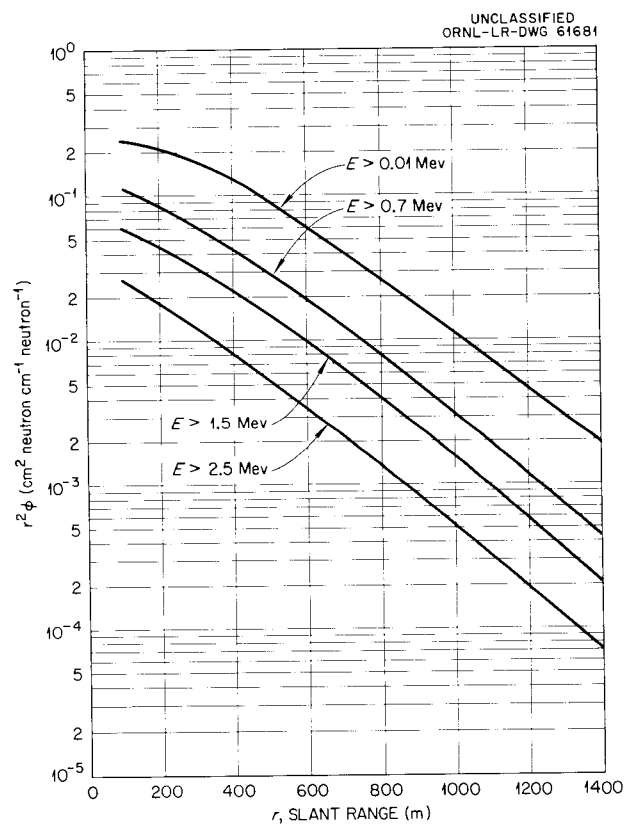

Fig. 3.12. Integral Fluxes vs Slant Range. Prompt fission source; air-ground geometry $H = 91.44$ m.

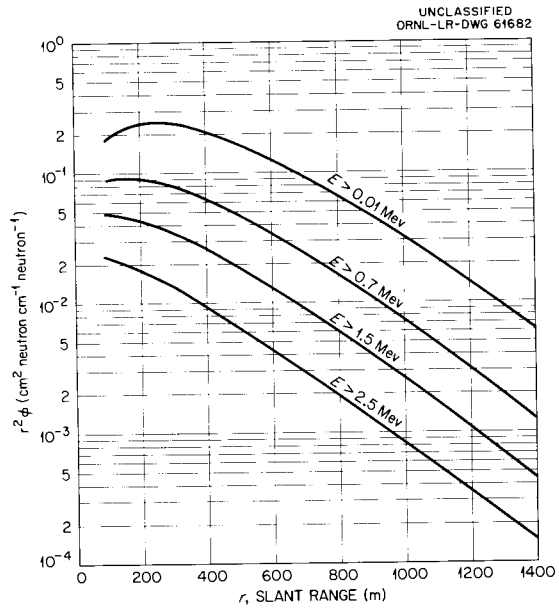

Fig. 3.13. Integral Flux vs Slant Range. Prompt fission source in infinite air medium.

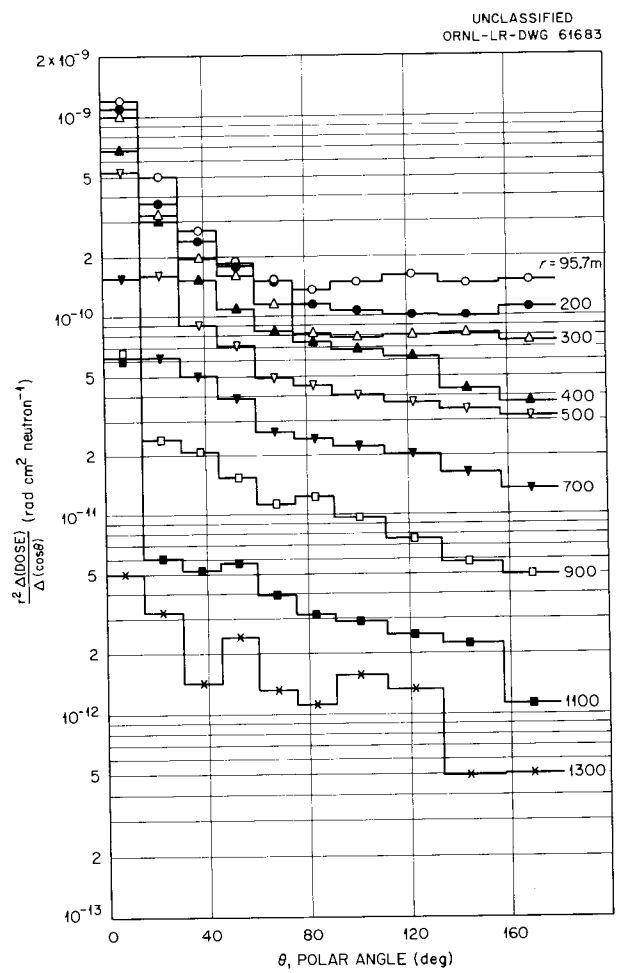

Fig. 3.14. Angular Distribution of Dose for Prompt Fission Source. Air-ground geometry $H = 91.44$ m.

Pulse Height from an Ionization Chamber Containing an Attaching Gas

When the pulse from a parallel-plate-electrode ionization chamber containing an attaching gas is examined with a linear pulse amplifier having the proper integration and differentiation time constants, the pulse height will be a simple analytic function of the attachment coefficient and the electron drift velocity.[24,25] Bortner and Hurst[26] have published the following expression for the time variation of the output pulse from such a chamber:

$$V(\tau) = \frac{A}{\tau_0 t_1} \int_0^{\tau} e^{-ft/\tau_0} (\tau - t)\, e^{-(\tau - t)/t_1}\, dt \qquad (\tau < \tau_0)\,, \quad (11)$$

$$V(\tau) = \frac{A}{\tau_0 t_1} \int_0^{\tau_0} e^{-ft/\tau_0} (\tau - t)\, e^{-(\tau - t)/t_1}\, dt \qquad (\tau > \tau_0)\,, \quad (12)$$

where

$f = \alpha f_1 P d$,

$\tau_0 = d/W$,

t_1 = differentiating and integrating time constant of the amplifier,

d = separation of electrode in chamber,

W = drift velocity of electrons in gas,

α = attachment coefficient of gas,

$f_1 p$ = partial pressure of attaching gas.

Equations (1) and (2) may be integrated to give:

$$V(\tau) = \frac{e^{-u}}{y}\left(-u + \frac{x}{y} e^{yu/x} - \frac{x}{y}\right) \qquad (u < x)\,, \quad (13)$$

$$V(\tau) = \frac{e^{-u}}{y}\left[(e^y - 1)\, u - e^y\left(x - \frac{x}{y}\right) - \frac{x}{y}\right] \qquad (u > x)\,, \quad (14)$$

where the following substitutions have been made:

$$u = \tau/t_1\,,$$
$$x = \tau_0/t_1\,,$$
$$y = (\tau_0/t_1) - f\,.$$

The maximum value of $V(\tau)$ gives the output pulse height which would be a function of both τ_0/t_1 and f. A program was developed for the IBM 7090 computer which calculated the pulse height for the following ranges of the parameters τ_0/t_1 and f:

$0 \leqq \tau_0/t_1$, in increments of 1.0,

$0 \leqq f \leqq 5$, in increments of 0.01 for $0 \leqq f \leqq 1.0$,
in increments of 0.02 for $1.0 < f \leqq 5.0$.

These results are to be published in tabular form in report ORNL-3090.

Some General Remarks on Radiation Dosimetry

Since the time of its establishment by the careful work of L. H. Gray, the Bragg-Gray principle has served as the main basis for practical radiation dosimetry measurements. The principle, originally limited to the relationship between the quantity of ionization produced in a gas-filled cavity and the amount of energy absorbed per gram of the gas, or per gram of suitably designed cavity enclosure, has, in effect, been extended to include arrangements employing means other than ionization for determining the energy absorbed in the sensitive volume. Thus, the use of calorimetric and chemical detectors has much in common with the use of ionization methods; in particular, all methods are based on indirect indications of the total amount of energy absorbed in the sensitive volume.

The purpose of this discussion is to formulate a more general basis for radiation dosimetry. The key to the additional generality arises from the fact that, whereas in the Bragg-Gray principle, one can deal only with the total energy absorbed in the sensitive volume (test system), in the more general statement one deals with a set of characteristic interactions of the radiation in question with the test system. In particular, in counting methods in which the distribution of energy-loss due to interaction of radiation with the test system can be measured, one may deal with various properties of the distribution itself. This generalization of the output (response) of the test

[24] T. E. Bortner and G. S. Hurst, *Health Phys.* 1, 39–45 (1958).

[25] G. S. Hurst and T. E. Bortner, *Capture of Electrons in Molecular Oxygen*, ORNL-2670 (Sept. 15, 1959).

[26] G. S. Hurst and T. E. Bortner, *Phys. Rev.* 114, 116 (1959).

system and the associated relaxation of the design of the test system provide additional parameters which make it possible to approximate various dose-energy responses with required accuracy.

When penetrating radiation of energy spectrum $N(E)$ interacts with any medium it may be desirable to characterize this interaction in at least one of several ways. Among these are: (1) the locally absorbed dose (or energy absorbed per gram) in an infinitesimal volume at an arbitrary point in the medium; (2) the distribution of absorbed dose with stopping power or the LET distribution; (3) special cases of (1), the absorbed dose at the point in the medium where it is a maximum, or the average of the dose at several specified points in the medium; (4) the energy imparted (in contrast to energy absorbed) per gram in an infinitesimal volume element of the medium, for example, the first collision dose; (5) the biologically significant dose for a specified biological medium; or (6) the biological dose for a specified medium and an adopted RBE-vs-LET curve, for example, the rem dose in man for particles of various specific ionizations. For future reference these dose–energy relationships are designated as $D_{jk}(E)$, where j refers to the medium and k refers to the type of dose or dose distribution.

Now consider the interaction of a given kind of radiation with a test system. Suppose that a beam of this radiation having energy E and unit flux impinges on the system. There will then be generated in the test system a certain distribution of interaction products. These products may be recoil nuclei, recoil electrons, radioactive nuclei, etc. Let $n_{l,\beta}^{(\alpha)}(\epsilon_l, E)\, d\epsilon_l$ be the number of these products of type l which dissipate an amount of energy in the range of energies between ϵ_l and $\epsilon_l + d\epsilon_l$ in the αth subsystem of the test system. The quantity β is understood to symbolize a set of parameters $\beta_1, \beta_2, \ldots \beta_n$ which characterizes the configuration of the test system, that is, its dimensions, nuclear composition, the physical distribution of subsystems, and any other quantities required to specify it completely.

Suppose that one wishes to measure the dose (or dose distribution) $D_{jk}(E)$ in this same beam of radiation. One may obtain a measure of the dose $D_{jk}(E)$ by utilizing a general test system which is unrelated, in a direct sense, to the jth material or the kth physical effect. In order to show how this may be done, one defines a response $R_i^{(\alpha)}(E)$ of the αth subsystem in terms of an operator $0_i^{(\alpha)}(\epsilon_l)$ which acts on the distribution $n_{l,\beta}^{(\alpha)}(\epsilon_l, E)$ as follows:

$$R_i^{(\alpha)}(E) = \sum_l 0_i^{(\alpha)}(\epsilon_l)\, n_{l,\beta}^{(\alpha)}(\epsilon_l, E)\,. \qquad (15)$$

(The functional dependence of $R_i^{(\alpha)}(E)$ upon the configuration parameters β is not shown explicitly.) This generalized response leads to considerable flexibility in practice, since for each operator 0_i a different response is at one's disposal. To illustrate the nature of the 0_i, consider the case

$$0_i^{(\alpha)} = \int_0^\infty d\epsilon_l\, \epsilon_l\,. \qquad (16)$$

Then the single-valued response $R_i^{(\alpha)}(E)$ is

$$R_i^{(\alpha)}(E) = \sum_l \int_0^\infty d\epsilon_l\, \epsilon_l n_{l,\beta}^{(\alpha)}(\epsilon_l, E) = \epsilon_T^{(\alpha)}(E)\,, \qquad (17)$$

where $\epsilon_T^{(\alpha)}(E)$ is the total energy absorbed in the subsystem. This will be recognized immediately as the conventional quantity measured in Bragg-Gray dosimetry since ionization chamber methods, calorimetric methods, and chemical methods all give a measure of the total absorbed energy. In contrast, if one uses pulse-counting methods in which the energy distribution function $n_{l,\beta}^{(\alpha)}(\epsilon_l, E)$ is available, one may employ different operators $0_i^{(\alpha)}$, each of which leads to a new response $R_i^{(\alpha)}(E)$.

A generalization of dosimetry may now be stated as follows:

> Let operators $0_i^{(\alpha)}$ act upon the energy-loss distribution function $n_{l,\beta}^{(\alpha)}(\epsilon_l, E)$ generated in a test system having a suitable configuration $\beta_1, \beta_2, \ldots \beta_n$. A given dose function $D_{jk}(E)$ is measurable with error less than δ in an energy range $E_1 \leqq E \leqq E_2$ provided there exist operators $0_i^{(\alpha)}$ and geometrical parameters $\beta_1, \beta_2, \ldots \beta_n$ such that the inequality
>
> $$\left[\sum_{l,\alpha} 0_i^{(\alpha)}(\epsilon_l)\, n_{l,\beta}^{(\alpha)}(\epsilon_l, E) - D_{jk}(E)\right] \leqq \delta \qquad (18)$$
>
> is satisfied for all energies E in the specified range.

In carrying out the matching process, one may choose an operator 0_i and find a configuration $\beta_1, \beta_2, \ldots \beta_n$ such that the inequality (18) is

satisfied, or alternatively one may fix the β and find an appropriate operator $0_i^{(\alpha)}$. An example of the use of each of these approaches will be illustrated.

Since no methods of dosimetry using the second moment of the energy–dose distribution have yet been devised, a conceptual theoretical design of such a device will be given as an illustration. The procedure involves first selecting the operator such that the response function is

$$R_i(E) = \int_B^\infty \epsilon^2 n(\epsilon, E)\, d\epsilon \,. \qquad (19)$$

Next, one tries to find a geometrical arrangement such that the inequality (18) holds with δ sufficiently small. For the present illustration, $D_{jk}(E)$ is specified as the first-collision dose curve for neutrons in tissue. Consider the simple geometry shown in Fig. 3.15 in which a plane beam of monoenergetic neutrons of energy E is incident on a series of plane slabs of indicated hydrogen concentrations. The distribution function $n(\epsilon, E)$ for a range of E was found by machine calculations[27] from which $R_i(E)$ as given by Eq. (19) was computed for various values of E. When B is set at 0.1 Mev, $R_i(E)$ as shown in Fig. 3.16 is obtained, which agrees quite well with the first-collision dose curve. Thus we see that a simple geometry may be found which may be associated with the second moment of the energy-loss distribution such that a direct indication of the first-collision dose is achieved.

The use of the generalized operator with fixed geometrical parameters β will be illustrated for a very simple geometry, that is, isotropic irradiation of a plane hydrogenous slab of $(CH_2)_n$ plastic whose thickness, E_w, is equal to the range of a 10-Mev proton and is in contact with a nonhydrogenous detector whose thickness, E_d, is equal to

[27] H. B. Eldridge, P. Flusser, and R. H. Ritchie, *Proton Recoil Energy Loss Distributions in Plane Geometry*, ORNL-3089 (to be published).

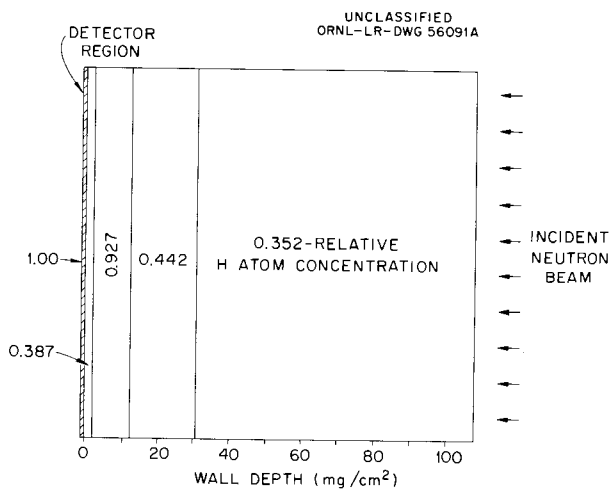

Fig. 3.15. Schematic Diagram of a Geometrical Arrangement for Obtaining the First-Collision-Dose Curve When Using the Second Moment of the Energy Loss Distribution. The relative hydrogen concentration and the thickness of each of the regions are shown. It is assumed that the proton range-energy relationship for each region is that of $(CH_2)_n$.

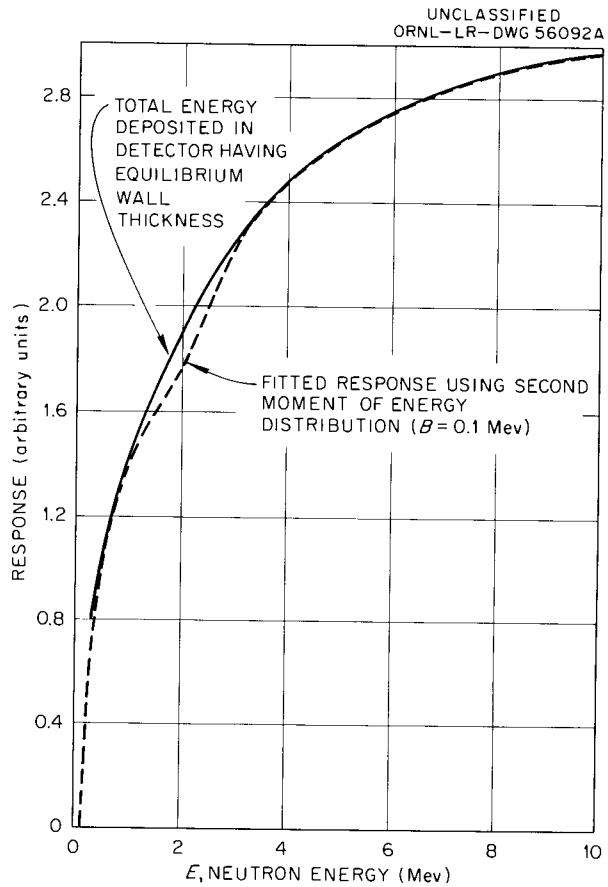

Fig. 3.16. Calculated Second-Moment Response of the Geometry Shown in Fig. 3.15 and Comparison with the Total Energy Deposited in Detector (Essentially the First-Collision Tissue Dose) as a Function of Neutron Energy.

the range of a 2-Mev proton. The distribution of energy losses in the detector is shown in Fig. 3.17 for various neutron energies ranging from 0.3 Mev to 14 Mev (ORNL Report 3089[27] gives energy loss distributions for several similar geometrical arrangements). For more complete illustration of the flexibility of the generalized operator we wish to

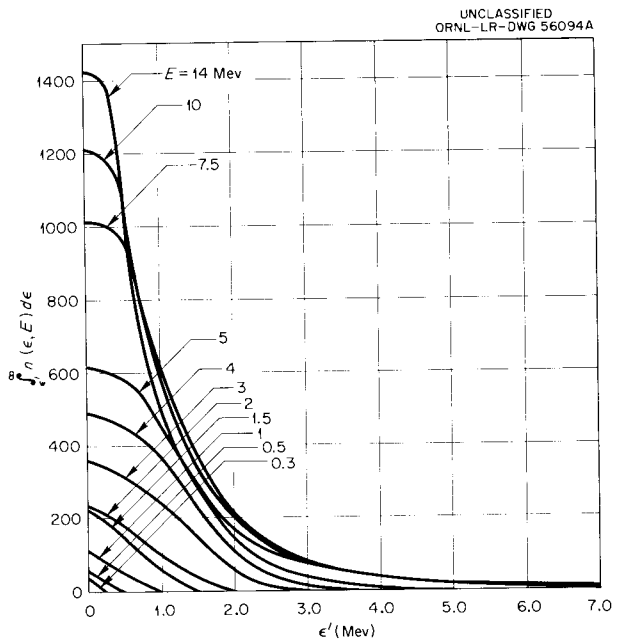

Fig. 3.17. Calculated Energy Loss Distributions for Isotropic Irradiation of a Plane Hydrogenous Slab of Wall Thickness E_w = 10 Mev in Contact with a Nonhydrogenous Detector of Thickness E_d = 2 Mev. The integral of the energy loss distribution is plotted as a function of the lower limit of integration, ϵ'.

find operators $0_i(E)$ such that the inequality expressed in (18) is satisfied when the function $D_{jk}(E)$ takes on two values, namely (1) the first-collision dose in standard tissue in rads, and (2) the maximum permissible dose limits for protection of man against radiation, in rems.

Electronic operations involving binary addition and subtraction are particularly simple; hence we will try response functions of the type,

$$R(E) = A \sum_{u=1}^{u=u_{max}} R_u(E)$$

$$= A \sum_{u=1}^{u=u_{max}} 2^{r(u)} (-1)^{m(u)} \int_{E_1(u)}^{E_2(u)} n(\epsilon, E)\, d\epsilon \,, \quad (20)$$

where A is an arbitrary constant, $r(u)$ is 0 or a positive integer, $m(u)$ is either 1 or 2, and the number of energy losses in the uth channel is determined by the range of integration $E_1(u)$ and $E_2(u)$. For a particular neutron energy E a choice may be made of five parameters: $r(u)$, $m(u)$, $E_1(u)$, $E_2(u)$, and u_{max}; thus it is expected that the conditions of inequality (18) can be satisfied over a wide range of energy. Table 3.1 shows the calculation of Eq. (20) for the tissue first collision dose $D_{t,f}(E)$ over an energy range from 0.3 Mev to 14 Mev, which from inspection of the last two columns is seen to be a good fit to the tissue first collision dose. Similarly it is seen from Table 3.2 that a good fit to the dose, $D_{mp}(E)$, in rems may be obtained simply by changing the energy-loss operator.

Table 3.1. Fit of Inequality (18) to the Tissue First-Collision Dose, $D_{t,f}(E)$ in Rad (NBS Handbook 75) for the Plane Slab Detector

(E_w = 10 Mev; E_d = 2.0 Mev; $A = 2.50 \times 10^{-11}$)

E (Mev)	u	E_1	E_2	$\int_{E_1(u)}^{E_2(u)} n(\epsilon, E)\, d\epsilon$	$r(u)$	$m(u)$	$R_u(E)$	Dose (rad neutrons^{-1} cm^{-2}) $R(E) \times 10^9$	$D_{t,f}(E) \times 10^9$
0.3	1	0.15	0.25	12	2	2	+48	1.20	1.21
0.5	1	0.15	0.25	13	2	2	+52	1.62	1.62
	2	0.25	0.37	13	0	2	+13		
1.0	1	0.15	0.25	12	2	2	+48	2.10	2.49
	2	0.25	0.37	16	0	2	+16		
	3	0.70	0.80	10	1	2	+20		
1.5	1	0.15	0.25	15	2	2	+60	2.89	2.70
	2	0.25	0.37	20	0	2	+20		
	3	0.70	0.80	18	1	2	+36		
2.0	1	0.15	0.25	10	2	2	+40	3.04	3.00
	2	0.25	0.37	14	0	2	+14		
	3	0.70	0.80	14	1	2	+28		
	4	1.65	1.95	20	1	2	+40		
3.0	1	0.15	0.25	10	2	2	+40	3.34	3.53
	2	0.25	0.37	12	0	2	+12		
	3	0.70	0.80	12	1	2	+24		
	4	1.65	1.95	54	1	2	+108		
	5	2.30	2.85	25	1	1	−50		
4.0	1	0.15	0.25	8	2	2	+32	3.41	4.00
	2	0.25	0.37	11	0	2	+11		
	3	0.70	0.80	16	1	2	+32		
	4	1.65	1.95	70	1	2	+140		
	5	2.30	2.85	46	1	1	−92		
	6	3.20	4.80	7	1	2	+14		
5.0	1	0.15	0.25	6	2	2	+24	4.86	4.23
	2	0.25	0.37	21	0	2	+21		
	3	0.70	0.80	24	1	2	+48		
	4	1.65	1.95	77	1	2	+154		
	5	2.30	2.85	51	1	1	−102		
	6	3.20	4.80	25	1	2	+50		
7.5	1	0.15	0.25	4	2	2	+16	4.34	4.70
	2	0.25	0.37	18	0	2	+18		
	3	0.70	0.80	82	1	2	+164		
	4	1.65	1.95	91	1	2	+182		
	5	2.30	2.85	63	1	1	−126		
	6	3.20	4.80	48	1	2	+96		
	7	5.00	∞	22	3	1	−176		

Table 3.1 (continued)

E (Mev)	u	E_1	E_2	$\int_{E_1(u)}^{E_2(u)} n(\epsilon, E)\, d\epsilon$	$r(u)$	$m(u)$	$R_u(E)$	Dose (rad neutrons^{-1} cm^{-2}) $R(E) \times 10^9$	$D_{t,f}(E) \times 10^9$
10.0	1	0.15	0.25	12	2	2	+48	5.23	5.28
	2	0.25	0.37	24	0	2	+24		
	3	0.70	0.80	100	1	2	+200		
	4	1.65	1.95	76	1	2	+152		
	5	2.30	2.85	60	1	1	−120		
	6	3.20	4.80	41	1	2	+82		
	7	5.00	∞	22	3	1	−176		
14.0	1	0.15	0.25	10	2	2	+40	5.80	6.06
	2	0.25	0.37	64	0	2	+64		
	3	0.70	0.80	100	1	2	+200		
	4	1.65	1.95	68	1	2	+136		
	5	2.30	2.85	50	1	1	−100		
	6	3.20	4.80	34	1	2	+68		
	7	5.00	∞	22	3	1	−176		

Table 3.2. Fit of Inequality (18) to the Dose, $D_{mp}(E)$ in Rem (NBS Handbook 63) for the Plane Slab Detector (E_w = 10 Mev; E_d = 2.0 Mev; $A = 1.2 \times 10^{-9}$)

E (Mev)	u	E_1	E_2	$\int_{E_1(u)}^{E_2(u)} n(\epsilon, E)\, d\epsilon$	$r(u)$	$m(u)$	$R_u(E)$	Dose (rem neutrons^{-1} cm^{-2}) $R(E) \times 10^8$	$D_{mp}(E) \times 10^8$
0.5	1	0.25	0.45	22	0	2	+22	2.6	2.3
1.0	1	0.25	0.45	28	0	2	+28	3.9	3.9
	2	0.90	0.96	5	0	2	+5		
2.0	1	0.25	0.45	24	0	2	+24	3.9	
	2	0.90	0.96	9	0	2	+9		
3.0	1	0.25	0.45	22	0	2	+22	3.8	
	2	0.90	0.96	10	0	2	+10		
5.0	1	0.25	0.45	18	0	2	+18	3.9	3.9
	2	0.90	0.96	26	0	2	+26		
	3	3.70	5.80	11	0	1	−11		
7.5	1	0.25	0.45	24	0	2	+24	4.1	4.1
	2	0.90	0.96	44	0	2	+44		
	3	3.70	5.80	33	0	1	−33		
10.0	1	0.25	0.45	50	0	2	+50	4.3	4.1
	2	0.90	0.96	46	0	2	+46		
	3	3.70	5.80	32	0	1	−32		
	4	7.50	∞	7	2	1	−28		

EXPERIMENTAL PHYSICS OF DOSIMETRY

R. D. Birkhoff

E. T. Arakawa
T. E. Bortner[28]
L. W. Cochran[28,29]
D. W. Forester[30]
H. H. Hubbell, Jr.
G. S. Hurst
R. M. Johnson
L. B. O'Kelly
T. D. Strickler[28]
L. de Franceschi[31]
J. M. Feola[31]
A. L. Frank[32]

The Spherical Electrostatic Analyzer

In two recent publications[33,34] the theoretical characteristics of an electrostatic, low-energy, high-transmission charged particle spectrometer have been described. In these papers it was shown that a transmission of 25% of all charged particles emitted from a point on the inner sphere could be obtained at a momentum resolution of 7%. Also, the corresponding values for a disk source of diameter 0.3 that of the inner sphere were found to be 16 and 7.7%.

Such a device has been designed and constructed for the high transmission characteristics mentioned above and is expected to operate for electron energies between a few electron volts and 45 kev. An electron gun of special design is being used to determine how the actual performance agrees with that predicted theoretically.

The basic design parameters chosen and the special features of the device will be described here, together with the performance expected under these conditions.

Three basic parameters may be chosen for such instruments:

1. the inner sphere radius,
2. the acceptance angle, which determines the transmission and the resolution,
3. the source size.

The over-all size was fixed by the inside dimensions of an available vacuum tank about 27 in. in diameter. For convenience the inner sphere, source, and detector are run at ground potential, and the outer sphere at high voltage. To reduce the danger of flashover, the outer sphere was spaced midway between the inner sphere and the tank wall. The exit slit was spaced 122.7° or $\pi - 1$ radians around the sphere from the source, thus giving a theoretical transmission of 25% for a point source. The ratio of the sphere radii is then 3:2, so the inner sphere is 12.5 in. in diameter and the outer is 18.75 inches. The source radius is 0.3 times the inner sphere radius, or 3.75 in. in diameter.

The spheres are made of sets of $\frac{1}{8}$-in. brass rods converging on the source. Rods were used instead of solid spheres in order to avoid as far as possible having electrons scattered from the spheres into the exit slit. Aluminum or magnesium rods were preferred because of their lower scattering, but were not readily available in alloys of sufficient elasticity to make accurate spheres.

The slit edges of the exit aperture are the inner sphere and an aluminum ring at 0.8 in. larger radius. Five field-terminating rings between the outer slit and the outer sphere are spaced to preserve the inverse-square field near the exit slit.

Because the transmission is expected to be quite high, between 16 and 25%, the detector is a Faraday cage consisting of a hollow cylinder placed behind the exit slit and hidden from the outer sphere. If a more sensitive detector is needed, space is available for a 4×4-in. cylindrical block of scintillating plastic, and a photomultiplier.

Fig. 3.18 is a photograph of the instrument before final assembly. The Faraday cage has been removed and appears at the left. The electron gun is shown projecting through the axial hole in the door in the outer sphere. When the door is closed, the projecting end of the gun just enters the corresponding hole in the door in the inner sphere.

The spectrograph is to be used to measure the electron spectrum in thick irradiated media. The first medium to be studied will be Cu^{64} where the primary positron flux may be readily separated experimentally from the secondary electron spectrum.

[28] Consultant.
[29] Temporary employee.
[30] Summer employee.
[31] Noncitizen guest.
[32] AEC Health Physics Fellow.
[33] R. H. Ritchie, J. S. Cheka, and R. D. Birkhoff, *Nuclear Instr. & Methods* 6, 157 (1960).
[34] R. D. Birkhoff *et al.*, *Nuclear Instr. & Methods* 8, 313 (1960).

Fig. 3.18. Photograph of Spherical Condenser Spectrometer.

Ionization of Gas Mixtures

The possibility of obtaining ionization efficiencies[35] for molecules highly excited by impact with metastable noble gases has encouraged the extension of previous work[36-38] on the alpha-particle ionization of binary gas mixtures. New apparatus has been constructed, and several sets of data for argon plus various molecular gases have been obtained. The ionization chamber is made of stainless steel and is pumped with a forepump trapped with a Linde molecular sieve, followed with a molecular sieve sorption pump. This system provides a means for maintaining high gas purity during the time of measurement with a Pu^{239} source of high disintegration rate (approximately 1.5×10^6 particles/min). Measuring the ionization current with a "rate-of-drift" method showed that the results reproduce to about ±0.1%.

Results have been obtained for mixtures of argon with nitrogen, ethylene, propane, ethane, acetylene, cyclopropane, butene-1, methane, krypton, and xenon. A representative set of data for argon mixed with nitrogen, acetylene, and krypton is shown in Fig. 3.19. Analysis of the data to obtain ionization efficiencies is in progress.

[35] R. L. Platzman, *J. phys. radium* **21**, 853 (1960).

[36] T. E. Bortner and G. S. Hurst, *Phys. Rev.* **93**, 1236 (1954).

[37] C. E. Melton, G. S. Hurst, and T. E. Bortner, *Phys. Rev.* **96**, 643 (1954).

[38] T. D. Strickler, *Average Energy Loss per Ion Pair Produced by Alpha Particles in Binary Gas Mixtures*, ORNL-3080 (July 3, 1961).

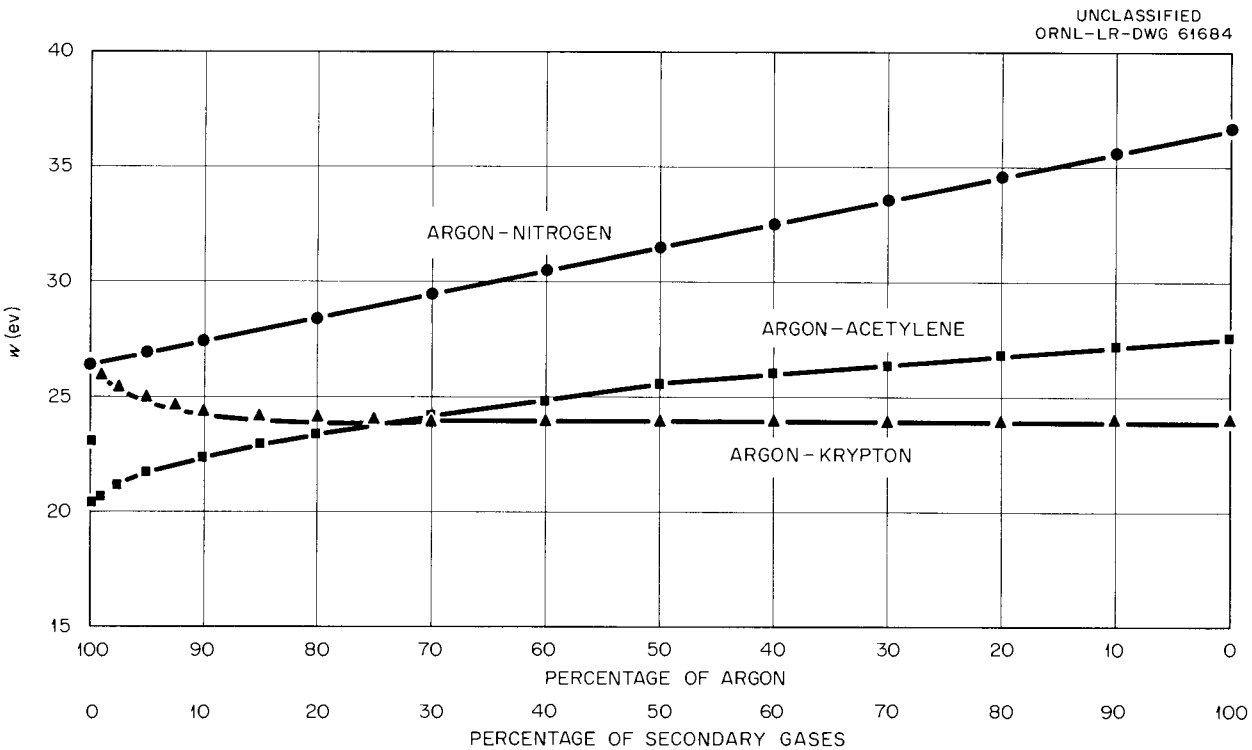

Fig. 3.19. Values of w for Mixtures of Argon with Nitrogen, Acetylene, and Krypton.

Dissociative Electron Capture in Water Vapor

The experimental results previously reported[39] for α_0 (probability of electron capture per cm of travel in the electrical field direction and per unit pressure of water vapor) have been interpreted in terms of the cross-section function $\sigma_c(\epsilon)$. The quantity α_0 can be written in terms of the capture cross section, $\sigma_c(\epsilon)$, at energy ϵ as follows,

$$\alpha_0(E/P) = \frac{N_0(2/m)^{1/2}}{w(E/P)} \int_0^\infty \epsilon^{1/2}\, \sigma_c(\epsilon)\, f(\epsilon, E/P)\, d\epsilon\,, \quad (1)$$

where $f(\epsilon, E/P)$ is the normalized energy distribution function for electrons in pure Ar, $w(E/P)$ is the electron drift velocity in Ar, m is the electron mass, and N_0 is the number of water molecules per cm^3 at 1 mm Hg.

Considering the fact that the mass spectrograph data[40-42] and the beam experiment[43] show a fairly narrow peak for the formation of H^- and that in all such experiments the electron beam has an appreciable spread in energy, it is reasonable to select a strongly peaked function as a trial solution for $\sigma_c(\epsilon)$ in Eq. (1). Hence,

$$\alpha_0(E/P) = \frac{N_0(2/m)^{1/2}}{w(E/P)}\, \epsilon_1^{1/2} f(\epsilon_1, E/P) \int_0^\infty \sigma_c(\epsilon)\, d\epsilon \quad (2)$$

where ϵ_1 is the energy at which the capture cross section peaks. Since the various observers are not in agreement on the energy at which the cross section peaks, we consider ϵ_1 as a variable and find a value which satisfies Eq. (2) for the experimental range of E/P. Tabulations of $w\alpha_0/f(\epsilon)$ for

[39] R. D. Birkhoff *et al.*, *Health Phys. Ann. Progr. Rept. July 31, 1960*, ORNL-2994, p 204.

[40] W. W. Lozier, *Phys. Rev.* **36**, 1417 (1930).

[41] M. M. Mann, Andrew Hustrulid, and J. T. Tate, *Phys. Rev.* **58**, 340 (1940).

[42] M. Cottin, *J. chim. phys.* **56**, 1024 (1959).

[43] N. E. Bradbury, *J. Chem. Phys.* **2**, 827 (1934); N. E. Bradbury and H. Tatel, *J. Chem. Phys.* **2**, 835 (1934).

various electron energies ϵ_1 are shown in Table 3.3. In these tabulations the drift velocity w for Ar was taken from Bortner, Hurst, and Stone.[44] The values of the electron energy distribution function for Ar were based on the solution of the Boltzman transport equation following the procedure of Barbiere[45] and Bowe,[46] and are conveniently tabulated[47] for future reference. It is seen from Table 3.3 that if we let $\epsilon_1 = 6.4$ ev, a good solution to Eq. (2) is found, while for values of $\epsilon_1 = 6.3$ or 6.5, the fit to Eq. (2) is less accurate. The magnitude of the cross section integral

$$A = \int_0^\infty \sigma_c(\epsilon)\, d\epsilon ,$$

corresponding to $\epsilon_1 = 6.4$ ev, is 7.7×10^{-18} cm^2 ev. The magnitude of A and the energy where the cross section is a maximum, ϵ_1, derived in this way compare favorably with the results obtained by Buchel'nikova.[48] From the curve published by Buchel'nikova, one may estimate $\epsilon_1 = 6.4$ ev and $A = 6.5 \times 10^{-18}$ cm^2 ev. The statistical errors for α_0 are not believed to be larger than ±5%, and statistical errors for w are approximately ±2%. These errors, as seen from Table 3.3 would not change appreciably the values quoted above for ϵ_1 and A. However, the significance of the consistence between the results of the beam experiment and the present swarm experiment is closely related to the validity of the electron energy distribution function used in the analysis of the swarm experiment. In support of the distribution function, we note that Bowe[46] has shown that for Ar the calculated distribution function gave values for the electron drift velocity which agree well with experiment.

A further consistency check, using the electron energy distribution functions in argon, was made by comparing the swarm results for electron capture in Ar-O_2 mixtures reported in ref 49 with the beam experiment reported in ref 48. Even though the check involved only a small fraction of the total number of electrons in the high-energy tail, both the magnitude and the dependence of α (for O_2) on E/P were in very good agreement with the beam experiment.

In summary, we have found no evidence of internal inconsistency between the swarm experiments and the beam experiments for electron capture in both H_2O and O_2, provided that the swarm experiments are conducted in mixtures with argon for which the electron energy distribution is established from independent considerations. This suggests the swarm method as a means of establishing the energy scale and absolute cross section for various electron capture reactions, provided that the swarm experiments are performed under conditions where good information is available on the electron energy distribution.

Low Energy Electron Attachment and Drift Velocity in Gas Mixtures Containing Water Vapor

Electron attachment and electron drift velocity in gas mixtures containing water vapor have been measured using techniques described previously.[50,51] The gases used were ethylene, nitrogen, methane, and carbon dioxide. At first there appeared to be electron attachment in some of these mixtures since the pulse from the ion chamber decreased in amplitude with the addition of water vapor in a manner characteristic of nondissociative capture. In most cases the addition of water vapor caused a considerable decrease in drift velocity. Figures 3.20 and 3.21 show drift velocity vs E/P for methane-water vapor and ethylene-water vapor mixtures respectively. A similar effect is observed when water vapor is added to carbon dioxide. The effect in nitrogen is rather surprising since the addition of water vapor causes an increase in drift velocity. This is shown in Fig. 3.22. Although the curve for pure nitrogen is smooth, the addition of water vapor causes a peak at low E/P that shifts upward and

[44] T. E. Bortner, G. S. Hurst, and W. G. Stone, *Rev. Sci. Instr.* 28, 103 (1957).

[45] D. Barbiere, *Phys. Rev.* 84, 653 (1951).

[46] J. C. Bowe, *Phys. Rev.* 117, 1416 (1960).

[47] R. H. Ritchie and G. E. Whitesides, *Electron Distribution Functions in Argon*, ORNL-3081 (June 2, 1961).

[48] I. S. Buchel'nikova, *Soviet Phys. JETP* 35(8), 783 (1959).

[49] T. E. Bortner and G. S. Hurst, *Health Phys.* 1, 39 (1958).

[50] G. S. Hurst and T. E. Bortner, *Capture of Electrons in Molecular Oxygen*, ORNL-2670 (Sept. 15, 1959).

[51] T. E. Bortner, G. S. Hurst, and W. G. Stone, *Rev. Sci. Instr.* 28, 103 (1957).

Table 3.3. Evaluation of the Ratio $w\alpha_0/f(\epsilon_1)$ for Various Values of ϵ_1

An E/P-independent ratio indicates a solution to Eq. (2)

E/P	α_0 [cm^{-1}(mm Hg)$^{-1}$]	$w\alpha_0 \times 10^{-6}$ [sec^{-1}(mm Hg)$^{-1}$]	$f(\epsilon_1)$ and Ratios at Electron Energies (ev) of:							
			6.3		6.4		6.5		6.6	
			$f(\epsilon_1)$	$w\alpha_0/f(\epsilon_1)$	$f(\epsilon_1)$	$w\alpha_0/f(\epsilon_1)$	$f(\epsilon_1)$	$w\alpha_0/f(\epsilon_1)$	$f(\epsilon_1)$	$w\alpha_0/f(\epsilon_1)$
				$\times 10^6$		$\times 10^6$		$\times 10^6$		$\times 10^6$
0.40	0.18	0.058	0.00224	25.9	0.00161	36.0	0.00114	50.9	0.000793	73.1
0.45	0.57	0.185	0.00615	30.1	0.00472	39.2	0.00358	51.7	0.00269	68.8
0.50	1.20	0.396	0.0126	31.4	0.0102	38.8	0.00813	48.7	0.00643	61.6
0.55	2.0	0.670	0.0213	31.5	0.0179	37.4	0.0149	45.0	0.0122	54.9
0.60	3.0	1.02	0.0317	32.2	0.0273	37.4	0.0233	43.8	0.0198	51.5
0.65	4.1	1.41	0.0428	32.9	0.0377	37.4	0.0330	42.7	0.0287	49.1
0.70	5.3	1.86	0.0540	34.4	0.0484	38.4	0.0432	43.1	0.0383	48.6
0.75	6.6	2.34	0.0647	36.2	0.0589	39.7	0.0533	43.9	0.0481	48.6

broadens as more water vapor is added. This is similar to the effect observed when water is mixed with argon.

When calculations of the attachment coefficient are corrected for the change in drift velocity, the attachment cross section for these gas mixtures appears to be quite low. An exception is the carbon dioxide-water vapor mixtures in which there may be a pressure-dependent capture process with a threshold at a water vapor pressure of about 8 mm Hg. The attachment then increases as either water vapor pressure or total pressure increases. The effect is small; however, if real it is consistent with the results of Bradbury[52] who observed heavy negative ions in water vapor-carbon dioxide mixtures. It could be caused possibly by a reaction between water and carbon dioxide resulting in the formation of a compound such as H_2CO_3 which could in turn capture electrons.

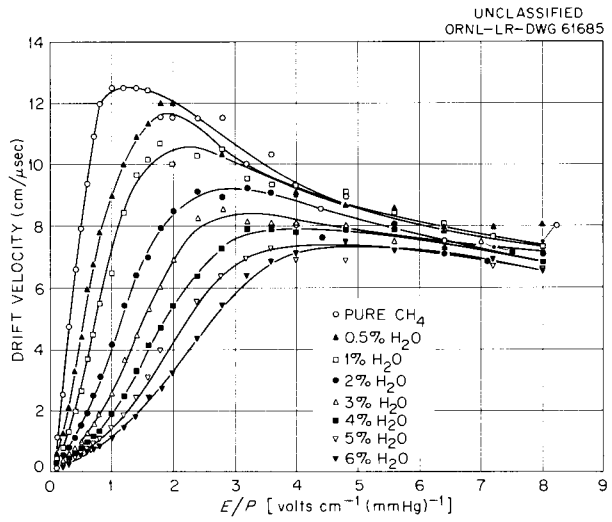

Fig. 3.20. Electron Drift Velocity in Methane–Water Vapor Mixtures.

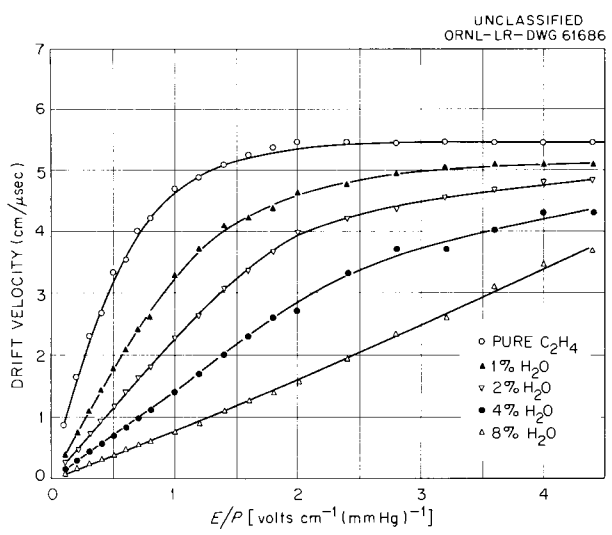

Fig. 3.21. Electron Drift Velocity in Ethylene–Water Vapor Mixtures.

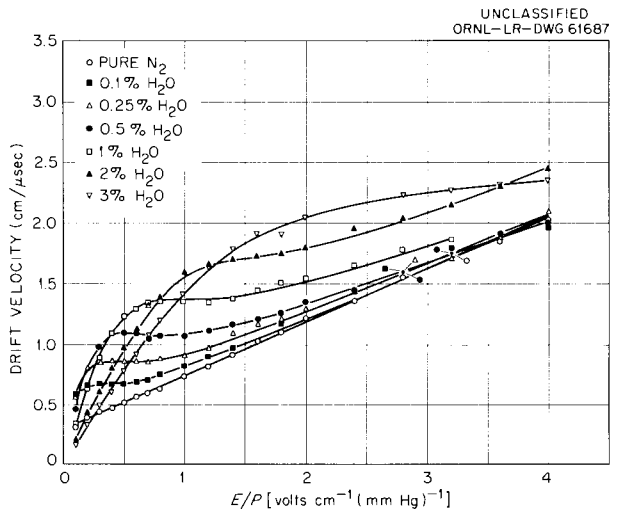

Fig. 3.22. Electron Drift Velocity in Nitrogen–Water Vapor Mixtures.

The Interference Filter Spectrograph

In the study of the fluorescence and thermoluminescence of irradiated biochemicals and metals, it has been found that conventional grating or prism spectrographs do not have enough transmission for spectroscopy of these very weak extended sources. In order to gather as much light as possible from sources as large as 5 cm in diameter, an interference filter spectrometer has been constructed which consists of a disk about one meter in diameter containing 50 holes in its periphery where filters may be mounted, and a light-tight enclosure for the disk supported so that the instrument may be used in either a vertical or horizontal position. Ports in the enclosure allow the light from the source to pass through any filter and strike the photomultiplier located on the opposite side. The device is shown in Fig. 3.23 with a motor and speed reducer which causes the wheel to rotate once every two minutes.

[52] N. E. Bradbury, *J. Chem. Phys.* 2, 827 (1934).

Fig. 3.23. Photograph of Interference Filter Spectrograph Showing Worm Drive and Beam and Access Ports.

Filters have been installed, each of which transmits a band about 100 A wide at half maximum. Together they span the spectral region from 2000 A to 7500 A. Maximum transmission for most filters is about 50%. Transmission characteristics of the interference filters for light incident at various angles were determined using a Cary Spectrophotometer. Transmission curves were obtained for a number of filters at angles 0, 5, 10, 15, 20, 25, and 30°. Some results for a 610-mμ filter are shown in Fig. 3.24. A code has been written which will give the transmission profile for any filter for any source size and source-filter distance. These profiles are being checked experimentally using a Beckman DU monochromator which provides monochromatic light to a translucent diffuser plate and thus simulates the sources to be used. Ultimately it is hoped that the disk may be rotated in about 10 sec in order to analyze the rapidly changing spectra of thermoluminescence from warming amino acids.

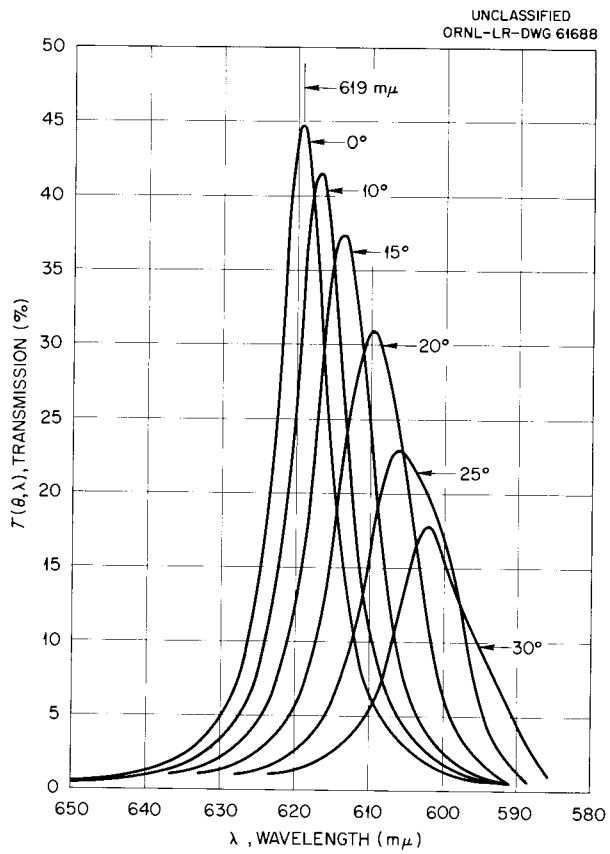

Fig. 3.24. Transmission of 619 mμ Interference Filter as a Function of Wavelength for Angles of Incidence of 0, 10, 15, 20, 25, and 30°.

Measurement of Light Emission from Irradiated Metal Foils

The theory of the emission of light from a film irradiated by a beam of charged particles has been discussed in the section of this report entitled "Theoretical Physics of Dosimetry." In brief, the light may arise from three interactions between the beam and the foil. Transition radiation occurs when an electron in the beam leaves a region of one dielectric constant and enters a region having a different dielectric behavior. Bremsstrahlung occurs when an electron in the beam experiences a deflection in a nuclear encounter in passing through the foil. Cherenkov radiation occurs when the velocity of the electron exceeds the velocity of light in the medium. The latter radiation was not observed because of the low energy of the electron beam (40 – 115 kev). Some indication of bremsstrahlung was noted experimentally as will be detailed later, but the intensity was low for the experimental situation employed here in comparison with the intensity of the transition radiation. Further, the theory of bremsstrahlung production has been derived only for isolated atoms and thus must be considered to be of orientation value only when applied to finite foils where optical interference effects are anticipated.

The experiment consisted in sending a monoenergetic beam of electrons from an accelerator through a foil and measuring the resulting optical spectrum with a Seya-Namioka vacuum ultraviolet spectrometer. Currents of about 15 μamp passed through foils a few hundred angstroms thick for periods of several hours with no apparent deterioration of the foils. Foils were vacuum evaporated either in a separate evaporator in the case of Ag and Au which oxidize slowly, or in the vacuum of the accelerator and spectrometer in the case of Al. Thicknesses were obtained by weighing and interferometrically. Spectra were taken over a spectral range from 2000 to 6000 A using an EMI 6256B photomultiplier as the detector. Transmission of the spectrometer and photomultiplier were determined by observation of the black-body radiation from a tungsten filament. The design of the irradiation chamber permitted observation of the spectra at angles of 0, 30, and 72° to the foil, normal on the beam exit side. The addition of a Glan prism to the entrance arm of the spectrometer allowed polarization measurements of the light to be made.

The results of the light emission measurements on silver foils were in approximate agreement with theoretical expectation. Thinner silver foils tended to have an emission peak in the region from 3400 to 3500 A for certain electron beam energies. This can be seen in Fig. 3.25 for $\theta = 30°$ and a thickness of 800 A. For thicker foils the sharp peak has disappeared into the broad continuum as seen in Fig. 3.26 for $\theta = 72°$ and $t = 2000$ A. The effect of foil thickness on peak intensity is shown again in Fig. 3.27. In Fig. 3.28 the data is compared with the Ritchie-Eldridge theory and agreement may be considered to be satisfactory if allowance is made for the experimental uncertainties involved.

The change in spectral distribution for different angles of emission shows as approximate agreement with the theory for the angular distribution. Figure 3.29 shows corrected data for three

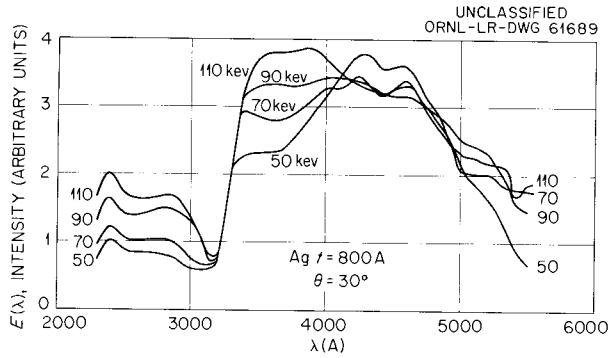

Fig. 3.25. Spectral Distributions from 800-A Ag Foil at 30° for Beam Energies of 50, 70, 90, and 110 kev.

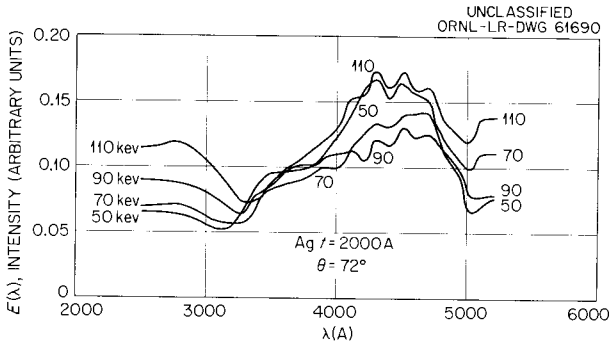

Fig. 3.26. Spectral Distributions from 2000-A Ag Foil at 72° for Beam Energies of 50, 70, 90, and 110 kev.

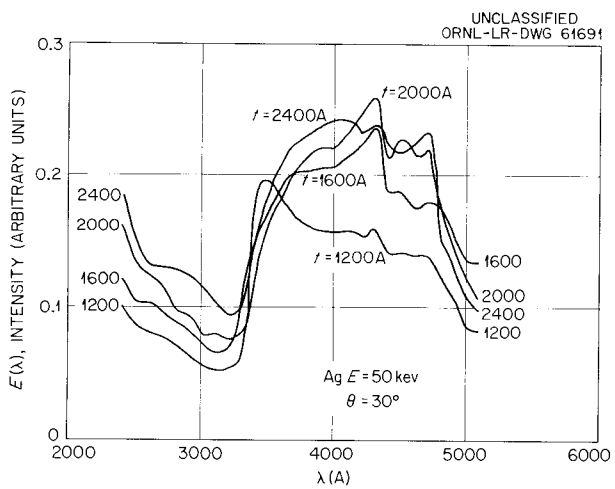

Fig. 3.27. Spectral Distributions at 30° from Ag Foils of Thicknesses 1200, 1600, 2000, and 2400 A for 50-kev Beam Energy.

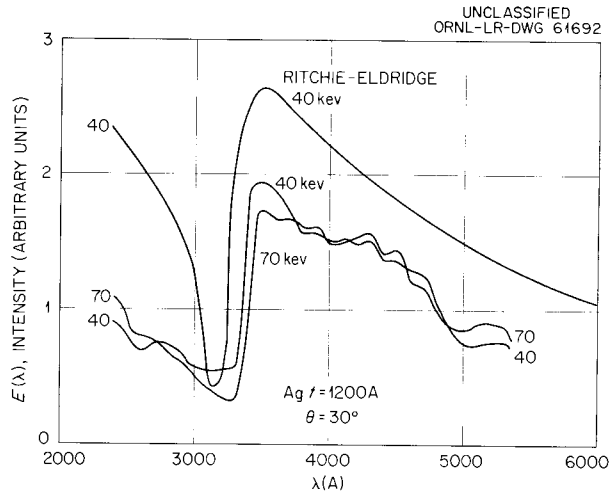

Fig. 3.28. Experimental Spectral Distributions for a 1200-A Ag Foil at 30° for Beam Energies of 40 and 70 kev and the Ritchie-Eldridge Theory at 40 kev.

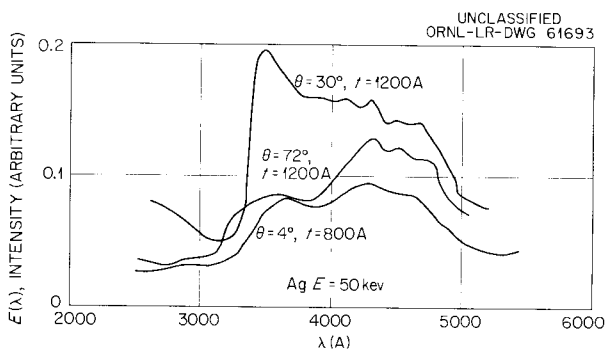

Fig. 3.29. Spectral Distributions for a Beam Energy of 50 kev for an 800-A Ag Foil at 4° and a 1200-A Foil at 30 and 72°.

angles of emission and Fig. 3.30 compared four experimental points with Ferrell's theoretical angular distribution.

The variation of light intensity with beam energy for the various foil thicknesses agreed approximately with theory. Fig. 3.31 contrasts experimental points from thin foil spectra at a wave length of 2400 A with the theory of Ritchie-Eldridge. Theory and experiment are normalized to agree at 80 kev. The theoretical curves are seen to have a greater slope than the experimental points. This could be an indication of the $1/E$ bremsstrahlung increase at the lower energies. Figure 3.32 shows the more complicated energy dependence found for thicker foils. The general shapes of the three curves seem to follow those of

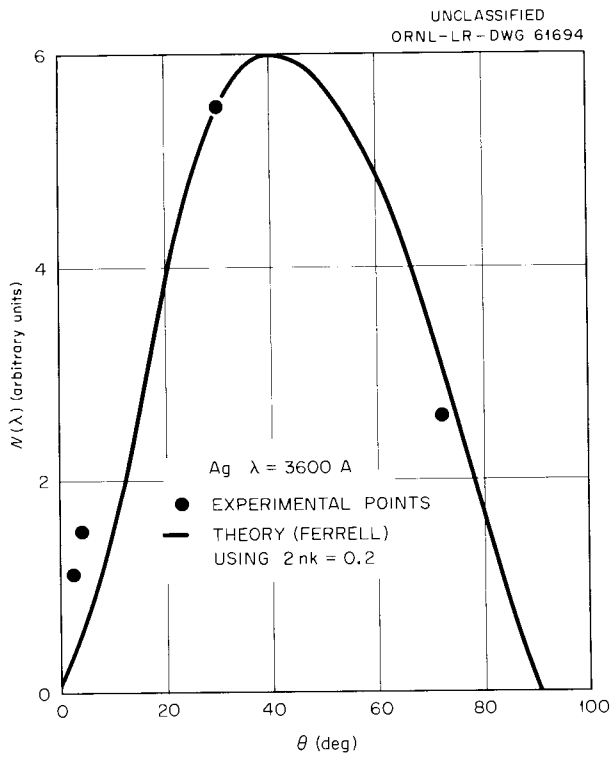

Fig. 3.30. Experimental Angular Distribution of Light at 3600 A from Ag and the Ferrell Theory.

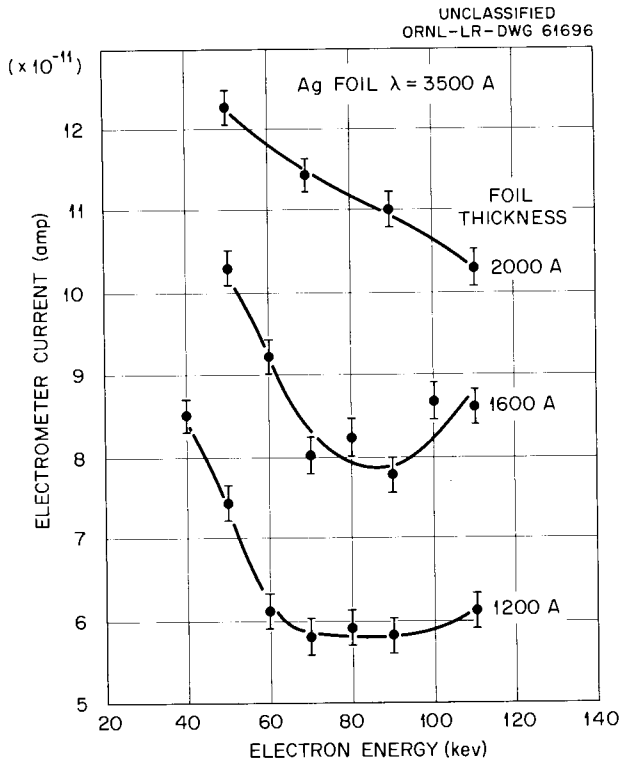

Fig. 3.32. Experimental Light Intensity at 3500 A as a Function of Beam Energy for Ag Foils of Thicknesses 1200, 1600, and 2000 A.

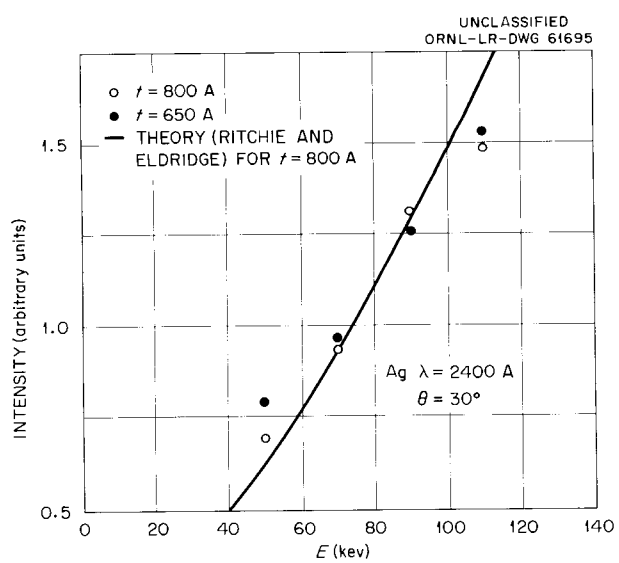

Fig. 3.31. Experimental Light Intensity at 2400 A as a Function of Beam Energy for Ag Foils of Thicknesses 650 and 800 A. Solid line is theory of Ritchie and Eldridge for 800-A foil.

theoretical curves for thicknesses between 1600 2000 A.

The determination of polarization of the silver light revealed that it was partially polarized in the plane of incidence. This seems to show that transition radiation is at least a sizeable part of the light detected since bremmstrahlung is polarized principally at 90° to this direction.

The results for aluminum foils follow some of general trends of theory, but there are some important differences in the spectral distributions. In the short-wave-length regions the only foil thicknesses which exhibited sizeable increases in emission were the thicker foils, whereas it was expected theoretically that the light from the thin foils should rise more sharply. Also, as shown by Fig. 3.33 a broad spectrum with its maximum at approximately 4400 A clearly exists. This maximum has the greatest intensity for the thicker foils. An artificially smoothed out spectral distribution for four foil thicknesses under identical conditions is shown by Fig. 3.34. It is noted also that a broad peak may exist in the silver foil

measurements which is similar to the peak in aluminum. This silver peak may be partially obscured by the presence of the maximum at ~3600 A.

The dependence of intensity on foil thickness and electron energy is shown in Figs. 3.35 and 3.36. The observation that the only curve in Fig. 3.35 which extrapolates to zero is the one based on measurements with the polarizer tends to give support to the idea that bremsstrahlung added significantly to the light at the lower beam energies. A polarizer would cut out the larger part of the bremsstrahlung while transmitting most of the polarized transition radiation. The absolute photon yields of the aluminum foils are low by a factor of approximately 4 when compared with theoretical predictions as seen on Fig. 3.37.

The spectrum from aluminum proved to be more highly polarized in the plane of incidence than that from silver. This would be expected if the component polarized out of the plane of incidence were bremsstrahlung whose intensity varies as Z^2.

Additional work is in progress.

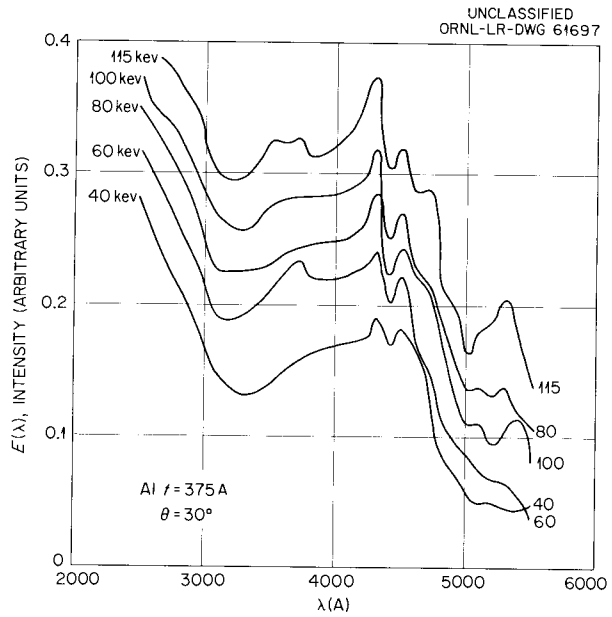

Fig. 3.33. Spectral Distributions from 375-A Al Foil at 30° for Beam Energies of 40, 60, 80, 100, and 115 kev.

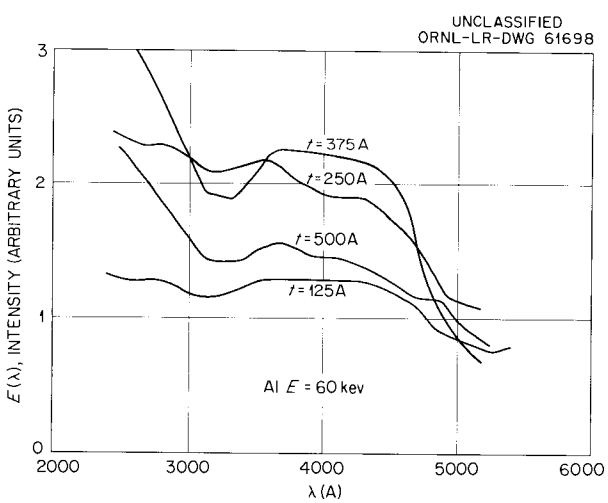

Fig. 3.34. Spectral Distributions for a 60-kev Beam Energy for Al Foils of Thicknesses 125, 250, 375, and 500 A.

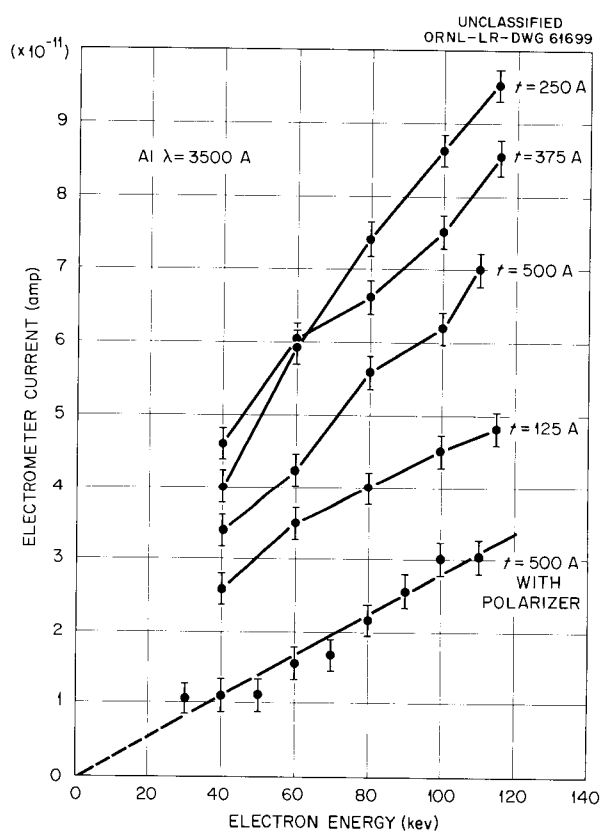

Fig. 3.35. Light Intensity at 3500 A as a Function of Beam Energy for Al Foils of Thicknesses 125, 250, 375, and 500 A.

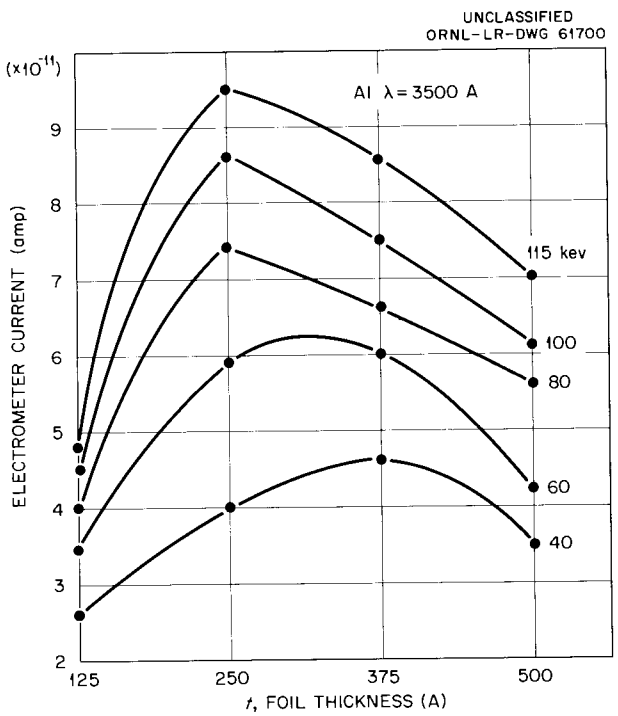

Fig. 3.36. Electrometer Current as a Function of Foil Thicknesses for 3500-A Light from Al Foils at Beam Energies of 40, 60, 80, 100, and 115 kev.

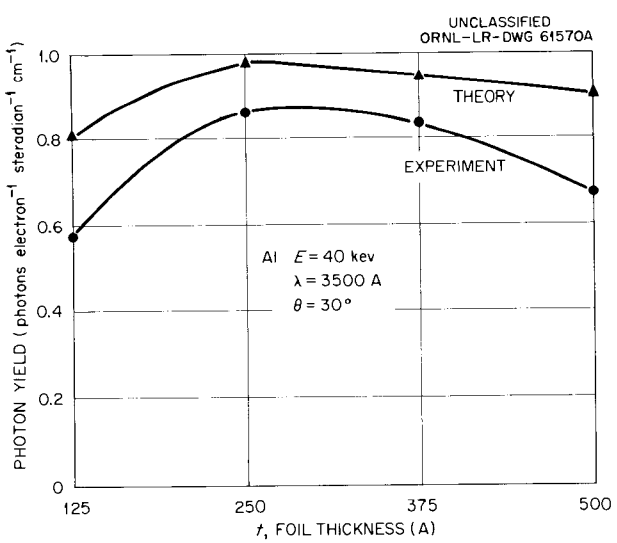

Fig. 3.37. Experimental and Theoretical Photon Yield as a Function of Foil Thickness for Al Foils at a Beam Energy of 40 kev.

DOSIMETRY METHODS

F. J. Davis

A. E. Carter
J. A. Harter
D. Pittman[53]
P. W. Reinhardt
R. M. Simmons
E. B. Wagner

Silicon-Gold Surface Barrier Fission Dosimeter

A composite fission foil suitable for measuring the fast-neutron dose of a typical fission spectrum has been prepared for testing. The foil is a nickel disk plated with a mixture of U^{235}, Np^{237}, and U^{238} in the proportions 1.0, 1.14, and 1.99. Fission fragments from the foil will be detected with a silicon diode which, when shielded with B^{10}, will give a total fission count proportional to the neutron dose. From previous measurements using U^{235} foils with silicon detectors in the thermal column, it is estimated that 3.5 cm^2 foil with density of 2.0 mg/cm^2 will have a sensitivity of approximately 3×10^3 counts/rad.

Radiation Measurements over Simulated Plane Sources

To assist in the interpretations of radiation measurements over area and point sources, a calibration test location was constructed in the Frenchman Flat area of the Nevada Test Site. The extended source area consisted of a square array 2000 ft on a side with source stations at 100-ft intervals. In the center, to assist in ground measurements, was a smaller array of 100 stations at 10-ft intervals and 1/100 the value of the outer stations. Two point-source stations were placed in positions making an equilateral triangle with the extended source area and 6000 ft apart.

Two arrangements of sources were used. In the first arrangement the sources in the outer array were each 15 mc Cs^{137} and those in the inner array 0.15 mc Cs^{137}. Point source *A* was 1.72 curies Cs^{137}, and point source *B* was 2.00 curies I^{131}. The second arrangement consisted of 4.5-mc Co^{60} sources in the outer array, 0.053-mc Co^{60} sources in the inner array, 1.2-curies Co^{60} at point *A*, and 2.00-curies I^{131} at point *B*.

The measurements were made with the equipment aboard the U.S. Geological Survey's twin-engine

[53] Engineering and Mechanical Division.

DC-3 aircraft. The regular radiation detection equipment carried aboard this aircraft[54] consists of six NaI(Tl) scintillation detectors used in parallel, each 4 in. in diameter by 2 in. thick. One-half inch of lead shielding is used on the sides and rear of the crystals with 1 in. of lead on the forward side. The pulses are fed through an amplifier and discriminator to a recording rate meter. The discriminator setting used allows pulses to be counted which are above those originating from 50-kev gamma rays. A radar altimeter records the altitude above ground and can also be coupled into the recording rate meter to compensate automatically for the height of the aircraft to give the gamma radiation intensity on the ground. Auxiliary equipment carried for this operation was a 256-channel analyzer which gave the pulse height distribution from a single unshielded 4-in.-diam by 2-in.-thick NaI(Tl) scintillation detector.

The dose measurements at 3 ft above ground level are shown in Table 3.4. The 4 × 2-in. crystal scintillometer was calibrated with Cs^{137}, Co^{60}, and Ra sources at a distance that gave a comparable scattering component with that in the field measurements.

Table 3.4. Dose Measurements at 3 ft Above Ground Level

Cs^{137} array, 16.2 μc/m^2; Co^{60} orray, 4.8 μc/m^2; background (4 × 2-in. crystal), 25 μr/hr

	Dose (μr/hr)	
	Cs^{137} Array	Co^{60} Array
4 × 2-in. crystal	225	200
Theoretical	228	234

The usual expression for the variation of intensity I_0 with height h above a point source is

$$I_0 = \frac{k S_0 e^{-\mu h} B(\mu h)}{h^2}, \qquad (1)$$

where μ is the absorption coefficient for air, S_0 the source strength, and $B(\mu h)$ the buildup factor due to scattered radiation. The function $B(\mu h)$ can usually be expressed empirically in a power series as

$$B(\mu h) = 1 + a(\mu h) + b(\mu h)^2 + \ldots , \qquad (2)$$

where a, b, etc. are constants depending on energy of radiation and the detector response function. For our purpose the first two terms are generally sufficient, and for soft radiation and altitude above 500 ft the second term, $a(\mu h)$, alone adequately expresses the buildup. If one integrates Eq. (1) using the first two terms of the buildup factor over an infinite plane source of S_A curies per unit area, the intensity relation

$$I_A = 2\pi k S_A \left[E_1(\mu h) + a e^{-\mu h}\right] \qquad (3)$$

is obtained.

Assuming an air density of 1.057 g/liter calculated from the air pressure and temperature at time of measurement, and the constants given in Table 3.5, we obtain the theoretical values given in Table 3.4. The values for Cs^{137} compare quite well, but the values for Co^{60} differ by 17%.

Table 3.5. Constants Used in Determining Theoretical Dose

	Cs^{137}	Co^{60}	Reference
S_A	16.2 μc/m^2	4.8 μc/m^2	
μ	0.077 cm^2/g	0.056 cm^2/g	*a*
$E_1(\mu h)$	4.32	4.65	
k	0.39 rhm	1.35 rhm	*b*
a	1.45	1.1	*c*

[a]W. S. Snyder and J. L. Powell, *Absorption of Gamma Rays*, ORNL-421, Suppl. 2 (Mar. 14, 1950).

[b]National Bureau of Standards Handbook 54, p 42, *Protection Against Radiation from Radium Cobalt-60 and Cesium-137* (Sept. 1, 1954).

[c]H. Goldstein and J. E. Wilkins, Jr., *Calculations of the Penetration of Gamma Rays*, NYO-3075, p 180 (June 30, 1954). Values are estimated from graph showing dose buildup factor vs *E*. Medium: water; source: point isotropic.

Aerial Measurements. – In Fig. 3.38 are shown the data obtained from flying over the three point sources. The ordinate is intensity times height plotted on semilog coordinates against height. These coordinates are chosen so that if the data fit a buildup factor proportional to height, they will appear as a straight line with slope equal to μ.

[54]F. J. Davis and P. W. Reinhardt, *Nuclear Sci. and Eng.* 2, 713 (1957).

For I^{131} the data fit the straight line from 400 ft on up; however, for the harder radiation of Co^{60}, the straight line only fits above 800 ft.

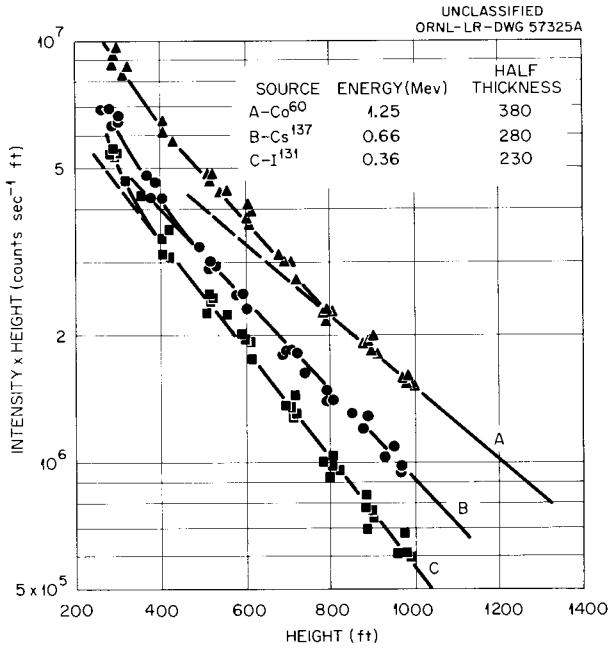

Fig. 3.38. Variation of Intensity with Height over Point Sources.

The relative experimental buildup factors vs height determined from flights over the point sources are shown in Fig. 3.39. The straight lines fitted to the points have the indicated equations when normalized to a unity intercept on the ordinate.

The values of a (coefficients of μh) shown on the graph are not values representing dose but values as measured with the scintillation detector which counts all pulses with equal weight. Consequently, the value of a for this detector will be higher than for a detector measuring dose.

If the second term of the buildup relation is the only one of significance, then Eq. (3) becomes simply an exponential variation with height. The data shown in Fig. 3.40 for the Cs^{137} extended sources show a good fit to the theoretical half thickness of air of 280 ft. The points falling below the curves at low altitudes are probably due to the side shielding of the crystals so they do not effectively see an infinite extended source. The Co^{60} extended source data seem to fit a half thickness of air of 340 ft better than the theoretical half-thickness of 380 ft. The discrepancy may be due to two causes: (1) the second term in the buildup relation is no longer the controlling term for the harder radiation of Co^{60}, so that significant contributions of the $E_1(\mu h)$ term would raise the

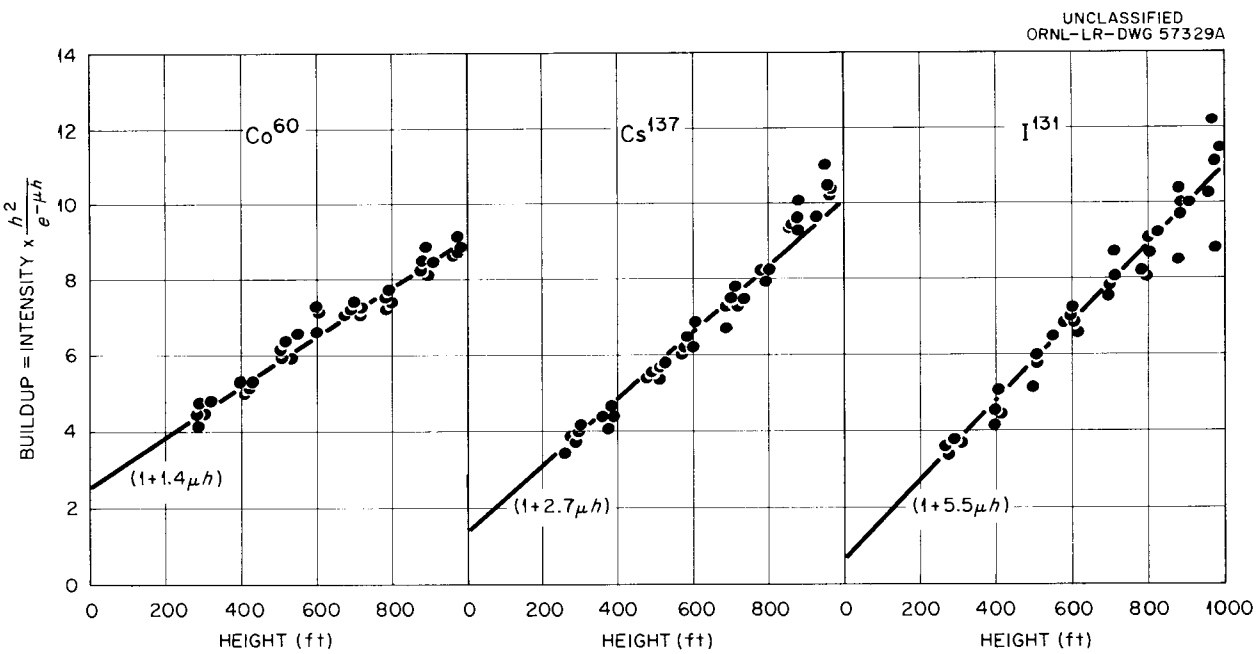

Fig. 3.39. Variation of Buildup of Radiation with Height from Point Sources.

curve for low altitudes; (2) the high-altitude measurements may be too low because of the limited area of the field. The count rates at 500 ft equivalent to a ground reading of 1 μr per hour for Cs^{137} and Co^{60} plane sources are 25 and 18 counts per second, respectively.

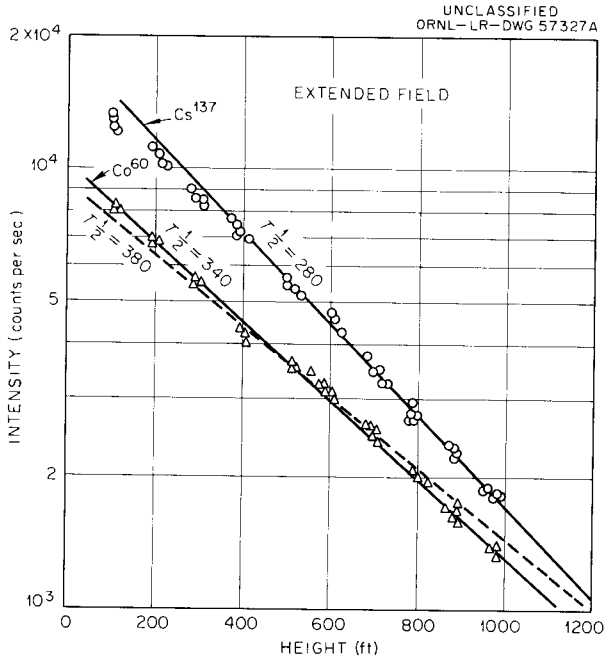

Fig. 3.40. Variation of Intensity with Height Above Extended Sources. (Six crystals; side shielded.)

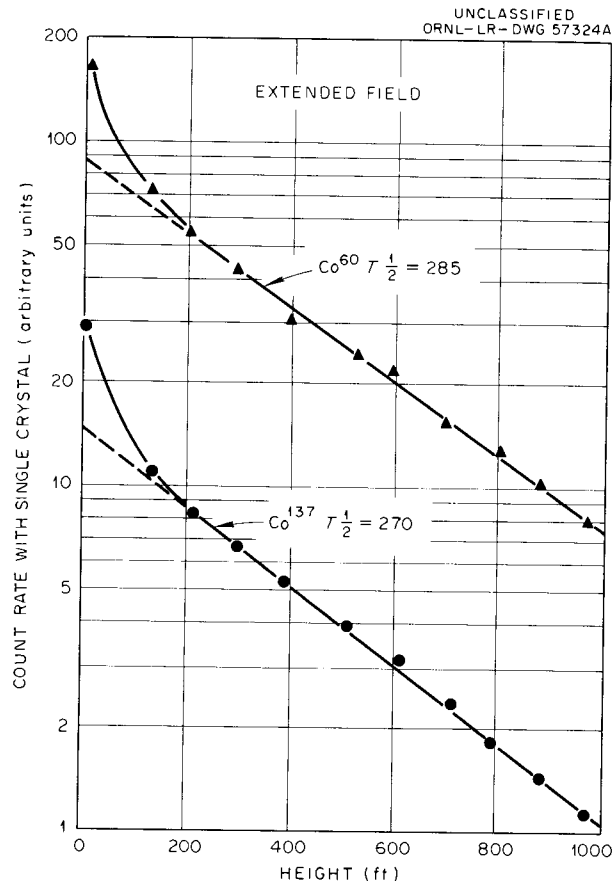

Fig. 3.41. Variation of Intensity with Height Above Extended Sources. (Single crystal.)

The use of the single 4 × 2-in. crystal with the 256-channel analyzer was mainly for spectral measurements. However, the integral of the pulse height distribution gives a means of comparison with the 6-crystal rate meter. The points shown in Fig. 3.41 are the total integrated count minus background of the five passes at each altitude over the extended source. The points shown at 3 ft were measurements made on the ground. It is to be noted that the curves turn up sharply on the low-altitude end due to the $E_1(\mu h)$ term in Eq. (3). Also, no shielding was used on the side of the crystal to cancel out this effect. The slope of the curves is steeper, especially for Co^{60}, than that of the corresponding curves in Fig. 3.40. This may be due to the effect of the time integral of the count which was started and stopped at the edges of the field.

If I_0 is the intensity over a point source of S_0 curies, then eliminating k in Eqs. (1) and (3) gives the relation,

$$I_A = 2\pi I_0 h^2 \frac{[E_1(\mu h) + ae^{-\mu h}]}{e^{-\mu h}(1 + a\mu h)} \frac{S_A}{S_0} . \qquad (4)$$

If the second term in the buildup factor is assumed to be the controlling term, this equation reduces to

$$I_A = 2\pi I_0 \frac{h}{\mu} \frac{S_A}{S_0} . \qquad (5)$$

If one calibrates an instrument and gets a reading I_0 over a source S_0 with an air absorption constant μ at a height h, then one should get a reading I_A over an infinite plane source of S_A per unit area at the same height h. In Table 3.6 are shown

Table 3.6. Ratio of Measurements over Point and Plane Sources*

	$1/\mu$ (ft) (ρ = 1.057 g/liter)	$(I_A/I_0)_{th}$ ($S_A = 10^{-3}\ S_0/m^2$)	$(I_A/I_0)_{exp}$ (Array)	$\frac{2 \times I_{edge}}{I_{center}}$	$(I_A/I_0)_{exp}$ (∞ Array)
I^{131}	334	94			
Cs^{137}	403	108	95	1.14	108
Co^{60}	554	131	94	1.33	125

*Values given are for 500 ft above ground.

the values for the ratio of I_A/I_0 for the three sources I^{131}, Cs^{137}, and Co^{60} for an altitude of 500 ft. In other words, at 500 ft one should get the same reading on an instrument flying over a 94-mc point source of I^{131} as over a field of a 1-μc/m^2 plane source. For the 6-crystal rate meter this would be a count rate of 360 counts/sec above background. The corresponding point sources for Cs^{137} and Co^{60} equivalent to a 1-μc/m^2 plane source at 500 ft altitude calculated from Eq. (4) are 108 mc and 131 mc respectively. The corresponding experimental values were 95 and 94 mc respectively.

The radiation intensity measurement made over the edge of the field averaged 57% for Cs^{131} and 66% for Co^{60} of the corresponding readings over the center line of the field. This would indicate that the field was not large enough and that the readings over the center should be increased by 14 and 33% or more to approximate readings over an infinite field. If these corrections are applied to the experimental point sources equivalent to a field of 1 μc/m^2, we obtain 108 μc for Cs and 125 μc for Co, which agree much better with the theoretical values given.

The pulse height distribution of the gamma rays from the Cs^{137} field is shown in Fig. 3.42. The experimental points show a prominent photo peak for the lower altitudes but nearly fade out at 1000 ft. Figure 3.43 shows the corresponding pulse height curves obtained from the Co^{60} field. It is noted in both Figs. 3.42 and 3.43 that the peak due to scattered radiation drifts to lower energies for the higher altitude. Figure 3.44 is a plot of the energy of the scatter peak obtained from the cesium field.

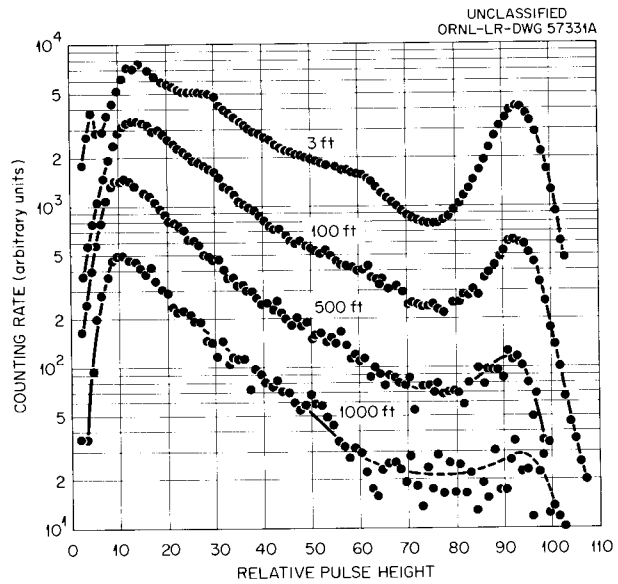

Fig. 3.42. Pulse Height Distribution Obtained over Cs^{137} Source Field.

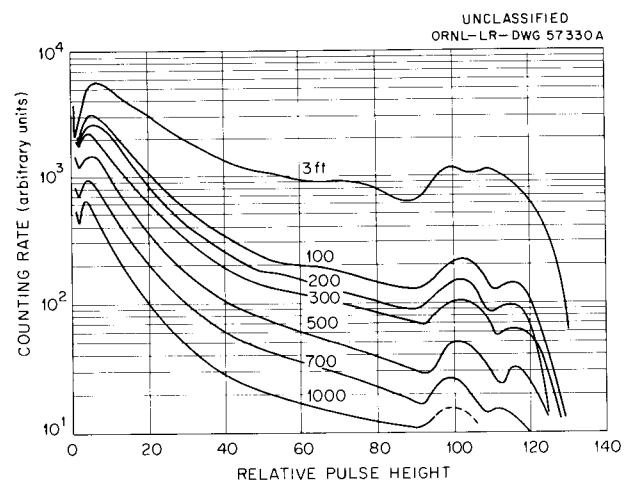

Fig. 3.43. Pulse Height Distribution Obtained over Co^{60} Source Field.

In Fig. 3.45 is plotted the ratio of the height of the scattering peak height to the photo peak height of the pulse height distribution curves. Also shown in Fig. 3.45 is the ratio of the total count rate to the count rate in the photo peak. These are obtained by integrating the pulse height distribution curves. It is to be noted that the curves approach linearity above 100-ft altitude. This is to be expected if one has a buildup factor linear with height.

By plotting the count rate of the photo peak against altitude, one should obtain the variation of the primary radiation with altitude with no buildup. This is shown in Fig. 3.46. Also shown is a plot of $E_1(\mu h)$ which is what is obtained theoretically when one integrates the intensity relation, Eq. (1), over a plane source with unity buildup factor.

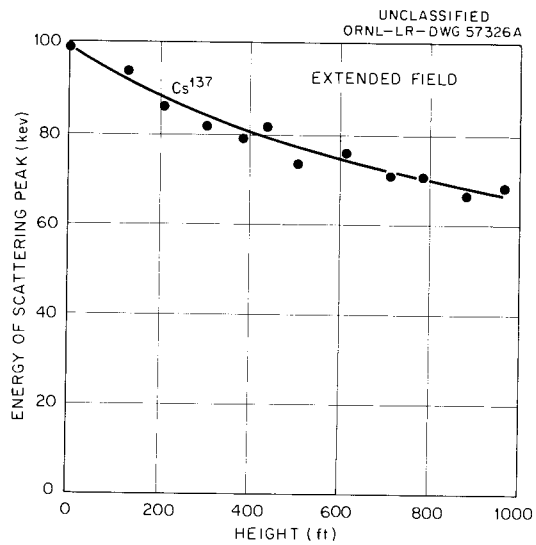

Fig. 3.44. Variation of the Energy of the Scattering Peak in the Pulse Height Distribution of Cs^{137}.

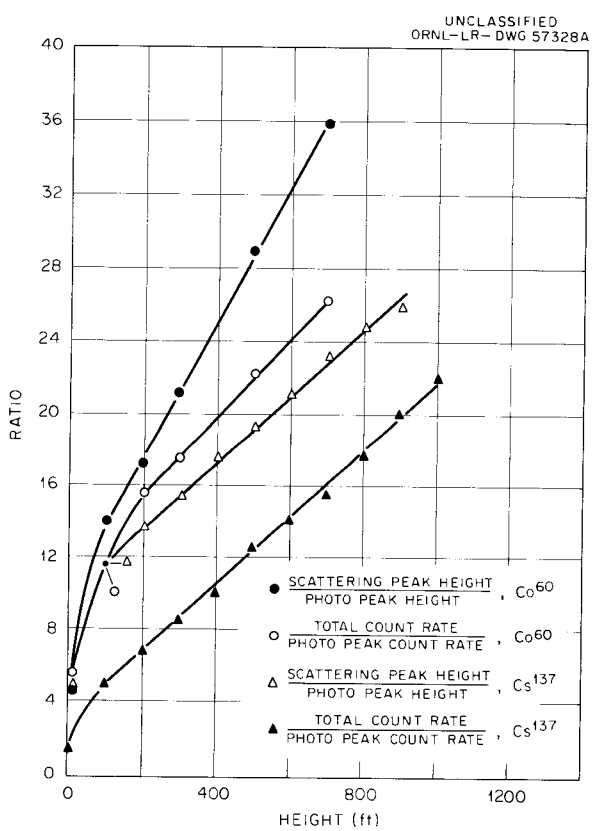

Fig. 3.45. Ratio of the Scattering Peak Heights to the Photopeaks.

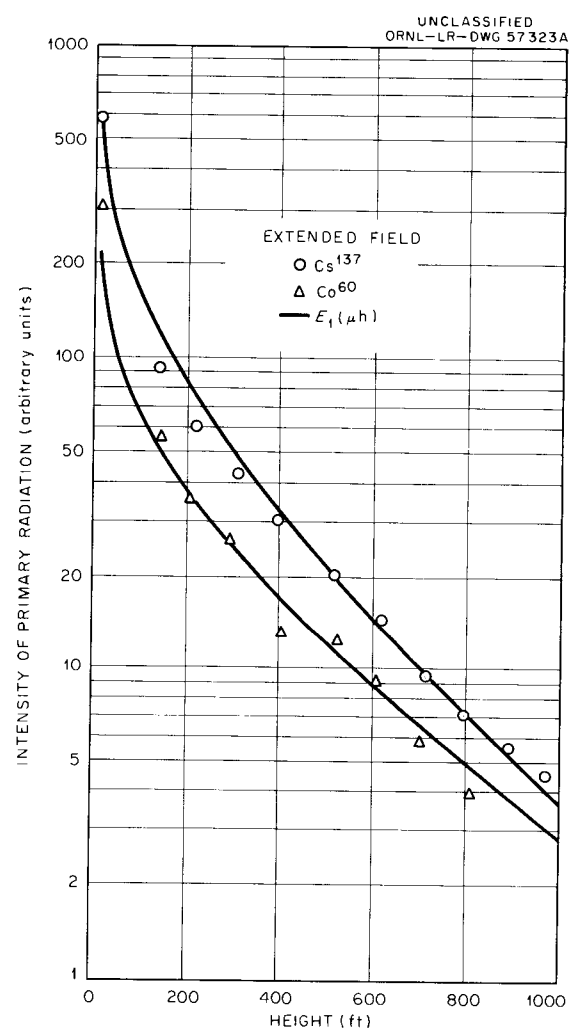

Fig. 3.46. Variation of Primary Radiation with Height Above Extended Source Field.

DOSIMETRY APPLICATIONS

J. A. Auxier

J. S. Cheka W. H. Shinpaugh, Jr.
F. W. Sanders J. H. Thorngate

Ichiban Program – the Atomic Bomb Hypocenter at Nagasaki

As part of the cooperative program between ORNL and the Atomic Bomb Casualty Commission (ABCC) in Hiroshima and Nagasaki, Japan, ORNL collaborated in 1959 with Shogo Nagaoka, Director of the Peace Memorial Museum in Hiroshima in a redetermination of the burst point of the atomic bomb over Hiroshima. This was reported in ABCC Technical Report 12-59. This program was extended, with the assistance of Sunao Tonaka and Shoichi Ueda of the Statistics Department of ABCC, with a similar redetermination for Nagasaki.

Granite, which best indicated "shadows" of the thermal rays of the bomb, was not used much in Nagasaki, so only about 300 measurements at 23 different locations were available. Some of the shadows are still visible, but many have disappeared. Not all the measurements at one location were truly independent, so the best method of statistical analysis was to average the shadow angle measurements at each location, usually a cemetery, and consider this angle and the coordinates of the location as the basic data. A least squares fit was made to the data to minimize the sum of the perpendicular distances from each projected shadow line to the hypocenter, the point on the ground under the burst point. The burst height was similarly determined.

In terms of the coordinates of the wartime U.S. Armp Map of Nagasaki, series AMS L902 number 138353 dated August 1945, these coordinates are:

$$x = 1293.633 \pm 0.142 \qquad (E-W),$$
$$y = 1065.953 \pm 0.064 \qquad (N-S).$$

The unit is 1000 yards, and the coordinates are in terms of the 1000-yard world polyconic grid band III N, Zone "C". The 95% confidence limits are those given.

The burst height and its standard deviation were:

$$H = 499.8 \pm 16.8 \text{ meters}.$$

The corresponding figures currently in use at ABCC are:

$$x = 1293.61,$$
$$y = 1065.92,$$
$$H = 490 \text{ meters}.$$

The differences between these and the new values are within the errors of measurement and calculation. Other methods of computation were tried, but these results are the most accurate in the opinion of the authors.

The coordinates on the U.S. Army map are the most useful for ABCC, since all survivors' locations at the time of bombing (ATB) are given in terms of these coordinates. However, other investigators may need to locate the hypocenter position on the ground, or in terms of other maps. Therefore a careful study was made of the Army map, of a post-war Nagasaki City planning map surveyed in 1950 and revised and issued by Nagasaki Prefecture in November 1955, and of pre- and post-bombing photographs made by the U.S. Air Force. Many small discrepancies were noted in the positions of and relative distances between various landmarks which could reasonably be presumed not to have moved. The latitude and longitude values for the same landmarks on the two maps differ somewhat, probably because of post-war resurveys of primary bench marks. Therefore, the following figures are less accurate than the Army map coordinates just given, but represent our best estimate from available data.

	Army Map	Japanese Map
Latitude	N 32° 46' 13.8"	N 32° 46' 12.3"
Longitude	E 129° 51' 57.4"	E 129° 51' 57.6"

At this latitude one second of latitude is 30.8 meters and one second of longitude is 26.0 meters, so that if the conversion to latitude and longitude were assumed to be exactly correct, the 95% confidence limits would be:

Latitude ± 1.9",
Longitude ± 5.0".

In terms of a position on the ground, further errors may be introduced in determining the location of presently existing reference landmarks. No primary bench marks are close enough to the hypocenter to permit an accurate survey without considerable expense and difficulty.

As nearly as can be determined from the maps and photographs mentioned, the hypocenter lies about 83 meters east and 20 meters south of the intersection of the main north-south street leading up the Urakami Valley, and the cross street leading to the Urakami Cathedral. The intersection of the projected curbstone lines at the southwest corner of the street crossing is here taken as the reference point. This description is the least accurate of those given here.

An ABCC Technical Report on this work is in preparation.

Evaluation of the Residual Radiation in Hiroshima and Nagasaki

The problem of biological disturbances from exposure to residual radiation appears periodically in the Hiroshima and Nagasaki atomic bomb studies. It is generally felt that the level of radiation present was not sufficient to cause any biological damage to persons who entered the cities for rescue work a day or more after the nuclear detonations, but no definitive substantiation of this belief is available. Therefore, an investigation was carried out to assess the amount of radiation present in the two cities after the bombings.

Two sources of radiation were considered, fission product fallout and neutron-induced radioactivity. The magnitude of fission product fallout was relatively well known from measurements made in the cities several weeks after the event. The calculations are based upon the $t^{-1.2}$ decay law which should be sufficiently accurate for this application. However, an assessment of the neutron-induced radiation was more difficult, chiefly due to the fact that the most active isotopes (Na^{24}, Mn^{56}, etc.) are generally those with short half-lives and these isotopes had decayed to undetectable levels within a few weeks of the event. The major portion of this present investigation involved a calculation by several methods of the quantity of radioisotopes produced. It was felt that the most precise result was obtained by irradiating samples of soil and roof tiles, which were the main constituents on the ground after the detonations, in a nuclear reactor. The activity produced was then determined by gamma-ray analysis using a scintillation detector.[55]

An exposure dose was then computed using the known decay schemes of these isotopes. The results obtained by this method give integrated infinity doses of 20.5 r and 3.6 r in Hiroshima and 1.2 r and 2.8 r in Nagasaki from Na^{24} and Mn^{56} respectively. A second gamma-ray analysis was performed on the soil samples a year after the original neutron irradiation. The most abundant radioisotopes present one year after the exposure of the soil samples were Sc^{46} (half-life of 85 days) and Co^{60} (half-life of 5.9 years). The exposure level due to these isotopes was calculated by the above methods and plotted in Fig. 3.47. It is seen that the experimentally measured values which were all made two weeks or more after detonation, are comparable both in magnitude and rate of decay with the activity calculated for Sc^{46} and Co^{60} since the Na^{24} and Mn^{56} activities had decayed to negligible levels by that time. This confirms the theory that most of the activity measured in the hypocenter area was not due to fallout but to neutron-induced activity in the ground and other materials on the ground.

The results of this investigation show that the radiation level in Hiroshima and Nagasaki after the detonations were of such levels that very few individuals, if any, were exposed to significant amounts of residual radiation.

A complete resume is being prepared as an ABCC Technical Report.

Fast Burst Reactor (Fast Critical Assembly)

Detailed design has been completed and construction is essentially completed for the ORNL fast critical assembly.[56] As the first such device to be constructed for health physics and bio-medical research, the design meets the needs for a wide dose rate range (variable by a factor of $\sim 10^{11}$) and high neutron-to-gamma dose ratio; the neutron-to-gamma dose ratio from the core is about 10 to 1 and large sources of Co^{60} and Cs^{137} will be available for simultaneous or independent exposures.

The assembly is designed for continuous operation at power levels up to 1 kw and brief operation ($\sim$10 min) at 10 kw, and in a pulse mode with pulses up to 10^{17} fissions/pulse. At 10^{17} fissions/pulse the expected pulse width at half-height is $\sim$40 μsec. The neutron dose rate at a

[55] This analysis was performed by J. F. Emery and and G. W. Leddicotte of the Analytical Chemistry Division of ORNL.

[56] Built under contract by Nuclear Development Associates, Inc., White Plains, New York.

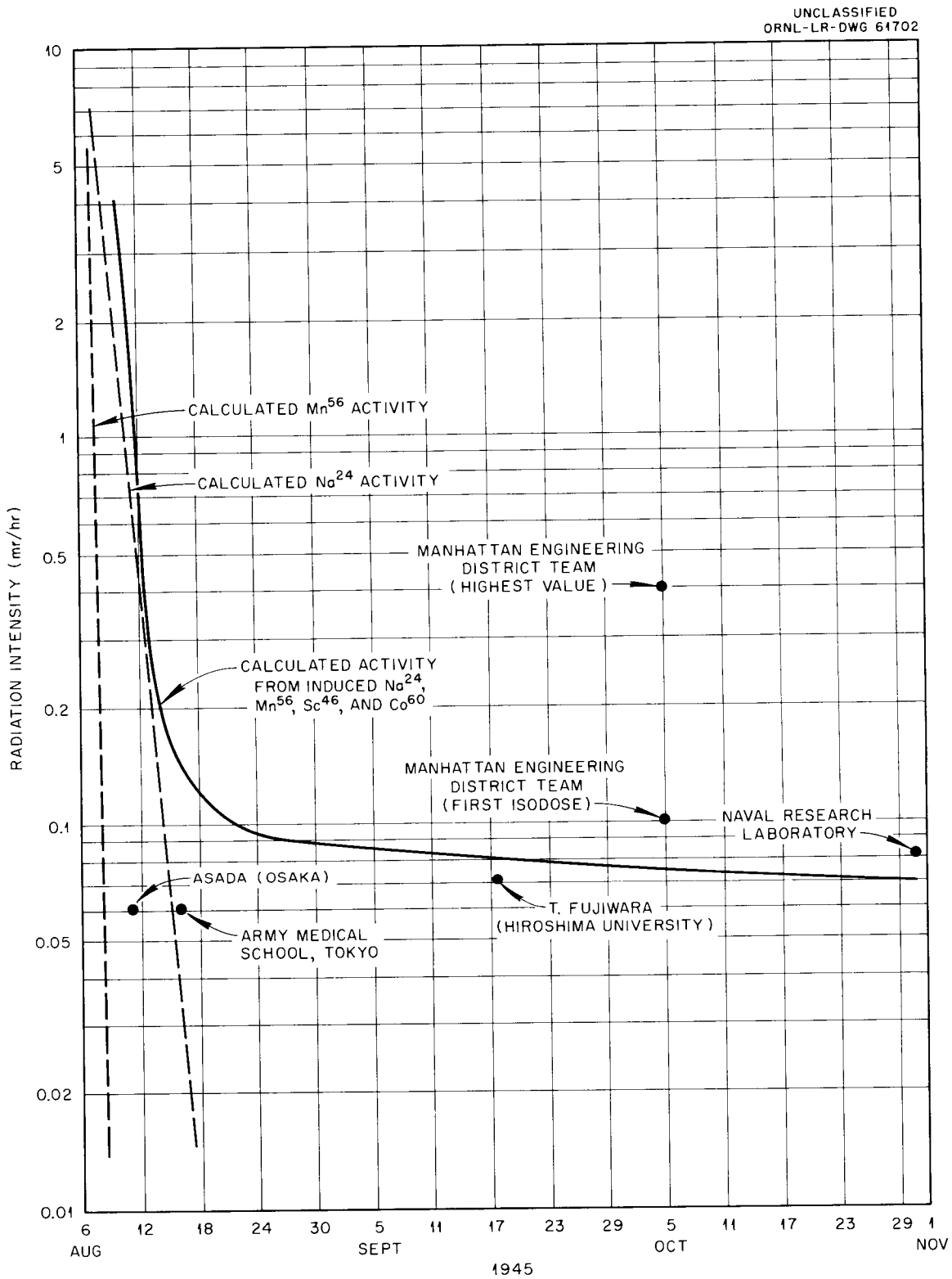

Fig. 3.47. Comparison of the Calculated Neutron Induced Activity vs the Experimentally Measured Values at the Hypocenter Area in Hiroshima.

distance of 1 m from the core during operation at 1 kw will exceed 2500 rads (tissue).

Figure 3.48 shows the critical assembly near completion. The core (shown in the lower half of the figure with safety block disengaged) is enriched uranium alloyed with 10% by weight molybdenum. The control console is shown in Fig. 3.49. Facility construction has commenced and the assembly is scheduled to be installed in mid-1962; in the interim it will be used for studies at the Nevada Test Site (Operation BREN).

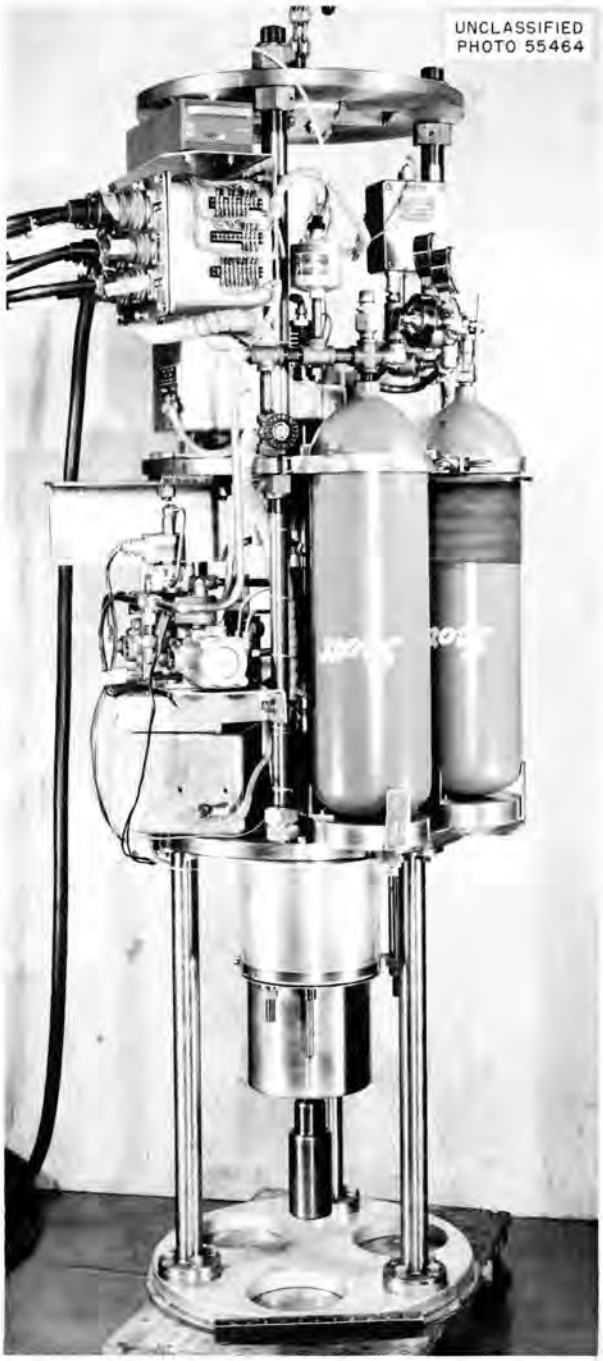

Fig. 3.48. Fast Burst Reactor During Checkout Operation.

Metaphosphate Glass Microdosimeters (Fluorods)

Metaphosphate glass rods are used in the ORNL badges for the purpose of accident monitoring since they can be used for evaluating gamma doses from a few to several thousand rads. If these fluorods retain their radiophotoluminescence for a reasonable length of time, they can also serve as long-term integrating dosimeters.

It has been shown[57] that this material changes its absorption characteristics with irradiation, and that the newly-formed absorption bands regress with time, but that the rate of regression is a function of radiation exposure. The fluorescence which is measured is the result of absorption of one of the ultraviolet lines, and would probably follow the same pattern. Since their dosages ranged from 10^5 reps upward, the regression at the small doses of interest to health physicists may be negligible. It was also of interest to determine whether the fluorods would integrate small doses.

In addition to the Schulman type "high-Z" glass, specimens of Bausch and Lomb's "low-Z" glass and Japanese (Tokyo Shibaura Electric Co., Ltd.) No. 2 glass rods were obtained and included in the investigation.

For single doses, the fluorescence of the high-Z glass increases after irradiation to reach a maximum in about 10 hr and after 24 hr begins to regress at an approximately logarithmic rate, losing about 20% in 120 days. Both the Bausch and Lomb low-Z glass and the Japanese glass have a different pattern. The fluorescence continues to increase, being about 3% higher in 20 days than in 24 hr. Thereafter, there appears a slow regression so that in 60 days the reading is approximately the same as at 24 hr.

The relative sensitivities of the high-Z, low-Z, and Japanese glass are as 1:1.2:2.3.

The pre-dose fluorescence readings (at approximately 6400 A) are about the same for the high- and low-Z glasses, but that of the Japanese glass is about one-half as much.

[57] B. E. Proctor, *et al.*, *Studies on Glass Dosimeters*, NYO 3345 (1955).

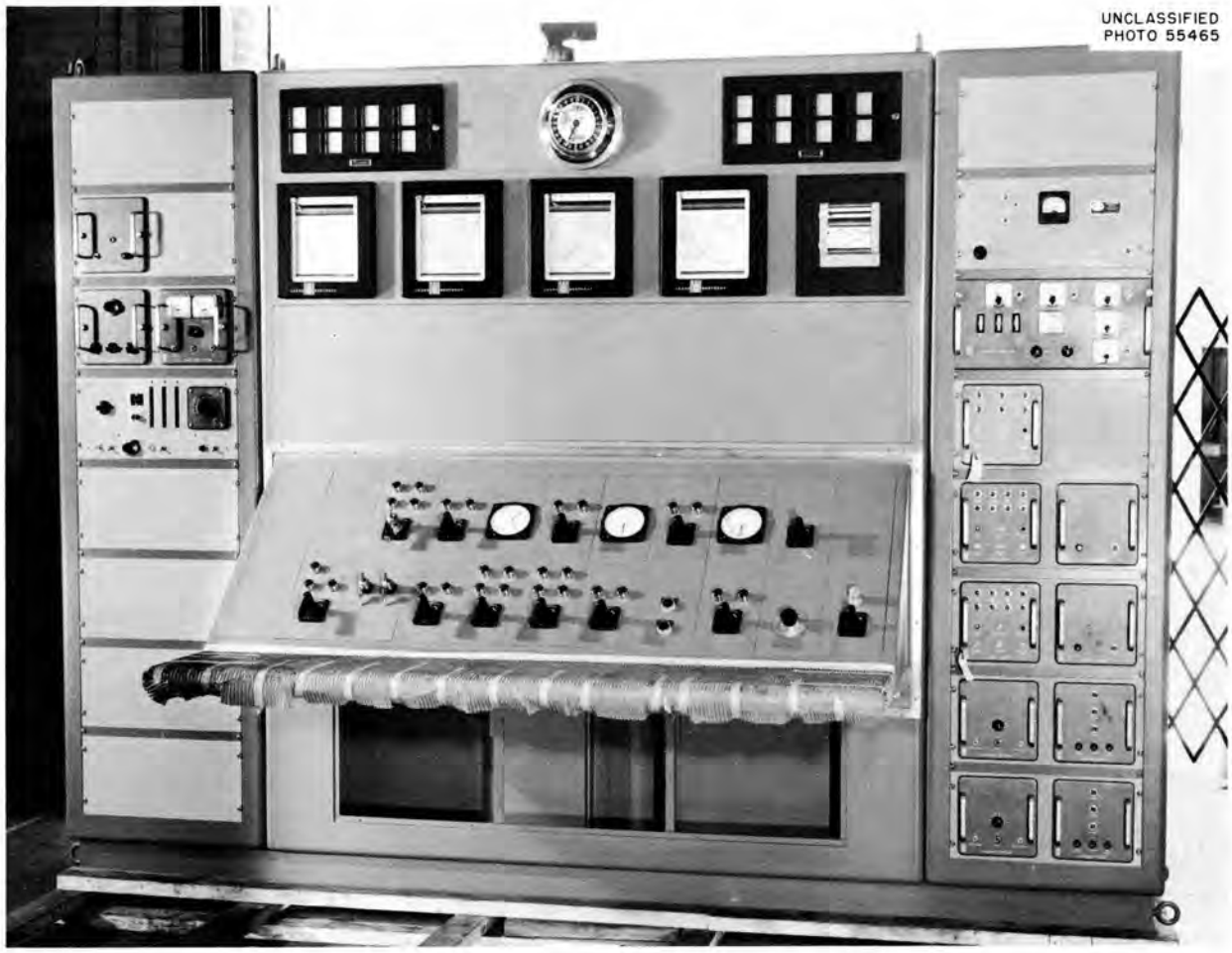

Fig. 3.49. Fast Burst Reactor. Front view of reactor control console during completion stages of wiring and assembly.

A study is underway wherein groups of the three types of glass are exposed to 500 mr of radium gamma rays per working day. These are read weekly. After three months both the Japanese and the low-Z fluorods indicate linear additivity, while regression is evident in the high-Z rods.

A difficulty with the fluorods is their frangibility. A chipped rod does not give a true or reproducible reading. The readout system also needs improvement; the chuck and its chamber should be cooled to room temperature as the reading is temperature dependent, and the rod requires minutes to reach equilibrium at the chuck temperature before reading.

Compton Gamma-Ray Spectrometer

In order to measure the gamma spectrum of the mixed radiation field which will be encountered during Operation BREN,[58] a neutron insensitive gamma-ray spectrometer has been developed. Neutron activation ruled out the use of any scintillation detector and prompted the study of a magnetic device. Reports have been published concerning many such devices. From the many possible devices the method chosen measures the momentum of the forward scattered Compton electrons which are produced by gamma rays incident upon a beryllium foil. The spectrometer which was designed is shown in Fig. 3.50. The sensitivity was increased at the cost of decreased resolution by the use of a relatively thick, 12 mil, radiator foil and a $\frac{1}{8}$- by $\frac{1}{2}$-in. counter opening.

The quantity measured by the spectrometer is the product of the magnetic field strength, H, and the

[58] BREN – Bare Reactor Experiment, Nevada, scheduled for late 1961 and early 1962 at the Nevada Test Site.

radius of curvature, ρ, through which the electron is bent by the magnetic field. A prototype spectrometer using a movable counter to vary ρ was found to be impractical due to the large amount of scattered radiation which was detected at small values of ρ. Therefore, a device with a fixed radius of curvature was built in which H is varied to measure the momentum spectrum of the recoiling electrons.

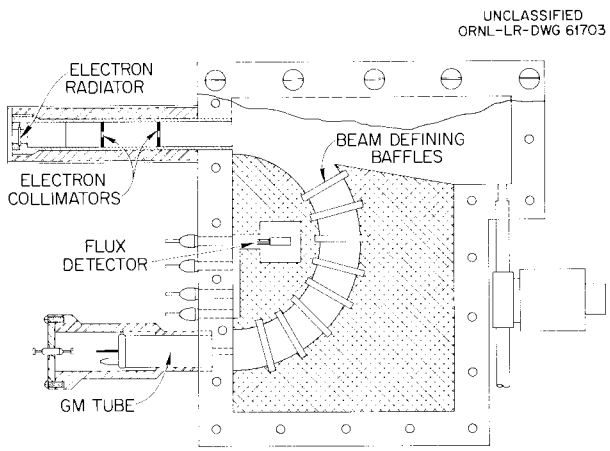

Fig. 3.50. Compton Gamma Spectrometer.

An incident gamma ray may, upon striking the beryllium radiator, undergo a Compton scattering. If the electron goes in the forward direction at a sufficiently small angle, it will pass through the electron collimator and into the magnetic field which is perpendicular to the plane of the spectrometer. The ρ in which the electron is bent upon entering the magnetic field depends upon the momentum of the electron and H. If H is adjusted so that ρ for the electron is defined by the baffles of the spectrometer, the electron is bent through 180° and is incident upon the face of the G-M counter. An electron of sufficient energy to pass through the window of the counter produces a count which is recorded with a scaler.

The lower gamma-ray energy limit of this spectrometer is 150 kev. This is set by the thickness of the counter window, the mechanism of the Compton scattering reaction, and the thickness of the beryllium radiator. The fixed ρ of 5.0 cm requires an H of 160 gauss to properly deflect the electrons resulting from 150-kev gamma rays. This field strength is near the residual field of the electromagnet being used. The upper gamma-ray energy limit of 8 Mev is set by the maximum field strength which the magnet will produce. This is about 6000 gauss.

In actual use the magnetic field is controlled by a Halltron semiconductor magnetic flux sensing device. The output of the Halltron is compared with a fixed voltage by a Brown amplifier and the magnet current varied by a servo to produce the desired H.

The momentum spectrum of the recoil electrons produced by a Cs^{137} gamma source as measured with a prototype spectrometer is shown in Fig. 3.51 as a function of magnet current. Calibration is necessary to convert magnet current or H into energy.

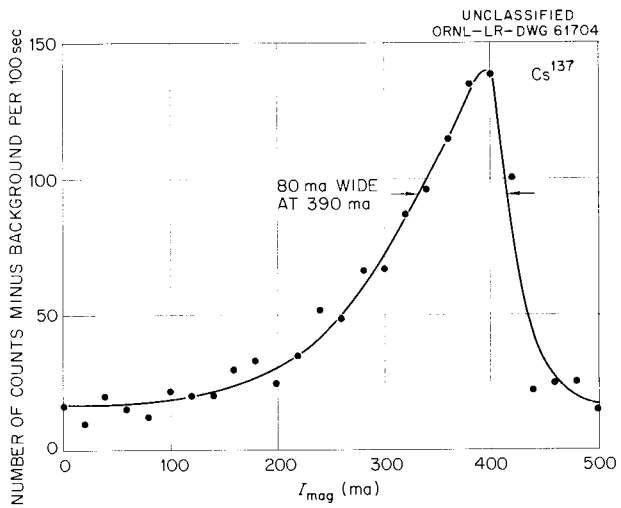

Fig. 3.51. Cs^{137} Response of Prototype Gamma Spectrometer.

Considerable shielding is necessary to reduce the background counts produced by gamma rays directly incident upon the G-M tube. At least 8 in. of lead in the front and 4 in. in the other directions is considered sufficient. For use in a mixed radiation field a neutron shield which consists of 20 in. of borated water surrounding the lead shield must be used. If no neutron shield is used, large numbers of gamma rays will be produced by the inelastic scattering of the neutrons in the lead.

Neutron Spectrometer

In order to measure the low dose rates expected during Operation BREN a fast-neutron spectrometer with greater than usual sensitivity was developed.

The method chosen was based closely on a thick-radiator recoil-proton–fast-neutron spectrometer developed by Mozely and Shoemaker.[59] Their unit utilized one anthracene scintillation crystal as a proton radiator and a second as the proton detector. A resolution of 7% was reported for this device.

Mozely and Shoemaker separated the anthracene crystals with a proportional counter as they found a triple coincidence scheme was necessary to reduce the chance gamma-ray contribution to their measurements. It has since been suggested[60] that such a triple coincidence scheme would not be necessary with the faster electronic and coincidence devices now available which would allow evacuating the chamber between the crystals.

The relatively fast coincidence circuits used in the experimental spectrometer have resulted in a gamma-ray rejection ratio of 100 to 1. This is not high enough for some applications but is quite satisfactory for the BREN experiments where a 1 to 1 neutron to gamma-ray ratio is expected. By tuning the coincidence circuits more carefully, better rejection ratios could be obtained.

The device constructed for field use is shown diagramatically in Fig. 3.52. The photo-multiplier tube which is used is normally supplied without a base and uses a Teflon socket. These precautions reduce the attenuation of the neutron beam before it reaches the proton radiator. The anthracene crystals are 76 mm in diam and 2 mm thick. A glass backing is used for added strength in mounting the crystals. The ridges on the spectrometer wall improve the proton collimation of the device by minimizing the proton scatter from the walls.

In operation the unit feeds the electronic system blocked out in Fig. 3.53. A proton which deposits enough energy in both crystals to produce a pulse in each and large enough to overcome the noise operates a coincidence gate. The coincidence gate signal opens the linear gate of a multichannel analyzer to allow the analysis of the sum of the pulses from the two detectors. Therefore the proton

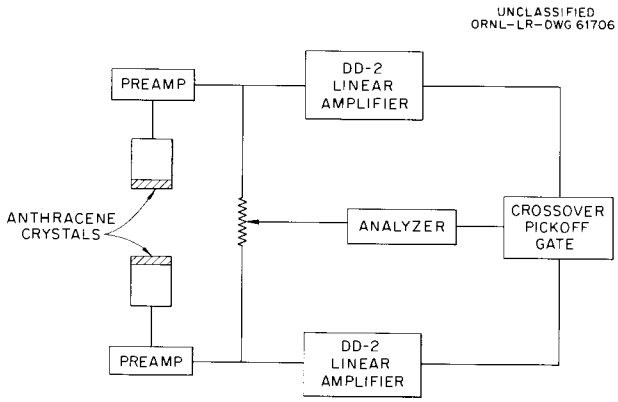

Fig. 3.53. Neutron Spectrometer Electronics.

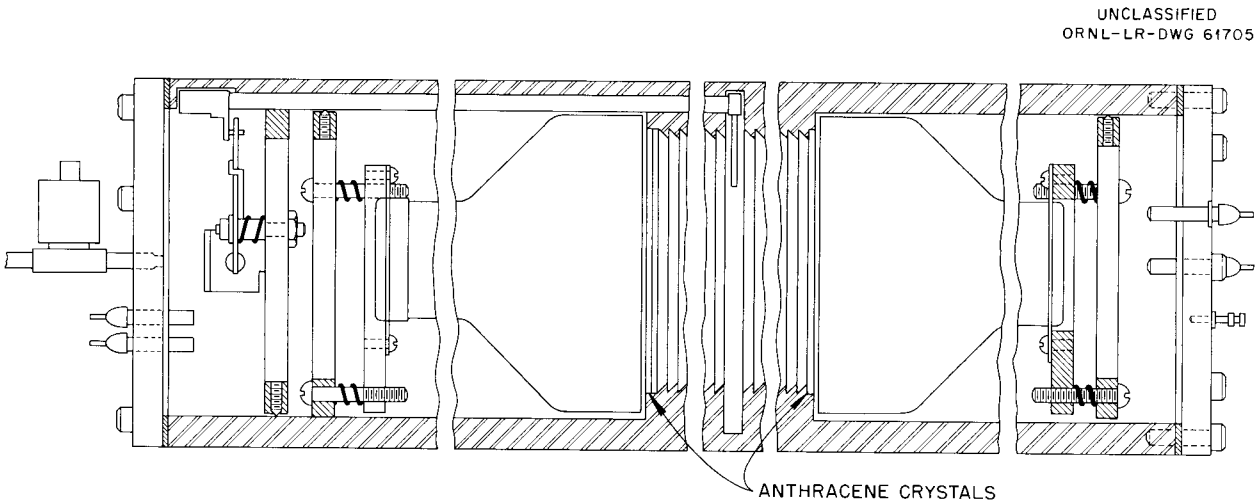

Fig. 3.52. Neutron Spectrometer.

[59] R. F. Mozely and F. C. Shoemaker, *Rev. Sci. Instr.* 23, 569 (1952).

[60] C. H. Johnson, *Fast Neutron Physics* (ed. by J. L. Fowler and J. B. Marion), sec II, chap. C, p 284, Interscience, New York, 1960.

radiator is essentially as thick as the range, in anthracene, of the proton being measured. This produces an increasing radiator thickness with increasing neutron energy with a resulting increase in spectrometer efficiency.

Because this is a recoil-proton–fast-neutron spectrometer the incident neutrons must be collimated. For Operation BREN this will be done with a cylindrical collimator which provides 25 in. of borated water shielding on the sides and has a conical entrance port.

This spectrometer has an energy range from 700 kev to 15 Mev. The lower energy limit is set by the system noise and the statistical limitations of proton detection with scintillation counters. The upper limit is set by the range of protons in anthracene and the thickness of the crystals. The 2-mm thick crystals used correspond to a proton range of 15 Mev. The pulse height vs energy relationship of the spectrometer is nonlinear due to the nonlinear light output of the anthracene crystal as a function of energy.

The basic experimental problem with these units is keeping the over-all gain of the detectors equal. In the field model the gains are balanced by putting the peak from a Pu^{239} alpha source at the same pulse height setting for both detectors. This is done primarily by adjusting the high voltage on the photomultiplier tubes. Another satisfactory method, used in the prototype, is to put the Compton edge from a Cs^{137} gamma source at the same pulse height for both detectors.

As noted briefly before, the efficiency of this spectrometer is a strong function of the incident neutron energy. The efficiency decreases slightly with increasing energy of incident neutrons due to the decreasing neutron collision cross section; the efficiency increases with increasing neutron energy due to the effective increased proton radiator thickness (which is a function of the range of recoil protons in anthracene). The over-all effect is an increase in efficiency.

The expected efficiency of the spectrometer which was built for the field is in the range of 10^{-3} to 10^{-4} counts per neutron. Experimental measurements on a smaller prototype with Van de Graaff and Po-Be neutrons are consistent with this figure.

PHYSICS OF TISSUE DAMAGE

D. R. Nelson

R. D. Birkhoff C. J. Weinberg[61]
J. G. Carter

Emission Spectra of the Low Temperature Thermoluminescence from Gamma-Irradiated Biochemicals

If some materials at low temperatures are irradiated with ionizing radiation, light is emitted when they are subsequently heated. The study of this thermoluminescence reveals the nature and behavior of metastable states in these materials. Of particular interest in radiobiology are radiation induced changes in proteins and their constituent amino acids as revealed by their thermoluminescence spectra.

Many molecules essential to normal biological functioning are extremely complex structures. Nevertheless from considerations of the constraints associated with macromolecular conformations, it has been postulated that excitation energy may become preferentially localized at only a few restricted sites within these structures. Previous investigations were in accord with this prediction.[62,63] However, consider first the thermoluminescence phenomenon in a somewhat simpler compound, NaCl. If a powdered sample of NaCl is irradiated with Co^{60} gamma rays at liquid-nitrogen temperature, light is emitted at a nonconstant rate when the irradiated material is subsequently heated at a linear rate. In fact, if a glow curve is constructed by plotting the intensity of the emitted light vs temperature, it is found that there are nine peaks between 77°K and 300°K. Presumably this indicates that there are a number of potential imperfections in the crystal at which displaced electrons and the corresponding holes can become trapped. This is in contrast to the situation which occurs when biochemicals are irradiated. Past research[62,63] demonstrated that a characteristic glow curve having only one very predominant peak at approximately 120°K is obtained from irradiated crystalline-protein preparations. The glow curves

[61] United States Air Force.

[62] L. Augenstine *et al.*, *Radiation Research Suppl.* 2, 19 (1960).

[63] L. Augenstine, J. Carter, D. Nelson, and H. Yockey, p 149 in *Free Radicals in Biological Systems*, ed. by M. S. Blois, Jr., Academic Press, New York, 1961.

from amino acids have peaks in this general temperature range and are also comparatively simple. That is, under comparable conditions, there are fewer "isolated" peaks in the glow curves from these substances than in those from the alkali halides.

Prior investigations have produced the following results:[64]

1. The thermoluminescence from proteins is apparently not the weighted sum of that from its complement of amino acids.

2. The intensity of thermoluminescence from the amino acids falls roughly into two classes. Those acids containing a ring structure have approximately three orders of magnitude greater intensities than those which do not contain this structure.

3. In the molecular crystals of the amino acids, the chemical structure is much more important in determining the nature of the thermoluminescence than such a gross parameter as the crystal space group.

4. Finally, the effects of purity level are least pronounced in the aromatic amino acids. This was a primary consideration in selecting this type amino acid for the present studies.

The present studies are concerned primarily with determining the spectral distribution of the thermoluminescence from amino acids, the enzyme trypsin, and bacillus megaterium spores and also with improving the estimates of the activation energies.

The procedures by which the glow curves, activation energies, and emission spectra of L-tyrosine, L-phenylalanine, L-tryptophan, trypsin, and spores were obtained are as follows:

The Glow Curves. – Dry, powdered samples of the highest grade purity, commerically available, aromatic amino acids; twice crystallized tryspin; and spores were used. One hundred milligrams of the powdered preparations were placed in brass containers, flushed with dry helium, and sealed under 8 lb of He pressure. The samples were then cooled to liquid-nitrogen temperature and given a dose of approximately 10^6 rads in the ORNL Cobalt Irradiation Facility. Within 24 hr after irradiation, the samples were heated at a linear rate of 12°C/min from 77°K and 300°K, and the emitted light was measured with a liquid-nitrogen cooled 1P21 photomultiplier and accessory circuits. An exposure dose of about 10^6 rads was used in these studies so that the intensity of thermoluminescence was adequate for studies of the spectral distribution. However in previous studies, characteristic glow curves were obtained with doses as low as 240 rads, and the shape of the glow curve was not changed significantly with doses as high as 10^7 rads.[62]

The Activation Energies. – To determine the energy required to release trapped electrons from their metastable energy states, an irradiated sample was warmed at the normal 12°C/min rate until the thermoluminescence achieved a predetermined intensity. It was then quenched by re-emersion in liquid nitrogen and the procedure repeated until a number of initial rise curves had been obtained. Estimates of the activation energies by the method of initial rise curves are based on the assumption that for all types of kinetics, the intensity of thermoluminescence can be expressed in the form of

$$I = F \exp(-E/kT)$$

where

I = intensity,
E = activation energy,
T = temperature in °K,
k = Boltzman's constant.

F is a function of the number of full electron traps and of empty centers, and the transition probabilities involved. F can be taken as constant for the initial part of a glow peak, when the change in the number of trapped carriers and empty centers may be neglected. One then obtains

$$\ln I = -E/kT + \text{constant}.$$

The plotting of $\ln I$ vs $1/T$ should give a straight line, and from the slope of this line E can be readily calculated. Fig. 3.54 shows a series of initial rise curves and their corresponding $\ln I$ vs $1/T$ plots.

Emission Spectra. – Difficulties in spectral analyses were experienced due to the weakness and rapid changes of the luminescence intensity. The system of spectral analysis employed consisted of a series of overlapping bandpass and cutoff filters inserted between the sample and photomultiplier. The photomultiplier output with a filter inserted is then a function of the emission spectrum, filter transmission, and photomultiplier spectral

[64] J. G. Carter, *Low-Temperature Thermoluminescence of the Gamma-Irradiated Amino Acids and Proteins*, ORNL-2970 (Nov. 16, 1960).

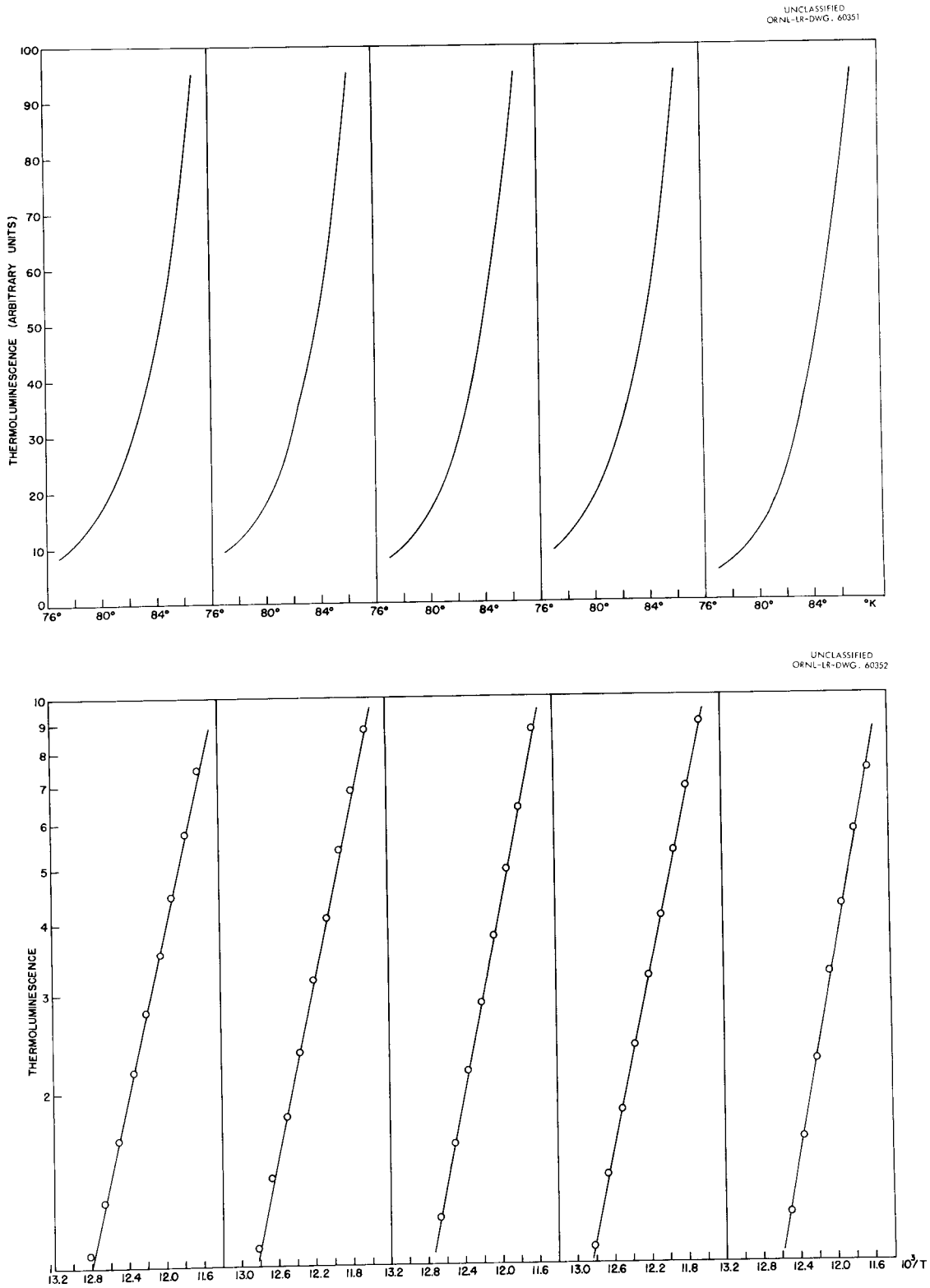

Fig. 3.54. A Series of Initial Rise Curves and Their Corresponding ln I vs $1/T$ Plots.

response. If the spectrum is divided into equal wavelength intervals, and a unique set of filters is chosen, a matrix type solution can be employed. The effective spectral sensitivity region of the tube from 3000 A to 6500 A was divided into 14 intervals 250 A wide, and a series of 13 filters and no filter gave a total of 14 current readings. The spectra were then obtained using a 14 × 14 matrix solution.

Results and Discussion. – The glow curves for tyrosine, tryptophan, phenylalanine, trypsin, and spores are shown in Fig. 3.55. The solid lines are the averages of at least eight glow curves for each substance. The dash lines are drawn through the maximum and minimum values observed and provide an indication of the variability to be expected with the present methods. This variability arises from factors such as spatial distribution of the sample on the bottom of the holder, and slight variations in the dose given to different samples due to the nonuniform radiation field. Table 3.7 gives the temperature at which the maximum intensity of the individual peaks of the glow curves occur and estimates of the activation energies associated with these peaks.

The spectra determined at a variety of temperatures for the five substances are shown in Figs. 3.56–3.60. It is to be emphasized that our choice of filters and phototube restricted our determinations to the spectral region 3000–6500 A. The thermoluminescence spectra are presented at ten degree intervals for the temperature range 77 to 280°K. The ordinate scale is chosen so that each spectrum will have unit area if each 250 A interval has unit width. Thus the contribution within each of these spectral intervals is expressed as per cent of total radiant flux at each temperature. In contrasting one spectrum with another, one compares the relative spectral composition at one temperature with that at another. If the contribution from a certain spectral interval has increased from one spectrum compared to that of another, it does not necessarily mean that the intensity of the glow curve has increased, but rather that the contribution of a particular spectral interval to the total radiant flux has increased. In order to simplify the description of the spectra, each spectral interval will be identified with its average wavelength; but it must be remembered that the resolution is at best only 250 A.

Thermoluminescence Spectra of L-Tyrosine. – The tyrosine thermoluminescence spectra are shown

Table 3.7. Estimates of Activation Energies and Glow Peak Temperatures

Biochemical	Temperature of a Peak of Glow Curve, T_g		Activation Energy,* E_i	
	°K	σ**	ev	σ
Tyrosine	112	1.9	0.16	0.009
	151	3.3	0.25	0.013
Tryptophan	105	4.6	0.19	0.012
	133	6.1	0.25	0.018
	177		0.39	0.013
Phenylalanine	118	2.9	0.22	0.019
	133	2.3	0.29	0.011
	174	1.6	0.31	0.006
Trypsin	122	4.1	0.044	0.009

*Estimated from initial rise curves.

**Standard deviation.

UNCLASSIFIED
ORNL-LR-DWG 60354

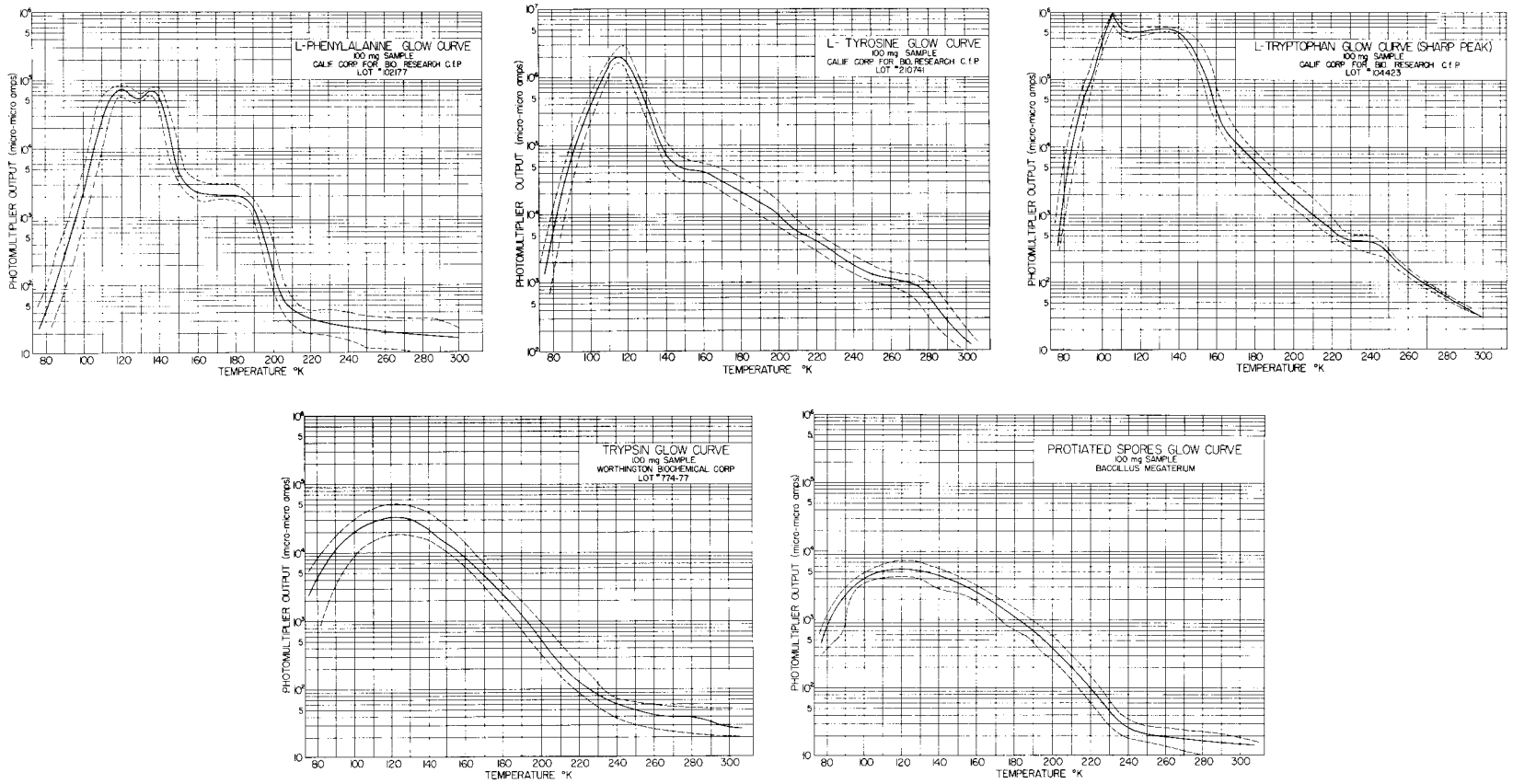

Fig. 3.55. A Composite of the Glow Curves of L-Phenylalanine, L-Tyrosine, L-Tryptophan, Trypsin, and Protiated Spores.

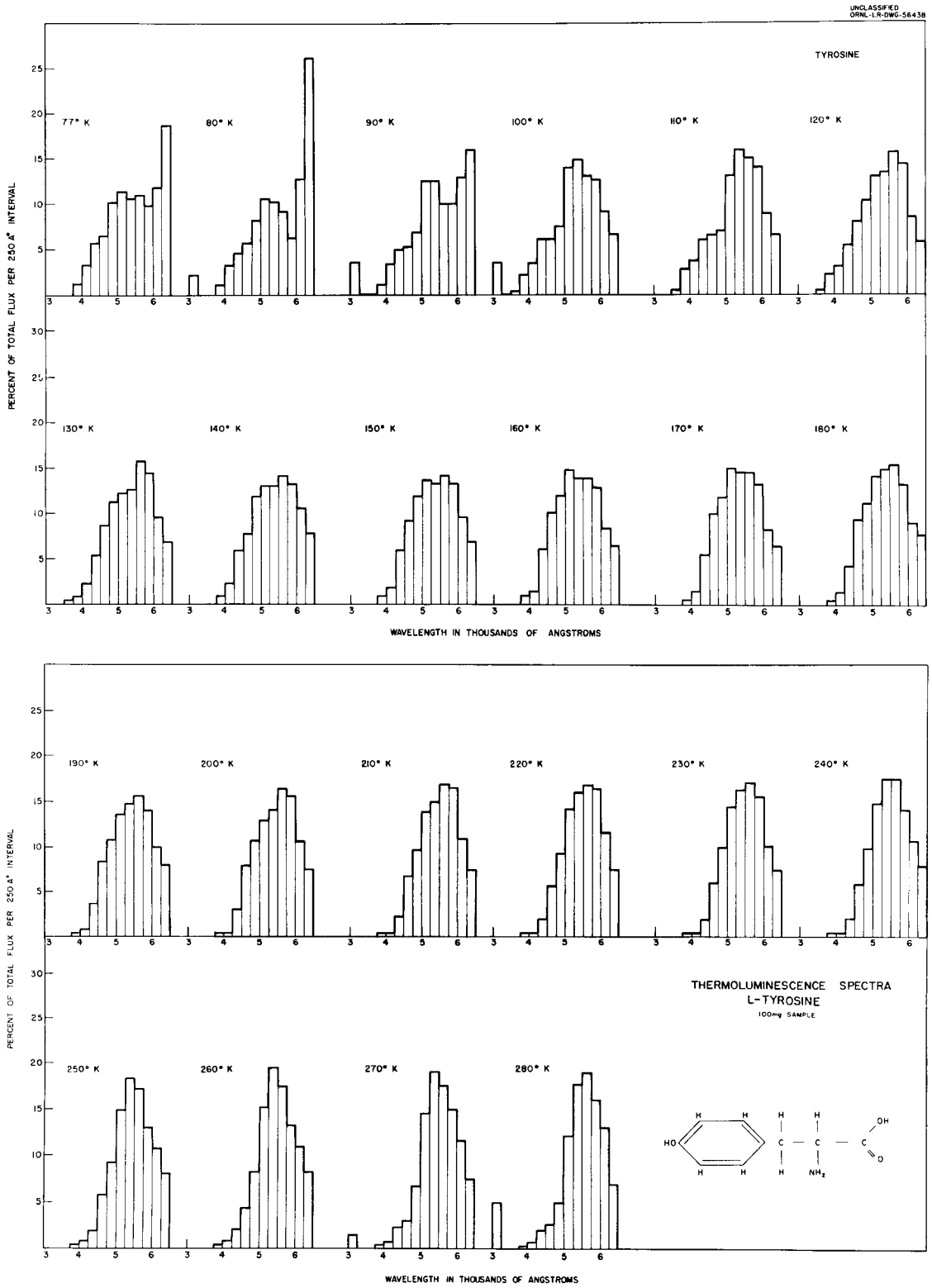

Fig. 3.56. Thermoluminescence Spectra of L-Tyrosine.

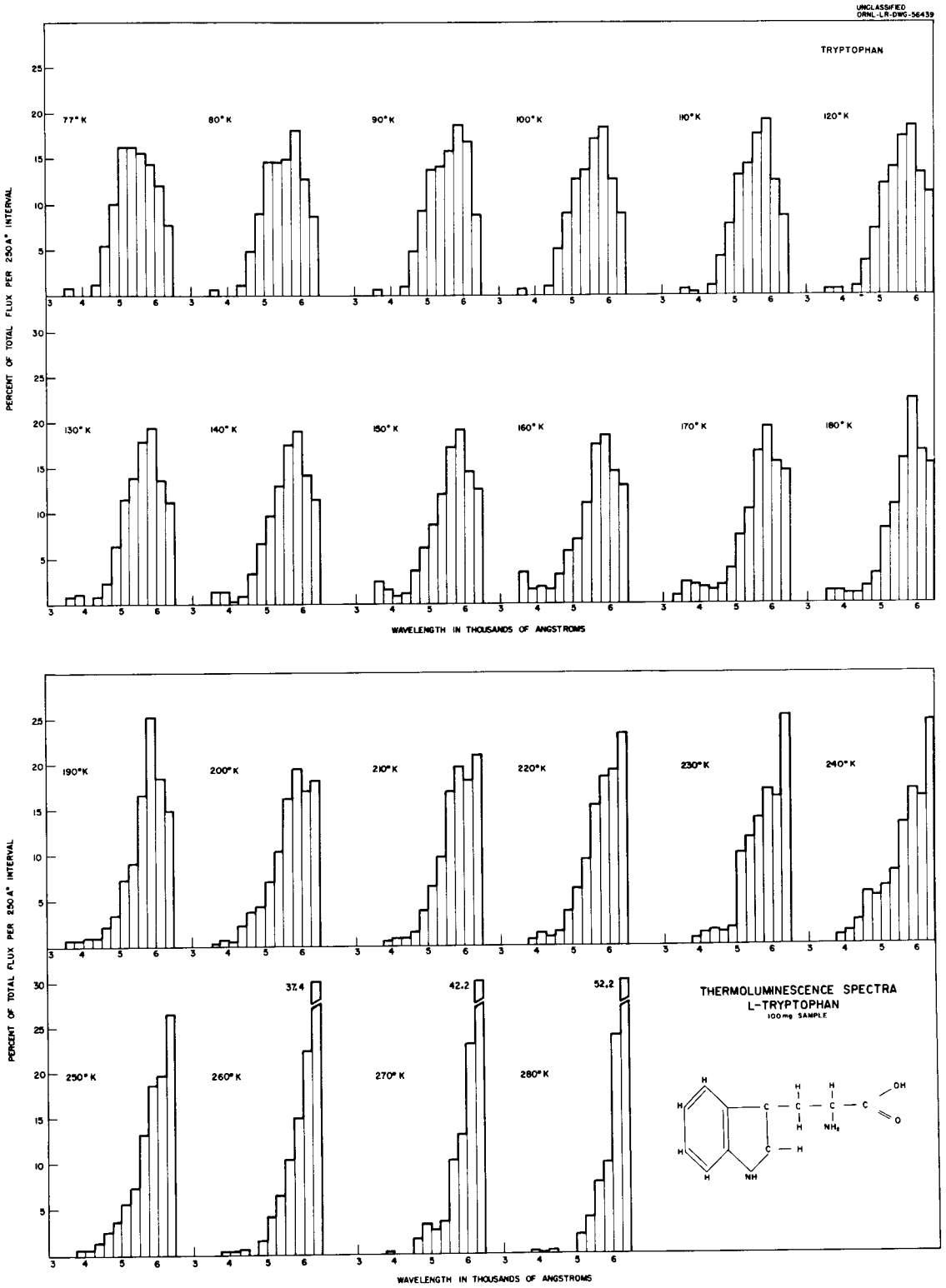

Fig. 3.57. Thermoluminescence Spectra of L-Tryptophan.

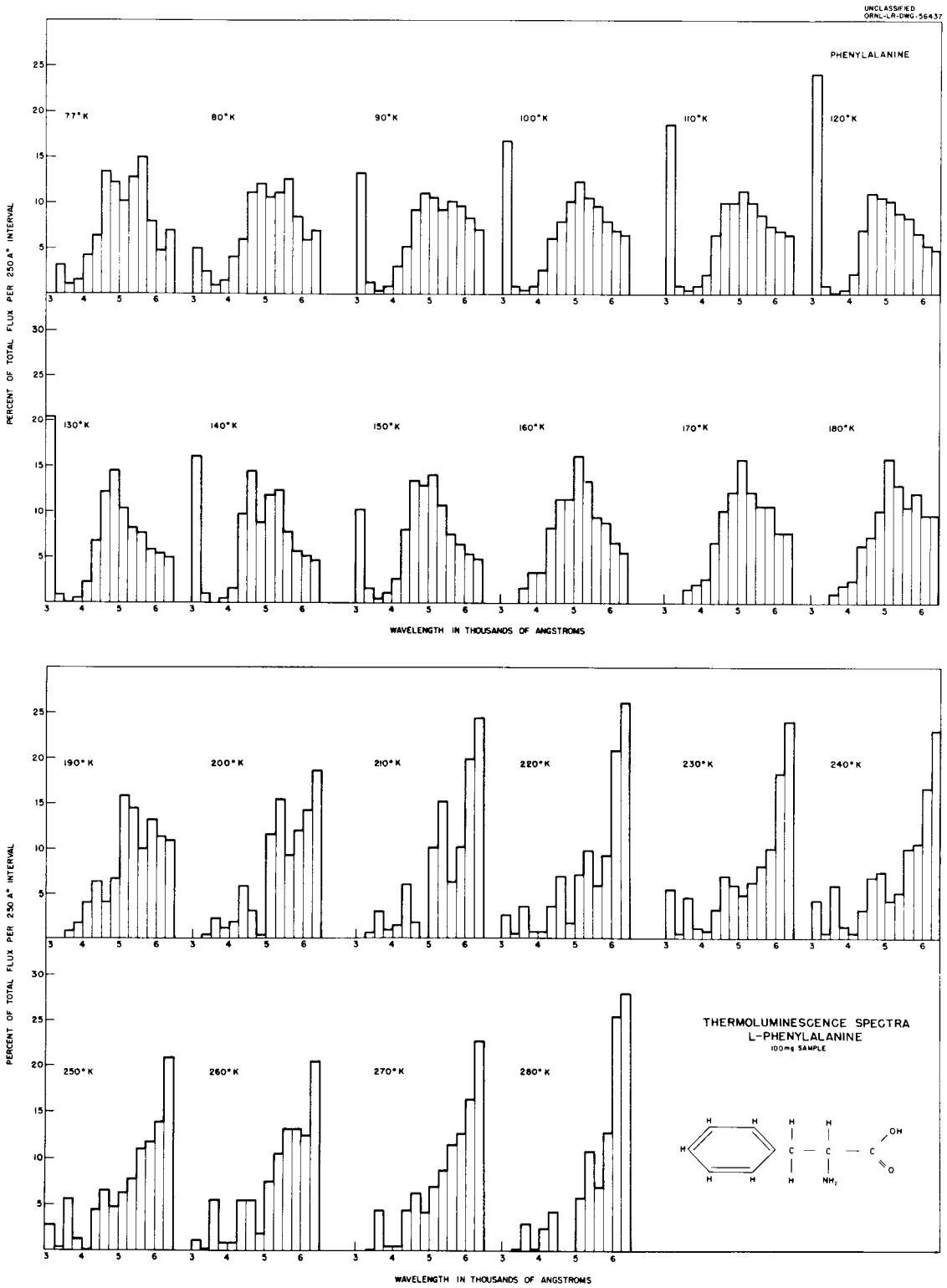

Fig. 3.58. Thermoluminescence Spectra of L-Phenylalanine.

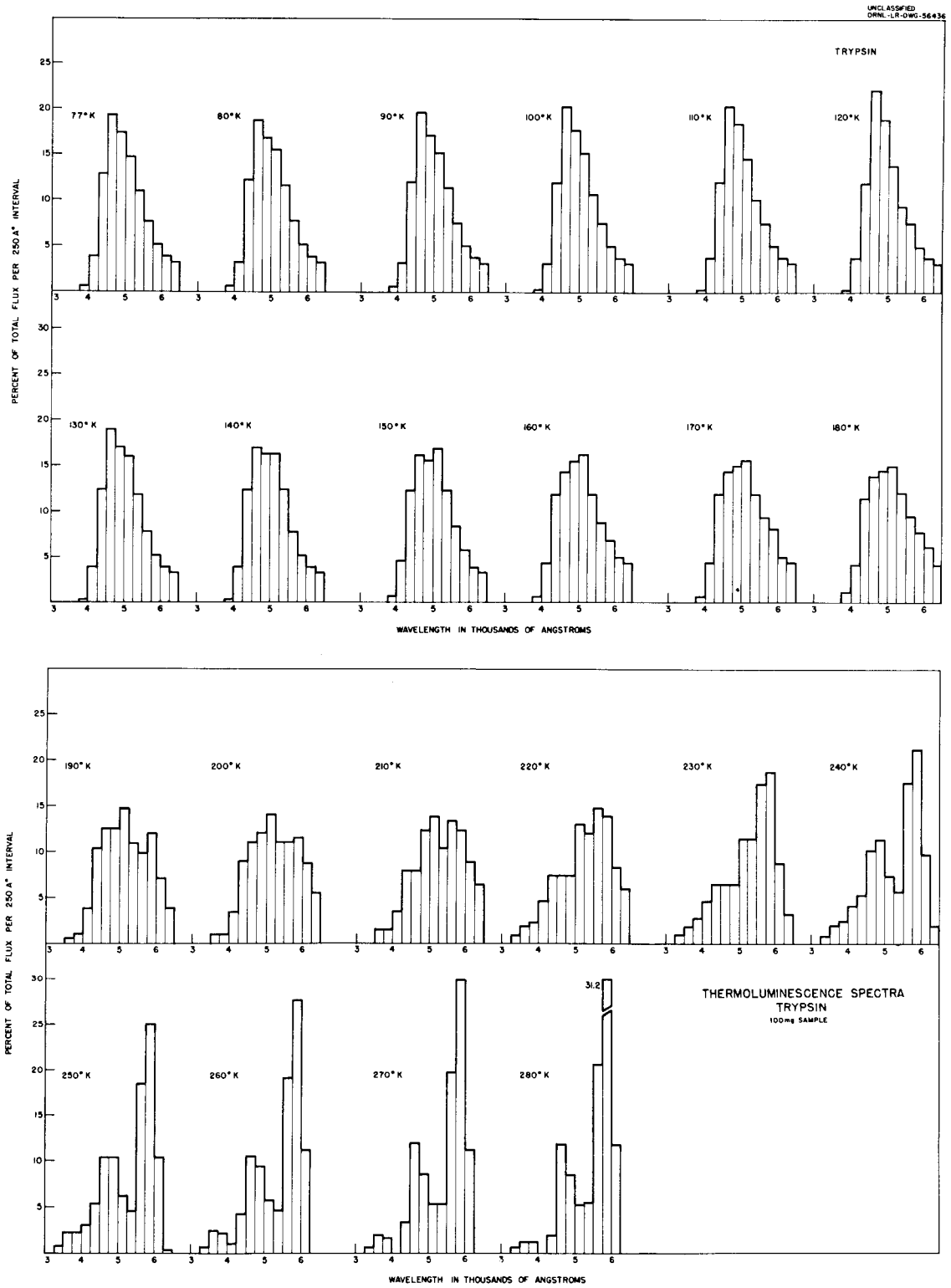

Fig. 3.59. Thermoluminescence Spectra of Trypsin.

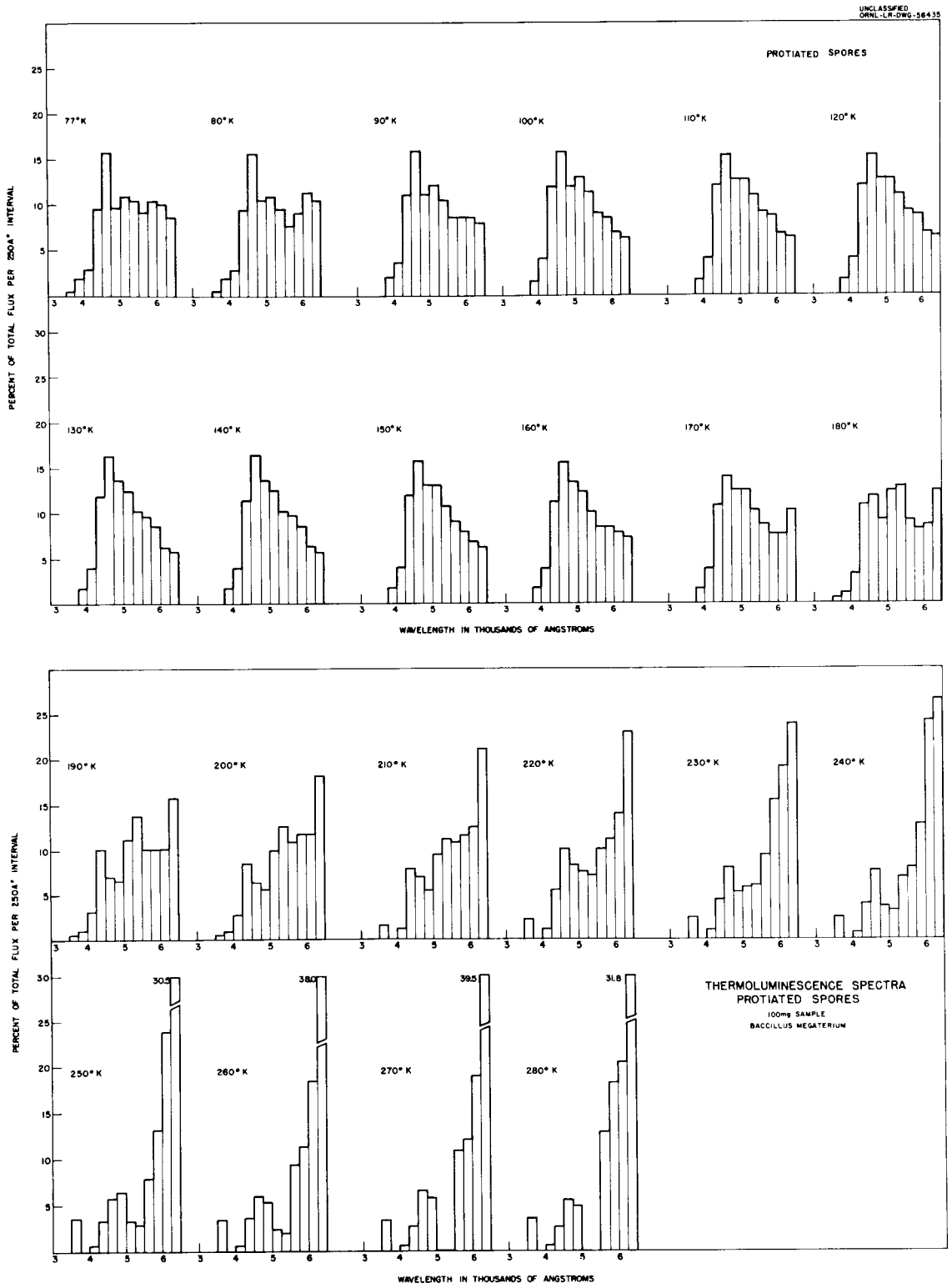

Fig. 3.60. Thermoluminescence Spectra of Protiated Spores.

in Fig. 3.56. It is of interest to note that tyrosine exhibited a glow prior to warmup. Since the time between irradiation and warmup was approximately one to two hours, this would indicate a long-lived low-temperature phosphorescence. This initial glow at 77°K appears to be mostly a broad band between 5000 and 6500 A and does not correspond to the spectrum for long-lived phosphorescence of tyrosine solutions at 77°K reported by Vladimirov.[65] Vladimirov reports the maximum at 4400 A with minor peaks at 4100 and 4600 A.

For the 115°K glow curve peak, the wavelength of greatest emission appears to be approximately 5500 A. The emission at 5125 A apparently corresponds to the glow curve peak at approximately 160°K. An emission at 5375 A begins to appear and reaches a maximum at 260°K. This would correspond to the glow curve peak at approximately 270°K.

Thermoluminescence Spectra of L-Tryptophan. – The thermoluminescence spectra for tryptophan are shown in Fig. 3.57. The correlation between the emission spectra and glow curve peaks is less striking for tryptophan than for tyrosine. The spectrum at 77°K appears to have a broad band emission centered about 5375 A. This is not in agreement with the spectrum for long-lived phosphorescence of tryptophan solutions reported by Vladimirov and Litvin[66] who reported a maximum at 3900 A. For the glow curve peak at 133°K, the major emission appears at 5875 A; and this same component can be noticed in all the spectra from 80 to 250°K. The small glow curve peak at 240°K is due to light emitted at 4625 A. The spectra then shift predominantly to the longer wavelengths until at 280° K approximately 50% of the radiant flux is in the 6375 A interval or longer.

Thermoluminescence Spectra of L-Phenylalanine. – The thermoluminescence spectra of phenylalanine are shown in Fig. 3.58. The initial spectrum at 77°K shows an emission in the near ultraviolet at approximately 4759 and 5625 A. As the sample is warmed, the emission at 3125 A becomes more predominant and reaches a maximum at 120°K. At the same time, there appears a broad emission band at approximately 5000 A. The spectrum appears to be essentially the same for both the 121 and the 136.5°K glow curve peaks. In order to confirm this result, a phenylalanine glow curve was obtained using narrow band interference filters. Three interference filters were used with peak transmissions at 3250, 4550, and 6010 A, and a total width of approximately 100 A at half of the maximum transmission. With all three filters, the characteristic double peaks of phenylalanine were evident. The 3250 A interference filter also confirmed that the ultraviolet component did not contribute to the third peak at 170–180°K. Above 180°K the spectra appear to shift to the red; however from 220°K on, the thermoluminescence is so close to the background of the photomultiplier that the spectra are subject to large errors, and no particular importance can be attached to the appearance of the numerous emission bands.

Thermoluminescence Spectra of Trypsin. – The thermoluminescence spectra for trypsin are shown in Fig. 3.59. Initially the predominant emission is at 4625 A and remains so to 140°K. This temperature range includes the glow curve peak at 122°K, and leads to the supposition that the high initial glow is due to a high probability of escape at 77°K. At 190°K an increased emission in the longer wavelengths appears at 5875 A, and the spectra then shift increasingly to this wavelength as the temperature rises.

Thermoluminescence Spectra of the Spores. – The thermoluminescence spectra for the spores are shown in Fig. 3.60. At 77°K, the emissions appear at 4625, 5250, and 6000 A. The longer wavelength emissions tend to diminish as the glow curve peak at 122°K is approached. The spectra remain essentially constant from 110 to 150°K, with the primary emission at 4625 A, and except for the longer wavelengths, the spectra resemble those of trypsin for the same temperature range. From 180°K on, there is an ever increasing shift to longer wavelengths. For trypsin, this shift was to 5875 A, where for the spores, it was to 6375 A or longer.

Conclusions. – The purpose of this study was the determination of the spectral distribution of thermoluminescence and the activation energies associated with peaks of the glow curves. The light emitted at a temperature corresponding to a maximum in the glow curve was found to have a spectral distribution characteristic of the biochemical at that temperature. In general the spectral distribution shifted to longer wavelengths

[65] Y. A. Vladimirov, *Izvest. Akad. Nauk S.S.S.R.* 23, 1, 85 (1959).

[66] Y. A. Vladimirov and F. F. Litvin, *Biophysics (U.S.S.R.) (English Translation)* 5, 151 (1960).

with increasing temperatures. This is expected if there is a partitioning of the potentially available energy between radiative and nonradiative processes. In the case of trypsin, however, the increase in wave length appears to be greater than can be accounted for by this partitioning. In some instances the appearance of characteristic spectral bands coincided with previously suspected peaks as indicated by inflections in the shape of the glow curves.

The thermoluminescence spectra for trypsin did not bear any obvious or predictable relationship to the thermoluminescence spectra of the aromatic amino acids. It was not a composite of the spectra from its constituent amino acids. This is also the case for the fluorescence and phosphorescence of trypsin, where, due to the transfer of energy among the amino acids, the light emission is dominated by the tryptophan. Tryptophan does not play this role with regard to the thermoluminescence. The thermoluminescence for tryptophan has a spectral distribution above 5500 A at all temperatures, whereas that for trypsin has a much shorter wavelength distribution.

The following statements briefly summarize the results and conclusions of this study.

1. Those electronic rearrangements which are initiated in the interaction of ionizing radiation with trypsin become preferentially localized in a very restricted number of metastable configurations.

2. The thermoluminescence from trypsin is not the sum of independent contributions of the thermoluminescence observed from the isolated constituent amino acids.

3. The thermoluminescence from the molecular crystals of aromatic amino acids is not attributable to those electronic transitions which account for fluorescence and phosphorescence due to ultraviolet excitation.

4. The energy resulting from the decay of the metastable configuration in trypsin may very well appear as tryptophan phosphorescence. Thus the recombination might involve either tyrosine or phenyalanine, and energy transfer to tryptophan would then account for the predominant emission at 4600 A.

5. With increasing temperature, the spectral distribution shifts toward longer wave lengths. The fact that these bands are shifted by as much as 0.6 ev makes it seem somewhat unlikely that this would represent an increasing partition of recombination energy into nonradiative modes.

6. There has been considerable controversy as to whether conduction bands exist in proteins. The present studies do not resolve this question. If such do exist, however, these results indicate that that the conduction and filled bands must be separated by at least 2.7 ev in trypsin.

4. INTERNAL DOSIMETRY

W. S. Snyder

ESTIMATION OF INTERNAL DOSE

Estimation of Pu Body Burdens on the Basis of Urinalysis Data

W. S. Snyder

Urinalysis data provide some of the more reliable and readily obtainable indications that an employee has accumulated a significant body burden of Pu^{239}. The problem of estimating the body burden quantitatively from such data is a very difficult one, and most methods involve a considerable degree of subjectivity. Nevertheless, Lawrence has developed a code[1] for the IBM 704 which provides an estimate of body burden of Pu^{239} from the entire urinalysis data of the employee.

In evaluating urinalysis data at ORNL, two methods of programming this problem were devised; these rest on the same basic assumptions as the work of Lawrence but differ somewhat in the mathematical treatment given the data. The available data are assumed to represent the counts C_i (expressed in dis/min) per 24-hr specimen obtained from n 24-hr urine specimens taken on days t_i, $i = 1, 2, \ldots, n$. In essence, the method of Lawrence assumes a single intake at some intermediate time between successive sample days and subtracts from the count C_i the estimated contributions to this count from all previously estimated intakes. In some cases, the estimated output from previously computed intakes exceeds the actual output, and some data points must be rejected. The methods outlined here do not require the rejection of any data points and consider the intake of Pu to the blood and the urinary output to be continuous functions. The data points are considered as sample values which serve to estimate these continuous functions.

Let exposure begin at time $t = 0$, and let $I(\tau)\,d\tau$ dis/min be the intake of Pu^{239} to the blood in a time interval $d\tau$. According to Langham[2] the urinary excretion of Pu^{239} on the tth day due to a single intake of $I(\tau)\,d\tau$ is $aI(\tau)\,d\tau(t-\tau)^{-\alpha}$ dis/min where $a = 0.0029$ and $\alpha = 0.76$. By integration the total urinary excretion of Pu^{239} on the tth day is then

$$U(t) = a\int_0^t I(\tau)\,(t-\tau)^{-\alpha}\,d\tau\,. \qquad (1)$$

Retention on the tth day following a single intake of a unit amount has been described[3] by

$$R(t) = 0.99t^{-0.01} \qquad (2)$$

or by

$$R(t) = 1 - \frac{bt^{1-\beta}}{1-\beta}\,. \qquad (2')$$

In the formula (2′), $b = 0.0079$ and $\beta = 0.94$; $R(t)$ equals 1 minus the accumulated excretion to the tth day as given by Langham.[2] For continuous intake of $I(\tau)$ dis min^{-1} day^{-1} on the τth day the total retention is given by

$$R(t) = 0.99\int_0^t I(\tau)\,(t-\tau)^{-0.01}\,d\tau \qquad (3)$$

or by

$$R(t) = \int_0^t I(\tau)\left[1 - \frac{b}{1-\beta}\,(t-\tau)^{1-\beta}\right]d\tau\,. \qquad (3')$$

[1] J. N. P. Lawrence, *PUQFUA: An IBM-704 Fortran Code for Determining Plutonium Body Burden from Urine Assays*, LA-2329 (1960).

[2] W. H. Langham *et al.*, *Distribution and Excretion of Plutonium Administered Intravenously to Man*, LA-1151 (1950).

[3] See p 38, "Report of ICRP Committee II on Permissible Dose for Internal Radiation (1959)," *Health Phys.* 3 (1960).

The equations (1) and (3) or (1) and (3′) apply the excretion formulas of Langham[2] or the ICRP formula to the case of a continuous intake function $I(\tau)$.

By simple mathematical procedures it is possible to eliminate the unknown function $I(\tau)$ from (1) and (3) or from (1) and (3′). The most elegant method is by the use of the Laplace transform. Using (1) and (3) one obtains

$$R(t) = \frac{b}{a}\frac{\Gamma(1-\beta)}{\Gamma(1-a)\Gamma(a-\beta)}\int_0^t U(\tau)(t-\tau)^{a-\beta-1}\,d\tau\,, \quad (4)$$

and by using (1) and (3′) one obtains

$$R(t) = \frac{1}{a\Gamma\alpha\Gamma(1-\alpha)}\int_0^t U(\tau)(t-\tau)^{\alpha-1}\,d\tau - \frac{b\Gamma(2-\beta)}{a(1-\beta)\Gamma(1-\alpha)\Gamma(1-\alpha-\beta)}\int_0^t U(\tau)(t-\tau)^{\alpha-\beta}\,d\tau\,. \quad (4')$$

Either (4) or (4′) offers a convenient mathematical formula for $R(t)$. Either formula demands data for $U(\tau)$ as a continuous function of time, and the values of $U(\tau)$ are known only at discrete times t_i, $i = 1, 2, \ldots, n$. Thus it is necessary to regard these as samples of the values of $U(\tau)$ and interpolate from these to the continuous case. Several methods of doing this have been explored. No substantial difference in the estimates has thus far resulted from the several schemes used, and so linear interpolation has been used for the code which programs these formulas for the IBM 7090.

A few cross-checks have been made by analyzing some cases by the method of Lawrence and by the present methods. The checks indicate agreement of the three methods to within 15 to 20% of the permissible body burden of Pu^{239} in most of the cases tried. Other tests are under way. The running time and machine costs per case are trivial.

On the $(MPC)_w$ for Rn^{222} and Its Comparison with Naturally Occurring Levels

S. R. Bernard

Introduction. – Recent measurements of Rn^{222} levels in waters from springs in the area surrounding Oak Ridge by Reynolds *et al.*[4] indicated a concentration range from 0.3×10^{-6} to 0.64×10^{-6} $\mu c/cc$. These levels are not evidently unusual when compared with other measured levels (Table 4.1). Waters from the Clinch River contain less Rn^{222}, while water taken from uranium mines in Canada contains more Rn^{222}.

Since some of the local springs supply drinking water to some towns surrounding this area, the question of whether these measured concentrations are in excess of the $(MPC)_w$ for Rn^{222} or whether these levels may be considered as background has been raised.

The latest publications of ICRP and NCRP do not cite an $(MPC)_w$ for Rn^{222}. However, the earlier publication of NCRP[5] cites a value of 2×10^{-6} $\mu c/cc$ for occupational workers exposed 168 hr per week. This $(MPC)_w$ is derived from consideration of the radiation exposure delivered to the GI tract due to its submersion in water containing Rn^{222}. For exposure of the population NCRP recommends (in Table 2, p 11 of ref 5) a provisional level of 10^{-7} $\mu c/cc$ for an alpha emitter. However, it is stated that this value does not refer to the natural background but to additions to the natural background caused by man.[5] Some of the levels appearing in Table 4.1 are in excess of these NCRP values. Whether these can be considered as natural background is not clear.

It is interesting to compare these levels with the recommendations approved by the State Sanitation Inspection of the USSR.[6] They recommend 10^{-9} curies per liter (1×10^{-6} $\mu c/cc$) for Rn^{222} plus daughters as the maximum permissible concentration in open bodies of water in work rooms. They also stipulate that in waters of subterranean springs utilized for the drinking-water supply system a concentration of only those radioactive elements which are of natural origin is permitted, in a quantity which does not exceed the maximum permissible amounts for open reservoirs. The basis for setting MPC values in the USSR is not

[4] S. A. Reynolds, C. L. Burros, and T. H. Handley, Chemistry Division, unpublished data.

[5] *NBS Handbook 52* (1953).

[6] D. I. Zakutinshie, *Toxicology Problems of Radioactive Materials*, AEC-tr-4031 (1959).

Table 4.1. Rn^{222} Concentrations in Various Spring and River Waters

Range or Average Rn^{222} Concentration (μc/cc)	Source or Origin of Water	Location of Water Body	Reference
$\times 10^{-6}$			
0.3–0.64	Spring	Oak Ridge, Tenn.	*a*
0.036–0.62	Spring	Rochester, N.Y.	*b*
0.166	Bath spa	Bath, England	*c*
0.031	Domesticated tap	Bath, England	*c*
0.003	Thames river	Bath, England	*c*
0.8	Warm and cold springs	Hot Springs, Ark.	*d*
15	Uranium-vanadium-niobium prospect	Hot Springs, Ark.	*d*
100	Uranium mine	Canada	*e*
16.1–25.9	Body of deep, still water	New York	*f*
0.086–24.6	Area containing radioactive anomalies	New York	*f*
0.001–3.1	Surface waters draining parts of Wasatch Mt.	Utah	*g*
0.003	Clinch River	Oak Ridge, Tenn.	*h*

[a]S. A. Reynolds, C. L. Burros, and T. H. Handley, Chemistry Division, ORNL, unpublished data.

[b]J. B. Hursh, *The Radium Content of Public Water Supplies*, UR-257 (1953).

[c]R. B. Jacobi, "The Determination of Radon and Radium in Water," *J. Chem. Soc. 1949*(S), 314.

[d]P. K. Kuroda, P. E. Damon, and H. E. Hyde, "Radioactivity of the Spring Water of Hot Springs National Park Vicinity in Arkansas," *Am. J. Sci.* 252(2), 76–78 (1954).

[e]S. D. Simpson, C. G. Stewart, G. R. Yourt, and H. Bloy, "Canadian Experience in the Measurement and Control of Radiation Hazards in Uranium Mines and Mills," *Health Phys.* 1, 81 (1958).

[f]J. Fresco, E. Hardy and J. Harley, *A Method for the Determination of Rn in Water*, NYO-4664 (1955).

[g]A. S. Rogers, "Physical Behavior and Geologic Control of Rn in Mountain Streams," Publications of U.S. Geological Survey, Bull. 1052-3, pp 187–211 (1958).

[h]L. F. Garcia, "Variations in the Radium and Radon Contents of the Clinch River," master's thesis, Vanderbilt University (1952).

altogether clear, but it would appear from the discussion of the computations of the MPC's that the first consideration is given to somatic effects of the radiation.[6]

ICRP has recently made a set of fairly detailed recommendations for permissible exposure of the population at large on the basis of somatic and genetic effects (Table 4.2). However, these recommendations pertain to the situation of contamination of the surroundings by an industrial source. Whether or not ICRP or NCRP would consider the levels of Rn^{222} in Table 4.1 as the natural background, or even what level for natural background should be chosen, is not clear. If these recommended dose rates (Table 4.2) are employed together with some recent (1957, 1959) experimental data, an $(MPC)_w$ for Rn^{222} plus daughters can be calculated. It is the purpose of this paper to determine this $(MPC)_w$ (with which to estimate the internal radiation exposure) and to compare it with the recommended level of 10^{-7} μc/cc prescribed for an alpha emitter by NCRP,[5] and

Table 4.2. Recommended Permissible Dose Rates (rems/week) for Population Exposure as Given by ICRP and NCRP

Organ	ICRP[a]		NCRP[b]	
	max	av	max	av
Gonads and whole body	0.01	0.001	0.01	0.001
Blood-forming organs	0.01	0.003	0.01	
Bone and thyroid	0.01	0.004	0.01	
Other organs	0.03	0.01	0.03	

[a] *Recommendations of the International Commission on Radiological Protection, 1959*, Pergamon, London, 1960; also see *Report on Decisions at the 1959 Meeting of the ICRP, Health Phys.* 2, 317 (1960).

[b] Addendum to *NBS Handbook 59*, "Permissible Dose from External Sources of Ionizing Radiation" (1958).

with naturally occurring levels. In the following, the considerations leading to the value of 16×10^{-5} μc/cc for occupational workers exposed 168 hours per week or 0.5×10^{-5} μc/cc for the population average are presented. Also, at this level it is indicated that the genetic dose will not be exceeded. The uncertainties in this value are discussed.

Calculated $(MPC)_w$ for Rn^{222}. – We save considerable space and effort by employing Eq. (3) of the ICRP Committee II Report:[7]

$$q = \frac{2.8 \times 10^{-3} mR}{f_2 \epsilon} . \qquad (1)$$

Here qf_2 is the number of μc in an organ of mass m grams which receives an RBE dose rate of R rems/week from a contained radionuclide whose effective energy is ϵ Mev per disintegration. Letting ϵ = 200 Mev for Rn^{222} plus daughters from Table 5*a* of ref 7 and rearranging (1), we find

$$\frac{qf_2}{m} = 1.4 \times 10^{-5} R , \qquad (2)$$

or the number of μc/cc in the organ assuming a density of 1 g/cc which produces an RBE dose rate of R rems/week. When R = 0.1 rem/week,

$$\frac{qf_2}{m} = 1.4 \times 10^{-6} \mu c/cc . \qquad (3)$$

If one makes the general assumption that the Rn concentration in the body organs will equilibrate with the concentration in the drinking water, then from (3) a concentration of 1.4×10^{-6} μc/cc in drinking water would deliver 0.1 rem/week to the body. This assumption is not tenable, however, in view of the fact that radon concentrates in fatty tissues, and it does not include the elimination of radon from the body by exhalation. To include these factors we assume that, in the steady state, the daily rate of intake of Rn^{222}, denoted by 2200 $(MPC)_w$, is balanced by the daily rate E of elimination by body elimination processes, plus the rate $\lambda_r q$ of radioactive decay processes (where λ_r is the radiological decay constant and q is the μc in the total body). Thus we may write

$$2200\ (MPC)_w = E + \lambda_r q . \qquad (4)$$

The rate E can be eliminated from this equation with the data cited by Turner *et al.*[8] From some early (1920) data reported by Meyer,[9] it is estimated that the half-life of radon in the body is ~1 hr. Turner *et al.* estimate that 0.75% of the ingested radon undergoes complete disintegration in the body. Rounding this off to ~1%, we see that 99% of the radon entering the body escapes by elimination processes.

Thus, setting $E = 0.99[2200\ (MPC)_w]$ in (4), using $\lambda_r = 0.693/3.8\ day^{-1}$, and rearranging, we find

$$(MPC)_w = 8.3 \times 10^{-3} q\ \mu c/cc . \qquad (5)$$

From (2) and (5) we obtain

$$(MPC)_w = 1.2 \times 10^{-7} \frac{mR}{f_2} . \qquad (6)$$

The value of R to be substituted in (6) depends upon the f_2 value. The $(MPC)_w$ for radon must be computed for those organs and tissues listed

[7] "Report of ICRP Committee II on Permissible Dose for Internal Radiation (1959)," *Health Phys.* 3 (1960).

[8] R. C. Turner, J. M. Radley, and W. V. Mayneord, "Naturally Occurring Alpha-Activity of Drinking Waters," *Nature* 4, 348 (1961).

[9] S. Meyer, Mitt. Des Institutes fur Radium Forshung, No. 238, Wien, 1929.

in Table 4.2, and the $(MPC)_w$ value must afford protection to all of the tissues.

The value of f_2, the ratio of the concentration of radon in an organ to that in the total body, can be determined from the experimental data of Nussbaum.[10] He measured the solubility coefficient, α', of radon in organs and tissues of rats after inhalation of radon-contaminated air. He extrapolates these values to man. Since α' is defined to be the $\mu\mu$c per ml of tissue divided by the $\mu\mu$c per ml of air, then if α'_x denotes the coefficient for organ x while $V_x\alpha'_x$ denotes the total $\mu\mu$c of radon per unit concentration (1 $\mu\mu$c/ml) in air in organ x whose volume or mass = V_x, f_2^x is given by

$$f_2^x = \frac{\alpha'_x V_x}{\alpha'_x V_x + \alpha'_y V_y + \ldots} . \qquad (7)$$

Inserting Nussbaum's α' values (from Table 33, page 135, ref 10) into (7) together with the appropriate values for V, we obtain

$$f_2 = 0.71 \text{ for fat}$$
$$= 0.11 \text{ for yellow marrow}$$
$$= 1.1 \times 10^{-4} \text{ for testes.}$$

Since fat concentrates more radon than other tissues, it is not necessary to determine f_2 for other organs. Inserting the f_2 values together with appropriate values for R and m into (6), we obtain the $(MPC)_w$. Table 4.3 presents the $(MPC)_w$ for occupational workers, while Table 4.4 presents the population $(MPC)_w$ values based on the average dose rates appearing in Table 4.2.

As can be noted from Tables 4.3 and 4.4, the value based on yellow marrow is lowest and thus affords protection to all the tissues. In Table 4.4 it is noted that the value of 5.0×10^{-6} μc/cc is higher than some of the "naturally" occurring levels appearing in Table 4.1.

Since Rn^{222} has the long-lived (7000-day) daughter Pb^{210} in its decay chain, we must determine whether or not the Pb^{210} level in the body will exceed the maximum permissible body burden. The number of atoms, N, of Rn^{222} entering the bloodstream each day is

Table 4.3. $(MPC)_w$ for Occupational Workers Exposed for 168 Hr Per Week

Organ	f_2	m (g)	R (rem/week)	$(MPC)_w$ (μc/cc)
				$\times 10^{-4}$
Fat	0.71	10^4	0.3	5.1
Yellow marrow	0.11	1500	0.1	1.6
Testes	1.1×10^{-4}	40	0.1	420

Table 4.4. Population $(MPC)_w$ Values Based on Average Permissible Dose Rates (See Table 4.2)

Organ	f_2	m (g)	R (rem/week)	$(MPC)_w$ (μc/cc)
				$\times 10^{-6}$
Fat	0.71	10^4	0.01	16
Yellow marrow	0.11	1500	0.003	5
Testes	1.1×10^{-4}	40	0.001	42

and, since 99% of these atoms will be eliminated by the body, only 1% will be converted to Pb^{210}. Hence, the number of μc of Pb^{210} produced in the body each day will be

$$\frac{N \dfrac{0.693}{7000} \text{day}^{-1}}{3.7 \times 10^4 \cdot 3600 \cdot 24 \cdot 100}$$
$$= \left(\frac{2200}{100}\right)\left(\frac{3.8}{7000}\right)(MPC)_w \ \mu\text{c of } Pb^{210} \text{ per day} .$$

Letting $(MPC)_w = 1.6 \times 10^{-5}$ μc/cc (ref 7), we obtain

$$\mu\text{c of } Pb^{210}/\text{day} = 1.9 \times 10^{-5} .$$

[10] E. Nussbaum, *Radon Solubility in Body Tissues and in Fatty Acids*, UR-503 (1957).

$$N = \frac{2200(MPC)_w \ \mu\text{c/day} \cdot 3.7 \times 10^4 \dfrac{\text{dis/sec}}{\mu\text{c}} \cdot 3600 \text{ sec/hr} \cdot 24 \text{ hr/day}}{0.693/3.8 \text{ day}^{-1}} ,$$

Now the permissible Pb^{210} daily intake into the blood is

$$2200(10^{-6})(0.08)\ \mu c/day = 18 \times 10^{-5}\ \mu c/day\ ,$$

where 10^{-6} is the $(MPC)_w$ for Pb^{210}, 0.08 is the fraction absorbed from the GI tract into the blood, and 2200 is the daily water intake.[7] As can be noted, the Rn^{222} will not produce an excess body burden of Pb^{210}, because the daily intake due to ingestion of Rn^{222} is less than the permissible intake for Pb^{210}.

Discussion and Conclusions. – Admittedly the $(MPC)_w$ lacks the desired certainty because of an inadequacy of experimental measurements on man. There are two interesting points for concern in regard to the uncertainty in the $(MPC)_w$ for Rn^{222}. The first has to do with the fact that Nussbaum finds that the ratio of radon concentration in fat to that in water is ~42, lower by a factor of ~3 than the ratio of ~125 reported in the earlier (1910–1930) literature.[11] Nussbaum mentions this in his report and is at a loss to explain it. The second has to do with the assumption of Nussbaum and Hursh[12] that equilibrium of radon in fat with that in air occurs in ~24 hr. When radon solubility coefficients in fat (α') are plotted vs time on semilog paper as done by Hursh and Nussbaum,[12] equilibration appears to occur at 24 hr. If these same measurements are plotted on log-log paper (Fig. 4.1) the measurements follow the equation $3.5t^{0.072}$ (t in hours), and the concept of equilibration is less easy to defend. With this relatively slow increase, extrapolation to 50 years, which extrapolation is admittedly dangerous, yields $\alpha' = 9.2$, different from the "equilibrium" value of 4.83 by only a factor of ~2. This relatively slow increase might be due to some metabolic process of the experimental animal – rat. It is possible that α' for man may increase this slowly too. Needless to say, there is a need for human data.

In conclusion it would appear that the value $5 \times 10^{-6}\ \mu c/cc$ of Rn^{222} of water can be suggested for the Rn^{222} $(MPC)_w$ but pending more reliable data on human beings. It can be said that some naturally occurring Rn^{222} concentrations are in excess of this $(MPC)_w$.

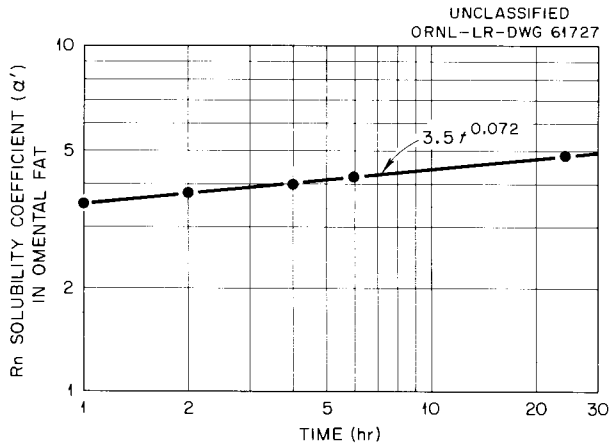

Fig. 4.1. Log Plot of Rn Solubility Coefficient (α') vs Time.

$(MPC)_a$ for Insoluble Ra^{226} Compounds

S. R. Bernard

An $(MPC)_a$ for insoluble Ra^{226} compounds based on lung as the organ of reference has been determined.[13] In calculating this $(MPC)_a$ it is necessary to assume a value for retention of Ra^{226} daughters in the tissue, because the effective energy per disintegration depends on the retention.

In experimental studies with dogs and from the data obtained on human beings who have long-term, skeletal-stored radium, a value of 30% retention has been observed.[14] If this value is assumed to apply to the case of lung-stored Ra^{226}, the effective energy (ϵ) is 110 Mev per disintegration and the $(MPC)_a$ is $5 \times 10^{-11}\ \mu c/cc$ (40-hr week). This might be considered to be a conservative value, because in bone the remodeling process and the resulting formation of new bone crystals produce conditions favoring a diffusion lock of radon, thereby increasing the retention. Actually, the retention at one day after injection is ~4%, and only after a considerable period (~2 decades) it takes on the value of 30%. If we

[11] As cited in *Medical Physics*, vol 3, p 21, Yearbook Publishers, Chicago, 1960.

[12] E. Nussbaum and J. B. Hursh, "Radon Solubility in Rat Tissues," *Science* 125(22), 552 (1957).

[13] S. R. Bernard and M. R. Ford, "Note on the ICRP and NCRP Recommended $(MPC)_a$ for Insoluble Ra^{226} Compounds," *Health Phys.* 4, 307 (1961).

[14] C. M. Mays *et al.*, "Radon Retention in Radium-Injected Beagles," *Rad. Res.* 8, 480–89 (1958).

determine the $(MPC)_a$ based on lung assuming 0% retention, then $\epsilon = 49$ Mev and the corresponding $(MPC)_a = 1 \times 10^{-10}$ $\mu c/cc$.

STABLE ELEMENT METABOLISM BY MAN

The Spectrographic Determination of Trace Elements in Human Tissue

S. R. Koirtyohann C. Feldman

Introduction. – The tissue analysis program which was carried out in the past by I. H. Tipton at the University of Tennessee has been transferred to the Analytical Chemistry Division of the Oak Ridge National Laboratory. The facilities for tissue ashing and those for the trace element determinations have been consolidated in one building, and the techniques described here are being used to expedite analysis. A more detailed report of these techniques has been made previously.[15]

Sample Preparation. – Before analysis, tissues were dissected to remove excess fat and connective tissue and then dried in silica dishes at 100°C for 24 hr. Samples too large to be ashed conveniently (> ~ 80 g) were cut into small cubes (~1 cm) and mixed. A 40-g sample was then taken for drying and ashing.

In order to reduce the quantity of tissue which must be ashed, a method has been developed for pulverizing dried tissue on an impact shaker. This pulverized material can be thoroughly mixed and a small (~1 g), but representative, sample then taken for ashing. Smaller samples ash more rapidly and greatly increase the sample capacity of the furnaces.

After drying, the samples were weighed and placed in a cold furnace which was provided with a stainless steel liner. A quartz plate was suspended about $\frac{1}{8}$ in. above the tops of the dishes to further reduce the danger of contamination. The furnace temperature was raised slowly (overnight) to 350°C, allowed to remain at 350°C for 4 to 6 hr, and then raised slowly (~10 hr) to 450°C. Ashing is normally completed in about 24 hr at 450°C. The ash was then weighed and prepared for spectrometric analysis. Tissues can be processed (dissected, dried, and ashed) at the rate of about 1.4 samples/man hr.

Odor Elimination. – The tissue preparation facility is located in the main research building at ORNL, which necessitates reliable control of the disagreeable odors created by the drying and ashing processes. This problem has been solved by completely oxidizing the odorous materials. The oxidation was performed by passing the fumes through a gas flame or an electrical resistance heater before exhausting them.[16]

Cross-Contamination. – Trace element concentrations in the various tissues are known to vary widely. Since the same silica dishes are used for many different samples, it was necessary to assess the danger of cross-contamination through the dishes. A sample of liver was ashed and the dish cleaned in the normal way (washed, soaked in a HNO_3-H_2SO_4 bath, soaked in a Na_2EDTA solution, and rinsed with deionized water). Ten grams of ammonium bisulfate (NH_4HSO_4) were then fused in the dish.[17] This salt was then vaporized at ~250°C and the residue dissolved and examined spectrographically by porous cup exposure. From this preliminary experiment, no evidence was found that any sample constituents which could be removed by NH_4HSO_4 fusion remained after the routine cleaning of the dish.

Spectrometric Examination of the Ash. – *Instrumentation.* – The instrument used for this work was a 1.5-m Applied Research Laboratories Industrial Research Quantometer with 32 fixed and 9 movable receivers. Any 32 of the channels can be used simultaneously. Fixed receivers were set for lines of Cd, As, Mg, Pb, Si, Fe, Al, Sn, Cu, Zn, Zr, Ni, Co, Mn, Sr, Cr, Ca, Ba, Na, Bi, Mo, V, Ti, and Ag. In general, the most sensitive arc lines for each element were employed. The movable receivers were used for special problems.

Preparation of Standards. – Pure KH_2PO_4, NaCl, MgO, $CaCO_3$, and Fe_2O_3 are required for the preparation of a synthetic soft tissue ash. Reagent grade KH_2PO_4 and NaCl were found to be sufficiently pure. Ether extraction was used to purify iron for the Fe_2O_3. Pure MgO was prepared from resublimed magnesium metal. $CaCO_3$ free from

[15] S. R. Koirtyohann and C. Feldman, "The Spectrographic Determination of Trace Elements in Human Tissue," *Analytical Chemistry in Nuclear Reactor Technology*, Fourth Conference, Gatlinburg, Tenn., Oct. 12–14, 1960, TID-7606, p 56.

[16] The use of combustion to eliminate odors was suggested by R. G. Pickard, Central Scientific Co., Chicago, Ill. (private communication).

[17] C. Feldman, *Analytical Chemistry* 32, 1727 (1960).

Sr and Ba was prepared by precipitating the Ca from alcoholic solution with 8-hydroxyquinoline, as described by Mitchell.[18] The purified $CaCO_3$ contained about 2 ppm Sr and less than 5 ppm Ba, compared with 250 ppm Sr and approximately 50 ppm Ba in the starting material.

The synthetic soft tissue ash consisted of 67% KH_2PO_4, 25% NaCl, 3.6% MgO, 3.0% $CaCO_3$, and 1.4% Fe_2O_3. These materials were mixed and heated at 500°C for 24 hr, after which they were thoroughly ground and used as a matrix for the standards.

A trace element mix was prepared which contained the trace elements to be determined (as the element or oxide in most cases) in the approximate proportions in which they are found in tissue ash. Portions of this mix were fused with 1 g of $K_2S_2O_7$ to provide greater homogeneity than could be achieved by dry grinding. The fusion cakes (one for each standard concentration) were ground and mixed with synthetic tissue ash to make 10 g of standard. Standards were prepared with trace element concentrations in the ratios of 0, 1, 3, and 5. Maximum concentrations of trace elements ranged from 25 ppm for Ag to 7500 ppm for Zn.

Exposure Conditions. – Samples and standards were mixed, using plastic vials and the mechanical shaker, with graphite and NaBr to give an arcing mixture consisting of ⅓ tissue ash, ⅓ graphite, and ⅓ sodium bromide. The buffer mixture contained 0.01% Pd to serve as the internal standard. The arcing mixture was loaded into a carbon electrode using a mechanical loader.[19] The filled electrodes were heated at 350°C for 1 hr just prior to the exposure to remove any adsorbed moisture from the arcing mixture. Exposures were made using an arc current of 11 amperes dc with the sample contained in the anode. The initial electrode spacing was 3 mm; the gap is not adjusted during the exposure. Arcing was continued until all the sample was consumed, which required about 75 sec. A Stallwood jet, operated with 8 liters/min of He and 2 liters/min O_2, was employed.

The Stallwood jet, which is frequently used to reduce selective volatility in mineralogical analysis,[20,21] was employed here primarily to increase arc stability. The use of helium and oxygen in the jet, rather than air, aids in reducing general background intensities and practically eliminates cyanogen bands.

Instrument Calibration. – Exposures were made of several standards which contained appropriate concentration ranges of the desired trace elements. Working curves consisted of a linear plot of scale deflection (corrected for variations in internal standard intensity) vs concentration in the ash. Figure 4.2 shows a typical working curve.

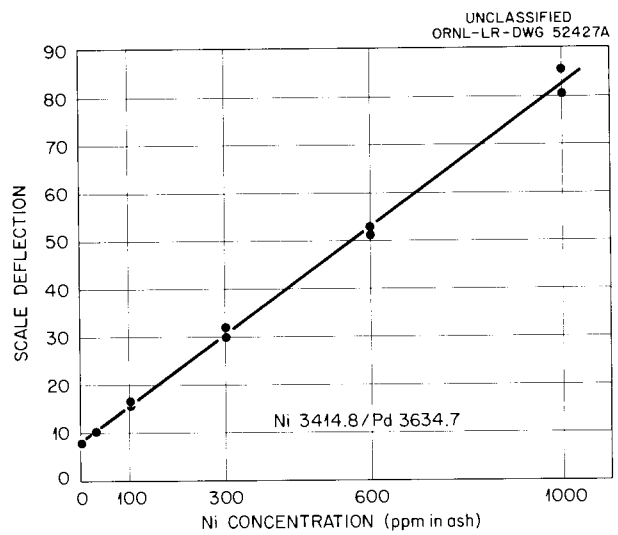

Fig. 4.2. Analytical Curve for Determining Nickel in Tissue Ash with Quantometer.

Precision and Sensitivity. – The precision figures given in Table 4.5 were calculated from 9 exposures of a standard containing 30% of the maximum concentration (top of the working curve) for each trace element.

The detection limits given in Table 4.5 were arbitrarily taken as the concentration giving a total signal of 1.5 times background. The validity of this figure as a detection limit depends, of course, on the observed variability of background intensity at a given wavelength from one exposure to the next. Such variations have amounted to approximately ±4 to 8% for replicate exposures of a given

[18] R. L. Mitchell, "The Spectrographic Analysis of Soils, Plants, and Related Materials," *Commonwealth Bur. Soil Sci.*, p 129, Tech. Comm. No. 44 (1948).

[19] A. Strasheim and E. J. Tappere, *Appl. Spec.* 13, 12 (1959).

[20] D. M. Shaw *et al.*, *Anal. Chim. Acta* 22, 398–400 (1960).

[21] B. J. Stallwood, *J. Opt. Soc. Am.* 44, 171–6 (1945).

Table 4.5. Sensitivity and Precision for Trace Elements

Detection limits arbitrarily taken as concentrations giving a total signal 1.5 × background

Element	Line	Detection Limit (ppm in ash)	Photographic Detection Limit (ppm in ash)	Coefficient of Variation (Element/Pd 3634.6)
Ag	3382.9	1.5	0.5	6.0
Al	3082.2	14	3	1.5
Ba	4554.0	3.5		2.1
Be	3130.4		1	7.0
Bi	3067.7	9	5	4.4
Cd	2288.0	7	5	6.4
Co	3453.5	6	2	2.9
Cr	4254.3	6	1	5.3
Cu	3274.0	~2	<1	9.4
Mo	3132.6	5	2	4.0
Mn	4030.8	5	2	3.3
Nb	4058.9		20	6.3
Ni	3114.8	9	2	4.7
Pb	2833.1	26	5	6.1
Sn	2840.0	27	4	5.3
Sr	4077.7	1	0.2	4.7
Ti	3361.2	11	5	1.8
V	3102.3	7	4	3.4
Zn	3345.0	150	50	6.8
Zr	3392.0		5	4.8
			Mean	4.8

sample or standard. Larger background variations (±15 to 20%) have been observed between different samples. It therefore seems reasonable to attribute any signal which is 50% above the normal background for that wavelength to the actual presence of the element in question.

Photographic Work. – Detection limits are, in general, about a factor of 3 lower when photographic light detection is used in place of the Quantometer. A photographic exposure was made of each sample on a 1.5-m Applied Research Laboratories Spectrograph. This allowed estimation of the concentrations of elements that are detectable photographically but not with the Quantometer. Semiquantitative estimates (±2X) of these values were obtained by visual comparison with standards.

Results. – The brain, heart, and diaphragm samples from 28 autopsies from San Francisco have been analyzed. The results are presented in Tables 4.6, 4.7, and 4.8.

Future Work. – Future plans for the program include completion of the development of a method for the determination of trace elements in bone, development of a method for the determination of the major constituents (Na, Ca, Mg, P, Fe) in the samples, and work to determine whether or not some trace elements are lost during ashing.

Table 4.6. Trace Element Concentrations in San Francisco Brain Samples

(Numbers in parentheses are semiquantitative estimates from photographic exposures)

ORNL Sample No.	Autopsy No.	Per Cent of Wet Sample Wt.		Concentration (μg per g of ash)														
		Dry	Ash	Co	Cu	Ni	Cr	Pb	Al	Mn	Mo	Sn	Ti	Sr	Ag	Bi	Zn	Cd
300 Br	M2062	24.9	1.4		490	(5)		(5)	14	19				2.8	2.4		1300	13
301 Br	M2063	27.6	1.5		450	(5)		(5)	(10)	21			(5)	3.0	(2)		1000	7
302 Br	M2075	25.9	1.9	8	350	(5)		(5)	14	12				2.9	(1)		1000	16
303 Br	M2076	22.9	1.4		460	63		1170	44	27				22.	2.5	12	1600	14
304 Br	M2077	27.9	1.4		610	(3)	(2)	(5)	26	23	(2)		(10)	3.1	(1)		1200	14
305 Br	M2081	29.7	1.7		340	(5)		(5)	14	12			(5)	2.8	(2)		950	11
306 Br	M2082	32.3	1.3		640			460	25	24				3.2			1200	10
307 Br	M2085	23.9	1.3	(2)	470	(5)		(5)	(10)	18	(5)		(5)	3.0	(1)		1700	21
308 Br	M2098	40.6	2.2		470	(3)		(5)	15	22	(5)		(5)	4.3	(1)		1100	10
309 Br	M2099	26.1	1.4		390	(2)	(2)	(5)	(10)	15	(2)		(5)	8.9	(0.5)		1200	11
310 Br	M2107	26.3	1.4	11	610	(2)	(1)	(5)	17	26	(2)			5.3	(1)		1200	11
311 Br	M2108	25.2	1.3		760	(5)		(5)	(20)	53	(2)		(5)	3.6	(1)		1200	10
312 Br	M2122	38.9	1.4		490	(2)		(5)	16	17				2.6	(1)		1000	8
314 Br	M2125	25.1	1.3		450	(2)		(5)	13	20	(4)	(4)	(5)	3.3	(2)		1300	11
315 Br	M2141	24.1	1.3		610	(2)		(5)	12	20	(2)			4.6	(0.5)		1200	11
316 Br	M2143	25.5	1.4		400	(2)		(5)	18	23	(2)			3.6	(1)		1500	16
318 Br	M2154	26.2	1.5		310				12	15	(2)			2.0	(0.5)		1100	8
319 Br	M2173	32.0	1.3		470	(2)		(5)	18	20	(5)		(5)	3.4	(0.5)		1200	8
320 Br	M2176	24.1	1.3		590			(10)	31	26	(2)			3.6	(0.5)		1200	10
321 Br	M2217	21.4	1.4	(4)	380	(2)		(5)	16	19	(2)		(5)	2.3	(0.5)		800	6
322 Br	M2221	26.2	2.3		240	(2)		(5)	14	10	(2)		(5)	2.4	(0.5)		850	19
323 Br	M2230	21.0	1.3		400	(2)		(10)	14	19	(2)			3.2	(1)		900	9
324 Br	M2232	27.0	1.4		510	(2)	(1)	(10)	15	20	(2)		(5)	2.6	(1)		1000	14
326 Br	M2248	23.7	1.4		390	(2)	(1)	(5)	11	19	(2)		(5)	2.9	(0.5)		1000	11
327 Br	M2261	29.3	1.8		330	(2)	(1)	(5)	16	14	(2)		(5)	3.2	(0.5)		900	13

Table 4.7. Trace Element Concentrations in San Francisco Diaphragm Samples

(Numbers in parentheses are semiquantitative estimates from photographic exposures)

ORNL Sample No.	Autopsy No.	Per Cent of Wet Sample Wt.		Concentration (μg per g of ash)																	
		Dry	Ash	Co	Cu	Ni	Cr	Pb	Al	Mn	Mo	Sn	Ti	Sr	Ba	Ag	Bi	Zn	Cd	Zr
301 D	M2063	34.3	1.4	(3)	180	24	36	42	184	24	(2)	48	(15)	10	11	1.5		3000	30	
302 D	M2075	21.6	0.62	27	140	16	(2)	(30)	58	12	(2)	33	(5)	22	7.0			4100	30	
303 D	M2076	28.7	0.72		160	24	(4)	(10)	64	13	(2)	(8)	(5)	9.4	3.7			5500	17	
304 D	M2077	29.4	0.58		200	(5)	(2)	(10)	53	14	(3)	43		14				6800	38	
305 D	M2081	29.4	0.66		190	10	(2)	(15)	39	22	(3)	42		9.6			(5)	5200	34	
306 D	M2082	27.1	0.68		150	10	(8)	(10)	47	13	(3)	42		8.3		(0.5)		5300	32	
307 D	M2085	25.5	0.88		170	20	(4)	(10)	34	19	(2)	(5)		5.2				4800	14	
308 D	M2098	34.7	0.67		190	13	11	(20)	58	21	(4)	(10)	(5)	8.4				5500	18	
309 D	M2099	25.4	0.49		210	26	22	34	140	29	7.0	56	14	27	4.0			4800	58	(5)
310 D	M2107	40.8	0.52		170	11	(4)	(10)	23	17	(2)	48		17	3.2	1.6		4400	24	
311 D	M2108	34.7	0.70		140	(5)	(1)	(10)	19	34	(2)	(4)		6.1				5900	38	
312 D	M2122	26.5	0.79	(2)	180	(5)	(4)	430	47	20	(2)	58	37	8.0	25.2	(0.5)		5000	8.0	
313 D	M2124	28.2	0.63		180	(5)	(2)	40	140	34	6.0	175	1600	15	100	14		3800	85	
314 D	M2125	23.9	0.85		115	(5)	(1)	(15)	28	8	(2)	100	(5)	8.3		10		3400	15	(5)
315 D	M2141	27.4	0.78		150	13	(2)	(10)	20	11	(3)	27		7.2				6700	45	
316 D	M2143	23.1	0.57		230	16	(6)	(15)	42	26	5.0	61		17	3.7			7500	41	(5)
317 D	M2148	39.2	0.77		125	(15)	(2)	(5)	23	10	(3)	28	(10)	7.4				3600	18	
318 D	M2154	22.9	1.1		110	(5)	(2)	(10)	(15)	(10)		(4)	(5)	4.1				5000	7.0	
319 D	M2173	27.1	0.57	(2)	200	(5)	(5)	54	66	20	5.0	500	17	12		36		3800	110	
320 D	M2176	27.1	0.56		160	19	(2)	(10)	160	18	(3)	27	(10)	15		2.0		5500	17	
321 D	M2217	27.5	0.798	8.6	140	26	(10)	(10)	28	17	(3)	40	(5)	6.9		2.5		5000	22	
322 D	M2221	24.7	0.83		160	16	(1)	(10)	16	7	(2)	36		6.0				7300	14	
323 D	M2230	28.8	0.74		160	(10)	(1)	(10)	19	24	(2)	(10)		9.9		(0.5)		4500	28	
324 D	M2232	33.2	0.64		180	(10)	(3)	(15)	150	18	(3)	42	(10)	12		8.0		4200	42	(5)
325 D	M2237	33.5	0.63		150	44	(5)	(10)	20	11	(3)	48		9.4		(0.5)		5200	18	
326 D	M2248	29.8	0.54		170	26	(20)	28	85	28	(2)	29	(10)	12	6.0			3800	67	(5)
327 D	M2261	35.2	0.65		170	34	(3)	(10)	30	12	(3)	57	(5)	8.1				4800	24	

Table 4.8. Trace Element Concentrations in San Francisco Heart Samples

(Numbers in parentheses are semiquantitative estimates from photographic exposures)

ORNL Sample No.	Autopsy No.	Per Cent of Wet Sample Wt.		Concentration (μg per g of ash)																
		Dry	Ash	Co	Cu	Ni	Cr	V	Pb	Al	Mn	Mo	Sn	Ti	Sr	Ba	Ag	Bi	Zn	Cd
300 H	M2062	22.4	0.86	(2)	420	10	(2)		(10)	30	19	4.0	23	(10)	6.4	3.2			3100	8.0
301 H	M2063	24.3	1.1	(4)	350	(5)	(4)		(10)	34	25	3.2	38	(10)	4.6				3000	6.2
302 H	M2075	22.3	0.79	16	480	17	(4)		(10)	32	17	4.6	47		13	3.0			4000	12
303 H	M2076	22.1	0.92	6.8	420	420	9.2	(4)	(20)	85	26	4.5	(10)		9.6				2900	14
304 H	M2077	23.7	0.89	(4)	420	(3)	(2)		(10)	28	18	4.1	44	(5)	6.8				3400	8.2
305 H	M2081	26.1	0.87	(4)	430	21	(2)		(10)	42	24	3.2	44		7.2				3100	7.8
306 H	M2082	22.8	0.84	(4)	450	44	(2)		(5)	23	22	3.2	47	(5)	6.5				3500	7.2
307 H	M2085	21.9	1.0	(2)	380	90	(2)		(5)	19	27	2.9	(4)	(5)	5.2			(10)	2700	7.0
308 H	M2098	23.3	0.87	(2)	350	(10)	(2)	(2)	(10)	39	25	3.2	(10)	(10)	7.6				3000	5.8
309 H	M2099	23.1	0.84	(4)	400	17	(2)		(5)	30	15	4.0	26	(10)	7.6				3400	7.8
310 H	M2107	22.5	1.0	(4)	340	200	(2)	(4)	(5)	18	32	3.6	(20)	(10)	7.4				3400	9.4
311 H	M2108	23.4	0.85	(10)	380	15	(1)		(10)	21	63	3.9	(4)	(5)	7.1				3200	11
312 H	M2122	48.3	0.498	(6)	360	(10)	(2)		(20)	100	26	3.0	79	(20)	11	5.9			2700	6.4
313 H	M2124	31.9	1.1	(2)	180	(5)	(4)		(10)	38	13	(2)	33	(20)	11		(0.5)		3400	7.2
314 H	M2125	34.0	0.59	(2)	320	89	(2)		(10)	40	22	3.9	66	(5)	11		6.1		3200	9.7
315 H	M2141	22.4	0.98	(4)	380	34	(2)		(5)	21	24	3.4	(4)	(10)	5.1				4000	10
316 H	M2143	28.2	0.88	(6)	380	15	(4)		(10)	22	21	3.5	47	(5)	6.0				3400	9.1
317 H	M2148	21.7	1.02	(2)	320	18	(2)		(5)	10	21	3.0	(10)		4.5				2800	(3)
318 H	M2154	25.3	0.99	(2)	410	19	(1)		(5)	17	14	3.4	34		5.1				3100	(2)
319 H	M2173	27.7	0.83	23	320	(3)			(5)	28	20	3.9	(4)	(10)	7.4				2900	6.9
320 H	M2176	22.0	0.93	(2)	380	16			(10)	15	30	5.6	(4)	(5)	4.3		10.9		4200	12
321 H	M2217	42.6	0.69	19	320	(5)	(1)		(20)	45	28	4.5	(15)	94	12				2600	5.5
322 H	M2221	23.2	0.96		460	(5)	(1)		(10)	17	17	3.9	(33)		4.2				3600	5.2
323 H	M2230	23.5	0.91	(2)	430	(5)	(2)		(5)	76	35	5.1	(10)	(5)	9.6				3100	7.4
324 H	M2232	22.5	0.89		300	15	(2)		(5)	19	23	3.8	28	(5)	7.4				4000	6.6
325 H	M2237	24.8	1.9	(2)	200	27	(2)		(5)	12	9	2.9	(20)	(5)	3.0				2400	11
326 H	M2248	21.9	0.798	(4)	320	75	(2)		(5)	28	21	3.3	(10)	(10)	7.6	3.3	(0.5)		3700	8.4
327 H	M2261	30.3	0.76	(4)	400	30	(2)	(2)	(5)	27	26	4.3	64	(10)	12				3800	6.6

Statistical Interpretation of Trace Element Concentrations in Human Tissue

I. H. Tipton M. J. Cook

At the present time the elements Mg, Ca, Mn, Fe, Cu, Zn, and Mo are designated "essential trace elements" – "trace," since they occur in concentrations of about 10 μg per g of wet tissue or less, and "essential," since each one has been demonstrated to be associated with one or more enzyme systems or to have some other vital function. At least 20 other elements have been observed in many mammalian tissues. They are designated "nonessential trace elements" since no function has been discovered for them. Ten of these – Sr, Ba, Al, Ti, Cr, Ni, Ag, Cd, Sn, Pb – have been observed within the limits of sensitivity of the method in at least one tissue of every adult subject (age >20 years) from the United States analyzed in the University of Tennessee – ORNL Health Physics Division cooperative program, and several of them (Sr, Al, Pb) in almost every sample of every tissue.

Table 4.10 includes data for these seven essential and ten nonessential elements in seven organs of 166 adult victims of instantaneous accidental death from eleven cities in the United States (see Table 4.9). The value for per cent occurrence is the per cent of the total number of samples analyzed in which an element was actually observed above the lower limit of sensitivity of the method. If an element is not observed in a sample this does not necessarily mean that the concentration is zero but only that it is less than the lowest observable value. Since the individual values for most elements were not distributed normally, and since for elements of less than 100% occurrence the concentration could not be quantitated in every sample, the median value in μg per g of tissue ash is reported instead of the mean. The total range, lowest to highest values, indicates the extent of the individual variation. To avoid a disproportionate effect from a few aberrant concentrations, which may have arisen from variations in sampling, loss in ashing, or contamination, the range of the central 80% of values instead of the total range has been used to estimate the variability.

As may be observed in Table 4.11, the variability (ratio of the extremes of the 80% range) of the essential elements is very much less than that of the nonessential elements. Of the 44 ratios for the essential elements, only eleven are over 3.5, and only four over 5. Of the 34 ratios for the nonessential elements which occur in measurable concentrations in 80% of the samples, only one is under 3.5 and three under 5.

Table 4.9. Number of Organs from Each City (Normal Adult)

	Liver	Kidney	Lung	Aorta	Heart	Spleen	Brain
Baltimore	21	21	21	22	21	21	20
Birmingham	0	1	0	0	1	1	0
Chicago	1	3	4	0	4	1	1
Columbus, Ohio	1	1	1	1	0	1	1
Dallas	26	25	26	21	26	25	24
Denver	26	25	25	13	22	23	23
Memphis	11	10	10	3	10	10	0
Miami	23	23	23	18	22	22	20
New York	9	13	10	5	10	10	9
Richmond	25	24	23	21	24	25	18
Seattle–Tacoma	19	18	17	5	18	16	16
Total U.S.	162	164	160	109	158	155	132

Table 4.10. A Summary of Data for Adults (Age >20 yr) from the United States

	Per Cent of Wet Sample Weight		Concentration (μg per g of tissue ash except as indicated)																
	Ash	Dry	Ag	Al	Ba	Ca (%)	Cd	Cr	Cu	Fe (%)	Mg (%)	Mn	Mo	Ni	Pb	Sn	Sr	Ti	Zn
Aorta																			
Occurrence, %	100	100	62	100	100	100	21	86	100	100	100	100	5	47	100	91	100	46	100
Median	1.4	33	0.1	28	7.0	5.5	<50	1.7	90	0.27	1.4	8	<4	<5	150	14	33	<5	1,800
Low	0.13	22	<0.1	5	0.8	0.55	<50	<0.1	5	0.07	0.25	4	<4	<5	10	<5	3.2	<5	400
High	5.6	56	33	310	60	11	250	56	320	1.1	3.9	110	350	190	520	560	200	430	7,300
10th percentile	0.76	27	<0.1	11	3.2	2.6	<50	<0.1	52	0.15	0.94	4	<4	<5	35	5	15	<5	1,100
90th percentile	3.0	45	0.9	140	16	8.5	50	10	140	0.60	2.0	25	<4	30	300	45	76	31	3,000
Brain																			
Occurrence, %	100	100	87	100	50	100		78	100	100	100	100	2	7	70	8	100	10	100
Median	1.5	25	0.5	15	0.2	0.52		0.3	370	0.32	0.90	18	<4	<5	5	<5	1.4	<5	800
Low	1.2	18	<0.1	4	<0.2	0.26		<0.1	38	0.15	0.49	6	<4	<5	<5	<5	0.1	<5	140
High	3.5	49	34	520	4.0	1.8		11	960	0.66	1.5	71	20	12	450	110	17	21	6,600
10th percentile	1.4	20	<0.1	7	<0.2	0.33		<0.1	240	0.22	0.62	10	<4	<5	<5	<5	0.5	<5	520
90th percentile	1.9	38	1.5	38	1.9	0.96		2.0	550	0.50	1.2	32	<4	<5	34	<5	4.0	5	1,200
Heart																			
Occurrence, %	100	100	22	100	67	100	6	93	100	100	100	100	17	42	62	65	100	28	100
Median	1.1	25	<0.1	19	0.5	0.38	<50	1.6	350	0.47	1.6	19	<4	<5	10	5	2.6	<5	2,700
Low	0.70	17	<0.1	4	<0.2	0.10	<50	<0.1	210	0.25	0.57	4	<4	<5	<5	<5	0.5	<5	1,500
High	3.3	45	65	270	9.3	3.2	190	44	760	1.4	3.5	57	38	130	180	270	19	100	8,000
10th percentile	0.90	22	<0.1	10	<0.2	0.21	<50	0.1	250	0.36	1.1	9	<4	<5	<5	<5	1.2	<5	2,000
90th percentile	1.2	33	0.5	70	2.7	0.80	<50	8.0	460	0.69	2.4	38	20	27	29	35	6.5	9	4,300
Kidney																			
Occurrence, %	100	100	46	100	84	100	100	84	100	100	100	100	97	28	100	96	100	28	100
Median	1.1	24	<0.1	28	1.3	0.80	2900	1.0	260	0.65	1.2	77	32	<5	98	20	5.0	<5	4,700
Low	0.44	14	<0.1	6	<0.2	0.27	570	<0.1	140	0.24	0.51	19	<4	<5	6	<5	0.6	<5	1,500
High	2.9	39	6.0	560	29	3.7	8000	36	770	1.6	2.6	350	120	80	680	480	28	140	10,000
10th percentile	0.98	19	<0.1	14	<0.2	0.46	1500	<0.1	190	0.39	0.86	41	20	<5	43	<5	2.3	<5	3,200
90th percentile	1.3	29	0.9	130	4.0	1.5	5100	4.5	360	1.1	1.6	150	57	16	220	50	12	10	7,700
Liver																			
Occurrence, %	100	100	94	100	46	100	98	81	100	100	100	100	100	22	100	96	100	29	100
Median	1.1	36	0.9	48	<0.2	0.37	180	1.5	530	1.4	1.2	99	76	<5	130	24	1.5	<5	3,500
Low	0.5	25	<0.1	9	<0.2	0.10	<50	<0.1	200	0.23	0.57	26	13	<5	22	<5	<0.1	<5	1,100
High	3.4	82	7.0	880	14	2.2	1500	15	5000	5.3	3.0	580	480	80	1000	180	16	100	13,000
10th percentile	1.0	30	0.1	19	<0.2	0.22	60	<0.1	330	0.59	0.80	55	28	<5	59	7	0.5	<5	2,200
90th percentile	1.8	49	3.3	140	2.0	0.70	350	3.2	1000	2.4	1.8	210	160	16	250	76	3.5	17	6,000
Lung																			
Occurrence, %	100	100	37	100	100	100	55	100	100	100	100	100	10	56	100	97	100	99	100
Median	1.1	22	<0.1	1,800	14	1.0	50	13	130	2.6	0.90	20	<4	5	49	39	8.5	240	1,400
Low	0.50	13	<0.1	170	0.5	0.33	<50	0.5	50	0.76	0.38	5	<4	<5	<5	<5	0.5	12	660
High	1.8	86	12	10,000	160	2.9	270	120	330	9.0	1.7	170	38	190	630	920	46	5500	3,100
10th percentile	1.0	20	<0.1	740	4.4	0.58	<50	3.4	94	1.2	0.62	8	<4	<5	17	13	4.7	68	900
90th percentile	1.2	28	0.5	4,000	40	1.6	150	50	200	5.2	1.2	55	4	43	140	110	19	1000	1,800
Spleen																			
Occurrence, %	100	100	33	100	61	100	14	78	100	100	100	100	12	19	98	84	100	31	100
Median	1.4	26	0.1	26	0.5	0.50	<50	0.5	90	2.3	0.95	10	<4	<5	28	11	2.2	<5	1,400
Low	0.40	20	<0.1	4	<0.2	0.18	<50	<0.1	30	0.40	0.30	4	<4	<5	<5	<5	0.26	<5	720
High	3.4	82	37	1,700	28	3.8	280	110	410	11	2.1	110	37	330	2000	200	60	110	4,600
10th percentile	1.1	23	<0.1	11	<0.2	0.27	<50	<0.1	68	0.91	0.68	5	<4	<5	10	<5	1.1	<5	1,100
90th percentile	1.6	34	0.5	270	2.5	0.78	50	3.8	120	4.3	1.5	28	4	10	110	36	6.0	33	1,900

Table 4.11. Variability of Metal Concentrations in Human Organs

Element	Concentration Variability $\left(\frac{\text{90th percentile}}{\text{10th percentile}}\right)$						
	Liver	Kidney	Lung	Aorta	Heart	Spleen	Brain
				Essential Elements			
Mg	2.2	1.9	1.9	2.1	2.2	2.2	1.9
Ca	3.2	3.3	2.8	3.3	3.8	2.9	2.9
Mn	4.0	3.7	6.9	6.2	4.2	6.5	3.2
Fe	4.5	2.8	4.3	4.0	1.9	4.8	2.3
Cu	3.0	1.9	2.1	2.7	1.8	1.9	2.3
Zn	2.7	2.4	2.0	2.8	2.2	1.9	2.3
Mo	5.7	2.9					
				Nonessential Elements			
Sr	6.9	5.2	4.0	5.1	5.4	5.5	8.0
Ba	>21	>20	9.1	5.0	> 3.5	5.0	> 9.5
Al	7.4	9.3	6.7	13	7.0	27	5.4
Ti	> 3.6*	> 2**	15	> 6.2*	> 1.8**	> 7*	
V			>27				
Cr	>40	45	15	>100	80	>38	>20
Ni	> 3.4	> 1.6**	> 8.6	> 6.0*	> 5.4*	> 2**	
Ag	35	9	> 5*	> 9.0	> 5*	> 5*	>15
Cd	5.8	3.4	> 3.0	> 1.0**			
Sn	12	>10	8.5	9.0	> 7.0	7.4	
Pb	4.2	5.1	8.2	8.5	> 5.8	10	> 6.8

*Indicates <50% occurrence.

**Indicates <50% occurrence, all measured values close to lower limit of sensitivity. Blanks indicate < 10% occurrence.

In general, the concentrations of the essential elements are one to three orders of magnitude greater than those of the nonessential elements. In Table 4.12 the *lower limit* of the 80% range of concentration (in micromoles per g of ash) for the essential elements and the *upper limit* of this range for nonessential elements is given. Despite the obvious tendency for essential metals to be more concentrated, Al is considerably higher in concentration than Mn in all organs, and Cd higher than Mo in kidney and liver. There is a marked tendency for Al and Ti to accumulate in the lung and for Cd to accumulate in the kidney and liver. The former may perhaps result from the continued inhalation of insoluble dust particles, but there is no obvious explanation for the latter.

Of course no conclusions as to the essentiality or nonessentiality of an element can be drawn from these data. Correlations between elements in a single tissue and between the concentrations of a single element in various tissues are also being investigated.

Table 4.12. Concentrations of Metals in Organs of U.S. Adults (>20 yrs)

Element	Concentration (micromoles per g of ash)							
	Liver	Kidney	Lung	Aorta	Heart	Spleen	Brain	Organ-to-Organ Variation
10th Percentile for 7 Essential Elements								
Mg	330	350	250	390	450	280	250	1.8
Ca	55	120	140	640	52	67	81	12
Mn	0.95	0.75	0.15	0.070	0.16	0.082	0.18	14
Fe	95	70	210	27	66	150	38	7.8
Cu	5.2	3.0	1.5	0.82	3.9	1.1	3.9	6.3
Zn	34	49	14	17	31	15	8.0	6.1
Mo	0.29	0.21						> 7
90th Percentile for 10 Nonessential Elements								
Sr	0.040	0.14	0.22	0.86	0.074	0.068	0.041	21
Ba	0.015	0.029	0.29	0.12	0.020	0.018	0.014	21
Al	5.2	4.8	150	5.2	2.6	10	1.4	110
Ti	0.38*	0.21*	21	0.65*	0.19*	0.72*		>210
Cr	0.077	0.087	0.96	0.19	0.15	0.073	0.038	25
Ni	0.29*	0.27*	0.73	0.51*	0.46*	0.17*		> 8.6
Ag	0.032	0.0083*	0.0046*	0.0083	0.0046*	0.0046*	0.014	7.0
Cd	3.1	46	1.3	0.44*				>100
Sn	0.69	0.42	0.92	0.38	0.30	0.31		> 22
Pb	1.2	1.1	0.68	1.4	0.14	0.53	0.16	10

*Indicates <50% occurrence.

Blanks indicate <10% occurrence.

Minimum measurable amounts: Mo, 0.04; Ni, 0.09; Cd, 0.4; Sn, 0.04; Ti, 0.1 micromole per g of ash.

Variability of Relative Organ Concentration of Trace Elements in Human Tissue

W. S. Snyder M. J. Cook

When animals of the same age and strain are exposed to a radionuclide, the amounts deposited in the various tissues of these animals vary considerably from one animal to another. No matter how carefully the conditions of exposure are regulated, there is generally considerable individual variation. The human data available suggest that man is perhaps as variable as other species in these respects. Since the dose a tissue receives from a radionuclide generally varies with the concentration of the isotope in the tissue, it is clear that doses to body tissues of similar individuals may differ even though the external conditions of exposure are identical. When differences in uptake and retention which correlate with age, sex, weight, habits, or other characteristics of the individual are considered, it is apparent that the doses different individuals in an exposed population receive may differ widely. Although these observations are practically truisms, there has been little attempt to arrive at an estimate of the extent of this variability or to correlate it with individual characteristics.

The Federal Radiation Council in its first report[22] recognized the problem. Section 5.4 of that report reads:

"Under certain conditions, such as widespread radioactive contamination of the environment,

[22] "Background Material for the Development of Radiation Protection Standards," *Staff Report of the Federal Radiation Council*, Report No. 1 (May 13, 1960).

the only data available may be related to average contamination or exposure levels. Under these circumstances, it is necessary to make assumptions concerning the relationship between average and maximum doses. The Federal Radiation Council suggests the use of the arbitrary assumption that the majority of individuals do not vary from the average by a factor greater than three. Thus, we recommend the use of 0.17 rem for yearly whole-body exposure of average population groups. (It is noted that this guide is also in essential agreement with current recommendations of the NCRP and the ICRP.) It is critical that this guide be applied with reason and judgment. Especially, it is noted that the use of the average figure, as a substitute for evidence concerning the dose to individuals, is permissible only when there is a probability of appreciable homogeneity concerning the distribution of the dose within the population included in the average. Particular care should be taken to assure that a disproportionate fraction of the average dose is not received by the most sensitive population elements. Specifically, it would be inappropriate to average the dose between children and adults, especially if it is believed that there are selective factors making the dose to children generally higher than that for adults."

This paper is an attempt to give a preliminary indication of the extent of this variability. The data offered here are not extensive enough to give definitive information on many points. A larger and more carefully chosen sample would be necessary to give a more complete answer on any of the points treated below. However, the methods used here may be of interest, and the data cited probably constitute the most extensive and valuable evidence we now have on this question of individual variation.

A project to determine the concentrations of various stable trace elements in human tissues was initiated in 1950 as a joint project of the University of Tennessee and the Oak Ridge National Laboratory. Samples of tissues from some 30 body organs have been obtained at autopsies of some 200 individuals in 9 major cities of the United States. In this paper only data on adults between the ages of 21 through 60 are considered. Each individual was judged as grossly normal by the pathologist in charge of the autopsy, and all are believed to have resided for at least 10 years in the urban area where they died. Most of them died as the result of an accident or by violence. The spectrographic analysis of the tissues was under the direction of I. H. Tipton of the Department of Physics at the University of Tennessee. Much of the data on trace elements in the standard man, as presented in ICRP Report of Committee II, is due to this program. The data presented here are only a small portion of the total data and are offered by way of illustration.

Figure 4.3 indicates the concentration of Cd, Cu, and Zn in liver, lung, and kidney by age decades. Only a mean value for each age decade is shown. It is questionable whether a real age trend exists in these data, although Cd and Zn in kidney may show a significant change. It is interesting that Cu and Zn show less variability than does Cd. So far as is known, Cd has no essential role in the body, but Cu and Zn are known to be essential in nearly all tissues. Nevertheless, a recent study by Gunn *et al.* indicates that Cd may replace Zn in some instances.[23]

As a more striking instance of an age trend, Fig. 4.4 shows the concentration of Al in liver, lung, and kidney. Again each point represents the mean of all samples for an age decade. The lines were fitted to these points by least squares.

Such data may be used to test the "rule of three" suggested by the Federal Radiation Council; that is, that the majority of individuals does not vary from the average by a factor greater than three. Since this was recommended only "when there is a probability of appreciable homogeneity concerning the distribution of the dose within the population included in the average," it seems desirable to classify the data according to the urban area in which the individual lived. It should be emphasized that no data are available on the diet of these individuals.

The data now available are not sufficient to determine the form of the distribution of values but suggest that it is not a normal distribution, generally being skewed on the high side. For this reason the statistics applied here will be of

[23] Samuel A. Gunn, Thelma C. Gould, and W. A. D. Anderson, "Competition of Cadmium for Zinc in Rat Testis and Dorsolateral Prostate," *Acta Endocrinologica* 37, 24–30 (1961).

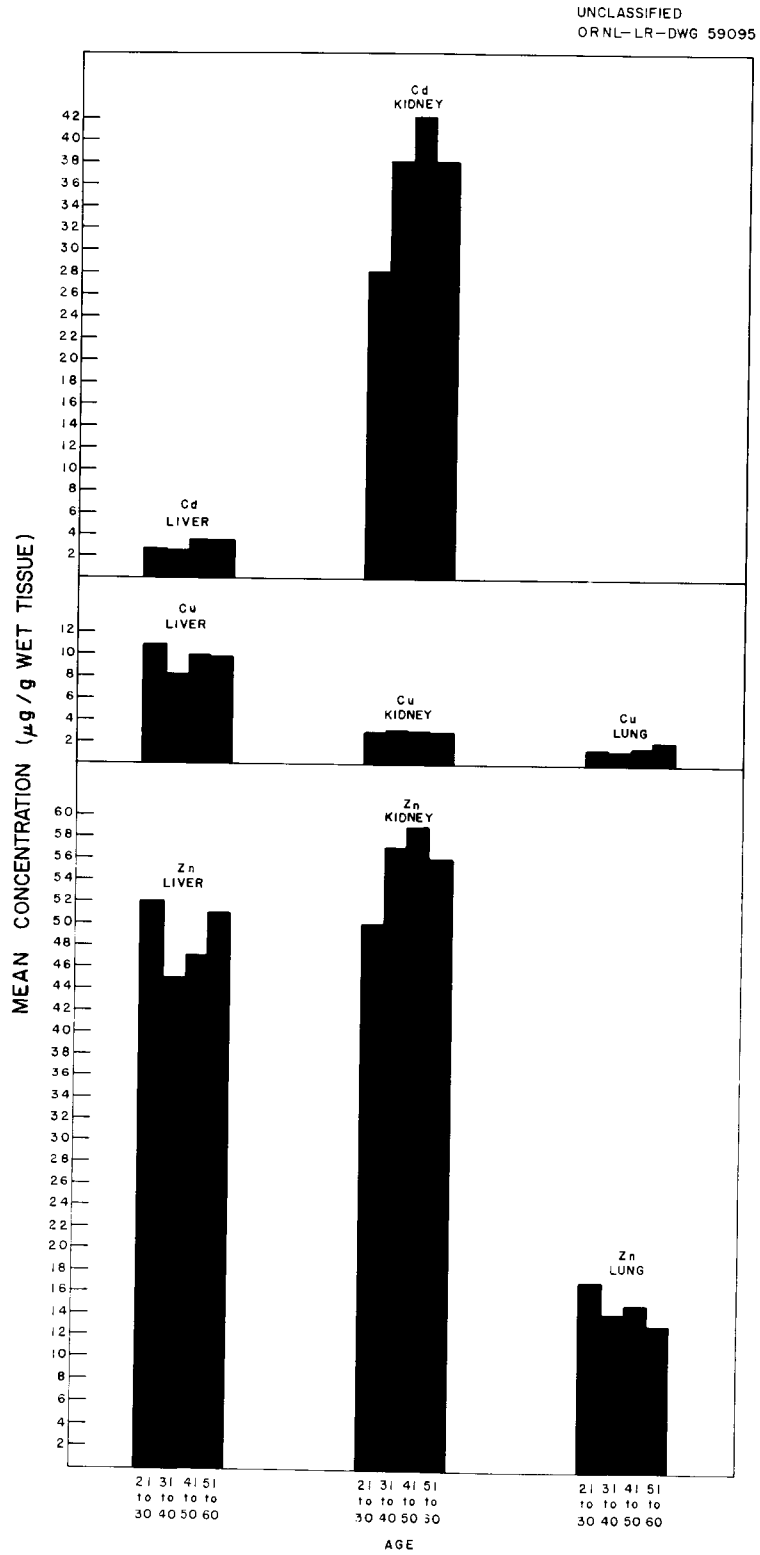

Fig. 4.3. Distribution by Age of Stable Cd, Cu, and Zn in Liver, Kidney, and Lung.

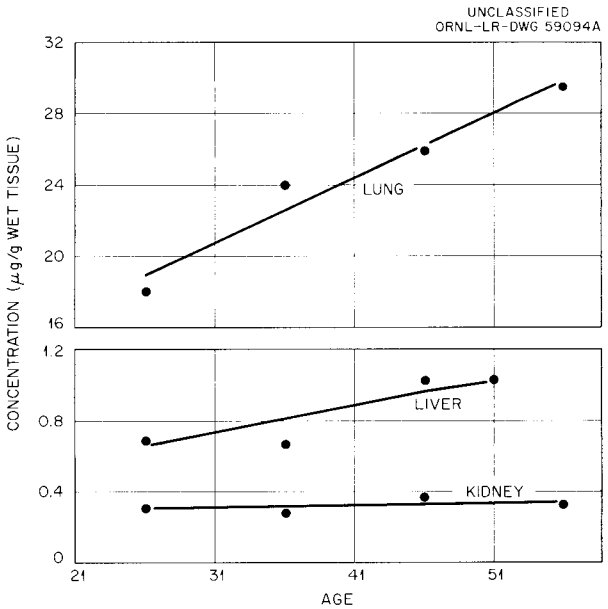

Fig. 4.4. Variation of Al in Lung, Liver, and Kidney of Adults in Urban Populations (Ages 21 Through 60).

nonparametric type; that is, they make no assumption concerning the form of the distribution of these values.

As an example of this approach, consider the question of estimating the per cent of a population group with a concentration value, say, of Cd in liver, above a certain value. Let the selected value be a and suppose a sample of n individuals is selected randomly and that k of these have sample values greater than a. It is desired to estimate the fraction of the population which exceeds a.

Assume the fraction p of the population exceeds a, and thus $1 - p$ is the fraction of the population with sample values less than a. The probability that a random sample of n individuals will contain r individuals above a is

$$\frac{n!}{r!(n-r)!} p^r (1-p)^{n-r} .$$

Thus the probability that k or fewer individuals above a will occur in the random sample of n is

$$\sum_{r=0}^{k} \frac{n!}{r!(n-r)!} p^r (1-p)^{n-r} . \qquad (1)$$

If p is large, this value will be small, and one may ask what values of p would be unlikely in view of the fact that no more than k individuals were above a in the sample. For example, if k is much less than n and p is very close to 1, the above probability is close to zero. Thus a value of p close to 1 is very unlikely since this assumption implies the sample is very exceptional and unlikely to occur. To fix the argument, suppose p_0 is chosen to satisfy the equation

$$\sum_{r=0}^{k} \frac{n!}{r!(n-r)!} p_0^r (1-p_0)^{n-r} = 0.05 .$$

Recalling that k is much less than n, it is clear that a value of p larger than p_0 decreases the value of the left side. Thus if the per cent of the population above a is greater than p_0, our sample is one which has a probability of 5% or less of occurring; that is, we have 95% probability that it did not occur. Consequently one may assert with 95% confidence that the per cent of the population above a does not exceed p_0.

This type of analysis may be applied to the concentration values of a given element in a selected tissue of the sampled individuals. Figure 4.5 shows the concentrations of Cu, Al, and Zn in kidney both for adults in the various urban areas and for the total sample of all these urban areas. The range of values, the mean of the sample, and the number of individuals in each sample are shown as well as the maximum estimate for the per cent of the population above three times the sample mean. It will be noted that these percentages range from 12 to 40% for the individual cities but reduce to 3 to 9% for the larger group, that is, the total sample. This is probably an artifact due to the small sample size. Indeed, the minimum value of p that can be obtained occurs when $k = 0$, that is, $(1-p)^n$. This corresponds to a value of

$$p_0 = 1 - \sqrt[n]{0.05} .$$

Figure 4.6 shows this relation graphically. A sample of about 300 is required to obtain an estimate of 1% for p_0 under the best circumstances. Thus the percentages for the individual cities are probably unnecessarily large. The sample size for the group of urban adults as a whole seems adequate, and thus the estimates of the percentages here are probably trustworthy.

The most serious limitation on the validity of the above analysis is that of sampling. The assumption was made that the sampling was random,

UNCLASSIFIED
ORNL-LR-DWG 59096

CITY	CU		ZN		AL	
	SAMPLE RANGE, MEAN AND NUMBER IN SAMPLE	MAXIMUM ESTIMATE (%) OF POPULATION ABOVE 3x MEAN (95% CONFIDENCE)	SAMPLE RANGE AND MEAN	MAXIMUM ESTIMATE (%) OF POPULATION ABOVE 3x MEAN (95% CONFIDENCE)	SAMPLE RANGE, MEAN AND NUMBER IN SAMPLE	MAXIMUM ESTIMATE (%) OF POPULATION ABOVE 3x MEAN (95% CONFIDENCE)
BALTIMORE	1.8, 3, 4.1 (18)	15.36	31, 50, 70 (19)	14.64	0.06, 0.4, 1.9 (18)	23.80
DALLAS	2.1, 2.8, 3.6 (22)	12.77	28, 46, 65 (22)	12.77	0.07, 0.3, 0.7 (22)	12.77
MIAMI	2.1, 3, 3.9 (20)	13.92	28, 51, 91 (20)	13.92	0.1, 0.3, 0.9 (20)	28.30
RICHMOND	2.3, 3.4, 5.4 (17)	16.20	46, 75, 130 (17)	16.20	0.07, 0.2, 0.4 (16)	17.11
SEATTLE	2.3, 3, 4.6 (10)	25.86	28, 60, 105 (10)	25.86	0.08, 0.4, 1.2 (10)	39.33
TOTAL SAMPLE	1.8, 3, 5.4 (87)	3.50	28, 55, 130 (88)	3.46	0.06, 0.3, 1.9 (86)	8.81

Fig. 4.5. Variation of Al, Cu, and Zn Concentrations in Kidneys of Adults in Urban Populations (Ages 21 Through 60).

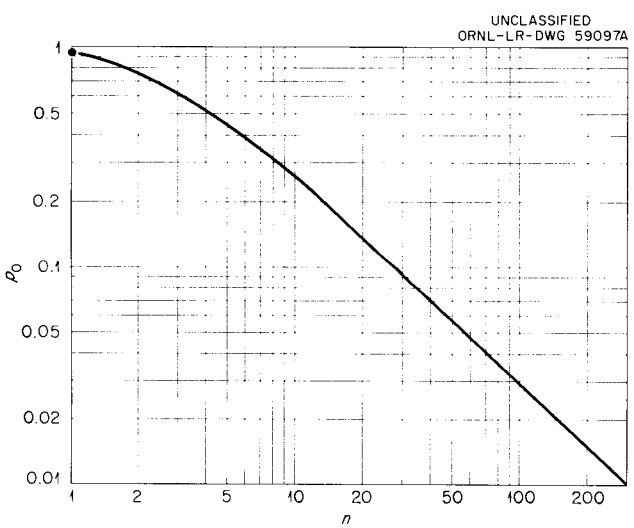

Fig. 4.6. Minimal Fraction of the Population as a Function of Sample Size.

and this is seldom, if ever, the case when human beings are being sampled. There is no known bias in the individuals sampled in this program, but there may be many hidden influences which are related to the procedure by which an individual enters the sample. It is likely that similar influences will be inherent in any sampling program set up to implement the recommendations of the Federal Radiation Council. Accidents of residence, habits, etc., may alter greatly an individual's chance of selection. This seems, in large measure, inescapable since one cannot control the selection arbitrarily.

MICROSCOPIC AND AUTORADIOGRAPHIC STUDIES OF URANIUM DISTRIBUTION IN RAT KIDNEY

E. S. Jones S. R. Bernard

Introduction

Studies of the distribution of uranium in rat kidney at the microscopic level were continued.[24] These were carried forward for the purpose of obtaining more information relating to the phenomenon of prolonged retention of uranium by kidneys of animals given an intravenous injection of a large mass of uranium. Muir,[25] in previous

[24] E. S. Jones, *Health Phys. Div. Ann. Progr. Rept. July 31, 1960*, ORNL-2994, p 274.

[25] J. R. Muir, *ibid.*, p 272.

reports, has presented kidney retention measurements in rats injected with levels ranging from 1000 μg/kg down to 1 μg/kg. A prolonged retention in kidneys is observed when levels of 100 to 1000 μg/kg are injected.

In the following there are presented graphs of the distribution of uranium concentrations observed in the cortex and medulla of rat kidney, data on the leaching of uranium from the kidney by fixing and dehydrating solutions, comparison of distribution after freeze-drying and after formalin fixation, and measurements of the diameters of proximal convoluted tubules and glomeruli. Additional values for the nonuniform distribution factor are presented also.

Distribution of Uranium in Rat Kidneys

In order to determine the distribution of uranium in rat kidney and the effect of uranium upon the parameters of the distribution curves, the number of uranium tracks were counted in 100 fields of cortex and 50 or 100 fields of medulla and classified by conventional statistical methods. The number of tracks per field was converted to uranium concentration in the following manner: Let d denote the diameter of the microscopic field, t the thickness of the field, c the number of tracks per field, and D the number of days of exposure. The volume of the field is

$$\frac{\pi d^2}{4} t \ .$$

Assuming the specific gravity of the tissue to be 1.05,[26] then the counts/min/g are

$$\text{counts/min/g} = \frac{10^{11} C}{(37.8) D \pi t d^2} \ .$$

Letting $d = 370\ \mu$, $t = 8\ \mu$, and using $D = 28$ days to correspond to the exposure period,

$$\text{counts/min/g} = 27.465c \ .$$

Assuming a geometry factor of 2, then the

$$\text{dis/min/g} = 2(27.5)c = 55c \ .$$

Figures 4.7–4.10 present the histograms of the uranium concentrations observed in kidneys of rats administered 1000 μg of uranium per kg of body weight killed at 1, 7, 10, and 28 days after injection respectively. Figures 4.11–4.14 show the distribution curves for rats administered 100 μg per kg of body weight and killed at the same times. Figures 4.15 and 4.16 show the distribution curves for animals injected with 10 μg per kg and killed at 1 and 7 days postinjection, respectively. All the rats were injected with approximately the same amount of activity, namely, ~50,000 dis/min, but with different masses of uranium, due to the 2.5 μg of U^{233}, the remaining mass amounts consisting of U^{238}.

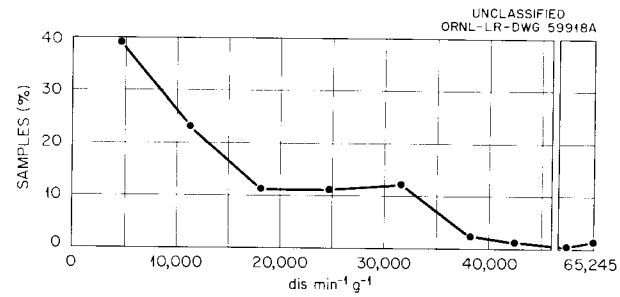

Fig. 4.7. Distribution of Uranium in Rat Cortex at One Day Following Intravenous Injection of 1000 μg U per kg of Body Weight.

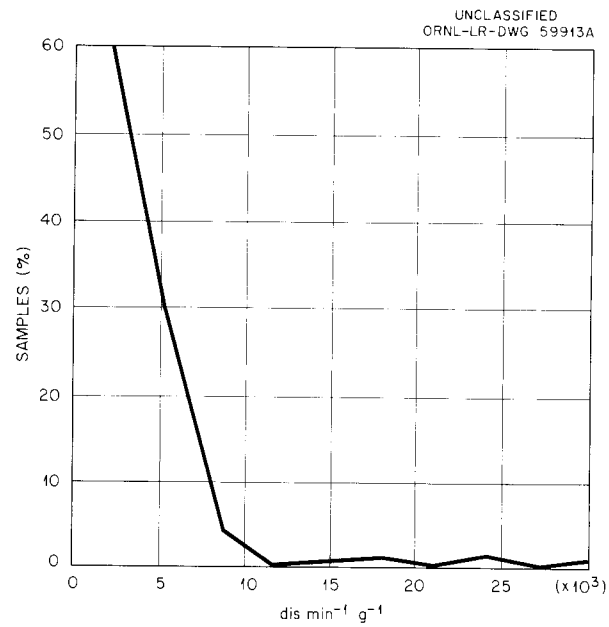

Fig. 4.8. Distribution of Uranium in Rat Kidney Cortex at Seven Days Following Intravenous Injection of 1000 μg U per kg of Body Weight.

[26] M. Arataki, *Am. J. Anat.* 36, 399 (1926).

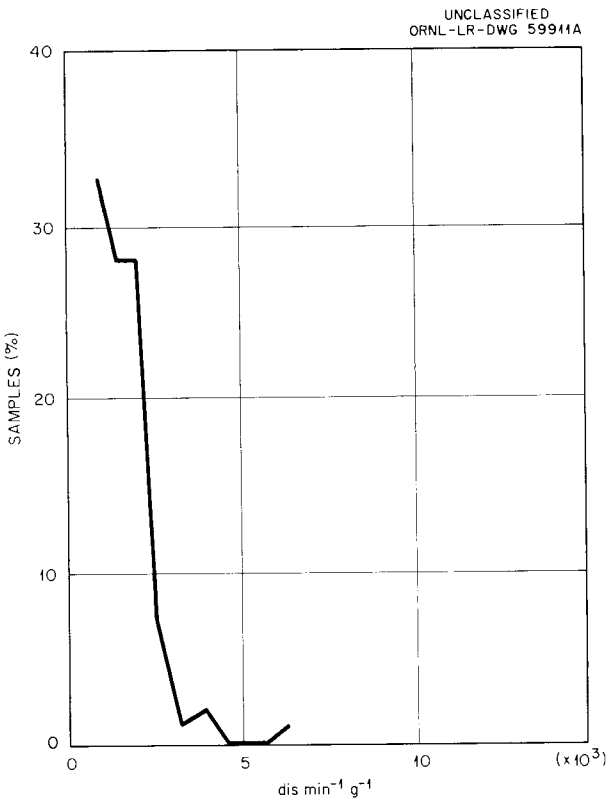

Fig. 4.9. Distribution of Uranium in Rat Kidney Cortex at Ten Days Following Intravenous Injection of 1000 μg U per kg of Body Weight.

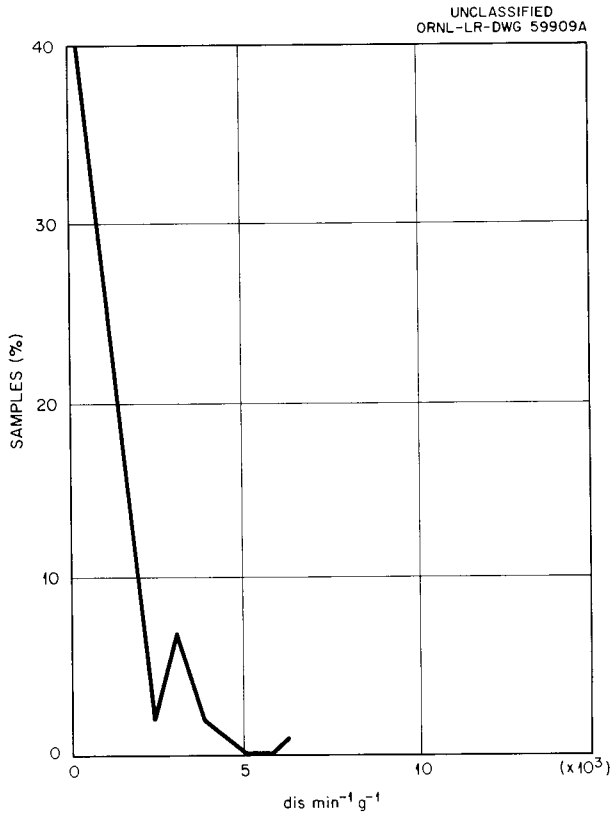

Fig. 4.10. Distribution of Uranium in Rat Kidney Cortex at 28 Days Following Intravenous Injection of 1000 μg U per kg of Body Weight.

The effect of mass of injected uranium on the distribution in the kidney is seen by comparing the data appearing in Figs. 4.7, 4.11, and 4.15 which present the distributions observed at 1 day after injection. At a kidney cortex concentration level of 10,000 dis/min/g, ~26% of the samples contained this level in rats administered 1000 μg/kg, whereas ~16% of the samples contained this level in rats administered 100 μg of U per kg, and only ~4% contained this level in rats administered 10 μg of U per kg. As can be seen then, in general, increasing the mass of injected uranium (Figs. 4.7, 4.11, and 4.15) produces a greater number of higher concentrations, resulting in a skewing of the distribution curve.

The dependency of the distribution on time after the injection can be observed in Figs. 4.7, 4.8, and 4.9; 4.10, 4.11, and 4.12, etc. Here it can be noted that as time increases the skewness of the curves decreases. The data crowd around the origin, showing a lower number of higher concentrations.

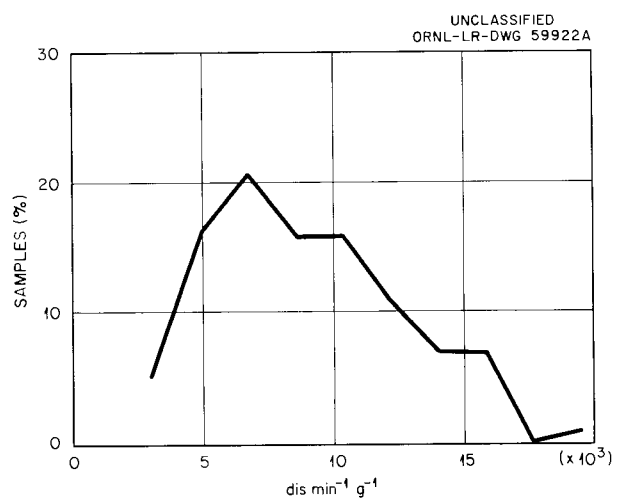

Fig. 4.11. Distribution of Uranium in Rat Kidney Cortex at One Day Following Intravenous Injection of 100 μg U per kg of Body Weight.

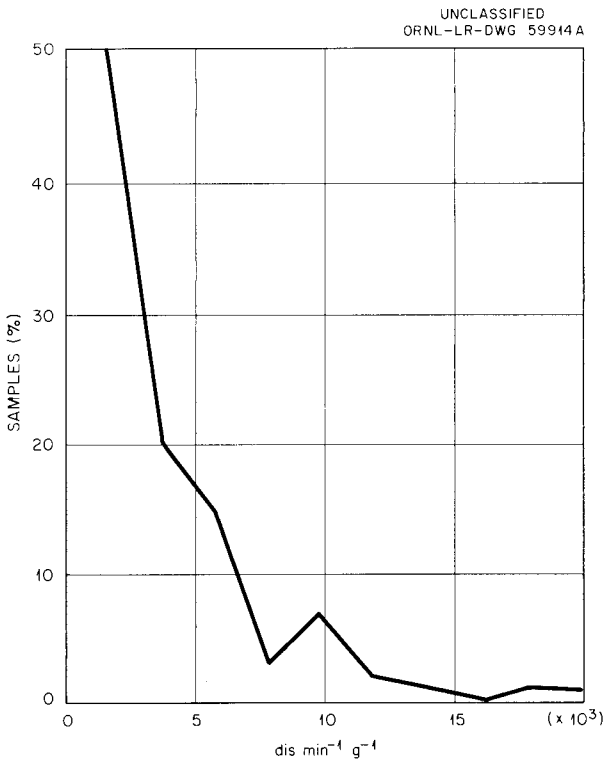

Fig. 4.12. Distribution of Uranium in Rat Kidney Cortex at Seven Days Following Intravenous Injection of 100 μg U per kg of Body Weight.

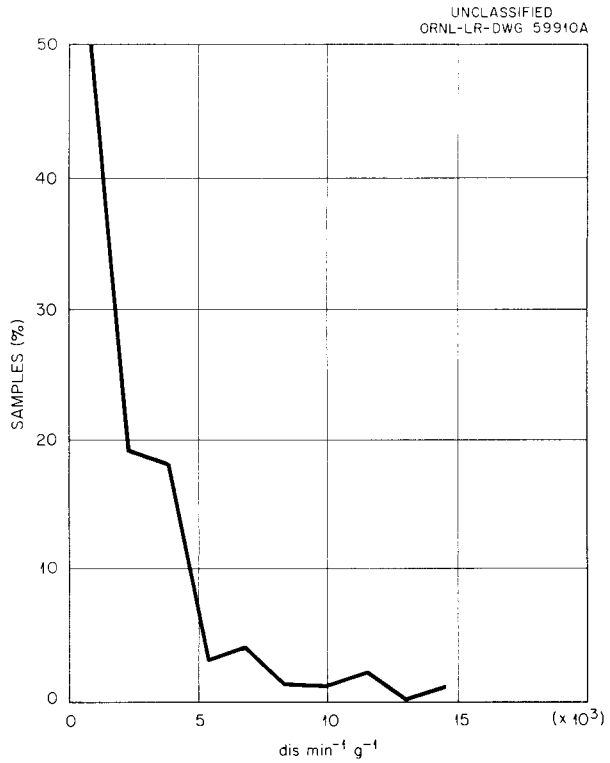

Fig. 4.14. Distribution of Uranium in Rat Kidney Cortex at 28 Days Following Intravenous Injection of 100 μg U per kg of Body Weight.

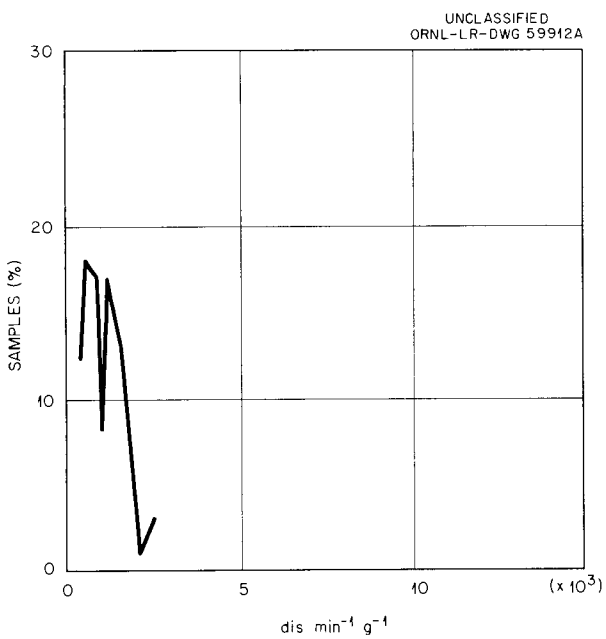

Fig. 4.13. Distribution of Uranium in Rat Kidney Cortex at Ten Days Following Intravenous Injection of 100 μg U per kg of Body Weight.

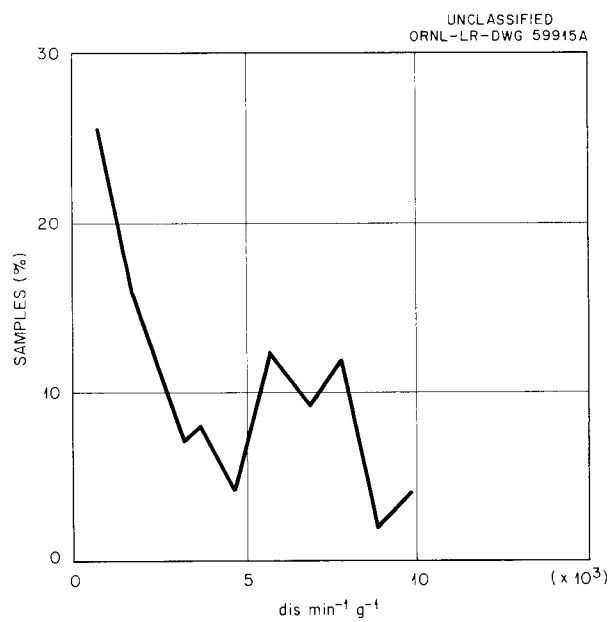

Fig. 4.15. Distribution of Uranium in Rat Kidney Cortex at One Day Following Intravenous Injection of 10 μg U per kg of Body Weight.

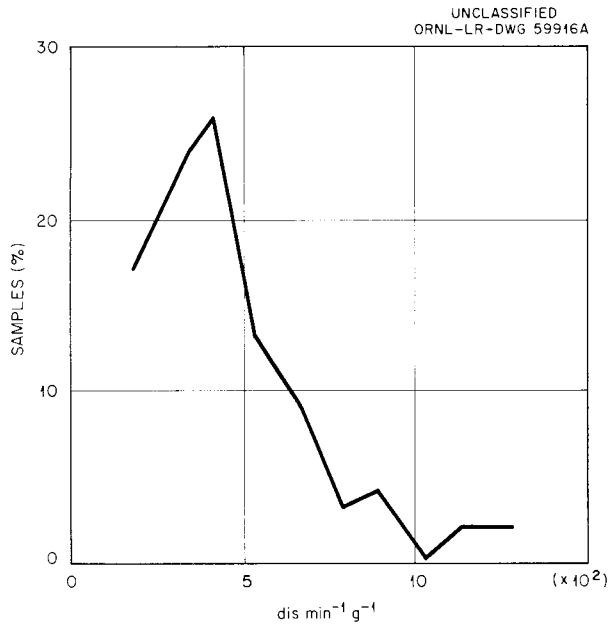

Fig. 4.16. Distribution of Uranium in Rat Kidney Cortex at Seven Days Following Intravenous Injection of 10 μg U per kg of Body Weight.

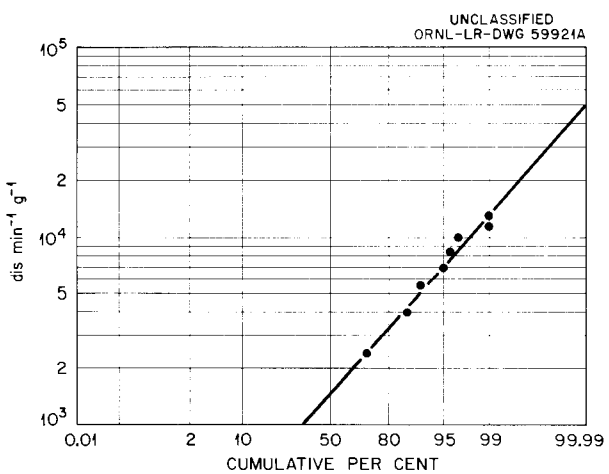

Fig. 4.17. Cumulative Log Probability Graph of Uranium Distribution in Cortex of Rat Kidney at 28 Days Following Intravenous Injection of 100 μg U per kg of Body Weight.

An effort to study this effect quantitatively has been made by fitting distribution curves to these data. When a log-normal distribution is assumed for the concentration and the cumulative per cent of samples is plotted on log-probability paper, the resulting plots appear as shown in Figs. 4.17,

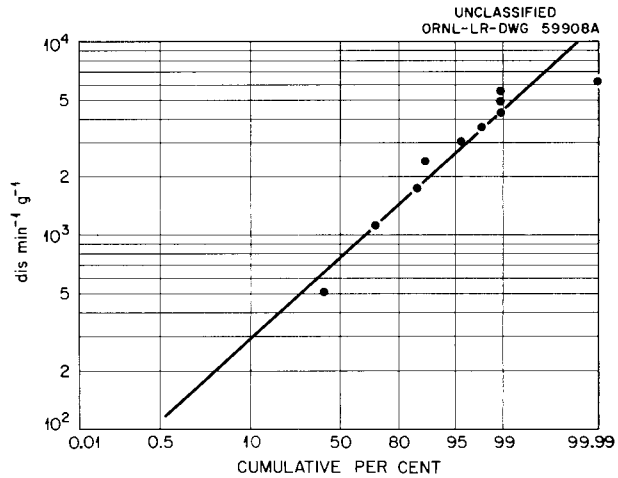

Fig. 4.18. Cumulative Log Probability Graph of Uranium Distribution in Cortex of Rat Kidney at 28 Days Following Intravenous Injection of 1000 μg U per kg of Body Weight.

4.18, and 4.19. As can be noted in these figures, the data do not always closely follow the straight line as required for a log-normal distribution (Fig. 4.19). Thus, the log-normal distribution cannot always be used to describe quantitatively the effect of masses of uranium on perturbing the distribution.

Some additional studies were carried out to determine the gradient in concentration of uranium in the cortex. From a section of a kidney which had been bisected into left and right halves and then bisected again into anterior and posterior quarters, measurements of the tracks along rays extending inward from the peripheral edge of the cortex were made. The schematic diagram, Fig. 4.20, illustrates the position of the section in the kidney and the location of the rays along which counts were made. As can be seen, the rays roughly converge at a point on the outer edge of the medulla. The first microscopic field was located on the periphery of the kidney. Tracks contained in this field were counted and recorded. The second microscopic field was located one diameter (370 μ) interior, bordering on the first field, and counted. The counts per field for the six rays are shown in Table 4.13. At the top of each column appears the distance from the periphery. In some cases measurements could not be made at depths of 2035 μ due to irregularities in the sections. The average counts per field

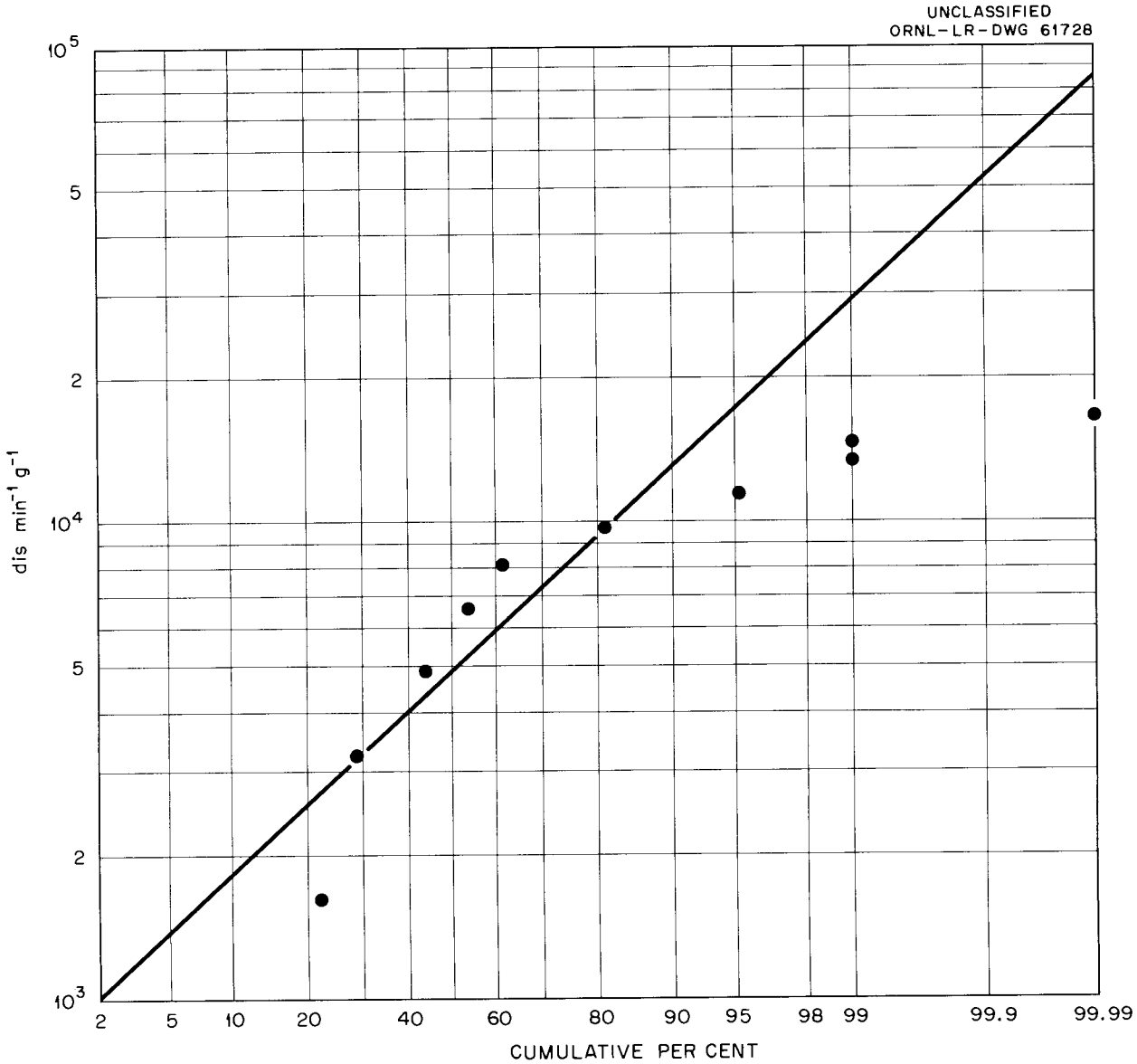

Fig. 4.19. Cumulative Log Probability Graph of Uranium Distribution in Cortex of Rat Kidney at One Day Following Intravenous Injection of 10 μg U per kg of Body Weight.

appear in the eighth row. These average counts per field decrease with increasing distance from the periphery of the cortex. Note also in the table that aggregates of activity occur at 185 and 555 μ. When the fields containing aggregates of activity are excluded and averages recomputed, the average counts per field appear to be relatively constant. By multiplying by 55 as explained above, the counts are thereby converted to dis/min/g. These values are plotted as a function of distance from the periphery of the kidney, and the graph appears in Fig. 4.21. The drop in concentration, for the case where aggregates are included, follows the expression

$$32{,}000 \text{ dis/min/g } e^{-0.693x/1240} ,$$

where x is the depth in microns. When aggregates are excluded, the concentrations appear to be relatively constant, as is noted in Fig. 4.21. This work is being continued to determine the gradient as a function of dose level administered to the animal and time after administration.

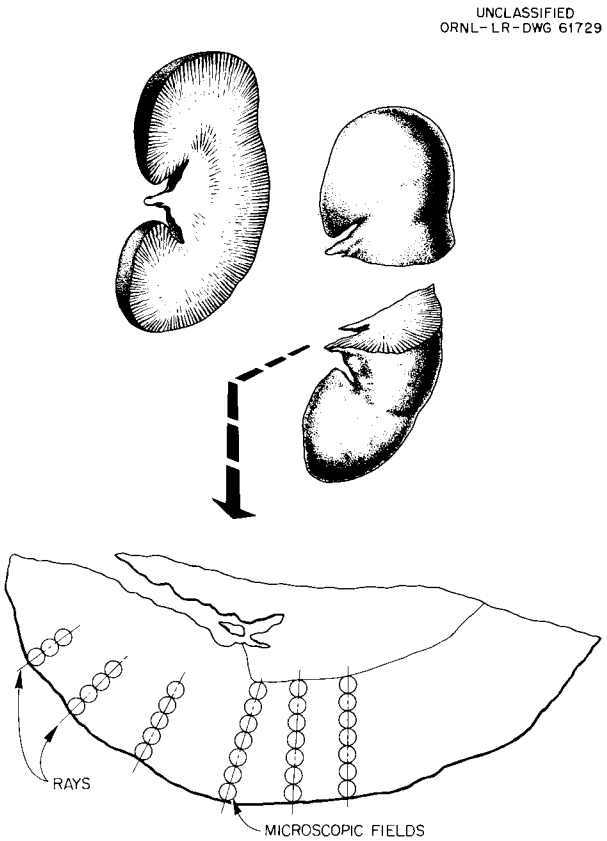

Fig. 4.20. Schematic Diagram.

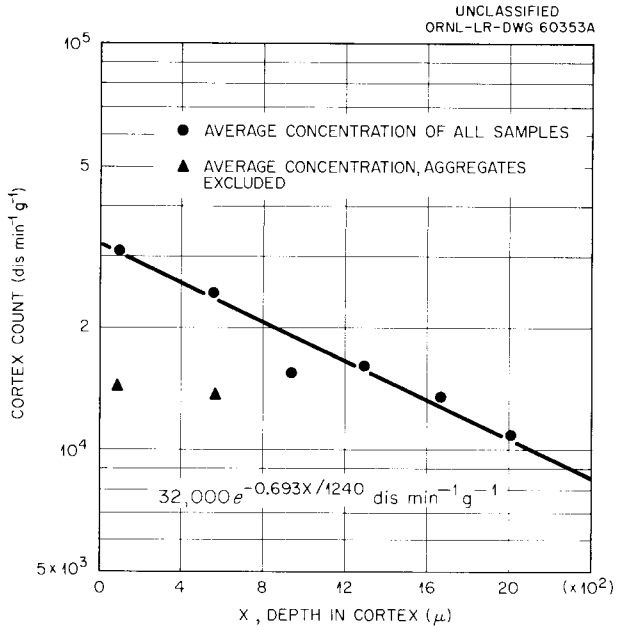

Fig. 4.21. Concentration in Rat Kidney as a Function of Distance from Outer Periphery of Cortex.

Table 4.13. Distribution of Uranium Concentrations in the Rat Kidney Cortex as a Function of Distance Along a Ray Extending from the Periphery Inward – High-Level Dose (1,000 μg/kg) at 1 Day Postinjection

Ray	Uranium Concentration (counts/field) at a Depth (μ) of					
	185	555	925	1295	1665	2035
1	132	87	234	244	235	199
2	653[a]	1,393[a]	332	217		
3	562	72	101			
4	822[a]	150	311	342	252	
5	78	394	384	351		
6	1,086	536	316			
Average						
counts/field	556 (257)[b]	438 (248)[b]	279	289	244	199
dis/min/g	30,580 (14,135)[c]	24,090 (13,640)[c]	15,345	15,895	13,420	10,945

[a]Denotes an aggregate was noted in the field.
[b]Denotes average of fields with aggregates excluded.
[c]Denotes average dis/min/g with aggregates excluded.

Studies to Determine Leaching of Uranium from Quartered Rat Kidney

In order to determine how much uranium is removed from the kidneys during fixing and dehydrating processes, all solutions of the latter were analyzed for their uranium content. Table 4.14 presents the data obtained in these studies. As can be noted at the bottom of the table, very little (0.3–4.7% of the total uranium) is leached by the solutions. In general, most leaching occurs when samples remain in the solution for extended (12–24-hr) periods.

Distribution of Uranium in Rat Kidney Tissues Prepared by the Freeze-Dry Method Compared with Formalin-Fixed Tissues

The purpose of this experiment was to observe the distribution of uranium in kidneys fixed by some method other than that employing 10% formalin in order to ascertain, if possible, whether formalin fixation was altering the distribution. Kidneys from 2 rats administered 1000 μg/kg and killed at 7 days and 1 day were bisected, the left half fixed with formalin and the right half freeze-dried. The freeze-dry method is a modification of that of

Table 4.14. Leaching of Uranium from Rat Kidneys in Fixing and Dehydrating Solutions

Composition of Solutions	Time in Solution (hr)	Uranium Activity of Solution (dis/min/sample)		
		For High Dose Level (1000 μg/kg)		For Low Dose Level (10 μg/kg)
		1 Day Postinjection	7 Days Postinjection	7 Days Postinjection
10% Formalin neutralized with excess of $CaCO_3$	24	14.8	2.7	1.8
35% Ethyl alcohol	1	7.4	2.1	0.9
	1	2.5	0.6	0.7
50% Ethyl alcohol	1	2.0	2.4	1.1
	1	0.7	0.7	0.5
70% Ethyl alcohol	1	1.1	0.5	0.3
	~17	9.0	0.4	4.5
80% Ethyl alcohol	0.5	0.8	0.4	0.3
	0.5	0.5	0.5	0.7
95% Ethyl alcohol	1	0.8	0.2	0.7
	1	0.4	0.1	0.2
N-Butyl alcohol	2	1.1	0.1	0.8
	2	3.1	0.1	0.4
Total:				
In solutions		44.2	10.7	12.8
In quartered kidney		8317.0	3591.0	254.0
Leached from kidney		0.5(%)	0.3(%)	4.7(%)

Pearse.[27] The formalin-fixation method is that usually employed in pathological laboratories,[28] the solutions being those shown in Table 4.14. Autoradiograms were made on the half kidneys.

Data obtained from both the formalin-fixed and the freeze-dried tissues were statistically classified and plotted. The distribution curves are shown in Figs. 4.22 and 4.23. Figure 4.22 shows the curves compiled from the data assembled from the tissues of the animal killed at 7 days postinjection. There is almost identical agreement between the one curve representing data from the freeze-dried tissue and the other from formalin-fixed tissue. Figure 4.23 shows the contrasting curves constructed from the data of the two differently prepared tissues from the animal killed at 1 day. These latter show a slight lack of agreement, perhaps due to the fewer number of samples obtainable with the more difficult technique from freeze-dried material.

[27] A. G. E. Pearse, *Histochemistry Theoretical and Applied*, 1960.

[28] R. D. Lillie, *Histopathologic Technic and Practical Histochemistry*, 1954.

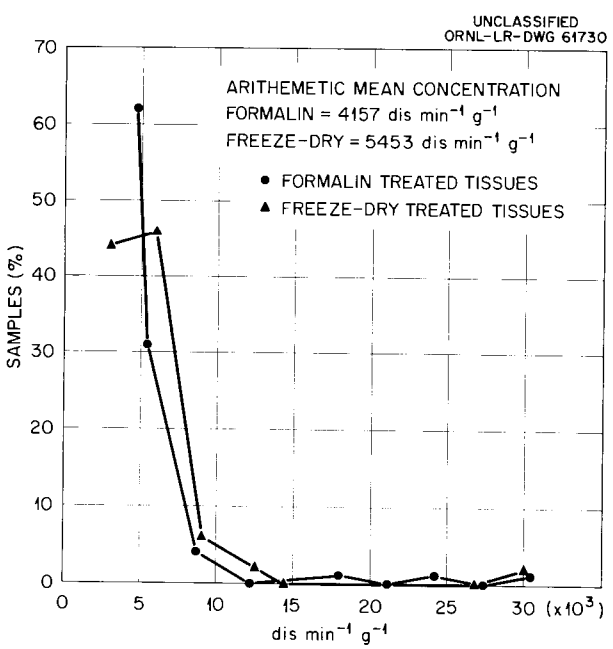

Fig. 4.22. Distribution of Uranium in Rat Kidney Cortex at Seven Days Following an Injection of 1000 μg U per kg as Estimated by the Freeze-Dry Method and the Formalin-Fixation Method.

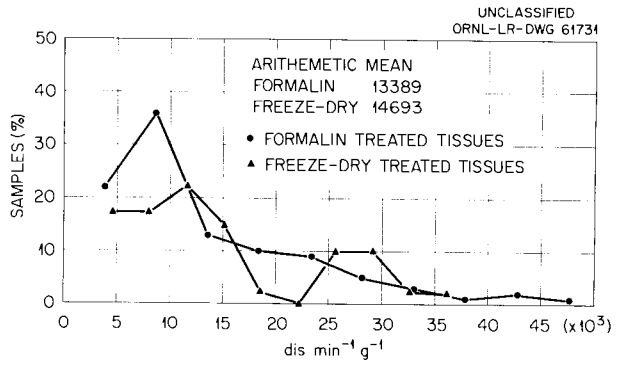

Fig. 4.23. Distribution of Uranium in Rat Kidney Cortex at One Day Following an Injection of 1000 μg U per kg as Estimated by the Freeze-Dry Method and the Formalin-Fixation Method.

The arithmetic means in dis/min/g, appearing on the graphs for the two animals estimated from counts made on formalin and freeze-dried tissue, agree quite closely. However, the mean dis/min/g based on freeze-dried data are slightly, but probably not significantly, higher. Additional autoradiograms are required to determine these distribution curves more accurately and to determine whether they differ significantly from each other.

Histological Changes in Proximal Tubules and Glomeruli of Uranium-Injected Rats

Some measurements of anatomical changes at the microscopic level were made on stained and autoradiographic sections of kidneys of animals injected with 1000 and 10 μg/kg. The diameters of normal-appearing proximal convoluted tubules, sectioned perpendicularly to their long axes, were measured. The tubules were not always uniformly circular, and thus a somewhat arbitrary procedure of measuring the narrowest diameter was adopted. Table 4.15 presents the measured diameters of 10 tubules observed in kidneys of control animals, animals injected with 10 μg of U per kg, and animals injected with 1000 μg of U per kg. All injected animals were killed at 4 days postinjection. The age of the control animal was unknown. As can be noted, the mean diameters of 10 tubules from experimental animals (42 and 40.5 μ) do not differ significantly from the mean of the controls (41.25). Measurements were made also on tubules of kidneys of rats killed at 7 days postinjection (Table 4.16). Here a slightly expanded tubule is evidenced in the injected animals relative to controls.

Table 4.15. Diameters of Proximal Rat-Kidney Tubules 4 Days After Injection of Uranium

	Tubule Diameter (μ)		
	Control*	Uranium Injected**	
		10 μg/kg	1000 μg/kg
	37.50	45.00	41.25
	37.50	45.00	37.50
	37.50	41.25	39.38
	33.75	43.13	43.13
	41.25	41.25	31.88
	39.38	37.50	50.63
	48.75	41.25	43.13
	48.75	33.75	39.38
	50.63	43.13	37.50
	37.50	48.75	41.25
Mean	41.25	42.00	40.50
Std. Dev.	1.85	1.3	1.5

*Periodic acid–Schiff stain.
**Hematoxylin and eosin stain.

Table 4.16. Diameters of Proximal Rat-Kidney Tubules 7 Days After Injection of Uranium

	Tubule Diameter (μ)		
	Control	Uranium Injected	
		10 μg/kg	1000 μg/kg
	41.25	43.13	46.88
	30.00	35.63	45.00
	41.25	50.63	37.50
	39.38	43.13	48.75
	43.13	45.00	48.75
	31.88	39.38	41.25
	33.75	33.75	41.25
	30.00	37.50	48.75
	33.75	33.75	33.75
	41.25	45.00	45.00
Mean	36.56	40.69	43.68
Std. Dev.	1.65	1.77	1.66

Measurements of diameters of glomeruli, following the method employed by Arataki,[26] were made on animals killed at 4 and 84 days postinjection. Arataki used the diameter of the Bowman's capsule as the maximum and the diameter of the glomerulus, in the strict sense, as the minimum. The average was obtained by taking the geometric mean of these quantities.

Table 4.17 presents the measurements of the diameters of glomeruli for control animals and for uranium-injected animals sacrificed at 4 and 84 days postinjection. The mean diameters, as defined by Arataki, appear at the bottom of the table. The means for the control animals are 96 μ determined on sections stained by the Periodic Acid–Schiff method and 104 μ determined on sections stained with hematoxylin and eosin. Appearing at the bottom of columns III, IV, and V are the mean diameters of animals injected with different levels of uranium. As can be seen, the mean diameter generally decreases as the amount injected into the animal increases. A dose level of 10 μg/kg produces $\sim$10% reduction in the diameters, while a dose level of 1000 μg/kg produces $\sim$16% reduction.

The effect of time on the diameters of animals injected with 100 μg/kg is evident. At 4 days the diameter is 81.7 μ (Col. IV), while at 84 days the diameter increases to 88.3 μ (Col. VI). Unfortunately, no control animals were sacrificed at 84 days. However, Arataki studied the change in diameter with age, and his data show that the mean diameters increase with age going from 94 μ for 90-day-old rats to 107 μ for 200-day-old rats. Since the uranium-injected rats were $\sim$90 days old when injected, then at 84 days postinjection they are $\sim$174 days old. Then, the measured diameter of 88.3 μ (Col. VI) for $\sim$174-day-old rats, although greater than 81.7 μ (Col. IV), still remains below the diameter of $\sim$100 μ (Cols. I and II) for $\sim$90-day-old control rats. Evidently the uranium has produced some long-term change in the glomerulus.

Nonuniform Distribution Factor

The work on the nonuniform distribution factor,[29] described in the report of 1960,[24] has been continued beyond that of the 10 kidneys discussed

[29] *Report of Committee II on Permissible Dose for Internal Radiation*, Pergamon Press, London, 1960.

Table 4.17. Diameters (in μ) of Glomeruli of Kidneys of Uranium-Injected Rats

Control				4 Days Postinjection						84 Days Postinjection	
				10 μg/kg		100 μg/kg		1000 μg/kg		100 μg/kg	
Max	Min	Max	Min	Max	Min	Max	Min	Max	Min	Max	Min
I[a]		II[b]		III		IV		V		VI	
86.25	73.13	93.75	82.50	103.13	80.63	106.88	86.25	84.38	65.63	80.63	73.13
127.50	93.75	120.00	103.13	108.75	90.00	80.63	71.25	91.88	71.25	103.13	90.00
108.75	93.75	103.13	84.38	90.00	75.00	71.25	60.00	103.13	84.38	75.00	50.63
112.50	78.75	84.38	56.25	91.88	82.50	82.50	71.25	84.38	61.88	90.00	63.75
86.25	67.50	112.50	93.75	90.00	69.38	103.13	82.50	110.63	69.38	90.00	80.63
106.88	84.38	131.25	108.75	90.00	56.25	90.00	75.00	78.75	61.88	105.00	86.25
78.75	63.75	103.13	90.00	90.00	65.63	88.13	82.50	93.75	78.75	105.00	86.25
127.50	97.50	127.50	108.75	108.75	71.25	90.00	69.38	93.75	71.25	103.13	71.25
101.25	75.00	120.00	108.75	108.75	75.00	71.25	56.25	78.75	78.75	93.75	67.50
108.75	88.13	112.50	112.50	93.75	58.13	82.50	67.50	103.13	75.00	75.00	75.00
120.00	120.00	125.63	108.75	108.75	88.13	112.50	93.75	106.88	84.38	103.13	80.63
90.00	71.25	135.00	123.75	97.50	76.88	93.75	80.63	93.75	73.13	80.63	60.00
125.65	93.75	108.75	93.75	101.25	75.00	90.00	78.75	84.38	76.88	98.38	80.63
121.88	103.13	108.75	97.50	112.50	93.75	90.00	63.75	112.50	88.13	78.75	67.50
112.50	90.00	112.50	93.75	82.50	69.38	93.75	71.25	112.50	88.13	65.63	56.25
112.50	101.25	131.25	123.75	112.50	97.50	80.63	75.00	103.13	84.38	116.25	112.50
103.13	84.38	98.38	90.00	112.50	93.75	63.75	56.25	90.00	60.00	90.00	82.50
93.75	75.00	71.25	63.75	97.50	84.38	86.25	76.88	88.13	67.50	135.00	118.13
112.50	84.38	138.75	123.75	105.00	75.00	98.38	88.13	101.25	71.25	121.88	110.63
108.75	90.00	108.75	86.25	103.13	82.50	106.88	93.72	78.75	63.75	121.88	103.13
Mean[c] 96		104		88.5		81.7		83.5		88.3	

[a]Periodic acid–Schiff stain.
[b]Hematoxylin and Eosin stain.
[c]See text for definition.

there. Counting has been completed on 29 half kidneys, the later counting being simplified by the use of a Reichert Micro-Viewscope.[30] Except for the two half kidneys in which the activity was found greater in the medulla, the average non-uniform distribution factor, N, estimated by autoradiographic counts on 27 half kidneys is the same as that reported earlier; namely, $N = 1.32$ with a range of 1.11 to 1.4. Except for one in which the activity was greater in the medulla, the average N, from 17 half kidneys, is 1.28 with a range of 1.06 to 1.48 when estimated by radiochemical methods. In analyzing these data for N, it should be noted that if the uranium were evenly distributed over the kidney, N would be 1, and that if 100% of the uranium were in the cortex and none in the medulla, N would be 1.43. Obviously $N = 1.3$ indicates that 90.9% of the uranium is localized in the cortex which comprises about 70% of the volume. This would lead one to conclude that for radioactive isotopes of uranium the absorbed radiation dose to the kidney, when the kidney is the critical organ, is approximately 1.4 times greater than when uniform distribution is assumed.

[30] Reichert Micro-Viewscope (Halco Co.).

5. HEALTH PHYSICS TECHNOLOGY

THE ORNL *IN VIVO* GAMMA-RAY SPECTROMETER FACILITY

B. R. Fish

P. E. Brown
J. M. Garner
J. L. Thompson
V. A. McKay[1]
S. A. Helf[2]
J. M. Robert[3]

Introduction

The ORNL *In Vivo* Gamma-Ray Spectrometer facility (IVGS) has been in operation since June 1960. At present, its primary use is as an aid in the detection and measurement of internal exposures. The facility is still under development, and all research connected with it is directed toward local problems. It is planned that, eventually, the program will include counting all new and terminating employees as well as accident cases and others having known potential exposures. As this routine function is met, more emphasis will be placed upon general research and development.

The IVGS Facility

A shielded room, 10 × 10 × 10 ft inside, was constructed of four layers of prewar steel armor plate having a total thickness of 14 in. Interior walls, ceiling, and floor are lined with ⅛ in. of low-radioactivity lead. Entrance to the shielded room is through a double-door airlock, which provides a buffer zone to reduce the loss of aged air from the counter area. Also accessible from the buffer zone is a 3 × 4 × 5-ft antechamber, called the "cubicle." This area has 14 in. of steel between it and the large counting room, and a 4-in.-diam by 4-in.-thick NaI(Tl) crystal is used to monitor the background during the time a subject is being counted in the big room. It may be possible, later on, to use this independent background to correct the subject's spectrum; however, presently the gross background is used merely to indicate that a recount is necessary. Because of the proximity of the IVGS facility to the reactor off-gas stacks, A^{41} has been observed in the subject's as well as the cubicle spectrum when the wind is from the northeast.

A recirculating air treatment system provides aged air for the steel room. Air from the big room is directed into the cubicle and then pumped through charcoal traps, cooling coils, and heaters to remove odors and excess moisture and to adjust the temperature. Slight positive pressure is maintained inside the steel rooms; hence, there is some loss of air because of leakage and opening the buffer-zone doors. Makeup air is provided by cylinders of breathing-air connected through a differential pressure controlled valve and a filtered line to the air recirculation system.

All the work, to date, has been with a 4-in.-diam × 4-in.-thick NaI(Tl) crystal, coupled through a 1.5-in.-thick Lucite light pipe to a 3-in. phototube (Dumont type 6363). The crystal assembly is manipulated by means of a manually operated positioning device (shown with the 8 × 4-in. crystal in Fig. 5.1). This crystal, canned in 0.005-in. aluminum, yields a resolution of 6.2% for K^{40} based upon the ratio of the width of the photopeak at half maximum to the energy corresponding to the photopeak (7.8% for Cs^{137}). Most of the routine counts have been made in the standard Argonne chair geometry. Background for the 4 × 4-in. crystal with a distilled-water-filled mannequin in the chair position is 498 counts/min for 0 to 1.50 Mev (σ = 5 counts/min). The 4 × 4-in. crystal has been used in conjunction with a 200-channel RIDL pulse height analyzer.

Routine Program

Before starting a limited counting schedule on February 27, 1961, work had been restricted to checking individuals in connection with known

[1]ORNL Instrumentation and Controls Division.

[2]Picatinny Arsenal; Dover, New Jersey.

[3]ORINS undergraduate trainee; Louisiana Polytechnic Institute.

Fig. 5.1. Crystal Positioning Device.

contaminating accidents. During this first phase of the program, 19 individuals were counted a total of 25 times. From the beginning of limited routine operation until July 1, 1961, 208 individuals were counted for a total of 235 times. Of the 208 persons checked in the routine program, 15 showed peaks in their gamma-ray spectra that could be identified as being different from the normal amounts of K^{40} and Cs^{137}. Isotopes recognized in these individuals are listed in Table 5.1. None of the human gamma-ray spectra have indicated as much as 50% of the maximum permissible body burden[4] of the isotopes identified.

[4]Report of ICRP Committee II. *Health Phys.* 3 (June 1960).

Status

The routine program has been suspended in order to install a Nuclear Data 512-channel analyzer and to install and calibrate the first of two 8-in.-diam × 4-in.-thick NaI(Tl) crystals (Fig. 5.2). The 8 × 4-in. crystals are each mounted in a 0.019-in. stainless steel can which has a matched window configuration embodying ORNL and Harshaw Chemical Company designs. Three 3-in.-diam phototubes (Dumont type 6363), selected for similarity of gain and resolution, are employed in parallel for each 8 × 4-in. crystal. The first 8 × 4-in. crystal will be mounted on the crystal manipulator (Fig. 5.1), and used instead of the 4 × 4-in. crystal in the routine counting program. When the second 8 × 4-in.

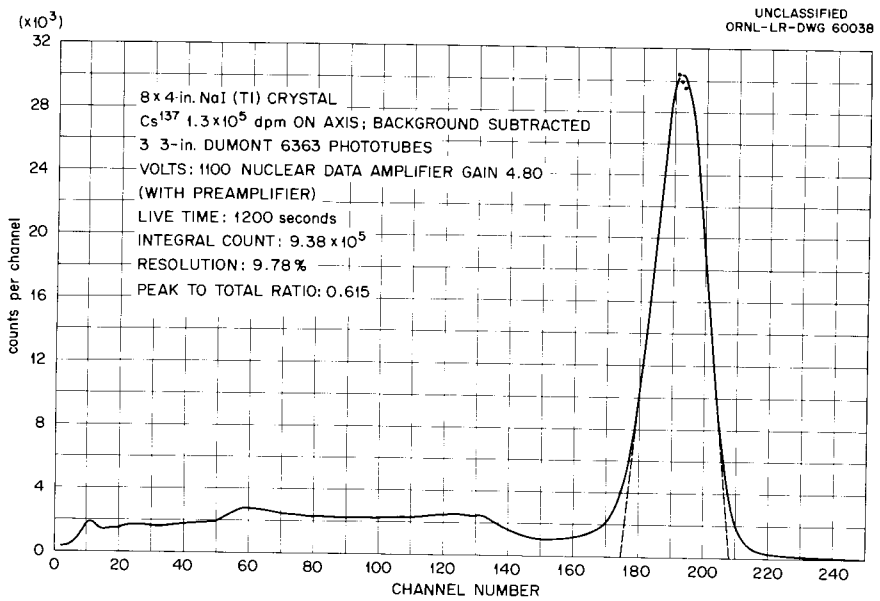

Fig. 5.2. Cesium-137 Spectrum.

Table 5.1. Measurable Contamination Found In Employees During Routine Whole Body Counting

Period February 27 to June 5, 1961

Isotope	Number of Individuals	Maximum Found (μc)	Per Cent of Maximum Permissible Body Burden
Cs^{137}	9	0.44	1.46
Co^{60}	7	0.08	0.8
Pa^{233}	3	2.8	7.0
Hg^{203}	2	0.8	20.0
I^{131}	1	0.012	1.7
Zr^{95}-Nb^{95}	1	0.03	0.2

crystal is completed, it will be suspended temporarily from a wall mount and used as an adjunct to the first crystal until a suitable floor mount can be fabricated. A digital computer program is being written to aid in the analysis of data accumulated in the routine program.

THE EXCRETION PATTERN OF Sr^{90} AND Ca^{45} IN MAN

L. B. Farabee

The most satisfactory way to estimate the internal body content of a beta-emitting radionuclide is to analyze the body excreta; however, the body burden can be determined only if the excretion pattern for this radioisotope has been established. A tenable way for estimating the body burden of Sr^{90} is of particular interest. Also of biological significance is the comparison of the metabolism and excretion of simultaneously injected Sr^{90} and Ca^{45}. Much experimental work has been done along this line with animals[5] as well as with humans.[6]

A study of the excretory pattern of Sr^{90} and Ca^{45} was carried out at Oak Ridge National Laboratory following an accident in which an employee received a puncture wound in the thumb with a hypodermic needle which had previously

[5] R. F. Palmer and R. C. Thompson, *Hanford Biology Research Annual Report for 1959*, HW-65500, pp 14–20 (1960).

[6] Margaret Bishop *et al.*, *Int. J. Rad. Biol.* 2, 125–42 (1960).

been used in a solution containing a mixture of Sr^{90} and Ca^{45}. Urine and fecal samples were submitted daily for several months and were analyzed for both radionuclides. The objectives of this study were to determine: (1) the distribution of Sr^{90} in urine and feces; (2) the initial dose of Sr^{90} from excretion data; and (3) the effect of increased calcium intake in the diet on the excretion of Sr^{90} and Ca^{45}. On the third day following the accident, the dietary calcium was increased to about 4 g/day and remained at this level during the study. This caused the urinary calcium level to double, while the bulk of the calcium was found in the feces.

Analyses of urine and feces for Sr^{90} were performed using a procedure which is described in ORNL-1932.[7] After separation of the Sr^{90}, the Ca^{45} was precipitated as calcium oxalate with the calcium normally present in the sample. All counting was done on a beta counter having a background of about 0.7 counts/min.

The amount of Sr^{90} initially injected into the finger was estimated by comparison with human excretion data reported by Margaret Bishop *et al.*[6] In that report two human subjects were injected with Sr^{85}, and the subsequent pattern of excretion was determined. During the first 22 days after injection, one individual excreted 64.5% of the injected Sr^{85} in the urine, while the other person excreted a total of 56.5%, giving an average for the two of 60.5%. During the first 22 days, the ORNL subject excreted an accumulative total of 9900 dis/min of Sr^{90} in the urine. Thus, assuming that this represents 60.5% of the initial amount, it is estimated that the exposed individual received approximately 1.64×10^4 dis/min of Sr^{90} initially. A comparison of the daily urinary excretion of the ORNL subject with the average of the two subjects of Bishop's study is shown in Fig. 5.3. The magnitude of the experimental excretion data was adjusted to correspond to an injection of 1.64×10^4 dis/min

[7] L. B. Farabee, *Procedure for the Radiochemical Analysis of Strontium and Barium in Human Urine*, ORNL-1932 (1957).

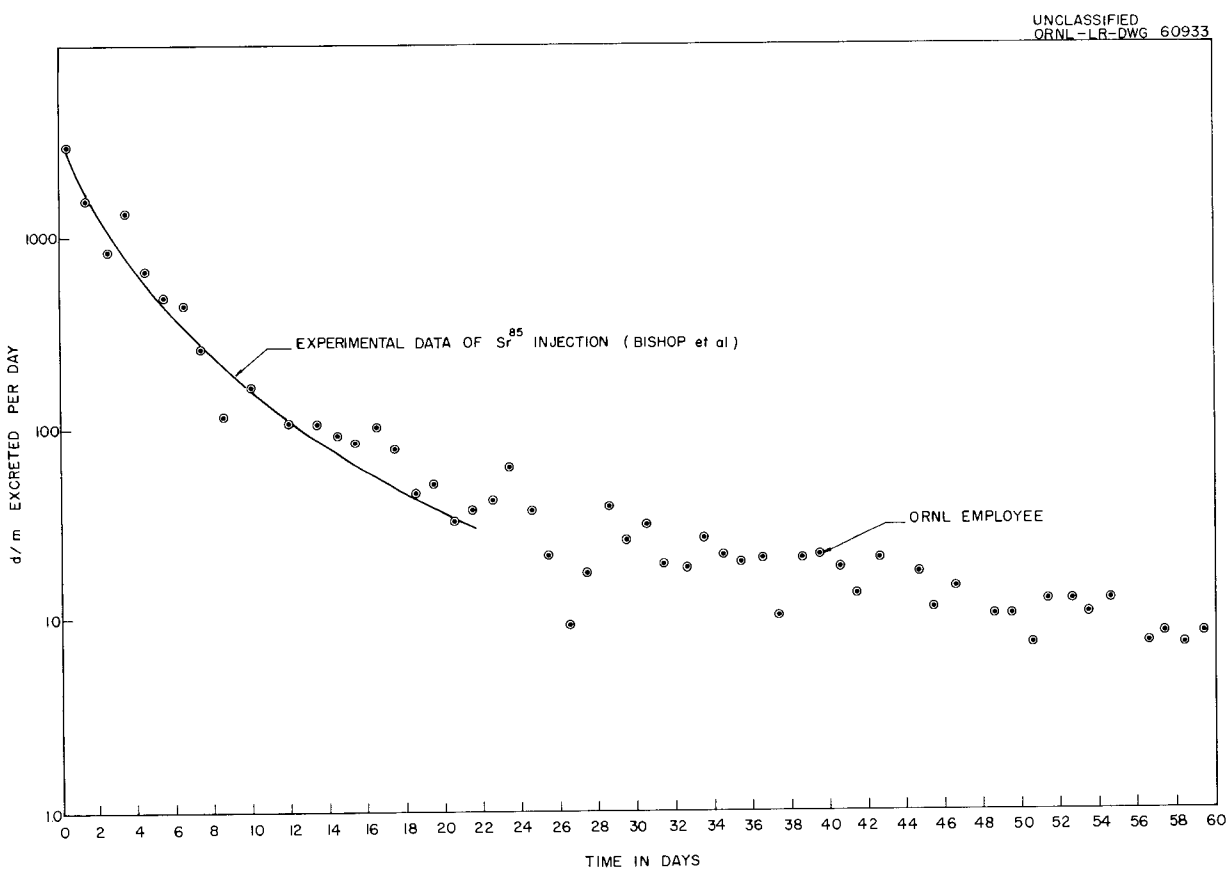

Fig. 5.3. Comparison of Sr^{90} Excreted in Urine by the ORNL Subject with Experimental Data (Bishop *et al.*).

of Sr^{90}. It is clearly shown that the patterns of urinary excretion in these cases are similar. The ratio of Ca^{45} to Sr^{90} was known to be 8; hence, the initially injected Ca^{45} dose was estimated to be 1.31×10^5 dis/min.

Elimination of Sr^{90} in the urine for the first 60 days (Fig. 5.3) appears to follow a typical strontium urinary excretion curve. Despite a greatly increased dietary calcium intake, no significant change in the strontium excretion pattern was observed. Fecal excretion of Sr^{90} by the ORNL subject was similar to that of the two experimental subjects and amounted to about 30% of the total excretion during the first 60 days.

Ca^{45} Excretion

The Ca^{45} excreted per day in both urine and feces, as well as the percentage of the estimated initial dose is listed in Table 5.2. Urinary excretion of Ca^{45} as a function of time after injection is shown in Fig. 5.4. The effect of a high calcium diet can be seen in the elevated peak of the excretion curve on the fourth day. This sudden increase in the Ca^{45} urinary excretion rate coincides with a deliberate increase in the stable calcium intake by a factor of approximately 2.

Discussion

Our results show clearly that the excretion pattern for Sr^{90} and Ca^{45} are not similar. Sr^{90} is predominantly excreted in the urine, whereas the ratio of urinary Ca^{45} to fecal Ca^{45} is about 1.6. A large increase in dietary intake of stable calcium has little effect on the excretion of Sr^{90}, but it apparently does increase Ca^{45} elimination as has been reported for animals.[5]

Table 5.2. Daily Urine and Fecal Excretions of Ca^{45} During the First 22 Days After Exposure

Days After Injection	Ca^{45} Excretion in Urine (dis min^{-1} day^{-1})	Per Cent of Dose/Day	Ca^{45} Excretion in Feces (dis min^{-1} day^{-1})	Per Cent of Dose/Day
1	6,187	4.80	3,636	2.78
2	4,886	3.73	3,636	2.78
3	3,764	2.88	1,760	1.34
4	6,652	5.08	1,760	1.34
5	4,955	3.79	1,760	1.34
6	3,933	3.00	5,460	4.17
7	3,139	2.40	3,212	2.38
8	2,510	1.92	975	0.74
9	2,475	1.89	968	0.74
10	1,632	1.25	(1,000)*	(0.76)
11	1,632	1.25	(1,000)*	(0.76)
12	1,652	1.26	1,038	0.79
13	1,652	1.26	1,038	0.79
14	1,492	1.14	1,920	1.47
15	966	0.74	556	0.43
16	983	0.75	(586)*	(0.45)
17	1,311	1.00	(586)*	(0.45)
18	1,028	0.63	617	0.47
19	555	0.42	1,142	0.87
20	645	0.49	(500)*	(0.38)
21	600	0.46	(500)*	(0.38)
22	552	0.42	439	0.34
Total	53,201	40.6	34,089	26.0

*Portions of these samples were lost; numbers in parentheses are estimates of the average excretion rates at the given times.

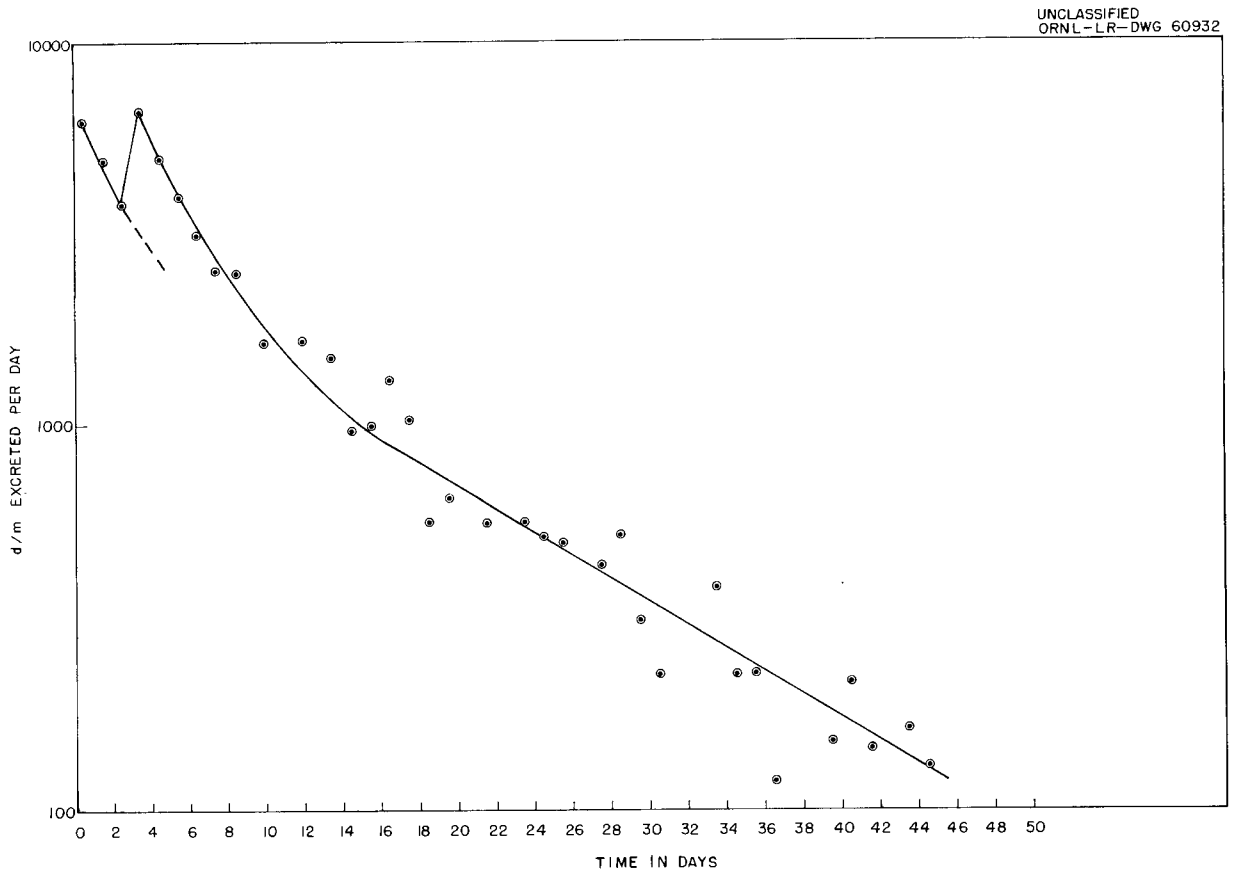

Fig. 5.4. The Excretion of Ca^{45} in Urine.

EXPLODING WIRE AEROSOL GENERATOR

F. G. Karioris[8] J. W. Youngblood

An aerosol generator based on the exploding wire phenomenon has been developed.[9] Although designed primarily for the production of uranium oxide aerosols for inhalation studies, the device is applicable to many other experiments, particularly those requiring a high-yield generator whose output is reproducible in concentration and particle size.

The generator, shown in Fig. 5.5, consists of a dc power supply, capacitor bank, triggered sphere gap, and an explosion chamber. Twenty GE Pyronal capacitors connected to give 20 μf capacitance may be charged to 20 kv by a variable voltage power supply. Maximum energy storage is approximately 4000 joules. The sphere gap consists of 1.125-in.-diam hardened steel spheres mounted on 0.50-in. threaded brass bolts and supported in a Lucite yoke mounted on standoff insulators. In tests thus far, the separation between the spheres has been set to support a potential difference of 30 kv, and the gap is triggered by ionizing the air between the spheres with a high-frequency leak detector. Surge currents up to 60,000 amp have been observed by means of a coaxial shunt of conventional design. For safety of operation and maintenance, all equipment is enclosed in a 68 × 70 × 25-in. cabinet equipped with safety interlocks which automatically discharge the capacitors through a resistor bank whenever a cabinet door is opened. As an additional safety device, grounding cables are provided for manually shorting the capacitors.

The explosion chamber consists of a 1-in.-thick disk of Lucite clamped between two Pyrex

[8]Consultant, Marquette University, Milwaukee, Wis.

[9]F. G. Karioris *et al.*, *Health Phys. Div. Ann. Progr. Rept. July 31, 1960*, ORNL-2994.

Fig. 5.5. Exploding Wire Aerosol Generator.

glass end-bells. There is a 1 × 5-in. rectangular slot in the center of the disk which supports 0.5-in.-diam stainless steel electrodes. Wire to be exploded is connected between the electrodes and lies along the principal axis of the slot. Electrode spacing may be adjusted to accommodate wires up to 4 cm in length. Gas ports provide for filling the explosion chamber with selected atmospheres and for withdrawing the aerosol.

Although the production of uranium oxide aerosols was the primary objective for building the device, 14 other metals have been exploded with the results shown in Table 5.3. Metallic particles are produced by noble metals and oxide particles by common metals when the explosion occurs in air. Electron diffraction has established that metallic particles are produced when copper is exploded in an atmosphere of argon. X-ray diffraction analysis has shown that the aerosol produced by the explosion of uranium in air consists of U_3O_8 with less than 5% contamination by β-UO_2 for explosions above 8 kv. This permits calculating the per cent yield from the weight of solid material collected after the explosion of a known weight of uranium. Over the range 6–15 kv, the yield increases slowly with capacitor charge, the average being 85.1 ± 3.9%. The composition of the other aerosols is being investigated by x-ray diffraction to permit calculation of yields. Table 5.3 indicates that, in general, a large fraction of the exploded wire is dispersed in the aerosol.

It is possible to produce aerosol concentrations as high as 10 g/m^3 within the 4.7-liter volume of the explosion chamber. This cor-

Table 5.3. Aerosols from Exploding Wire Generator

(All explosions at 10 kv with 20 μf; 2.5 cm length of wire)

Metal	Amount Exploded (mg)	Amount Aerosol Collected on Millipore (mg)	Color of Smoke	Color of Deposit on Millipore	Composition by X-Ray Diffraction
Ag	32.6	24.6	Black	Black	Ag
Al	3.9	8.6	White	Gray	Al_2O_3
	10.9	24.0			
Au*	108.3	63.4	Brown	Chocolate	Au
Cu**	25.8	7.3	Red	Velvet black	Cu
Cu	26.0	20.4	Brown	Brown	Cu_2O, CuO
Fe	8.3	9.1	White	Brown	
Mg	20.3	20.2	White	Gray	
Mo	31.4	30.5	Blue-white	Teal blue	
Ni	47.4	34.5	White	Gray	
Pb	70.2	57.9	White	Cream	
Pt*	156.8	62.5	Brown	Black	Pt
Sn*	25.5	27.1	White	Pale tan	SnO_2
Ta	91.9	39.2	White	Gray	
Th	11.0	11.3	White	Violet	ThO_2
U	10.0	10.0	White	Gray	U_3O_8, β-UO_2
W	95.8	52.1	White	Purple	Complex mixture

*Electron micrographs of thermal precipitator samples show isolated spheres. All others show spheres, chains and agglomerates.
**In argon atmosphere. All other exploded in air.

responds initially to about 3×10^{11} particles/cm^3. Electron micrography shows that the aerosols are typical smokes consisting of small spherical particles, chains, and agglomerates. The count median diameter for uranium exploded at 15 kv is 0.02 μ. Nitrogen adsorption analysis of U_3O_8 particles produced at 10 kv gave a specific surface of 15.2 m^2/g, corresponding to an effective diameter of 0.05 μ. Median particle size tends to decrease, although very slowly, with increasing voltage; and the size distribution function appears to be intermediate between normal and log-normal. Additional work is required to establish these relations quantitatively.

An aerosol of isolated spherical particles rather than chains or agglomerates has been produced by diluting freshly prepared U_3O_8 smoke in a 200-liter chamber and fanning for one hour. Although the mass concentration decreases exponentially with a 30-min half-life during fanning, the resulting aerosol can be stored for several hours after preparation. The median diameter of the particles is about 0.02 μ, with the result that the settling velocity of the aerosol is so small that concentration in the chamber remains relatively constant for long periods after fanning is discontinued. Aerosol produced in this manner, enriched in U^{235}, has been administered to mice to determine its distribution, retention, and excretion characteristics.

STUDIES OF SURFACE CONTAMINATION

G. W. Royster, Jr.

Introduction

In recognition of obvious gaps in the knowledge of the significance of radioactive surface contamination, a study was initiated in January 1961. Usually, it is agreed that "loose" radioactive contamination is undesirable in the working environment; however, there is no generally accepted definition of the term "loose" contamination, nor is there any agreement on methods to measure "removability." After surveying the very meager literature on the subject, it was decided that the first step should be to examine available methods of measuring "removable" contamination.

Intercomparison of Methods for Measuring "Removable" Contamination

Thorium dioxide dust, 3 μ in diameter, was allowed to settle onto 16 different test surfaces, and the loose contamination was sampled by smears and adhesive papers. These sampling techniques were compared with a new method developed by the aerosol group. This third procedure employs air impingement to redisperse loose contamination from the surface, and the resulting airborne material is collected on a filter (the "smair" sampler, Fig. 5.6). Results of this study are reported elsewhere[10–12] and may be summarized as follows: No one method of sample removal is representative of the other mechanisms of redispersion; the adhesive paper samples consistently removed the largest fraction of the total contamination. The efficiency of each sampling technique was observed as a function of the area measured per sample. For example, smear samples were taken by the standard method[10] except that a single sample paper was rubbed over one or more than one standard area. There is no loss in the sampling efficiency of the smair technique

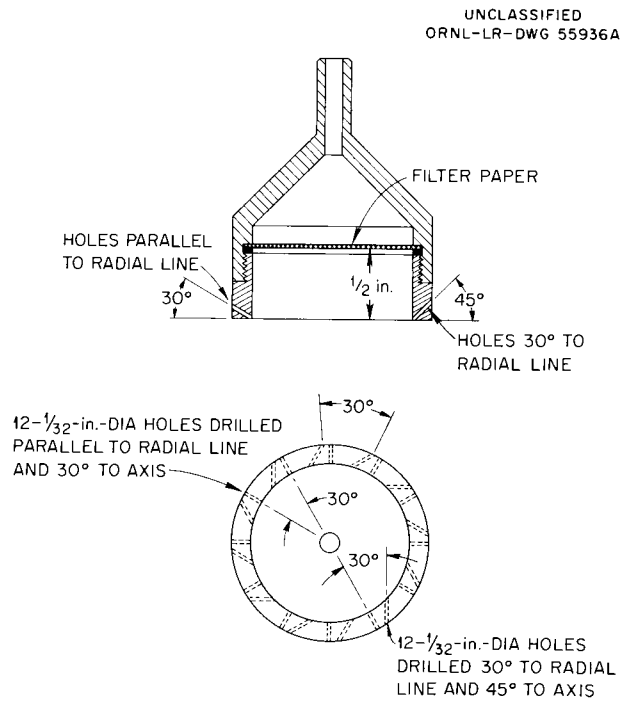

Fig. 5.6. Smair Sampler.

as the area is increased from 20 to 200 cm^2 per sample. Smear samples show a relatively rapid decrease in removal efficiency initially, and then seem to decrease in efficiency more slowly. Adhesive samples also show a decrease in removal efficiency as the measured area increases. Increasing the concentration of the contaminant on the surface (constant area per sample), reduces the removal efficiency of a smear even more rapidly than the effect of increasing the area (constant concentration). Adhesive paper samples also show a decrease in the removal of ThO_2 from surfaces as the concentration on the surface increases. In contrast, the smair samples show essentially no change in removal efficiency as surface dustiness increases.

Effect of Surface Roughness on the Fraction Removable

In order to compare the roughness of the test materials, negative replicas were made of several representative surfaces and were studied with the aid of electron and of light microscopy. Figure 5.7 shows microphotographs (180X) of the replicas of fiberboard, asphalt tile, waxed asphalt tile, and Plexiglas surfaces using oblique illumination.

---

[10] G. W. Royster, Jr., and B. R. Fish, ORNL CF-61-3-39 (1960).

[11] G. W. Royster, Jr., and B. R. Fish, *Studies of Contamination. I. Intercomparison of Methods for Measuring "Removable" Contamination,* presented at Annual Health Physics Society Meeting, June 12–16, 1961, Las Vegas, Nev.

[12] B. R. Fish *et al., Health Phys. Technology Section Quart. Progr. Rept., January–March 1961,* ORNL CF-61-7-67.

UNCLASSIFIED
PHOTO 55015

FIBER BOARD (80*)

ASPHALT TILE (55*)

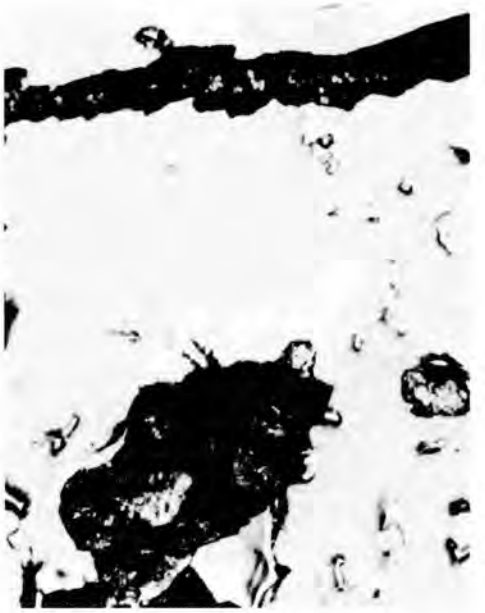

ASPHALT TILE WAXED (35*)

PLEXIGLAS (8*)

*ROOT MEAN SQUARE DEVIATION IN MICROINCHES

Fig. 5.7. Microphotographs of Surface Replicas.

Plexiglas, representative of a smooth surface, yields a high per cent removal by the smear technique (71.3%). Fiberboard, a rough surface consisting of a matrix of overlapping fibers, yields a low per cent (23.5%) removed by the same technique. It should be pointed out that what appears to be macrostructural detail on the Plexiglas surface is, in the main, sub-surface structure in the replica. Dark areas on the photographs represent pits and crevices. Further evidence of the effect of roughness on the fraction removed per sample is shown in Fig. 5.8. The per cent recovery is plotted as a function of surface roughness measured by means of a stylus-type Surfindicator.[13] With this instrument, a diamond stylus is moved across the surface, and the root mean square deviation of the test surface is recorded electronically. Regression lines, calculated by the method of least squares, for the adhesive paper and smair measuring techniques have slopes of −0.095 (σ = 0.11) and −0.15 (σ = 0.15) respectively. These results imply that the slopes of the two curves do not significantly deviate from zero at the 95% confidence level. However, data obtained by the smear technique, as a function of surface roughness, yield a slope of −0.60 (σ = 0.18), indicating that the slope of the smear data is different from zero. Student's t test applied to the smear sample data shows that the slope is significantly different from zero at the 98% confidence level.

These studies are being continued to include the effects of temperature, humidity, static electrical charges on surfaces, aging the deposit, particle size, and surface hardness using thorium dioxide and other compounds.

[13]Brush Instrument Company, Surfindicator Model BL-110.

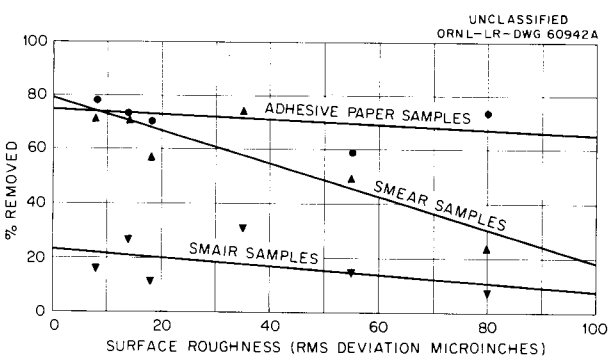

Fig. 5.8. Effect of Surface Roughness on Per Cent of Total Contamination Removed per Sample.

A STUDY OF METHODS FOR MONITORING THE I^{131} CONTAMINATION IN THE ENVIRONMENT

J. W. Youngblood
P. E. Brown G. W. Royster, Jr.
J. L. Thompson S. L. Wood[14]

The high fission yield and the volatility of I^{131} make it one of the more probable and in many cases the controlling radio-contaminant in gaseous wastes from nuclear installations. Analyses of stack effluent samples have shown this to be true at ORNL. This particular fission product, although volatile at ordinary temperatures, is strongly adsorbed on typical pasture grasses. Thus, for cattle grazing several hundreds of square meters daily, the intake represents the deposition of I^{131} from thousands of cubic meters of air. Unlike many fission products, iodine is readily assimilated from the gastrointestinal tract and is highly concentrated in the thyroid gland. In the case of cattle a significant quantity is also secreted in milk (approximately 3% of the daily intake is secreted per day).[15] Thus, in addition to being a hazard to the grazing animal, I^{131} deposited on pasture grasses may also result in a hazard to human beings, particularly infants whose diets consist largely of milk. Chamberlain has conducted a series of experiments to determine the deposition rate of airborne I^{131} onto grass.[16] Assuming a maximum permissible level of 10^{-4} μc/g of grass, the deposition rate leads to an equilibrium air concentration of 10^{-12} μc/cc, lower by a factor of 3000 than the recommended $(MPC)_a$ value for continuous occupational exposure. This fact, along with the impending possibility that considerably more stringent limits may be placed by the Federal Radiation Council on the allowable levels of I^{131} exposure to the general population, prompted our investigation into monitoring methods for evaluating the extent of I^{131} contamination in

[14]ORINS research participant, Austin Peay State College, Clarksville, Tenn.

[15]A. C. Chamberlain *et al.*, Paper No. 393 in *Proc. Intern. Conf. Peaceful Uses Atomic Energy, Geneva 1955*, 13.

[16]A. C. Chamberlain and R. C. Chadwick, AERE H/R 993 (1952).

the environment as a result of ORNL operations.

Monitoring techniques selected for study include the collection and analysis of grass and cattle thyroid samples. This type of monitoring program requires considerable manpower for sample collection and analysis and necessitates the fulltime use of a gamma-ray spectrometer. Nevertheless, some monitoring technique of comparable sensitivity will definitely be needed if the proposed lower I^{131} limits are established officially. A significant reduction in sampling frequency might be achieved through the application of atmospheric dispersion models for predicting quantitatively the distribution of I^{131} in the environment. Therefore the purpose of this study was to establish criteria for the detection of $\mu\mu c$ levels of I^{131} on grass and in cattle thyroids, and to compare the analytical values with those predicted using Culkowski's modification of Sutton's and Chamberlain's atmospheric diffusion equations.[17] Culkowski's model affords a finer breakdown of wind behavior by using the mean wind speed for each of six speed groups and the fraction of the total time the wind is represented in each class.

Grass and thyroid samples were collected from a number of locations and analyzed with an RIDL 200-channel gamma-ray spectrometer. To minimize background, a narrow energy increment containing only the center portion of the 0.364-Mev photopeak was used. Thyroid samples were first digested in a solution of 20 g NaOH and 20 ml H_2O before counting with either a 4 × 2-in. or a 3 × 3-in. NaI(Tl) crystal. Counting efficiencies of the crystals for I^{131} were 15% and 9.5% respectively. At the 95% confidence level, the lower limit of detectability was 8 $\mu\mu c$ per thyroid for a 60-min count. Grass samples were collected from an area of one square meter and a portion (150 g) of the grass was counted with the 4 × 2-in. crystal. Counting efficiency in this case was 9.1% and the lower limit of detectability was 12 $\mu\mu c$ per 150-g sample.

A total of 158 cattle thyroid samples from 12 different grazing areas was obtained from a local meat packing company and analyzed during the period from August 1960 through March 1961. The grazing areas ranged from 6 to 100 miles from ORNL. In only 15% of the samples was the I^{131} concentration below the lower limit of detection. The method of procuring samples provided useful data on the I^{131} background within a 100-mile radius of ORNL, but the randomness of sampling locations complicated an evaluation of the diffusion model for predicting the buildup of radioactivity in the environment. For sampling locations at known distances in the prevailing wind directions from ORNL and not separated from it by large topographical features, the ratio between the amount of I^{131} found in the thyroid and the predicted deposition per square meter of grass averaged 550. For sampling stations separated from ORNL by major topographic features and lying along minor wind axes, this ratio was erratic and generally less than 100. However, this might be expected from the infrequency of winds in those directions and because of the increased dilution achieved from the turbulence produced by the presence of ridges. Results show a gradual decrease in I^{131} with increasing distance from ORNL; values ranges from 100 $\mu\mu c$ per g of thyroid for cattle grazing at a distance of 6 miles to a general ambient level of 2 $\mu\mu c/g$ at distances of 50 to 100 miles from the Laboratory. From July 1960 through October 1960 there was no over-all increase or decrease in the levels of I^{131} found in the thyroids; however, after November there was a general decrease in thyroid radioactivity. This may reflect the result of increased supplementary feeding during the winter months.

A total of 130 grass samples was collected and analyzed for I^{131}. Fifty-two of these were from areas within 6 miles of ORNL, while the majority of the others corresponded to thyroid sampling sites and contained an insufficient quantity of I^{131} for detection. The close-in grass samples were collected from 10 locations over the period from August 1960 through December 1960. The average ratio between the measured and predicted quantities of I^{131} per square meter of grass was 0.4 ± 0.19.

The consistency with which the predicted deposition values exceeded the measured ones is probably a result of the values assigned to the diffusion coefficients in the dispersion equation.

[17] W. M. Culkowski, *Sixth AEC Air Cleaning Conference*, TID-7593.

Other possible sources of error affecting the I^{131} deposition predictions are:

(1) *Inaccuracies in the available data on I^{131} releases from the stack.* Effluent samples were collected with a filter paper at the end of 70 ft of 1-in.-diam stainless steel pipe. An earlier study had shown that a varying fraction of the iodine is retained on both the filter paper and pipe walls. In an effort to account for these losses it was assumed that the filter collection efficiency was 10% and that 55% of the I^{131} was deposited on the conduit walls.

(2) *The assumption of a constant retention half-life and deposition velocity for I^{131} on grass.* A deposition velocity onto grass of 0.025 m/sec was assumed. In order to account for the disappearance of I^{131} from grass due to weathering effects and radioactive decay, a half-life of five days was used in the calculations.

(3) *Lack of accurate information on the location of sampling sites.* This was particularly true in regard to the grazing area of the cattle from which thyroids were obtained.

Despite these sources of error, the ratios between the measured and the predicted I^{131} values suggest that further investigations under better conditions would yield an acceptable system for predicting and monitoring I^{131} in the ORNL environment. In anticipation of such a study, steps have been taken to reduce the sources of error. An isokinetic effluent sampling system employing an absolute filter and an activated charcoal cartridge has been installed inside the appropriate stack. Analysis of the collected activity provides data on the release of the other effluent contaminants as well as I^{131}. Arrangements have been made, with the help of M. C. Bell,[18] to obtain thyroids from cattle in selected grazing areas, as well as to collect grass samples from these locations. In addition, F. A. Gifford and W. M. Culkowski, local U.S. Weather Bureau, have devised and are testing an instrument for more accurately determining atmospheric dispersion coefficients. Arrangements are being made to obtain this information for use in predicting the dispersion and distribution of I^{131} in the environment.

[18] Dr. M. C. Bell, University of Tennessee-AEC Agricultural Research Farm.

ESTIMATION OF FAST NEUTRON DOSE TO MAN BY THE ANALYSIS OF HAIR FOR P^{32}

L. B. Farabee W. T. Thornton

Introduction

A nuclear accident may expose personnel to significant amounts of ionizing radiation. The measurement of such an exposure involves the use of many instruments of dosimetry designed to measure the neutron and the gamma-ray dose. The method which has been found to be most reliable for evaluating the neutron dose of persons exposed to mixed radiation fields is that obtained from the formation of Na^{24} in the body via the reaction $Na^{23}(n,\gamma)Na^{24}$. However, the spectrum of incident neutrons must be known. In the Hurst threshold detector system this is determined by means of detector units located at fixed dosimeter stations in conjunction with data from gold, indium, and sulfur in the employee film badge or in a radiation dose orientation belt.[19,20]

Despite advances in physical dosimetry, serious exposures to neutrons have consistently occurred in the absence of adequate means of evaluating total radiation dose to man. As a supplement to present physical dosimetry methods, it is proposed that postexposure analysis of hair for P^{32}, which arises via the reaction $S^{32}(n,p)P^{32}$, will aid in evaluating the fast neutron dose (> 2.5 Mev) and give information relative to the orientation of the exposed person. Human hair contains about 49 ± 1.4 mg of sulfur per g of hair, and this composition has been found to be constant regardless of color, consistency, and anatomical distribution.[20] The phosphorus content was found to be 0.15 ± 0.04 mg per g of hair. Since the activation cross sections of sulfur and of phosphorus are essentially the same, almost all the P^{32} activity present in the hair sample will be derived from fast neutron capture by sulfur.

Analytical Procedure

A chemical procedure has been developed which isolates the P^{32} from a 1-g hair sample with a

[19] G. S. Hurst and R. H. Ritchie, *Radiation Accidents: Dosimetric Aspects of Neutron and Gamma-Ray Exposures*, ORNL-2748 (Part A) (Nov. 2, 1959).

[20] D. F. Peterson, V. E. Mitchell, and W. H. Langham, "Estimation of Fast Neutron Doses in Man," (Los Alamos Scientific Laboratory) (to be published in Health Physics Journal).

chemical yield of 99%. The hair sample is placed in a 125-ml Erlenmeyer flask fitted with an air-cooled reflux condenser. About 10 to 15 ml of concentrated HNO_3 is added and heat applied until most of the organic material is destroyed. After cooling the flask, 5 ml of perchloric acid is added, and the flask is heated to about 190°C until white fumes of $HClO_4$ appear. The sample is cooled, diluted to 50 ml, and an aliquot is taken for sulfur analysis. The P^{32} analysis is made on the rest of the sample as follows:

(1) 5 mg of lanthanum is added and the phosphate of the hair is precipitated as $LaPO_4$ in a basic medium;
(2) this precipitate is filtered and washed several times with small aliquots of water;
(3) the precipitate is dissolved from the filter with 50 ml of hot 0.2 *N* HNO_3;
(4) this solution is then passed over a cation exchange resin column, which is 1.0 cm in diameter and contains 3 ml of Dowex-50 × 12 (H^+ cycle), at a flow rate of 3 ml/min, followed by three 10-ml washes of 0.2 *N* HNO_3; and
(5) the effluent which contains the P^{32} is evaporated and transferred to a stainless steel dish for counting.

Sample counting is done on a low-background beta counter for which the counting efficiency is 31% and the background is 0.8 counts/min. Since 1 rad of fast neutrons produces only 1.9 dis/min of P^{32} in a 1-g hair sample, good sensitivity depends upon using a beta counter with a low background and upon obtaining adequate separation of the P^{32} from fission products which might contaminate the hair in an accidental exposure. The use of larger samples of hair will increase the sensitivity for fast neutrons. It has been shown that this procedure is equally as good for 3- and 5-g hair samples as for 1-g samples.

Exposure Studies

Individual 1-g hair samples sealed in polyethylene envelopes were placed on a plastic mannequin filled with tissue-equivalent solution. Sulfur pellets, spaced at 90° intervals, were placed in a belt around the waist of the same mannequin. These samples were exposed in a field of mixed neutron and gamma radiation at the Tower Shielding Reactor in Test No. 1 on February 18, and in Test No. 2 on March 4. The P^{32} in the sulfur detectors was measured by the Radiation Dosimetry Section, and these were the referee dosimeters for fast neutrons in positions around the waist of the mannequins.

Results

Rad doses of fast neutrons, estimated by hair activation, were remarkably close to the referee dosimetry measured by activation of sulfur (Table 5.4). Differences in orientation produced significant differences in estimated dose depending upon the location of the hair sample; for example, the average of the front-to-back ratios of three phantoms was about 10. This work has demonstrated the ease of estimating fast neutron dose down to about 5 rad and of establishing the approximate orientation of the person by means of hair analysis for P^{32}. Additional studies now under way include testing the analysis procedure for discrimination against possible fission product contamination.

Table 5.4. Comparison of Fast-Neutron Dose Estimates (>2.5 Mev), Based on Hair Sulfur Activation Measurements, with Other Physical Dosimetry

Sample Number	Hair Analysis Dose (rad)	Referee Dosimetry Dose (rad)	Per Cent of Referee Dose
	Test No. 1		
1	32.7	32.6	100
2	35.3	32.6	108
3	35.6	33.4	107
4	31.6	33.4	95
5	32.0	31.9	100
6	36.8	31.9	115
7	33.6	32.6	103
8	37.6	32.6	115
9	30.0	33.4	90
10	30.7	33.4	92
11	34.4	31.9	108
12	4.8	4.9	98
	Test No. 2		
1	69.5	68.6	101
2	70.1	68.6	102
3	66.6	68.1	98
4	65.6	71.4	92
5	63.4	63.6	100
6	67.6	63.6	106
7	67.0	68.8	97
8	61.1	68.8	89
		Average	100.8 (σ = 7.5)

6. EDUCATION, TRAINING, AND CONSULTATION

AEC FELLOWSHIP PROGRAM

E. E. Anderson M. F. Fair
C. E. Breckinridge K. Z. Morgan

Twenty-six students completed the course in Applied Radiation Physics at Vanderbilt University in May 1961. Twenty of these were AEC Fellows, four were from the Nuclear Engineering Department of the University, one was a student from Indonesia, and one was a student from the Philippines. The 20 AEC Fellows reported to the Health Physics Division in June for their applied health physics training.

Eleven of the Fellows were granted extensions to the Fellowship to complete the requirements for the MS degree. Of these, two have chosen to do their research at the Health Physics Division, and nine will return to Vanderbilt University. The AEC Fellows for the 1961-62 program were selected in March 1961, and a group of 17 will enroll at Vanderbilt University in September 1961.

OTHER ACTIVITIES

E. E. Anderson M. F. Fair
C. E. Breckinridge

A ten-week course in health physics was conducted by the Health Physics Division of the Oak Ridge National Laboratory and the Special Training Division of the Oak Ridge Institute of Nuclear Studies for personnel of the Atomic Energy Commission and from state departments of health. Thirteen participants attended the course from March 6, 1961 to May 12, 1961.

A 60-hr course in health physics was presented by the Division for the ORSORT Program. This was a combined lecture and laboratory course covering all aspects of health physics.

Members of the Section gave lectures on various topics in health physics to NSF-AEC Institutes in Radiation Biology for High School Teachers, to university groups under the ORINS-ORNL lecture program, and to professional societies.

During the year a total of nine trainees associated with nuclear energy programs in this country and abroad trained in various phases of applied health physics. The name and home agency for each individual assigned for training follow: James F. Bresson, The Martin Company, Baltimore, Maryland; Jose Ferrer-Monge, Puerto Rico Nuclear Center, Puerto Rico; Lester Skolil, San Diego College, San Diego, California; Jose Feola, IAEA student, Argentina; Stelio Marchi and Luciano de Franceschi, CAMEN, Livorno, Italy; A. L. Mohan, AEET, Bombay, India; S. Joedoatmodjo, ICA student, Indonesia; and Samuel Helf, Picatinny Arsenal, New Jersey.

Lectures and discussion periods on particular phases of health physics were given for the following:

1. U.S. Public Health Service
2. ORNL Orientation Program
3. MIT Practice School
4. ORINS Radioisotope Techniques Course
5. ORINS Medical Division – Courses in Clinical Techniques
6. ORNL Radiation Safety and Control Lecture Series

A member of the staff arranged and conducted Health Physics Division seminars and organized programs for visitors to the Division.

PUBLICATIONS

E. T. Arakawa, "Radiation Dosimetry in the Hiroshima and Nagasaki Atomic Bomb Survivors," *New Engl. J. Med.* **263**, 488–93 (1960).

W. T. Atyeo, E. B. Baker, and D. A. Crossley, Jr., "The Genus *Raphignathus* Dugès (Acarina, Raphignathidae) in the United States with Notes on the Old World Species," *Acarologia* **3**, 14–20 (1961).

W. T. Atyeo and D. A. Crossley, Jr., "Labidostommidae from Australia (Acarina, Prostigmata) with the Description of the New Species," *Trans. Roy. Soc. S. Australia* **84**, 83–86 (1961).

S. I. Auerbach and D. A. Crossley, Jr., "A Sampling Device for Soil Microarthropods," *Acarologia* **3**, 279–87 (1961).

J. A. Auxier, C. H. Bernard, and W. T. Thornton, "Silver Metaphosphate Glass for Gamma-Ray Measurements in Co-Existent Neutron and Gamma-Radiation Fields," pp 503–10 in *Selected Topics in Radiation Dosimetry*, Brüder Rosenbaum, Vienna, Austria, 1961.

J. A. Auxier, J. S. Cheka, and F. W. Sanders, WT-1725 (Mar. 17, 1961) classified.

J. A. Auxier, F. W. Sanders, and P. N. Hensley, "A Device for Determining the Orientation of Persons Exposed to Neutron and/or Gamma Radiation," *Health Phys.* **5**, 226 (1961).

J. A. Auxier, F. W. Sanders, and W. S. Snyder, "Na^{24} Activation in the Dosimetry of Nuclear Accidents," pp 201–11 in *Radioactivity in Man* (ed. by G. R. Meneely, M.D.), Thomas, Springfield, Ill., 1961.

C. H. Bernard, W. T. Thornton, and J. A. Auxier, "Silver Metaphosphate Glass for Gamma-Ray Measurements in Coexisting Neutron and Gamma Radiation Fields," *Health Phys.* **4**, 236–43 (1961).

S. R. Bernard, "Mathematical Studies of the Interaction of Respiratory Gases with Whole Blood. I. O_2 Absorption," *Bull. Math. Biophys.* **22**, 391–415 (1960).

S. R. Bernard, "Mathematical Studies of the Interaction of Respiratory Gases with Whole Blood. II. CO_2 Absorption," *Bull. Math. Biophys.* **23**, 1–14 (1961).

S. R. Bernard and M. R. Ford, "Note on the ICRP and NCRP Recommended MPC_a for Insoluble Ra^{226} Compounds," *Health Phys.* **4**, 307–8 (1961).

R. D. Birkhoff, "Dosimetry of Beta-Rays and Electrons," pp 1328–38 in *Proceedings of Ninth International Congress for Radiology* (ed. by B. Rajewsky), Thieme, Stuttgart, 1960.

R. D. Birkhoff, J. M. Cohen, H. B. Eldridge, and R. H. Ritchie, "The Spherical Condenser as a High Transmission Particle Spectrometer: II. Disc Source," *Nuclear Instr. & Methods* **8**, 313–19 (1960).

R. E. Blanco and E. G. Struxness, *Waste Treatment and Disposal Progress Report for April and May 1961*, ORNL CF-61-7-3 (July 1961).

W. J. Boegly, Jr., R. L. Bradshaw, F. M. Empson, and F. L. Parker, "Disposal of Radioactive Wastes in Natural Salt – Field Experiments," pp 577–90 in *Proceedings of the Fifteenth Industrial Waste Conference, May 3–5, 1960, Purdue University, Lafayette, Ind.* (March 1961).

R. L. Bradshaw, J. J. Perona, J. T. Roberts, and J. O. Blomeke, *Evaluation of Ultimate Disposal Methods for Liquid and Solid Radioactive Wastes, Part I – Interim Liquid Storage*, ORNL-3128 (July 31, 1961).

J. G. Carter, *Low Temperature Thermoluminescence of the Gamma Irradiated Amino Acids and Proteins*, ORNL-2970 (Nov. 16, 1960).

R. S. Caswell, G. R. Ringo, R. H. Ritchie, and E. Tochilin, *Measurements of Neutron Flux and Spectra for Physical and Biological Applications*, National Bureau of Standards Handbook 72, Washington, D.C. (July 15, 1960).

K. E. Cowser, "Treatment of Low-Activity-Level Waste Water," *Nuclear Safety* **2**, 59–63 (1960).

K. E. Cowser, T. F. Lomenick, and W. M. McMaster, *Status Report on Evaluation of Solid Waste Disposal at ORNL: I*, ORNL-3035 (Feb. 8, 1961).

D. A. Crossley, Jr., "Comparative External Morphology and Taxonomy of Nymphs of the Trombiculidae," *Univ. Kansas Sci. Bull.* **40**, 135–321 (1960).

D. A. Crossley, Jr., and K. K. Bohnsack, "Long-Term Ecological Study in the Oak Ridge Area. III – The Oribatid Mite Fauna in Pine Litter," *Ecology* **41**, 785–90 (1960).

D. A. Crossley, Jr., and H. F. Howden, *Insect Species on Vegetation of White Oak Lake Bed, Oak Ridge, Tennessee*, ORNL-3094 (1961).

D. A. Crossley, Jr., and H. F. Howden, "Insect-Vegetation Relationships in a Radioactive Waste Area," *Ecology* **42**, 302–17 (1961).

D. A. Crossley, Jr., and M. E. Pryor, "The Uptake and Elimination of Cesium-137 by a Grasshopper – *Romelea microptera*," *Health Phys.* **4**, 16–20 (1960).

D. A. Crossley, Jr., and J. H. Schnell, "Comparative Elimination of Radiostrontium and Radiocesium by Grasshoppers," *Ann. Entomol. Soc. Am.* **54**, 459–61 (1961).

F. J. Davis, "Neutron Dose Determinations with Threshold Detectors," pp 399–404 in *Selected Topics in Radiation Dosimetry*, Brüder Rosenbaum, Vienna, Austria, 1961.

F. J. Davis, "System for Dose Measurements in Radiation Incidents," *Nuclear Safety* **2**, No. 1 (September 1960).

W. de Laguna and E. G. Struxness, "Disposal of Radioactive Wastes into Deep Geologic Formation" (abstract of paper, American Nuclear Society, 1960 Winter Meeting, December 14, 1960), *Trans. Am. Nuclear Soc.* **3**(2), 548–50 (1960).

P. B. Dunaway and S. V. Kaye, "Cotton Rat Mortality During Severe Winter," *J. Mammalogy* **42**, 265–68 (1961).

F. M. Empson (ed.), W. J. Boegly, Jr., R. L. Bradshaw, H. Kubota, F. L. Parker, and E. G. Struxness, *Status Report on Waste Disposal in Natural Salt Formations: III*, ORNL-3053 (July 11, 1961).

B. R. Fish, "Inhalation of Uranium Aerosols by Mouse, Rat, Dog, and Man," *Inhaled Particles and Vapours*, pp 151–65, Pergamon, London, 1961.

B. R. Fish and S. R. Bernard, "Studies to Determine Uranium Retention in Man and Small Animals," *Industrial Hygiene News Report* **4**(3), 1 (1961).

D. G. Gardiner and K. E. Cowser, "Optimization of Radionuclide Removal from Low-Level Process Wastes by the Use of Response Surface Methods," *Health Phys.* **5**, 70–78 (1961).

William Happer and R. D. Birkhoff, "Angular Response of a Partially Shielded Cylindrical Dosimeter," *Health Phys.* **4**, 62–64 (1960).

J. C. Howell, "Birds of a Valley," *Audubon Magazine*, November-December, 283–86 (1960).

H. H. Hubbell, Jr., A. P. Hull, and R. D. Birkhoff, *A Small Wrist Dosimeter for Beta and Gamma Radiation*, ORNL-2730 (Sept. 30, 1960).

G. S. Hurst, "Mixed Radiation Dosimetry and Its Application in Determining the Dose Received by the Japanese at Hiroshima and Nagasaki," pp 1361–74 in *Proceedings of Ninth International Congress for Radiology* (ed. by B. Rajewsky), Thieme, Stuttgart, 1960.

G. S. Hurst, R. S. Caswell, F. C. Maienschein, H. H. Rossi, J. A. Sayeg, R. H. Schuler, and R. W. Wallace, *Measurements of Absorbed Dose of Neutrons and Mixtures of Neutrons and Gamma Rays*, National Bureau of Standards Handbook 75, Washington, D.C., 1961.

G. S. Hurst, R. H. Ritchie, F. W. Sanders, P. W. Reinhardt, J. A. Auxier, E. B. Wagner, A. D. Callihan, and K. Z. Morgan, "Dosimetric Investigation of the Yugoslav Radiation Accident," *Health Phys.* **5**, 179–202 (1961).

G. S. Hurst and E. B. Wagner, "Special Counting Techniques in Mixed Radiation Dosimetry," pp 409–17 in *Selected Topics in Radiation Dosimetry*, Brüder Rosenbaum, Vienna, Austria, 1961.

D. G. Jacobs, "Sorption of Cesium by Conasauga Shale," *Health Phys.* **4**, 157–63 (1960).

D. G. Jacobs, "Strontium Movement in the Soil," *Nuclear Safety* **2**(2), 63–65 (1960).

H. Kubota and T. Tamura, *Waste Disposal in Salt: I. The HNO_3-NaCl Reaction*, ORNL-2984 (Sept. 15, 1960).

K. Z. Morgan, "Dosimetry Requirements for Protection from Ionizing Radiation," pp 3–23 in *Selected Topics in Radiation Dosimetry*, Brüden Rosenbaum, Vienna, Austria, 1961.

R. J. Morton *et al.* (eds.), *Status Report No. 1 on Clinch River Study*, ORNL-3119 (July 27, 1961).

D. J. Nelson, "Biological Concentration of Radioisotopes from Aquatic Environments," *Nuclear Safety* **2**, 81–83 (1960).

D. J. Nelson, "Improved Chlorophyll Extraction Method," *Science* **132**, 351 (1960).

D. R. Nelson, R. D. Birkhoff, R. H. Ritchie, and H. H. Hubbell, Jr., "Measurement of Electron Flux in Media Bombarded by X-Rays," *Health Phys.* **5**, 203–11 (1961).

Jacob Neufeld and P. S. Doyle, "Electromagnetic Interaction of a Beam of Charged Particles with Plasma," *Phys. Rev.* **121**, 654–58 (1960).

Jacob Neufeld and W. S. Snyder, "Estimates of Energy Dissipation by Heavy Charged Particles in Tissue," pp 35–44 in *Selected Topics in Radiation Dosimetry*, Brüder Rosenbaum, Vienna, Austria, 1961.

F. L. Parker, W. J. Boegly, Jr., R. L. Bradshaw, F. M. Empson, L. Hemphill, E. G. Struxness, and T. Tamura, "Disposal of Radioactive Wastes in Natural Salt," pp 365–86 in *Disposal of Radioactive Wastes, Proceedings of the Scientific Conference on the Disposal of Radioactive Wastes, Monaco, Nov. 16–21, 1959*, vol 2, International Atomic Energy Agency, Vienna, 1960.

R. H. Ritchie and H. B. Eldridge, "Thermal Neutron Flux Depression by Absorbing Foils," *Nuclear Sci. and Eng.* **8**, 300–11 (1960).

R. H. Ritchie, H. B. Eldridge, and E. E. Anderson, "Calculation of the Radiation Yield from Fission Assemblies and Comparison with Experiments," pp 657–66 in *Selected Topics in Radiation Dosimetry*, Brüder Rosenbaum, Vienna, Austria, 1961.

R. H. Ritchie and G. E. Whitesides, *Equilibrium Electron Distributions in Elastically Scattering Gases*, ORNL-3081 (June 2, 1961).

G. W. Royster, Jr., and B. R. Fish, *Studies of Surface Contamination. I. Intercomparison of Methods for Measuring "Removable" Contamination*, ORNL CF-61-3-39 (1961).

R. E. Shanks and J. S. Olson, "First-Year Breakdown of Leaf Litter in Southern Appalachian Forests," *Science* **134**, 194–95 (1961).

W. S. Sndyer, "Estimation of Dose Distribution within the Body from Exposures to a Criticality Accident," pp 647–56 in *Selected Topics in Radiation Dosimetry*, Brüden Rosenbaum, Vienna, Austria, 1961.

T. D. Strickler, *Average Energy Loss Per Ion Pair Produced by Alpha Particles in Binary Gas Mixtures*, ORNL-3080 (July 3, 1961).

E. G. Struxness, K. E. Cowser, and W. de Laguna, "Radioactive Waste Management and Disposal at Oak Ridge" (abstract of paper, American Nuclear Society, December 14, 1960), *Trans. Am. Nuclear Soc.* **3**(2), 543–45 (1960).

T. Tamura and D. G. Jacobs, "Improving Cesium Selectivity of Bentonites by Heat Treatment," *Health Phys.* 5, 149–54 (1961).

T. Tamura and E. G. Struxness, *Removal of Strontium from Wastes*, ORNL CF-60-10-43 (Nov. 28, 1960).

K. T. Thomas, D. G. Jacobs, T. Tamura, and E. G. Struxness, *Strontium Sorption Using Naturally Occurring Ion Exchange Materials*, ORNL CF-60-10-35 (Dec. 5, 1960).

J. H. Thorngate, *The Cosine-Cubed Neutron Spectrometer*, ORNL-2969 (Apr. 19, 1961).

W. T. Thornton and J. A. Auxier, *Some X-Ray and Fast Neutron Response Characteristics of Silver Metaphosphate Glass Dosimeters*, ORNL-2912 (Aug. 11, 1961).

E. G. Wagner and G. S. Hurst, "A G-M Tube Gamma-Ray Dosimeter with Low Neutron Sensitivity," *Health Phys.* 5, 20–26 (1961).

N. Wald, M.D., and G. E. Thoma, M.D., *Radiation Accidents: Medical Aspects of Neutron and Gamma-Ray Exposures*, ORNL-2748, Part B (Feb. 21, 1961).

PAPERS

E. T. Arakawa

Some Physical Considerations in the Atomic Bomb Investigations, Atomic Bomb Casualty Commission, January 28, 1960, Nagasaki, Japan.

E. T. Arakawa, A. L. Frank, R. D. Birkhoff, and R. H. Ritchie

Optical Emission of Irradiated Ag and Al Foils, Americal Physical Society, April 24–27, 1961, Washington, D.C.

J. A. Auxier

Dosimetric Considerations in Criticality Exposures, Scientific Meeting on the Diagnosis and Treatment of Acute Radiation Injury, October 17–21, 1960, Geneva, Switzerland.

J. A. Auxier and F. W. Sanders

Application of Phantoms to Blood Sodium Activation Studies, Health Physics Society, Sixth Annual Meeting, June 11–16, 1961, Las Vegas, Nevada.

S. R. Bernard

Recent Studies of Uranium Distribution and Excretion in Man and Small Animals, Sixth Conference on Industrial Hygiene and Air Pollution, University of Texas, December 3, 1960, Austin, Texas.

R. D. Birkhoff

Slowing Down Spectra and Light Emission of Irradiated Metals, Vanderbilt University, October 19, 1960, Nashville, Tennessee.

J. S. Cheka

Glass as a Long-Term Personnel Dosimeter, Conference on Microdosimetry, February 14–15, 1961, Rochester, New York.

M. J. Cook and W. S. Snyder

Variability of Relative Organ Concentration of Trace Elements in Human Tissue, Health Physics Society, Sixth Annual Meeting, June 11–16, 1961, Las Vegas, Nevada.

K. E. Cowser

Hydrological and Geochemical Aspects of Fission Product Retention and Movement in the White Oak Creek Drainage Basin, Meeting of the Advisory Committee for Biology and Medicine, May 12, 1961, Oak Ridge, Tennessee

K. E. Cowser and T. Tamura

Significant Results in Low-Level Waste Treatment at ORNL, Health Physics Society, Sixth Annual Meeting, June 11–16, 1961, Las Vegas, Nevada.

D. A. Crossley, Jr.

Fission Product Accumulation by White Oak Lake Bed Insects, Ecological Society of America, August 29, 1960, Stillwater, Oklahoma.

F. J. Davis and P. W. Reinhardt

Radiation Measurements Over Simulated Plane Sources, Health Physics Society, Sixth Annual Meeting, June 11–16, 1961, Las Vegas, Nevada.

W. de Laguna and E. G. Struxness

Disposal of Radioactive Wastes to Deep Geological Formations, American Nuclear Society, 1960 Winter Meeting, December 12–15, 1960, San Francisco, California.

P. B. Dunaway

Bioaccumulation of Radioisotopes by Mammals in a Radioactive Environment, American Society of Mammalogists, Forty-First Annual Meeting, June 12–15, 1961, Urbana, Illinois.

P. B. Dunaway and S. V. Kaye

Studies of Small-Mammal Populations on the Radioactive White Oak Lake Bed, Wildlife Management Institute, Twenty-Sixth North American Wildlife and Natural Resources Conference, March 6–8, 1961, Washington, D.C.

H. B. Eldridge, R. H. Ritchie, and V. E. Anderson

Radiation Yield from Some Bare Critical Assemblies, Health Physics Society, Sixth Annual Meeting, June 11–16, 1961, Las Vegas, Nevada.

B. R. Fish and S. R. Bernard

Studies to Determine Uranium Retention in Man and Small Animals, Sixth Conference on Industrial Hygiene and Air Pollution, December 2–3, 1960, University of Texas, Austin, Texas

B. R. Fish and F. G. Karioris

Inhalation of U_3O_8 Smoke from Exploding Wires, Health Physics Society, Sixth Annual Meeting, June 11–16, 1961, Las Vegas, Nevada.

G. S. Hurst

Human Data Derived from Radiation Accidents, St. Louis University Hospital, August 12, 1960, St. Louis, Missouri.

Some Molecular Biophysics Experiments at ORNL, Donner Laboratory, June 19, 1961, Berkeley, California.

G. S. Hurst, L. B. O'Kelly, and T. E. Bortner

Dissociative Electron Capture in Water Vapor, Radiation Research Society, May 15–17, 1961, Washington, D.C.

G. S. Hurst and R. H. Ritchie

Some General Remarks on Radiation Dosimetry, Health Physics Society, Sixth Annual Meeting, June 11–16, 1961, Las Vegas, Nevada.

D. G. Jacobs

Cesium Exchange Properties of Vermiculite, Health Physics Society, Sixth Annual Meeting, June 11–16, 1961, Las Vegas, Nevada.

D. G. Jacobs and T. Tamura

The Mechanism of Ion Fixation Using Radioisotope Techniques, 7th International Congress of Soil Science, August 14–24, 1960, Madison, Wisconsin.

Mineral Reactions Pertinent to the Treatment and Disposal of Radioactive Wastes, 2d AEC Working Meeting on Fixation of Radioactive Wastes, Stable Solid Media, September 27–29, 1960, Idaho Falls, Idaho.

S. V. Kaye and P. B. Dunaway

Bioaccumulation of Radioactive Isotopes by Herbivorous Small Mammals, Health Physics Society, Sixth Annual Meeting, June 11–16, 1961, Las Vegas, Nevada.

Small Mammal Population Dynamics and Bioaccumulation of Fission Products on White Oak Lake Bed, American Association for the Advancement of Science, One Hundred Twenty-seventh Meeting, December 26–31, 1960, New York, New York.

R. J. Morton

Problems and Practice in Radioactive Waste Disposal, Monthly Meeting of Chattanooga Branch, American Society of Civil Engineers, January 10, 1961, Chattanooga, Tennessee

D. R. Nelson, J. G. Carter, and C. J. Weinberg (presented by J. G. Carter)

Thermoluminescence from Gamma-Irradiated Biochemicals: Investigation of Emission Spectra, Radiation Research Society, May 15–17, 1961, Washington, D.C.

D. R. Nelson and C. J. Weinberg (presented by C. J. Weinberg)

Thermoluminescence Curves, Spectra, and Activation Energies of Aromatic Amino Acids, Trypsin, and Spores, American Physical Society, Southeastern Section, March 30–April 1, 1961, Louisville, Kentucky.

G. W. Royster, Jr.

Electrodeposition of Uranium from Urine, Sixth Annual Meeting of the Bio-Assay and Analytical Chemistry Group, October 13–14, 1960, Sandia Base, New Mexico.

G. W. Royster, Jr., and B. R. Fish

Studies of Surface Contamination. I. Intercomparison of Methods for Measuring "Removable" Contamination, Health Physics Society, Sixth Annual Meeting, June 11–16, 1961, Las Vegas, Nevada.

F. W. Sanders

A Complete Dosimetry System for Monitoring Nuclear Accidents; Nuclear Accident at the Oak Ridge Y-12 Plant; Nuclear Accident at the Boris Kidric Institute; and, ORNL's Role in the Atomic Bomb Casualty Commission Program, Japan Atomic Energy Research Institute, December 15, 1960, Tokai-Mura, Japan,

The Problem of Dosimetry, Radiation Research Society, May 15–17, 1961, Washington, D.C.

E. G. Struxness, K. E. Cowser, and W. de Laguna

Radioactive Waste Management and Disposal at Oak Ridge, American Nuclear Society, 1960 Winter Meeting, December 12–15, 1960, San Francisco, California.

T. Tamura

Waste-Sorbent Interactions for Strontium Removal, Health Physics Society, Sixth Annual Meeting, June 11–16, 1961, Las Vegas, Nevada.

LECTURES

E. E. Anderson

Health Physics Society, Symposium on University Curricula in Radiological Health, August 2, 1960, Princeton Inn, Princeton, New Jersey.

Radiation Hazards and Current Practices in Radiation Protection (3 lectures), August 4–5, 1960, University of Wyoming, Laramie, Wyoming.

Radiation Protection Problems Today, August 4, 1960, Public Lecture, Laramie, Wyoming.

Radiation Hazards Today, November 5, 1960, University of Tennessee, Knoxville, Tennessee.

Radiation Hazards and Current Practices in Radiation Protection, November 15, 1960, Lander College, Greenwood, South Carolina.

S. I. Auerbach

Ecology and Radioactivity (5 lectures), Institute for College Teachers of Animal Ecology, August 1–6, 1960, Boulder, Colorado.

The Effect of Radiation on Ecological Systems, Research Information Meeting, Headquarters Staff, Office of Civil Defense Mobilization, September 22, 1960, Battle Creek, Michigan.

Ecology and the Radioactive Problem, Department of Biological Sciences, Western Illinois University, January 12–14, 1961, Macomb, Illinois.

Research Opportunities in National Laboratories, Physics Department, Western Illinois University, January 12–14, 1961, Macomb, Illinois.

Implications of Radioecology for Wildlife Research, Annual Meeting Cooperative Wildlife Research Unit Leaders, U.S. Fish and Wildlife Service, March 2–4, 1961, Washington, D.C.

Panel – *Effect of Radiation on Ecological System of the Biosphere Due to Atomic Industry Operations,* International Atomic Energy Agency, March 30, 1961, Vienna, Austria.

Ecology, ORINS Course in Health Physics, April 11, 1961, Oak Ridge, Tennessee.

The Ecology Program of the Oak Ridge National Laboratory, Biology Department, Northwestern University, April 20–22, 1961, Evanston, Illinois.

Radioecology, Animal Ecology Class, University of Tennessee, May 23, 1961, Knoxville, Tennessee.

J. A. Auxier

Neutron Dosimetry, Summer Postgraduate Course in Medical Aspects of Radiological Health, St. Louis University Hospital, July 20, 1961, St. Louis, Missouri.

Nuclear Accidents, Summer Postgraduate Course in Medical Aspects of Radiological Health, St. Louis University Hospital, July 21, 1961, St. Louis, Missouri.

W. J. Boegly, Jr.

Radiation Problems Related to Public Health, College of Education, University of Tennessee, May 15, 1961, Knoxville, Tennessee.

R. L. Bradshaw

Engineering and Hazards Evaluation, Short Course in Health Physics for Public Health Personnel, presented for AEC and ORINS at ORNL, April 28, 1961, Oak Ridge, Tennessee.

C. E. Breckinridge

A Study of Inverse Isotope Dilution Analyses of Chlortetracycline, AAAS Meeting, December 29, 1960, New York, New York.

Health Physics, ORINS Medical Division, May 4, 1961, Oak Ridge, Tennessee.

P. H. Carrigan, Jr.

The Hydrologic Cycle, ORSORT, April 5, 7, 1961, Oak Ridge, Tennessee.

Dispersion in Surface Waters, Short Course in Health Physics for Public Health Personnel, presented for AEC and ORINS at ORNL, April 18, 1961, Oak Ridge, Tennessee.

K. E. Cowser

Process Waste Water Treatment, Health Physics Course for ORSORT Foreign Students, December 30, 1960, Oak Ridge, Tennessee.

Handling, Treatment, and Disposal of Chemical Processing Wastes at ORNL, Regional Conference on Radiological Health, U.S. Public Health Service, April 5, 1961, New York, New York; Short Course in Health Physics for Public Health Personnel for AEC and ORINS, April 17, 1961, Oak Ridge, Tennessee; U.S. Public Health Service Course on Environmental Health Aspects of Nuclear Reactor Operations, May 9, 1961, Oak Ridge, Tennessee.

D. A. Crossley, Jr.

Insect-Vegetation Relationships in a Radioactive Waste Area, Department of Entomology, University of Nebraska, November 7, 1960, Lincoln, Nebraska.

W. de Laguna

Radioactive Waste Disposal, Sigma Xi Lecture, Carnegie Institute of Technology, April 12, 1961, Pittsburgh, Pennsylvania.

F. M. Empson

Radiation Problems Related to Public Health, College of Education, University of Tennessee, December 7, 1960, Knoxville, Tennessee.

M. F. Fair

Health Physics (2 lectures), Duke University Marine Laboratory, August 3–4, 1960, Beaufort, North Carolina; ASEE-AEC Summer Institute, ORNL, August 8, 1960, Oak Ridge, Tennessee; ORINS, September 15, 1960, January 19, and May 11, 1961, Oak Ridge, Tennessee; Soil Conservation Group, ORINS, October 10, 1960, Oak Ridge, Tennessee; ORINS Medical Division, December 15, 1960, April 27, and May 25, 1961, Oak Ridge, Tennessee; (5 lectures) Florida State University, July 19–20, 1961, Tallahassee, Florida; (5 lectures) University of Wyoming, July 26–27, 1961, Laramie, Wyoming.

L. Hemphill

Origin and Nature of Fuel Process Wastes, U.S. Public Health Service Course on Reactor Environmental Health Problems, ORNL, May 10, 1961, Oak Ridge, Tennessee.

G. S. Hurst

Methods of Mixed Radiation Dosimetry, ORSORT Lecture, July 21, 1960, Oak Ridge, Tennessee.

Dosimetry of Mixtures of Neutrons and Gamma Radiation-Counting Methods, Summer Postgraduate Course in Medical Aspects of Radiological Health, St. Louis University Hospital, August 11, 1960, St. Louis, Missouri.

Dosimetry of Neutrons and Gamma Radiation – Integrating Methods: Application to Radiation Accidents, Summer Postgraduate Course in Medical Aspects of Radiological Health, St. Louis University Hospital, August 12, 1960, St. Louis, Missouri.

T. F. Lomenick

Ground Disposal of Solids and Liquids, Short Course in Health Physics for Public Health Personnel, presented for AEC and ORINS at ORNL, April 18, 1961, Oak Ridge, Tennessee; ORSORT, January 4, 1961, Oak Ridge, Tennessee.

K. Z. Morgan

Permissible Exposure and Ionizing Radiation with Reactors, Oak Ridge High School, July 27, 1960, Oak Ridge, Tennessee

Maximum Permissible Body Burdens of Radionuclides, St. Louis University School of Medicine, August 16–18, 1960, St. Louis, Missouri.

Radiation Safety, Radiation Safety Training Program, ORNL, September 28, 1960, Oak Ridge, Tennessee; Staff Conference Training Program, ORNL, October 17–21, 1960, Oak Ridge, Tennessee.

The Significance of the Tissue Analysis Program for the Estimation of Internal Dose, ORNL, October 25, 1960, Oak Ridge, Tennessee.

Remarks for Information Meeting, Health Physics Division Information Meeting, ORNL, October 27, 1960, Oak Ridge, Tennessee.

Maximum Permissible Internal Dose of Radionuclides, Donner Laboratory, University of California, November 28, 1960, Berkeley, California.

Health Physics, ORSORT Lecture, December 18, 21, 1960, Oak Ridge, Tennessee.

Idaho Accident, Safety Building, ORNL, January 16, 1961, Oak Ridge, Tennessee; ORSORT, February 3, 1961, Oak Ridge, Tennessee.

Permissible Exposure to Ionizing Radiation, University of North Carolina, January 31, 1961, Chapel Hill, North Carolina.

Permissible Exposure to Radiation and Allowable Environmental Contamination, Radiation Safety Training Program, ORNL, February 27–28, 1961, Oak Ridge, Tennessee; Chemistry and Physics Division Seminar, ORNL, March 24, 1961, Oak Ridge, Tennessee.

Maximum Permissible Exposure to External and Internal Ionizing Radiation, Medical College of Virginia, March 2, 1961, Richmond, Virginia.

The SL-1 Accident, Society of Nuclear Medicine, Academy of Medicine, March 11, 1961, Atlanta, Georgia.

Permissible Exposure, University of Kentucky, March 15, 1961, Lexington, Kentucky; ORINS Training Class in Health Physics, ORNL, April 26–28, 1961, Oak Ridge, Tennessee.

Permissible Dose for External Radiation, Refresher Course on Permissible Dose for AIHA, April 10, 1961, Detroit, Michigan.

Control of Radiation Exposure to Humans – Radiation Guidance Limits – Why?, Health Physics Society, Oak Ridge Section, April 20, 1961, Oak Ridge, Tennessee.

Internal Dose Lecture, Vanderbilt University, May 1–2, 1961, Nashville, Tennessee.

Civil Defense Lecture, ORNL, May 3, 1961, Oak Ridge, Tennessee.

R. J. Morton

Oak Ridge National Laboratory Waste Disposal Facilities and Field Studies (tour and lecture), ORNL, August 12, 1960, Oak Ridge, Tennessee; ORSORT 1960 ASEE-AEC Summer Institute for College Professors, August 8–12, 1960, Oak Ridge, Tennessee.

Radioactive Waste Problems in Environmental Health Programs, Staff Meeting of Division of Sanitation, Kansas State Board of Health, September 29, 1960, Hutchinson, Kansas.

J. S. Olson

Movement of Radioactive Isotopes in Ecosystems, Duke University, December 7, 1960, Durham, North Carolina; Sigma Xi, University of Alabama Medical Center, and Southern Research Institute, January 5, 1961, Birmingham, Alabama; Sigma Xi, University of Alabama, January 6, 1961, Tuscaloosa,

Alabama; Sigma Xi and Botany Department, University of Georgia, March 1, 1961, Athens, Georgia; Biology Department, Florida State University, March 6, 1961, Tallahassee, Florida; Vanderbilt University, April 13, 1961, Nashville, Tennessee; Biology Department, St. Mary's College, April 26, 1961, South Bend, Indiana.

Professional Opportunities in Radiation Ecology, Ecology Seminar, Botany Department, Duke University, December 8, 1960, Durham, North Carolina.

Gamma Spectrometry and Other Techniques of Using Multiple Tracers in Field Conditions, Isotopes Techniques Class and staff and visitors to Biology Department, University of Alabama, January 6, 1961, Tuscaloosa, Alabama.

Advantages and Limitations of Individual Isotopes in Ecological Research, Graduate Seminar, Zoology Department, University of Georgia, Athens, Georgia.

Uses of Isotopes in Forestry Research, Forestry School and Sigma Xi, University of Georgia, March 2, 1961, Athens, Georgia.

Sand Dune Development, Graduate Ecology Field Trip, Institute of Marine Studies, University of Georgia, March 3, 1961, Sapelo Island, Georgia.

Ecological and Social Significance of Radioactive Contamination of the Environment, Botany Department, University of Chicago, April 24, 1961, Chicago, Illinois.

Ecological Impact of a Nuclear Attack, Particularly on Vegetation, Discussion for NAS-NRC Advisory Committee on Civil Defense, May 6, 1961, Washington, D.C.

W. S. Snyder

Neutron Dose in Tissue Phantoms, Vanderbilt University, November 16, 1960, Nashville, Tennessee.

Single Exposure Dose, Neutron Dose, Federal Radiation Council, International Commission on Radiological Protection, National Committee on Radiation Protection, Vanderbilt University, April 24–25, 1961, Nashville, Tennessee.

Estimation of Neutron Dose, Societe de Radiation Protection, April 7, 1961, Saclay, France.

E. G. Struxness

Waste Handling and Research and Development Concerning Waste Disposal, Short Course in Health Physics for Public Health Personnel, presented for AEC and ORINS at ORNL, May 11, 1961, Oak Ridge, Tennessee.

Radioactive Waste Disposal (two 2-hr lectures), Health Physics Fellowship Program, Vanderbilt University, May 1, 2, 1961, Nashville, Tennessee.

Subterranean Disposal of Radioactive Wastes, Second Colloquium on Public Health and the Problems of Radioactive Waste Disposal, Section of Nuclear Medicine, University of Chicago, November 30–December 2, 1960, Chicago, Illinois.

Studies on Disposal of Radioactive Wastes in Natural Salt Formations, Staff Meeting of Division of Sanitation, Kansas State Board of Health, September 29, 1960, Hutchinson, Kansas.

T. Tamura

Structural Implications of Cesium Sorption by Alumino-Silicate Clays, Chemistry Department Seminar, University of North Carolina, May 13, 1961, Chapel Hill, North Carolina.

INTERNAL DISTRIBUTION

1. C. E. Larson
2. Biology Library
3–5. Central Research Library
6. Reactor Division
7–56. Laboratory Records Department
57. Laboratory Records, ORNL R.C.
58. J. P. Murray (K-25)
59. R. G. Jordan (Y-12)
60. A. M. Weinberg
61. J. A. Swartout
62. K. Z. Morgan
63. M. L. Nelson
64. S. C. Lind
65. A. S. Householder
66. C. S. Harrill
67. C. E. Winters
68. E. H. Taylor
69. W. H. Jordan
70. T. A. Lincoln
71. A. Hollaender
72. F. L. Culler
73. H. E. Seagren
74. D. Phillips
75. M. T. Kelley
76. R. S. Livingston
77. C. D. Susano
78. R. J. Morton
79. E. G. Struxness
80. W. E. Cohn
81. M. L. Randolph
82. M. J. Skinner
83. J. C. Hart
84. T. H. J. Burnett
85. G. S. Hurst
86. S. R. Bernard
87. J. A. Lane
88. W. S. Snyder
89. L. B. Holland
90. J. L. Gabbard
91. A. C. Upton
92. D. M. Davis
93. R. L. Clark
94. L. C. Johnson
95. O. D. Teague
96. E. J. Kuna
97. A. D. Warden
98. J. A. Auxier
99. S. I. Auerbach
100. F. C. Maienschein
101. B. Fish
102. C. E. Breckinridge
103. R. D. Birkhoff
104. J. A. Harter
105. R. W. Peelle
106. R. M. Richardson
107. J. S. Olson
108. D. Bagwell (consultant)
109. T. E. Bortner (consultant)
110. P. H. Doyle (consultant)
111. U. Fano (consultant)
112. T. D. Strickler (consultant)
113. J. C. Frye (consultant)
114. W. H. Langham (consultant)
115. G. M. Fair (consultant)
116. R. E. Zirkle (consultant)
117. L. S. Taylor (consultant)
118. R. L. Platzman (consultant)
119. N. Wald (consultant
120. ORNL – Y-12 Technical Library, Document Reference Section

EXTERNAL DISTRIBUTION

121. Physics and Engineering Group, Balcones Research Center, RFD 4, Box 189, Austin, Texas
122. G. E. Thoma, St. Louis University Hospital, 135 South Grand Boulevard, St. Louis, Missouri
123. Vanderbilt University (Physics Library)
124. H. LeGrande, U.S. Geological Survey, Washington, D.C.
125. Lola Lyons, Librarian, Olin Industries, Inc., East Alton, Illinois
126. Jack Story, Health Physicist, North Carolina State College, Raleigh, North Carolina
127. J. H. Ebersole, USSS Nautilus, c/o Fleet Post Office, New York, New York

128. David S. Smith, Health and Safety Division, U.S. Atomic Energy Commission, Chicago Operations Office, P.O. Box 59, Lemont, Illinois
129. Research and Development Division, AEC, ORO
130. S. C. Sigoloff, Edgerton, Germeshausen and Grier, Inc., P. O. Box 98, GoLeta, California
131. Robert Wood, Department of Physics, Memorial Center, 444 E. 68th St., New York 21, New York
132. John Wolfe, Division of Biology and Medicine, U.S. Atomic Energy Commission, Washington, D.C.
133. Orlando Park, Department of Biology, Northwestern University, Evanston, Illinois
134. Eugene Odum, Department of Zoology, University of Georgia, Athens, Georgia
135. W. T. Ham, Medical College of Virginia, Richmond, Virginia
136. F. H. W. Noll, Department of Physics, Berea College, Berea, Kentucky
137. Herbert E. Stokinger, Bureau of State Service, Department of Health Education and Welfare, Penn 14 Broadway, Cincinnati 2, Ohio
138. J. B. Lackey, University of Florida, Gainesville, Florida
139. J. J. Davis, Biology Operation, Hanford Atomic Power Operations, Seattle, Washington
140. Robert B. Platt, Department of Biology, Emory University, Atlanta, Georgia
141. C. H. Bernard, Physics Department, Texas A&M College Station, Texas
142. C. E. Dady, Watertown Arsenal, Ordinance Material Research Office, Watertown, Massachusetts
143. John I. Hopkins, Davidson College, Department of Physics, P.O. Box 327, Davidson, North Carolina
144. W. J. Lacy, Office of Civil Defense Mobilization, Battle Creek, Michigan
145. G. A. Andrews, Oak Ridge Institute of Nuclear Studies, Oak Ridge, Tennessee
146. E. P. Resner, States Marine Lines, c/o New York Shipbuilding Corp., Camden, New Jersey
147–151. J. A. Lieberman, Division of Reactor Development, AEC, Washington, D.C.
152. H. J. Carey, Jr., The Carey Salt Company, Hutchinson, Kansas
153. C. Orr, Georgia Institute of Technology, Atlanta, Georgia
154. E. F. Gloyna, Department of Civil Engineering, University of Texas, Austin 12, Texas
155. J. S. Cragwall, Jr., U.S. Geological Survey, Surface Water Branch, 823 Edney Building, Chattanooga, Tennessee
156. H. H. Waesche, AEC Liaison Officer, Geochemical and Petrology Branch, U.S. Geological Survey, Naval Gun Factory, Building 213, Washington 25, D.C.
157. S. Leary Jones, Tennessee Department of Public Health, Cordell Hull Building, Nashville, Tennessee
158. H. C. Thomas, Chemistry Department, University of North Carolina, Chapel Hill, North Carolina
159. Glenn Gentry, Fish Management Division, Game and Fish Commission, Cordell Hull Building, Nashville, Tennessee
160. Vincent Schultz, Environmental Sciences Branch, Division of Biology and Medicine, U.S. Atomic Energy Commission, Washington 25, D.C.
161. O. W. Kochtitzky, Tennessee Valley Authority, 717 Edney Building, Chattanooga, Tennessee
162. Leslie Silverman, Industrial Engineering, Department of Industrial Hygiene School of Public Health, Harvard University, 55 Shattuck Street, Boston 15, Massachusetts
163. J. Wade Watkins, U.S. Bureau of Mines, Bartlesville, Oklahoma
164. Kansas State Board of Health, Topeka, Kansas (Dwight F. Metzler)
165. Kansas State Geological Survey, Lawrence, Kansas (Frank C. Foley)
166. W. R. Thurston, Executive Secretary, Division of Earth Sciences, National Academy of Sciences – National Research Council, Washington, D.C.
167. C. S. Shoup, Biology Division, U.S. Atomic Energy Commission, Oak Ridge, Tennessee
168. L. Garcia, Naval Research Laboratory, Washington, D.C.
169–831. Given distribution as shown in TID-4500 (16th ed. Rev.) under Health and Safety category (100 copies – OTS)